CHROMATIN STRUCTURE AND FUNCTION

EDITED BY: Laxmi Narayan Mishra, Christophe Thiriet and Dileep Vasudevan

PUBLISHED IN: Frontiers in Genetics and Frontiers in Cell and Developmental Biology

frontiers Research Topics

ISSN 1664-8714
ISBN 978-2-83250-785-8
DOI 10.3389/978-2-83250-785-8

About Frontiers

Frontiers is more than just an open-access publisher of scholarly articles: it is a pioneering approach to the world of academia, radically improving the way scholarly research is managed. The grand vision of Frontiers is a world where all people have an equal opportunity to seek, share and generate knowledge. Frontiers provides immediate and permanent online open access to all its publications, but this alone is not enough to realize our grand goals.

Frontiers Journal Series

The Frontiers Journal Series is a multi-tier and interdisciplinary set of open-access, online journals, promising a paradigm shift from the current review, selection and dissemination processes in academic publishing. All Frontiers journals are driven by researchers for researchers; therefore, they constitute a service to the scholarly community. At the same time, the Frontiers Journal Series operates on a revolutionary invention, the tiered publishing system, initially addressing specific communities of scholars, and gradually climbing up to broader public understanding, thus serving the interests of the lay society, too.

Dedication to Quality

Each Frontiers article is a landmark of the highest quality, thanks to genuinely collaborative interactions between authors and review editors, who include some of the world's best academicians. Research must be certified by peers before entering a stream of knowledge that may eventually reach the public - and shape society; therefore, Frontiers only applies the most rigorous and unbiased reviews.
Frontiers revolutionizes research publishing by freely delivering the most outstanding research, evaluated with no bias from both the academic and social point of view. By applying the most advanced information technologies, Frontiers is catapulting scholarly publishing into a new generation.

What are Frontiers Research Topics?

Frontiers Research Topics are very popular trademarks of the Frontiers Journals Series: they are collections of at least ten articles, all centered on a particular subject. With their unique mix of varied contributions from Original Research to Review Articles, Frontiers Research Topics unify the most influential researchers, the latest key findings and historical advances in a hot research area! Find out more on how to host your own Frontiers Research Topic or contribute to one as an author by contacting the Frontiers Editorial Office: frontiersin.org/about/contact

CHROMATIN STRUCTURE AND FUNCTION

Topic Editors:
Laxmi Narayan Mishra, Regeneron Pharmaceuticals, Inc., United States
Christophe Thiriet, UMR6286 Unité de fonctionnalité et Ingénierie des Protéines (UFIP), France
Dileep Vasudevan, Institute of Life Sciences (ILS), India

Citation: Mishra, L. N., Thiriet, C., Vasudevan, D., eds. (2022). Chromatin Structure and Function. Lausanne: Frontiers Media SA. doi: 10.3389/978-2-83250-785-8

Table of Contents

frontiers | Frontiers in Genetics

TYPE Editorial
PUBLISHED 07 February 2023
DOI 10.3389/fgene.2023.1140534

OPEN ACCESS

EDITED AND REVIEWED BY
Michael E. Symonds,
University of Nottingham, United Kingdom

*CORRESPONDENCE
Laxmi Narayan Mishra,
mishrabiotech@gmail.com
Christophe Thiriet,
Christophe.Thiriet@univ-rennes1.fr,
Dileep Vasudevan,
dileep@ils.res.in

†Present address:
Laxmi Narayan Mishra, Regeneron Pharmaceuticals Inc, Tarrytown, NY, United States

SPECIALTY SECTION
This article was submitted to Epigenomics and Epigenetics, a section of the journal Frontiers in Genetics

RECEIVED 09 January 2023
ACCEPTED 25 January 2023
PUBLISHED 07 February 2023

CITATION
Mishra LN, Thiriet C and Vasudevan D (2023), Editorial: Chromatin structure and function.
Front. Genet. 14:1140534.
doi: 10.3389/fgene.2023.1140534

Editorial: Chromatin structure and function

Laxmi Narayan Mishra[1*†], Christophe Thiriet[2*] and Dileep Vasudevan[3*]

[1]Albert Einstein College of Medicine, Bronx, NY, United States, [2]Université de Rennes 1, CNRS-UMR6290 Institut génétique et développement de Rennes (IGDR), Rennes, France, [3]DBT-Institute of Life Sciences, Bhubaneswar, India

KEYWORDS

chromatin, histone, histone posttranslational modifications, chromatin remodeling, DNA damage repair

Editorial on the Research Topic
Chromatin structure and function

Chromatin dynamics influence DNA-dependent processes such as transcription, repair, replication, and recombination (Hübner and Spector, 2010; Galvani and Thiriet, 2015). Because disorganized chromatin affects gene expression and eventually leads to disease onset, scientists are eager to learn more about the roles of histone PTMs, DNA methylation, and chromatin remodeling factors in chromatin dynamics. In eukaryotes, how genes are packaged in chromatin determines whether or not the genes can be expressed to produce the encoded product. Typically, DNA-binding factors cannot access DNA within the nucleosome, and nucleosomes must be disassembled for them to gain access to the underlying DNA (Mishra and Hayes, 2018; Sundaram and Vasudevan, 2020). Various high-throughput technologies have emerged to aid researchers in understanding chromatin structure and function (Marr et al., 2022). This Research Topic contains numerous articles on chromatin dynamics, transcription, DNA damage repair, and drug resistance.

In their study, Vinaychandran and Bhargava describe how the structural characteristics of nucleosomal DNA affect transcription factor binding and effective translation. Shi et al. reviewed recent advances in determining chromatin dynamics and their modulation by factors such as PTMs, histone variant incorporation, and effector protein binding. Seharawat et al. discuss how histone PTMs affect nucleosome structure and regulate chromatin accessibility in a review. Pavlenko et al.'s review article summarizes current knowledge on the functions of lysine-specific demethylase-5 and focuses on molecular interactions and their potential implications. They also bring unanswered questions about histone demethylation that require the scientific community's attention to understand it fully.

Genome attacks are common throughout cell life, and various factors can cause DNA damage. When a DNA lesion occurs, the cell repairs it to preserve the genetic material's integrity. Because the genome has been condensed into chromatin, the repair must occur within the context of chromatin structure to access and repair damaged DNA (Hauer and Gasser, 2017). Bisht et al. in their research article, show that the interaction of SMARCAL1 and BRG1, two chromatin remodeling factors that collaborate in the promoter region during double-stranded DNA repair, is dependent on their ATPase activity. Based on BRCA1 and 53BP1 abundance and organization, Abate and Hendzel's study demonstrates the presence of multiple classes of DNA double-strand break (DSB) repair compartments. Roemer et al. discuss constitutive heterochromatin accessibility. They studied the chromocenter concentrations and diffusion of several DSB sensors, mediators, and effector proteins in

mice without DNA damage using fluorescently labeled proteins involved in DNA damage detection and repair. In their review, Aricthota et al. discuss the role of histone acetylation in altering chromatin organization and promoting the recruitment of DSB repair proteins to DNA damage sites.

On the other hand, nucleosome assembly is required to restore the native nucleosomal template and the correct epigenetic landscape, which is most visible during DNA replication. The newly synthesized DNA must be packaged in a consistent, complementary, and epigenetically tagged fashion. At the replication fork, a highly orchestrated mechanism not only creates templates and produces an identical copy of DNA but also removes nucleosomes in front and reassembles histones into nucleosomes behind (Verreault, 2000). Zhao et al. reconstituted nucleosomes *in vitro* using the nucleosome positioning sequence Widom 601 and proposed a chemical-kinetic model of nucleosome assembly and disassembly using precise biophysical methods such as FRET and FTS assays. Gene regulation, recombination, and other fundamental processes rely on large-scale chromatin interactions, including chromosome interactions. Krajewski discusses how bulky post-translational histone modifications like ubiquitination, internucleosomal dynamics, and DNA stress work together to functionalize nucleosomes in a large nucleosome array in his hypothesis and theory paper.

Methylation of DNA regulates gene expression by generally turning the gene off (Moore and Fan, 2013). Li et al. discuss the limitations of identifying N6-methyladenine, a poorly studied DNA methylation in eukaryotes. They also discuss the potential applications of this recently discovered DNA modification. In a systematic review, Rawat et al. discuss the coexisting mutations and gene expression trends associated with K13-mediated artemisinin resistance in *Plasmodium falciparum*. They analyzed a large dataset of single nucleotide polymorphisms (SNPs) to determine the prevalence, geographic distribution, and coexistence patterns of genetic markers associated with artemisinin resistance.

Overall, the breadth of the articles in this Research Topic demonstrates the remarkable progress being made in understanding the critical roles of chromatin structure in transcription, replication, and DNA damage repair. These articles also raise numerous unanswered questions that must be addressed in the near future to fully understand the disease biology associated with altered chromatin structure.

Author contributions

As guest editors, LM, CT, and DV organized the Research Topic, invited authors, and oversaw manuscript review. LM wrote the editorial. LM, CT, and DV edited and approved the publication. All listed authors contributed significantly, directly, and intellectually to the work and approved its publication.

Conflict of interest

LM is employed by Regeneron Pharmaceuticals Inc.

The remaining authors declare that the research was conducted in the absence of any commercial or financial relationships that could be construed as a potential conflict of interest.

Publisher's note

References

Galvani, A., and Thiriet, C. (2015). Nucleosome dancing at the tempo of histone tail acetylation. *Genes. (Basel)* 6 (3), 607–621. doi:10.3390/genes6030607

Hauer, M. H., and Gasser, S. M. (2017). Chromatin and nucleosome dynamics in DNA damage and repair. *Genes. Dev.* 31 (22), 2204–2221. doi:10.1101/gad.307702.117

Hübner, M. R., and Spector, D. L. (2010). Chromatin dynamics. *Annu. Rev. Biophys.* 39, 471–489. doi:10.1146/annurev.biophys.093008.131348

Marr, L. T., Jaya, P., Mishra, L. N., and Hayes, J. J. (2022). Whole-genome methods to define DNA and histone accessibility and long-range interactions in chromatin. *Biochem. Soc. Trans.* 50, 199–212. doi:10.1042/BST20210959

Mishra, L. N., and Hayes, J. J. (2018). A nucleosome-free region locally abrogates histone H1–dependent restriction of linker DNA accessibility in chromatin. *J. Biol. Chem.* 293 (50), 19191–19200. doi:10.1074/jbc.RA118.005721

Moore, L., and Fan, G. (2013). DNA methylation and its basic function. *Neuropsychopharmacol* 38, 23–38. doi:10.1038/npp.2012.112

Sundaram, R., and Vasudevan, D. (2020). Structural basis of nucleosome recognition and modulation. *Bioessays* 42 (9), e1900234. doi:10.1002/bies.201900234

Verreault, A. (2000). De novo nucleosome assembly: New pieces in an old puzzle. *Genes. Dev.* 14 (12), 1430–1438. doi:10.1101/gad.14.12.1430

frontiers in Cell and Developmental Biology

ORIGINAL RESEARCH
published: 07 October 2021
doi: 10.3389/fcell.2021.762571

Nucleosome Assembly and Disassembly *in vitro* Are Governed by Chemical Kinetic Principles

Hongyu Zhao[1,2], Mingxin Guo[1,2], Fenghui Zhang[1,2], Xueqin Shao[1,2], Guoqing Liu[1,2], Yongqiang Xing[1,2], Xiujuan Zhao[1,2], Liaofu Luo[1,2] and Lu Cai[1,2]**

[1] School of Life Science and Technology, Inner Mongolia University of Science and Technology, Baotou, China, [2] Inner Mongolia Key Laboratory of Functional Genome Bioinformatics, Inner Mongolia University of Science and Technology, Baotou, China

OPEN ACCESS

Edited by:
Christophe Thiriet, UMR 6286 Unité de Fonctionnalité et Ingénierie des Protéines (UFIP), France

Reviewed by:
Andrew Bowman, University of Warwick, United Kingdom
Rodolfo Negri, Sapienza University of Rome, Italy

***Correspondence:**
Liaofu Luo
lolfcm@imu.edu.cn
Lu Cai
nmcailu@163.com

Specialty section:
This article was submitted to Epigenomics and Epigenetics, a section of the journal Frontiers in Cell and Developmental Biology

Received: 22 August 2021
Accepted: 17 September 2021
Published: 07 October 2021

Citation:
Zhao H, Guo M, Zhang F, Shao X, Liu G, Xing Y, Zhao X, Luo L and Cai L (2021) Nucleosome Assembly and Disassembly in vitro Are Governed by Chemical Kinetic Principles. Front. Cell Dev. Biol. 9:762571. doi: 10.3389/fcell.2021.762571

As the elementary unit of eukaryotic chromatin, nucleosomes *in vivo* are highly dynamic in many biological processes, such as DNA replication, repair, recombination, or transcription, to allow the necessary factors to gain access to their substrate. The dynamic mechanism of nucleosome assembly and disassembly has not been well described thus far. We proposed a chemical kinetic model of nucleosome assembly and disassembly *in vitro*. In the model, the efficiency of nucleosome assembly was positively correlated with the total concentration of histone octamer, reaction rate constant and reaction time. All the corollaries of the model were well verified for the Widom 601 sequence and the six artificially synthesized DNA sequences, named CS1–CS6, by using the salt dialysis method *in vitro*. The reaction rate constant in the model may be used as a new parameter to evaluate the nucleosome reconstitution ability with DNAs. Nucleosome disassembly experiments for the Widom 601 sequence detected by Förster resonance energy transfer (FRET) and fluorescence thermal shift (FTS) assays demonstrated that nucleosome disassembly is the inverse process of assembly and can be described as three distinct stages: opening phase of the (H2A–H2B) dimer/$(H3–H4)_2$ tetramer interface, release phase of the H2A–H2B dimers from $(H3–H4)_2$ tetramer/DNA and removal phase of the $(H3–H4)_2$ tetramer from DNA. Our kinetic model of nucleosome assembly and disassembly allows to confirm that nucleosome assembly and disassembly *in vitro* are governed by chemical kinetic principles.

Keywords: nucleosome reconstitution *in vitro*, nucleosome disassembly, chemical kinetic model, nucleosome structure, nucleosome dynamics

INTRODUCTION

The nucleosome is the elementary repeating unit of chromatin in eukaryotes. Approximately 147 base pairs (bp) of DNA in a left-handed superhelix wrap approximately 1.75 turns on an octamer containing two copies of four histone proteins to form a nucleosome core (Luger et al., 1997). In addition to serving as the building blocks of chromatin to pack DNA, nucleosome structure can also

dynamically regulate many biological processes, such as transcription, DNA replication, repair, and recombination (Völker-Albert et al., 2016; Liu et al., 2019).

Nucleosomes are highly dynamic *in vivo*. Eviction of histones and reconstruction of nucleosomes occur frequently upon chromatin rearrangement (Kameda et al., 2019). Nucleosome positioning is malleable and movable along the DNA (Lai and Pugh, 2017; Liu et al., 2018). These dynamic nucleosomes can be regulated by posttranslational modifications (PTMs), replacing of their component histones, histone chaperones interacting with nucleosomes and remodeling devices. Gene expression involves nucleosomal rearrangement. In turn, changes in nucleosome positioning can also modulate gene expression by adjusting the DNA accessibility of regulatory proteins (Kameda et al., 2019).

Several works have investigated the dynamic process of nucleosomes. Ranjith et al. (2007) presented a kinetic model based on *Xenopus* egg extract solutions without added adenosine triphosphate (ATP) to describe the force-dependent on- and off-kinetics for nucleosomes and diffusion of nucleosomes along DNA. Förster resonance energy transfer (FRET) assays showed that the steps of nucleosome disassembly include the opening of the $(H3–H4)_2$ tetramer/(H2A–H2B) dimer interface, H2A–H2B dimer release from the DNA and $(H3–H4)_2$ tetramer removal (Gansen et al., 2009; Böhm et al., 2011). Remodeling kinetics models described the dynamics of chromatin remodeling driven by chromatin remodelers (Padinhateeri and Marko, 2011; Florescu et al., 2012). However, the intrinsic kinetics of the nucleosome assembly reaction without any chaperone remain elusive.

In view of the complexity of participation factors in nucleosome dynamics and the detection difficulty of nucleosome assembly and disassembly *in vivo*, nucleosome reconstitution *in vitro* by salt dialysis is the ideal model to elucidate the dynamic characteristics of nucleosome assembly and disassembly. Nucleosome assembly and disassembly by salt dialysis is not a strictly reversible chemical reaction. Based on the kinetic theory of chemical reactions, we proposed a chemical kinetic model to describe nucleosome assembly by salt dialysis *in vitro*. In the model, the efficiency of nucleosome assembly was positively correlated with the total concentration of histone octamer, reaction rate constant and reaction time. The reaction rate constant in the model may be used as a new parameter to evaluate the affinity of DNA to histones. The model was well tested for the Widom 601 sequence and the six artificially synthesized sequences, named CS1–CS6, by the salt dialysis method *in vitro*. Nucleosome disassembly experiments using the Widom 601 sequence detected by FRET and fluorescence thermal shift (FTS) assays demonstrated that nucleosome disassembly is the inverse process of assembly and can be described as three distinct stages: the opening phase of the (H2A–H2B) dimer/$(H3–H4)_2$ tetramer interface, the release phase of the H2A–H2B dimers from $(H3–H4)_2$ tetramer/DNA and the removal phase of the $(H3–H4)_2$ tetramer from DNA. The present work elucidated that nucleosome assembly and disassembly *in vitro* are governed by chemical kinetic principles, and could provide deeper insight into the mechanism of nucleosome dynamics *in vivo*.

MATERIALS AND METHODS

Preparation of DNAs and Recombinant Histone Octamer

To investigate the relation between N/S and underlying factors in assembly, 147-bp- length 601 DNA was labeled with Cy3 for canonical gel detection of nucleosomes (Lowary and Widom, 1998). The forward primer of polymerase chain reaction (PCR) was 5′-Cy3-CAGGATGTA TATATCTGACACGTGCCT-3′, and the reverse primer was 5′-CTGGAGAATCCCGGTGCCGAGGCC-3′. In addition, six artificially synthesized CS1–CS6 DNA sequences were used for experimental verification. Detailed sequence information is shown in our previous paper (Zhao et al., 2019). The forward primer of PCR was 5′-Cy3- ACGGCCAGTGAATTCGAGG-3′, and the reverse primer was 5′- GCCAAGCTTCTGAGATC GGAT-3′.

To reveal the nucleosome disassembly phases using gel electrophoresis and FRET analysis, 169-bp-long Widom 601 DNA fragments labeled by Cy3 and Cy5 of double fluorescence molecules with a Förster distance of ∼54 Å were prepared by PCR from a plasmid containing the 601 sequence. Forward primer: 5′-ACAGTACTGGCCGCCCTGGAGAATCCCGGTG CCGAGGCCGC***T***(Cy3)CAATTG-3′; reverse primer: 5′-TAC ATGCACAGGATGTATATATCTGACACGTGCCTGGAGAC***T***(Cy5)AGGGAG-3′.

To understand the disassembly mechanism using FTS, 147-bp-long 601 fragments without any labeling marker were prepared by PCR from a plasmid containing the 601 sequence. The forward primer of PCR was 5′-CAGGA TGTAT ATAT CTGACA CGTGCCT-3′, and the reverse primer was 5′-CTGGA GAATC CCGG TGC CGAGGCC-3′.

All primers were synthesized in Sangon Biotech, China.

The expression and purification of histones were performed as described previously (Zhao et al., 2015, 2019). Briefly, four histones (H2A, H2B, H3, and H4) were expressed and purified from *Escherichia coli* BL21 cells containing pET-histone expression plasmids. To reconstitute the histone octamer, four histones with equimolar ratios were mixed in refolding buffer (2 M NaCl, 10 mM Tris–HCl, pH 7.5, 1 mM Na-EDTA, and 5 mM 2-mercaptoethanol). Histone octamers were purified through a Superdex S200 filtration column (GE Healthcare). Confirmation of the purity and stoichiometry of the histone octamers was performed using SDS-PAGE on 15% gels with Coomassie Brilliant Blue staining, and the concentration was determined using an extinction coefficient at 276 nm.

Nucleosome Assembly Reaction *in vitro*

For *in vitro* structure investigation, mononucleosomes were assembled by using the salt-dialysis method as described previously (Zhao et al., 2015, 2019). Each DNA fragment was incubated in reconstitution reactions containing 10 mM Tris–HCl (pH 8.0), 1 mM EDTA (pH 8.0), 2 M NaCl, and histone octamers. The samples were placed in a microdialysis apparatus with 6–8 kDa dialysis tubing (Thermo Scientific, Slide-A-Lyzer MINI Dialysis Units, 7,000 MWCO). Then, they were placed in a beaker containing high-salt buffer (10 mM Tris–HCl, pH

8.0, 2 M NaCl, and 1 mM EDTA), which was continuously diluted by slowly pumping in TE buffer (10 mM Tris–HCl, pH 8.0, 1 mM EDTA) to a lower concentration of NaCl from 2 to 0.6 M over a period of 16 h. After this period, the samples were further dialyzed for an additional minimum of 3 h in TE buffer (10 mM Tris–HCl, pH 8.0, 1 mM EDTA) for gel analysis or in 10 mM HEPES buffer for FTS and FRET analysis. Dialysis was performed in a darkroom for the assembly reaction on fluorescence-labeled DNA templates. All of the steps were performed at 4°C.

In the reaction system, 3 μg DNA templates in total 60 μL reaction volume was used to assemble nucleosome. The molar concentration of 601 DNA sequence is 5.09×10^{-7} mol/L, and the molar concentration of CS DNA sequences is 4.62×10^{-7} mol/L in reaction system. As shown in **Table 1**, the concentrations of histone octamer and the ratios of histone octamer to DNA in reaction system have a change of gradient.

Gel Analysis of Nucleosome Assembly Efficiency

For Cy3-labeled DNA templates, the reaction mixtures were resolved on 5% native polyacrylamide gels in 0.5 × TBE. The Cy3 fluorescence of nucleosome DNA and the free DNA band in the gel was measured and quantified at an emission wavelength of 605 nm and excitation wavelength of 520 nm (GE Healthcare, Amersham Imager 600RGB and Image Quant TL).

While Widom 601 DNA templates were labeled by Cy3 and Cy5 of double fluorescence molecule, the Cy5 fluorescence signal of nucleosome DNA and free DNA band in the gel was detected and quantified at an emission of 705 nm and excitation of 630 nm (GE Healthcare, Amersham Imager 600RGB and ImageQuant TL).

For nonlabeled DNA templates in FTS analysis, the reconstituted samples were loaded on 5% native polyacrylamide gels in 0.5 × TBE and stained with ethidium bromide.

TABLE 1 | The concentrations of histone octamer and the ratios of histone octamer to DNA in reaction system.

Mass concentrations of histone octamer (μg/mL)	Molar concentrations of histone octamer (mol/L)	Molecular ratio of histone octamer to 601 sequence	Molecular ratio of histone octamer to CS sequences
5	0.46×10^{-7}	0.090	0.100
10	0.92×10^{-7}	0.181	0.199
15	1.38×10^{-7}	0.271	0.299
20	1.84×10^{-7}	0.361	0.398
25	2.30×10^{-7}	0.452	0.498
30	2.76×10^{-7}	0.542	0.597
35	3.22×10^{-7}	0.633	0.697
40	3.68×10^{-7}	0.723	0.797
45	4.14×10^{-7}	0.813	0.896
50	4.60×10^{-7}	0.904	0.996
55	5.06×10^{-7}	0.994	1.095
60	5.52×10^{-7}	1.084	1.195

Förster Resonance Energy Transfer Analysis

The double-fluorescence-labeled Widom 601 DNA templates were reconstituted into mononucleosomes using the salt dialysis method as described above. FRET experiments were performed at 20°C on a fluorescence spectrometer (Bio-Tek, Cytation5).

For the temperature-dependent dissociation detection by FRET assay, reconstituted samples with different incubation time at 70°C were detected. The difference in fluorescence intensity between the donor and acceptor emissions was normalized. Then, the temperature-dependent dissociation curves of nucleosomes were generated between fluorescence intensity and incubation time.

For the salt-dependent dissociation study, samples with different concentrations of NaCl were excited at 485 nm, and the emission was recorded from 570 to 800 nm. The difference in the fluorescence intensity between the donor and acceptor emissions was plotted against the concentration of NaCl, which generated the salt-dependent dissociation curves of nucleosomes (Chen et al., 2013). The change rate of fluorescence was calculated by the difference of fluorescence against difference of ion concentration.

Thermal Stability Assay

The stabilities of nucleosome dissociation were evaluated by a thermal stability shift assay as described previously (Sueoka et al., 2017; Arimura et al., 2018). A 147-bp-long 601 fragments without any labeling-marker were used. The thermal stability assay was performed in a solution containing, 0.25 M NaCl, 10 mM HEPES, 1 mM β-mercaptoethanol, and 5 × SYPRO Orange. The nucleosomes were equivalent to 375 ng DNA in each reaction. The total volume was adjusted to 30 μL.

The fluorescence signals of SYPRO Orange were recorded in the VIC channel of real-time PCR detection system (ABI 7500), and a temperature gradient was used from 25 to 95°C at each 1°C.

Raw fluorescence intensity data were normalized using the formula of $NF_i = \frac{F_i - F_{min}}{F_{max} - F_{min}}$, where F_i, F_{min}, and F_{max} indicate each fluorescence at a certain temperature, minimum and maximum of fluorescence intensity, respectively. The change rate of fluorescence was calculated by the formula of $CF_i = \frac{NF_{i+1} - NF_i}{T_{i+1} - T_i}$, where NF and T indicate normalized-fluorescence and temperature, respectively. The temperature range is 55–95°C.

RESULTS

A Chemical Reaction Kinetics Model of Nucleosome Assembly

The nucleosome assembly reaction consists of three stages *in vitro*. First, the assembly and dissociation reaction of the histone octamer with its H3/H4 tetramer and two H2A/H2B dimers is not a strictly reversible process. Second, DNAs bind to H3/H4 tetramers to partially assemble an intermediate complex of nucleosomes. Third, two copies of the H2A/H2B dimer successively integrate into the intermediate complex to assemble

a complete nucleosome. The above processes can be written in a set of reaction equations as follows.

$$\begin{cases} P \leftrightarrow P_4 + P_2 + P_2' \quad ① \\ D + P_4 \leftrightarrow N_a \quad ② \\ N_a + P_2 \leftrightarrow N_b \quad ③ \\ N_b + P_2' \leftrightarrow N \quad ④ \end{cases} \tag{1}$$

where P, P_4, P_2, and P_2' represent the histone octamer, H3/H4 tetramer, and two H2A/H2B dimers, respectively. Na and Nb are two nucleosome intermediates. DNA molecules and the intact nucleosomes are denoted as D and N, respectively.

Using the mass action law of chemical reaction, we obtain a set of differential equations about the change of concentration of eight reaction components P, P_4, P_2, P_2', D, Na, Nb, and N. The equations are too complicated to obtain an analytical solution.

For the sake of simplicity, we propose a simplified model to describe the macrokinetics of the reaction process, namely, we study the overall reaction directly.

$$D + P \leftrightarrow N \tag{2}$$

where the rate constants k and k' of the forward and reverse reactions in Eq. 2 are assumed to be time-dependent, $k = k(t)$ and $k' = k'(t)$, respectively. Using the same notation of molecule to represent its concentration, we obtain two differential equations on the concentration of nucleosomes, DNAs and histone octamers.

$$\frac{dN}{dt} = kPD - k'N \tag{3}$$

$$\frac{dD}{dt} = \frac{dP}{dt} = -kPD + k'N \tag{4}$$

where the total amount of DNA and histone octamer in the reaction system, named as S and Q, should be constant. Hence, we obtain Eq. 5

$$\begin{aligned} N + D &= S\,(constant) \\ N + P &= Q(constant) \end{aligned} \tag{5}$$

N/S is defined as the efficiency of nucleosome assembly. It is interesting to uncover the underlying factors affecting N/S and obtain analytic functions.

Combining Eqs. 3, 5, we obtain

$$\frac{dN}{dt} = kN^2 - \left(k' + kS + kQ\right)N + kQS \tag{6}$$

To integrate Eq. 6, one obtains

$$\int_0^N \frac{dN}{N^2 - (\frac{k'}{k} + S + Q)N + QS} = \int_0^T kdt \tag{7}$$

where T is the total dialysis time and the integral $\int_0^T kdt$ can be denoted as $\theta\,(T)$.

In the process of dialysis *in vitro*, k(t) and k'(t) are known since the concentration change of NaCl has been controlled. Thus, the integral in Eq. 7 can be calculated. In experiments, the total nucleosome reconstitution reaction can be split into several steps. The rate constant of the i-th step of the reaction is defined as k_i, and the corresponding reaction time is denoted as τ_i. One has $\theta = \sum_i k_i\tau_i = \bar{k}\sum \tau_i$ where $\bar{k}$ is the mean reaction constant and $\sum \tau_i = T_{ef}$ is the total efficient time of the reaction. The efficient time T_{ef} is an increasing function of the total dialysis time T. In our dialysis experiment, T changes in a relatively small range (approximately in the range from 0.01 to 0.02 h). Therefore, T_{ef} can be approximated as

$$T_{ef} = \alpha + \varepsilon T \tag{8}$$

and we have

$$\theta(T) = \int_0^T kdt = \bar{k}T_{ef} = \bar{k}(\alpha + \varepsilon T) \tag{9}$$

Considering that the gradient descent of NaCl concentration mainly promotes the nucleosome assembly, as a first order approximation, we assume k' to be ignored in Eq. 7. We obtain:

$$\int_0^N \frac{dN}{N^2 - (S+Q)N + QS} = \frac{1}{Q-S}\left(ln\frac{N-Q}{N-S} - ln\frac{Q}{S}\right) = \theta(T)$$

It leads to

$$\frac{N}{S} = \frac{\frac{Q}{S}\left\{1 - exp\left[(Q-S)\theta(T)\right]\right\}}{1 - \frac{Q}{S}exp\left\{(Q-S)\theta(T)\right\}} \tag{10}$$

Under $(Q-S)\,\theta\,(T) = 1$, the exponential function in Eq. 10 is expanded to 2nd order of $(Q-S)\theta(T)$, and it follows

$$\frac{N}{S} \cong \frac{Q\vartheta(T)}{1 + Q\vartheta(T)} = \frac{Q\bar{k}T_{ef}}{1 + Q\bar{k}T_{ef}} = \frac{Q\bar{k}(\alpha + \varepsilon T)}{1 + Q\bar{k}(\alpha + \varepsilon T)} \tag{10.1}$$

which shows N/S approaches to 1 as Q>>S and approaches to 0 as Q<<S. A simplified form of Eq. 10.1 for not-too-large Q is the linear relation between N/S and Q

$$\frac{N}{S} = Q\bar{k}(\alpha + \varepsilon T) \tag{11}$$

which is useful in analyzing experimental data.

Otherwise, if k' cannot be ignored in Eq. 7, then we obtain

$$\frac{1}{Q - S + \gamma\frac{Q+S}{Q-S}}ln\left(\frac{\left\{N - Q\left(1 + \frac{\gamma}{Q-S}\right)\right\}\left\{S\left(1 - \frac{\gamma}{Q-S}\right)\right\}}{\left\{Q\left(1 + \frac{\gamma}{Q-S}\right)\right\}\left\{N - S\left(1 - \frac{\gamma}{Q-S}\right)\right\}}\right) = \bar{k}(\alpha + \varepsilon T) \tag{12}$$

where γ is the integral median of (k'/k). As $\frac{\gamma}{|Q-S|} \ll 1$, Eq. 12 returns to Eq. 10.

Equation 12 gives a rigor expression of N/S depending on the total concentration of DNA and histone octamer, reaction rate constant and reaction time. Eq. 10 is a simplified representation under the condition of ignoring the disassembly reaction, and Eq. 11 provides a simplified linear relation for analyzing experimental data.

The Efficiency of Nucleosome Assembly Is Proportional to Histone Concentration

By using the nucleosome reconstitution method *in vitro* and the canonical gel detection of nucleosomes we shall test the relation between assembly efficiency N/S and histone concentration Q deduced from the chemical kinetic model. First, the Widom 601 DNA sequence (Lowary and Widom, 1998) was labeled by the fluorescence molecular probe Cy3 (**Figure 1A**). A recombinant histone octamer, that lacked all PTMs, was expressed and purified from bacteria (**Figure 1B**). Then, we assembled the mononucleosomes on 601 DNA templates with a concentration gradient of histone octamers. As shown in **Figure 1C**, after separation by gel electrophoresis, the nucleosome-assembled DNAs appeared as retarded bands compared to free DNAs. The ratio of nucleosome DNA in the assembled sample showed an increasing trend with the histone octamer concentration. We then quantified the ratio of nucleosome DNA to total DNA (N/S in Eq. 10) as an assembly efficiency to evaluate the nucleosome formation ability of each assembled sample. The nucleosome assembly efficiency was positively correlated with the histone octamer concentration (**Figure 1D**). This result of nucleosome assembly on the 601 DNA template *in vitro* indicated that N/S has a significant linear correlation with Q for not-too-large Q, which is consistent with Eq. 11.

Then, we examined the nucleosome assembly efficiency for six CS DNA sequences with a histone octamer concentration gradient (**Supplementary Figure 1**). CS DNA templates were designed with different sequence features in our previous work (Zhao et al., 2019). CS1 sequences consist of uninterrupted 11 copies of RRRRRYYYYY (named the R5Y5 motif, here R = purine, Y = pyrimidine), but do not contain a 10.5-bp periodicity of TA dinucleotides. CS2 and CS3 fit with 11 uninterrupted units of the R5Y5 motif and visible 10.5-bp periodicity of TA dinucleotides. Sequences CS4, CS5, and CS6 contain 10.5 bp periodic TA dinucleotides but do not contain the R5Y5 motif. We found that nucleosome assembly efficiency (N/S) is proportional to histone octamer concentration (Q) for CS1–CS6 at the same reaction condition and time, which is the same as that for the Widom 601 sequence.

Parameter $\bar{k}$ Can Be Used to Evaluate the Affinity of DNA Fragments to Histone Octamers

In the model, parameter $\bar{k}$ is the mean reaction rate constant in the process of nucleosome assembly. The slope coefficient of linear fitting in Eq. 11 is $\varepsilon\bar{k}$, where ε should be a constant under the same experimental condition for the reconstituted reaction on six CS sequences. We may directly use the slope coefficient to evaluate the nucleosome formation ability with DNA sequences. To examine this hypothesis, we used six CS sequences to assemble mononucleosomes *in vitro* by salt-dialysis (**Supplementary Figure 1**). Our previous work demonstrated that CS2 and CS3 sequences containing both the R5Y5 motif and TA repeats with 10.5-bp periodicity have a stronger ability to assemble nucleosomes, and the CS1 sequence with only the R5Y5 motif has a lower affinity to histones *in vitro* among the six DNA sequences (Zhao et al., 2019).

The slope coefficients of linear fitting on CS2 and CS3 were significantly higher than those on other CS sequences (**Figure 2**, paired-sample t-test, $p < 0.01$), which suggested that CS2 and CS3 have a higher affinity for histone octamers. The slope coefficient on CS1 was only 0.01272, which was the lowest among the six CS sequences (**Figure 2**, paired-sample t-test, $p < 0.01$). These results were highly consistent with our previous report (Zhao et al., 2019) and suggested that the parameter $\bar{k}$ can be used to evaluate the affinity between histones and DNA sequences.

The Efficiency of Nucleosome Assembly Is Proportional to Dialysis Time

In our nucleosome assembly kinetics model, assembly reaction time was one of the parameters affecting the nucleosome assembly efficiency *in vitro*. We then assembled nucleosomes on a Widom 601 sequence with a concentration gradient of histone octamers under dialysis times of 10, 12, 14, and 16 h (**Supplementary Figure 2**). As shown in **Figure 3A**, the nucleosome assembly efficiency displayed a significant linear correlation with histone octamer concentration at four dialysis times ($p < 0.01$). Interestingly, the fitting curve between slope coefficient in **Figure 3A** and assembly reaction time showed a high linear dependence (**Figure 3B**, $p < 0.01$). This result confirmed the linear relationship between N/S and T in Eq. 11.

Nucleosome Disassembly Can Be Described as Three Distinct Stages *in vitro*

In our initial reaction Eq. 1, nucleosome assembly contains two key stages: the binding of the $(H3/H4)_2$ tetramer to DNA and the (H2A/H2B) dimer to $(H3/H4)_2$/DNA. In salt dialysis, gradient descent of salty ions can promote the binding of negatively charged DNAs to histones. It is easier to understand the kinetic mechanism from nucleosome disassembly than from assembly.

We employed a FRET assay to monitor the dynamic change in nucleosome structure in the disassembly process. In this assay, we labeled Widom 601 DNA sequences with a donor Cy3 and an acceptor Cy5 over a 96-bp separation. Because of the over 30 nm length between the two dyes, FRET signals on free DNA templates cannot be detected (**Supplementary Figure 3**). While the nucleosome is reconstituted on the Widom 601 DNA template, the spatial distance of the two fluorescent molecules is reduced to approximately 4.6 nm (**Figure 4A**), which enables the well-organized nucleosome to be excited to produce efficient FRET signals (**Supplementary Figure 3**).

Nucleosome disassembly under high temperature was detected by FRET assay. The reconstituted nucleosomes were incubated at the temperature of 70°C. We used both native polyacrylamide gel electrophoresis (PAGE) and FRET to detect nucleosome disassembly. In the first 80 min of the disassembly reaction, the amount of nucleosome DNA in the total DNA showed no obvious change by PAGE (**Figure 4B**). In other words, we cannot detect the physical separation between DNA and histones in this stage. However, as the disassembly reaction

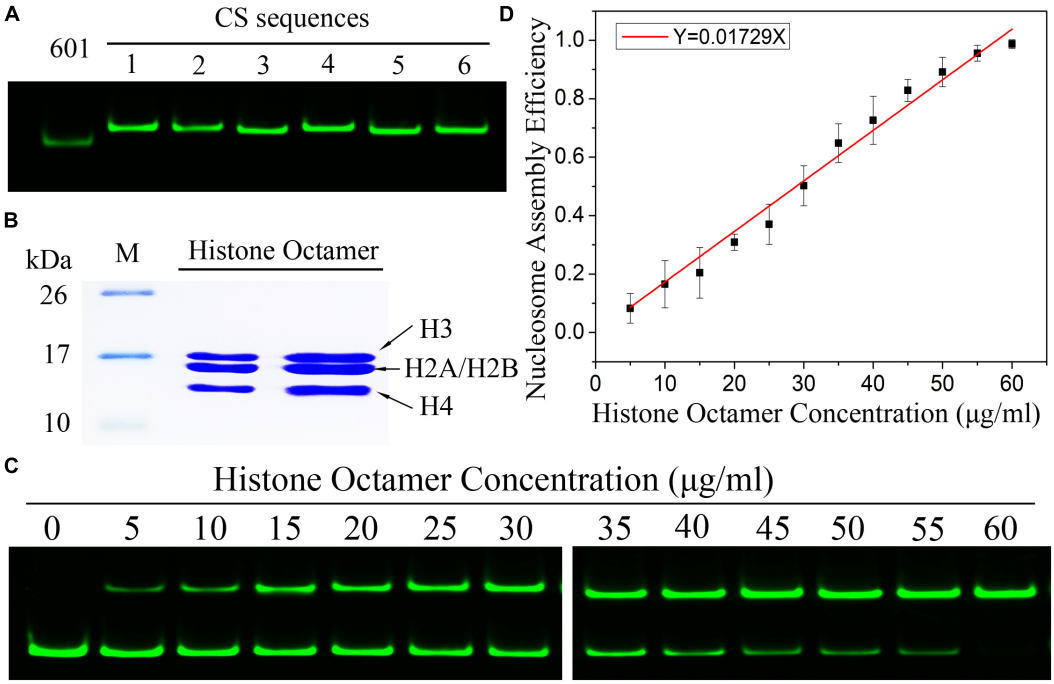

FIGURE 1 | The efficiency of nucleosome assembly on the Widom 601 sequence *in vitro* by salt dialysis is dependent on histone concentration. **(A)** Preparation of Widom 601 DNAs and CS DNAs. The Cy3-labeled DNA sequences were detected by native-PAGE. **(B)** Preparation of histone octamer. The reconstituted canonical histone octamer was analyzed by SDS-PAGE. **(C)** Detection results of nucleosome assembly *in vitro*. The reconstituted nucleosomes with different histone octamers were analyzed by native PAGE. In each lane of the gel, the top band is nucleosome DNAs, and the bottom band is free DNAs. **(D)** The relation curves of nucleosome assembly efficiency vs. histone octamer concentration for the Widom 601 sequence. Nucleosome assembly efficiency was calculated by the ratio of nucleosome DNAs to total DNAs from panel **(C)** for each reconstituted sample. For each sample, five independent repeats were performed.

started, the FRET signals quickly decreased and then remained unchanged for ∼60 min. These results implied that the DNA wrapping on the histone octamer has become loose, but the nucleosome does not depolymerize at this primary stage. After ∼80 min of incubation at 70°C, the amount of nucleosome DNA in PAGE detection decreased with increasing disassembly reaction time. FRET signals also display a similar downtrend at this quick disassembly stage. Combining the results of PAGE and FRET assays, one can conclude that relaxation of the nucleosome spatial structure begins before the physical separation of DNA from histones is completed.

Quantitative FRET signals were used to monitor the NaCl-dependent disassembly process of nucleosomes (**Supplementary Figure 4**). The normalized FRET signal has two rapid descent stages with increasing NaCl concentration (**Figure 4C**). Then, we calculated the change rate of fluorescence to NaCl concentration. Two obvious peaks of the change rate of fluorescence were observed at ∼0.6 and 1.0 mol/L NaCl (**Figure 4C**). This result suggested that H2A/H2B dimer disassembly (reverse reaction in Eq. 1-③④) and H3/H4 tetramer depolymerization (reverse reaction in Eq. 1-②) may contribute to the first peak and second peak, respectively.

Then, we employed an FTS assay to detect thermal stability-dependent nucleosome disassembly. The nucleosomes were reconstituted on 147-bp 601 DNA templates without any fluorescence labeling. We then performed FTS experiments with SYPRO Orange. This method monitors the fluorescence signal from SYPRO Orange, which binds hydrophobically to the proteins by thermal denaturation. In this assay, the histones that thermally dissociate from the nucleosome are detected by fluorescent signals of SYPRO Orange (Arimura et al., 2018). As shown in **Figure 4D**, the fluorescence signal intensity began to increase significantly after 55°C, which suggested that the nucleosomes started to decompose. The first rapid increase in the fluorescence from 68 to 75°C indicates the removal of the H2A/H2B dimer, and the later peak from 83 to 87°C indicates the dissociation of the H3/H4 tetramer from DNA. These results also support staged characteristics of nucleosome disassembly in our initial reaction Eq. 1.

In summary, nucleosome disassembly can be described as three distinct stages: the opening phase of the $(H3–H4)_2$ tetramer/(H2A–H2B) dimer interface, the release phase of H2A–H2B dimer from $(H3–H4)_2$ tetramer/DNA and the removal phase of $(H3–H4)_2$ tetramer from DNA.

DISCUSSION

In this work, we proposed a chemical kinetic model of nucleosome assembly. Nucleosome reconstitution assays by salt dialysis *in vitro* demonstrated that the efficiency of nucleosome assembly was positively correlated with the concentration of histone octamer, reaction rate constant, and reaction time in

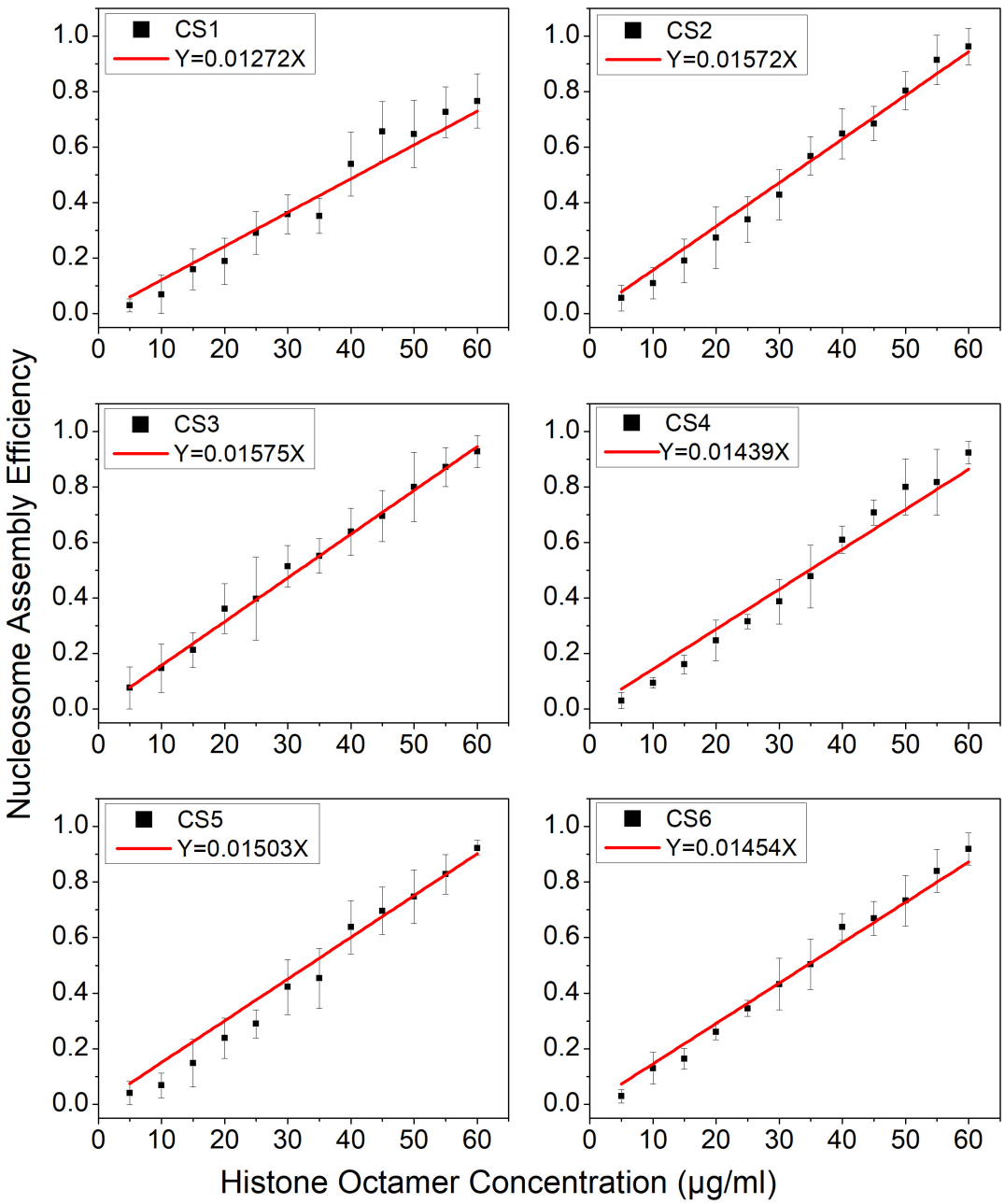

FIGURE 2 | The regression curve of nucleosome assembly efficiency vs. histone octamer concentration for six CS sequences. The nucleosomes were reconstituted on CS1–CS6 DNAs with different histone octamer concentrations. Reconstituted nucleosomes were analyzed by native-PAGE and quantized to calculate the nucleosome assembly efficiency. For each sample, five independent repeats were performed.

this model. All the conclusions of the kinetic model were well confirmed for selected sequences by using the salt dialysis method *in vitro*. Our theoretical model and experimental test reveal that nucleosome assembly and disassembly *in vitro* are governed by chemical kinetic principles.

In the derivation process of Eq. 11, we bring in hypothesis $(Q-S)\theta(T) \ll 1$ to expand the exponential function by the Taylor mean value theorem. For the extreme case of $Q \gg S$, the condition $(Q-S)\theta(T) \ll 1$ is not met. While we take the limit of Eq. 10, $\frac{N}{S} = \frac{\frac{Q}{S}(exp(-(Q-S)\theta)-1)}{exp(-(Q-S)\theta)-\frac{Q}{S}} \approx 1$ can be obtained. In our reconstituted nucleosome assays, the supersaturated concentration of histone octamer in the reaction system can lead all DNAs to assemble nucleosomes, in other words, $\frac{N}{S}$ should be 1 in this case. On the other hand, for the extreme case of $Q \ll S$, one can obtain $\frac{N}{S} = \frac{\frac{Q}{S}\{1-exp[(Q-S)\theta(T)]\}}{1-\frac{Q}{S}exp\{(Q-S)\theta(T)\}} \approx \frac{Q}{S} \approx 0$ in Eq. 10.

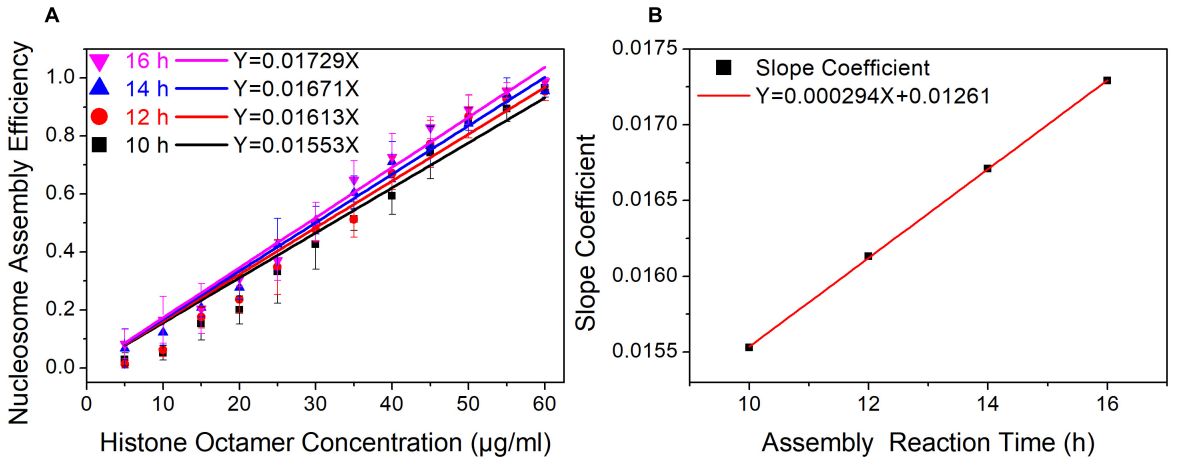

FIGURE 3 | The regression curve of nucleosome assembly efficiency vs. reaction time for 601 DNA sequence under different assembly reaction times. **(A)** Regression curves of nucleosome assembly efficiency vs. histone octamer concentration under 10, 12, 14, and 16 h of dialysis time. For each sample, five independent repeats were performed. **(B)** Linear regression curve between the slope coefficient in panel **(A)** and assembly reaction time.

While the concentration of histone octamers was far less than the concentration of DNAs, the DNAs could hardly reconstitute into nucleosomes. This experimental observation is consistent with the theoretical calculation result. Therefore, the condition $(Q - S)\,\theta(T) \ll 1$ is reasonable for the nucleosome assembly *in vitro*.

In a previous study, the affinity of DNAs to histones was usually quantified by the ratio of nucleosome DNA to free DNA in reconstituted nucleosome samples and/or the relative Gibbs free energy of reconstituted reaction under only one specific concentration of histone octamer (Thåström et al., 2004a; Volle and Delaney, 2012). However, the nucleosome assembly efficiency is associated with histone octamer. In the present kinetic model, reaction rate constant $\bar{k}$ is an important parameter. Comparing the difference of reaction rate constant $\bar{k}$ among different DNAs is a systematic evaluation method for the affinity of DNAs to histone, which can provide a more comprehensive understanding from the reconstituted reaction under gradient concentration of histone octamer than previous method only from one concentration of histone octamer.

Our model describes the chemical kinetics of nucleosomes based on nucleosome assembly and disassembly assays *in vitro*. Nucleosome reconstitution, dissociation and remodeling *in vivo* are more complicated than that *in vitro*. Nucleosome assembly chaperonin and chromatin remodeler are intimately involved in the dynamics of nucleosomes *in vivo*. Our kinetics model may not be directly used to describe the apparent kinetics of nucleosome dynamics *in vivo*. However, the intrinsic kinetics, which only involve the interaction of DNAs and histones, may elucidate the basic rule in the kinetic principle of nucleosome assembly and could provide the ideal model to develop further an apparent kinetics model of nucleosomes.

Our experiments showed that nucleosome disassembly can be described as three distinct stages: opening phase of the (H2A/H2B) dimer/$(H3/H4)_2$ tetramer interface, release phase of the H2A/H2B dimers from $(H3/H4)_2$ tetramer/DNA and removal phase of the $(H3/H4)_2$ tetramer from DNA. This result may be helpful for the understanding the effects of different physiological variables on dimers stability. H2A/H2B dimers dissociation can be crucial in the efficiency of transcription elongation, and the process *in vivo* is often regulated by transcription factor, such as FACT (facilitates chromatin transcription) complex. Hsieh et al. (2013) revealed that FACT can induce global accessibility of nucleosomal DNA without histone H2A/H2B displacement and thus can facilitate action of processive enzymes on DNA, such as transcription through chromatin. Chen et al. (2018) demonstrated that FACT displays dual functions in destabilizing the nucleosome and maintaining the original histones and nucleosome integrity at the single-nucleosome level. At early 1990s, researchers attempted to understand the mechanical behavior in the interaction between DNA and histones. DNA topological parameters, such as DNA linking variants, torsional stress, were used to elucidate mechanism of nucleosome structure (Negri et al., 1994; Negri and Di Mauro, 1997). PTMs in histone proteins play essential roles in nucleosome dynamics. The results from three-color single-molecule FRET showed that H2A/H2B dimer displacement process has a slight difference between in the salt-induced case and in the Nap1-mediated case. For the Nap1-mediated dimer dissociation, the acetylation at histone H4K16 or H3K56 facilitates the process both kinetically and thermodynamically (Lee and Lee, 2017). Sueoka et al. (2017) uncovered that phosphorylation at H2A Tyr57 changes the stability of the H2A-H2B dimer but does not interfere with histone-DNA interactions, an facilitate the dissociation of H2A/H2B dimer from the nucleosome structure. The acetylation and ubiquitination of histones H2A and H2B.1 weaken their interaction with the (H3-H4)2 tetramer and/or nucleosomal DNA, while histones H2A.Z and H2B.2 strengthen these interactions (Li et al., 1993). So far, how these complex factors regulate the H2A/H2B dimers dissociation *in vivo* is not fully understood.

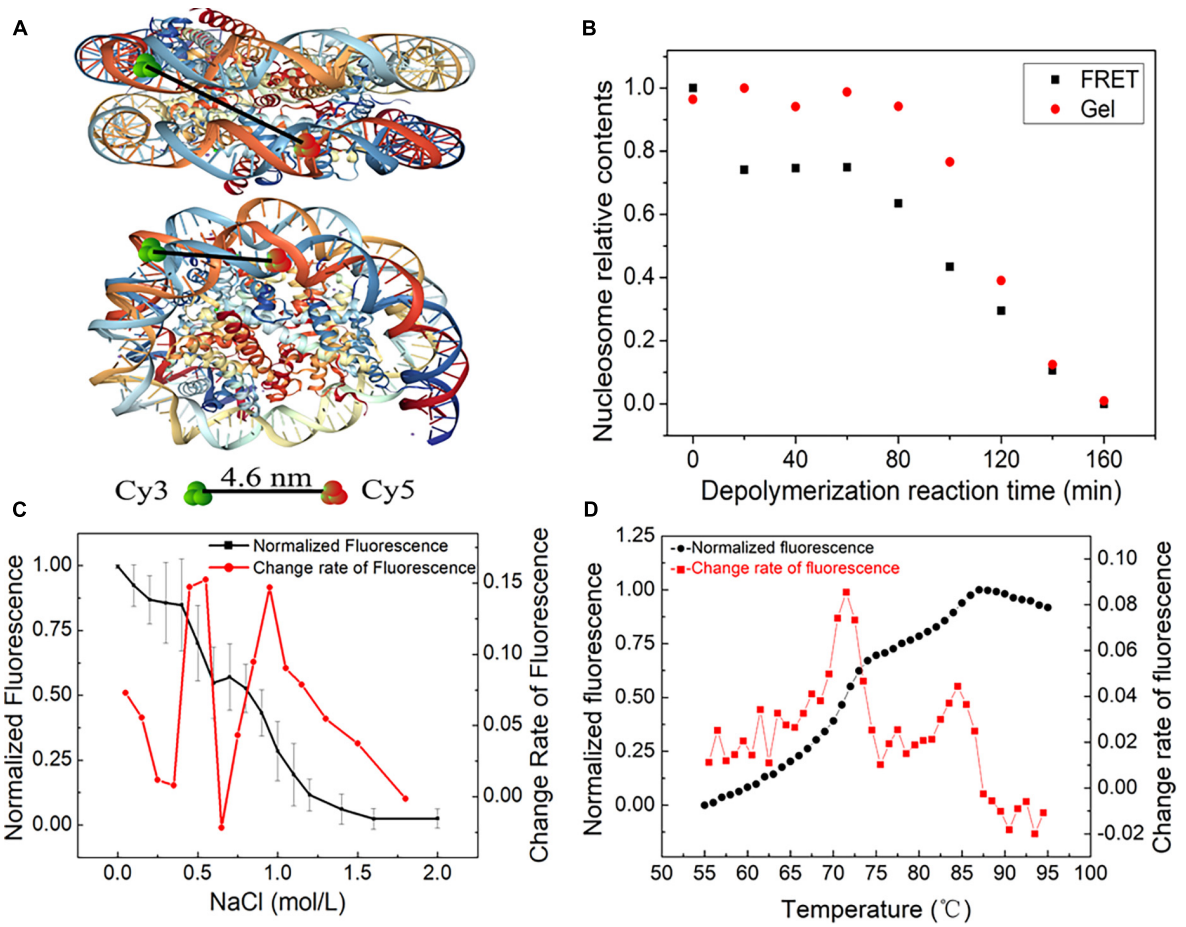

FIGURE 4 | The dynamic stages of nucleosome disassembly *in vitro* using the Widom 601 sequence. **(A)** Top and side views of the nucleosome with the position of donor Cy3 and acceptor Cy5 (structural outline of nucleosome: PDB ID 3 L Z1). **(B)** Nucleosome disassembly after incubation at 70°C. Red dots denote the amount of nucleosome DNA in total DNA detected by native PAGE, and black dots denote the relative signals of Förster resonance energy transfer (FRET) generated in nucleosomes. **(C)** FRET analysis of NaCl-dependent dissociation of nucleosomes. The black dots denote the normalized FRET signals obtained by monitoring the fluorescence difference between the donor and acceptor emissions upon donor excitation at 480 nm. The red dots are the change rate of FRET signals to NaCl concentration. **(D)** Thermal shift assays with the nucleosome using SYPRO Orange. The relative fluorescence intensity at each temperature is plotted as a black dot. The red dots show the differential values of the thermal stability curves presented in the black dots.

Taking into account the irreversible of nucleosome assembly/disassembly process and the cooperative behavior of the increases in [NaCl] or temperature in salt-dialysis method, Thåström et al. (2004b) emphasized that equilibrium affinities cannot be obtained from these measurements. The chemical kinetics discussed in present work is regarded to the nucleosome assembly driven by NaCl dilution. As we know, different from equilibrium thermodynamics, the chemical kinetics generally discusses the time-dependent process and does not require the reversibility of the process. Experiments on increase in [NaCl] influencing assembly/disassembly are not the reversal process of that we discussed. Therefore, there is no conflict between Thåström's work and our model.

The ATP-dependent assembly of periodic nucleosome arrays and the ATP-independent random deposition of histones onto DNA (such as salt-dialysis method) are two kinds of popular strategies in the reconstitution of chromatin *in vitro* (Lusser and Kadonaga, 2004). Some simplification is inevitable in nucleosome assembly system *in vitro*. The central question is whether this simplification can reveal the laws of nucleosome assembly. The ATP-dependent assembly reaction can produce periodic nucleosome arrays, similar to those seen in bulk native chromatin. This assembly method requires ATP-utilizing chromatin assembly factors, such as ACF (ATP-utilizing chromatin assembly and remodeling factor) or RSF (remodeling and spacing factor), etc., (Lusser and Kadonaga, 2004). Even so, this assembly reaction *in vitro* is still not a complete simulation of the complex nucleosome assembly *in vivo*. The salt-dialysis method, in which the reaction temperature and concentration gradient of saline ions is constant, is one of ATP-independent strategy to assemble the nucleosomes *in vitro*. The only biological molecules in this reaction system are DNA and histones. The nucleosome assembly efficiency is not affected by the other

factors, such as chromatin remodelers, histone chaperones. Thus, the salt-dialysis method of nucleosome assembly can be regarded as a simple model of nucleosome assembly *in vivo*. In this work, more attention was paid on the affinity between DNA and histone octamer in nucleosome assembly reaction. So, employing the salt-dialysis method should be sounder and more feasible. We used the salt-dialysis experimental system *in vitro* to well uncover the relation between nucleosome assembly efficiency and DNA sequences, concentration of histone octamer, and reaction time. These results suggest that nucleosome assembly/disassembly *in vitro* is governed by chemical kinetic principles. This conclusion has merit for further understanding the nucleosome dynamics *in vivo*. In recent years, several studies revealed that nucleosome organizations *in vivo* are dominantly encoded in the genomic sequence and nucleosomes' intrinsic DNA sequence preferences vary greatly between differing DNA sequences (Field et al., 2008; Kaplan et al., 2009). These results imply that the roughly nucleosome position *in vivo* can be determined by the affinity between DNA and histone octamer, which can be simulated by the salt-dialysis method of nucleosome assembly *in vitro*, and the accurate nucleosome position is modulated by other factors, such as histone chaperone, histone modification. Taking into account other factors, our further research will focus on the simulation of the nucleosome assembly *in vivo*.

In future, we can integrate DNAs, histone octamer, histone chaperones, and chromatin remodelers into a complex model for further understanding the mechanism of nucleosome assembly. In the model, we can investigate the effect of mechanical characteristics of DNAs, histone variables and physiological variables on nucleosome assembly. Meanwhile, a complex system of nucleosome reconstitution *in vitro* can be constructed by combining salt dialysis, histone chaperones and ATP-dependent assembly factors. This nucleosome reconstitution system can be used to examine more complicated factors in theoretical model. The new model may get closer to nucleosome dynamics *in vivo*. Further, we can also introduce RNA polymerase II into nucleosome assembly model and nucleosome assembly reaction system. By analyzing the competitive binding to DNAs of RNA polymerase II and histone, we can attempt to understand the coupling mechanism of transcription elongation and nucleosome dynamics.

Taken together, we propose a chemical kinetics model to describe the dynamic nucleosome assembly, and the results reveal that nucleosome assembly and disassembly *in vitro* are governed by chemical kinetic principles. We provide a novel evaluation method in which parameter $\bar{k}$ can be used to evaluate the affinity of DNAs to histones. In addition, we further confirmed that there exist three distinct stages in nucleosome dynamics, which is consistent with the conclusions of previous work (Gansen et al., 2009; Böhm et al., 2011). These results will contribute to further understanding the dynamics of nucleosomes *in vivo*.

DATA AVAILABILITY STATEMENT

The original contributions presented in the study are included in the article/**Supplementary Material**, further inquiries can be directed to the corresponding author/s.

AUTHOR CONTRIBUTIONS

LC, LL, and HZ designed the research, contributed to the theoretical model, and wrote the manuscript. HZ, MG, FZ, and XS performed the experiment. GL, YX, and XZ analyzed the data. All authors contributed to the article and approved the submitted version.

FUNDING

This work was funded by the National Natural Science Foundation of China (31760247 to HZ, 62071259 and 61671256 to LC) and the Natural Science Foundation of Inner Mongolia (2021MS03007 to HZ).

SUPPLEMENTARY MATERIAL

The Supplementary Material for this article can be found online at: https://www.frontiersin.org/articles/10.3389/fcell.2021.762571/full#supplementary-material

REFERENCES

Arimura, Y., Ikura, M., Fujita, R., Noda, M., Kobayashi, W., Horikoshi, N., et al. (2018). Cancer-associated mutations of histones H2B, H3.1 and H2A.Z.1 affect the structure and stability of the nucleosome. *Nucleic Acids Res.* 46, 10007–10018. doi: 10.1093/nar/gky661

Böhm, V., Hieb, A. R., Andrews, A. J., Gansen, A., Rocker, A., Tóth, K., et al. (2011). Nucleosome accessibility governed by the dimer/tetramer interface. *Nucleic Acids Res.* 39, 3093–3102. doi: 10.1093/nar/gkq1279

Chen, P., Dong, L., Hu, M., Wang, Y. Z., Xiao, X., Zhao, Z., et al. (2018). Functions of FACT in breaking the nucleosome and maintaining its integrity at the single-nucleosome level. *Mol. Cell* 71, 284–293.e4. doi: 10.1016/j.molcel.2018.06.020

Chen, P., Zhao, J., Wang, Y., Wang, M., Long, H., Liang, D., et al. (2013). H3.3 actively marks enhancers and primes gene transcription via opening higher-ordered chromatin. *Genes Dev.* 27, 2109–2124. doi: 10.1101/gad.222174.113

Field, Y., Kaplan, N., Fondufe-Mittendorf, Y., Moore, I. K., Sharon, E., Lubling, Y., et al. (2008). Distinct modes of regulation by chromatin encoded through nucleosome positioning signals. *PLoS Comput. Biol.* 4:e1000216. doi: 10.1371/journal.pcbi.1000216

Florescu, A. M., Schiessel, H., and Blossey, R. (2012). Kinetic control of nucleosome displacement by ISWI/ACF chromatin remodelers. *Phys. Rev. Lett.* 109:118103. doi: 10.1103/PhysRevLett.109.118103

Gansen, A., Valeri, A., Hauger, F., Felekyan, S., Kalinin, S., Tóth, K., et al. (2009). Nucleosome disassembly intermediates characterized by single-molecule FRET. *Proc. Natl. Acad. Sci. U.S.A.* 106, 15308–15313. doi: 10.1073/pnas.0903005106

Hsieh, F. K., Kulaeva, O. I., Patel, S. S., Dyer, P. N., Luger, K., Reinberg, D., et al. (2013). Histone chaperone FACT action during transcription through chromatin by RNA polymerase II. *Proc. Natl. Acad. Sci. U.S.A.* 110, 7654–7659. doi: 10.1073/pnas.1222198110

Kameda, T., Awazu, A., and Togashi, Y. (2019). Histone tail dynamics in partially disassembled nucleosomes during chromatin remodeling. *Front. Mol. Biosci.* 6:133. doi: 10.3389/fmolb.2019.00133

Kaplan, N., Moore, I. K., Fondufe-Mittendorf, Y., Gossett, A. J., Tillo, D., Field, Y., et al. (2009). The DNA-encoded nucleosome organization of a eukaryotic genome. *Nature* 458, 362–366. doi: 10.1038/nature07667

Lai, W. K. M., and Pugh, B. F. (2017). Understanding nucleosome dynamics and their links to gene expression and DNA replication. *Nat. Rev. Mol. Cell Biol.* 18, 548–562. doi: 10.1038/nrm.2017.47

Lee, J., and Lee, T. H. (2017). Single-molecule investigations on histone H2A-H2B dynamics in the nucleosome. *Biochemistry* 56, 977–985. doi: 10.1021/acs.biochem.6b01252

Li, W., Nagaraja, S., Delcuve, G. P., Hendzel, M. J., and Davie, J. R. (1993). Effects of histone acetylation, ubiquitination and variants on nucleosome stability. *Biochem. J.* 296, 737–744. doi: 10.1042/bj2960737

Liu, G., Liu, G. J., Tan, J. X., and Lin, H. (2019). DNA physical properties outperform sequence compositional information in classifying nucleosome-enriched and -depleted regions. *Genomics* 111, 1167–1175. doi: 10.1016/j.ygeno.2018.07.013

Liu, G., Xing, Y., Zhao, H., Cai, L., and Wang, J. (2018). The implication of DNA bending energy for nucleosome positioning and sliding. *Sci. Rep.* 8:8853. doi: 10.1038/s41598-018-27247-x

Lowary, P. T., and Widom, J. (1998). New DNA sequence rules for high affinity binding to histone octamer and sequence-directed nucleosome positioning. *J. Mol. Biol.* 276, 19–42. doi: 10.1006/jmbi.1997.1494

Luger, K., Mäder, A. W., Richmond, R. K., Sargent, D. F., and Richmond, T. J. (1997). Crystal structure of the nucleosome core particle at 2.8 A resolution. *Nature* 389, 251–260. doi: 10.1038/38444

Lusser, A., and Kadonaga, J. T. (2004). Strategies for the reconstitution of chromatin. *Nat. Methods* 1, 19–26. doi: 10.1038/nmeth709

Negri, R., Costanzo, G., Buttinelli, M., Venditti, S., and Di Mauro, E. (1994). Effects of DNA topology in the interaction with histone octamers and DNA topoisomerase I. *Biophys. Chem.* 50, 169–181. doi: 10.1016/0301-4622(94)85029-1

Negri, R., and Di Mauro, E. (1997). Nucleosomes as topological rheostats. *J. Biomol. Struct. Dyn.* 14, 741–746. doi: 10.1080/07391102.1997.10508176

Padinhateeri, R., and Marko, J. F. (2011). Nucleosome positioning in a model of active chromatin remodeling enzymes. *Proc. Natl. Acad. Sci. U.S.A.* 108, 7799–7803. doi: 10.1073/pnas.1015206108

Ranjith, P., Yan, J., and Marko, J. F. (2007). Nucleosome hopping and sliding kinetics determined from dynamics of single chromatin fibers in Xenopus egg extracts. *Proc. Natl. Acad. Sci. U.S.A.* 104, 13649–13654. doi: 10.1073/pnas.0701459104

Sueoka, T., Hayashi, G., and Okamoto, A. (2017). Regulation of the stability of the histone H2A-H2B dimer by H2A Tyr57 phosphorylation. *Biochemistry* 56, 4767–4772. doi: 10.1021/acs.biochem.7b00504

Thåström, A., Bingham, L. M., and Widom, J. (2004a). Nucleosomal locations of dominant DNA sequence motifs for histone-DNA interactions and nucleosome positioning. *J. Mol. Biol.* 338, 695–709. doi: 10.1016/j.jmb.2004.03.032

Thåström, A., Gottesfeld, J. M., Luger, K., and Widom, J. (2004b). Histone-DNA binding free energy cannot be measured in dilution-driven dissociation experiments. *Biochemistry* 43, 736–741. doi: 10.1021/bi0302043

Völker-Albert, M. C., Pusch, M. C., Fedisch, A., Schilcher, P., Schmidt, A., and Imhof, A. (2016). A quantitative proteomic analysis of in vitro assembled chromatin. *Mol. Cell Proteomics* 15, 945–959. doi: 10.1074/mcp.M115.053553

Volle, C. B., and Delaney, S. (2012). CAG/CTG repeats alter the affinity for the histone core and the positioning of DNA in the nucleosome. *Biochemistry* 51, 9814–9825. doi: 10.1021/bi301416v

Zhao, H., Xing, Y., Liu, G., Chen, P., Zhao, X., Li, G., et al. (2015). GAA triplet-repeats cause nucleosome depletion in the human genome. *Genomics* 106, 88–95. doi: 10.1016/j.ygeno.2015.06.010

Zhao, H., Zhang, F., Guo, M., Xing, Y., Liu, G., Zhao, X., et al. (2019). The affinity of DNA sequences containing R5Y5 motif and TA repeats with 10.5-bp periodicity to histone octamer in vitro. *J. Biomol. Struct. Dyn.* 37, 1935–1943. doi: 10.1080/07391102.2018.1477621

Conflict of Interest: The authors declare that the research was conducted in the absence of any commercial or financial relationships that could be construed as a potential conflict of interest.

Publisher's Note: All claims expressed in this article are solely those of the authors and do not necessarily represent those of their affiliated organizations, or those of the publisher, the editors and the reviewers. Any product that may be evaluated in this article, or claim that may be made by its manufacturer, is not guaranteed or endorsed by the publisher.

frontiers | Frontiers in Genetics

MINI REVIEW
published: 05 April 2022
doi: 10.3389/fgene.2022.870640

Recent Advances in Investigating Functional Dynamics of Chromatin

Xiangyan Shi[1], Ziwei Zhai[1], Yinglu Chen[1], Jindi Li[1] and Lars Nordenskiöld[2]**

[1]*Department of Biology, Shenzhen MSU-BIT University, Shenzhen, China,* [2]*School of Biological Sciences, Nanyang Technological University, Singapore, Singapore*

Dynamics spanning the picosecond-minute time domain and the atomic-subcellular spatial window have been observed for chromatin *in vitro* and *in vivo*. The condensed organization of chromatin in eukaryotic cells prevents regulatory factors from accessing genomic DNA, which requires dynamic stabilization and destabilization of structure to initiate downstream DNA activities. Those processes are achieved through altering conformational and dynamic properties of nucleosomes and nucleosome–protein complexes, of which delineating the atomistic pictures is essential to understand the mechanisms of chromatin regulation. In this review, we summarize recent progress in determining chromatin dynamics and their modulations by a number of factors including post-translational modifications (PTMs), incorporation of histone variants, and binding of effector proteins. We focus on experimental observations obtained using high-resolution techniques, primarily including nuclear magnetic resonance (NMR) spectroscopy, Förster (or fluorescence) resonance energy transfer (FRET) microscopy, and molecular dynamics (MD) simulations, and discuss the elucidated dynamics in the context of functional response and relevance.

Keywords: NMR, FRET, MD simulations, dynamics of nucleosomes, nucleosome conformational dynamics

OPEN ACCESS

Edited by:
Dileep Vasudevan,
Institute of Life Sciences (ILS), India

Reviewed by:
Thomas Schalch,
University of Leicester,
United Kingdom
Pétur Heidarsson,
University of Iceland, Iceland

****Correspondence:***
Xiangyan Shi
xyshi@smbu.edu.cn
Lars Nordenskiöld
larsnor@ntu.edu.sg

Specialty section:
This article was submitted to Epigenomics and Epigenetics, a section of the journal Frontiers in Genetics

Received: *07 February 2022*
Accepted: *11 March 2022*
Published: *05 April 2022*

Citation:
Shi X, Zhai Z, Chen Y, Li J and Nordenskiöld L (2022) Recent Advances in Investigating Functional Dynamics of Chromatin. Front. Genet. 13:870640. doi: 10.3389/fgene.2022.870640

INTRODUCTION

Chromatin in eukaryotic cells is organized in the form of 147 bp DNA wrapping the histone octamer (HO) complex to form nucleosome core particles (NCPs), connected by linker DNA to form a "beads-on-a-string," which in the presence of linker histone and/or physiological salt, condenses to higher ordered structures (Zhou et al., 2019; Baldi et al., 2020). This condensed structure acts as the barrier for protein factors necessary for accessing DNA during downstream genomic activities and requires dynamic stabilization and destabilization for maintaining cellular homeostasis. The accomplishment of genomic DNA activities in eukaryotic cells is propagated from the modulation of dynamic spatiotemporal organization of chromatin, which is achieved through factors including post-translational modifications (PTMs) (Jenuwein and Allis, 2001; Bannister and Kouzarides, 2011; Bowman and Poirier, 2014; Fenley et al., 2018), incorporation histone variants (Talbert and Henikoff, 2016; Martire and Banaszynski, 2020), remodelers, and other effector proteins (Tyagi et al., 2016; Armeev et al., 2019; Reyes et al., 2021). Since the first atomic resolution structure was obtained 24 years ago (Luger et al., 1997), well over a hundred structures of NCPs with different DNA sequences or histone variants and in complex with protein factors have been determined by X-ray diffraction (XRD) and cryogenic electron microscopy (cryo-EM) (Luger et al., 1997; Korolev et al., 2018; Zhou et al., 2019; Soman et al., 2020; Lobbia et al., 2021). The atomic structure information opened the door to understanding the molecular basis of genomic DNA regulation processes. Various NCPs adopt structures with high similarity and minor local conformational

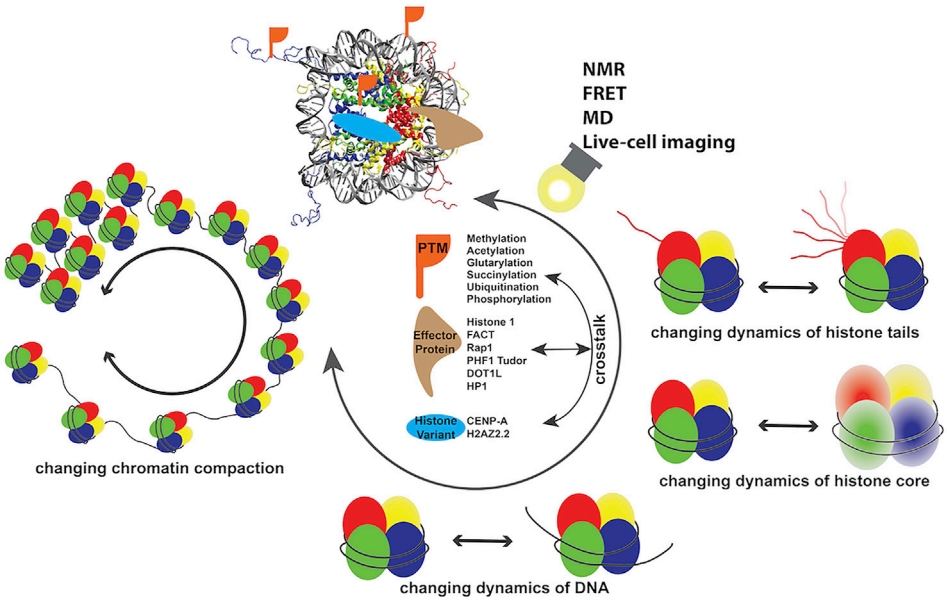

FIGURE 1 | Dynamics of chromatin modulated by a number of factors discussed in this review.

differences, suggesting that molecular characteristics beyond structure also play dominant roles in the biological behaviors of chromatin associated with incorporation of different histone variants, modifications, and DNA sequences. Recent studies have determined the dynamics properties of several nucleosomes and nucleosome–protein complexes, revealing the link between biological function and dynamics properties. Dynamics of chromatin span from picosecond to minute timescales at atomic to subcellular levels, which greatly contribute to regulating various DNA processes and remain largely unclear at high spatiotemporal resolution. With the recent development of high-resolution techniques primarily including nuclear magnetic resonance (NMR) spectroscopy, Förster (or fluorescence) resonance energy transfer (FRET) microscopy, and molecular dynamics (MD) simulations, increasing information on dynamics of nucleosomes and nucleosome–protein complexes have been determined, suggesting the functional components of this important molecular property. In this review, we focus on recent research investigating the dynamics of chromatin systems (**Figure 1**) and we discuss the biological roles of these functional dynamics features.

Advanced Techniques for Characterizing Chromatin Dynamics

Recent development of advanced techniques primarily including NMR, FRET, and MD simulations has significantly stimulated *in vitro* research on chromatin dynamics. NMR allows for quantifying the motional amplitudes and timescales for dynamics covering second-picosecond timescales at atomic resolution (Krushelnitsky et al., 2013; Kovermann et al., 2016; Shi and Rienstra, 2016). Solution-state NMR has been successfully implemented to determine the conformation and dynamics of nucleosomes. It mainly provides information of the highly flexible histone tails (Zhou et al., 2012; Morrison et al., 2018; Ohtomo et al., 2021; Rabdano et al., 2021) or methyl sites in the rigid histone core (Kato et al., 2011; Kitevski-LeBlanc et al., 2018) because of its limitation in detecting rigid structural components of large molecules. This intrinsic size limitation is overcome by using solid-state NMR (SSNMR) that has developed as an emerging powerful technique in studying chromatin. This revealed structure and dynamics for several nucleosomes and nucleosome–protein complexes (Ackermann and Debelouchina, 2021; le Paige et al., 2021). NMR techniques require isotope labeling to gain sufficient sensitivity and sometimes also require fragment labeling (e.g., labeling one of the histones) to reduce signal complexity. Preparation of large amounts (milligrams) of homogenous nucleosome complexes with isotope labeling for NMR characterization is not always trivial and demands plenty of effort. FRET, particularly single-molecule FRET (smFRET), offers a highly sensitive and suitable approach to probe the conformational dynamics of chromatin (Buning and van Noort, 2010; Sasmal et al., 2016; Kilic et al., 2018). Typically, the fluorophore pairs are installed at specific sites of the DNA in nucleosomes and their distances between 1 and 10 nm can be derived from the FRET efficiency. The experimental data reflect the transitions of distinguished states originating from dynamics such as DNA wrapping/unwrapping in nucleosomes (Kilic et al., 2018). Site-specific labeling at particular sites with suitable fluorophores is generally a challenging task for nucleosomes and nucleosome–protein complexes. The spatial resolution limit of FRET prevents its access to local structural details at the atomic resolution (Sasmal et al., 2016). For this reason, it is often integrated with other techniques such as NMR and/or MD to delineate the atomistic pictures of conformations. Another

superior technique, MD simulation, permits investigating structure and multi-scale dynamics at the atomic level for chromatin (Huertas and Cojocaru, 2021). All-atom MD simulations of mononucleosomes have reached a timescale of up to 15 ms (Armeev et al., 2021; Huertas and Cojocaru, 2021) and can detect key atomistic characteristics that modulate the dynamics of nucleosomes. Because of the limitation of all-atom MD, coarse-grained MD has been established to simulate nucleosomes at a longer timescale and capture the organization and dynamics of nucleosome arrays (Voltz et al., 2008; Huertas and Cojocaru, 2021). Future development of force fields, water models, and supercomputer systems is required to improve the accuracy of MD. This will enable extension of the simulation timescale toward milliseconds and studying longer nucleosome arrays that can capture important functionally relevant atomistic features. Despite the current technical limitations, the application of these three techniques provides substantial new insights into the dynamics of chromatin with various modulators as discussed in the following sections.

The dynamics of chromatin *in vivo* cover a wide spatiotemporal window across the entire cell cycle, which is hardly detectable in real time by conventional characterization tools. FRET-based visualization of chromatin is a powerful tool to track the dynamic states of chromatin in live cells. To date, the focus in this field has been largely placed on designing proper biosensors (Llères et al., 2009; Sasaki et al., 2009; Sanchez et al., 2017; Peng et al., 2018; Gong et al., 2021; Mendonca et al., 2021). With the recent efforts toward this direction, studies detected dynamic fluctuations in histone H4K5 and K8 acetylation in living cells and confirmed that H4K5 acetylation is significantly reduced during mitosis (Sasaki et al., 2009). Another study revealed that H3S10p attenuates H3K9me3 at the onset of mitosis during a cell cycle, and demethylation of H3K9me3 is accompanied by the reduction of heterochromatin-like structures and thereby may increase the accessibility and promote the recruitment of chromatin remodelers (Peng et al., 2018). Although the design of proper biosensors is tedious and challenging, those examples of FRET-based visualization demonstrate its advances in tracking spatial distribution and abundance of epigenetic marks at the subcellular levels, which provides indispensable information in chromatin biology research.

Functional Dynamics of Nucleosomes

Recent molecular level NMR and MD studies covering nanosecond to millisecond timescales successfully demonstrated that in addition to structural characteristics, nucleosome dynamics provide important functional relevance. NMR studies determined conformational dynamics in NCPs for both highly flexible N-terminal tails and plastic histone core (Kitevski-LeBlanc et al., 2018; Shi et al., 2018; Xiang et al., 2018; Shi et al., 2020a; Shi et al., 2020b; Rabdano et al., 2021; Zandian et al., 2021). Histone tails in nucleosomes are the most well-characterized regions in studies of dynamics at the atomic level. Because of the highly flexible properties of these N-terminal tails, the atomistic pictures of conformations and dynamics are primarily captured by NMR and MD simulations (Massiah et al., 2013; Musselman et al., 2013; Morrison et al., 2018; Armeev et al., 2019; Abramov et al., 2020; Shi et al., 2020a; Ohtomo et al., 2021). A recent solution-state NMR study characterized the H2A and H2B tails in nucleosomes using deuterated samples at an ultra-high magnetic field (950 MHz), which observed two conformations of the tails corresponding to states interacting with different DNA regions (Ohtomo et al., 2021). It was noted that the observed stable conformations represent the averaged conformations of a large assembly of N-terminal tail states that likely involve fast exchange. Recent advances in SSNMR studies of chromatin allows elucidating the structure and dynamics for both the highly flexible tails and the rigid core for samples in compact states, where the water contents of the nucleosome samples are around 50–90% (Gao et al., 2013; Shi et al., 2018; Xiang et al., 2018; Ackermann and Debelouchina, 2021; Zandian et al., 2021). The determined motional amplitudes for amino acid backbone groups of histones in the NCPs suggest that motions at the nanosecond-microsecond timescale closely correlate with the structures (Shi et al., 2018; Shi et al., 2020a). More importantly, it revealed that there are collective microsecond-millisecond motions present at multiple regions of histones that form particular pathways to possibly transmit epigenetic signals form the NCP core to DNA sites distant from the histone sites (Shi et al., 2018; Shi et al., 2020b). Such studies of dynamics at the molecular level allow us to understand the functional dynamic properties and their contributions in DNA regulation activities. Consistent with this, a solution-state NMR study of nucleosomes harboring tetra-acetylated H4 revealed that acetylation shifts H3 tail dynamic conformations to being more dominant in the DNA–histone contact state, suggesting the existence of a histone tail network (Furukawa et al., 2020). Taken together, these studies suggest that dynamic networks likely extended from the HO to remote DNA sites. The coupling between DNA and histone conformation and dynamics on the microsecond timescale was directly observed by MD studies (Shaytan et al., 2016; Winogradoff and Aksimentiev, 2019; Armeev et al., 2021). The 15-microsecond all-atom MD simulation captured the atomistic details and illustrated that DNA breathing/unwrapping events occur at multi-microsecond timescale and are governed by histone dynamics (Armeev et al., 2021), which also demonstrated the functional roles of the plasticity of histone core in nucleosomes. Sub-nucleosomes including hexsomes and tetrasomes are species that also contribute to the regulation of DNA processes. The combination of NMR and MD studies elucidated that the H3 tails in hexasome possess distinct and asymmetric formations, and dynamics of the tails are increased with the loss of H2A/H2B dimer in nucleosome (Morrison et al., 2021). Similarly, a FRET study proposed a step-wise disassembly process and determined a shorter opening timescale for hexasomes in comparison with nucleosomes, indicating that the dissociation of a H2A/H2B dimer led to a more accessible DNA (Gansen et al., 2018). In addition to internal dynamics faster than microseconds, motions of hundreds of milliseconds were detected for nucleosome arrays (a mimic of chromatin fiber), which is the interconverting of different tetranucleosome stacking registers that can be modulated through long-range regulation factors to accomplish biological functions (Kilic et al., 2018).

Post-Translational Modifications

PTMs are one of the most common epigenetic regulatory mechanisms in eukaryotic proteins (Jenuwein and Allis, 2001).

The modifications typically occur at signal amino acid sites of histones and, in some cases, establish crosstalk (Tropberger et al., 2013; Wojcik et al., 2018; Kirsch et al., 2020), which introduce minor conformational alterations, allowing the recognition by PTM readers and initiation of the downstream activities (Taverna et al., 2007; Sanchez and Zhou, 2011). The dysregulation of PTMs can cause severe health issues such as cancers, neurodevelopmental disorders, and cardiovascular diseases (Schwartzentruber et al., 2012; Kim et al., 2017; Wickramasekara and Stessman, 2019; Zhao and Shilatifard, 2019; Bryant et al., 2020; Bagert et al., 2021). Furthermore, many nucleosome binding proteins recognize PTMs and cooperate with the modifications to accomplish biological functions, for example, H3K9me3 with HP1α, the PWWP domain with H3K36me3, and the SAGA complex with H3K4me3 (Vermeulen et al., 2010; Horn and van Ingen, 2020). Methylation is the most studied histone PTM at both molecular and genome levels. Structural studies showed that the dimethylation or trimethylation of H4K79 in NCPs result in subtle lysine sidechain structural rearrangements without global structural changes (Lu et al., 2008). It was recently revealed that the monomethylation of H4K20 leads to enhanced mobility of histones and less folded nucleosome arrays (Shoaib et al., 2021). This provides a molecular basis for the *in vivo* observation that H4K20me1 and H4K20me3 are accumulated at transcriptional active and suppression regions, respectively, which illustrate that the biological consequences of modifications are achieved through altering the dynamics of nucleosomes and, therefore, changing the compaction of nucleosome and the accessibility of DNA.

Acetylation is another prevalently occurring PTM that is crucial for DNA activities and reduces the net positive charge on histones. H4 tail acetylation likely leads to destabilizing chromatin at DNA double-strand breaks and dynamic changes of different modifications of the tail potentially regulate the repair pathways (Dhar et al., 2017). The genetically encoding acetyl-lysine strategy was used to provide large quantities of H3K56Ac, allowing a smFRET study that revealed the seven-fold increase in DNA breathing by this epigenetic modification (Neumann et al., 2009). An all-atom 5- to 6-microsecond MD simulation illustrated that acetylation of H3K56 weakens DNA–histone interactions and leads to further increase in mobility and exposure of DNA sites in lesion-containing nucleosomes, suggesting that this modification prepares the complex for DNA repair (Cai et al., 2020; Fu et al., 2021). In line with this, the combination of magnetic tweezers and FRET measurements showed that nucleosomes containing acetylation at the entry-exit site H3K56 or H4K77/K79 exhibited significantly enhanced DNA unwrapping (partial peeling of DNA ends from HO) and no change in disassembly (complete dissociation of DNA from HO) in comparison with unmodified NCPs (Simon et al., 2011). On the other hand, opposite effects were observed for nucleosomes harboring acetylation at the dyad site H3K115/K122 (Simon et al., 2011). Similarly, a FRET study of 170 bp Widom 601 nucleosomes revealed that acetylation of H3 and H4 induce different effects on nucleosome stability, where the former enhances DNA end unwrapping and the latter leads to opposite effects on disassembly and dimer exchange (Gansen et al., 2015). Those observations suggest that acetylation modifications occur at individual histone tail positions and independently modulate nucleosome dynamics through distinct mechanisms.

Besides acetylation, other lysine acylation modifications such as glutarylation and succinylation were also detected for histones *in vivo* (Li and Li, 2021). Glutarylation is a novel histone modification mark that was recently identified at 27 sites of histones (Tan et al., 2014; Bao et al., 2019). A study showed that glutarylation of H4K91 was highly enriched in active genes and the de-glutarylation was associated with chromatin condensation (Bao et al., 2019). FRET experiments revealed that glutarylation of H4K91 led to less stable nucleosomes in comparison with the acetylation of this site and the wild-type, and promoted the separation of H2A/H2B dimers from H3/H4 tetramers during nucleosome disassembly (Bao et al., 2019) Succinylation was first observed for all four histones by isotope labeling and HPLC/MS/MS analysis, and mutations on the succinylation sites led to functional consequences as demonstrated in budding yeast (Zhang et al., 2010; Xie et al., 2012). In comparison with acetylation, the succinylation introduces a longer sidechain and further reduction of the charge by one more unit due to the introduction of a negative carboxylate at the modified lysine site, therefore likely leading to greater alteration on structure and dynamics of the histones. The first site-specific succinylation-modified histones were obtained using thiol-ene addition at the H2BK34 site, and a smFRET study showed that the modification greatly attenuated DNA–histone interactions and reduced nucleosome structural stability (Jing et al., 2018). Succinylation of a nucleosome lateral surface residue, H3K122, leads to enhancing chromatin dynamics, which explains its transcription stimulation effects *in vitro* and enrichments in promoters of active genes *in vivo* (Zorro Shahidian et al., 2021).

Ubiquitination has been identified for tens of sites in histones and often establishes crosstalk with other modifications to regulate chromatin (Han et al., 2013; Mattiroli and Penengo, 2021). The unfolding of the outer DNA wrap in the nucleosomes harboring unmodified and ubiquitinated H2A required a free energy of 32 kJ/mol and 210 kJ/mol, respectively (Xiao et al., 2020). This ubiquitination achieves such effects through suppressing DNA unwrapping and, therefore, modulating the stability of nucleosomes. A study suggested that H2BK120Ub impairs the divalent cation-induced chromatin fiber compaction by affecting the later stage of compaction, while H4 acetylation disrupts the process *via* altering the electrostatic interactions at the early stage of compaction (Fierz et al., 2011). By combining a hydrogen–deuterium exchange strategy with NMR, it was revealed that H2BK120Ub results in decompaction of fibers likely mediated by the glutamate patch and ubiquitin fragments of neighboring mononucleosomes, interacting to hinder chromatin fiber association (Debelouchina et al., 2016). Phosphorylation increases the capability of forming electrostatic interactions with spatially closed chemical groups and contributes to DNA processes such as apoptosis, replication (Baker et al., 2010), stimulation-induced transcription (Armache et al., 2020), and telomere silencing (Zhang et al.,

2021). The combination of adding negative charges and a bulkier side chain by phosphorylation of H3T118 resulted in a reduction of DNA–histone binding by 2 kcal/mol, an increase in DNA accessibility near the dyad by six folds, and the promotion of nucleosome disassembly by a remodeler (North et al., 2011).

The composition of DNA in nucleosomes is one of the dominant factors dictating the architecture, compactness, and accessibility of chromatin. Varying DNA sequences lead to changes in nucleosome structure, dynamics, positioning, and compactness (Shaytan et al., 2017; Shi et al., 2020b; Soman et al., 2020). For example, our recent study revealed that the telomeric NCPs exhibit higher mobility in both histone N-terminal tails and core regions in comparison with the Widom 601 NCPs (Shi et al., 2020b). Alteration of DNA flexibility by changing the sequence was found to modulate the unwrapping direction, where DNA unwraps more from the stiffer end, which can be facilitated by the stability of the inner turn of the DNA (Ngo et al., 2015). MD simulations of DNA minicircles yielded an energy landscape analysis showing that changing DNA sequence and methylation states induced conformational and energetic perturbations for the systems (Yoo et al., 2021). Experimental studies of structure and dynamics for DNA methylations have been lagging behind, partially due to the difficulty of large-scale methylated DNA preparation. A recently developed synthetic strategy utilized $^{13}CH_3$-methionine, S-adenosylmethionine synthase, ATP, methyltransferase, and target DNA to produce $^{13}CH_3$-methyl-labeled for solution-state NMR experiments. It successfully observed structure and dynamics information for DNA-methylated mononucleosomes (Abramov et al., 2020). The 5-hydroxymethylated cytosine (5 hmC) naturally occurs 10–100 times less than 5-methylcytosine (5 mC) and, different from 5 mC, it likely accumulates at euchromatin (Chen et al., 2014). The combination of FRET with a biochemical study observed that 5 hmC decreases nucleosome stability (Mendonca et al., 2014). These studies lead the way to understanding the mechanisms of chromatin activities modulated by post-translation modifications of DNA.

Effector Proteins Altering the Dynamics of Nucleosome–Protein Complexes

DNA regulation is achieved through consecutive processes precisely cooperating at the temporal and spatial domain. For example, "writers" generate histone PTMs to open or tighten nucleosomes, which will be responded to by "readers" to incorporate regulatory proteins to interact with chromatin to trigger the downstream activities. The binding of effector proteins typically introduces essential changes to the structure, dynamics, and/or fiber compaction of chromatin, which often correlates with contacting interfaces. Yeast pioneer transcription factor Rap1 binds to chromatin fiber, resulting in no substantial structural disruption to the nucleosomes; instead, it interferes with the neighboring nucleosome interaction and opens chromatin (Mivelaz et al., 2020). Linker histone H1 is a key chromatin high-order structure modulating protein and contains the globular domain that binds to the nucleosome on the dyad (Bednar et al., 2017; Hao et al., 2021; Wang et al., 2021; Zhou et al., 2021), an N-terminal tail enhancing DNA binding (Collepardo-Guevara et al., 2020), and a C-terminal region interacting with linker DNA (Bednar et al., 2017; Hao et al., 2021; Wang et al., 2021; Zhou et al., 2021). The C-terminal domain retains high flexibility that allows H1 interacting with prothymosin α through highly disordered regions, promoting the dissociation of H1 from nucleosomes (Heidarsson et al., 2022). H1 undergoes structure changes upon binding to nucleosomes and alters the DNA accessibility by combining with PTMs and effector proteins (Collepardo-Guevara et al., 2020). H1 could bind to nucleosomes with on-dyad and off-dyad modes with the former more energetically favorable and the latter more dynamic (Wereszczynski and Woods, 2020; Rudnizky et al., 2021). The transition between the two modes may combine with other factors and serve as a switch for modulating DNA processes. PTMs spanning the entire protein are widely identified for H1 and many are revealed as linked to chromatin condensation/decondensation (Izzo and Schneider, 2016; Roque et al., 2016; Andrés et al., 2020). The acetylation of H1K85 likely results in a more condensed chromatin organization *via* enhancing its interaction with the histone core as demonstrated by using the modification mimic H1K85Q and also facilitates recruiting HP1 onto chromatin (Li et al., 2018). Phosphorylation modulates the structure of the H1 C-terminal domain and disrupts the condensation states of chromatin depending on the degree of modification (Roque et al., 2008; Izzo and Schneider, 2016). Comprehensive characterization of how H1 PTMs impact chromatin compaction and dynamics at the molecular level is generally lacking and awaits future investigation. The FACT complex is a histone chaperone that facilitates nucleosome assembly and disassembly, of which the mechanisms were recently revealed by cryo-EM structures of FACT–subnuclosome complexes (Liu et al., 2019). The binding of yeast FACT to a mononucleosome led to ATP-independent reversible DNA uncoiling involving >70% of the nucleosomal DNA as observed by FRET measurements for nucleosomes fluorescently labeled at three different sites (Valieva et al., 2016). A study combining solution-state NMR and FRET suggested that the human PHF1 Tudor domain binding to H3K36me3 containing NCP lead to the increase in nucleosome dynamics by shifting the population to the nucleosome opening state (Musselman et al., 2013). Cryo-EM combined with smFRET experiments showed that human methyltransferase DOT1L destabilizes nucleosome without alteration of HO conformation, and the effect is further enhanced by H2BK120 ubiquitination (Jang et al., 2019). In contrast to those effector proteins, chromatin-associated proteins such as HP1 contribute to the compaction of the chromatin fiber. Three isoforms, HP1α, HP1β, and HP1γ exist in mammalian cells. A recent cryo-EM study resolved 11.5–23.9 Å structures for the non-phosphorylated HP1 in complex with H3K9me3-containing dinucleosome, and revealed that HP1 forms a dimer that bridges two nucleosomes with linker DNA exposed to solvent (Machida et al., 2018). Another smFRET study elucidated that HP1α binds to nucleosomes on the 50–500 ms timescale and stabilizes chromatin fibers but introduces structural fluctuation on the sub-second timescale (Kilic et al., 2018). Taken together, the association of effector proteins with chromatin typically introduce changes to the dynamics and compaction of chromatin, preparing for downstream

activities. There are often critical conformational changes occurring in many of those interactions, which are not fully characterized due to the limitation of techniques and await future studies.

Histone Variants

Cells utilize the incorporation of histone variants to regulate gene events such as gene expression, DNA repair, and X chromosome inactivation (Sarma and Reinberg, 2005; Biterge and Schneider, 2014; Martire and Banaszynski, 2020). The histone variants, H3.2, H3.3 and CENP-A, H2AZ, H2AZ, and microH2A, share similarities of 50–99% with canonical ones and introduce unique compaction and accessibility features to chromatin (Sarma and Reinberg, 2005; Biterge and Schneider, 2014; Nechemia-Arbely et al., 2017). CENP-A is found at the active centromeres and its misregulation is observed in cancers. In comparison with the canonical NCP, the human CENP-A–containing NCP possesses a structure with thirteen base pairs at both ends of DNA absent and CENP-A αN loop shortened, suggesting increased flexibility of those regions (Tachiwana et al., 2011). As elucidated by FRET, the replacement of H3 by CENP-A leads to a destabilized and reshaped nucleosome structure and requires the binding of CENP-C to stabilize to a similar shape to that of the canonical nucleosomes (Falk et al., 2015; Falk et al., 2016). H2AZ2.2, a histone H2AZ variant, is demonstrated to be existing *in vivo*, and it functions by destabilizing nucleosomes, mainly attributed to its C-terminal region weakening the interactions with H3 (Bönisch et al., 2012).

CONCLUSION

Our understanding of the atomistic details of structure and dynamics of nucleosomes and nucleosome–protein complexes has been significantly expanded with the last two decades' development of high-resolution techniques. Here, we summarized studies and their importance pertaining to the dynamics of nucleosomes and their changes induced by the presence of modulation factors including PTMs, histone variants, and effector proteins. The functional relevant motions in chromatin typically span from the microsecond to the sub-second window, and the dynamics alterations introduced by modulation factors are achieved by the cooperation of multiple dynamical regions. Due to technical limitations, particularly FRET, much of the currently elucidated dynamics information is still limited by spatiotemporal resolution; however, it indubitably illustrates that dynamics play dominant roles in chromatin regulation processes. In addition, because subtle conformational changes are hard to capture in many of those studies discussed here, we cannot exclude the significance of structure contribution in this context. Ideally, combining atomic structure and dynamics characterization in the future will allow the complete understanding of chromatin regulation mechanisms at the molecular level.

AUTHOR CONTRIBUTIONS

XS and LN designed and wrote the manuscript. All authors contributed to the article and approved the submitted version.

FUNDING

This work was supported by the research funding from Shenzhen MSU-BIT University and Singapore Ministry of Education (MOE) Academic Research Fund (AcRF) Tier 2 (MOE2018-T2-1-112).

REFERENCES

Abramov, G., Velyvis, A., Rennella, E., Wong, L. E., and Kay, L. E. (2020). A Methyl-TROSY Approach for NMR Studies of High-Molecular-Weight DNA with Application to the Nucleosome Core Particle. *Proc. Natl. Acad. Sci. U.S.A.* 117 (23), 12836–12846. doi:10.1073/pnas.2004317117

Ackermann, B. E., and Debelouchina, G. T. (2021). Emerging Contributions of Solid-State NMR Spectroscopy to Chromatin Structural Biology. *Front. Mol. Biosci.* 8. doi:10.3389/fmolb.2021.741581

Andrés, M., García-Gomis, D., Ponte, I., Suau, P., and Roque, A. (2020). Histone H1 Post-Translational Modifications: Update and Future Perspectives. *Ijms* 21 (16), 5941. doi:10.3390/ijms21165941

Armache, A., Yang, S., Martínez de Paz, A., Robbins, L. E., Durmaz, C., Cheong, J. Q., et al. (2020). Histone H3.3 Phosphorylation Amplifies Stimulation-Induced Transcription. *Nature* 583 (7818), 852–857. doi:10.1038/s41586-020-2533-0

Armeev, G. A., Gribkova, A. K., Pospelova, I., Komarova, G. A., and Shaytan, A. K. (2019). Linking Chromatin Composition and Structural Dynamics at the Nucleosome Level. *Curr. Opin. Struct. Biol.* 56, 46–55. doi:10.1016/j.sbi.2018.11.006

Armeev, G. A., Kniazeva, A. S., Komarova, G. A., Kirpichnikov, M. P., and Shaytan, A. K. (2021). Histone Dynamics Mediate DNA Unwrapping and Sliding in Nucleosomes. *Nat. Commun.* 12 (1). doi:10.1038/s41467-021-22636-9

Bagert, J. D., Mitchener, M. M., Patriotis, A. L., Dul, B. E., Wojcik, F., Nacev, B. A., et al. (2021). Oncohistone Mutations Enhance Chromatin Remodeling and Alter Cell Fates. *Nat. Chem. Biol.* 17 (4), 403–411. doi:10.1038/s41589-021-00738-1

Baker, S. P., Phillips, J., Anderson, S., Qiu, Q., Shabanowitz, J., Smith, M. M., et al. (2010). Histone H3 Thr 45 Phosphorylation Is a Replication-Associated post-translational Modification in *S. cerevisiae*. *Nat. Cel Biol.* 12 (3), 294–298. doi:10.1038/ncb2030

Baldi, S., Korber, P., and Becker, P. B. (2020). Beads on a String-Nucleosome Array Arrangements and Folding of the Chromatin Fiber. *Nat. Struct. Mol. Biol.* 27 (2), 109–118. doi:10.1038/s41594-019-0368-x

Bannister, A. J., and Kouzarides, T. (2011). Regulation of Chromatin by Histone Modifications. *Cell Res* 21 (3), 381–395. doi:10.1038/cr.2011.22

Bao, X., Liu, Z., Zhang, W., Gladysz, K., Fung, Y. M. E., Tian, G., et al. (2019). Glutarylation of Histone H4 Lysine 91 Regulates Chromatin Dynamics. *Mol. Cel* 76 (4), 660–675. e669. doi:10.1016/j.molcel.2019.08.018

Bednar, J., Garcia-Saez, I., Boopathi, R., Cutter, A. R., Papai, G., Reymer, A., et al. (2017). Structure and Dynamics of a 197 Bp Nucleosome in Complex with Linker Histone H1. *Mol. Cel* 66 (3), 384–397. e388. doi:10.1016/j.molcel.2017.04.012

Biterge, B., and Schneider, R. (2014). Histone Variants: Key Players of Chromatin. *Cell Tissue Res* 356 (3), 457–466. doi:10.1007/s00441-014-1862-4

Bönisch, C., Schneider, K., Pünzeler, S., Wiedemann, S. M., Bielmeier, C., Bocola, M., et al. (2012). H2A.Z.2.2 Is an Alternatively Spliced Histone H2A.Z Variant that Causes Severe Nucleosome Destabilization. *Nucleic Acids Res.* 40 (13), 5951–5964. doi:10.1093/nar/gks267

Bowman, G. D., and Poirier, M. G. (2014). Post-translational Modifications of Histones that Influence Nucleosome Dynamics. *Chem. Rev.* 115 (6), 2274–2295. doi:10.1021/cr500350x

Bryant, L., Li, D., Cox, S. G., Marchione, D., Joiner, E. F., Wilson, K., et al. (2020). Histone H3.3 beyond Cancer: Germline Mutations in Histone 3 Family 3A and 3B Cause a Previously Unidentified Neurodegenerative Disorder in 46 Patients. *Sci. Adv.* 6 (49). doi:10.1126/sciadv.abc9207

Buning, R., and van Noort, J. (2010). Single-pair FRET Experiments on Nucleosome Conformational Dynamics. *Biochimie* 92 (12), 1729–1740. doi:10.1016/j.biochi.2010.08.010

Cai, Y., Geacintov, N. E., and Broyde, S. (2020). Variable Impact of Conformationally Distinct DNA Lesions on Nucleosome Structure and Dynamics: Implications for Nucleotide Excision Repair. *DNA Repair* 87, 102768. doi:10.1016/j.dnarep.2019.102768

Chen, Y., Damayanti, N. P., Irudayaraj, J., Dunn, K., and Zhou, F. C. (2014). Diversity of Two Forms of DNA Methylation in the Brain. *Front. Genet.* 5. doi:10.3389/fgene.2014.00046

Debelouchina, G. T., Gerecht, K., and Muir, T. W. (2016). Ubiquitin Utilizes an Acidic Surface Patch to Alter Chromatin Structure. *Nat. Chem. Biol.* 13 (1), 105–110. doi:10.1038/nchembio.2235

Dhar, S., Gursoy-Yuzugullu, O., Parasuram, R., and Price, B. D. (2017). The Tale of a Tail: Histone H4 Acetylation and the Repair of DNA Breaks. *Phil. Trans. R. Soc. B* 372 (1731), 20160284. doi:10.1098/rstb.2016.0284

Falk, S. J., Guo, L. Y., Sekulic, N., Smoak, E. M., Mani, T., Logsdon, G. A., et al. (2015). CENP-C Reshapes and Stabilizes CENP-A Nucleosomes at the Centromere. *Science* 348 (6235), 699–703. doi:10.1126/science.1259308

Falk, S. J., Lee, J., Sekulic, N., Sennett, M. A., Lee, T.-H., and Black, B. E. (2016). CENP-C Directs a Structural Transition of CENP-A Nucleosomes Mainly through Sliding of DNA Gyres. *Nat. Struct. Mol. Biol.* 23 (3), 204–208. doi:10.1038/nsmb.3175

Fenley, A. T., Anandakrishnan, R., Kidane, Y. H., and Onufriev, A. V. (2018). Modulation of Nucleosomal DNA Accessibility via Charge-Altering post-translational Modifications in Histone Core. *Epigenetics & Chromatin* 11 (1). doi:10.1186/s13072-018-0181-5

Fierz, B., Chatterjee, C., McGinty, R. K., Bar-Dagan, M., Raleigh, D. P., and Muir, T. W. (2011). Histone H2B Ubiquitylation Disrupts Local and Higher-Order Chromatin Compaction. *Nat. Chem. Biol.* 7 (2), 113–119. doi:10.1038/nchembio.501

Fu, I., Geacintov, N. E., and Broyde, S. (2021). Molecular Dynamics Simulations Reveal How H3K56 Acetylation Impacts Nucleosome Structure to Promote DNA Exposure for Lesion Sensing. *DNA Repair* 107, 103201. doi:10.1016/j.dnarep.2021.103201

Furukawa, A., Wakamori, M., Arimura, Y., Ohtomo, H., Tsunaka, Y., Kurumizaka, H., et al. (2020). Acetylated Histone H4 Tail Enhances Histone H3 Tail Acetylation by Altering Their Mutual Dynamics in the Nucleosome. *Proc. Natl. Acad. Sci. U.S.A.* 117 (33), 19661–19663. doi:10.1073/pnas.2010506117

Gansen, A., Felekyan, S., Kühnemuth, R., Lehmann, K., Tóth, K., Seidel, C. A. M., et al. (2018). High Precision FRET Studies Reveal Reversible Transitions in Nucleosomes between Microseconds and Minutes. *Nat. Commun.* 9 (1). doi:10.1038/s41467-018-06758-1

Gansen, A., Tóth, K., Schwarz, N., and Langowski, J. (2015). Opposing Roles of H3- and H4-Acetylation in the Regulation of Nucleosome Structure-A FRET Study. *Nucleic Acids Res.* 43 (3), 1433–1443. doi:10.1093/nar/gku1354

Gao, M., Nadaud, P. S., Bernier, M. W., North, J. A., Hammel, P. C., Poirier, M. G., et al. (2013). Histone H3 and H4 N-Terminal Tails in Nucleosome Arrays at Cellular Concentrations Probed by Magic Angle Spinning NMR Spectroscopy. *J. Am. Chem. Soc.* 135 (41), 15278–15281. doi:10.1021/ja407526s

Gong, Y., Wei, C., Cheng, L., Ma, F., Lu, S., Peng, Q., et al. (2021). Tracking the Dynamic Histone Methylation of H3K27 in Live Cancer Cells. *ACS Sens.* 6 (12), 4369–4378. doi:10.1021/acssensors.1c01670

Han, J., Zhang, H., Zhang, H., Wang, Z., Zhou, H., and Zhang, Z. (2013). A Cul4 E3 Ubiquitin Ligase Regulates Histone Hand-Off during Nucleosome Assembly. *Cell* 155 (4), 817–829. doi:10.1016/j.cell.2013.10.014

Hao, F., Kale, S., Dimitrov, S., and Hayes, J. J. (2021). Unraveling Linker Histone Interactions in Nucleosomes. *Curr. Opin. Struct. Biol.* 71, 87–93. doi:10.1016/j.sbi.2021.06.001

Heidarsson, P. O., Mercadante, D., Sottini, A., Nettels, D., Borgia, M. B., Borgia, A., et al. (2022). Release of Linker Histone from the Nucleosome Driven by Polyelectrolyte Competition with a Disordered Protein. *Nat. Chem.* 14 (2), 224–231. doi:10.1038/s41557-021-00839-3

Horn, V., and van Ingen, H. (2020). Recognition of Nucleosomes by Chromatin Factors: Lessons from Data-Driven Docking-Based Structures of Nucleosome-Protein Complexes. doi:10.5772/intechopen.81016

Huertas, J., and Cojocaru, V. (2021). Breaths, Twists, and Turns of Atomistic Nucleosomes. *J. Mol. Biol.* 433 (6), 166744. doi:10.1016/j.jmb.2020.166744

Izzo, A., and Schneider, R. (2016). The Role of Linker Histone H1 Modifications in the Regulation of Gene Expression and Chromatin Dynamics. *Biochim. Biophys. Acta (Bba) - Gene Regul. Mech.* 1859 (3), 486–495. doi:10.1016/j.bbagrm.2015.09.003

Jang, S., Kang, C., Yang, H.-S., Jung, T., Hebert, H., Chung, K. Y., et al. (2019). Structural Basis of Recognition and Destabilization of the Histone H2B Ubiquitinated Nucleosome by the DOT1L Histone H3 Lys79 Methyltransferase. *Genes Dev.* 33 (11-12), 620–625. doi:10.1101/gad.323790.118

Jenuwein, T., and Allis, C. D. (2001). Translating the Histone Code. *Science* 293 (5532), 1074–1080. doi:10.1126/science.1063127

Jing, Y., Liu, Z., Tian, G., Bao, X., Ishibashi, T., and Li, X. D. (2018). Site-specific Installation of Succinyl Lysine Analog into Histones Reveals the Effect of H2BK34 Succinylation on Nucleosome Dynamics. *Cel Chem. Biol.* 25 (2), 166–174. e167. doi:10.1016/j.chembiol.2017.11.005

Kato, H., van Ingen, H., Zhou, B.-R., Feng, H., Bustin, M., Kay, L. E., et al. (2011). Architecture of the High Mobility Group Nucleosomal Protein 2-nucleosome Complex as Revealed by Methyl-Based NMR. *Proc. Natl. Acad. Sci. U.S.A.* 108 (30), 12283–12288. doi:10.1073/pnas.1105848108

Kilic, S., Felekyan, S., Doroshenko, O., Boichenko, I., Dimura, M., Vardanyan, H., et al. (2018). Single-molecule FRET Reveals Multiscale Chromatin Dynamics Modulated by HP1α. *Nat. Commun.* 9 (1). doi:10.1038/s41467-017-02619-5

Kim, J.-H., Lee, J., Lee, I.-S., Lee, S., and Cho, K. (2017). Histone Lysine Methylation and Neurodevelopmental Disorders. *Ijms* 18 (7), 1404. doi:10.3390/ijms18071404

Kirsch, R., Jensen, O. N., and Schwämmle, V. (2020). Visualization of the Dynamics of Histone Modifications and Their Crosstalk Using PTM-CrossTalkMapper. *Methods* 184, 78–85. doi:10.1016/j.ymeth.2020.01.012

Kitevski-LeBlanc, J. L., Yuwen, T., Dyer, P. N., Rudolph, J., Luger, K., and Kay, L. E. (2018). Investigating the Dynamics of Destabilized Nucleosomes Using Methyl-TROSY NMR. *J. Am. Chem. Soc.* 140 (14), 4774–4777. doi:10.1021/jacs.8b00931

Korolev, N., Lyubartsev, A. P., and Nordenskiöld, L. (2018). A Systematic Analysis of Nucleosome Core Particle and Nucleosome-Nucleosome Stacking Structure. *Sci. Rep.* 8 (1). doi:10.1038/s41598-018-19875-0

Kovermann, M., Rogne, P., and Wolf-Watz, M. (2016). Protein Dynamics and Function from Solution State NMR Spectroscopy. *Quart. Rev. Biophys.* 49, e6. doi:10.1017/S0033583516000019

Krushelnitsky, A., Reichert, D., and Saalwächter, K. (2013). Solid-State NMR Approaches to Internal Dynamics of Proteins: From Picoseconds to Microseconds and Seconds. *Acc. Chem. Res.* 46 (9), 2028–2036. doi:10.1021/ar300292p

le Paige, U. B., Xiang, S., Hendrix, M. M. R. M., Zhang, Y., Folkers, G. E., Weingarth, M., et al. (2021). Characterization of Nucleosome Sediments for Protein Interaction Studies by Solid-State NMR Spectroscopy. *Magn. Reson.* 2 (1), 187–202. doi:10.5194/mr-2-187-2021

Lemak, A., Yee, A., Wu, H., Yap, D., Zeng, H., Dombrovski, L., et al. (2013). Solution NMR Structure and Histone Binding of the PHD Domain of Human MLL5. *PLoS ONE* 8 (10), e77020. doi:10.1371/journal.pone.0077020

Li, X., and Li, X. D. (2021). Integrative Chemical Biology Approaches to Deciphering the Histone Code: A Problem-Driven Journey. *Acc. Chem. Res.* 54 (19), 3734–3747. doi:10.1021/acs.accounts.1c00463

Li, Y., Li, Z., Dong, L., Tang, M., Zhang, P., Zhang, C., et al. (2018). Histone H1 Acetylation at Lysine 85 Regulates Chromatin Condensation and Genome Stability upon DNA Damage. *Nucleic Acids Res.* 46 (15), 7716–7730. doi:10.1093/nar/gky568

Liu, Y., Zhou, K., Zhang, N., Wei, H., Tan, Y. Z., Zhang, Z., et al. (2019). FACT Caught in the Act of Manipulating the Nucleosome. *Nature* 577 (7790), 426–431. doi:10.1038/s41586-019-1820-0

Llères, D., James, J., Swift, S., Norman, D. G., and Lamond, A. I. (2009). Quantitative Analysis of Chromatin Compaction in Living Cells Using FLIM-FRET. *J. Cel Biol.* 187 (4), 481–496. doi:10.1083/jcb.200907029

Lobbia, V. R., Trueba Sanchez, M. C., and van Ingen, H. (2021). Beyond the Nucleosome: Nucleosome-Protein Interactions and Higher Order Chromatin Structure. *J. Mol. Biol.* 433 (6), 166827. doi:10.1016/j.jmb.2021.166827

Lu, X., Simon, M. D., Chodaparambil, J. V., Hansen, J. C., Shokat, K. M., and Luger, K. (2008). The Effect of H3K79 Dimethylation and H4K20 Trimethylation on Nucleosome and Chromatin Structure. *Nat. Struct. Mol. Biol.* 15 (10), 1122–1124. doi:10.1038/nsmb.1489

Luger, K., Mäder, A. W., Richmond, R. K., Sargent, D. F., and Richmond, T. J. (1997). Crystal Structure of the Nucleosome Core Particle at 2.8 Å Resolution. *Nature* 389 (6648), 251–260. doi:10.1038/38444

Machida, S., Takizawa, Y., Ishimaru, M., Sugita, Y., Sekine, S., Nakayama, J.-i., et al. (2018). Structural Basis of Heterochromatin Formation by Human HP1. *Mol. Cel* 69 (3), 385–397. e388. doi:10.1016/j.molcel.2017.12.011

Martire, S., and Banaszynski, L. A. (2020). The Roles of Histone Variants in fine-tuning Chromatin Organization and Function. *Nat. Rev. Mol. Cel Biol.* 21 (9), 522–541. doi:10.1038/s41580-020-0262-8

Mattiroli, F., and Penengo, L. (2021). Histone Ubiquitination: An Integrative Signaling Platform in Genome Stability. *Trends Genet.* 37 (6), 566–581. doi:10.1016/j.tig.2020.12.005

Mendonca, A., Chang, E. H., Liu, W., and Yuan, C. (2014). Hydroxymethylation of DNA Influences Nucleosomal Conformation and Stability *In Vitro*. *Biochim. Biophys. Acta (Bba) - Gene Regul. Mech.* 1839 (11), 1323–1329. doi:10.1016/j.bbagrm.2014.09.014

Mendonca, A., Sánchez, O. F., Xie, J., Carneiro, A., Lin, L., and Yuan, C. (2021). Identifying Distinct Heterochromatin Regions Using Combinatorial Epigenetic Probes in Live Cells. *Biochim. Biophys. Acta (Bba) - Gene Regul. Mech.* 1864 (8), 194725. doi:10.1016/j.bbagrm.2021.194725

Mivelaz, M., Cao, A.-M., Kubik, S., Zencir, S., Hovius, R., Boichenko, I., et al. (2020). Chromatin Fiber Invasion and Nucleosome Displacement by the Rap1 Transcription Factor. *Mol. Cel* 77 (3), 488–500. e489. doi:10.1016/j.molcel.2019.10.025

Morrison, E. A., Baweja, L., Poirier, M. G., Wereszczynski, J., and Musselman, C. A. (2021). Nucleosome Composition Regulates the Histone H3 Tail Conformational Ensemble and Accessibility. *Nucleic Acids Res.* 49 (8), 4750–4767. doi:10.1093/nar/gkab246

Morrison, E. A., Bowerman, S., Sylvers, K. L., Wereszczynski, J., and Musselman, C. A. (2018). The Conformation of the Histone H3 Tail Inhibits Association of the BPTF PHD finger with the Nucleosome. *eLife* 7. doi:10.7554/eLife.31481

Musselman, C. A., Gibson, M. D., Hartwick, E. W., North, J. A., Gatchalian, J., Poirier, M. G., et al. (2013). Binding of PHF1 Tudor to H3K36me3 Enhances Nucleosome Accessibility. *Nat. Commun.* 4 (1). doi:10.1038/ncomms3969

Nechemia-Arbely, Y., Fachinetti, D., Miga, K. H., Sekulic, N., Soni, G. V., Kim, D. H., et al. (2017). Human Centromeric CENP-A Chromatin Is a Homotypic, Octameric Nucleosome at All Cell Cycle Points. *J. Cel Biol.* 216 (3), 607–621. doi:10.1083/jcb.201608083

Neumann, H., Hancock, S. M., Buning, R., Routh, A., Chapman, L., Somers, J., et al. (2009). A Method for Genetically Installing Site-specific Acetylation in Recombinant Histones Defines the Effects of H3 K56 Acetylation. *Mol. Cel* 36 (1), 153–163. doi:10.1016/j.molcel.2009.07.027

Ngo, T. T. M., Zhang, Q., Zhou, R., Yodh, J. G., and Ha, T. (2015). Asymmetric Unwrapping of Nucleosomes under Tension Directed by DNA Local Flexibility. *Cell* 160 (6), 1135–1144. doi:10.1016/j.cell.2015.02.001

North, J. A., Javaid, S., Ferdinand, M. B., Chatterjee, N., Picking, J. W., Shoffner, M., et al. (2011). Phosphorylation of Histone H3(T118) Alters Nucleosome Dynamics and Remodeling. *Nucleic Acids Res.* 39 (15), 6465–6474. doi:10.1093/nar/gkr304

Ohtomo, H., Kurita, J.-i., Sakuraba, S., Li, Z., Arimura, Y., Wakamori, M., et al. (2021). The N-Terminal Tails of Histones H2A and H2B Adopt Two Distinct Conformations in the Nucleosome with Contact and Reduced Contact to DNA. *J. Mol. Biol.* 433 (15), 167110. doi:10.1016/j.jmb.2021.167110

Peng, Q., Lu, S., Shi, Y., Pan, Y., Limsakul, P., Chernov, A. V., et al. (2018). Coordinated Histone Modifications and Chromatin Reorganization in a Single Cell Revealed by FRET Biosensors. *Proc. Natl. Acad. Sci. U.S.A.* 115 (50), E11681–E11690. doi:10.1073/pnas.1811818115

Rabdano, S. O., Shannon, M. D., Izmailov, S. A., Gonzalez Salguero, N., Zandian, M., Purusottam, R. N., et al. (2021). Histone H4 Tails in Nucleosomes: a Fuzzy Interaction with DNA. *Angew. Chem. Int. Ed.* 60 (12), 6480–6487. doi:10.1002/anie.202012046

Reyes, A. A., Marcum, R. D., and He, Y. (2021). Structure and Function of Chromatin Remodelers. *J. Mol. Biol.* 433 (14), 166929. doi:10.1016/j.jmb.2021.166929

Roque, A., Ponte, I., Arrondo, J. L. R., and Suau, P. (2008). Phosphorylation of the Carboxy-Terminal Domain of Histone H1: Effects on Secondary Structure and DNA Condensation. *Nucleic Acids Res.* 36 (14), 4719–4726. doi:10.1093/nar/gkn440

Roque, A., Ponte, I., and Suau, P. (2016). Post-translational Modifications of the Intrinsically Disordered Terminal Domains of Histone H1: Effects on Secondary Structure and Chromatin Dynamics. *Chromosoma* 126 (1), 83–91. doi:10.1007/s00412-016-0591-8

Rudnizky, S., Khamis, H., Ginosar, Y., Goren, E., Melamed, P., and Kaplan, A. (2021). Extended and Dynamic Linker Histone-DNA Interactions Control Chromatosome Compaction. *Mol. Cel* 81 (16), 3410–3421. e3414. doi:10.1016/j.molcel.2021.06.006

Sanchez, O. F., Mendonca, A., Carneiro, A. D., and Yuan, C. (2017). Engineering Recombinant Protein Sensors for Quantifying Histone Acetylation. *ACS Sens.* 2 (3), 426–435. doi:10.1021/acssensors.7b00026

Sanchez, R., and Zhou, M.-M. (2011). The PHD finger: a Versatile Epigenome Reader. *Trends Biochem. Sci.*. doi:10.1016/j.tibs.2011.03.005

Sarma, K., and Reinberg, D. (2005). Histone Variants Meet Their Match. *Nat. Rev. Mol. Cel Biol.* 6 (2), 139–149. doi:10.1038/nrm1567

Sasaki, K., Ito, T., Nishino, N., Khochbin, S., and Yoshida, M. (2009). Real-time Imaging of Histone H4 Hyperacetylation in Living Cells. *Proc. Natl. Acad. Sci. U.S.A.* 106 (38), 16257–16262. doi:10.1073/pnas.0902150106

Sasmal, D. K., Pulido, L. E., Kasal, S., and Huang, J. (2016). Single-molecule Fluorescence Resonance Energy Transfer in Molecular Biology. *Nanoscale* 8 (48), 19928–19944. doi:10.1039/c6nr06794h

Schwartzentruber, J., Korshunov, A., Liu, X.-Y., Jones, D. T. W., Pfaff, E., Jacob, K., et al. (2012). Driver Mutations in Histone H3.3 and Chromatin Remodelling Genes in Paediatric Glioblastoma. *Nature* 482 (7384), 226–231. doi:10.1038/nature10833

Shaytan, A. K., Armeev, G. A., Goncearenco, A., Zhurkin, V. B., Landsman, D., and Panchenko, A. R. (2016). Coupling between Histone Conformations and DNA Geometry in Nucleosomes on a Microsecond Timescale: Atomistic Insights into Nucleosome Functions. *J. Mol. Biol.* 428 (1), 221–237. doi:10.1016/j.jmb.2015.12.004

Shaytan, A. K., Xiao, H., Armeev, G. A., Wu, C., Landsman, D., and Panchenko, A. R. (2017). Hydroxyl-radical Footprinting Combined with Molecular Modeling Identifies Unique Features of DNA Conformation and Nucleosome Positioning. *Nucleic Acids Res.* 45 (16), 9229–9243. doi:10.1093/nar/gkx616

Shi, X., Prasanna, C., Nagashima, T., Yamazaki, T., Pervushin, K., and Nordenskiöld, L. (2018). Structure and Dynamics in the Nucleosome Revealed by Solid-State NMR. *Angew. Chem. Int. Ed.* 57 (31), 9734–9738. doi:10.1002/anie.201804707

Shi, X., Prasanna, C., Pervushin, K., and Nordenskiöld, L. (2020a). Solid-state NMR 13C, 15N Assignments of Human Histone H3 in the Nucleosome Core Particle. *Biomol. NMR. Assign.* 14, 99–104. doi:10.1007/s12104-020-09927-w

Shi, X., Prasanna, C., Soman, A., Pervushin, K., and Nordenskiöld, L. (2020b). Dynamic Networks Observed in the Nucleosome Core Particles Couple the Histone Globular Domains with DNA. *Commun. Biol.* 3 (1). doi:10.1038/s42003-020-01369-3

Shi, X., and Rienstra, C. M. (2016). Site-specific Internal Motions in GB1 Protein Microcrystals Revealed by 3D 2H-13C-13C Solid-State NMR Spectroscopy. *J. Am. Chem. Soc.* 138 (12), 4105–4119. doi:10.1021/jacs.5b12974

Shoaib, M., Chen, Q., Shi, X., Nair, N., Prasanna, C., Yang, R., et al. (2021). Histone H4 Lysine 20 Mono-Methylation Directly Facilitates Chromatin Openness and Promotes Transcription of Housekeeping Genes. *Nat. Commun.* 12 (1). doi:10.1038/s41467-021-25051-2

Simon, M., North, J. A., Shimko, J. C., Forties, R. A., Ferdinand, M. B., Manohar, M., et al. (2011). Histone Fold Modifications Control Nucleosome Unwrapping and Disassembly. *Proc. Natl. Acad. Sci. U.S.A.* 108 (31), 12711–12716. doi:10.1073/pnas.1106264108

Soman, A., Liew, C. W., Teo, H. L., Berezhnoy, N. V., Olieric, V., Korolev, N., et al. (2020). The Human Telomeric Nucleosome Displays Distinct Structural and Dynamic Properties. *Nucleic Acids Res.* 48 (10), 5383–5396. doi:10.1093/nar/gkaa289

Sridhar, A., Orozco, M., and Collepardo-Guevara, R. (2020). Protein Disorder-To-Order Transition Enhances the Nucleosome-Binding Affinity of H1. *Nucleic Acids Res.* 48 (10), 5318–5331. doi:10.1093/nar/gkaa285

Tachiwana, H., Kagawa, W., Shiga, T., Osakabe, A., Miya, Y., Saito, K., et al. (2011). Crystal Structure of the Human Centromeric Nucleosome Containing CENP-A. *Nature* 476 (7359), 232–235. doi:10.1038/nature10258

Talbert, P. B., and Henikoff, S. (2016). Histone Variants on the Move: Substrates for Chromatin Dynamics. *Nat. Rev. Mol. Cel Biol.* 18 (2), 115–126. doi:10.1038/nrm.2016.148

Tan, M., Peng, C., Anderson, K. A., Chhoy, P., Xie, Z., Dai, L., et al. (2014). Lysine Glutarylation Is a Protein Posttranslational Modification Regulated by SIRT5. *Cel Metab.* 19 (4), 605–617. doi:10.1016/j.cmet.2014.03.014

Taverna, S. D., Li, H., Ruthenburg, A. J., Allis, C. D., and Patel, D. J. (2007). How Chromatin-Binding Modules Interpret Histone Modifications: Lessons from Professional Pocket Pickers. *Nat. Struct. Mol. Biol.* 14 (11), 1025–1040. doi:10.1038/nsmb1338

Tropberger, P., Pott, S., Keller, C., Kamieniarz-Gdula, K., Caron, M., Richter, F., et al. (2013). Regulation of Transcription through Acetylation of H3K122 on the Lateral Surface of the Histone Octamer. *Cell* 152 (4), 859–872. doi:10.1016/j.cell.2013.01.032

Tyagi, M., Imam, N., Verma, K., and Patel, A. K. (2016). Chromatin Remodelers: We Are the Drivers!!. *Nucleus* 7 (4), 388–404. doi:10.1080/19491034.2016.1211217

Valieva, M. E., Armeev, G. A., Kudryashova, K. S., Gerasimova, N. S., Shaytan, A. K., Kulaeva, O. I., et al. (2016). Large-scale ATP-independent Nucleosome Unfolding by a Histone Chaperone. *Nat. Struct. Mol. Biol.* 23 (12), 1111–1116. doi:10.1038/nsmb.3321

Vermeulen, M., Eberl, H. C., Matarese, F., Marks, H., Denissov, S., Butter, F., et al. (2010). Quantitative Interaction Proteomics and Genome-wide Profiling of Epigenetic Histone marks and Their Readers. *Cell* 142 (6), 967–980. doi:10.1016/j.cell.2010.08.020

Voltz, K., Trylska, J., Tozzini, V., Kurkal-Siebert, V., Langowski, J., and Smith, J. (2008). Coarse-grained Force Field for the Nucleosome from Self-Consistent Multiscaling. *J. Comput. Chem.* 29 (9), 1429–1439. doi:10.1002/jcc.20902

Wang, S., Vogirala, V. K., Soman, A., Berezhnoy, N. V., Liu, Z. B., Wong, A. S. W., et al. (2021). Linker Histone Defines Structure and Self-Association Behaviour of the 177 Bp Human Chromatosome. *Sci. Rep.* 11 (1). doi:10.1038/s41598-020-79654-8

Wickramasekara, R., and Stessman, H. (2019). Histone 4 Lysine 20 Methylation: A Case for Neurodevelopmental Disease. *Biology* 8 (1), 11. doi:10.3390/biology8010011

Winogradoff, D., and Aksimentiev, A. (2019). Molecular Mechanism of Spontaneous Nucleosome Unraveling. *J. Mol. Biol.* 431 (2), 323–335. doi:10.1016/j.jmb.2018.11.013

Wojcik, F., Dann, G. P., Beh, L. Y., Debelouchina, G. T., Hofmann, R., and Muir, T. W. (2018). Functional Crosstalk between Histone H2B Ubiquitylation and H2A Modifications and Variants. *Nat. Commun.* 9 (1). doi:10.1038/s41467-018-03895-5

Woods, D. C., and Wereszczynski, J. (2020). Elucidating the Influence of Linker Histone Variants on Chromatosome Dynamics and Energetics. *Nucleic Acids Res.* 48 (7), 3591–3604. doi:10.1093/nar/gkaa121

Xiang, S., le Paige, U. B., Horn, V., Houben, K., Baldus, M., and van Ingen, H. (2018). Site-Specific Studies of Nucleosome Interactions by Solid-State NMR Spectroscopy. *Angew. Chem. Int. Ed.* 57 (17), 4571–4575. doi:10.1002/anie.201713158

Xiao, X., Liu, C., Pei, Y., Wang, Y.-Z., Kong, J., Lu, K., et al. (2020). Histone H2A Ubiquitination Reinforces Mechanical Stability and Asymmetry at the Single-Nucleosome Level. *J. Am. Chem. Soc.* 142 (7), 3340–3345. doi:10.1021/jacs.9b12448

Xie, Z., Dai, J., Dai, L., Tan, M., Cheng, Z., Wu, Y., et al. (2012). Lysine Succinylation and Lysine Malonylation in Histones. *Mol. Cell Proteomics* 11 (5), 100–107. doi:10.1074/mcp.M111.015875

Yoo, J., Park, S., Maffeo, C., Ha, T., and Aksimentiev, A. (2021). DNA Sequence and Methylation Prescribe the Inside-Out Conformational Dynamics and Bending Energetics of DNA Minicircles. *Nucleic Acids Res.* 49 (20), 11459–11475. doi:10.1093/nar/gkab967

Zandian, M., Gonzalez Salguero, N., Shannon, M. D., Purusottam, R. N., Theint, T., Poirier, M. G., et al. (2021). Conformational Dynamics of Histone H3 Tails in Chromatin. *J. Phys. Chem. Lett.* 12 (26), 6174–6181. doi:10.1021/acs.jpclett.1c01187

Zhang, S., Yu, X., Zhang, Y., Xue, X., Yu, Q., Zha, Z., et al. (2021). Metabolic Regulation of Telomere Silencing by SESAME Complex-Catalyzed H3T11 Phosphorylation. *Nat. Commun.* 12 (1). doi:10.1038/s41467-020-20711-1

Zhang, Z., Tan, M., Xie, Z., Dai, L., Chen, Y., and Zhao, Y. (2010). Identification of Lysine Succinylation as a New post-translational Modification. *Nat. Chem. Biol.* 7 (1), 58–63. doi:10.1038/nchembio.495

Zhao, Z., and Shilatifard, A. (2019). Epigenetic Modifications of Histones in Cancer. *Genome Biol.* 20 (1). doi:10.1186/s13059-019-1870-5

Zhou, B.-R., Feng, H., Ghirlando, R., Kato, H., Gruschus, J., and Bai, Y. (2012). Histone H4 K16Q Mutation, an Acetylation Mimic, Causes Structural Disorder of its N-Terminal Basic Patch in the Nucleosome. *J. Mol. Biol.* 421 (1), 30–37. doi:10.1016/j.jmb.2012.04.032

Zhou, B.-R., Feng, H., Kale, S., Fox, T., Khant, H., de Val, N., et al. (2021). Distinct Structures and Dynamics of Chromatosomes with Different Human Linker Histone Isoforms. *Mol. Cel* 81 (1), 166–182. e166. doi:10.1016/j.molcel.2020.10.038

Zhou, K., Gaullier, G., and Luger, K. (2019). Nucleosome Structure and Dynamics Are Coming of Age. *Nat. Struct. Mol. Biol.* 26 (1), 3–13. doi:10.1038/s41594-018-0166-x

Zorro Shahidian, L., Haas, M., Le Gras, S., Nitsch, S., Mourão, A., Geerlof, A., et al. (2021). Succinylation of H3K122 Destabilizes Nucleosomes and Enhances Transcription. *EMBO Rep.* 22 (3). doi:10.15252/embr.202051009

Conflict of Interest: The authors declare that the research was conducted in the absence of any commercial or financial relationships that could be construed as a potential conflict of interest.

Publisher's Note: All claims expressed in this article are solely those of the authors and do not necessarily represent those of their affiliated organizations, or those of the publisher, the editors, and the reviewers. Any product that may be evaluated in this article, or claim that may be made by its manufacturer, is not guaranteed or endorsed by the publisher.

frontiers | Frontiers in Genetics

SYSTEMATIC REVIEW
published: 06 April 2022
doi: 10.3389/fgene.2022.824483

Identification of Co-Existing Mutations and Gene Expression Trends Associated With K13-Mediated Artemisinin Resistance in *Plasmodium falciparum*

Mukul Rawat[1*†‡], *Abhishek Kanyal*[1†], *Deepak Choubey*[2†], *Bhagyashree Deshmukh*[1], *Rashim Malhotra*[1], *DV Mamatharani*[1], *Anjani Gopal Rao*[1] *and Krishanpal Karmodiya*[1*]

[1]*Department of Biology, Indian Institute of Science Education and Research, Pune, India,* [2]*Life Science Research Unit, Persistent Systems Limited, Pune, India*

Plasmodium falciparum infects millions and kills thousands of people annually the world over. With the emergence of artemisinin and/or multidrug resistant strains of the pathogen, it has become even more challenging to control and eliminate the disease. Multiomics studies of the parasite have started to provide a glimpse into the confounding genetics and mechanisms of artemisinin resistance and identified mutations in Kelch13 (K13) as a molecular marker of resistance. Over the years, thousands of genomes and transcriptomes of artemisinin-resistant/sensitive isolates have been documented, supplementing the search for new genes/pathways to target artemisinin-resistant isolates. This meta-analysis seeks to recap the genetic landscape and the transcriptional deregulation that demarcate artemisinin resistance in the field. To explore the genetic territory of artemisinin resistance, we use genomic single-nucleotide polymorphism (SNP) datasets from 2,517 isolates from 15 countries from the MalariaGEN Network (The Pf3K project, pilot data release 4, 2015) to dissect the prevalence, geographical distribution, and co-existing patterns of genetic markers associated with/enabling artemisinin resistance. We have identified several mutations which co-exist with the established markers of artemisinin resistance. Interestingly, K13-resistant parasites harbor α-ß hydrolase and putative HECT domain–containing protein genes with the maximum number of SNPs. We have also explored the multiple, publicly available transcriptomic datasets to identify genes from key biological pathways whose consistent deregulation may be contributing to the biology of resistant parasites. Surprisingly, glycolytic and pentose phosphate pathways were consistently downregulated in artemisinin-resistant parasites. Thus, this meta-analysis highlights the genetic and transcriptomic features of resistant parasites to propel further exploratory studies in the community to tackle artemisinin resistance.

Keywords: malaria, *Plasmodium falciparum*, artemisinin resistance, Kelch13 mutations, genomics, transcriptomics

OPEN ACCESS

Edited by:
Laxmi Narayan Mishra, Albert Einstein College of Medicine, United States

Reviewed by:
Jun Miao, University of South Florida, United States
Chenqi Wang, University of South Florida, United States

****Correspondence:***
Mukul Rawat
mr21@sanger.ac.uk
Krishanpal Karmodiya
krish@iiserpune.ac.in

‡Present Address:
Mukul Rawat, Wellcome Sanger Institute, Wellcome Genome Campus, Hinxton, United Kingdom

†These authors have contributed equally to this work

Specialty section:
This article was submitted to Epigenomics and Epigenetics, a section of the journal Frontiers in Genetics

Received: *29 November 2021*
Accepted: *08 February 2022*
Published: *06 April 2022*

Citation:
Rawat M, Kanyal A, Choubey D, Deshmukh B, Malhotra R, Mamatharani DV, Rao AG and Karmodiya K (2022) Identification of Co-Existing Mutations and Gene Expression Trends Associated With K13-Mediated Artemisinin Resistance in Plasmodium falciparum. Front. Genet. 13:824483. doi: 10.3389/fgene.2022.824483

INTRODUCTION

Malaria, a disease caused by a unicellular parasite belonging to the genus *Plasmodium*, has plagued mankind since times immemorial. *Plasmodium falciparum* is perhaps the most virulent species of the genus and is also associated with the more morbid and often lethal manifestations of malaria. The World Health Organization (WHO), which keeps a close tab on the global prevalence of the disease, reported an estimated 229 million cases of malaria and 409,000 deaths in 2019 alone (World Health Organization, 2020). Clinical observations in the field and *in vitro* studies of drug pressure regimens have shown the parasite's ability to evolve drug resistance rapidly (Bakhiet et al., 2019; Uwimana et al., 2020). WHO recommended use of artemisinin-based combination therapies (ACTs) in 2001. However, several studies have shown the selection of mutations associated with resistance to multiple drugs in *P. falciparum*, leading to the Accelerated Resistance to Multiple Drug phenotype (Rathod et al., 1997; Le Bras et al., 2003).

Artemisinin is a sesquiterpene lactone derived from the wormwood plant *Artemisia annua*. It is highly potent in reducing' the asexual stage parasite load in infected humans with no major side-effects. Owing to its short plasma half-life, it is often coupled with other longer lasting compounds in an ACT to prevent the relapse of parasites leading to emergence of resistance. The drug carries an endoperoxide bridge that is cleaved in the presence of free Fe^{2+} ions in the parasite, generated by digestion of hemoglobin in the food vacuole. Upon activation the drug goes into a free radical cascade that forms adduct with and damages biomolecules in the parasite cell. Recent click chemistry–based experiments designed to tag and identify molecular interactions of artemisinin in cells have identified factors involved in chaperoning, cellular transport, nucleic acid synthesis, and antigenic variation (Ismail et al., 2016a). Clinical resistance to artemisinin was first reported by Arjen Dondorp et al. in 2009 (Dondorp et al., 2009). It was identified as a delay in the clearance of parasite following treatment with artemisinin. Furthermore, to confound a clear definition of artemisinin resistance, *in vitro* drug sensitivity studies were shown to have little or no changes in artemisinin IC_{50} values even in field isolates with delayed clinical clearance times. Hence, a new standard of artemisinin sensitivity assay was developed called the ring-stage survival assay (RSA), which mimics the pharmacokinetic properties of the drug, including peak plasma concentrations and exposure cycles normally observed for artemisinin in patients (Witkowski et al., 2013). A survival of >1% of parasites in the RSA deems them resistant to artemisinin in *in vitro* settings. *In vitro* studies established that artemisinin resistance is associated primarily with the ring stage of *Plasmodium* life cycle; it is considered as "partial resistance" due to its stage specific nature. Artemisinin-resistant parasites, i.e., those with delayed clearance phenotype, result from the ability of the ring stage to enter into a "dormant state" induced by artemisinin stress. Parasites stay in a dormant stage for different duration depending on the genetic back ground (Teuscher et al., 2010).

Mutations in the PfKelch13 (K13) gene were identified to be definitively associated with artemisinin resistance (Ariey et al., 2014). One of the first studies to identify the role of K13 mutations in artemisinin resistance showed the enhancement of PI3P enriched vesicles carrying proteostatic factors in K13 mutant artemisinin resistance parasites (**Figure 1**) (Bhattacharjee et al., 2018). Some of the very recent studies identify K13-enriched endosomal compartments that directly regulate the endocytosis of hemoglobin into the host cell (Birnbaum et al., 2020). Mutations in K13 or its associated partner proteins in this vacuolar compartment tend to reduce the endocytosis of hemoglobin into parasite cells resulting in reduced drug activation (**Figure 1**) (Birnbaum et al., 2020). K13 mutations may, however, be predominant only in a subset of global populations, especially from Southeast Asia (SEA) (MalariaGEN Plasmodium falciparum Community Project, 2016). Although reports of artemisinin resistance from other parts of the world are gradually emerging, a strong correlation with K13 mutations is not observed. Subsequent independent drug adaptation studies have identified numerous mutational markers associated with artemisinin resistance *in vitro* (Wang et al., 2020). As such, there may be no one "universal identifier" of artemisinin resistance, but a number of them each specifically built/selected upon a complicated genetic background shaped by years of differential evolution in the field (Wilairat et al., 2016).

Furthermore, considering the sheer abundance of cellular targets for artemisinin in the cell, it is plausible to assume that modes of developing resistance must be prolific as well. An insight into the possible systemic mechanisms for artemisinin resistance has come from population transcriptomic studies (Mok et al., 2015). The parasite shows distinct gene expression changes, allowing for delayed progression of the ring stage of parasite, where it is transcriptionally least active and presents very limited proteome for damage (Mok et al., 2015). The parasite then seems to subsequently enter into a state of heightened stress response by enhancing the production of stress response factors pertaining to reactive oxygen stress complex, T-complex protein 1 ring complex, endoplasmic reticulum–resident unfolded protein response (UPR) pathway, and the ER-associated degradation (Mok et al., 2015). Studies have also linked the activated UPR in the endoplasmic reticulum to a downstream translational arrest (**Figure 1**) (Mok et al., 2015; Suresh and Haldar, 2018). The transcriptional profiles unique to resistant parasites are believed to be overlaid on a complex interaction of environmental pressures and selective evolution of genotypes (Mok et al., 2011; Dwivedi et al., 2017). Epigenetic factors that can respond to environmental perturbations in real time and evoke rapid responses in parasites may also contribute to resistance as shown in a recent study (Rawat et al., 2021). Identifying the markers and mechanisms of resistance in K13-independent resistance is also the next challenge and comparative multiomics can bolster investigations into these questions. Artemisinin combination therapy while highly effective and less susceptible to complete failure is nonetheless prone to gradual failure by accumulation of progressive single-nucleotide polymorphisms (SNPs) mediating resistance to not only artemisinin but also the partner drug (Wang et al., 2016). Several SNPs have been profiled in association with failure of the partner drugs currently employed in the ACT alongside artemisinin (Antony et al., 2016; Jiang et al., 2021). Few such

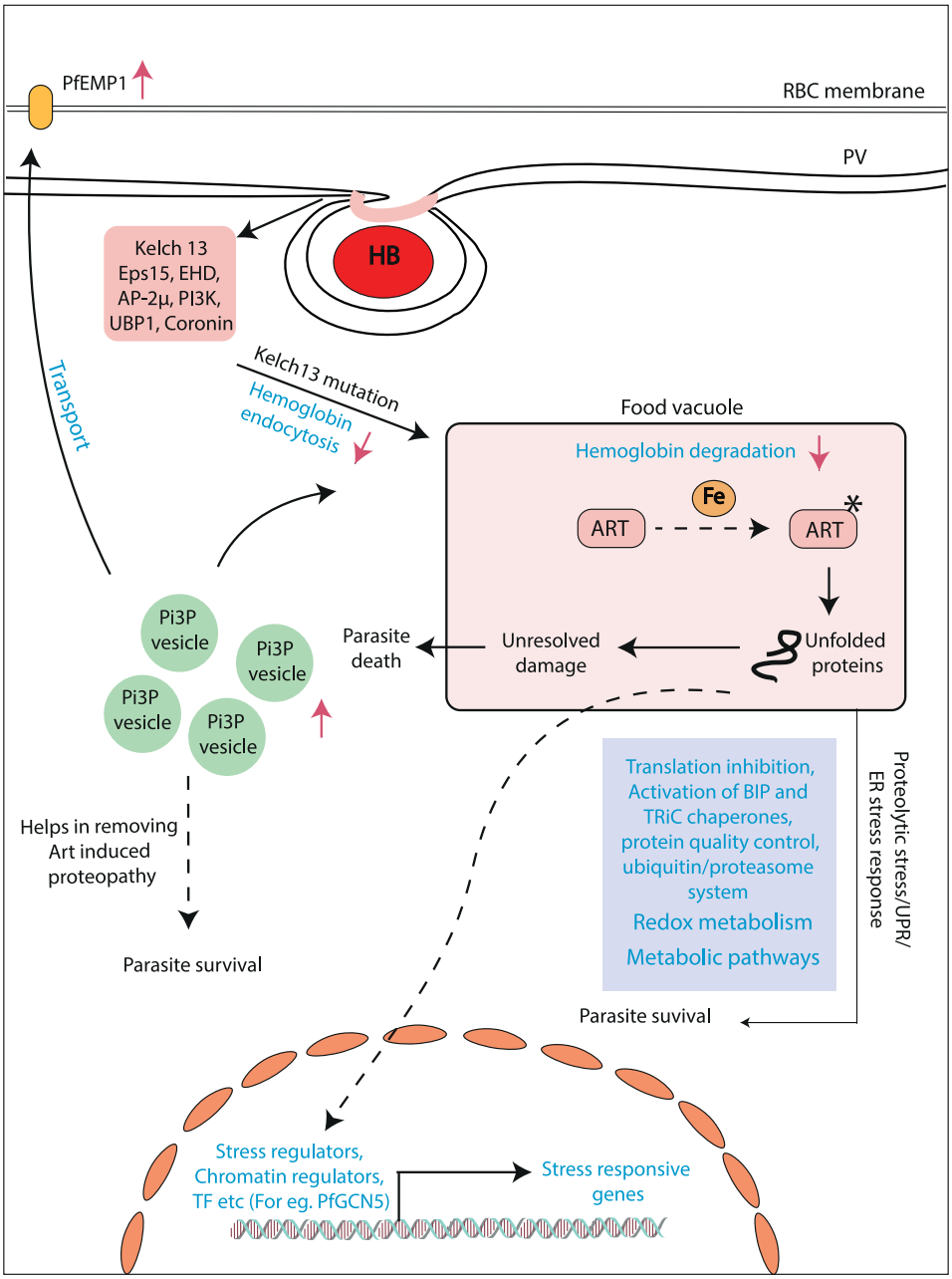

FIGURE 1 | Mechanisms proposed for artemisinin resistance in *P. falciparum*. Model showing the different mechanism proposed for artemisinin resistance generation. Artemisinin treatment results alkylation of several proteins resulting in the state of stress within the parasites. Different pathways like unfolded protein response and ubiquitin/proteasome system. Stress-like state results in the upregulation of stress induced genes by transcriptional regulators (e.g., PfGCN5). Another mechanism addresses the role of upregulated PI3P levels in the artemisinin-resistant parasites. Increased level of this lipid results in increased PI3P vesicles, which houses various proteins helps in the removing artemisinin induced proteopathy. Recent studies have identified decreased hemoglobin uptake and degradation. This ultimately results in decreased artemisinin activation and, hence, decreased artemisinin sensitivity.

examples are lumefantrine (mutations in the chloroquine resistance transporter, Pfcrt K76T, and multidrug resistance gene Pfmdr1 N86Y), amodiaquine (mutations in the Pfcrt K76T and Pfmdr1 N86Y), piperaquine (copy number variations in plasmepsin 2-3), and sulfadoxine-piperaquine dihydrofolate reductase gene pfdhfr (51I, 59R, and 108N), and the double mutant in dihydrofolate pteroate synthase gene pfdhps (437G and 540E) have been reported to be rendered useless by mutations (Slater et al., 2016).

With the ever-increasing usage of ACT worldwide, it becomes especially important to screen isolates from the field and perform genotype–phenotype screenings to assess

the efficacy of drugs currently employed in the field. The markers emerging out of these molecular epidemiology studies also need validation by *in vitro* studies that aim at observing the effects to engineering these mutations on parasite phenotypes (Stokes et al., 2021). Such studies highlight the need of system-wide analysis, characterization, and validation of resistance marker data.

The purpose of this analysis cum review is to revisit the ample genomic and transcriptional datasets described for artemisinin resistance in the Greater Mekong Subregion in SEA and Africa. We aim to summarize our current understanding of the genotypic landscape and highlight the transcriptomic trends in artemisinin-resistant parasites. Our focus has been to summarize the genetic markers associated with artemisinin resistance and their geographical prevalence and to investigate the patterns of their co-existence in isolates reported with artemisinin resistance. Initial transcriptome studies have provided us valuable insights into the possible physiological adaptations of the parasites to artemisinin and highlighting key factors from these datasets may fuel future investigations. In our review of the transcriptomic dataset, we aim at identifying specific factors that show consistent deregulation in association with artemisinin resistance. These highlighted factors can be further investigated for their role in emergence of drug resistance and be potentially considered for lead candidates for targeting in ongoing/future pharmacological intervention strategies on artemisinin resistance. With this review, we also aim to shift focus of investigations from broad biological pathways to specific factors that may have important roles to play in artemisinin drug resistance generation and sustenance.

MATERIALS AND METHODS

Whole Genome Sequencing Data Access and Analysis

SNP data were downloaded from Pf3K (Pilot data release 4) MalariaGEN (The Pf3K project, 2015) to analyze key mutations present in the PfKelch13 gene (PF3D7_1343700) (located on Chromosome number 13) (MalariaGEN Plasmodium falciparum Community Project, 2016). Genomes of 2517 isolates were available from 15 different geographical locations, majorly categorized into Africa (1,501) and Asia (1,010) subcontinents and some lab strains (6). Variant annotation for the data was done using snpEff version 4.3 (Cingolani et al., 2012). Fourteen of the K13 SNPs known to be associated with artemisinin resistance were assessed for their prevalence across different geographical region and co-existence among the 424 isolates they were found in.

Four SNPs from chloroquine resistance transporter Pfcrt gene (K76T, A220S, I356T, and R371I) and five SNPs for multidrug resistance Pfmdr gene (N86Y, E130K, Y184F, S1043C, and N1042D) were analyzed for co-existence with three definitive K13 markers of artemisinin resistance (C580Y, R539T, and I543T). Further exploration of background genomic variants co-existing with the K13 mutations in artemisinin resistance was identified using the 359 samples, which show one of the three major K13 mutations (C580Y, R539T, and Y493H). For an SNP to be filtered for co-existence with K13 mutations it had to be present in at least 75% of K13 mutant isolates (2 sigma value is 81.27%, covering more than 95% of the population). We performed a chi-squared test by comparing the combination wild-type (WT)/mutant instances of K13 with WT/mutant instances of the candidate genes in a 2 × 2 grid format. We applied the chi-squared independence test with a p-value cutoff of 0.05 and degree of freedom 1 (standard for a 2 × 2 grid) (**Supplementary Table S1**). In-house Perl and R scripts were used to analyze the data for co-existence. Variant annotation was done for all the SNPs using the tool snpEFF and only those SNPs that were non-synonymous mutation were considered for further analysis (Cingolani et al., 2012). Plots were generated using R and GraphPad (Swift and sciences, 1997; Tippmann, 2015).

Transcriptome Data Access and Review

We reviewed transcriptomic datasets from three studies with the aim to identify genes that were deregulated consistently across multiple studies. Gene list for the different protocol was drafted from the previously published literature as well as using PlasmoDB Malaria Parasite Metabolic Pathway (MPMP) database. The studies of Mok et al. and Rocomora et al. were used to identify genes that were deregulated (Mok et al., 2015; Mok et al., 2011; Rocamora et al., 2018). The studies of Mok et al. (2011 and 2015) are the *ex vivo* transcriptomic dataset, whereas Rocamora 2018 study used *in vitro*–selected artemisinin-resistant isolates (Chan and Walmsley, 1997). We chose to extract the list of genes mentioned as significantly deregulated in the respective studies as per the statistical criteria set by the original authors and as described in **Supplementary Table S2**. For this review, we considered genes mentioned in these studies with at least two-fold differential expression. Those that showed consistent deregulation across at least two of the three independent studies were shortlisted. The aim of this transcriptomic review is to identify genes (relevant to important biological pathways contributing to drug resistance), showing consistent deregulation.

RESULTS AND DISCUSSION

Genomic Landscape of Artemisinin Resistance: Geographical Prevalence and Trends of Co-Existence

To explore the genetic landscape relevant to artemisinin and multidrug resistance, we focused on the validated genetic markers associated strongly with drug resistance across the world. We laid special emphasis on the K13, the chloroquine resistance transporter (Pfcrt) and the multidrug resistance (Pfmdr) SNPs to identify their 1) abundance, 2) co-existence in isolates, and 3) geographical prevalence. We downloaded the Pf3K SNP dataset for 2,517 isolates from 15 countries in the SEA, South Asia, and Africa and six lab strains of the parasite. To have a better understanding of the genotype associated with artemisinin resistance, we focused on the isolates harboring any of the 14 K13 mutations confirmed to be correlated with artemisinin

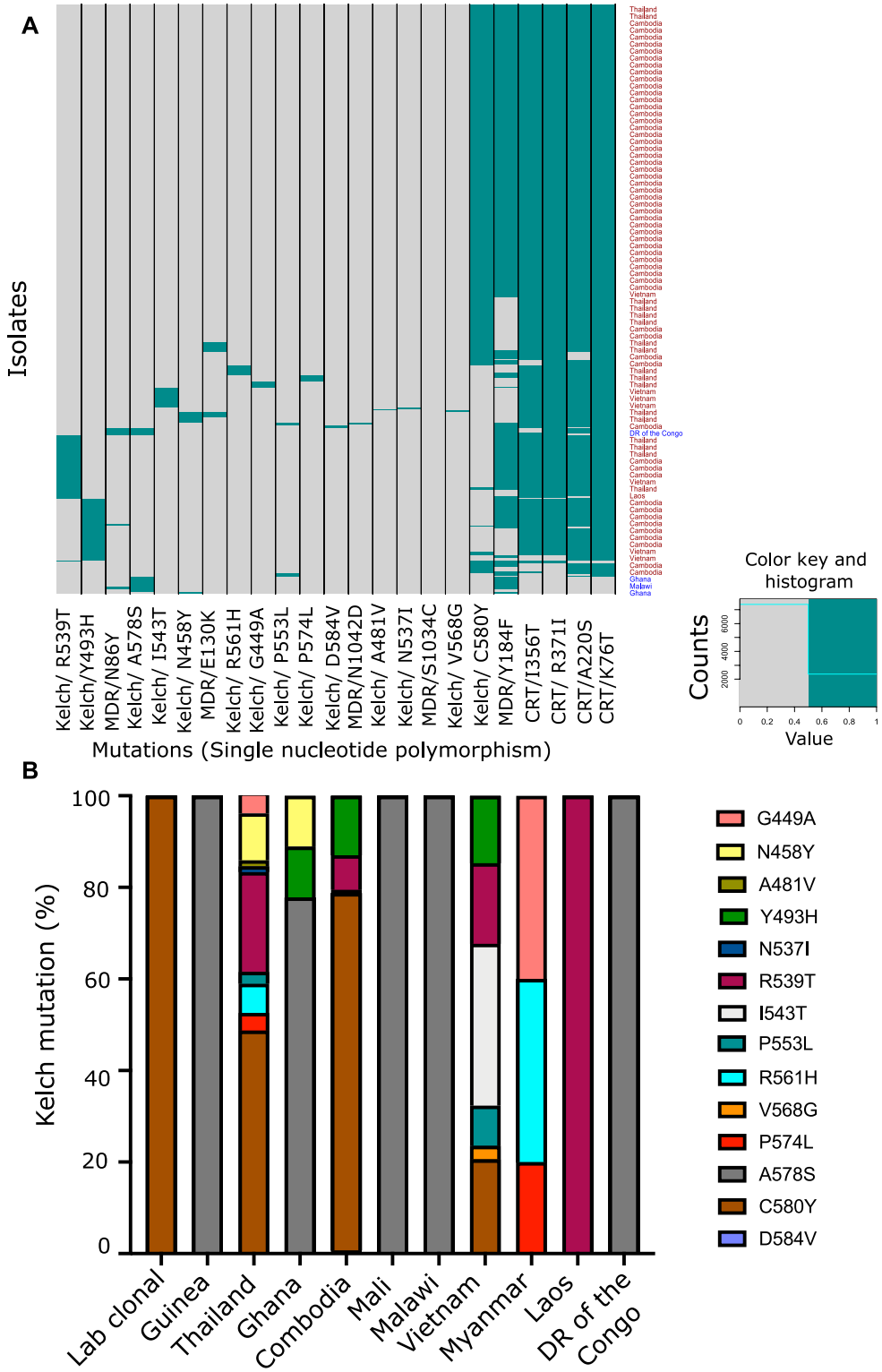

FIGURE 2 | Co-prevalence of the PfKelch13 mutations with other markers of multidrug resistance. **(A)** SNP data were downloaded from Pf3K (Pilot data release 4) MalariaGEN to analyze key mutations present in the K13 gene (PF3D7_1343700). Genomes of 2,517 isolates were available from 15 different geographical locations, majorly categorized into Africa (1,501) and Asia (1,010) subcontinents and some lab strains (6). Variant annotation for the data was done using snpEff version 4.3. Heatmap representing the mutation present in the different isolates from different geographical areas. Pfcrt (Chloroquine Resistance Transporter) and Pfmdr (Multidrug Resistance Transporter) mutations were also plotted along with the known K13 mutations to understand the co-prevalence of these mutations. **(B)** Fourteen of the Kelch SNPs known to be associated with artemisinin resistance were assessed for their prevalence across different geographical region and co-existence among the 424 isolates they were found in. Percentage proportion of different K13 mutation prevalent in the different countries used for the study.

resistance in GWAS (**Supplementary Table S3**) (Miotto et al., 2015). Among these, the C580Y SNP was found to be the most abundant, followed by R539T and Y493H (**Figure 2A** and **Supplementary Table S3**). Most of the other SNPs were at very low frequency as summarized in the (**Figure 2A** and **Supplementary Table S3**). It is speculated that mutations in the K13 protein result in either depletion of function or destabilization of the protein itself (Ariey et al., 2014; Coppée et al., 2019). A dysfunctional, mutant K13 or even lower amounts of WT K13 have been linked to impediments in the hemoglobin endocytosis leading to a subsequently lower activation of artemisinin as a result (Birnbaum et al., 2020). Although this protects the parasites from the damage caused by the drug, it infers a cost of poor growth and proliferation defects due to lack of amino acids obtained from hemoglobin catabolism. This explains why C580Y, which has low resistance to offer in RSA (~8% survival in RSA), is far more abundantly spread across SEA as compared to the other mutations (R539T or I543T) that offer more survival under drug pressure but may cause proliferation bottlenecks due to limited nutrient availability (Ariey et al., 2014; Nair et al., 2018; Tirrell et al., 2019; Birnbaum et al., 2020). Furthermore, we looked for co-existence of the K13 SNPs with other drug resistance markers, if any. Although mutations in the markers for chloroquine resistance (Pfcrt and Pfmdr) and sulfadoxine and pyrimethamine (Pfdhfr/Pfdhps) can often co-exist, the same does not hold true for mutations of the K13 gene (**Figure 2A**). We observed prevalence of only one variant of K13 at a time in the isolates. This may well be because harboring even two individually destabilizing mutations in the core K13 protein may amplify the overall instability of the protein, thus resulting in non-viability of the parasites. Interestingly, from SEA, Cambodia reported three isolates with co-existence of C580Y/Y493H K13 SNPs; two isolates with C580Y and one isolate from Thailand reported a double mutation (C580Y + R539T) (**Figure 2A** and **Supplementary Table S3**). However, presence of multiple K13 mutations can also be result of multiclonal infections. Among the SEA countries alone, the most prominent K13 mutations stood as C580Y, R539T, Y493H, and I543T in the decreasing order (**Figure 2B** and **Supplementary Table S3**). The countries in Africa reported scarcity of K13 mutations with A578S being the only predominant variant (**Figure 2B** and **Supplementary Table S3**). The regionally distinct enrichment of K13 mutations between African and Southeast Asian countries is striking.

Inspection of Genetic Backgrounds Against Which Specific K13 SNPs are Co-Existed

We proceeded to analyze the co-existence of K13 polymorphisms with markers associated with resistance to drugs that have been previously employed in the field and have subsequently been taken out of active usage. Pfcrt and Pfmdr SNPs were assessed for chloroquine resistance (**Supplementary Table S3**) (Venkatesan et al., 2014). We prepared a matrix with binary representation (0 for absent; 1 for present) for the prevalence of various SNPs in isolates from across the world. From this, we filtered out the isolates for distinct K13 mutations and calculated the percentage of isolates that reported co-existing mutations in the MDR or CRT locus. CQ resistance SNPs are among the most prevalent in the field, owing to rampant uncontrolled usage of CQ in the past decades, which led to widespread and rapid development of resistance that spread across the world. It is believed that these SNPs may form a genotypic background, which stabilizes the selection of K13 SNPs (Miotto et al., 2015). We observed a trend of co-existence of K13, Pfcrt, and Pfmdr mutations among the isolates (**Table 1**). A majority of the Pfcrt mutations were prevalent in the background of the K13 genotype and might be even permissive for establishment of K13, whereas only one Pfmdr mutation (Y184F) was found to share its existence with the K13 SNPs (**Figure 2A**, **Table 1** and **Supplementary Table S3**). When we sorted the samples to filter out for the prominent Pfcrt SNPs, we found enrichment of isolates from African countries. These isolates were enriched for the K13 A578S (**Supplementary Table S3**). It is plausible that the decade-long withdrawal of chloroquine from the African subcontinent may have diminished the abundance of popular Pfcrt mutations in the region. It is also plausible that A578S K13 mutations are more easily selected for in this unique genetic background (marked by absence of the popular Pfcrt markers).

Genomic Variants Co-Existing With the Artemisinin Resistance Markers

To detect the genomic variants that co-existed along with K13 mutations in artemisinin-resistant isolates, we screened the background genotype of the three major K13 mutants (C580Y, Y493H, and R539T). The SNP data were downloaded from MalariaGEN Network (The Pf3K project, pilot data release 5, 2016) repositories for all the *P. falciparum* chromosomes (MalariaGEN Plasmodium falciparum Community Project, 2016). A total of 359 isolates carried one of the three major K13 SNPs and flagged as "resistant", whereas the rest of the isolates lacking definitive K13 mutations were marked as "sensitive". Variant annotation was done using the tool snpEFF, and the non-synonymous SNPs were considered for further assessment (Cingolani et al., 2012). To consider an SNP as co-existing alongside K13 mutation, we set a cutoff criterion of co-existence in at least 75% resistant isolates (269 genomes) and absence in 75% sensitive isolates (1,619 genomes). We identified a total of 337 SNPs enriched across a pool of 207 genes from different chromosomes (**Figure 3A**). Normalized for the chromosome length, chromosome 13 harbored the maximum number of mutations followed by chromosome 14 (**Figure 3B** and **Supplementary Table S3**). This might be due to enhanced selection of patches of the chromosome 13 that favors the emergence of resistance. Among the genes that harbored the most mutations were a putative α-ß hydrolase (PF3D7_1328500) and a putative HECT domain–containing protein (PF3D7_0628100) (**Supplementary Table S4**). Of note were also an RNA-binding protein (PF3D7_0723900), a SET domain containing protein (PF3D7_0629700), autophagy-related protein 18 (PF3D7_1012900), and an AP2-domain transcription factor (PF3D7_1222400) (**Supplementary Table S4**). To further validate the co-existence of these distinct gene mutants with K13 mutations, we performed a chi-squared test to assess the relation between mutant/WT K13 with individual mutant/WT gene variants. We found that the association between K13 mutations

TABLE 1 | Co-prevalence of the K13 mutations with other markers of multidrug resistance.

K13 genotype	CRT genotype (% positive)				MDR genotype (% positive)				
	K76T	A220S	I356T	R371I	N86Y	E130K	Y184F	S1034C	N1042D
C580Y	99.2	97	96.3	97.4	0	2.5	83.5	0	0
Y493H	100	98	91	91	2	0	52	0	0
R539T	98	96	98	98	0	0	90	0	0

and the candidate background gene mutations identified by us was statistically significant for all except the Pfmdr1 mutation (**Supplementary Table S1**). Although several mutations have already been reported to be selected in the background of K13 mutations like ferrodoxin (PF3D7_1318100) and ubiquitin C-terminal hydrolase (PF3D7_0722330), we report several novel mutations hitherto undescribed. An investigation of the possible pathways connected with these mutations using the GO analysis revealed SNPs enriched upon genes associated with endocytosis, host cell invasion/exit, and signal transduction (**Figure 3C**). These pathways have also been implicated as contributing to artemisinin resistance as per recent studies. Thus, it is possible that mutations in these genes (like those in K13) affect the protein functionality/abundance and may thus trigger/support resistance to artemisinin.

Artemisinin Resistance Transcriptome: Investigation of Key Regulatory Factors and Processes

Next, we reviewed the transcriptome of artemisinin-sensitive and artemisinin-resistant parasites to identify the co-regulatory factors and processes. The datasets on field isolates from SEA in 2011 and 2015 (Mok et al.) were used as source for the *ex vivo* transcriptomes, whereas data from Rocamora et al. (2018) were used a source for the *in vitro*–selected artemisinin-resistant isolates (Mok et al., 2011; Mok et al., 2015; Rocamora et al., 2018). To investigate the transcriptional profile of genes from various pathways, we drafted a list of genes from each pathway from relevant publications and PlasmoDB gene MPMP database. Moreover, genes that showed at least two-fold differential expression and deregulated (both up and downregulated) across at least two of the three independent studies (Mok et al., 2011; Mok et al., 2015; Rocamora et al., 2018) were discussed and highlighted in the following sections. Heatmaps were generated for representing the deregulated expression of selected genes from key biological pathways in *Plasmodium* contributing to artemisinin resistance. **Figure 4** is generated from transcriptomic dataset of the study of Mok et al. (2011) comparing three artemisinin-resistant and seven artemisinin-sensitive parasite isolates. The genes were selected on the basis of their deregulation in this dataset and at least one other transcriptomic dataset that we reviewed. Similarly, **Supplementary Figure S2** is generated from the study of Mok et al. (2015). The genes were selected on the basis of their deregulation in the dataset of Mok et al. (2015) and at least one other transcriptomic dataset (Mok et al., 2015 or Rocomora et al., 2018), which we reviewed.

Global Transcriptional Regulators: Transcription Factors and Chromatin-Associated Factors

P. falciparum relies on a host of general [RNA polymerase II (RNA Pol II) core subunits/accessory proteins and general coactivators involved in initiation/elongation] and specific transcription-associated factors (apicomplexan AP2 factors, zinc finger proteins, and Helix turn helix motif proteins) for transcriptional control (Coulson et al., 2004; Balaji et al., 2005; Callebaut et al., 2005; Bischoff and Vaquero, 2010; Painter et al., 2011; Tuteja et al., 2011; Jeninga et al., 2019). Genetic ablation studies of a few of these factors, especially the ApiAP2 family of TFs, have hinted at strong roles of proteins in invasion into host red blood cells, governing the expression of exported proteins, gametocytogenesis, and liver-stage development (Iwanaga et al., 2012; Modrzynska et al., 2017; Santos et al., 2017; Van Biljon et al., 2019). Given the wide range of processes that transcription factors can govern, we were interested in identifying changes in their expression profile associated with artemisinin resistance. We procured a list of transcription factors, transcription-associated proteins, and chromatin-associated factors that aid in transcription from the PlasmoDB gene search database (Aurrecoechea et al., 2009). A list of high confidence transcription factors and associated proteins was also referenced from a bioinformatic study by Vaquero et al. (Bischoff and Vaquero, 2010). Our cross-dataset comparison revealed numerous factors that were commonly found to be deregulated across multiple studies. The RNA Pol II subunit RBP9 (PF3D7_0110400) and zinc finger protein (Ran-binding domain containing) (PF3D7_0408300) were upregulated, and CCR4-associated factor 1 (PF3D7_0811300), zinc finger protein (PF3D7_1205500), RNA Pol II subunit RBP11 (PF3D7_1304900), and conserved protein (PF3D7_1320700) were found to be downregulated in artemisinin-resistant parasites (**Figure 4**). In general, we see a strong correlation of the deregulation of multiple ZnF proteins and DNA-dependent RNA Pol II subunits with the artemisinin resistance phenotype both in the field and *in vitro* settings (**Supplementary Table S5**). These factors are higher up in the gene expression/regulation hierarchy and may have numerous genes (and consequently biological processes) under their direct regulation. Thus, they would be of value to investigate and understand the widespread transcriptional deregulation that precedes the establishment of artemisinin resistance in parasites.

We surveyed literature related to chromatin-associated proteins (CAPs) in *P. falciparum*. Primary gene set was

A

Chromosome number	Number of SNPS	Number of Genes
1	4	4
2	6	4
3	5	5
4	10	9
5	16	11
6	27	14
7	20	11
8	19	14
9	21	18
10	26	13
11	26	19
12	22	15
13	67	30
14	68	40

B

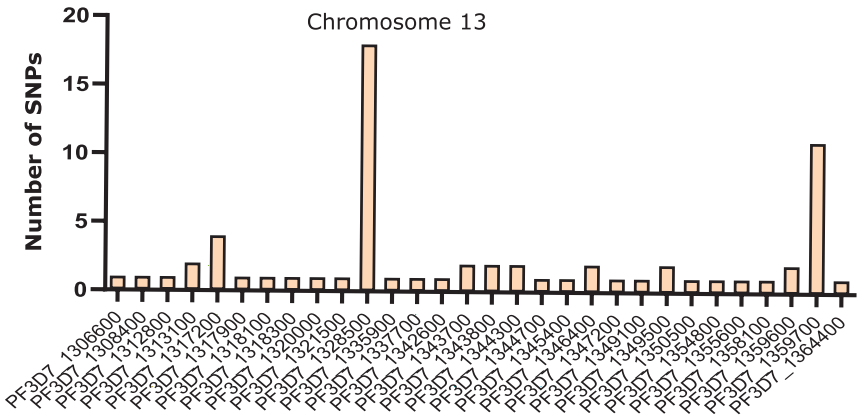

C

GO ID	GO Term	Percentage of bkgd genes in our results	P - value
GO:0006897	Endocytosis	30	0.006
GO:0044091	Entry into host	13	0.0008
GO:0009187	Cyclic nucleotide metabolic process	33.3	0.004
GO:0098657	Import into cell	27.3	0.008

FIGURE 3 | Co-existence of different SNPs along with PfKelch13 mutations. **(A)** Exploration of background genomic variants co-existing with the K13 mutations in artemisinin resistance was identified using the 359 samples, which show one of the three prime K13 mutations (C580Y, R539T, and Y493H). In order for an SNP to be filtered for co-existence with K13 mutations, it had to be present in at least 75% of K13 mutant isolates. Variant annotation was done for all the SNPs using the tool snpEFF and only those SNPs that were non-synonymous mutation were considered for further analysis. Table presenting the number of SNPs identified present in the 75% of the K13 mutants isolates and present in less than 25% of the sensitive (K13 mutant absent) isolates in various chromosomes. **(B)** Bar graph showing the number of SNPs present on the different genes over chromosome 13. **(C)** Gene ontology performed for the genes showing SNP co-existing with K13 mutations. Different biological processes like "endocytosis", "locomotion", "cell division", and "response to drug" were found to be enriched. Plots were generated using R and GraphPad.

procured from the dataset by Batugedara et al. (Batugedara et al., 2020), who utilized a combination of *in silico* methods and Chromatin Enrichment for Proteomics (ChEP) to identify a bona fide set of CAPs (Batugedara et al., 2020). These CAPS were identified to enrich for various biological processes in GO analysis, *viz.*, cell division, mRNA processing, protein modifications, ubiquitin-associated, and chromatin-associated (Batugedara et al., 2020). We decided to filter for CAPs that were enriched for chromatin specific functions exclusively, considering their potential role in regulation of gene expression. We also supplemented our dataset of candidate genes from the MPMP database, filtering specifically for

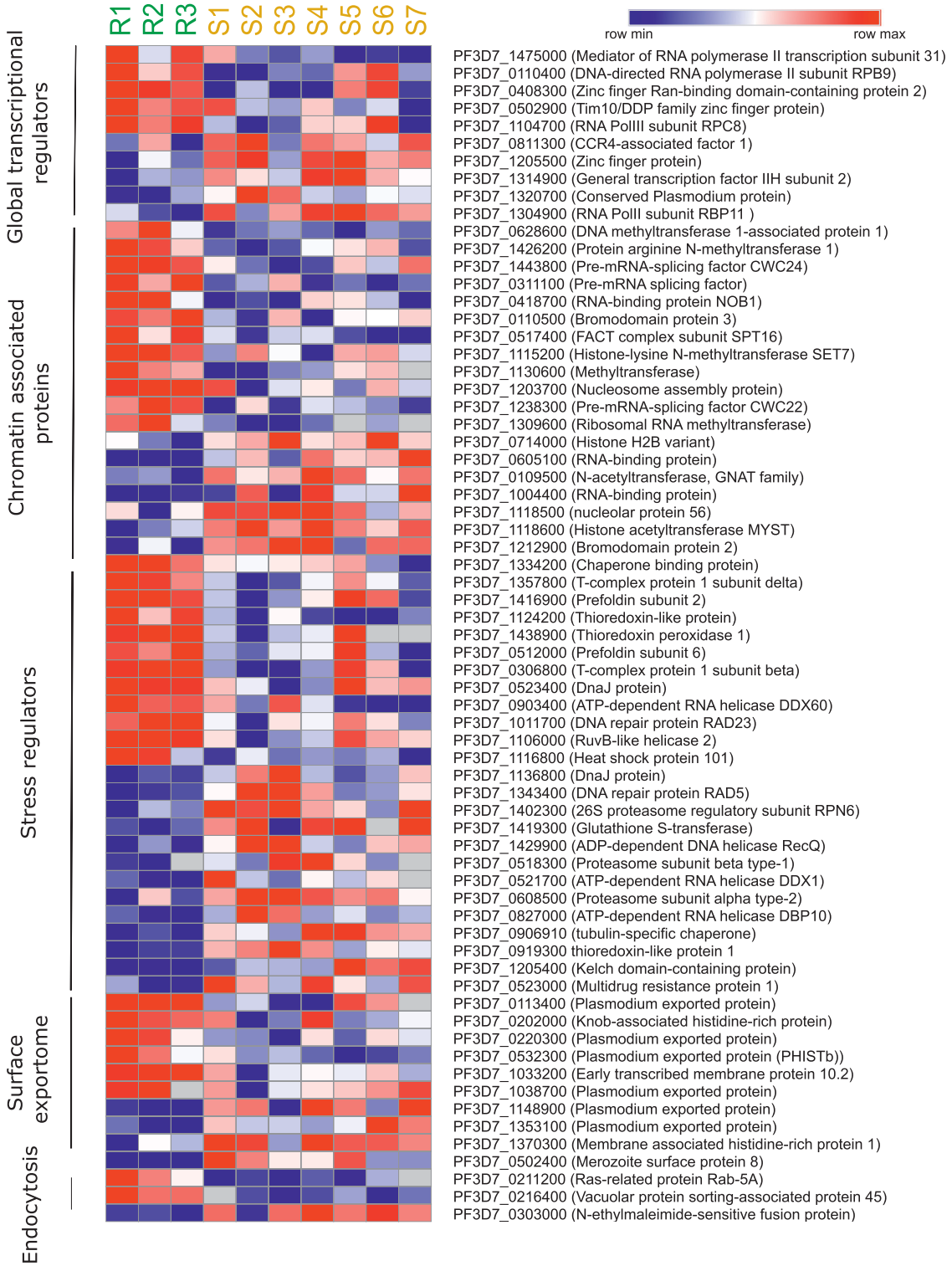

FIGURE 4 | Artemisinin resistance transcriptome of different biological pathways. Heatmap representing the deregulated expression of select genes from key biological pathways in *Plasmodium* contributive to artemisinin resistance. The heatmap is generated from transcriptomic dataset of Mok et al., 2011 study comparing three artemisinin-resistant and seven artemisinin-sensitive parasite isolates. The genes were selected on the basis of their deregulation in this dataset and at least one other transcriptomic dataset that we reviewed (Mok et al., 2015 and Rocamora et al., 2018).

TABLE 2 | Pathways and gene implicated in artemisinin resistance. Genes in red are upregulated in resistant parasites, whereas those represented in blue are downregulated.

Processes/Pathways	Key genes deregulated
Transcription Factors	DNA-directed RNA polymerase II subunit RPB9 (PF3D7_0110400)
	Zinc finger Ran-binding domain–containing protein 2 (PF3D7_0408300)
	Tim10/DDP family zinc finger protein (PF3D7_0502900)
	PF3D7_0811300 (CCR4-associated factor 1)
Chromatin-Associated Factors	Methyltransferase (PF3D7_1130600, PF3D7_1115200, PF3D7_1309600, PF3D7_1426200)
	Putative DNMT1 associated protein (PF3D7_0628600)
	Pre-mRNA splicing factor (PF3D7_1238300, PF3D7_1443800, PF3D7_0311100)
	Bromodomain protein 3 (PF3D7_0110500)
	Nucleosome assembly protein (PF3D7_1203700).
	Histone acetyl transferase MYST (PF3D7_1118600)
	GNAT family member acetyl transferase (PF3D7_0109500
	RNA-binding proteins (PF3D7_0605100 and PF3D7_1004400)
	Bromodomain protein (PF3D7_1212900)
Global stress regulators	DNA repair protein RAD23 (PF3D7_1011700)
	RAD54 DNA recombination and repair protein (PF3D7_1343400)
	The T-complex 1 subunit beta (PF3D7_0306800) and subunit delta (PF3D7_1357800)
	Prefoldin subunit 6 (PF3D7_0512000)
	Prefoldin subunit 2 (PF3D7_1416900)
	DnaJ protein (PF3D7_0523400)
	Thioredoxin peroxidase 1 (PF3D7_1438900) Thioredoxin-like protein (PF3D7_1124200)
Surface exportome	PHISTb (PF3D7_0532300, PF3D7_0731300, PF3D7_1477500 trophozoite exported protein 1 (PF3D7_0603400)
Endocytosis	Ras-related protein Rab-5a (PF3D7_0211200)
	Vacuolar protein sorting–associated protein 45 (PF3D7_0216400)
	Multidrug resistance protein 1 (MDR1) (PF3D7_0523000)
	Kelch domain–containing protein (PF3D7_1205400)
Metabolic enzymes	Glycine cleavage H protein (PF3D7_1132900)
	Glycine cleavage T protein (PF3D7_1365500)

chromatin modifying proteins (Aurrecoechea et al., 2009). We finally curated a set of 57 proteins belonging to various classes of epigenetic modifiers (histone acetyltransferase, histone deacetylase, histone lysine methyltransferase, protein arginine methyltransferase, and histone demethylase), chromatin remodelers, and nuclear architecture proteins. The CAPs were observed to be often downregulated in association with artemisinin-resistant parasites. Importantly, the RNA-binding protein NOB1 (PF3D7_0418700), a putative methyltransferase (PF3D7_1130600), a pre-mRNA splicing factor CWC22 (PF3D7_1238300), and a ribosomal RNA methyl transferase (PF3D7_1309600) were all found to be upregulated (**Figure 4** and **Table 2**). Interestingly, the histone acetyltransferase MYST (PF3D7_1118600) and the GNAT family member acetyltransferase (PF3D7_0109500) were downregulated in the resistant parasites (**Supplementary Table S5**). The histone H2B variant (PF3D7_0714000), two putative RNA-binding proteins (PF3D7_0605100 and PF3D7_1004400), and a putative bromodomain protein (PF3D7_1212900) were also downregulated in artemisinin-resistant parasites (**Supplementary Table S5**). The deregulation of histone PTM code modifiers allows for widespread changes to take place in the gene expression profile, which may hold true for resistant parasites as well.

Stress Regulators

The extreme reactive nature of artemisinin leads to the build of reactive oxygen species and toxic misfolded proteins in the parasite cell (Mok et al., 2015; Rocamora et al., 2018; Suresh and Haldar, 2018). In the eventuality of insufficient management or clearance of these toxic aggregates, the parasite succumbs. Furthermore, artemisinin is also speculated to impart direct damage to the parasite DNA either by free radical mechanisms or by forming direct adducts (Gopalakrishnan and Kumar, 2015; Kadioglu et al., 2017). Thus, the damage to proteins and DNA are the major consequences of artemisinin exposure in parasites and need to be dealt with rapidly. As a

consequence, the parasite must invest significantly in mechanisms that can help it survive under inhospitable conditions and proliferate on the host cell resources.

RNA helicases in *P. falciparum* have been reported to participate in major RNA metabolic processes including ribosome biogenesis, transcriptional control and fidelity, splicing, and translation (Tuteja and Pradhan, 2006; Tuteja, 2010). These are the biological processes that see major dysregulation during the artemisinin treatment. Studies suggest the deregulation of RNA helicases upon exposure to stresses, especially therapeutic (chloroquine) (Thélu et al., 1994). Thus, it becomes especially relevant to study their expression profiles in relevance to artemisinin resistance. The ATP-dependent RNA Helicase DDX60 (PF3D7_0903400) and DNA repair protein RAD23 (PF3D7_1011700) and RuvB like helicase (PF3D7_1106000) were found to be upregulated in the artemisinin-resistant parasites from the study of Mok et al. (2011) and in the *in vitro* generated resistant line 6A-R (Rocamora, 2018) (**Supplementary Table S5**). Conversely, the ATP-dependent RNA helicase DBP9 (PF3D7_1429900), the DEAD box helicase PF3D7_1439100, and the RAD54 DNA recombination and repair protein (PF3D7_1343400) were downregulated in the resistant parasites (**Supplementary Table S5**). Because helicases tend to perform a diversity of regulatory functions, it would be important to investigate them individually for any specific contribution to artemisinin resistance.

Heat-shock proteins (HSPs)/chaperones are among the prime candidates for cytoprotective functions and cellular repairs (Daniyan et al., 2019). HSPs play a crucial role as biomolecular chaperones by performing various functions like folding, unfolding, assembly of proteins, and transport of proteins into correct subcellular compartments (Joshi et al., 1992; Akide-Ndunge et al., 2009). Artemisinin exposure also damages the parasite proteome extensively and compromises cellular functions (Prieto et al., 2008). This makes the functions of homeostatic chaperone protein even more important in parasite survival. The chaperone proteins and the protein homeostasis-associated machinery are reported to be extensively involved in emergence of artemisinin resistance and thus interesting molecular candidates to follow (Rawat et al., 2021). The T-complex 1 subunit beta (PF3D7_0306800) and subunit delta (PF3D7_1357800), putative chaperone binding protein (PF3D7_1334200), prefoldin subunit 6 (PF3D7_0512000), and DnaJ protein (PF3D7_0523400), Hsp101 (PF3D7_1116800; ClpB2), and prefoldin subunit 2 (PF3D7_1416900) were upregulated in artemisinin-resistant parasites (**Supplementary Table S5**). Interestingly, a tubulin specific chaperone (PF3D7_0906910) and DnaJ protein (PF3D7_1136800) were downregulated in resistant isolates (**Supplementary Table S5**). The upregulation of numerous proteostasis factors (especially chaperones) has been highlighted for their role in mitigating the damage invoked by artemisinin and proteostasis.

Redox systems are known to play an important role in the survival of parasites under any oxidative stress conditions (Kehr et al., 2010; Nepveu and Turrini, 2013). *P. falciparum* possesses thioredoxin and glutathione redox systems, which constitutes the thiol-based antioxidant defense system along with superoxide dismutase (Jortzik and Becker, 2012). Recent studies have highlighted the significance of these pathways in artemisinin-resistant parasites because they play an important role in the maintenance of homeostasis in presence of free radicals during artemisinin activation (Rocamora et al., 2018). Rocomora et al. (2018) identified several genes involved in redox metabolism to be upregulated in *in vitro* lab-generated resistant strain like thioredoxin-like protein (PF3D7_1124200), thioredoxin 1 (PF3D7_1457200), thioredoxin peroxidase 1 (PF3D7_1438900), and glutathione reductase (PF3D7_1419800) (**Supplementary Table S5**). Surprisingly, most of the members of proteins belonging to thioredoxin and glutathione systems were found to be downregulated in the clinical isolates of resistant parasites, except thioredoxin peroxidase 1 (PF3D7_1438900) and thioredoxin-like protein (PF3D7_1124200) (**Supplementary Table S5**). Understanding the role of redox proteins in oxidative stress will be useful in targeting these proteins to overcome artemisinin resistance.

Surface Exportome

The parasite employs some remarkable strategies of host cell remodeling to enable it to thrive and survive in this niche environment (Schulze et al., 2015; de Koning-Ward et al., 2016; Warncke et al., 2019). It has been shown that ~8%–10% of the *P. falciparum* proteome is exported; collectively, these proteins are referred to as the "exportome" (Mundwiler-Pachlatko and Beck, 2013). The parasite-derived exported proteins play an important role in determining the rigidity of the RBC, permeating it for nutrients and metabolites along with imparting new attributes such as adherence, and clumping to avoid immune and splenic clearance (Mundwiler-Pachlatko and Beck, 2013). Antigenic gene families such as PfEMP1, rifins, stevors, surfins, and PfMC-2TM are known to cause the phenomenon such as cytoadherence, rosetting, and clumping (Dzikowski and Deitsch, 2009). Whereas, *Plasmodium* helical interspersed subtelomeric (PHIST) family proteins are known to remodel the RBC surface through incorporation into host cytoskeleton (Prajapati and Singh, 2013; Warncke et al., 2016). It is known that artemisinin-resistant parasites having K13 mutation with elevated PI3P show enriched PfEMP1 containing export proteome (Mbengue et al., 2015). This provides resistant parasites with better cytoadherence and hence successful immune evasion as compared to sensitive ones (Bhattacharjee et al., 2018). In concordance, we observed upregulation of a large number of exported proteins PF3D7_1038700 and PF3D7_0220300 (exported proteins of unknown function), a knob-associated histidine-rich protein (PF3D7_0202000), the early transcribed membrane protein 10.2 (PF3D7_1033200), and several HISTb proteins (**Supplementary Table S5**). On the other hand, the merozoite surface protein 8 (PF3D7_0502400), two exported proteins of unknown function (PF3D7_1148900 and PF3D7_1353100), and the membrane-associated histidine-rich protein 1 (PF3D7_1370300) were found to be downregulated in

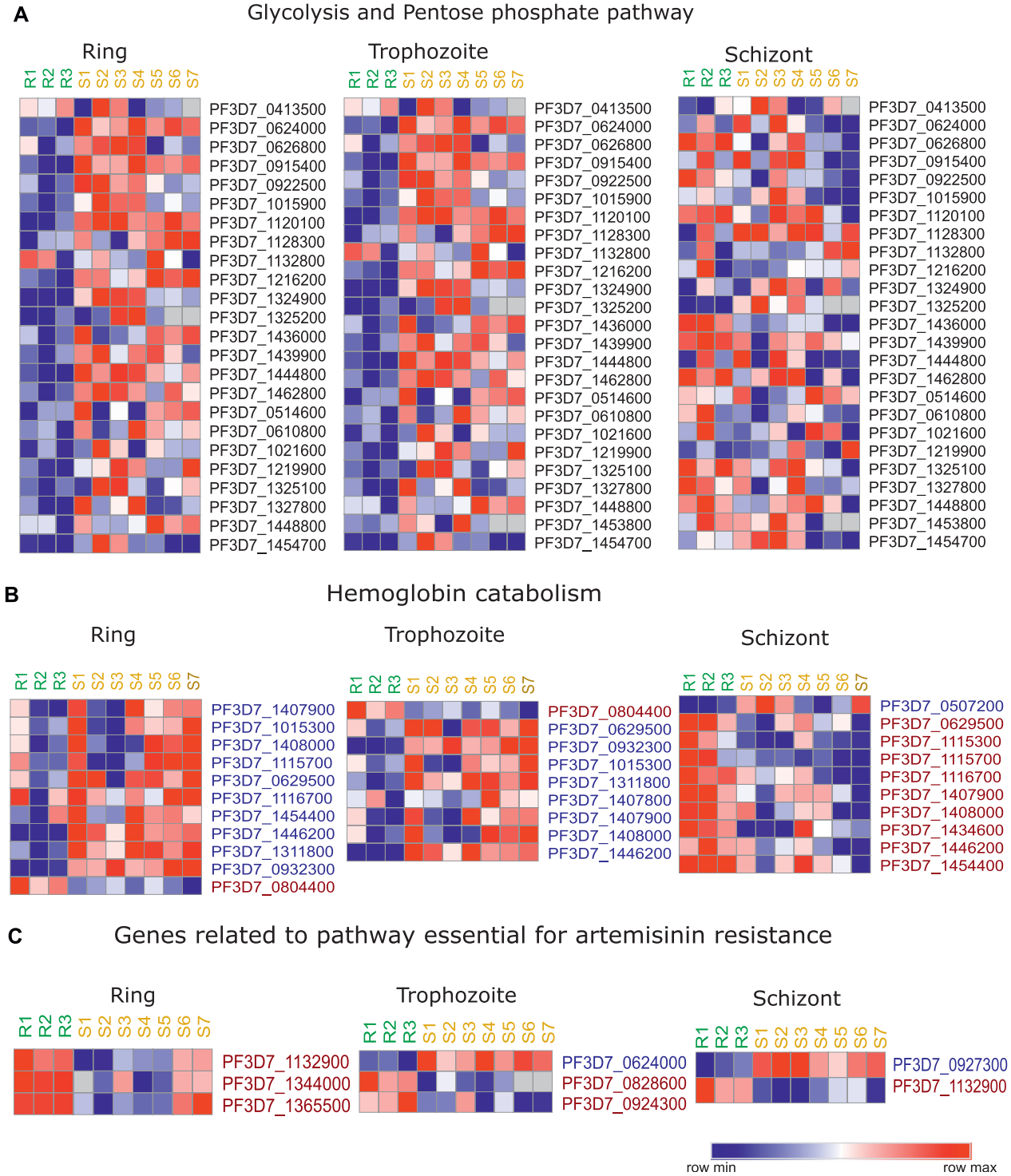

FIGURE 5 | Artemisinin resistance transcriptome for hemoglobin catabolism related genes and metabolic genes. Heatmap representing the stage specific trends in deregulation of expression of key genes implicated in **(A)** glycolysis and pentose phosphate pathway, **(B)** hemoglobin catabolism, and **(C)** genes related to pathway important for artemisinin resistance. The heatmap is generated from the expression values from the study of Mok et al. (2011). The list of genes themselves has been selected on the basis of deregulation of these genes across artemisinin-resistant vs. artemisinin-sensitive isolates in this and at least one other transcriptomic dataset reviewed in this study. R1–R3 represent the three artemisinin-resistant isolates, whereas S1–S7 represent the artemisinin-sensitive isolates.

artemisinin-resistant parasites (**Supplementary Table S5**). Although we did observe dramatic changes in expression of exported proteins associated with artemisinin resistance especially in the *in vitro*–selected resistant lines from the study of Rocamora et al. (2018), these changes were not found to be conserved across observations made from other studies.

Cytostomal Invagination Pathway

Plasmodium utilizes cytostome to imports chunks of host cell cytoplasm rich in hemoglobin *via* endocytic process which subsequently fuses to the food vacuole for further processing (Spielmann et al., 2020). Recent studies have highlighted the localisation of K13 protein in close proximity of the vesicular complex (Birnbaum et al., 2020). It was shown that parasites with inactivated K13 or a resistance-conferring K13 mutation displayed reduced hemoglobin endocytosis and resistance to artemisinin (Birnbaum et al., 2020). ARTs are activated by degradation products of hemoglobin. Hence, reduced activity of K13 and its interactors diminishes hemoglobin endocytosis and thereby artemisinin activation, resulting in parasite resistance (Siddiqui et al., 2017). This suggests that the process of endocytosis is critical to resistance generation in *P. falciparum*. In this regard, we were interested to investigate the role of endocytosis-related proteins across the artemisinin-resistant *Plasmodium* parasites. Our analysis found the Ras-related protein Rab-5a (PF3D7_0211200) and the vacuolar protein sorting–associated protein 45 (PF3D7_0216400) upregulated and a solitary N-ethylmaleimide-sensitive fusion protein (PF3D7_0303000) downregulated in the artemisinin-resistant parasites (**Supplementary Table S5**). Interestingly, not many endosome-associated proteins were found to be transcriptionally deregulated in artemisinin-resistant parasites. Fewer still were deregulated across multiple datasets.

Metabolic Pathways

Plasmodium is known to undergo metabolic alterations under different environmental and physiological conditions that are regulated by genetic and epigenetic mechanism (Lang-Unnasch and Murphy, 1998; Srivastava et al., 2016; Tewari et al., 2020). Being extensively adapted for a parasitic mode of life *Plasmodium* relies on the host for nutrients (Olszewski et al., 2009; Kafsack and Llinás, 2010; Zuzarte-Luís and Mota, 2018; Tougan et al., 2020). Several reports have indicated the role of metabolism in *P. falciparum* artemisinin resistance emergence (Carey et al., 2017; Guggisberg et al., 2018; Mok et al., 2021). Upon artemisinin treatment, *P. falciparum* is known to enter morphologically distinct quiescent stage that is characterized by reduced metabolism as a mean to resist unfavorable conditions (Teuscher et al., 2010; Chen et al., 2014). Metabolomics studies have identified the accumulation of glutathione and its precursor, gamma-glutamylcysteine, and significant depletion of one other putative metabolite in resistant strains (Siddiqui et al., 2017). Interestingly, dihydroartemisinin (DHA) treatment interferes with hemoglobin catabolism and pyridine biosynthesis (Cobbold et al., 2016). Covelli et al. in in their metabolomics study found significant reduction in the levels of Orate, which is a metabolite product of pyrimidine biosynthesis (Covelli et al., 2016). In addition, metabolites derived from lipid and cholesterol were significantly higher in DHA-exposed sensitive parasites (Covelli et al., 2016). Under DHA-induced dormancy, most of the metabolic pathways were found to be downregulated except fatty acid and pyruvate metabolic pathways that were active during phenomenon of dormancy (Chen et al., 2014). Inhibition studies of fatty acid and pyruvate metabolic pathway have been corelated with delayed recovery of dormant parasites (Chen et al., 2014). Hence, despite several studies available in the literature, the mechanism by which these metabolites conferring resistance to parasites is unclear. We looked at the transcriptional profile of the metabolic pathway genes in artemisinin-resistant isolates. We observed a clear downregulation of major metabolic pathways (glycolysis and pentose phosphate pathway) during intra erythrocytic life cycle in artemisinin-resistant parasites (**Figure 5A**).

Hemoglobin (Hb) digestion within the food vacuole results in the supply of amino acid to the parasite (Goldberg et al., 1990). Recent studies have shown that reduced hemoglobin digestion is responsible for reduced sensitivity to artemisinin, owing to lower availability of Fe^{2+} ions (generated by Hb catabolism) (Yang et al., 2019). Therefore, we looked at the stage specific expression of the genes that are involved in the digestion of hemoglobin in the dataset of Mok et al. (2011). Interestingly, these genes were downregulated in the resistant parasites during ring and trophozoite stages and upregulated during the schizont stage (**Figure 5B**). The downregulation of genes like aminopeptidase P (PF3D7_1454400), M1-family alanyl aminopeptidase (PF3D7_1311800), and cysteine proteinase falcipain 2a (PF3D7_1115700) is indicative of the fact that resistant parasites have reduced hemoglobin digestion (**Figure 5B**). Importantly, knockout of cysteine protease falcipain 2a (PF3D7_1115700) is reported to result in delayed sensitivity of parasites to artemisinin (Siddiqui et al., 2018). Moreover, mutations in cysteine falcipain 2a gene are also identified in *in vitro*–selected artemisinin-resistant parasites (Siddiqui et al., 2018). We looked at the expression level of these genes coding the enzyme vital for the resistant parasites and compared it to the sensitive parasites (Carey et al., 2017). Interestingly, out of the 11 genes reported to be essential for the artemisinin resistance, three genes were found to be highly expressed in resistant parasites: glycine cleavage H protein (PF3D7_1132900), glycine cleavage T protein (PF3D7_1365500), and aminomethyltransferase (PF3D7_1344000) during the ring stage of the parasites (**Figure 5C**). Similarly, we found folate transporter 1 (PF3D7_0828600) and thiamine pyrophosphokinase (PF3D7_0924300) to be upregulated and hexokinase (PF3D7_0624000) to be downregulated in resistant isolates from the study of Mok et al. (2011) during trophozoite stage (**Figure 5C**). Among chemical reactions unique to sensitive parasites, pyruvate kinase (PF3D7_0626800) was found to be significantly downregulated in resistant parasites. Two lipid metabolism-related genes phosphatidylinositol transfer protein (PF3D7_1351000) and phosphoinositide-binding protein

(PF3D7_0720700) were found to be upregulated in artemisinin-resistant parasites.

Artemisinin Resistance Proteome

Similar to the transcriptome, the proteome of *P. falciparum* varies with the stage of the parasite, and this has been the subject of many proteomic studies. Because proteins are the actual effector molecules in the cells, in recent years, the focus has shifted to a careful proteomic analysis of the artemisinin-resistant parasites. A finely tuned protein turnover machinery can help parasite to adapt under changing environment and drug treatment and should thus be properly studied to identify factors that can be crucial and be targeted. Artemisinin resistance mediated by K13 mutations is known to result in a dramatic upregulation of PI3P molecules and its vesicular structures (Mbengue et al., 2015; Bhattacharjee et al., 2018). Global peptidomics analysis suggested the lower levels of peptides derived from hemoglobin (HBα and HBβ) in artemisinin-resistant parasites (Siddiqui et al., 2017). Interestingly, hemoglobin catabolism–related genes were found to be downregulated in artemisinin-resistant lines that show a protein level validation of the downregulation in hemoglobin catabolism (Siddiqui et al., 2017). Recently, Ismail et al. (2016) identified protein targets of artemisinin drug using click chemistry (Ismail et al., 2016b). Interestingly, some of the proteins like M1-family alanyl aminopeptidase (PF3D7_1311800), Plasmepsin I (PF3D7_1407900), and II (PF3D7_1408000), which assist in hemoglobin digestion, were found to be direct target of artemisinin (Ismail et al., 2016b). This establishes a potential link between downregulation in hemoglobin peptide on DHA treatment and direct alkylation and inhibition of these proteases by artemisinin drug.

Bhattacharjee et al. recently reported the presence of the amplified PI3P vesicles, which helps in neutralizing the protein damage due to artemisinin (Bhattacharjee et al., 2018). These vesicles house proteins like K13, PfEMP1, and BiP and other proteins useful for maintaining homeostasis during artemisinin treatment. Out of the 502 proteins identified in their proteomic analysis of PI3P vesicles, approximately 72 are also reported to be upregulated at transcript level in transcriptomic study of artemisinin-resistant patient samples (Birnbaum et al., 2020).

CONCLUSION

A close inspection of the genomic and transcriptomic features of artemisinin-resistant isolates has identified/reaffirmed peculiar trends of genetic selection and gene expression patterns. K13 mutations still predominantly mark artemisinin resistance phenotype with the C580Y, R539T, and Y493H genotype in decreasing order of global prevalence (Ménard et al., 2016). Although the K13 mutations are dominant in the Southeast Asian countries, there is minor presence in Africa as well. African nations, however, report a distinct K13 mutations A578S being the major player (Ménard et al., 2016). Interestingly, only a few isolates showed double/triple K13 mutations perhaps, owing to the strong destabilizing effect individual mutations impose on parasite viability. In our efforts to explore the genetic markers/polymorphisms supporting K13 mutations, we identify a strong selection against a backdrop of Pfcrt mutations (K76T, A220S, I536T, and R571I) but not so much with Pfmdr mutations (only Y184F seemed to co-exist with K13 mutations). Pf mutations seem to have reduced in prevalence over decades of discontinued usage of chloroquine in the region. It might be possible that the lack of common Pfcrt markers over the recent years has reduced the selection of common K13 mutations, thus explaining their poor presence in the region while also allowing for novel mutations in K13 to emerge. Finally, we interrogated the co-existence of K13 mutations with other key SNPs in the genomic background of resistant isolates. With a 75% resistant vs. 25% sensitive filter, we identified a host of SNPs that exist alongside the three prominent K13 mutations. An α-ß hydrolase and a putative HECT domain–containing gene were found to harbor the maximum number of SNPs, with chromosome 13 bearing the maximum SNP load. It is quite possible that these genes showing high mutational burden may be playing some role as background mutations to support the Kelch-resistant mutation. Significant enrichment of endocytosis and host cell entry/egress pathways was noted. The spatial and temporal selection dynamics of genetic polymorphisms and their interplay toward deciding the fate of drug therapy across the globe shall be very interesting to follow up further.

A thorough investigation of the transcriptomic datasets of the artemisinin-resistant field isolates and *in vitro*–selected strains has helped us narrow down on key genes whose expression changes may be interesting to follow up for validation and subsequent studies. In our top-down approach, we focused on transcription regulatory protein, the broader chromatin associated proteome and stress response factors particularly because of their speculated roles in bringing about artemisinin resistance in the parasite. We observed a consistent deregulation of several transcription factors (ZnF proteins) and numerous epigenetic regulator (PfMYST and PfSET7) proteins that dictate the temporal expression of genes. Owing to their higher placement in the hierarchy of gene expression and a plethora of biological pathways under their regulation, some of these may be key to the broader deregulation that is characteristic of artemisinin resistance. We also found a strong deregulation of RNA Pol II–associated proteins across the IDC that may account for the redistribution of RNA expression observed in resistance (low in early stages and a burst of transcriptional activity toward the mature stages). We further looked out for stress responsive factors in the parasites. We observed a robust change in the expression profile of specific ATP-dependent RNA helicases that govern key processes like transcriptional fidelity and splicing. This may, in turn, have implications on the overall RNA output and quality control. HSPs were found to be significantly among the upregulated genes cohort testimony of their role in controlling protein damage in resistant isolates. An interesting aspect that we wanted to investigate was the

expression of exported protein genes, but, although these genes show deregulation in individual datasets, we did not observe a very consistent change across studies. Expression of exported proteins is often very sensitive to changes in environmental parameters that change across studies dramatically.

Our investigation of the metabolic pathway genes expression showed consistent downregulation of glycolytic and pentose phosphate pathway–associated genes. This strongly reiterates the metabolic slowdown that is characteristically associated with the ring stage parasites that are resistant to artemisinin. Also notable is the consistent downregulation of numerous aminopeptidases associated with hemoglobin catabolism. This follows course with numerous recent investigations, highlighting reduction of heme metabolism to be associated with artemisinin resistance in parasites. In addition, of note was the dramatic upregulation of genes associated with the folate metabolism in resistant parasites. We also reaffirm the overexpression of numerous redox pathway–associated genes in multiple studies. Our analysis highlights the aberrant expression of specific genes from pathways that have been implicated in mediating resistance. Numerous such examples have been highlighted in **Table 2**.

There is still a dearth of proteomic data relevant to investigating artemisinin resistance. However, the handful of studies that exist seem to suggest the parasite's attempts to reduce hemoglobin catabolism perhaps in attempts to suppress activation of drug. This also matches with transcriptomic investigations that seem to hint at a decline in the abundance of hemoglobin catabolism enzymes. Simultaneously, the parasite does seem to enrich its proteome (especially in PI3P marked vesicles) with proteostatic factors associated with chaperoning, translation, and quality control functions. More proteomic studies need follow to better understand the interplay between well documented transcriptional changes and the little known proteome.

DATA AVAILABILITY STATEMENT

The original contributions presented in the study are included in the article/**Supplementary Material**, further inquiries can be directed to the corresponding authors.

AUTHOR CONTRIBUTIONS

MR, AK, and DC designed and analyzed data. MR, AK, RM, BD, MDV, and AR performed transcriptome analysis. DC performed genome analysis. MR, AK, and KK wrote the manuscript. MR and KK planned, coordinated, and supervised the project. All authors read and approved the final manuscript.

FUNDING

This work was supported by a grant from DBT-Genome Engineering Technologies program (BT/PR25858/GET/119/169/2017) from the Government of India to KK.

SUPPLEMENTARY MATERIAL

The Supplementary Material for this article can be found online at: https://www.frontiersin.org/articles/10.3389/fgene.2022.824483/full#supplementary-material

REFERENCES

Akide-Ndunge, O. B., Tambini, E., Giribaldi, G., McMillan, P. J., Müller, S., Arese, P., et al. (2009). Co-ordinated Stage-dependent Enhancement of Plasmodium Falciparum Antioxidant Enzymes and Heat Shock Protein Expression in Parasites Growing in Oxidatively Stressed or G6PD-Deficient Red Blood Cells. *Malar. J.* 8, 113–115. doi:10.1186/1475-2875-8-113

Antony, H. A., Das, S., Parija, S. C., and Padhi, S. (2016). Sequence Analysis of Pfcrt and Pfmdr1 Genes and its Association with Chloroquine Resistance in Southeast Indian Plasmodium Falciparum Isolates. *Genomics Data* 8, 85–90. doi:10.1016/j.gdata.2016.04.010

Ariey, F., Witkowski, B., Amaratunga, C., Beghain, J., Langlois, A.-C., Khim, N., et al. (2014). A Molecular Marker of Artemisinin-Resistant Plasmodium Falciparum Malaria. *Nature* 505, 50–55. doi:10.1038/nature12876

Aurrecoechea, C., Brestelli, J., Brunk, B. P., Dommer, J., Fischer, S., Gajria, B., et al. (2009). PlasmoDB: a Functional Genomic Database for Malaria Parasites. *Nucleic Acids Res.* 37, D539–D543. doi:10.1093/nar/gkn814

Bakhiet, A. M. A., Abdelraheem, M. H., Kheir, A., Omer, S., Gismelseed, L., Abdel-Muhsin, A.-M. A., et al. (2019). Evolution of Plasmodium Falciparum Drug Resistance Genes Following Artemisinin Combination Therapy in Sudan. *Trans. R. Soc. Trop. Med. Hyg.* 113, 693–700. doi:10.1093/trstmh/trz059

Balaji, S., Babu, M. M., Iyer, L. M., and Aravind, L. J. N. a. r. (2005). Discovery of the Principal Specific Transcription Factors of Apicomplexa and Their Implication for the Evolution of the AP2-Integrase DNA Binding Domains. *Nucleic Acids Res.* 33, 3994–4006. doi:10.1093/nar/gki709

Batugedara, G., Lu, X. M., Saraf, A., Sardiu, M. E., Cort, A., Abel, S., et al. (2020). The Chromatin Bound Proteome of the Human Malaria Parasite. *Microb. Genom* 6, e000327. doi:10.1099/mgen.0.000327

Bhattacharjee, S., Coppens, I., Mbengue, A., Suresh, N., Ghorbal, M., Slouka, Z., et al. (2018). Remodeling of the Malaria Parasite and Host Human Red Cell by Vesicle Amplification that Induces Artemisinin Resistance. *Blood* 131, 1234–1247. doi:10.1182/blood-2017-11-814665

Birnbaum, J., Scharf, S., Schmidt, S., Jonscher, E., Hoeijmakers, W. A. M., Flemming, S., et al. (2020). A Kelch13-Defined Endocytosis Pathway Mediates Artemisinin Resistance in Malaria Parasites. *Science* 367, 51–59. doi:10.1126/science.aax4735

Bischoff, E., and Vaquero, C. (2010). In Silico and Biological Survey of Transcription-Associated Proteins Implicated in the Transcriptional Machinery during the Erythrocytic Development of Plasmodium Falciparum. *BMC Genomics* 11, 34–20. doi:10.1186/1471-2164-11-34

Callebaut, I., Prat, K., Meurice, E., Mornon, J. P., and Tomavo, S. (2005). Prediction of the General Transcription Factors Associated with RNA Polymerase II in Plasmodium Falciparum: Conserved Features and Differences Relative to Other Eukaryotes. *BMC Genomics* 6, 100–120. doi:10.1186/1471-2164-6-100

Carey, M. A., Papin, J. A., and Guler, J. L. (2017). Novel Plasmodium Falciparum Metabolic Network Reconstruction Identifies Shifts Associated with Clinical Antimalarial Resistance. *BMC Genomics* 18, 543–619. doi:10.1186/s12864-017-3905-1

Chan, Y., and Walmsley, R. P. (1997). Learning and Understanding the Kruskal-Wallis One-Way Analysis-Of-Variance-By-Ranks Test for Differences Among Three or More Independent Groups. *Phys. Ther.* 77, 1755–1761. doi:10.1093/ptj/77.12.1755

Chen, N., LaCrue, A. N., Teuscher, F., Waters, N. C., Gatton, M. L., Kyle, D. E., et al. (2014). Fatty Acid Synthesis and Pyruvate Metabolism Pathways Remain Active in Dihydroartemisinin-Induced Dormant Ring Stages of Plasmodium Falciparum. *Antimicrob. Agents Chemother.* 58, 4773–4781. doi:10.1128/aac.02647-14

Cingolani, P., Platts, A., Wang, L. L., Coon, M., Nguyen, T., Wang, L., et al. (2012). A Program for Annotating and Predicting the Effects of Single Nucleotide Polymorphisms, SnpEff. *Fly* 6, 80–92. doi:10.4161/fly.19695

Cobbold, S. A., Chua, H. H., Nijagal, B., Creek, D. J., Ralph, S. A., and McConville, M. J. (2016). Metabolic Dysregulation Induced inPlasmodium Falciparumby Dihydroartemisinin and Other Front-Line Antimalarial Drugs. *J. Infect. Dis.* 213, 276–286. doi:10.1093/infdis/jiv372

Coppée, R., Jeffares, D. C., Miteva, M. A., Sabbagh, A., and Clain, J. (2019). Comparative Structural and Evolutionary Analyses Predict Functional Sites in the Artemisinin Resistance Malaria Protein K13. *Sci. Rep.* 9, 10675–10717. doi:10.1038/s41598-019-47034-6

Coulson, R. M. R., Hall, N., and Ouzounis, C. A. (2004). Comparative Genomics of Transcriptional Control in the Human Malaria Parasite Plasmodium Falciparum. *Genome Res.* 14, 1548–1554. doi:10.1101/gr.2218604

Covelli, V., Cooper, J., Carey, M., and Guler, J. (2016). Metabolomics for the *In Vitro* Study of Artemisinin-Resistant Malaria Parasites. *Paper presented Open Forum Infect. Dis.* 3.

Daniyan, M. O., Przyborski, J. M., and Shonhai, A. (2019). Partners in Mischief: Functional Networks of Heat Shock Proteins of Plasmodium Falciparum and Their Influence on Parasite Virulence. *Biomolecules* 9, 295. doi:10.3390/biom9070295

de Koning-Ward, T. F., Dixon, M. W. A., Tilley, L., and Gilson, P. R. (2016). Plasmodium Species: Master Renovators of Their Host Cells. *Nat. Rev. Microbiol.* 14, 494–507. doi:10.1038/nrmicro.2016.79

Dondorp, A. M., Nosten, F., Yi, P., Das, D., Phyo, A. P., Tarning, J., et al. (2009). Artemisinin Resistance inPlasmodium falciparumMalaria. *N. Engl. J. Med.* 361, 455–467. doi:10.1056/nejmoa0808859

Dwivedi, A., Reynes, C., Kuehn, A., Roche, D. B., Khim, N., Hebrard, M., et al. (2017). Functional Analysis of Plasmodium Falciparum Subpopulations Associated with Artemisinin Resistance in Cambodia. *Malar. J.* 16, 493–517. doi:10.1186/s12936-017-2140-1

Dzikowski, R., and Deitsch, K. W. (2009). Genetics of Antigenic Variation in Plasmodium Falciparum. *Curr. Genet.* 55, 103–110. doi:10.1007/s00294-009-0233-2

Goldberg, D. E., Slater, A. F., Cerami, A., and Henderson, G. B. (1990). Hemoglobin Degradation in the Malaria Parasite Plasmodium Falciparum: an Ordered Process in a Unique Organelle. *Proc. Natl. Acad. Sci.* 87, 2931–2935. doi:10.1073/pnas.87.8.2931

Gopalakrishnan, A. M., and Kumar, N. (2015). Antimalarial Action of Artesunate Involves DNA Damage Mediated by Reactive Oxygen Species. *Antimicrob. Agents Chemother.* 59, 317–325. doi:10.1128/aac.03663-14

Guggisberg, A. M., Frasse, P. M., Jezewski, A. J., Kafai, N. M., Gandhi, A. Y., Erlinger, S. J., et al. (2018). Suppression of Drug Resistance Reveals a Genetic Mechanism of Metabolic Plasticity in Malaria Parasites. *MBio* 9, e01193. doi:10.1128/mbio.01193-18

Ismail, H. M., Barton, V. E., Panchana, M., Charoensutthivarakul, S., Biagini, G. A., Ward, S. A., et al. (2016). A Click Chemistry-Based Proteomic Approach Reveals that 1,2,4-Trioxolane and Artemisinin Antimalarials Share a Common Protein Alkylation Profile. *Angew. Chem. Int. Ed.* 55, 6401–6405. doi:10.1002/anie.201512062

Ismail, H. M., Barton, V., Phanchana, M., Charoensutthivarakul, S., Wong, M. H. L., Hemingway, J., et al. (2016). Artemisinin Activity-Based Probes Identify Multiple Molecular Targets within the Asexual Stage of the Malaria Parasites Plasmodium Falciparum 3D7. *Proc. Natl. Acad. Sci. USA* 113, 2080–2085. doi:10.1073/pnas.1600459113

Iwanaga, S., Kaneko, I., Kato, T., and Yuda, M. (2012). Identification of an AP2-Family Protein that Is Critical for Malaria Liver Stage Development. *PLoS ONE* 7, e47557. doi:10.1371/journal.pone.0047557

Jeninga, M., Quinn, J., and Petter, M. (2019). ApiAP2 Transcription Factors in Apicomplexan Parasites. *Pathogens* 8, 47. doi:10.3390/pathogens8020047

Jiang, T., Huang, Y., Cheng, W., Sun, Y., Wei, W., Wu, K., et al. (2021). Multiple Single-Nucleotide Polymorphism Detection for Antimalarial Pyrimethamine Resistance via Allele-specific PCR Coupled with Gold Nanoparticle-Based Lateral Flow Biosensor. *Antimicrob. Agents Chemother.* 65, e01063–20. doi:10.1128/aac.01063-20

Jortzik, E., and Becker, K. (2012). Thioredoxin and Glutathione Systems in Plasmodium Falciparum. *Int. J. Med. Microbiol.* 302, 187–194. doi:10.1016/j.ijmm.2012.07.007

Joshi, B., Biswas, S., and Sharma, Y. D. (1992). Effect of Heat-Shock on Plasmodium Falciparum Viability, Growth and Expression of the Heat-Shock Protein 'PFHSP70-I' Gene. *FEBS Lett.* 312, 91–94. doi:10.1016/0014-5793(92)81417-k

Kadioglu, O., Chan, A., Cong Ling Qiu, A., Wong, V. K. W., Colligs, V., Wecklein, S., et al. (2017). Artemisinin Derivatives Target Topoisomerase 1 and Cause DNA Damage In Silico and *In Vitro*. *Front. Pharmacol.* 8, 711. doi:10.3389/fphar.2017.00711

Kafsack, B. F. C., and Llinás, M. (2010). Eating at the Table of Another: Metabolomics of Host-Parasite Interactions. *Cell Host & Microbe* 7, 90–99. doi:10.1016/j.chom.2010.01.008

Kehr, S., Sturm, N., Rahlfs, S., Przyborski, J. M., and Becker, K. (2010). Compartmentation of Redox Metabolism in Malaria Parasites. *Plos Pathog.* 6, e1001242. doi:10.1371/journal.ppat.1001242

Lang-Unnasch, N., and Murphy, A. D. (1998). Metabolic Changes of the Malaria Parasite during the Transition from the Human to the Mosquito Host. *Annu. Rev. Microbiol.* 52, 561–590. doi:10.1146/annurev.micro.52.1.561

Le Bras, J., Durand, R., and pharmacology, c. (2003). The Mechanisms of Resistance to Antimalarial Drugs in Plasmodium Falciparum. *Fundam. Clin. Pharmacol.* 17, 147–153. doi:10.1046/j.1472-8206.2003.00164.x

MalariaGEN Plasmodium falciparum Community Project (2016). Genomic Epidemiology of Artemisinin Resistant Malaria. *Elife* 5, e08714. doi:10.7554/eLife.08714

Mbengue, A., Bhattacharjee, S., Pandharkar, T., Liu, H., Estiu, G., Stahelin, R. V., et al. (2015). A Molecular Mechanism of Artemisinin Resistance in Plasmodium Falciparum Malaria. *Nature* 520, 683–687. doi:10.1038/nature14412

Ménard, D., Khim, N., Beghain, J., Adegnika, A. A., Shafiul-Alam, M., Amodu, O., et al. (2016). A Worldwide Map ofPlasmodium falciparumK13-Propeller Polymorphisms. *N. Engl. J. Med.* 374, 2453–2464. doi:10.1056/nejmoa1513137

Miotto, O., Amato, R., Ashley, E. A., MacInnis, B., Almagro-Garcia, J., Amaratunga, C., et al. (2015). Genetic Architecture of Artemisinin-Resistant Plasmodium Falciparum. *Nat. Genet.* 47, 226–234. doi:10.1038/ng.3189

Modrzynska, K., Pfander, C., Chappell, L., Yu, L., Suarez, C., Dundas, K., et al. (2017). A Knockout Screen of ApiAP2 Genes Reveals Networks of Interacting Transcriptional Regulators Controlling the Plasmodium Life Cycle. *Cell Host & Microbe* 21, 11–22. doi:10.1016/j.chom.2016.12.003

Mok, S., Imwong, M., Mackinnon, M. J., Sim, J., Ramadoss, R., Yi, P., et al. (2011). Artemisinin Resistance in Plasmodium Falciparum Is Associated with an Altered Temporal Pattern of Transcription. *BMC Genomics* 12, 391–414. doi:10.1186/1471-2164-12-391

Mok, S., Ashley, E. A., Ferreira, P. E., Zhu, L., Lin, Z., Yeo, T., et al. (2015). Population Transcriptomics of Human Malaria Parasites Reveals the Mechanism of Artemisinin Resistance. *Science* 347, 431–435. doi:10.1126/science.1260403

Mok, S., Stokes, B. H., Gnädig, N. F., Ross, L. S., Yeo, T., Amaratunga, C., et al. (2021). Artemisinin-resistant K13 Mutations Rewire Plasmodium Falciparum's Intra-erythrocytic Metabolic Program to Enhance Survival. *Nat. Commun.* 12, 1–15. doi:10.1038/s41467-020-20805-w

Mundwiler-Pachlatko, E., and Beck, H.-P. (2013). Maurer's Clefts, the enigma of Plasmodium Falciparum. *Proc. Natl. Acad. Sci.* 110, 19987–19994. doi:10.1073/pnas.1309247110

Nair, S., Li, X., Arya, G. A., McDew-White, M., Ferrari, M., Nosten, F., et al. (2018). Fitness Costs and the Rapid Spread of Kelch13-C580y Substitutions Conferring Artemisinin Resistance. *Antimicrob. Agents Chemother.* 62, e00605–18. doi:10.1128/AAC.00605-18

Nepveu, F., and Turrini, F. (2013). Targeting the Redox Metabolism of Plasmodium Falciparum. *Future Med. Chem.* 5, 1993–2006. doi:10.4155/fmc.13.159

Olszewski, K. L., Morrisey, J. M., Wilinski, D., Burns, J. M., Vaidya, A. B., Rabinowitz, J. D., et al. (2009). Host-parasite Interactions Revealed by Plasmodium Falciparum Metabolomics. *Cell Host & Microbe* 5, 191–199. doi:10.1016/j.chom.2009.01.004

Painter, H. J., Campbell, T. L., Llinás, M., and parasitology, b. (2011). The Apicomplexan AP2 Family: Integral Factors Regulating Plasmodium Development. *Mol. Biochem. Parasitol.* 176, 1–7. doi:10.1016/j.molbiopara.2010.11.014

Prajapati, S. K., and Singh, O. P. (2013). Remodeling of Human Red Cells Infected with Plasmodium Falciparum and the Impact of PHIST Proteins. *Blood Cell Mol. Dis.* 51, 195–202. doi:10.1016/j.bcmd.2013.06.003

Prieto, J. H., Koncarevic, S., Park, S. K., Yates, J., III, and Becker, K. (2008). Large-Scale Differential Proteome Analysis in Plasmodium Falciparum under Drug Treatment. *PLoS ONE* 3, e4098. doi:10.1371/journal.pone.0004098

Rathod, P. K., McErlean, T., and Lee, P.-C. (1997). Variations in Frequencies of Drug Resistance in Plasmodium Falciparum. *Proc. Natl. Acad. Sci.* 94, 9389–9393. doi:10.1073/pnas.94.17.9389

Rawat, M., Kanyal, A., Sahasrabudhe, A., Vembar, S. S., Lopez-Rubio, J.-J., and Karmodiya, K. J. S. r. (2021). Histone Acetyltransferase PfGCN5 Regulates Stress Responsive and Artemisinin Resistance Related Genes in Plasmodium Falciparum. *Scientific Rep.* 11, 1–13. doi:10.1038/s41598-020-79539-w

Rocamora, F., Zhu, L., Liong, K. Y., Dondorp, A., Miotto, O., Mok, S., et al. (2018). Oxidative Stress and Protein Damage Responses Mediate Artemisinin Resistance in Malaria Parasites. *Plos Pathog.* 14, e1006930. doi:10.1371/journal.ppat.1006930

Santos, J. M., Josling, G., Ross, P., Joshi, P., Orchard, L., Campbell, T., et al. (2017). Red Blood Cell Invasion by the Malaria Parasite Is Coordinated by the PfAP2-I Transcription Factor. *Cell Host & Microbe* 21, 731–741. e10. doi:10.1016/j.chom.2017.05.006

Schulze, J., Kwiatkowski, M., Borner, J., Schlüter, H., Bruchhaus, I., Burmester, T., et al. (2015). ThePlasmodium Falciparumexportome Contains Non-canonical PEXEL/HT Proteins. *Mol. Microbiol.* 97, 301–314. doi:10.1111/mmi.13024

Siddiqui, F. A., Cabrera, M., Wang, M., Brashear, A., Kemirembe, K., Wang, Z., et al. (2018). Plasmodium Falciparum Falcipain-2a Polymorphisms in Southeast Asia and Their Association with Artemisinin Resistance. *J. Infect. Dis.* 218, 434–442. doi:10.1093/infdis/jiy188

Siddiqui, G., Srivastava, A., Russell, A. S., and Creek, D. J. (2017). Multi-omics Based Identification of Specific Biochemical Changes Associated with PfKelch13-Mutant Artemisinin-Resistant Plasmodium Falciparum. *J. Infect. Dis.* 215, 1435–1444. doi:10.1093/infdis/jix156

Slater, H. C., Griffin, J. T., Ghani, A. C., and Okell, L. C. (2016). Assessing the Potential Impact of Artemisinin and Partner Drug Resistance in Sub-saharan Africa. *Malar. J.* 15, 1–11. doi:10.1186/s12936-015-1075-7

Spielmann, T., Gras, S., Sabitzki, R., and Meissner, M. (2020). Endocytosis in Plasmodium and Toxoplasma Parasites. *Trends Parasitol.* 36, 520–532. doi:10.1016/j.pt.2020.03.010

Srivastava, A., Philip, N., Hughes, K. R., Georgiou, K., MacRae, J. I., Barrett, M. P., et al. (2016). Stage-specific Changes in Plasmodium Metabolism Required for Differentiation and Adaptation to Different Host and Vector Environments. *Plos Pathog.* 12, e1006094. doi:10.1371/journal.ppat.1006094

Stokes, B. H., Rubiano, K., Dhingra, S. K., Mok, S., Straimer, J., Gnädig, N. F., et al. (2021). Plasmodium Falciparum K13 Mutations in Africa and Asia Present Varying Degrees of Artemisinin Resistance and an Elevated Fitness Cost in African Parasites. *Elife* 10, e66277. doi:10.7554/eLife.66277

Suresh, N., and Haldar, K. (2018). Mechanisms of Artemisinin Resistance in Plasmodium Falciparum Malaria. *Curr. Opin. Pharmacol.* 42, 46–54. doi:10.1016/j.coph.2018.06.003

Swift, M. L., and sciences, c. (1997). GraphPad Prism, Data Analysis, and Scientific Graphing. *J. Chem. Inf. Comput. Sci.* 37, 411–412. doi:10.1021/ci960402j

Teuscher, F., Gatton, M. L., Chen, N., Peters, J., Kyle, D. E., and Cheng, Q. (2010). Artemisinin-Induced Dormancy inPlasmodium Falciparum: Duration, Recovery Rates, and Implications in Treatment Failure. *J. Infect. Dis.* 202, 1362–1368. doi:10.1086/656476

Tewari, S. G., Swift, R. P., Reifman, J., Prigge, S. T., and Wallqvist, A. (2020). Metabolic Alterations in the Erythrocyte during Blood-Stage Development of the Malaria Parasite. *Malar. J.* 19, 94–18. doi:10.1186/s12936-020-03174-z

Thélu, J., Burnod, J., Bracchi, V., Ambroise-Thomas, P., and biology, c. (1994). Identification of Differentially Transcribed RNA and DNA Helicase-Related Genes ofPlasmodium Falciparum. *DNA Cell Biol.* 13, 1109–1115. doi:10.1089/dna.1994.13.1109

Tippmann, S. (2015). Programming Tools: Adventures with R. *Nature* 517, 109–110. doi:10.1038/517109a

Tirrell, A. R., Vendrely, K. M., Checkley, L. A., Davis, S. Z., McDew-White, M., Cheeseman, I. H., et al. (2019). Pairwise Growth Competitions Identify Relative Fitness Relationships Among Artemisinin Resistant Plasmodium Falciparum Field Isolates. *Malar. J.* 18, 295–313. doi:10.1186/s12936-019-2934-4

Tougan, T., Edula, J. R., Morita, M., Takashima, E., Honma, H., Tsuboi, T., et al. (2020). The Malaria Parasite Plasmodium Falciparum in Red Blood Cells Selectively Takes up Serum Proteins that Affect Host Pathogenicity. *Malar. J.* 19, 155–213. doi:10.1186/s12936-020-03229-1

Tuteja, R., Ansari, A., and Chauhan, V. S. (2011). Emerging Functions of Transcription Factors in Malaria Parasite. *J. Biomed. Biotechnol.* 2011, 461979. doi:10.1155/2011/461979

Tuteja, R. (2010). Genome Wide Identification of Plasmodium Falciparum Helicases: a Comparison with Human Host. *Cell Cycle* 9, 104–120. doi:10.4161/cc.9.1.10241

Tuteja, R., and Pradhan, A. (2006). Unraveling the 'DEAD-Box' Helicases of Plasmodium Falciparum. *Gene* 376, 1–12. doi:10.1016/j.gene.2006.03.007

Uwimana, A., Legrand, E., Stokes, B. H., Ndikumana, J.-L. M., Warsame, M., Umulisa, N., et al. (2020). Emergence and Clonal Expansion of *In Vitro* Artemisinin-Resistant Plasmodium Falciparum Kelch13 R561H Mutant Parasites in Rwanda. *Nat. Med.* 26, 1602–1608. doi:10.1038/s41591-020-1005-2

Van Biljon, R., Van Wyk, R., Painter, H. J., Orchard, L., Reader, J., Niemand, J., et al. (2019). Hierarchical Transcriptional Control Regulates Plasmodium Falciparum Sexual Differentiation. *BMC Genomics* 20, 920–1016. doi:10.1186/s12864-019-6322-9

Venkatesan, M., Gadalla, N. B., Stepniewska, K., Dahal, P., Nsanzabana, C., Moriera, C., et al. (2014). Polymorphisms in Plasmodium Falciparum Chloroquine Resistance Transporter and Multidrug Resistance 1 Genes: Parasite Risk Factors that Affect Treatment Outcomes for P. Falciparum Malaria after Artemether-Lumefantrine and Artesunate-Amodiaquine. *falciparum Malar. after artemether-lumefantrine artesunate-amodiaquine* 91, 833–843. doi:10.4269/ajtmh.14-0031

Wang, S., Xu, S., Geng, J., Si, Y., Zhao, H., Li, X., et al. (2020). Molecular Surveillance and *In Vitro* Drug Sensitivity Study of Plasmodium Falciparum Isolates from the China-Myanmar Border. *Am. J. Trop. Med. Hyg.* 103, 1100–1106. doi:10.4269/ajtmh.20-0235

Wang, Z., Cabrera, M., Yang, J., Yuan, L., Gupta, B., Liang, X., et al. (2016). Genome-wide Association Analysis Identifies Genetic Loci Associated with Resistance to Multiple Antimalarials in Plasmodium Falciparum from China-Myanmar Border. *Sci. Rep.* 6, 33891–33912. doi:10.1038/srep33891

Warncke, J. D., Beck, H.-P. J. M., and Reviews, M. B. (2019). Host Cytoskeleton Remodeling throughout the Blood Stages of Plasmodium Falciparum. *Microbiol. Mol. Biol. Rev. MMBR* 83. doi:10.1128/mmbr.00013-19

Warncke, J. D., Vakonakis, I., Beck, H.-P., and Reviews, M. B. (2016). Plasmodium Helical Interspersed Subtelomeric (PHIST) Proteins, at the center of Host Cell Remodeling. *Microbiol. Mol. Biol. Rev.* 80, 905–927. doi:10.1128/mmbr.00014-16

Wilairat, P., Kümpornsin, K., and Chookajorn, T. (2016). Plasmodium Falciparum Malaria: Convergent Evolutionary Trajectories towards Delayed Clearance Following Artemisinin Treatment. *Med. Hypotheses* 90, 19–22. doi:10.1016/j.mehy.2016.02.022

Witkowski, B., Amaratunga, C., Khim, N., Sreng, S., Chim, P., Kim, S., et al. (2013). Novel Phenotypic Assays for the Detection of Artemisinin-Resistant Plasmodium Falciparum Malaria in Cambodia: *In-Vitro* and *Ex-Vivo* Drug-Response Studies. *Lancet Infect. Dis.* 13, 1043–1049. doi:10.1016/s1473-3099(13)70252-4

World Health Organization (2020). *World Malaria Report 2020: 20 Years of Global Progress and Challenges*. Geneva, Switzerland: World Health Organization.

Yang, T., Yeoh, L. M., Tutor, M. V., Dixon, M. W., McMillan, P. J., Xie, S. C., et al. (2019). Decreased K13 Abundance Reduces Hemoglobin Catabolism and Proteotoxic Stress, Underpinning Artemisinin Resistance. *Cell Rep.* 29, 2917–2928. e5. doi:10.1016/j.celrep.2019.10.095

Zuzarte-Luís, V., and Mota, M. M. (2018). Parasite Sensing of Host Nutrients and Environmental Cues. *Cell Host & Microbe* 23, 749–758. doi:10.1016/j.chom.2018.05.018

Conflict of Interest: Author DC was employed by the company Persistent Systems Limited.

The remaining authors declare that the research was conducted in the absence of any commercial or financial relationships that could be construed as a potential conflict of interest.

Publisher's Note: All claims expressed in this article are solely those of the authors and do not necessarily represent those of their affiliated organizations or those of the publisher, the editors, and the reviewers. Any product that may be evaluated in this article, or claim that may be made by its manufacturer, is not guaranteed or endorsed by the publisher.

frontiers | Frontiers in Genetics

HYPOTHESIS AND THEORY
published: 28 April 2022
doi: 10.3389/fgene.2022.873398

Histone Modifications, Internucleosome Dynamics, and DNA Stresses: How They Cooperate to "Functionalize" Nucleosomes

Wladyslaw A. Krajewski *

N.K. Koltsov Institute of Developmental Biology of Russian Academy of Sciences, Moscow, Russia

Tight packaging of DNA in chromatin severely constrains DNA accessibility and dynamics. In contrast, nucleosomes in active chromatin state are highly flexible, can exchange their histones, and are virtually "transparent" to RNA polymerases, which transcribe through gene bodies at rates comparable to that of naked DNA. Defining mechanisms that revert nucleosome repression, in addition to their value for basic science, is of key importance for the diagnosis and treatment of genetic diseases. Chromatin activity is largely regulated by histone posttranslational modifications, ranging from small chemical groups up to the yet understudied "bulky" ubiquitylation and sumoylation. However, it is to be revealed how histone marks are "translated" to permissive or repressive changes in nucleosomes: it is a general opinion that histone modifications act primarily as "signals" for recruiting the regulatory proteins or as a "neutralizer" of electrostatic shielding of histone tails. Here, we would like to discuss recent evidence suggesting that histone ubiquitylation, in a DNA stress–dependent manner, can directly regulate the dynamics of the nucleosome and their primary structure and can promote nucleosome decomposition to hexasome particles or additionally stabilize nucleosomes against unwrapping. In addition, nucleosome repression/ derepression studies are usually performed with single mononucleosomes as a model. We would like to review and discuss recent findings showing that internucleosomal interactions could strongly modulate the dynamics and rearrangements of nucleosomes. Our hypothesis is that bulky histone modifications, nucleosome inherent dynamics, internucleosome interactions, and DNA torsions could act in cooperation to orchestrate the formation of different dynamic states of arrayed nucleosomes and thus promote chromatin functionality and diversify epigenetic programming methods.

Keywords: nucleosomes, histones, hexasomes, ubiquitylation, histone modifications, histone code, DNA stresses

OPEN ACCESS

Edited by:
Dileep Vasudevan,
Institute of Life Sciences (ILS), India

Reviewed by:
Li Wei,
Institute of Physics (CAS), China
Sanxiong Liu,
NYU Grossman School of Medicine, United States

***Correspondence:**
Wladyslaw A. Krajewski
wkrajewski@hotmail.com

Specialty section:
This article was submitted to Epigenomics and Epigenetics, a section of the journal Frontiers in Genetics

Received: *10 February 2022*
Accepted: *28 March 2022*
Published: *28 April 2022*

Citation:
Krajewski WA (2022) Histone Modifications, Internucleosome Dynamics, and DNA Stresses: How They Cooperate to "Functionalize" Nucleosomes. Front. Genet. 13:873398. doi: 10.3389/fgene.2022.873398

INTRODUCTION

Many diseases and behavioral pathologies such as cancer (Espinosa, 2008; Cao and Yan, 2012; Johnsen, 2012; Cole et al., 2015), metabolic disorders (Gluckman et al., 2009; Gao et al., 2014), cardiovascular and autoimmune diseases, and diabetes (Dieker and Muller, 2010; Zou et al., 2014) are the results of gene deregulation (Gray, 2006; Perini and Tupler, 2006; Bhaumik et al., 2007; Weake, 2014; Mirabella et al., 2016). However, despite the critical importance of gene regulatory principles

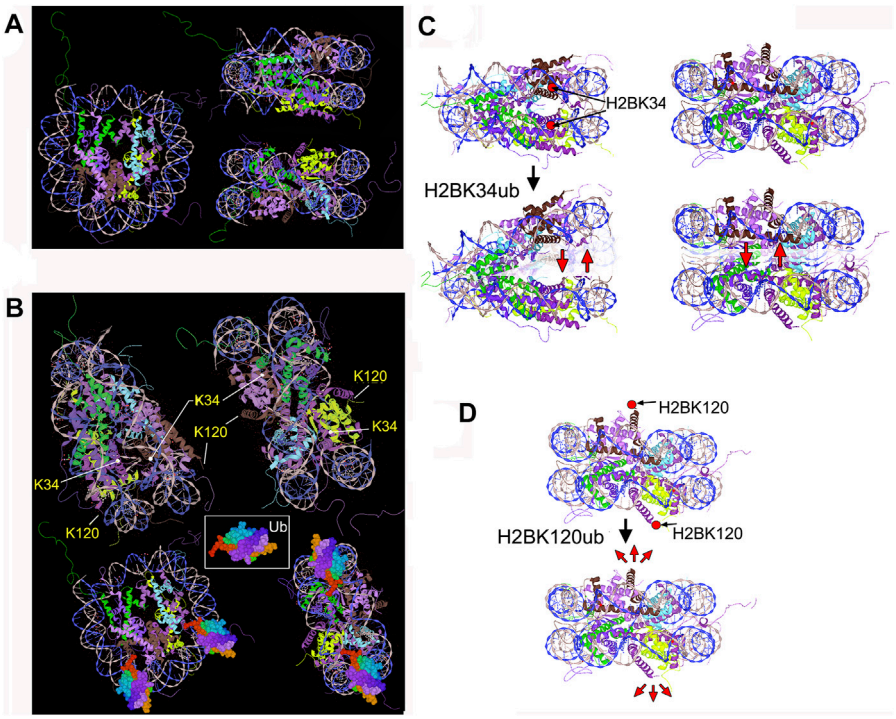

FIGURE 1 | (A) Nucleosome (1kx5) front, top, and side view. ●● H3.2 (chains A,E), ●● H2B 1.1 (chains D,H), ●● H2A type 1 (chains C,G), and ●● H4 (chains B,F) **(B)** Positions of H2B K34 and K120 indicated by arrows. Drafts at the bottom illustrate the H2BK34ub nucleosome (Ubiquitin PDB: 1ubq). **(C,D)** Sketches, depicting the potential mechanisms of nucleosome-destabilizing effects by H2BK34-/ K120-ubiquitylation. **(C)** H2BK34ub installed in the occluded nucleosome region could act as a "wedge", facilitating DNA gyre–gyre separation ("gaping"). **(D)** Mechanistic forces applied to the H2A-H2B dimer by ubiquitin deposited to H2B termini could weaken the nucleosome through stochastic motions of bulky ubiquitin and/or its steric clashes with the nucleosome surface. This could also promote nucleosome breathing and DNA-dimer opening motions.

for the diagnosis, prevention, and therapy of genetic diseases (and, in general, for directed manipulation of gene activity), many aspects of gene regulation have not been well-elucidated thus far and remain unclear on how DNA processing machineries overcome the tight multilevel packaging of DNA in cell nuclei.

In eukaryotes, the genetic information required to control all life processes exists in the form of chromatin, a complex hierarchical structure of DNA super-helices, stabilized by a multitude of protein–DNA and protein–protein interactions. On the first level of compaction, 147 bp of every ~200 bp of DNA are wrapped in 1.75 turns around an octamer of histone proteins, comprising one H3-H4 tetramer flanked on each side by H2A-H2B dimers (**Figure 1A**), thus forming nucleosomes, the basic repeated chromatin units (Luger et al., 1997; Vasudevan et al., 2010). Nucleosome arrays fold into 'solenoids (Kruithof et al., 2009; Kepper et al., 2011; Victor et al., 2012) or "zig-zag"-like (Dorigo et al., 2004; Grigoryev, 2004; Schalch et al., 2005; Grigoryev et al., 2009) arrangements to form the 25–34 nm chromatin fiber, stabilized by linker histones H1/H5 (Robinson and Rhodes, 2006). The 30-nm fiber further self-associates and condenses into higher-order tertiary structures.

Nucleosomes in their "canonic" state (as seen by X-ray studies (Luger et al., 1997; Richmond and Davey, 2003; Vasudevan et al., 2010) are rather robust static units, refractory to DNA-binding proteins, and thus, literary should present an "immovable barrier" even for the "irresistible force" of progressing RNA polymerases (Kornberg and Lorch, 1991). So, despite the nucleosomes being the key elements in gene regulation (Gibney and Nolan, 2010), it is still understudied how they relieve their intrinsically repressive effects on DNA expression.

Due to the structural tensions associated with the bending of the stiff (Manning, 2006) 147 bp core nucleosomal DNA around the histone globule, nucleosomes retain some degree of dynamicity and undergo spontaneous fluctuations of nucleosome wrapping, which range from 10–250 ms "breathing" and more slow "opening" motions (Koopmans et al., 2007; Armeev et al., 2018), up to the lo 1–10 min nucleosome hinge-like "gaping" openings (Zlatanova et al., 2009; Ngo and Ha, 2015). Fluctuations in nucleosome wrapping and transiently increasing DNA exposure (Polach and Widom, 1996) play important role in regulating the accessibility of transcription factors to the nucleosome DNA (Li et al., 2005) and alleviating RNA polymerases entering the nucleosome (Hodges et al., 2009; Selth et al., 2010). It is possible that any stimuli increasing the basic level of inherent nucleosome dynamics will contribute to the derepression of the nucleosome.

Nucleosomal histones are subjected to a multitude of reversible posttranslational modifications (PTMs) which, supposedly, control virtually all aspects of chromatin functioning. According to the "histone code" concept, PTMs "acting in a combinatorial or

sequential fashion on one or multiple histone tails specify unique downstream function" (Strahl and Allis, 2000). Many PTMs are dynamically deposited during the cell cycle to control particular cellular processes, whereas certain histone PTMs are thought to program the transcription memory transmitted to the progeny cells. A different (though debatable (Alabert et al., 2015; Reveron-Gomez et al., 2018)) view that histone PTMs are not transmitted to progeny chromatin but instead persistently bound histone-modifiers reestablish the PTM pattern on the daughter chromatin (Petruk et al., 2012; Petruk et al., 2013) came from histone H3K4me3/ H3K27me3 "inheritance" studies, which used (probably insufficiently sensitive) proximity-ligation assay to monitor the modified histones on replicated DNA. Finally, several recent studies (Reinberg and Vales, 2018; Escobar et al., 2019; Escobar et al., 2021) provided evidence that the repressive histone modifications but not active ones are inherited upon DNA replication.

In a classic view, both "small" (methylation and acetylation) (Rothbart and Strahl, 2014) and "bulky" (ubiquitin and SUMO-1,2/3 polypeptides (Cubenas-Potts and Matunis, 2013; Weake, 2014)) histone PTMs are considered binding targets for effector proteins (Rothbart and Strahl, 2014; Andrews et al., 2016) or as regulators of chromatin higher-order folding (acting by modulation of internucleosome interactions (Pepenella et al., 2014b; Prakash and Fournier, 2018)) but not as direct triggers of primary nucleosome structure reversing DNA repression. By tuning histone charges and deposition of a modest steric bulk, "small" histone PTMs only moderately affect the spontaneous fluctuations of nucleosomes without affecting their stability (PTMs at the nucleosome entry-exit) or modestly decrease nucleosome stability without affecting nucleosome dynamics (PTMs near the nucleosome dyad axis) (Bowman and Poirier, 2015; Armeev et al., 2018).

However, recent data suggest that currently understudied large polypeptide PTMs could play an active role in directly altering the nucleosome primary structure and dynamics. In addition, since intrinsic chromatin organization is based on a hierarchy of DNA helices (DNA double helix, nucleosome DNA wrapping, and chromatin fiber), the chromatin structure is subjected to superhelical stresses in DNA, which could significantly affect the nucleosome properties and functionality. Furthermore, due to multiple internucleosome interactions, the model describing a nucleosome array just as a polymer of individual "canonic" nucleosomes does not adequately recapitulate nucleosome functionalities. The interaction between nucleosomes *via* flexible histone termini could significantly affect nucleosome structural transitions (Krajewski, 2016). We would like to discuss these phenomena in view of the recent and older literature data.

NUCLEOSOMES AS KEY ELEMENTS IN EPIGENETIC REGULATION OF CHROMATIN ACTIVITY

What differentiates nucleosomes in transcriptionally active chromatin from the canonic ones? In both cases, these particles possess the same composition and share the same organizational principles. However, in transcribed chromatin regions, nucleosomes are dynamic and (Zlatanova et al., 2009; Armeev et al., 2018) exhibit high conformational flexibility (Saavedra and Huberman, 1986; Morse et al., 1987; Krajewski and Luchnik, 1991), easily exchange their histone subunits (Zlatanova et al., 2009; Venkatesh and Workman, 2015), and support fast progression of RNA polymerases (Singh and Padgett, 2009) that is accompanied by nucleosome unfolding and unshielding of histone H3 sulfhydryls which are otherwise buried at the nucleosome dyad and inaccessible in the canonic nucleosome state (Prior et al., 1983; Chen et al., 1991).

A notable hallmark of the transcribed chromatin is the dynamic monoubiquitylation of histone H2B at lysines K120 (K123 in yeast) (Batta et al., 2011; Fleming et al., 2008; Trujillo and Osley, 2012; Wright and Kao, 2015) and K34 (Li et al., 2017; Wu et al., 2011; Wu et al., 2013; Wu et al., 2014) (**Figure 1B**). This feature would be consistent with a series of recent findings showing that K34-ubiquitylation of histone H2B (and H2BK120ub to a lesser degree) can significantly enhance nucleosome dynamics, decrease nucleosome stability, and promote eviction of one histone H2A-H2B dimer (Krajewski et al., 2018; Krajewski W. A., 2020), especially in the presence of histone chaperons. This effect is likely due to the steric hindrances by "bulky" ubiquitin moieties, which destabilize the nucleosome (Krajewski, 2019; Krajewski WA., 2020). The resulting hexasome particle was stable, suggesting that dissociation of one ubiquitylated histone dimer is sufficient to relieve the steric stresses incurred by massive ubiquitin moieties (Krajewski et al., 2018; Krajewski W. A., 2020).

The 8.6 kD ubiquitin (Renatus et al., 2006) and 10–12 kD SUMO (Bayer et al., 1998; Huang et al., 2004) are close in size to histones that principally distinguishes these PTMs from "small" chemical modifications. A steric bulk deposited by ubiquitylation and sumoylation could act to "mechanically" alter the canonic nucleosomes. Nucleosome-destabilizing forces would be stronger when bulky PTMs are deposited within the nucleosome lateral surface and so, directly conflict with the compact nucleosome structure. For example, ubiquitylation of histone H2B at lysine K34, which is "buried" between two DNA gyres (Li et al., 2017; Wu et al., 2011) (**Figure 1B**), could act as a "wedge", facilitating DNA gyre–gyre opening (**Figure 1C**). Bulky PTMs at histone termini (e.g., H2BK120ub, **Figure 1B**) disturb the nucleosome core less but could affect intra-nucleosomal interactions, for example, by electrostatic repulsion (**Figure 1D**). The association of H2A-H2B dimers on the nucleosome interface could be weakened by stochastic (Brownian) motions of the attached PTMs, which will tend to "tear-off" one histone dimer out from the nucleosome interface (**Figure 1D**). Of note, it has been shown that dynamic nucleosome conformations could be shifted to more unwrapped structures by binding bulky objects to the nucleosome periphery (Polach and Widom, 1996; Buning et al., 2015), such as the transcription factors (Polach and Widom, 1996), an adjacent nucleosome, or long linker DNA (Buning et al., 2015). Due to the interactions between histone tails and nucleosome-associated core DNA (Cutter and Hayes, 2015; Shaytan et al., 2016; Chakraborty and Loverde, 2017; Morrison et al., 2018) or linker DNA

(Davey et al., 2002; Cutter and Hayes, 2015; Schunter et al., 2017), bulky PTMs of histone termini could destabilize the intra-nucleosome interactions either directly or by colliding with the nucleosome surface.

These results suggest a hypothesis (Krajewski, 2019; Krajewski WA., 2020) that in contrast to "small" histone PTMs, attachment to nucleosomes at certain positions of ubiquitin (and, supposedly, other bulky PTMs) could potentially represent an *in vivo* mechanism to functionalize canonic nucleosomes by strikingly increasing their dynamics and triggering the conversion of a nucleosome to a more functionally active hexasome particle.

Interestingly, recent single-molecule magnetic tweezer experiments (Xiao et al., 2020) have shown that H2AK119ub, on the contrary, dramatically prevents the peeling of the DNA from the histone octamer that stabilizes the nucleosome. The stabilizing effect of ubH2A was not a result of the enhanced stability of the octamer (ibid) but likely relies on the Ub-mediated steric clashes that prevent nucleosome unfolding. Although these results would benefit from refinement with more relevant biochemical approaches, it could be supposed that at some nucleosome positions, "hindrances" caused by bulky modifications could strongly stabilize and "lock" the nucleosome unwrapped state. With this example, one can propose that "bulky" modifications could create a stable "code" of both active and repressed chromatin states.

Histone ubiquitylation is one of the key epigenetic marks with a wide spectrum of action (Weake, 2014), so the functions of H2BK120ub and H2BK34ub (and H2A119ub) are not only limited to the proposed "direct" nucleosome-regulatory role but also involve other ubiquitylation-mediated binding events for the chromatin regulators (Vaughan et al., 2021). There are still less data available on H2BK34ub; therefore, we will just mention here two recent studies on the interactions of Dot1L and H2BK120ub nucleosomes, which are critical to direct H3K79 methylation (Anderson et al., 2019; Valencia-Sanchez et al., 2019).

Previous work showed that H2B-ubiquitylation is sufficient to directly enhance the nucleosome dynamics and nucleosome-hexasome transition *in vitro* (the effects were comparable to those produced by ATP-driven chromatin remodelers) and, supposedly, *in vivo*. But, however, the "direct" and "indirect" (*via* other regulatory factors) nucleosomal effects of the bulky PTMs are not self-exclusive. There also might be an interplay between histone ubiquitylation and another histone PTMs and their corresponding co-factors regulating chromatin dynamics *in vivo*. One example is that PRC2 co-factors JARID2 and AEBP2 play a crucial role in both the recruitment and activation of PRC2 through their recognition of H2AK119ub1 (Kasinath et al., 2021), which further orchestrates the local chromatin environment.

The tight link of H2BK120/ K34-ubiquitylation with transcription and replication shows a plausible mechanism assisting RNA and DNA polymerases to overcome the nucleosome barrier. The MOF–MSL complex, which deposits H2BK34ub (Krajewski and Vassiliev, 2019; Wu et al., 2011), plays a critical role in transcription, initiation, and elongation and is enriched at transcription start sites (Wu et al., 2014). Regardless of the exact mechanism, it could be hypothesized that H2BK34ub-facilitated destabilization and a dimer eviction in +1 nucleosome (which presents a greater transcription barrier *in vivo* than downstream nucleosomes (Adelman and Lis, 2012; Gilmour, 2009; Teves and Henikoff, 2014; Weber et al., 2014)) assists transient uncoiling of the promoter-proximal boundary of the +1 nucleosome and facilitates the release of Pol II from pausing and its transition to elongation step (**Figures 2A,B**). PAF1 associated with MOF–MSL and RNF20/40 (which deposit H2BK120ub (Hwang et al., 2003)) progresses together during transcription and elongation (Wu et al., 2014) that supposes that H2B-ubiquitylation, in cooperation with histone chaperones (Hsieh et al., 2013; Hsieh et al., 2015; Gurova et al., 2018), orchestrates unwrapping/rewrapping of transcribed nucleosomes by facilitating coordinated sequential dissociation and rebinding of the nucleosome-proximal and nucleosome-distal H2A-H2B dimer—steps required for RNA Pol II to traverse the nucleosome (Kulaeva et al., 2013). In contrast, H2AK119ub (associated with silenced genes (Meas and Mao, 2015)) could prevent Pol II progression and block remodeling activities (i.e., Swi-Snf and related) that act through peeling on DNA from the nucleosome.

In general, the consequences of histone ubiquitylation and sumoylation on the nucleosome primary structure are still understudied, although the experimental data support the direct, destabilizing, or stabilizing effects of bulky PTMs. *In vitro* H4K34-monoubiquitylation moderately destabilizes nucleosomal association of the H3–H4 tetramer, supposedly, due to the clash between DNA phosphate backbone and deposited ubiquitin (Machida et al., 2016). *In vivo* H3K4-polyubiquitylation by RNF8 promotes nucleosome disassembly and eviction from the DNA (Xia et al., 2017), although it is not clear whether this could be a direct effect of histone ubiquitylation. UV-irradiation activates the ubiquitylation of histones H3 and H4 by CUL4-DDB, promoting the eviction of histones and stimulating the recruitment of XPC repair protein (Wang et al., 2006). In biochemical studies, H2AK119-monoubiquitylation had marginal nucleosome stabilizing/ destabilizing effects (Fierz et al., 2012) but could directly alter the nucleosome interface *in vivo* and protect the H3K36 residue from modification (Bi et al., 2016). Using single-molecule magnetic tweezers, it has been shown that H2AK119ub stabilizes the nucleosome from unwrapping (Xiao et al., 2020) (see above).

There is less data on histone sumoylation. In yeast cells, genetically engineered multiple sumoylation of histone H2B had only a minor structural effect on nucleosomes (Chandrasekharan et al., 2009). The H4K12su is a gene silencing marker (Shiio and Eisenman, 2003; Nathan et al., 2006), despite the H4K12 position being near the H4 basic patch where the steric bulk and hindrances by installed SUMO polypeptides could affect the critical (for chromatin compaction) interaction between H4 tails and the H2A-H2B acidic patch on the adjoining nucleosome (Allahverdi et al., 2011; Pepenella et al., 2014b). Indeed, spFRET studies have shown that H4K12su destabilizes long-range internucleosome interactions and moderately represses the formation of compact chromatin (Dhall et al., 2014).

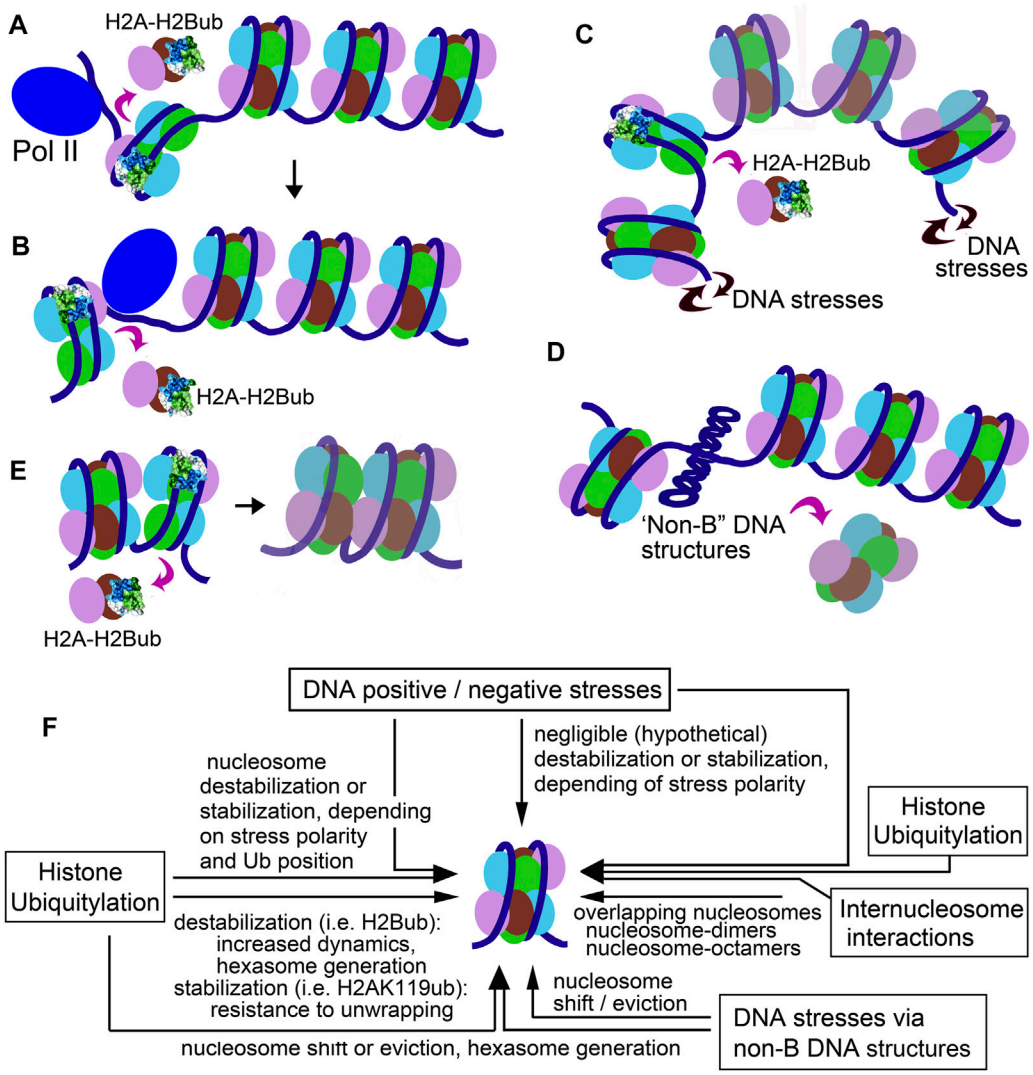

FIGURE 2 | Sketches illustrating the nucleosomal effects of H2Bub. **(A,B)** RNA Pol II traversing the H2B-ubiquitylated nucleosome. **(A)** Eviction of the promoter-proximal H2A-H2B dimer promotes the polymerase complex to enter the nucleosome; **(B)** Eviction of the promoter-distal H2A-H2B dimer promotes RNA Pol II to successfully elongate through the nucleosome. **(C)** Hexasome generation by DNA stresses. **(D)** Nucleosome rearrangement by transition of a DNA segment to a cruciform structure. **(E)** Formation of "overlapping" nucleosomes. **(F)** Schematic figure, depicting how different mechanisms (histone ubiquitylation, DNA stress, and internucleosome interaction) could cooperate to regulate chromatin dynamics and function.

DNA STRESSES AND DNA NON-CANONIC STRUCTURES IN EPIGENETIC CONTROL

Virtually any process that manipulates DNA strands can generate positive or negative DNA torsional stress (Esposito and Sinden, 1988; Baranello et al., 2012; Gilbert and Allan, 2014; Corless and Gilbert, 2016). For example, waves of positive and negative supercoiling are generated ahead and behind the RNA polymerase, respectively (Liu and Wang, 1987), which may be directly observed *in vivo* (e.g., (Lee and Garrard, 1991; Ljungman and Hanawalt, 1995; Naughton et al., 2013; Gerasimova et al., 2016)) and *in vitro* (Pfaffle and Jackson, 1990; Jackson, 1993; Bancaud et al., 2007). It is assumed that negative DNA stresses favor DNA wrapping on the histone octamer, while positive supercoiling destabilizes nucleosomes (Esposito and Sinden, 1988; Pfaffle and Jackson, 1990; Clark et al., 1993; Jackson, 1993; Bancaud et al., 2007). It would be appealing to attribute to DNA stresses an active role in the regulation of a primary nucleosome structure. Indeed, the generation of artificially high levels of positive DNA torsions in a single chromatin fiber by magnetic tweezers can break histone dimer–tetramer docking and induce transient, reversible nucleosome reorganization (Bancaud et al., 2007); the authors assume that a wave of such nucleosome chiral transitions can propagate ahead of a transcribing polymerase *in vivo*. However, after decades of studies, there is still no consensus whether the "physiological" levels of DNA torsions under physiologically relevant conditions could have any substantial effect on the nucleosome structure.

Both supporting (Garner et al., 1987; Jackson, 1993; Sheinin et al., 2013; Teves and Henikoff, 2014) and opposing (Clark et al., 1993; Sheinin et al., 2013) observations were published. The "physiological" levels of DNA supercoiling only marginally affected the stability of unmodified nucleosomes *in vitro*—such that histone octamers assembled on negatively supercoiled DNA with only a slight preference compared to that of positively supercoiled DNA (Clark and Felsenfeld, 1991; Clark et al., 1993). This question is of particular importance since years of studies accumulated mounting evidence of how cells could regulate DNA stresses. In addition, numerous "non-canonical" DNA structures have been discovered, which are capable of adopting non-B DNA conformation to absorb or enhance DNA torsions (Smith, 2008; Baranello et al., 2012; Kaushik et al., 2016).

A different situation could be if a nucleosome structure is already intrinsically destabilized by deposited bulky histone modification. We propose that DNA topology, favoring or disfavoring nucleosome wrapping, may contribute to the structural effects of histone ubiquitylation (Krajewski, 2019; Krajewski WA., 2020) (**Figure 2C**). In our experiments, "physiological" negative and positive supercoiling in long DNA templates had opposing (stimulating or inhibitory, respectively) effects on the hexasome generation upon assembly of H2BK34ub nucleosomes (Krajewski et al., 2018) but had no effect on unmodified nucleosomes. We suppose that nucleosome "unfolding" using moderate positive DNA stress restrains the steric hindrances in ubiquitylated nucleosomes, while nucleosome compaction by negative stresses enhances the hindrances (Krajewski et al., 2018). More strong DNA topology effects in short (298 bp) minicircle DNAs have diverse effects on unmodified, H2BK34ub and H2BK120ub nucleosomes (Krajewski, 2018), suggesting that DNA topology states can strongly and selectively (and, likely, bi-directionally) affect nucleosome stability and dynamics depending on the type of H2B-ubiquitylation. It is notable that certain DNA topologies increased the stability of H2BK120ub nucleosomes over unmodified ones (see (Xiao et al., 2020) and discussion above). The H2BK34- and H2BK120-ubiquitylated nucleosomes exhibited quite selective sensitivity and sustainability to positive and negative DNA stresses (Krajewski, 2018; Krajewski et al., 2018), implying that bulky PTMs could play an active role in amplifying or mitigating the nucleosomal effects of DNA torque (including those by translocating RNA Pol II) and, thus, highlighting the nucleosome-regulatory role of DNA stresses. It could be interesting to see how positive and negative DNA stresses could affect "DNA-peeling refractory" H2AK119ub nucleosomes.

In addition to their direct nucleosome stability effects, DNA stresses could also affect the nucleosomes "indirectly" by generating non-standard DNA structures. Even relatively short stretches of alternating (CG) pairs and inverted repeat DNA sequences can form different structural isomers (left-handed helices and cruciforms) in response to superhelical stress at low "physiological" densities (Esposito and Sinden, 1988; McLean and Wells, 1988; Smith, 2008; Wells, 1988). These structures can regulate (absorb) superhelical stresses in DNA and also can affect nucleosome distribution by "translationally shifting" histone octamers along with DNA or displacing nucleosomes from the DNA (**Figure 2D**). Many studies suggest that Z-DNA and cruciforms cannot be organized in the nucleosome. Deposition of nucleosomes on supercoiled DNA containing a region of Z-DNA or a cruciform leads to the exclusion of regions of Z-DNA from the interiors of nucleosome cores *in vitro* and *in vivo* (Krajewski, 1996).

INTERNUCLEOSOME INTERACTION AS AN ADDITIONAL SOURCE OF CHROMATIN FUNCTIONALITY

A "nucleosome-octamer" and "nucleosome-dimer" structure in which a nucleosome particle is associated with an additional histone octamer (Voordouw and Eisenberg, 1978; Stein, 1979; Daban and Cantor, 1982; Ausio et al., 1984; Aragay et al., 1988; Aragay et al., 1991) or another nucleosome (Tatchell and Van Holde, 1979; Ausio et al., 1984; Yager et al., 1989), respectively, was described years ago, although since then was forgotten for decades. Both the nucleosome-octamers and nucleosome-dimers are likely to be formed *via* trans-interactions between histone octamers. The site-directed histone-DNA and histone–histone cross-linking (Zheng and Hayes, 2003a; Zheng and Hayes, 2003b; Kan et al., 2007; Kan and Hayes, 2007; Kan et al., 2009; Pepenella et al., 2014a) revealed multitude interactions between histone tails and DNA of neighboring nucleosomes (reviewed in: (Luger et al., 2012; Pepenella et al., 2014b; Krajewski, 2016)). The nuclease digestion pattern and digestion kinetics of nucleosome-octamers and nucleosome-dimers are similar to those in single nucleosomes; therefore, it could be supposed that these particles largely retain the basic features of nucleosomal organization (Stein, 1979; Eisenberg and Felsenfeld, 1981; Krajewski and Vassiliev, 2012).

The ability of a nucleosome to bind extra histone octamers/dimers could play an important gene regulatory role during transient chromatin disassembly–reassembly through DNA replication or transcription. For example, a nucleosome behind the RNA Pol II could transiently bind a histone octamer or the evicted histone H2A/H2B dimer from the nucleosome being transcribed—this could be a possible mechanism of how the nucleosome reinstates its initial position on the DNA after the passage of the RNA Pol II complex.

The interaction between nucleosomes could, supposedly, affect chromatin remodeling and deposition of histone modifications. In polynucleosomes, human and yeast Swi/Snf complexes can generate structurally altered 'asymmetric' pairs of adjacent nucleosomes (Ulyanova and Schnitzler, 2005; Krajewski and Vassiliev, 2010). These "autosome" structures contain intact histone core octamers, but their nuclease cleavage pattern indicates the association of one internucleosomal and one subnucleosomal (220 and 70 bp, respectively) DNA fragment. In dinucleosomes, Isw1a/b and Isw2 generate extra structural alterations compared to mononucleosomes (Krajewski, 2013; Krajewski, 2014). Remodeling of the nucleosome-dimer particles by yeast Isw2 facilitated *in vitro* the association of

nucleosome-dimers with the MLL SET-domain polypeptide (Krajewski and Vassiliev, 2012). SET7 and ALL-1 SET polypeptides showed binding preferences for dinucleosomes (but not mononucleosomes) remodeled with yIsw1/Isw2. The assembly of nucleosomes in oligonucleosomes promoted histone H3 methylation by the EZH2/EED, which only inefficiently modifies single mononucleosomes (Martin et al., 2006). Furthermore, reorganization of di- and oligonucleosomes (but not mononucleosomes) by binding of histone H1 further increased H3 methylation by EZH2 (Martin et al., 2006). However, there is no direct evaluation of the significance of internucleosomal interactions in promoting increased PRC2 HMTase activity as of yet. It could be that dinucleosome-enhanced PRC2 HMTase activity is largely due to the mechanism of allosteric activation (Jiao and Liu, 2015; Yu et al., 2019), and incorporation of H1 further facilitates positioning and activity of the PRC2 complex (that is indirectly supported by strong inhibition of methylation with over-stoichiometric amounts of H1 (Martin et al., 2006)). In general, the reports showed that adjusting the internucleosome spacing could affect the activity of the writers of histone PTMs including PRC2, but many of these studies were performed in an artifactual manner by changing the nucleosome spacing length.

It could be supposed that spontaneous movements of nucleosomes along the DNA, nucleosome dynamic fluctuations, and nucleosome instability incurred by histone ubiquitylation, even in absence of chromatin remodeling activities, could result in transient relocation of a histone H2A-H2B dimer from one nucleosome to the surface of the neighboring nucleosome, thus facilitating the formation of hexasomes and other subnucleosomal structures. Similarly, the hexasome particle generated by histone ubiquitylation could transiently associate with the adjacent nucleosome to form the structurally altered "autosome-like" arrangement. Owen-Hughes' lab has shown that interactions between two nucleosomes could generate partial unwrapping of one nucleosome with the eviction of one H2A/H2B dimer and "merging" the resulting hexasome and a nucleosome into a single particle in which overlapping octamers and hexasomes invade each other's space (Engeholm et al., 2009). The authors supposed (ibid) that nucleosome overlapping could be promoted by the eviction of H2A-H2B dimer and by exposure of the nucleosome DNA-binding surfaces. Engeholm et al. supposed that this could occur by the action of Swi-/Snf-related remodeling activities, which can reduce the stability of nucleosomal association of the histone dimer (Bruno et al., 2003; Vicent et al., 2004) and unravel up to 50 bp from the edge of the nucleosomes (Fan et al., 2003; Flaus and Owen-Hughes, 2003; Kassabov et al., 2003; Krajewski and Vassiliev, 2010), such that the nucleosomes may associate through the exposed DNA-binding surfaces to form dinucleosome-like particle (Schnitzler et al., 2001; Ulyanova and Schnitzler, 2005; Ulyanova and Schnitzler, 2007). It is possible that other pathways resulting in destabilized binding of histone dimers with the nucleosome and promoting hexasome generation, such as histone ubiquitylation and nucleosome-destabilizing DNA stresses, could facilitate nucleosome colliding and overlapping (**Figure 2E**).

CONCLUSION

Here, we tried to briefly overview the evidence showing that cooperation between bulky histone modifications, DNA stresses, DNA non-canonic structure, and internucleosomal interactions could create an additional "layer" of chromatin activity determinants Figure 4E. We hypothesize that in such manner, these factors could create a "code" of chromatin activity states, in addition to the histone code of chromatin activity signals, which could promote the formation and stabilization of a highly dynamic, accessible structure of a nucleosome array. The proposed models stress the diversity of mechanisms by which histone PTMs, DNA conformations, and internucleosomal interactions regulate chromatin functionality.

DATA AVAILABILITY STATEMENT

The original contributions presented in the study are included in the article/Supplementary Materials, further inquiries can be directed to the corresponding author.

AUTHOR CONTRIBUTIONS

The author confirms being the sole contributor of this work and has approved it for publication.

FUNDING

This work was conducted in the frame of IDB RAS government programs of basic research in 2022 No. 0088-2021-0007.

REFERENCES

Adelman, K., and Lis, J. T. (2012). Promoter-proximal Pausing of RNA Polymerase II: Emerging Roles in Metazoans. *Nat. Rev. Genet.* 13, 720–731. doi:10.1038/nrg3293

Alabert, C., Barth, T. K., Reverón-Gómez, N., Sidoli, S., Schmidt, A., Jensen, O. N., et al. (2015). Two Distinct Modes for Propagation of Histone PTMs across the Cell Cycle. *Genes Dev.* 29, 585–590. doi:10.1101/gad.256354.114

Allahverdi, A., Yang, R., Korolev, N., Fan, Y., Davey, C. A., Liu, C.-F., et al. (2011). The Effects of Histone H4 Tail Acetylations on Cation-Induced Chromatin Folding and Self-Association. *Nucleic Acids Res.* 39, 1680–1691. doi:10.1093/nar/gkq900

Anderson, C. J., Baird, M. R., Hsu, A., Barbour, E. H., Koyama, Y., Borgnia, M. J., et al. (2019). Structural Basis for Recognition of Ubiquitylated Nucleosome by Dot1L Methyltransferase. *Cel Rep.* 26, 1681–1690. doi:10.1016/j.celrep.2019.01.058

Andrews, F. H., Strahl, B. D., and Kutateladze, T. G. (2016). Insights into Newly Discovered marks and Readers of Epigenetic Information. *Nat. Chem. Biol.* 12, 662–668. doi:10.1038/nchembio.2149

Aragay, A. M., Diaz, P., and Daban, J.-R. (1988). Association of Nucleosome Core Particle DNA with Different Histone Oligomers. *J. Mol. Biol.* 204, 141–154. doi:10.1016/0022-2836(88)90605-5

Aragay, A. M., Fernandez-Busquets, X., and Daban, J. R. (1991). Different Mechanisms for *In Vitro* Formation of Nucleosome Core Particles. *Biochemistry* 30, 5022–5032. doi:10.1021/bi00234a026

Armeev, G. A., Gribkova, A. K., Pospelova, I., Komarova, G. A., and Shaytan, A. K. (2018). Linking Chromatin Composition and Structural Dynamics at the Nucleosome Level. *Curr. Opin. Struct. Biol.* 56, 46–55. doi:10.1016/j.sbi.2018.11.006

Ausio, J., Seger, D., and Eisenberg, H. (1984). Nucleosome Core Particle Stability and Conformational Change. *J. Mol. Biol.* 176, 77–104. doi:10.1016/0022-2836(84)90383-8

Bancaud, A., Wagner, G., Conde e Silva, N., Lavelle, C., Wong, H., Mozziconacci, J., et al. (2007). Nucleosome Chiral Transition under Positive Torsional Stress in Single Chromatin Fibers. *Mol. Cel* 27, 135–147. doi:10.1016/j.molcel.2007.05.037

Baranello, L., Levens, D., Gupta, A., and Kouzine, F. (2012). The Importance of Being Supercoiled: How DNA Mechanics Regulate Dynamic Processes. *Biochim. Biophys. Acta (Bba) - Gene Regul. Mech.* 1819, 632–638. doi:10.1016/j.bbagrm.2011.12.007

Batta, K., Zhang, Z., Yen, K., Goffman, D. B., and Pugh, B. F. (2011). Genome-wide Function of H2B Ubiquitylation in Promoter and Genic Regions. *Genes Dev.* 25, 2254–2265. doi:10.1101/gad.177238.111

Bayer, P., Arndt, A., Metzger, S., Mahajan, R., Melchior, F., Jaenicke, R., et al. (1998). Structure Determination of the Small Ubiquitin-Related Modifier SUMO-1. *J. Mol. Biol.* 280, 275–286. doi:10.1006/jmbi.1998.1839

Bhaumik, S. R., Smith, E., and Shilatifard, A. (2007). Covalent Modifications of Histones during Development and Disease Pathogenesis. *Nat. Struct. Mol. Biol.* 14, 1008–1016. doi:10.1038/nsmb1337

Bi, X., Yang, R., Feng, X., Rhodes, D., and Liu, C.-F. (2016). Semisynthetic UbH2A Reveals Different Activities of Deubiquitinases and Inhibitory Effects of H2A K119 Ubiquitination on H3K36 Methylation in Mononucleosomes. *Org. Biomol. Chem.* 14, 835–839. doi:10.1039/c5ob02323h

Bowman, G. D., and Poirier, M. G. (2015). Post-translational Modifications of Histones that Influence Nucleosome Dynamics. *Chem. Rev.* 115, 2274–2295. doi:10.1021/cr500350x

Bruno, M., Flaus, A., Stockdale, C., Rencurel, C., Ferreira, H., and Owen-Hughes, T. (2003). Histone H2A/H2B Dimer Exchange by ATP-dependent Chromatin Remodeling Activities. *Mol. Cel* 12, 1599–1606. doi:10.1016/s1097-2765(03)00499-4

Buning, R., Kropff, W., Martens, K., and van Noort, J. (2015). spFRET Reveals Changes in Nucleosome Breathing by Neighboring Nucleosomes. *J. Phys. Condens. Matter* 27, 064103. doi:10.1088/0953-8984/27/6/064103

Cao, J., and Yan, Q. (2012). Histone Ubiquitination and Deubiquitination in Transcription, DNA Damage Response, and Cancer. *Front. Oncol.* 2, 26. doi:10.3389/fonc.2012.00026

Chakraborty, K., and Loverde, S. M. (2017). Asymmetric Breathing Motions of Nucleosomal DNA and the Role of Histone Tails. *J. Chem. Phys.* 147, 065101. doi:10.1063/1.4997573

Chandrasekharan, M. B., Huang, F., and Sun, Z.-W. (2009). Ubiquitination of Histone H2B Regulates Chromatin Dynamics by Enhancing Nucleosome Stability. *Proc. Natl. Acad. Sci. U.S.A.* 106, 16686–16691. doi:10.1073/pnas.0907862106

Chen, T. A., Smith, M. M., Le, S. Y., Sternglanz, R., and Allfrey, V. G. (1991). Nucleosome Fractionation by Mercury Affinity Chromatography. Contrasting Distribution of Transcriptionally Active DNA Sequences and Acetylated Histones in Nucleosome Fractions of Wild-type Yeast Cells and Cells Expressing a Histone H3 Gene Altered to Encode a Cysteine 110 Residue. *J. Biol. Chem.* 266, 6489–6498. doi:10.1016/s0021-9258(18)38145-6

Clark, D. J., and Felsenfeld, G. (1991). Formation of Nucleosomes on Positively Supercoiled DNA. *EMBO J.* 10, 387–395. doi:10.1002/j.1460-2075.1991.tb07960.x

Clark, D. J., Ghirlando, R., Felsenfeld, G., and Eisenberg, H. (1993). Effect of Positive Supercoiling on DNA Compaction by Nucleosome Cores. *J. Mol. Biol.* 234, 297–301. doi:10.1006/jmbi.1993.1585

Cole, A. J., Clifton-Bligh, R., and Marsh, D. J. (2015). Histone H2B Monoubiquitination: Roles to Play in Human Malignancy. *Endocr. Relat. Cancer* 22, T19–T33. doi:10.1530/erc-14-0185

Corless, S., and Gilbert, N. (2016). Effects of DNA Supercoiling on Chromatin Architecture. *Biophys. Rev.* 8, 245–258. doi:10.1007/s12551-016-0210-1

Cubeñas-Potts, C., and Matunis, M. J. (2013). SUMO: a Multifaceted Modifier of Chromatin Structure and Function. *Develop. Cel* 24, 1–12. doi:10.1016/j.devcel.2012.11.020

Cutter, A. R., and Hayes, J. J. (2015). A Brief Review of Nucleosome Structure. *FEBS Lett.* 589, 2914–2922. doi:10.1016/j.febslet.2015.05.016

Daban, J.-R., and Cantor, C. R. (1982). Structural and Kinetic Study of the Self-Assembly of Nucleosome Core Particles. *J. Mol. Biol.* 156, 749–769. doi:10.1016/0022-2836(82)90140-1

Davey, C. A., Sargent, D. F., Luger, K., Maeder, A. W., and Richmond, T. J. (2002). Solvent Mediated Interactions in the Structure of the Nucleosome Core Particle at 1.9Å Resolution. *J. Mol. Biol.* 319, 1097–1113. doi:10.1016/s0022-2836(02)00386-8

Dhall, A., Wei, S., Fierz, B., Woodcock, C. L., Lee, T.-H., and Chatterjee, C. (2014). Sumoylated Human Histone H4 Prevents Chromatin Compaction by Inhibiting Long-Range Internucleosomal Interactions. *J. Biol. Chem.* 289, 33827–33837. doi:10.1074/jbc.m114.591644

Dieker, J., and Muller, S. (2010). Epigenetic Histone Code and Autoimmunity. *Clinic Rev. Allerg Immunol.* 39, 78–84. doi:10.1007/s12016-009-8173-7

Dorigo, B., Schalch, T., Kulangara, A., Duda, S., Schroeder, R. R., and Richmond, T. J. (2004). Nucleosome Arrays Reveal the Two-Start Organization of the Chromatin Fiber. *Science* 306, 1571–1573. doi:10.1126/science.1103124

Eisenberg, H., and Felsenfeld, G. (1981). Hydrodynamic Studies of the Interaction between Nucleosome Core Particles and Core Histones. *J. Mol. Biol.* 150, 537–552. doi:10.1016/0022-2836(81)90379-x

Engeholm, M., de Jager, M., Flaus, A., Brenk, R., van Noort, J., and Owen-Hughes, T. (2009). Nucleosomes Can Invade DNA Territories Occupied by Their Neighbors. *Nat. Struct. Mol. Biol.* 16, 151–158. doi:10.1038/nsmb.1551

Escobar, T. M., Loyola, A., and Reinberg, D. (2021). Parental Nucleosome Segregation and the Inheritance of Cellular Identity. *Nat. Rev. Genet.* 22, 379–392. doi:10.1038/s41576-020-00312-w

Escobar, T. M., Oksuz, O., Saldaña-Meyer, R., Descostes, N., Bonasio, R., and Reinberg, D. (2019). Active and Repressed Chromatin Domains Exhibit Distinct Nucleosome Segregation during DNA Replication. *Cell* 179, 953–963. doi:10.1016/j.cell.2019.10.009

Espinosa, J. M. (2008). Histone H2B Ubiquitination: the Cancer Connection. *Genes Dev.* 22, 2743–2749. doi:10.1101/gad.1732108

Esposito, F., and Sinden, R. R. (1988). DNA Supercoiling and Eukaryotic Gene Expression. *Oxf Surv. Eukaryot. Genes* 5, 1–50.

Fan, H.-Y., He, X., Kingston, R. E., and Narlikar, G. J. (2003). Distinct Strategies to Make Nucleosomal DNA Accessible. *Mol. Cel* 11, 1311–1322. doi:10.1016/s1097-2765(03)00192-8

Fierz, B., Kilic, S., Hieb, A. R., Luger, K., and Muir, T. W. (2012). Stability of Nucleosomes Containing Homogenously Ubiquitylated H2A and H2B Prepared Using Semisynthesis. *J. Am. Chem. Soc.* 134, 19548–19551. doi:10.1021/ja308908p

Flaus, A., and Owen-Hughes, T. (2003). Dynamic Properties of Nucleosomes during thermal and ATP-Driven Mobilization. *Mol. Cel Biol.* 23, 7767–7779. doi:10.1128/mcb.23.21.7767-7779.2003

Fleming, A. B., Kao, C.-F., Hillyer, C., Pikaart, M., and Osley, M. A. (2008). H2B Ubiquitylation Plays a Role in Nucleosome Dynamics during Transcription Elongation. *Mol. Cel* 31, 57–66. doi:10.1016/j.molcel.2008.04.025

Gao, C., Huang, W., Kanasaki, K., and Xu, Y. (2014). The Role of Ubiquitination and Sumoylation in Diabetic Nephropathy. *Biomed. Res. Int.* 2014, 160692. doi:10.1155/2014/160692

Garner, M. M., Felsenfeld, G., O'Dea, M. H., and Gellert, M. (1987). Effects of DNA Supercoiling on the Topological Properties of Nucleosomes. *Proc. Natl. Acad. Sci. U.S.A.* 84, 2620–2623. doi:10.1073/pnas.84.9.2620

Gerasimova, N. S., Pestov, N. A., Kulaeva, O. I., Clark, D. J., and Studitsky, V. M. (2016). Transcription-induced DNA Supercoiling: New Roles of Intranucleosomal DNA Loops in DNA Repair and Transcription. *Transcription* 7, 91–95. doi:10.1080/21541264.2016.1182240

Gibney, E. R., and Nolan, C. M. (2010). Epigenetics and Gene Expression. *Heredity* 105, 4–13. doi:10.1038/hdy.2010.54

Gilbert, N., and Allan, J. (2014). Supercoiling in DNA and Chromatin. *Curr. Opin. Genet. Develop.* 25, 15–21. doi:10.1016/j.gde.2013.10.013

Gilmour, D. S. (2009). Promoter Proximal Pausing on Genes in Metazoans. *Chromosoma* 118, 1–10. doi:10.1007/s00412-008-0182-4

Gluckman, P. D., Hanson, M. A., Buklijas, T., Low, F. M., and Beedle, A. S. (2009). Epigenetic Mechanisms that Underpin Metabolic and Cardiovascular Diseases. *Nat. Rev. Endocrinol.* 5, 401–408. doi:10.1038/nrendo.2009.102

Gray, S. G. (2006). DMMC Workshop: Unravelling Chromatin and the Role of Epigenetics in Disease. *Epigenetics* 1, 187–189. doi:10.4161/epi.1.4.3399

Grigoryev, S. A., Arya, G., Correll, S., Woodcock, C. L., and Schlick, T. (2009). Evidence for Heteromorphic Chromatin Fibers from Analysis of Nucleosome Interactions. *Proc. Natl. Acad. Sci. U.S.A.* 106, 13317–13322. doi:10.1073/pnas.0903280106

Grigoryev, S. A. (2004). Keeping Fingers Crossed: Heterochromatin Spreading through Interdigitation of Nucleosome Arrays. *FEBS Lett.* 564, 4–8. doi:10.1016/s0014-5793(04)00258-3

Gurova, K., Chang, H. W., Valieva, M. E., Sandlesh, P., and Studitsky, V. M. (2018). Structure and Function of the Histone Chaperone FACT - Resolving FACTual Issues. *Biochim. Biophys. Acta Gene Regul. Mech.* 1861 (9), 892–904. doi:10.1016/j.bbagrm.2018.07.008

Hodges, C., Bintu, L., Lubkowska, L., Kashlev, M., and Bustamante, C. (2009). Nucleosomal Fluctuations Govern the Transcription Dynamics of RNA Polymerase II. *Science* 325, 626–628. doi:10.1126/science.1172926

Hsieh, F.-K., Kulaeva, O. I., Patel, S. S., Dyer, P. N., Luger, K., Reinberg, D., et al. (2013). Histone Chaperone FACT Action during Transcription through Chromatin by RNA Polymerase II. *Proc. Natl. Acad. Sci. U.S.A.* 110, 7654–7659. doi:10.1073/pnas.1222198110

Hsieh, F.-K., Kulaeva, O. I., and Studitsky, V. M. (2015). Experimental Analysis of hFACT Action during Pol II Transcription *In Vitro*. *Methods Mol. Biol.* 1276, 315–326. doi:10.1007/978-1-4939-2392-2_19

Huang, W.-C., Ko, T.-P., Li, S. S.-L., and Wang, A. H.-J. (2004). Crystal Structures of the Human SUMO-2 Protein at 1.6 Å and 1.2 Å Resolution. *Eur. J. Biochem.* 271, 4114–4122. doi:10.1111/j.1432-1033.2004.04349.x

Hwang, W. W., Venkatasubrahmanyam, S., Ianculescu, A. G., Tong, A., Boone, C., and Madhani, H. D. (2003). A Conserved RING finger Protein Required for Histone H2B Monoubiquitination and Cell Size Control. *Mol. Cel* 11, 261–266. doi:10.1016/s1097-2765(02)00826-2

Jackson, V. (1993). Influence of Positive Stress on Nucleosome Assembly. *Biochemistry* 32, 5901–5912. doi:10.1021/bi00073a024

Jiao, L., and Liu, X. (2015). Structural Basis of Histone H3K27 Trimethylation by an Active Polycomb Repressive Complex 2. *Science* 350, aac4383. doi:10.1126/science.aac4383

Johnsen, S. A. (2012). The Enigmatic Role of H2Bub1 in Cancer. *FEBS Lett.* 586, 1592–1601. doi:10.1016/j.febslet.2012.04.002

Kan, P.-Y., Caterino, T. L., and Hayes, J. J. (2009). The H4 Tail Domain Participates in Intra- and Internucleosome Interactions with Protein and DNA during Folding and Oligomerization of Nucleosome Arrays. *Mol. Cel Biol.* 29, 538–546. doi:10.1128/mcb.01343-08

Kan, P.-Y., Lu, X., Hansen, J. C., and Hayes, J. J. (2007). The H3 Tail Domain Participates in Multiple Interactions during Folding and Self-Association of Nucleosome Arrays. *Mol. Cel Biol.* 27, 2084–2091. doi:10.1128/mcb.02181-06

Kan, P., and Hayes, J. (2007). Detection of Interactions between Nucleosome Arrays Mediated by Specific Core Histone Tail Domains. *Methods* 41, 278–285. doi:10.1016/j.ymeth.2006.08.012

Kasinath, V., Beck, C., Sauer, P., Poepsel, S., Kosmatka, J., Faini, M., et al. (2021). JARID2 and AEBP2 Regulate PRC2 in the Presence of H2AK119ub1 and Other Histone Modifications. *Science* 371, abc3393. doi:10.1126/science.abc3393

Kassabov, S. R., Zhang, B., Persinger, J., and Bartholomew, B. (2003). SWI/SNF Unwraps, Slides, and Rewraps the Nucleosome. *Mol. Cel* 11, 391–403. doi:10.1016/s1097-2765(03)00039-x

Kaushik, M., Kaushik, S., Roy, K., Singh, A., Mahendru, S., Kumar, M., et al. (2016). A Bouquet of DNA Structures: Emerging Diversity. *Biochem. Biophys. Rep.* 5, 388–395. doi:10.1016/j.bbrep.2016.01.013

Kepper, N., Ettig, R., Stehr, R., Marnach, S., Wedemann, G., and Rippe, K. (2011). Force Spectroscopy of Chromatin Fibers: Extracting Energetics and Structural Information from Monte Carlo Simulations. *Biopolymers* 95, 435–447. doi:10.1002/bip.21598

Koopmans, W. J. A., Brehm, A., Logie, C., Schmidt, T., and van Noort, J. (2007). Single-pair FRET Microscopy Reveals Mononucleosome Dynamics. *J. Fluoresc.* 17, 785–795. doi:10.1007/s10895-007-0218-9

Kornberg, R. D., and Lorch, Y. (1991). Irresistible Force Meets Immovable Object: Transcription and the Nucleosome. *Cell* 67, 833–836. doi:10.1016/0092-8674(91)90354-2

Krajewski, W. A. (2020a). "Direct" and "Indirect" Effects of Histone Modifications: Modulation of Sterical Bulk as a Novel Source of Functionality. *Bioessays* 42, e1900136. doi:10.1002/bies.201900136

Krajewski, W. A. (2013). Comparison of the Isw1a, Isw1b, and Isw2 Nucleosome Disrupting Activities. *Biochemistry* 52, 6940–6949. doi:10.1021/bi400634r

Krajewski, W. A. (2018). Effects of DNA Superhelical Stress on the Stability of H2B-Ubiquitylated Nucleosomes. *J. Mol. Biol.* 430, 5002–5014. doi:10.1016/j.jmb.2018.09.014

Krajewski, W. A. (1996). Enhancement of Transcription by Short Alternating CG Tracts Incorporated within a Rous Sarcoma Virus-Based Chimeric Promoter: *In Vivo* Studies. *Mol. Gen. Genet.* 252, 249–254. doi:10.1007/s004380050226

Krajewski, W. A., Li, J., and Dou, Y. (2018). Effects of Histone H2B Ubiquitylation on the Nucleosome Structure and Dynamics. *Nucleic Acids Res.* 46, 7631–7642. doi:10.1093/nar/gky526

Krajewski, W. A., and Luchnik, A. N. (1991). High Rotational Mobility of DNA in Animal Cells and its Modulation by Histone Acetylation. *Mol. Gen. Genet.* 231, 17–21. doi:10.1007/bf00293816

Krajewski, W. A. (2016). On the Role of Inter-nucleosomal Interactions and Intrinsic Nucleosome Dynamics in Chromatin Function. *Biochem. Biophys. Rep.* 5, 492–501. doi:10.1016/j.bbrep.2016.02.009

Krajewski, W. A. (2020b). The Intrinsic Stability of H2B-Ubiquitylated Nucleosomes and Their *In Vitro* Assembly/disassembly by Histone Chaperone NAP1. *Biochim. Biophys. Acta (Bba) - Gen. Subjects* 1864, 129497. doi:10.1016/j.bbagen.2019.129497

Krajewski, W. A. (2019). Ubiquitylation: How Nucleosomes Use Histones to Evict Histones. *Trends Cel Biol.* 29, 689–694. doi:10.1016/j.tcb.2019.06.002

Krajewski, W. A., and Vassiliev, O. L. (2019). Analysis of Histone Ubiquitylation by MSL1/MSL2 Proteins *In Vitro*. *Arch. Biochem. Biophys.* 666, 22–30. doi:10.1016/j.abb.2019.03.015

Krajewski, W. A., and Vassiliev, O. L. (2012). Remodeling of Nucleosome-Dimer Particles with yIsw2 Promotes Their Association with ALL-1 SET Domain *In Vitro*. *Biochemistry* 51, 4354–4363. doi:10.1021/bi201645c

Krajewski, W. A., and Vassiliev, O. L. (2010). The *Saccharomyces cerevisiae* Swi/Snf Complex Can Catalyze Formation of Dimeric Nucleosome Structures *In Vitro*. *Biochemistry* 49, 6531–6540. doi:10.1021/bi1006157

Krajewski, W. A. (2014). Yeast Isw1a and Isw1b Exhibit Similar Nucleosome Mobilization Capacities for Mononucleosomes, but Differently Mobilize Dinucleosome Templates. *Arch. Biochem. Biophys.* 546, 72–80. doi:10.1016/j.abb.2014.02.003

Kruithof, M., Chien, F.-T., Routh, A., Logie, C., Rhodes, D., and van Noort, J. (2009). Single-molecule Force Spectroscopy Reveals a Highly Compliant Helical Folding for the 30-nm Chromatin Fiber. *Nat. Struct. Mol. Biol.* 16, 534–540. doi:10.1038/nsmb.1590

Kulaeva, O. I., Hsieh, F.-K., Chang, H.-W., Luse, D. S., and Studitsky, V. M. (2013). Mechanism of Transcription through a Nucleosome by RNA Polymerase II. *Biochim. Biophys. Acta (Bba) - Gene Regul. Mech.* 1829, 76–83. doi:10.1016/j.bbagrm.2012.08.015

Lee, M. S., and Garrard, W. T. (1991). Positive DNA Supercoiling Generates a Chromatin Conformation Characteristic of Highly Active Genes. *Proc. Natl. Acad. Sci. U.S.A.* 88, 9675–9679. doi:10.1073/pnas.88.21.9675

Li, G., Levitus, M., Bustamante, C., and Widom, J. (2005). Rapid Spontaneous Accessibility of Nucleosomal DNA. *Nat. Struct. Mol. Biol.* 12, 46–53. doi:10.1038/nsmb869

Li, J., He, Q., Liu, Y., Liu, S., Tang, S., Li, C., et al. (2017). Chemical Synthesis of K34-Ubiquitylated H2B for Nucleosome Reconstitution and Single-Particle Cryo-Electron Microscopy Structural Analysis. *Chembiochem* 18, 176–180. doi:10.1002/cbic.201600551

Liu, L. F., and Wang, J. C. (1987). Supercoiling of the DNA Template during Transcription. *Proc. Natl. Acad. Sci. U.S.A.* 84, 7024–7027. doi:10.1073/pnas.84.20.7024

Ljungman, M., and Hanawalt, P. C. (1995). Presence of Negative Torsional Tension in the Promoter Region of the Transcriptionally Poised Dihydrofolate Reductase Gene *In Vivo*. *Nucleic Acids Res.* 23, 1782–1789. doi:10.1093/nar/23.10.1782

Luger, K., Dechassa, M. L., and Tremethick, D. J. (2012). New Insights into Nucleosome and Chromatin Structure: an Ordered State or a Disordered Affair? *Nat. Rev. Mol. Cel Biol.* 13, 436–447. doi:10.1038/nrm3382

Luger, K., Mäder, A. W., Richmond, R. K., Sargent, D. F., and Richmond, T. J. (1997). Crystal Structure of the Nucleosome Core Particle at 2.8 Å Resolution. *Nature* 389, 251–260. doi:10.1038/38444

Machida, S., Sekine, S., Nishiyama, Y., Horikoshi, N., and Kurumizaka, H. (2016). Structural and Biochemical Analyses of Monoubiquitinated Human Histones H2B and H4. *Open. Biol.* 6, 1–9. doi:10.1098/rsob.160090

Manning, G. S. (2006). The Persistence Length of DNA Is Reached from the Persistence Length of its Null Isomer through an Internal Electrostatic Stretching Force. *Biophysical J.* 91, 3607–3616. doi:10.1529/biophysj.106.089029

Martin, C., Cao, R., and Zhang, Y. (2006). Substrate Preferences of the EZH2 Histone Methyltransferase Complex. *J. Biol. Chem.* 281, 8365–8370. doi:10.1074/jbc.m513425200

McLean, M. J., and Wells, R. D. (1988). The Role of DNA Sequence in the Formation of Z-DNA versus Cruciforms in Plasmids. *J. Biol. Chem.* 263, 7370–7377. doi:10.1016/s0021-9258(18)68652-1

Meas, R., and Mao, P. (2015). Histone Ubiquitylation and its Roles in Transcription and DNA Damage Response. *DNA Repair* 36, 36–42. doi:10.1016/j.dnarep.2015.09.016

Mirabella, A. C., Foster, B. M., and Bartke, T. (2016). Chromatin Deregulation in Disease. *Chromosoma* 125, 75–93. doi:10.1007/s00412-015-0530-0

Morrison, E. A., Bowerman, S., Sylvers, K. L., Wereszczynski, J., and Musselman, C. A. (2018). The Conformation of the Histone H3 Tail Inhibits Association of the BPTF PHD finger with the Nucleosome. *Elife* 7. doi:10.7554/eLife.31481

Morse, R. H., Pederson, D. S., Dean, A., and Simpson, R. T. (1987). Yeast Nudeosomes Allow thermal Untwisting of DNA. *Nucl. Acids Res.* 15, 10311–10330. doi:10.1093/nar/15.24.10311

Nathan, D., Ingvarsdottir, K., Sterner, D. E., Bylebyl, G. R., Dokmanovic, M., Dorsey, J. A., et al. (2006). Histone Sumoylation Is a Negative Regulator in *Saccharomyces cerevisiae* and Shows Dynamic Interplay with Positive-Acting Histone Modifications. *Genes Dev.* 20, 966–976. doi:10.1101/gad.1404206

Naughton, C., Avlonitis, N., Corless, S., Prendergast, J. G., Mati, I. K., Eijk, P. P., et al. (2013). Transcription Forms and Remodels Supercoiling Domains Unfolding Large-Scale Chromatin Structures. *Nat. Struct. Mol. Biol.* 20, 387–395. doi:10.1038/nsmb.2509

Ngo, T. T. M., and Ha, T. (2015). Nucleosomes Undergo Slow Spontaneous Gaping. *Nucleic Acids Res.* 43, 3964–3971. doi:10.1093/nar/gkv276

Pepenella, S., Murphy, K. J., and Hayes, J. J. (2014a). A Distinct Switch in Interactions of the Histone H4 Tail Domain upon Salt-dependent Folding of Nucleosome Arrays. *J. Biol. Chem.* 289, 27342–27351. doi:10.1074/jbc.m114.595140

Pepenella, S., Murphy, K. J., and Hayes, J. J. (2014b). Intra- and Inter-nucleosome Interactions of the Core Histone Tail Domains in Higher-Order Chromatin Structure. *Chromosoma* 123, 3–13. doi:10.1007/s00412-013-0435-8

Perini, G., and Tupler, R. (2006). Altered Gene Silencing and Human Diseases. *Clin. Genet.* 69, 1–7. doi:10.1111/j.1399-0004.2005.00540.x

Petruk, S., Black, K. L., Kovermann, S. K., Brock, H. W., and Mazo, A. (2013). Stepwise Histone Modifications Are Mediated by Multiple Enzymes that Rapidly Associate with Nascent DNA during Replication. *Nat. Commun.* 4, 2841. doi:10.1038/ncomms3841

Petruk, S., Sedkov, Y., Johnston, D. M., Hodgson, J. W., Black, K. L., Kovermann, S. K., et al. (2012). TrxG and PcG Proteins but Not Methylated Histones Remain Associated with DNA through Replication. *Cell* 150, 922–933. doi:10.1016/j.cell.2012.06.046

Pfaffle, P., and Jackson, V. (1990). Studies on Rates of Nucleosome Formation with DNA under Stress. *J. Biol. Chem.* 265, 16821–16829. doi:10.1016/s0021-9258(17)44835-6

Polach, K. J., and Widom, J. (1996). A Model for the Cooperative Binding of Eukaryotic Regulatory Proteins to Nucleosomal Target Sites. *J. Mol. Biol.* 258, 800–812. doi:10.1006/jmbi.1996.0288

Prakash, K., and Fournier, D. (2018). Evidence for the Implication of the Histone Code in Building the Genome Structure. *Biosystems* 164, 49–59. doi:10.1016/j.biosystems.2017.11.005

Prior, C. P., Cantor, C. R., Johnson, E. M., Littau, V. C., and Allfrey, V. G. (1983). Reversible Changes in Nucleosome Structure and Histone H3 Accessibility in Transcriptionally Active and Inactive States of rDNA Chromatin. *Cell* 34, 1033–1042. doi:10.1016/0092-8674(83)90561-5

Reinberg, D., and Vales, L. D. (2018). Chromatin Domains Rich in Inheritance. *Science* 361, 33–34. doi:10.1126/science.aat7871

Renatus, M., Parrado, S. G., D'Arcy, A., Eidhoff, U., Gerhartz, B., Hassiepen, U., et al. (2006). Structural Basis of Ubiquitin Recognition by the Deubiquitinating Protease USP2. *Structure* 14, 1293–1302. doi:10.1016/j.str.2006.06.012

Reverón-Gómez, N., González-Aguilera, C., Stewart-Morgan, K. R., Petryk, N., Flury, V., Graziano, S., et al. (2018). Accurate Recycling of Parental Histones Reproduces the Histone Modification Landscape during DNA Replication. *Mol. Cel* 72, 239–249. doi:10.1016/j.molcel.2018.08.010

Robinson, P. J., and Rhodes, D. (2006). Structure of the '30nm' Chromatin Fibre: A Key Role for the Linker Histone. *Curr. Opin. Struct. Biol.* 16, 336–343. doi:10.1016/j.sbi.2006.05.007

Rothbart, S. B., and Strahl, B. D. (2014). Interpreting the Language of Histone and DNA Modifications. *Biochim. Biophys. Acta (Bba) - Gene Regul. Mech.* 1839, 627–643. doi:10.1016/j.bbagrm.2014.03.001

Saavedra, R. A., and Huberman, J. A. (1986). Both DNA Topoisomerases I and II Relax 2 μm Plasmid DNA in Living Yeast Cells. *Cell* 45, 65–70. doi:10.1016/0092-8674(86)90538-6

Schalch, T., Duda, S., Sargent, D. F., and Richmond, T. J. (2005). X-ray Structure of a Tetranucleosome and its Implications for the Chromatin Fibre. *Nature* 436, 138–141. doi:10.1038/nature03686

Schnitzler, G. R., Cheung, C. L., Hafner, J. H., Saurin, A. J., Kingston, R. E., and Lieber, C. M. (2001). Direct Imaging of Human SWI/SNF-remodeled Mono- and Polynucleosomes by Atomic Force Microscopy Employing Carbon Nanotube Tips. *Mol. Cel Biol.* 21, 8504–8511. doi:10.1128/mcb.21.24.8504-8511.2001

Schunter, S., Villa, R., Flynn, V., Heidelberger, J. B., Classen, A.-K., Beli, P., et al. (2017). Ubiquitylation of the Acetyltransferase MOF in Drosophila melanogaster. *Plos. One.* 12, e0177408. doi:10.1371/journal.pone.0177408

Selth, L. A., Sigurdsson, S., and Svejstrup, J. Q. (2010). Transcript Elongation by RNA Polymerase II. *Annu. Rev. Biochem.* 79, 271–293. doi:10.1146/annurev.biochem.78.062807.091425

Shaytan, A. K., Armeev, G. A., Goncearenco, A., Zhurkin, V. B., Landsman, D., and Panchenko, A. R. (2016). Coupling between Histone Conformations and DNA Geometry in Nucleosomes on a Microsecond Timescale: Atomistic Insights into Nucleosome Functions. *J. Mol. Biol.* 428, 221–237. doi:10.1016/j.jmb.2015.12.004

Sheinin, M. Y., Li, M., Soltani, M., Luger, K., and Wang, M. D. (2013). Torque Modulates Nucleosome Stability and Facilitates H2A/H2B Dimer Loss. *Nat. Commun.* 4, 2579. doi:10.1038/ncomms3579

Shiio, Y., and Eisenman, R. N. (2003). Histone Sumoylation Is Associated with Transcriptional Repression. *Proc. Natl. Acad. Sci. U.S.A.* 100, 13225–13230. doi:10.1073/pnas.1735528100

Singh, J., and Padgett, R. A. (2009). Rates of *In Situ* Transcription and Splicing in Large Human Genes. *Nat. Struct. Mol. Biol.* 16, 1128–1133. doi:10.1038/nsmb.1666

Smith, G. R. (2008). Meeting DNA Palindromes Head-To-Head. *Genes Dev.* 22, 2612–2620. doi:10.1101/gad.1724708

Stein, A. (1979). DNA Folding by Histones: the Kinetics of Chromatin Core Particle Reassembly and the Interaction of Nucleosomes with Histones. *J. Mol. Biol.* 130, 103–134. doi:10.1016/0022-2836(79)90421-2

Strahl, B. D., and Allis, C. D. (2000). The Language of Covalent Histone Modifications. *Nature* 403, 41–45. doi:10.1038/47412

Tatchell, K., and Van Holde, K. E. (1979). Nucleosome Reconstitution: Effect of DNA Length on Nucleosome Structure. *Biochemistry* 18, 2871–2880. doi:10.1021/bi00580a031

Teves, S. S., and Henikoff, S. (2014). Transcription-generated Torsional Stress Destabilizes Nucleosomes. *Nat. Struct. Mol. Biol.* 21, 88–94. doi:10.1038/nsmb.2723

Trujillo, K. M., and Osley, M. A. (2012). A Role for H2B Ubiquitylation in DNA Replication. *Mol. Cel* 48, 734–746. doi:10.1016/j.molcel.2012.09.019

Ulyanova, N. P., and Schnitzler, G. R. (2005). Human SWI/SNF Generates Abundant, Structurally Altered Dinucleosomes on Polynucleosomal Templates. *Mol. Cel Biol.* 25, 11156–11170. doi:10.1128/mcb.25.24.11156-11170.2005

Ulyanova, N. P., and Schnitzler, G. R. (2007). Inverted Factor Access and Slow Reversion Characterize SWI/SNF-altered Nucleosome Dimers. *J. Biol. Chem.* 282, 1018–1028. doi:10.1074/jbc.m609473200

Valencia-Sanchez, M. I., De, I. P., Wang, M., Vasilyev, N., Chen, R., Nudler, E., et al. (2019). Structural Basis of Dot1L Stimulation by Histone H2B Lysine 120 Ubiquitination. *Mol. Cel* 74 (5), 1010–1019. doi:10.1016/j.molcel.2019.03.029

Vasudevan, D., Chua, E. Y. D., and Davey, C. A. (2010). Crystal Structures of Nucleosome Core Particles Containing the '601' strong Positioning Sequence. *J. Mol. Biol.* 403, 1–10. doi:10.1016/j.jmb.2010.08.039

Vaughan, R. M., Kupai, A., and Rothbart, S. B. (2021). Chromatin Regulation through Ubiquitin and Ubiquitin-like Histone Modifications. *Trends Biochem. Sci.* 46, 258–269. doi:10.1016/j.tibs.2020.11.005

Venkatesh, S., and Workman, J. L. (2015). Histone Exchange, Chromatin Structure and the Regulation of Transcription. *Nat. Rev. Mol. Cel Biol.* 16, 178–189. doi:10.1038/nrm3941

Vicent, G. P., Nacht, A. S., Smith, C. L., Peterson, C. L., Dimitrov, S., and Beato, M. (2004). DNA Instructed Displacement of Histones H2A and H2B at an Inducible Promoter. *Mol. Cel* 16, 439–452. doi:10.1016/j.molcel.2004.10.025

Victor, J. M., Zlatanova, J., Barbi, M., and Mozziconacci, J. (2012). Pulling Chromatin Apart: Unstacking or Unwrapping? *BMC. Biophys.* 5, 21. doi:10.1186/2046-1682-5-21

Voordouw, G., and Eisenberg, H. (1978). Binding of Additional Histones to Chromatin Core Particles. *Nature* 273, 446–448. doi:10.1038/273446a0

Wang, H., Zhai, L., Xu, J., Joo, H.-Y., Jackson, S., Erdjument-Bromage, H., et al. (2006). Histone H3 and H4 Ubiquitylation by the CUL4-DDB-ROC1 Ubiquitin Ligase Facilitates Cellular Response to DNA Damage. *Mol. Cel* 22, 383–394. doi:10.1016/j.molcel.2006.03.035

Weake, V. M. (2014). "Histone Ubiquitylation Control of Gene Expression," in *Fundamentals of Chromatin*. Editors J. Workman and S. Abmayr (New York, NY: Springer), 257–307. doi:10.1007/978-1-4614-8624-4_6

Weber, C. M., Ramachandran, S., and Henikoff, S. (2014). Nucleosomes Are Context-specific, H2A.Z-Modulated Barriers to RNA Polymerase. *Mol. Cel* 53, 819–830. doi:10.1016/j.molcel.2014.02.014

Wells, R. D. (1988). Unusual DNA Structures. *J. Biol. Chem.* 263, 1095–1098. doi:10.1016/s0021-9258(19)57268-4

Wright, D. E., and Kao, C.-F. (2015). (Ubi)quitin' the H2bit: Recent Insights into the Roles of H2B Ubiquitylation in DNA Replication and Transcription. *Epigenetics* 10, 122–126. doi:10.1080/15592294.2014.1003750

Wu, L., Lee, S. Y., Zhou, B., Nguyen, U. T. T., Muir, T. W., Tan, S., et al. (2013). ASH2L Regulates Ubiquitylation Signaling to MLL: Trans-regulation of H3 K4 Methylation in Higher Eukaryotes. *Mol. Cel* 49, 1108–1120. doi:10.1016/j.molcel.2013.01.033

Wu, L., Li, L., Zhou, B., Qin, Z., and Dou, Y. (2014). H2B Ubiquitylation Promotes RNA Pol II Processivity via PAF1 and pTEFb. *Mol. Cel* 54, 920–931. doi:10.1016/j.molcel.2014.04.013

Wu, L., Zee, B. M., Wang, Y., Garcia, B. A., and Dou, Y. (2011). The RING finger Protein MSL2 in the MOF Complex Is an E3 Ubiquitin Ligase for H2B K34 and Is Involved in Crosstalk with H3 K4 and K79 Methylation. *Mol. Cel* 43, 132–144. doi:10.1016/j.molcel.2011.05.015

Xia, Y., Yang, W., Fa, M., Li, X., Wang, Y., Jiang, Y., et al. (2017). RNF8 Mediates Histone H3 Ubiquitylation and Promotes Glycolysis and Tumorigenesis. *J. Exp. Med.* 214, 1843–1855. doi:10.1084/jem.20170015

Xiao, X., Liu, C., Pei, Y., Wang, Y.-Z., Kong, J., Lu, K., et al. (2020). Histone H2A Ubiquitination Reinforces Mechanical Stability and Asymmetry at the Single-Nucleosome Level. *J. Am. Chem. Soc.* 142, 3340–3345. doi:10.1021/jacs.9b12448

Yager, T. D., McMurray, C. T., and Van Holde, K. E. (1989). Salt-induced Release of DNA from Nucleosome Core Particles. *Biochemistry* 28, 2271–2281. doi:10.1021/bi00431a045

Yu, J.-R., Lee, C.-H., Oksuz, O., Stafford, J. M., and Reinberg, D. (2019). PRC2 Is High Maintenance. *Genes Dev.* 33, 903–935. doi:10.1101/gad.325050.119

Zheng, C., and Hayes, J. J. (2003a). Intra- and Inter-nucleosomal Protein-DNA Interactions of the Core Histone Tail Domains in a Model System. *J. Biol. Chem.* 278, 24217–24224. doi:10.1074/jbc.m302817200

Zheng, C., and Hayes, J. J. (2003b). Structures and Interactions of the Core Histone Tail Domains. *Biopolymers* 68, 539–546. doi:10.1002/bip.10303

Zlatanova, J., Bishop, T. C., Victor, J.-M., Jackson, V., and Van Holde, K. (2009). The Nucleosome Family: Dynamic and Growing. *Structure* 17, 160–171. doi:10.1016/j.str.2008.12.016

Zou, B., Yang, D.-L., Shi, Z., Dong, H., and Hua, J. (2014). Monoubiquitination of Histone 2B at the Disease Resistance Gene Locus Regulates its Expression and Impacts Immune Responses in Arabidopsis. *Plant Physiol.* 165, 309–318. doi:10.1104/pp.113.227801

Conflict of Interest: The author declares that the research was conducted in the absence of any commercial or financial relationships that could be construed as a potential conflict of interest.

Publisher's Note: All claims expressed in this article are solely those of the authors and do not necessarily represent those of their affiliated organizations, or those of the publisher, the editors, and the reviewers. Any product that may be evaluated in this article, or any claim that may be made by its manufacturer, is not guaranteed or endorsed by the publisher.

frontiers | Frontiers in Genetics

BRIEF RESEARCH REPORT
published: 13 May 2022
doi: 10.3389/fgene.2022.870700

Structural Features of the Nucleosomal DNA Modulate the Functional Binding of a Transcription Factor and Productive Transcription

*Vinesh Vinayachandran and Purnima Bhargava**

Centre for Cellular and Molecular Biology (Council of Scientific and Industrial Research), Hyderabad, India

A small non-histone protein of budding yeast, Nhp6 has been reported to specifically influence the transcription of a yeast gene, *SNR6*. The gene is essential, transcribed by the enzyme RNA polymerase III, and codes for the U6snRNA required for mRNA splicing. A translationally positioned nucleosome on the gene body enables the assembly factor TFIIIC binding by juxtaposing its otherwise widely separated binding sites, boxes A and B. We found histone depletion results in the loss of U6 snRNA production. Changing the rotational phase of the boxes and the linear distance between them with deletions in 5 bp steps displayed a helical periodicity in transcription, which gradually reduced with incremental deletions up to 40 bp but increased on further deletions enclosing the pseudoA boxes. Nhp6 influences the transcription in a dose-dependent manner, which is modulated by its previously reported co-operator, an upstream stretch of seven T residues centered between the TATA box and transcription start site. Nhp6 occupancy on the gene *in vivo* goes up at least 2-fold under the repression conditions. Nhp6 absence, T_7 disruption, or shorter A–B box distance all cause the downstream initiation of transcription. The right +1 site is selected with the correct placement of TFIIIC before the transcription initiation factor TFIIIB. Thus, the T_7 sequence and Nhp6 help the assembly and placement of the transcription complex at the right position. Apart from the chromatin remodelers, the relative rotational orientation of the promoter elements in nucleosomal DNA, and Nhp6 regulate the transcription of the *SNR6* gene with precision.

Keywords: chromatin structure, Nhp6, pol III, rotational phase, T_7 element, U6 snRNA, transcription

OPEN ACCESS

Edited by:
Laxmi Narayan Mishra, Regeneron Pharmaceuticals, Inc., United States

Reviewed by:
Chhabi Govind, Oakland University, United States
Ralf Blossey, UMR8576 Unité de Glycobiologie Structurale et Fonctionnelle (UGSF), France

****Correspondence:***
Purnima Bhargava
purnima@ccmb.res.in

†Present Address:
Vinesh Vinayachandran, Division of Cardiovascular Biology, School of Medicine, Case Western Reserve University, Cleveland, Ohio

Specialty section:
This article was submitted to Epigenomics and Epigenetics, a section of the journal Frontiers in Genetics

Received: *07 February 2022*
Accepted: *08 April 2022*
Published: *13 May 2022*

Citation:
Vinayachandran V and Bhargava P (2022) Structural Features of the Nucleosomal DNA Modulate the Functional Binding of a Transcription Factor and Productive Transcription. Front. Genet. 13:870700. doi: 10.3389/fgene.2022.870700

INTRODUCTION

The packaging of the eukaryotic genome into chromatin affects all the DNA-templated processes. The *in vivo* chromatin structure often reflects on the recent transcription activity of a locus. Nucleosomal arrays are non-randomly punctuated by the nucleosome-free regions (NFRs), which are generally hotspots of high transcription activity, promoter and enhancer elements, replication origins, fragile genomic sites, etc. The U6 snRNA gene is one of the few examples where positioned nucleosomes have been shown to cause its transcriptional activation (Stnkel et al., 1997; Bhargava 2013). The gene is transcribed by RNA polymerase (pol) III, which transcribes short, non-coding genes such as 5S rRNA, U6snRNA (Didychuk et al., 2018), and tRNAs, which form the bulk of the pol III transcriptome. Although yeast tRNA genes are found in the NFR (Kumar and Bhargava 2013), the chromatin structure around these genes is shown to have a regulatory influence on their

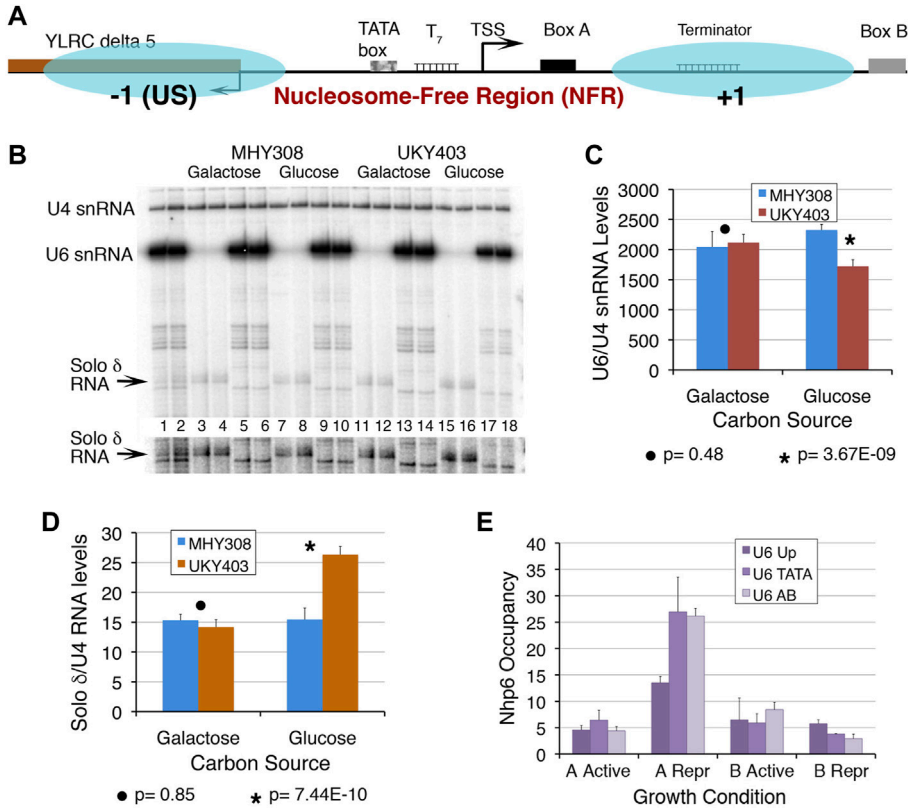

FIGURE 1 | Chromatin at the *SNR6* locus affects the U6 snRNA levels. **(A)** Schematic representation of the *SNR6* locus. Blue ovals show two positioned nucleosomes mapped earlier in the gene region (Arimbasseri and Bhargava 2008). Box B is found at the 3′-end of the gene body (+1) nucleosome whereas the −1 nucleosome is found upstream (US) of the TATA box at the −30 bp position. The TATA box, T_7 element, TSS (bent arrow), and box A are found in the NFR region. The US nucleosome by virtue of blocking the 5′ end of the Ty1 solo δ element (*YLRCδ5*) represses its expression. **(B)** A typical gel showing the primer extension products from duplicate samples. Disruption of the chromatin structure perturbs transcription at the *SNR6* locus. Yeast strains MHY308 and UKY403 (**Supplementary Table S1**) carry histone H4 genes under their own promoter or the *GAL1* promoter. When UKY403 cells are shifted to glucose for growth, H4 is depleted causing a loss of 50–60% of nucleosomes (Kim et al., 1988) by the time the cells get arrested. Cells were grown and processed for total RNA extraction as described earlier (Arimbasseri and Bhargava 2008). RNA was measured by the primer extension method using end-labeled gene-specific primers for cDNA synthesis in three independent experiments. U4 snRNA (pol II-transcribed) levels were used as the normalizer. Lanes 1 and 2 show primer extension products on total RNA from MHY308 and UKY403 using primers for U4, U6 snRNAs, and solo δ RNA, added together in the same extension reaction. Alternate pairs of the remaining lanes received primers of either solo δ (lanes 3, 4, 7, 8, 11, 12, 15 and 16) or U6 (lanes 5, 6, 9, 10, 13, 14, 17 and 18) along with the probe for U4 snRNA, which was used as the normalizer. A higher exposure of the gel area, cropped to visualize the solo δ RNA better, is given below the gel image. The significance of changes was confirmed by Student's two-tail *t*-test. The *p* values are given below the graphs. Quantification results for U6 snRNA **(C)** and solo δ RNA **(D)** showing average levels and scatter for four biological replicates. A large difference in the *y* axis scale is due to the very low level of solo δ RNA. **(E)** Occupancies of Nhp6A and B were measured at three parts of the *SNR6* locus in cells expressing HA-tagged Nhp6 A or B proteins. ChIP sample preparation, real-time PCR primers, amplicons, and fold enrichment calculation using TELVIR as the normalizer were as described earlier (Arimbasseri and Bhargava 2008). Samples were prepared from cells grown in an enriched medium (active) or under nutrient-deprivation (Repr; repressed) conditions.

transcription (Shukla and Bhargava 2018). The genes characteristically have intragenic promoter elements, boxes A and B (typically 50–60 bp apart in tRNA genes), to which the transcription factor (TF) IIIC binds in the first step and recruits the initiation factor TFIIIB in the next step, and pol III joins next (Geiduschek and Kassavetis 2001). Correct positioning of TFIIIB, for which box A is important, decides the transcription start site (TSS) to be selected (Gerlach et al., 1995).

The yeast U6snRNA (*SNR6*) gene has an unusual organization (**Figure 1A**) in having an upstream TATA box and an unusually long linear distance (202 bp) between box A and extragenic box B found downstream of the gene terminator (Brow and Guthrie 1990; Eschenlauer et al., 1993). The TATA box enables the TFIIIC-independent recruitment of TBP-containing TFIIIB and naked DNA (ND) transcription on *SNR6*. However, TFIIIC binding to boxes A and B is absolutely essential for chromatin transcription (Burnol et al., 1993). A positioned nucleosome brings the two boxes closer in space, situating them near the entry and exit points of DNA in the nucleosome (Shivaswamy et al., 2004; Arimbasseri and Bhargava 2008). Additionally, a stretch of 7 T residues, the T_7 element, centered between the TATA box and TSS (**Figure 1A**) is reported to support the role of a small non-histone protein Nhp6 in the pre-initiation complex (PIC) assembly on *SNR6* (Martin et al., 2001). Out of all pol III targets, yeast Nhp6 was shown to specifically influence *SNR6*. It activates the transcription of *SNR6*

in vitro and *in vivo* (Kruppa et al., 2001; Lopez et al., 2001; Martin et al., 2001). On tRNA genes, Nhp6 was shown to improve the fidelity of transcription and loading of the basal transcription factor TFIIIC (Kassavetis and Steiner 2006) with a reduction of non-specific transcriptions. Nhp6 was also found to influence the transcription of a subset of tRNA genes in a dose-dependent manner (Braglia et al., 2007). However, none of the studies probed the role of Nhp6 in the chromatin context, and the mechanism by which Nhp6 specifically activates *SNR6* remains unclear.

Nhp6 was reported to promote the pol II PIC assembly *in vivo* (Paull et al., 1996). Both Nhp6 and positioned nucleosomes are reported to influence the pol III PIC assembly involving the correct placement of TFIIIB and TFIIIC on the U6 snRNA gene (Kruppa et al., 2001; Lopez et al., 2001; Martin et al., 2001; Zhao et al., 2001; Shivaswamy and Bhargava 2006). The relative spatial orientation and distance between A and B boxes may influence the stability of simultaneous TFIIIC binding to them. As opposed to earlier genetic and *in vitro* transcription experiments, in this study, the role of Nhp6 in the transcriptional activation of *SNR6* is investigated under the aforementioned two conditions in the chromatin context. The distance between A and B boxes was reduced in 5 bp increments, which generated a shorter distance and a helical phase difference between them, causing a gradual reduction of transcription. We found that Nhp6 activates TFIIIC-dependent chromatin transcription in a T_7 stretch- and dose-dependent manner. Nhp6, together with the TATA box, T_7 element, and optimal distance between A and B boxes rightly positions the TFIIIC and TFIIIB, which results in accurate TSS selection along with transcriptional activation.

MATERIALS AND METHODS

Yeast Strains and Plasmid Templates

Yeast strains are described in **Supplementary Tables S1**. A total of 15 plasmids (named d5-d70 and dT_7) were derived from the plasmid pCS6 (**Supplementary Figures S1A, B** and **Supplementary Table S2**). Three of them, d25, d35, and d70 were not used for most of the experiments because of very low transcription from them. The histone H4 depletion strain UKY 403 and control strain MHY308 (gifts from Michael Grunstein) were grown till 0.8 OD_{600nm} in YEPGal and then in YEPD for 3 h before harvesting and RNA extraction as described earlier (Arimbasseri and Bhargava 2008).

ChIP and Real-Time Polymerase Chain Reaction

Yeast Nhp6A and B were HA-tagged at the C-terminal using the PCR toolbox (Janke et al., 2004). Both strains were used to measure Nhp6 occupancy over *SNR6* by using the ChIP and real-time PCR method (Arimbasseri and Bhargava 2008) as described earlier.

DNA Templates and *in vitro* Transcription

The recombinant Nhp6A protein, with the N-terminal 6XHis-tag, was purified using an overexpression clone (gift from David Stillman, United States). The chromatin was assembled using the well-established *Drosophila* embryonic S-190 extract system, which gives equally spaced nucleosomal arrays over plasmids (Shivaswamy et al., 2004). The *in vitro* transcription using lab stocks of pure proteins TFIIIC, pol III, and recombinant TFIIIB was carried out as described in detail earlier and the transcripts were visualized by the primer-extension method (Shivaswamy et al., 2004). All transcript yields were normalized with corresponding levels from pCS6 in each experiment. At least three or more independent experiments were performed for all the measurements. The *p*-values were calculated by two-tailed Student's t-test.

RESULTS

Chromatin is an Integral Part of *SNR6* Transcription *in vivo*

A positioned nucleosome between boxes A and B of the *SNR6* gene was shown to enable the binding of TFIIIC and high transcriptional activation *in vitro* (Shivaswamy et al., 2004). The nucleosome positioned upstream (US) of the TATA box is regulatory in nature (Arimbasseri and Bhargava 2008), where it also blocks the 5′end of a solo *δ* element (*YLRCdelta5*) (**Figure 1A**). The PIC assembly occurs in the NFR, which encompasses the TATA box, TSS, T_7 element, and box A (**Figure 1A**). We had earlier reported the loss of the overall chromatin organization at the *SNR6* locus under histone depletion conditions (Arimbasseri and Bhargava 2008). We found that under this condition, U6 snRNA levels are significantly reduced whereas the upstream solo *δ* element (pol II transcribed) is activated (**Figures 1B–D**), confirming that *SNR6* transcription requires a properly configured chromatin organization *in vivo*.

Nhp6, a protein belonging to the HMG1 class has two 89% identical isoforms in yeast Nhp6A and B (Stillman 2010). The Nhp6 presence has been reported earlier on the *SNR6* and some tRNA genes *in vivo* (Braglia et al., 2007). Our Nhp6 occupancy measurements by the ChIP and real-time PCR method found a similar enrichment of Nhp6A and Nhp6B on the TATA box and A–B box region of the *SNR6* gene locus (**Figure 1E**). Under starvation, the repression of pol III transcription (Moir and Willis 2013) is found to be accompanied by increased occupancy of specifically Nhp6A and a small loss of Nhp6B on the *SNR6* gene (**Figure 1E**). This suggests a repressive role of Nhp6A and a differential, non-redundant role of the Nhp6 isoforms on the *SNR6* gene.

Distance Between Boxes A and B Affects Transcription of the *SNR6* Gene

The deletion of 30–45 bp resulted in partial removal whereas longer deletions of 50 bp upwards in the complete removal of the pseudoA boxes (**Supplementary Table S2**). As expected, reducing the distance between the binding sites of TFIIIC resulted in somewhat periodic up and down levels of transcription (**Supplementary Figure S1C**), which reflect the

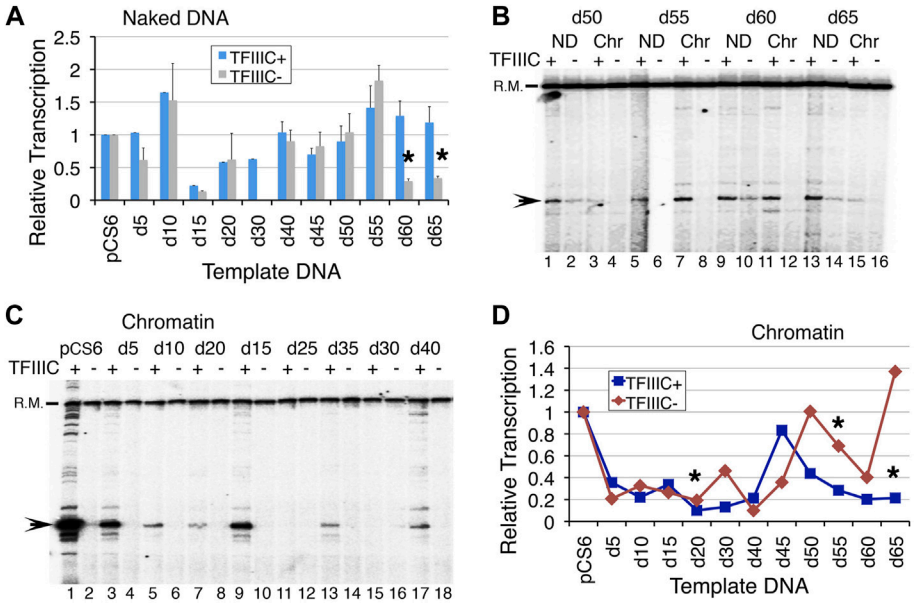

FIGURE 2 | Reducing the distance between boxes A and B in 5 bp increments affects *SNR6* transcription. Plasmids as naked DNA or assembled into chromatin were used as templates for *in vitro* transcription assays with or without the addition of pure TFIIIC. A radiolabeled probe of a non-U6 sequence externally added before transcript extraction was used as the recovery marker (R.M.) and normalizer. Positions of R. M. and U6 transcript are marked on the left-hand side of the gel images. Gels were scanned in a PhosphorImager machine and the Image Guage (Fuji) software was used for quantifications of the transcripts. **(A)** Average and scatter of the measured U6 transcripts from three independent experiments. All levels were normalized against the respective pCS6 transcription levels in the absence/presence of TFIIIC. Asterisks mark the significant differences between the TFIIIC- and TFIIIC + transcription for d60 ($p = 0.0016$) and d65 ($p = 0.0178$). **(B)** Comparison of transcription from chromatin (Chr) and naked DNA (ND) in the presence/absence of TFIIIC. ND shows transcripts from all but the chromatin is not equally repressed in each case. **(C)** Comparison of the transcription from chromatinized deletion clones in the presence and absence of TFIIIC. **(D)** Comparison of quantifications of chromatin transcription shows different expressions from all the deletion clones. All measurements were normalized against the respective pCS6 levels. Asterisks mark the significant changes for d20 ($p = 0.014$), d55 ($p = 0.023$), and d65 ($p = 0.004$).

changing helical phase of the DNA with deletions in 5 bp steps. TFIIIC- in dependent transcription was lowest for d15, d30, d60, and d65, while d10 and d55 were higher than pCS6 with/without TFIIIC (**Figure 2A**). The rest of the deletion clone NDs could be similarly transcribed with/without TFIIIC addition, staying below the pCS6 level (**Figure 2A**). This is not surprising since the transcription of *SNR6* ND is TFIIIC-independent. TFIIIC is known to slightly inhibit the naked pCS6 transcription. However, deleting one helical turn immediately next to the pseudoA boxes in the d10 plasmid gives ~1.5-fold gain of transcription, whereas deletions of 5 bp or more than 15 bp up to 50 bp deletion, return only ~60–90% of pCS6 transcription levels (**Figure 2A**). Interestingly, the transcription of d55–d65 increases to more than pCS6 levels with TFIIIC (**Figure 2B**, **Supplementary Figure S1C, D**). More than 50 bp deletions may reduce the linear distance between A and B boxes, but also constrain the steric flexibility of the intervening DNA, turning them out of phase on looping. Accordingly, d40–d55 are similarly transcribed with/without TFIIIC, and TFIIIC-dependent transcription increases for d55 whereas TFIIIC-independent transcription decreases for d60 and d65 with respect to the pCS6 level (**Figures 2A,B**, **Supplementary Figures S1C, D**). The increase on longer deletions with the deletion of the pseudoA boxes (**Supplementary Figure S1A**; **Supplementary Table S2**), suggests that the reduced TFIIIC-dependent transcription of pCS6 could be due to the sequestration of TFIIIC by the pseudoA boxes.

Phasing out of Boxes A and B Affects Transcription of the *SNR6* Chromatin

The chromatin transcription of the deletion clones with and without TFIIIC showed an undulating pattern (**Figures 2B–D**, **Supplementary Figures S1E, F**) with a gradual decrease of TFIIIC-dependent transcriptional activation (**Figure 2D**, **Supplementary Figure S1E**). A decrease in transcription was seen followed by an increase with every 5 bp deletion in the next step up to 50 bp deletions. As a 5 bp deletion reduces the distance from optimal to less optimal, boxes A and B also fall out of phase with each other. With the next 5bp deletion, the boxes may again come in phase, resulting in a gain of transcription, although not to the original level. Therefore, an alternating decrease and increase suggests a change in the phase as the reason behind the pattern, which could directly influence the simultaneous binding of the multi-subunit TFIIIC to its two widely separated binding sites.

Earlier studies reported that a 42-bp deletion between the terminator and B box (Δ42) reduces transcription from *SNR6* more than an 84-bp deletion (Δ84) could (Eschenlauer et al., 1993). In agreement with this, transcription was found at very low levels when 20–40 bp were deleted (**Figures 2C,D**), with the

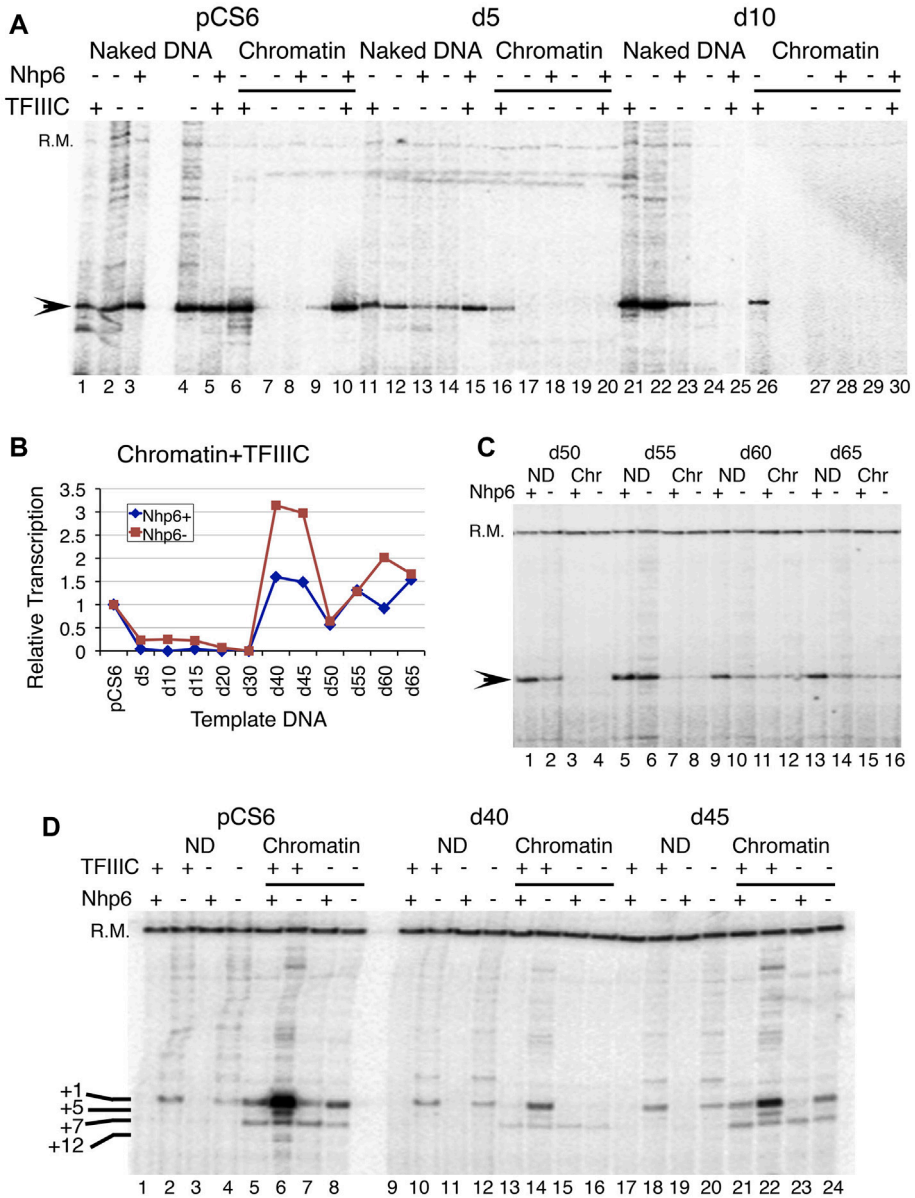

FIGURE 3 | Effect of Nhp6 on transcription of deletion clones. **(A)** Effect of a 180-ng Nhp6 addition on the transcription of naked and chromatinized pCS6, d5, and d10 plasmids *in vitro*. Nhp6 supports the TFIIIC-dependent transcription of pCS6 but not of d5 and d10. **(B)** Quantification results of Nhp6 effect on the chromatin transcriptions of pCS6 and all deletion clones in the presence of TFIIIC with (180 ng) and without Nhp6 are plotted. Measured transcript levels were obtained by first normalizing with the recovery marker (R.M.) and then with the corresponding pCS6 levels. **(C)** TFIIIC-dependent transcriptions of d50-d65 ND and chromatin (Chr) are compared in the presence (108 ng) and absence of Nhp6. **(D)** Comparison of transcription from the ND and chromatin pCS6, d40, and d45 templates with/without TFIIIC are shown. Added amount of Nhp6 was 120 ng. The recovery marker (R.M.) and downstream-initiated transcripts from +5, +7, and +12 bp positions are marked along with the +1 transcript on the left-hand side of the panel.

lowest observed levels from the d40 plasmid (**Supplementary Figure S1E**). Moreover, although TFIIIC-independent transcription increased with further deletions, the TFIIIC-dependent chromatin transcription remained lower than the pCS6 level (**Figures 2B,D**, **Supplementary Figure S1F**). In the absence of TFIIIC, the highest transcription was seen from d50, on both the chromatin and ND, but the highest activation was on the d45 chromatin (**Figure 2D**, **Supplementary Figure S1E**). Surprisingly, transcription from the d20, d30, and d50–d65 chromatin remains repressed with TFIIIC addition, suggesting severe compromise of TFIIIC binding to these templates (**Figures 2B–D**, **Supplementary Figure S1E**). The aforementioned results show a very subtle effect of the intervening DNA in the transcription of *SNR6* according to the gap length, DNA phase, and hence, the orientation of TFIIIC binding sites as discussed later. The results agree with earlier studies

suggesting TFIIIC-dependence of transcriptional activation by Nhp6.

Nhp6 Increases Fidelity and TFIIIC-Dependent Transcription

Nhp6 showed a dose-dependent effect on the *in vitro* chromatin transcription of a tRNA gene (Mahapatra et al., 2011). We found that the addition of 60 ng Nhp6 activated two of the templates, d40 and d45, more than two-fold (**Supplementary Figure S2A**). As the Nhp6 amount is increased further, chromatin activation in the presence of TFIIIC is reduced (**Supplementary Figure S2A**), suggesting that Nhp6 influences *SNR6* transcription in a dose-dependent manner. Nhp6 is reported to work through the stabilization of the TFIIIC-DNA complex (Kassavetis and Steiner 2006), which is essential for chromatin transcription. Much of the non-specific transcription from naked pCS6 is suppressed in the presence of TFIIIC or Nhp6, which together increased the initiation from the +1 site (**Figure 3A**, lanes 1–5). Similar to previous reports (Lopez et al., 2001), Nhp6 gave a 1.5- to 2-fold increase of the naked pCS6 transcription but inhibited d5-d15 ND or chromatin transcription with/without TFIIIC (**Figures 3A,B**, **Supplementary Figure S2B**). ND transcription of *SNR6* with further deletions could not be enhanced by Nhp6 without/with TFIIIC addition (**Figure 3C**, **Supplementary Figures S2C, D**). Surprisingly, Nhp6 activated d50 and d65 ND transcription by ~2- to 2.5-fold in the presence of TFIIIC (**Figure 3C**, **Supplementary Figure S2C**); their chromatin form is not activated by TFIIIC (**Figure 2D**).

Nhp6 Reduces TFIIIC-dependent Activation of Chromatin Transcription

No activation of chromatin by Nhp6 could be seen in the absence of TFIIIC (**Figures 3A–C**). TFIIIC binding to the repressed *SNR6* chromatin results in its high activation (Shivaswamy et al., 2004). On pCS6, ~10-fold TFIIIC-dependent activation of transcription is inhibited to ~2.4-fold with Nhp6 addition (**Figure 3D**, lanes 5 and 6). As compared with the pCS6 chromatin, comparatively lower activation with TFIIIC (**Figure 2**) is further reduced on shorter deletion clones by Nhp6 (**Figures 3A,B**). While on longer deletion clones, Nhp6 addition to the d40, d45, and d60 chromatin reduced the TFIIIC-dependent activation to almost pCS6 level, and d30, d50, and d65 were unaffected (**Figures 3B–D**). One reason for the observed differences in the Nhp6 effect on the longer deletion clones (**Figure 3B**) could be the differential effects of Nhp6 on their ND transcription (**Supplementary Figure S2C**).

We also noticed that chromatin formation on the deletion plasmids suppressed the +1 transcription, giving a downstream initiated transcript instead, which is seen in all the conditions (**Figure 3D**, chromatin lanes). On the d50 plasmid, which showed the lowest (of all longer deletion clones) activation of chromatin transcription with TFIIIC (**Figures 2B**, **3C**, **Supplementary Figure S2E**), Nhp6 addition could not restore the transcription from the right TSS (+1 transcript). The persistence of downstream initiation of transcription from the +7 bp position suggests altered TFIIIC and hence, TFIIIB placement upstream, which has been earlier suggested as the cause of different TSS selections in TATA box–A box double mutants (Eschenlauer et al., 1993).

The aforementioned results demonstrate that the Nhp6 effect is stronger on longer deletion clones where the pseudoA boxes are deleted and it generally represses the chromatin transcription in a TFIIIC-dependent manner. It appears that the pseudoA boxes may be serving as a guide to TFIIIC for binding to the upstream, right A boxes. Therefore, with a perturbation in TFIIIC binding in their absence, chromatin activation and right +1 site selection are both compromised on the plasmids d45–d65.

Nhp6 Requires the T_7 Promoter Element for Transcriptional Activation of *SNR6*

The T_7 promoter element, positioned between the TATA box and TSS is reported to co-operate with Nhp6 in the transcriptional activation of yeast *SNR6* (Martin et al., 2001). The chromatin transcription shows higher sensitivity to Nhp6 levels (**Figure 3**). Nhp6 clearly showed stronger inhibition of pCS6 than dT_7 transcription in a dose-dependent manner (**Supplementary Figure S3**), suggesting that the T_7 sequence may not be required for normal transcription but enhances the effects of Nhp6 on *SNR6*. In the presence of TFIIIC, Nhp6 suppresses the downstream transcription initiation from the pCS6 chromatin and dT_7 ND templates (**Figure 4A**, lanes 6 vs. 10 and 11 vs. 15). Consistent with the previously reported role of Nhp6 in increasing the transcriptional fidelity of PoI III on tRNA genes (Kassavetis and Steiner 2006; Mahapatra et al., 2011), Nhp6 could abolish downstream initiation of the pCS6 ND and chromatin. In contrast, transcription was completely inhibited by Nhp6 on the dT_7 chromatin (**Figure 4A**), suggesting a role for T_7 deletion in the chromatin repression. Thus, apart from the reported roles of TATA and A boxes (Gerlach et al., 1995), the T_7 stretch promoter element may also have a role in the TSS selection and TFIIIC binding.

As compared with ~1.9-fold Nhp6-dependent activation of ND transcription on pCS6, T_7 disruption returned only ~1.25-fold ($p < 0.1$) activation in the presence of TFIIIC (**Figure 4B**). With respect to pCS6+TFIIIC, ~0.7-fold ($p = 0.0082$) activation for dT_7 -TFIIIC resulted in repression (**Figure 4B**). TFIIIC absence and T_7 disruption influence Nhp6 similarly. Additive effects of the three components demonstrate that both Nhp6 and the T_7 element co-operate with TFIIIC to activate transcription on ND.

The Nhp6 effects on the TFIIIC-dependent dT_7 chromatin and ND transcription activation were opposite. The T_7 disruption gave ~2.7-fold gain ($p = 0.006$) of transcription in the absence of Nhp6 (**Figure 4C**), whereas Nhp6 addition significantly reduced this gain (cf. pCS6 and dT_7, Nhp6+ condition, **Figure 4C**) to only ~1.6-fold ($p = 0.028$), indicating a reduced TFIIIC binding to the dT_7 chromatin. Consistent with an earlier report (Martin et al., 2001), the results show that Nhp6 requires the T_7 element to manifest its influence fully on the transcription of *SNR6*.

The aforementioned results show that the T_7 sequence regulates the dose-dependent effects of Nhp6 on the TFIIIC-dependent chromatin transcription of the *SNR6* gene. Taken together, this

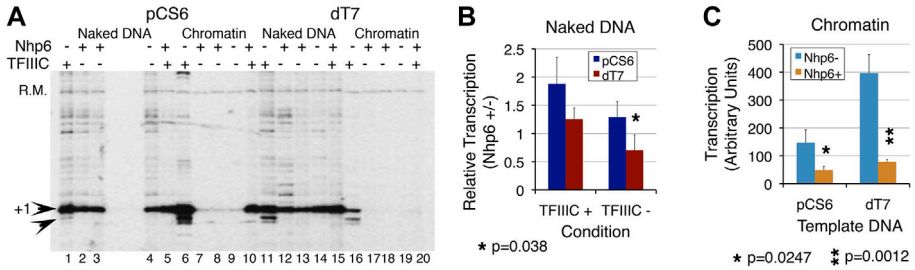

FIGURE 4 | T7 promoter element is required for transcription repression effects of Nhp6. Transcription of pCS6 and dT_7 was followed with or without Nhp6 addition (Nhp6+/–) in the presence/absence of TFIIIC. Measured transcript levels were obtained by normalizing with the recovery marker and the ratios of transcript levels in the presence/absence of Nhp6 were obtained separately for the transcription performed with/without TFIIIC (TFIIIC + or TFIIIC-) addition. **(A)** Nhp6 effect was followed with the addition of 108 ng Nhp6 in the lanes 3, 5, 8, and 10 for pCS6 and 13, 15, 18, and 20 for dT_7 templates. Arrowheads mark the position of transcripts initiated at +1 and +5 bp positions. Nhp6 abolishes background, non-specific transcription seen only in the presence of TFIIIC. The results were analyzed for ND and chromatin separately. Read-out of the Nhp6 effect for naked DNA **(B)** is given as the ratio of transcript yield in the presence/absence of Nhp6 (Nhp6 +/-). Values of ratios less than 1 denote repression by Nhp6 whereas those more than 1 denote activation, over the transcription level in the absence of Nhp6. The *p* values for measurements from 3–4 independent experiments are given; *p* value 0.038 compares the transcript levels from pCS6 and dT_7 in the absence of TFIIIC. In contrast to ~1.29-fold ($p = 0.13$) activation for pCS6, dT_7 transcription shows further 44% loss in the TFIIIC absence ($p = 0.032$). **(C)** Close to background chromatin transcription in the absence of TFIIIC gives high scatter in measurements. Because of this, only TFIIIC-dependent transcription in the absence or presence of Nhp6 was quantified. Nhp6 addition reduced the transcription similarly for pCS6 (3-fold, $p = 0.0247$) and dT_7 (~5-fold, $p = 0.0012$). Asterisk marks the significant differences; the *p* values are given at the bottom of the panels.

study has demonstrated that reducing the distance by short 5–40 bp deletions between the terminator and box B does not improve transcription; a longer deletion including extragenic pseudoA boxes does. Chromatin transcription from yeast *SNR6* is activated at lower and repressed at higher Nhp6 levels. Nhp6 increases transcription fidelity by abolishing non-canonical initiations in favor of +1 transcription. This transcriptional activation depends on TFIIIC and the cis promoter element T_7 stretch. Occupancy of specifically the Nhp6A isoform on the gene goes up under repression, attributing a repressive role to Nhp6 in keeping the highly active *SNR6* gene expression under check *in vivo*.

DISCUSSION

Distance Between Boxes A and B Influences Transcription From Chromatin

Reducing the distance between the terminator and box B may constrain the TFIIIC binding whenever the A–B boxes do not fall in phase. For a particular DNA sequence wound over the nucleosome surface, rotational positioning decides the DNA phase accessible for a DNA-binding factor (Albert et al., 2007), while proximity of the two far apart binding sites may become possible by the looping out of intervening naked DNA (Bhargava and Chaterji, 1992) and winding of nucleosomal DNA (Pusarla et al., 2007). The *SNR6* gene sequence directs the assembly of nucleosomes with unique rotational settings on the whole gene (Vinayachandran et al., 2009). The nucleosome between boxes A and B, which is both rotationally and translationally placed on the gene body, gives a clear 145-bp nucleosomal footprint (Shivaswamy and Bhargava 2006). Considering the possibility of change in this position with reduced spacing, the nucleosome may or may not support TFIIIC binding and interaction with the TFIIIB upstream. Our earlier measurements on a template with multiple operator sites for the binding of a lac repressor found that for a nucleosome to translationally and symmetrically position between two protein-binding sites, a minimum of 165 bp should be freely available such that a 145-bp core DNA length leaves 10 bp free DNA room from the protein binding sites at both ends (Pusarla et al., 2007). Therefore, we predict that the nucleosome position between A and B boxes may remain unaltered till 35 bp deletions, while on d40, d45, and d50 it may be difficult to fit in, which may hamper the juxtaposing of the boxes. This nay result in inefficient TFIIIC binding and loss of transcription, as observed in this study.

Further deletions may either include the A/B boxes in the core DNA wound over the nucleosome making TFIIIC/B binding non-productive, or the TFIIIC binding may exclude the nucleosome, alleviating the chromatin repression. The increase in TFIIIC-dependent ND transcription on d55, d60, and d65 plasmids may be explained by the absence of the interfering pseudoA boxes, whereas the opposite results on the chromatin may be the outcome of two effects. First, the TFIIIC binding may lead to nucleosome exclusion but a steric obstruction of the gene body may reduce transcription. Alternatively, in the TFIIIC absence, the nucleosome may be found only downstream of the +85 bp position, as seen earlier *in vivo* (Marsolier et al., 1995). This would enable the gene to be transcribed as naked DNA, without chromatin repression.

Nhp6 and T7 Effects on U6 Transcription are Manifested via TFIIIC and TFIIIB

The chromatin footprint on *SNR6* in a strain with deletion of 42 bp between boxes A and B, was found similar to that in a strain with a lethal point mutation on box B (Gerlach et al., 1995). The recognition of box A by TFIIIC in *SNR6* is reported to be an inefficient step during transcription complex assembly *in vitro* (Gerlach et al., 1995) and Nhp6A is shown to stabilize the TFIIIC-box A interaction (Kassavetis and Steiner 2006). A positive effect of Nhp6 specifically on *SNR6* transcription and synthetic lethality of Nhp6 with a 42 bp deletion between the terminator and box B, reducing the

distance between boxes A and B to the near subnucleosomal size (Kruppa et al., 2001; Lopez et al., 2001; Martin et al., 2001), synthetic lethality with *SNR6* TATA box mutations (Gerlach et al., 1995), and *nhp6ΔΔ* condition (Martin et al., 2001), all could be explained by increased TFIIIC binding and single-round transcription with Nhp6 addition to *SNR6 in vitro* (Kruppa et al., 2001). The *in vivo* chromatin structure altered around the TATA box region of *SNR6* in the nhp6ΔΔ cells was taken as an indication of altered TFIIIB binding, which could be a reason for the transcriptional repression of *SNR6* (Lopez et al., 2001). Therefore, the reduced transcription in deletion clones could be due to a loss or non-productive TFIIIC/TFIIIB binding to *SNR6*. This may be the reason that earlier a deletion of 42 bp between the terminator and box B showed synthetic lethality with several other promoter mutations in *SNR6* (Gerlach et al., 1995).

The T_7 mutations do not abolish the TFIIIB footprint but show lethality in the absence of Nhp6 (Martin et al., 2001). While the TATA box and T_7 stretch are found near the exit point of DNA in the US nucleosome, box A sits close to the DNA entry spot in the A–B box nucleosome. Nhp6 is generally found in the NFR near the entry/exit points of nucleosomal DNA (Dowell et al., 2010) and Nhp6A/B can cause looping and bending of DNA by at least 90° (Paull and Johnson 1995). Together, these observations raise the possibility that Nhp6 might be recruited to the T_7 stretch, just upstream of TSS and stabilize the TFIIIC interaction with box A in turn. This is consistent with the highest association of Nhp6 with TFIIIC, out of all the components of the pol III transcription complex (Bhalla et al., 2019; Shukla et al., 2021). The inherent rigidity of a stretch of T's confers inflexibility to DNA, which may allow their presence only at the entry/exit or dyad axis positions in the nucleosome. Thus, T_7 may interfere with the encroachment of NFR by the US regulatory nucleosome on *SNR6* (Arimbasseri and Bhargava 2008).

Nhp6 Influence on *SNR6* Transcription *in vivo* is Repressive

Transcription was found refractory to ~300 ng Nhp6, whereas after saturation at ~100 ng, higher Nhp6 additions inhibited chromatin transcription (Mahapatra et al., 2011). No transcription inhibition of *SNR6* ND was seen even up to 500-ng Nhp6 addition (Kruppa et al., 2001), whereas we found more than 180 ng Nhp6 as inhibitory for chromatin transcription *in vitro*. At lower levels, it caused even activation by enhancing the +1 transcription initiation. The requirement of both the upstream T_7 stretch and TFIIIC for transcription activation by Nhp6 implies a balancing role for the T_7 element in the dose-dependent effects of Nhp6. As Nhp6A is an abundant, non-sequence-specific DNA-binding protein, its effects may easily be dose-dependent *in vivo*. Increased Nhp6A occupancy on the *SNR6* gene under repression is consistent with a role for Nhp6 in further establishing the repressed chromatin state of *SNR6*.

Yeast *SNR6* is regulated by its unique chromatin organization and targeted by a plethora of epigenetic regulatory complexes (Bhargava 2013). This study shows that TFIIIC sequestration by pseudoA boxes, difficulty in chromatin formation, or TFIIIC binding due to distance/phase differences between A and B boxes also influence the *SNR6* transcription. The effects are individually small but subtle and significant when together. Enhancing transcription activation on the *SNR6* chromatin by Nhp6 is the outcome of a combined influence of TFIIIC and the T_7 element on chromatin transcription while T_7 stretch also affects TFIIIC binding. It appears that every part of the *SNR6* gene sequence has evolved with a unique role in fine-tuning its chromatin expression levels, making *SNR6* a specific target for Nhp6.

DATA AVAILABILITY STATEMENT

The original contributions presented in the study are included in the article and **Supplementary Files**, further inquiries can be directed to the corresponding author.

AUTHOR CONTRIBUTIONS

VV designed the strategy for deletions and constructed the plasmid clones, performed *in vitro* transcription assays, and collated the data. PB conceived the study, analyzed the data, generally supervised the experimental work, and wrote the manuscript.

FUNDING

This work was supported by the in-house institutional funding of CCMB-CSIR, Govt. of India. VV was a recipient of the CSIR Senior Research Fellowship.

ACKNOWLEDGMENTS

We thank David Stillman for the overexpression clone of His-tagged NHp6A and Michael Grunstein for the histone depletion strains.

SUPPLEMENTARY MATERIAL

The Supplementary Material for this article can be found online at: https://www.frontiersin.org/articles/10.3389/fgene.2022.870700/full#supplementary-material

REFERENCES

Albert, I., Mavrich, T. N., Tomsho, L. P., Qi, J., Zanton, S. J., Schuster, S. C., et al. (2007). Translational and Rotational Settings of H2A.Z Nucleosomes across the *Saccharomyces cerevisiae* Genome. *Nature* 446, 572–576. doi:10.1038/nature05632

Arimbasseri, A. G., and Bhargava, P. (2008). Chromatin Structure and Expression of a Gene Transcribed by RNA Polymerase III Are Independent of H2A.Z Deposition. *Mol. Cel. Biol.* 28, 2598–2607. doi:10.1128/MCB.01953-07

Bhalla, P., Vernekar, D. V., Gilquin, B., Couté, Y., and Bhargava, P. (2019). Interactome of the Yeast RNA Polymerase III Transcription Machinery Constitutes Several Chromatin Modifiers and Regulators of the Genes Transcribed by RNA Polymerase II. *Gene* 702, 205–214. doi:10.1016/j.gene.2018.12.037

Bhargava, P., and Chatterji, D. (1992). DNA Intervention in Transcriptional Activation. *FEBS Letts* 307, 245–248. doi:10.1016/0014-5793(92)80687-c

Bhargava, P. (2013). Epigenetic Regulation of Transcription by RNA Polymerase III. *Biochim. Biophys. Acta (Bba) - Gene Regul. Mech.* 1829, 1015–1025. doi:10.1016/j.bbagrm.2013.05.005

Braglia, P., Dugas, S. L., Donze, D., and Dieci, G. (2007). Requirement of Nhp6 Proteins for Transcription of a Subset of tRNA Genes and Heterochromatin Barrier Function in *Saccharomyces cerevisiae*. *Mol. Cel. Biol.* 27, 1545–1557. doi:10.1128/MCB.00773-06

Brow, D. A., and Guthrie, C. (1990). Transcription of a Yeast U6 snRNA Gene Requires a Polymerase III Promoter Element in a Novel Position. *Genes Dev.* 4, 1345–1356. doi:10.1101/gad.4.8.1345

Burnol, A.-F. o., Margottin, F., Huet, J., Almouzni, G., Prioleau, M.-N., Méchali, M., et al. (1993). TFIIIC Relieves Repression of U6 snRNA Transcription by Chromatin. *Nature* 362, 475–477. doi:10.1038/362475a0

Didychuk, A. L., Butcher, S. E., and Brow, D. A. (2018). The Life of U6 Small Nuclear RNA, from Cradle to Grave. *RNA* 24, 437–460. doi:10.1261/rna.065136.117

Dowell, N. L., Sperling, A. S., Mason, M. J., and Johnson, R. C. (2010). Chromatin-dependent Binding of the *S. cerevisiae* HMGB Protein Nhp6A Affects Nucleosome Dynamics and Transcription. *Genes Dev.* 24, 2031–2042. doi:10.1101/gad.1948910

Eschenlauer, J. B., Kaiser, M. W., Gerlach, V. L., and Brow, D. A. (1993). Architecture of a Yeast U6 RNA Gene Promoter. *Mol. Cel. Biol.* 13, 3015–3026. doi:10.1128/mcb.13.5.3015-3026.1993

Geiduschek, E. P., and Kassavetis, G. A. (2001). The RNA Polymerase III Transcription apparatus11Edited by P. E. Wright. *J. Mol. Biol.* 310, 1–26. doi:10.1006/jmbi.2001.4732

Gerlach, V. L., Whitehall, S. K., Geiduschek, E. P., and Brow, D. A. (1995). TFIIIB Placement on a Yeast U6 RNA Gene *In Vivo* Is Directed Primarily by TFIIIC rather Than by Sequence-specific DNA Contacts. *Mol. Cel. Biol.* 15, 1455–1466. doi:10.1128/MCB.15.3.1455

Janke, C., Magiera, M. M., Rathfelder, N., Taxis, C., Reber, S., Maekawa, H., et al. (2004). A Versatile Toolbox for PCR-Based Tagging of Yeast Genes: New Fluorescent Proteins, More Markers and Promoter Substitution Cassettes. *Yeast* 21, 947–962. doi:10.1002/yea.1142

Kassavetis, G. A., and Steiner, D. F. (2006). Nhp6 Is a Transcriptional Initiation Fidelity Factor for RNA Polymerase III Transcription *In Vitro* and *In Vivo*. *J. Biol. Chem.* 281, 7445–7451. doi:10.1074/jbc.M512810200

Kim, U. J., Han, M., Kayne, P., and Grunstein, M. (1988). Effects of Histone H4 Depletion on the Cell Cycle and Transcription of *Saccharomyces cerevisiae*. *EMBO J.* 7, 2211–2219. doi:10.1002/j.1460-2075.1988.tb03060.x

Kruppa, M., Moir, R. D., Kolodrubetz, D., and Willis, I. M. (2001). Nhp6, an HMG1 Protein, Functions in *SNR6* Transcription by RNA Polymerase III in *S. cerevisiae*. *Mol. Cel.* 7, 309–318. doi:10.1016/s1097-2765(01)00179-4

Kumar, Y., and Bhargava, P. (2013). A Unique Nucleosome Arrangement, Maintained Actively by Chromatin Remodelers Facilitates Transcription of Yeast tRNA Genes. *BMC Genomics* 14, 402. doi:10.1186/1471-2164-14-402

Lopez, S., Livingstone-Zatchej, M., Jourdain, S., Thoma, F., Sentenac, A., and Marsolier, M.-C. (2001). High-mobility-group Proteins NHP6A and NHP6B Participate in Activation of the RNA Polymerase III *SNR6* Gene. *Mol. Cel. Biol.* 21, 3096–3104. doi:10.1128/MCB.21.9.3096-3104.2001

Mahapatra, S., Dewari, P. S., Bhardwaj, A., and Bhargava, P. (2011). Yeast H2A.Z, FACT Complex and RSC Regulate Transcription of tRNA Gene through Differential Dynamics of Flanking Nucleosomes. *Nucleic Acids Res.* 39, 4023–4034. doi:10.1093/nar/gkq1286

Marsolier, M. C., Tanaka, S., Livingstone-Zatchej, M., Grunstein, M., Thoma, F., and Sentenac, A. (1995). Reciprocal Interferences between Nucleosomal Organization and Transcriptional Activity of the Yeast *SNR6* Gene. *Genes Dev.* 9, 410–422. doi:10.1101/gad.9.4.410

Martin, M. P., Gerlach, V. L., and Brow, D. A. (2001). A Novel Upstream RNA Polymerase III Promoter Element Becomes Essential when the Chromatin Structure of the Yeast U6 RNA Gene Is Altered. *Mol. Cel. Biol.* 21, 6429–6439. doi:10.1128/MCB.21.19.6429-6439.2001

Moir, R. D., and Willis, I. M. (2013). Regulation of Pol III Transcription by Nutrient and Stress Signaling Pathways. *Biochim. Biophys. Acta (Bba) - Gene Regul. Mech.* 1829, 361–375. doi:10.1016/j.bbagrm.2012.11.001

Paull, T. T., and Johnson, R. C. (1995). DNA Looping by *Saccharomyces cerevisiae* High Mobility Group Proteins NHP6A/B. *J. Biol. Chem.* 270, 8744–8754. doi:10.1074/jbc.270.15.8744

Paull, T. T., Carey, M., and Johnson, R. C. (1996). Yeast HMG Proteins NHP6A/B Potentiate Promoter-specific Transcriptional Activation *In Vivo* and Assembly of Preinitiation Complexes *In Vitro*. *Genes Dev.* 10, 2769–2781. doi:10.1101/gad.10.21.2769

Pusarla, R.-H., Vinayachandran, V., and Bhargava, P. (2007). Nucleosome Positioning in Relation to Nucleosome Spacing and DNA Sequence-specific Binding of a Protein. *FEBS J.* 274, 2396–2410. doi:10.1111/j.1742-4658.2007.05775.x

Shivaswamy, S., and Bhargava, P. (2006). Positioned Nucleosomes Due to Sequential Remodeling of the Yeast U6 Small Nuclear RNA Chromatin Are Essential for its Transcriptional Activation. *J. Biol. Chem.* 281, 10461–10472. doi:10.1074/jbc.M512425200

Shivaswamy, S., Kassavetis, G. A., and Bhargava, P. (2004). High-level Activation of Transcription of the Yeast U6 snRNA Gene in Chromatin by the Basal RNA Polymerase III Transcription Factor TFIIIC. *Mol. Cel. Biol.* 24, 3596–3606. doi:10.1128/MCB.24.9.3596-3606.2004

Shukla, A., and Bhargava, P. (2018). Regulation of tRNA Gene Transcription by the Chromatin Structure and Nucleosome Dynamics. *Biochim. Biophys. Acta (Bba) - Gene Regul. Mech.* 1861, 295–309. doi:10.1016/j.bbagrm.2017.11.008

Shukla, A., Bhalla, P., Potdar, P. K., Jampala, P., and Bhargava, P. (2021). Transcription-dependent Enrichment of the Yeast FACT Complex Influences Nucleosome Dynamics on the RNA Polymerase III-Transcribed Genes. *RNA* 27, 273–290. doi:10.1261/rna.077974.120

Stillman, D. J. (2010). Nhp6: a Small but Powerful Effector of Chromatin Structure in *Saccharomyces cerevisiae*. *Biochim. Biophys. Acta (Bba) - Gene Regul. Mech.* 1799, 175–180. doi:10.1016/j.bbagrm.2009.11.010

Stünkel, W., Kober, I., and Seifart, K. H. (1997). A Nucleosome Positioned in the Distal Promoter Region Activates Transcription of the Human U6 Gene. *Mol. Cel. Biol.* 17, 4397–4405. doi:10.1128/MCB.17.8.4397

Vinayachandran, V., Pusarla, R.-H., and Bhargava, P. (2009). Multiple Sequence-Directed Possibilities Provide a Pool of Nucleosome Position Choices in Different States of Activity of a Gene. *Epigenetics & Chromatin* 2, 4. doi:10.1186/1756-8935-2-4

Zhao, X., Pendergrast, P. S., and Hernandez, N. (2001). A Positioned Nucleosome on the Human U6 Promoter Allows Recruitment of SNAPc by the Oct-1 POU Domain. *Mol. Cel.* 7, 539–549. doi:10.1016/s1097-2765(01)00201-5

Conflict of Interest: The authors declare that the research was conducted in the absence of any commercial or financial relationships that could be construed as a potential conflict of interest.

Publisher's Note: All claims expressed in this article are solely those of the authors and do not necessarily represent those of their affiliated organizations, or those of the publisher, the editors, and the reviewers. Any product that may be evaluated in this article, or claim that may be made by its manufacturer, is not guaranteed or endorsed by the publisher.

frontiers | Frontiers in Cell and Developmental Biology

ORIGINAL RESEARCH
published: 16 June 2022
doi: 10.3389/fcell.2022.870815

On the Interaction Between SMARCAL1 and BRG1

*Deepa Bisht, Ketki Patne, Radhakrishnan Rakesh and Rohini Muthuswami**

Chromatin Remodeling Laboratory, School of Life Sciences, JNU, New Delhi, India

SMARCAL1 and BRG1, both classified as ATP-dependent chromatin remodeling proteins, play a role in double-strand break DNA damage response pathways. Mutations in SMARCAL1 cause Schimke Immuno-osseous Dysplasia (SIOD) while mutations in BRG1 are associated with Coffin-Siris Syndrome (CSS4). In HeLa cells, SMARCAL1 and BRG1 co-regulate the expression of *ATM*, *ATR,* and RNAi genes on doxorubicin-induced DNA damage. Both the proteins are found to be simultaneously present on the promoter of these genes. Based on these results we hypothesized that SMARCAL1 and BRG1 interact with each other forming a complex. In this paper, we validate our hypothesis and show that SMARCAL1 and BRG1 do indeed interact with each other both in the absence and presence of doxorubicin. The formation of these complexes is dependent on the ATPase activity of both SMARCAL1 and BRG1. Using deletion constructs, we show that the HARP domains of SMARCAL1 mediate interaction with BRG1 while multiple domains of BRG1 are probably important for binding to SMARCAL1. We also show that SIOD-associated mutants fail to form a complex with BRG1. Similarly, CSS4-associated mutants of BRG1 fail to interact with SMARCAL1, thus, possibly contributing to the failure of the DNA damage response pathway and pathophysiology associated with SIOD and CSS4.

Keywords: SMARCAL1-BRG1 interaction, SMARCAL1, BRG1, protein-protein interaction, SIOD, CSS4

OPEN ACCESS

Edited by:
Dileep Vasudevan,
Institute of Life Sciences (ILS), India

Reviewed by:
Arvind Panday,
Harvard Medical School, United States
Ann-Kristin Östlund Farrants,
Stockholm University, Sweden

****Correspondence:***
Rohini Muthuswami
rohini_m@mail.jnu.ac.in

Specialty section:
This article was submitted to Epigenomics and Epigenetics, a section of the journal Frontiers in Cell and Developmental Biology

Received: *07 February 2022*
Accepted: *30 May 2022*
Published: *16 June 2022*

Citation:
Bisht D, Patne K, Rakesh R and Muthuswami R (2022) On the Interaction Between SMARCAL1 and BRG1. Front. Cell Dev. Biol. 10:870815. doi: 10.3389/fcell.2022.870815

INTRODUCTION

The ATP-dependent chromatin remodeling proteins use the energy released from ATP hydrolysis to remodel nucleosomes, a process necessary for gene regulation as well as DNA damage repair (Osley et al., 2007; Clapier and Cairns, 2009; Hargreaves and Crabtree, 2011). The ATP-dependent chromatin remodeling proteins are grouped into helicases family due to the presence of seven helicase motifs that confer the DNA binding and ATP hydrolysis properties (Flaus et al., 2006). However, none of these proteins possess any helicase activity (Côté et al., 1994; Muthuswami et al., 2000). Instead, they use the energy liberated from ATP hydrolysis in altering the position of the nucleosome and maintaining chromatin architecture (Clapier and Cairns, 2009). The only exception is the INO80 complexes that show helicase activity due to the presence of Rvb1 and Rvb2 proteins (Shen et al., 2000; Conaway and Conaway, 2009). Phylogenetic analysis has identified six sub-families of which BRG1 is placed in the Snf2 class and SMARCAL1 has been classified as a distant member of the ATP-dependent chromatin remodeling protein family (Flaus et al., 2006).

BRG1 is a transcriptional modulator forming many complexes within the cell (Trotter and Archer, 2008). The protein also plays a role in DNA double-strand break repair where it is recruited to the break site via the interaction between bromodomain of BRG1 and acetylated H3 (Park et al., 2006; Lee et al., 2010; Kwon et al., 2015). This interaction is essential for remodeling nucleosomes at

the site of DNA damage and for spreading the acetylated H3 (Lee et al., 2010). BRG1 has been also shown to co-localize with γH2AX (Lee et al., 2010). Mutations in BRG1 are associated with lung, liver, prostate, breast, and pancreatic cancers (Wong et al., 2000; Reisman et al., 2003; Roy et al., 2015; Wu et al., 2017; Muthuswami et al., 2019; Wang et al., 2020). In addition, mutations in BRG1 also leads to Coffin-Siris Syndrome (CSS4), an autosomal dominant disorder, that is characterized by kidney abnormalities and azoospermia (Tsurusaki et al., 2012).

SMARCAL1 is an annealing helicase that promotes replication fork regression when double-strand breaks are induced in DNA (Bansbach et al., 2009; Postow et al., 2009; Bétous et al., 2012). During DNA damage the protein is recruited to the replication fork by RPA and the ATPase activity is used for re-annealing the single-stranded DNA. This protein too co-localizes with γH2AX (Bansbach et al., 2009; Ciccia et al., 2009). Mutations in SMARCAL1 cause Schimke Immuno-osseous Dysplasia (SIOD), an autosomal recessive disorder characterized by renal dysfunction, spondyloepiphyseal dysplasia, and T-cell immunodeficiency (Boerkoel et al., 2002).

Previously, we have shown that SMARCAL1 and BRG1 are co-regulated such that downregulation of SMARCAL1 results in reduced expression of BRG1 and downregulation of BRG1 results in repression of SMARCAL1 expression (Haokip et al., 2016). We further showed that this co-regulation is important for the functioning of the DNA damage response pathway as SMARCAL1 and BRG1 transcriptionally co-regulate the expression of *ATM* and *ATR* in HeLa cells (Sethy et al., 2018). They also co-regulate the expression of *DROSHA*, *DGCR8*, and *DICER*, thus, transcriptionally regulating the expression of damage response ncRNA that mediate the formation of 53BP1 foci (Patne et al., 2017).

The experimental evidence that both SMARCAL1 and BRG1 are present together on gene promoters led us to hypothesize that these proteins interact with each other forming a complex. In this paper, we present evidence that SMARCAL1 and BRG1 interact with each other both in the absence and presence of doxorubicin-induced DNA damage. We show that this interaction is dependent on the ATPase activity of both the ATP-dependent chromatin remodeling proteins. This interaction is abrogated in SIOD-associated and CSS4-associated mutants suggesting that the pleiotropic effects observed in SIOD and CSS4 patients could also stem from the impaired complex formation by SMARCAL1 and BRG1.

MATERIAL AND METHODS

Chemicals: All chemicals and reagents required for cell culture were purchased from Hi-media (United States). Sodium bicarbonate, Hoechst 33342, doxorubicin was purchased from Sigma-Aldrich (United States). Cell culture-grade dishes were purchased from Corning (Germany). For western blotting, PVDF membrane was purchased from Merck-Millipore (United States). X-ray sheets, fixer, and developer were purchased from Kodak (United States). Luminol, Coumaric acid, and hydrogen peroxide were purchased from Hi-media (United States). Turbofect was purchased from Thermo Scientific (United States). Protein G Beads was purchased from Merck-Millipore (United States).

Antibodies: Antibodies against BRG1 (Catalog #B8184) and γH2AX (Catalog #H5912) were purchased from Sigma-Aldrich

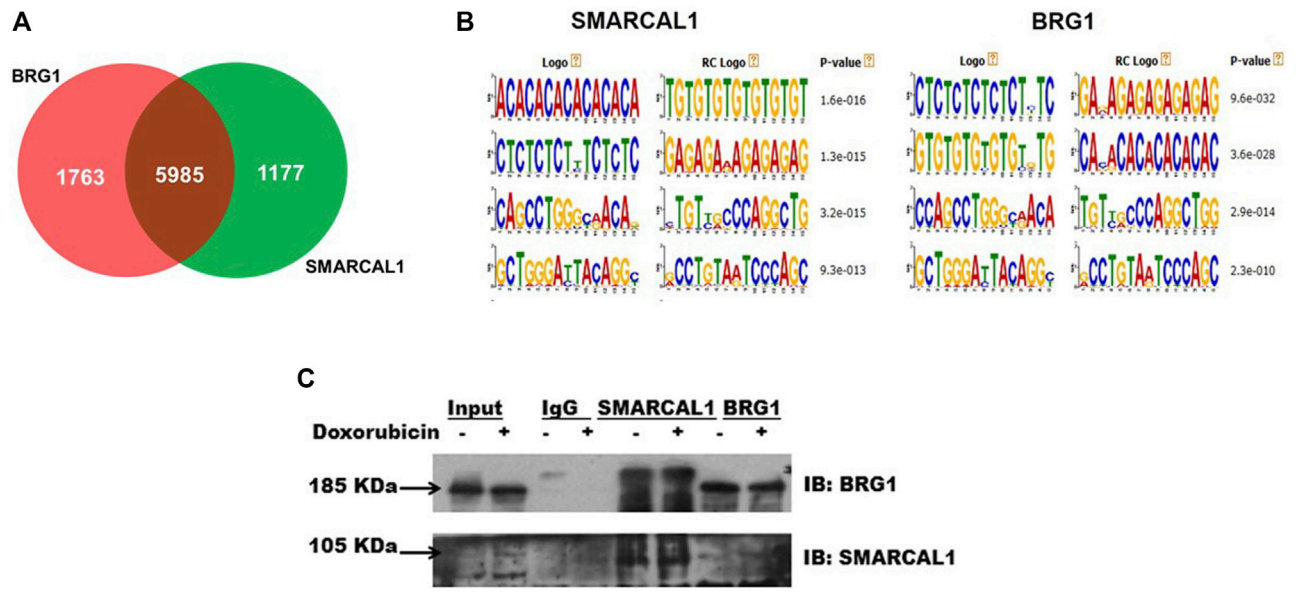

FIGURE 1 | SMARCAL1 and BRG1 co-immunoprecipitate, in the absence and presence of DNA damage: Genome-wide occupancy of SMARCAL1 and BRG1 identified by ChIP-seq analysis **(A)**. Venn diagram showing the intersection of the majority of genes **(B)**. Identical DNA motifs occupied by SMARCAL1 and BRG1 **(C)** Co-immunoprecipitation experiments were performed with anti SMARCAL1 and anti-BRG1 in untreated and treated protein samples with 2 μM doxorubicin for 10 min. The pull-down protein samples were probed for both proteins. IgG antibody was used for negative control. HeLa cells were used for the experiments. The experiment was performed using two independent biological samples and a representative blot has been included.

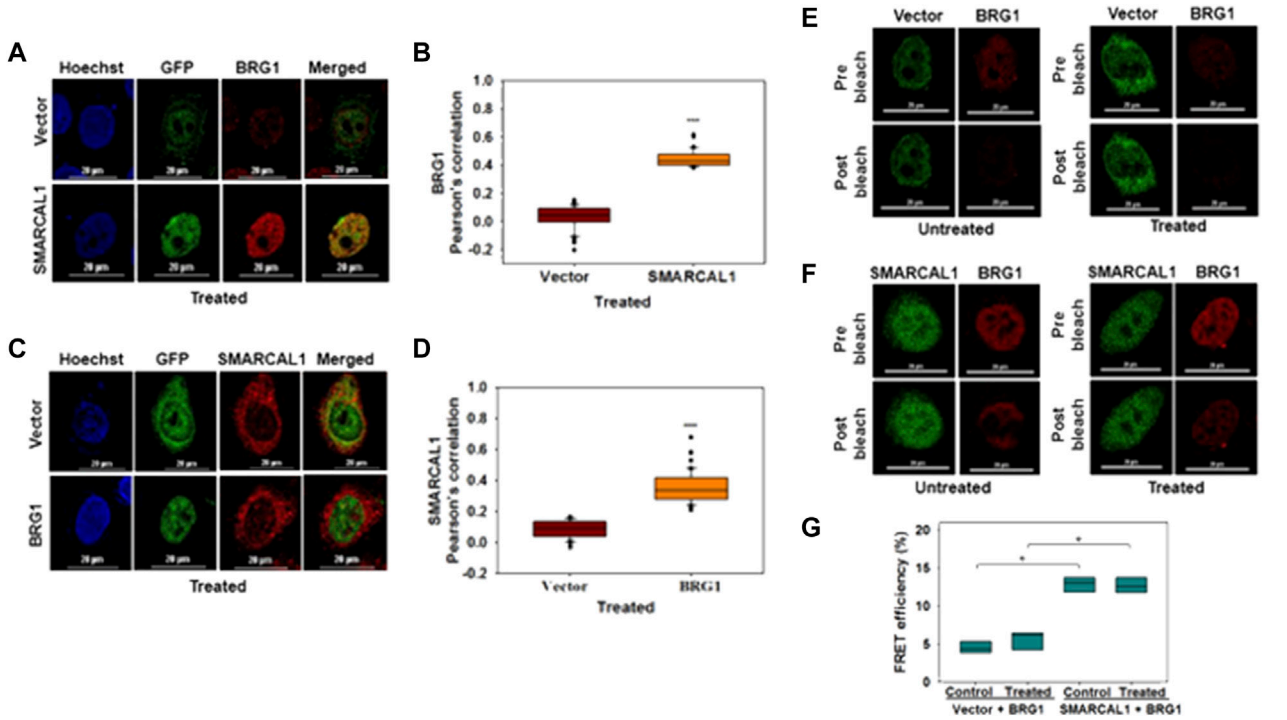

FIGURE 2 | SMARCAL1 and BRG1 interact with each other both in the absence and presence of DNA damage **(A)**. Co-localization between GFP-SMARCAL1 and endogenous BRG1 was monitored in the presence of doxorubicin-induced DNA damage in HeLa cells **(B)**. Pearson's coefficient for the co-localization of GFP SMARCAL1 with BRG1 **(C)**. Co-localization between GFP-BRG1 and endogenous SMARCAL1 was monitored in the presence of doxorubicin-induced DNA damage in HeLa cells **(D)**. Pearson's coefficient the interaction of GFP-BRG1 with SMARCAL1 **(E)**. Acceptor Photobleach FRET of GFP-vector alone signal after bleaching endogenous BRG1 in the absence and presence of doxorubicin treatment **(F)**. Acceptor photobleach FRET of GFP-SMARCAL1 signal after bleaching endogenous BRG1 in the absence and presence of doxorubicin treatment **(G)**. Quantitation of the FRET efficiency for the interaction of GFP-SMARCAL1 with BRG1. In all the co-localization experiments, HeLa cells were treated with 2 μM doxorubicin for 10 min and n ≥ 90 cells for GFP-SMARCAL1 and BRG1 and n ≥ 40 cells for GFP-BRG1 and SMARCAL1 were analyzed. In the FRET experiments, n ≥ 8 cells were analyzed and 2 μM doxorubicin treatment was given for 10 min. In the FRET experiments, n ≥ 8 cells were analyzed and 2 μM doxorubicin treatment was given for 10 min. Star indicates significance with **p*-value < 0.05, ***p*-value < 0.005, ****p* value <0.0001. The scale in the images is 20 μm.

(United States). SMARCAL1 antibody was custom raised against purified recombinant HARP1 domain (Catalog # 106014; Merck, India) (Haokip et al., 2016). TRITC and FITC-conjugated anti-mouse and anti-rabbit (Catalog# RTC2 and FTC3), as well as HRP-conjugated anti-rabbit IgG (Catalog#HPO3) and anti-mouse IgG (Catalog# HPO5) antibodies, were purchased from Merck (India).

Cell culture: HeLa and THP-1 cells, purchased from NCCS, Pune, were maintained in DMEM and RPMI media, respectively, containing 10% (v/v)) FBS and an antibiotic cocktail of penicillin, streptomycin, and amphotericin.

Co-immunoprecipitation: HeLa cells were grown to 70–80% confluency and resuspended in 300 μL of RIPA buffer (250 mM NaCl, 50 mM Tris. Cl pH 8.0, 2 mM EDTA, 1 mM PMSF, 1X protease inhibitor, 1% NP-40). After incubating at 4°C for 15 min, the cells were lysed by sonication (20 s ON; 30 s OFF- 10 cycles). The supernatant was obtained by centrifugation at 12,000 rpm for 30 min at 4°C. The process was repeated with the cell pellet and the combined supernatant was stored at −80°C till required.

The prepared extract was incubated with 20 μL protein G beads for 1 h at 4°C. After incubation, the supernatant was collected by centrifugation at 2000 rpm and quantified using Bradford reagent. 2 μg of antibodies was added to ~300 μg pre-cleared extract and incubated using a rotator at 4°C for 16 h. The next day, 20 μL protein G beads blocked with salmon sperm ssDNA and BSA was added to the extract-antibody mix and incubated for 4 h. The beads were then centrifuged at 2000 rpm and washed 4 times with lysis buffer. For analysis, the beads were boiled in Laemmli buffer (2% (v/v) SDS, 10% (v/v) glycerol, 60 mM Tris. Cl, pH 6.8) for 15 min. The supernatant was loaded on either 6 or 7% SDS polyacrylamide gel with a pre-stained loading marker and processed for western blotting.

Western Blotting: The gel was transferred on to PVDF membrane. After transfer, the membrane was washed 1X PBS buffer and blocked using 5% (w/v) BSA in 1X PBST (PBS containing 0.05% (v/v) Tween 20) for 1 h at 37°C. After blocking, the membrane was incubated with primary antibody solution with recommended dilution at 4°C overnight. The next day, the membrane was washed 4 times in 1X PBST for 5 min each on a rocker. The membrane was next incubated with secondary antibody solution (1:4000 dilution) for 1 h at 37°C. After incubation, the membrane was washed 4 times in 1X PBST for 5 min each on a rocker. A final wash was given with 1X PBS, and the membrane was developed using an Enhanced Chemiluminescence solution.

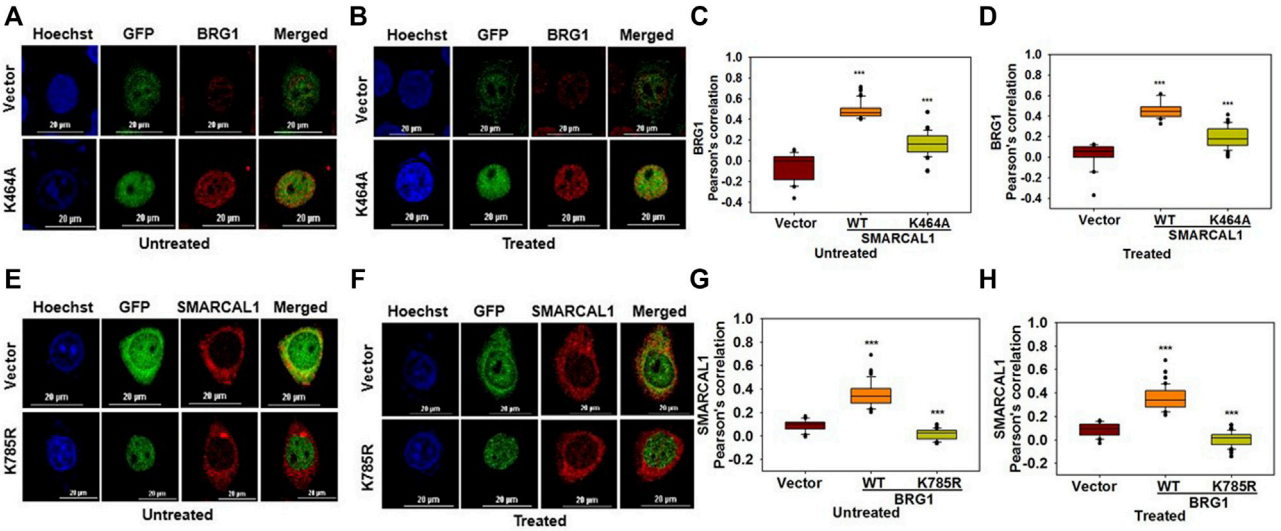

FIGURE 3 | The ATPase activity of SMARCAL1 and BRG1 is required for their co-localization **(A)**. Co-localization of GFP-SMARCAL1 K464A with BRG1 in the absence of doxorubicin treatment **(B)**. Co-localization of GFP-SMARCAL1 K464A with BRG1 in the presence of 2 μM doxorubicin treatment for 10 min **(C)**. Pearson's coefficient for the interaction in the absence of doxorubicin treatment **(D)**. Pearson's coefficient for the interaction in the presence of doxorubicin treatment **(E)**. Co-localization of GFP-BRG1 K785R with SMARCAL1 in the absence of doxorubicin treatment **(F)**. Co-localization of GFP-BRG1 K785R with SMARCAL1 in the presence of 2 μM doxorubicin treatment for 10 min **(G)**. Pearson's coefficient for the interaction in the absence of DNA damage **(H)** Pearson's coefficient for the interaction in the presence of DNA damage. In all these experiments, HeLa cells were treated with 2 μM doxorubicin for 10 min and n ≥ 40 cells for GFP-SMARCAL1 K464A and BRG1 and n ≥ 60 cells for GFP-BRG1 K785R and SMARCAL1 were analyzed. Star indicates significance with **p*-value < 0.05, ***p*-value < 0.005, ****p* value <0.0001. The wild-type data used in the analysis has been shown in **Figure 2** The scale in the images is 20 μm.

Oligonucleotides: The primers for cloning were designed from Ensemble Database and NCBI nucleotide and were synthesized from GCC Biotech (India). The primer sequences are provided in **Supplementary Table S1**.

Constructs: pcDNA3.1 Zeo-LAP-SMARCAL1 vector was cloned as explained in Haokip et al. (Haokip et al., 2016). BRG1 was sub-cloned from BJ5-BRG1 into pcDNA3.1 Zeo-LAP. Deletion constructs of SMARCAL1 and BRG1 were made using primers (**Supplementary Table S1**) spanning the deletion sites and amplified by PCR using Pfu DNA polymerase.

SMARCAL1 mutants corresponding to those observed in SIOD patients and BRG1 mutants corresponding to CSS4 patients were cloned as explained previously (Gupta et al., 2015; Sethy et al., 2018).

Transfections: HeLa cells were seeded in a 35 mm cell culture grade dish with a glass coverslip and incubated for 12 h so that they reached 60% confluency. THP-1 cells (10^6 cells/ml) were seeded 35 mm cell culture grade dish with a glass coverslip and differentiated using PMA. For each 35 mm dish, 1.5 μg plasmid DNA was mixed with 3 μL Turbofect reagent and transfection was done as per the manufacturer's instructions.

Immunofluorescence: For immunofluorescence, the cells were seeded on a coverslip placed inside the 35 mm dish. The cells were washed twice with 1X PBS and fixed with ice-cold acetone and methanol (1:1) for 15 min. The acetone: methanol solution was discarded and replaced with ice-cold 1X PBS added gently. After a brief incubation on ice, Triton X-100 (SRL India) at final concentration of 0.5% (v/v) was added for permeabilization. The cells were incubated in dark at 4°C for 10 min. After permeabilization, the coverslip was blocked using 2% (w/v) BSA for 1 h at 37°C. Subsequently, the coverslips were incubated with primary antibody solution (1:250) overnight at 4°C. The next day, the coverslip was washed 4–5 times in 1X PBS containing 0.2% Triton X-100 for 5 min each. After washing, the coverslip was incubated in secondary antibody (1:1000 dilution) solution and Hoechst 33,342 dye for 30–45 min at 37°C. The coverslips were washed 4–5 times with 1X PBS containing Triton X-100 for 5 min each and studied under a microscope.

Fixed cell FRET: These experiments were performed using Nikon A1R HD confocal microscope equipped with all four lasers (405, 488, 567, and 637 nm). The pictures were taken with a 60X objective lens with 1.5 times zoom. The pinhole was set at one Airy unit. The laser power was kept 100% for bleaching and 5% for capturing the image. The ROI was annotated, and a pre-bleached image was captured for 10 s using 488 and 561 nm lasers. The same area was bleached for the 30 s using 100% power of 561 nm laser. The post-bleached image was also captured using both the lasers used for pre-bleached images. The change in the pre-bleached and post-bleached donor intensities was measured using Nikon A1R analysis software. The FRET efficiencies were calculated using the formula (FRET efficiency = (1- Donor pre/ Donor post) and plotted with the help of Sigma plot version 10.0.

SMARCAL1 and BRG1 co-immunoprecipitate both in the absence and presence of DNA damage: The ChIP-sequencing were performed using HeLa cells. The raw reads of ChIP-sequencing data (GSE137250) were processed on the Galaxy (https://usegalaxy.org) platform. The adaptor sequences were trimmed from raw reads using trimmomatic (version 0.36.5), followed by quality control analysis using FastQC. The processed reads were aligned to the

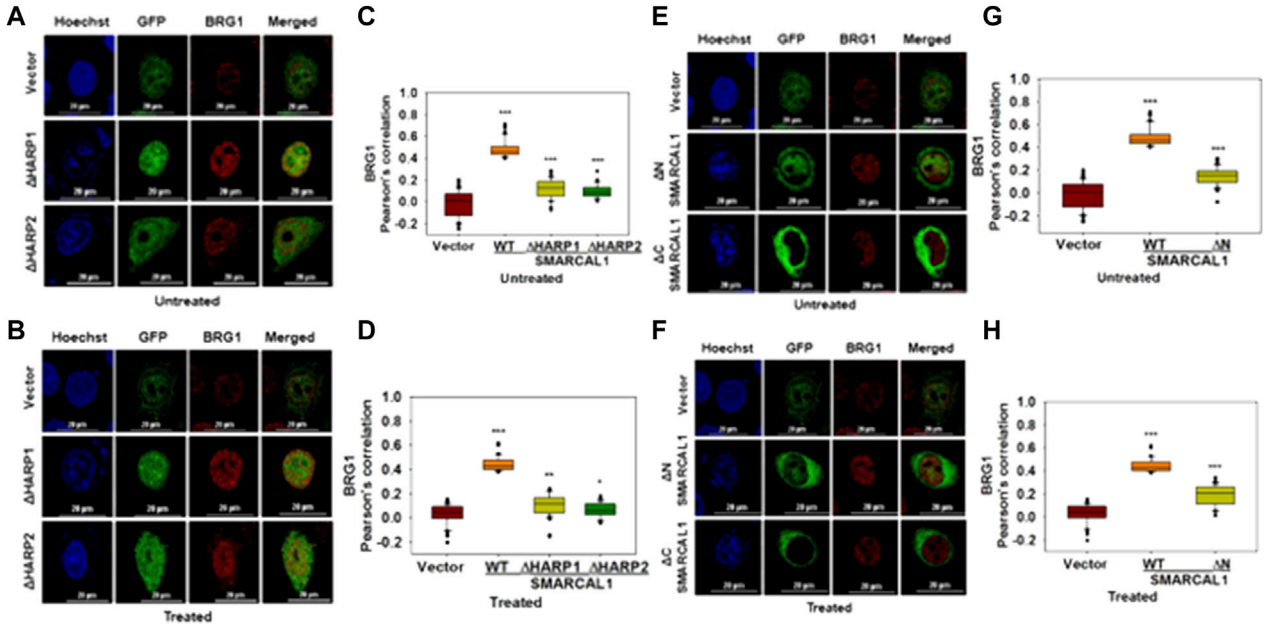

FIGURE 4 | HARP domains of SMARCAL1 are required for interaction with BRG1 **(A)**. Co-localization of GFP-ΔHARP1 and GFP-ΔHARP2 with BRG1 in the absence of doxorubicin treatment **(B)**. Co-localization of GFP-ΔHARP1 and GFP-ΔHARP2 with BRG1 in the presence of 2 μM doxorubicin treatment for 10 min **(C)**. Pearson's coefficient for the interaction of GFP-ΔHARP1 and GFP-ΔHARP2 with BRG1 in the absence of doxorubicin treatment **(D)**. Pearson's coefficient for the interaction of GFP-ΔHARP1 and GFP-ΔHARP2 with BRG1 in the presence of 2 μM doxorubicin treatment for 10 min **(E)**. Co-localization of GFP-ΔN and GPF-ΔC with endogenous BRG1 in the absence of doxorubicin treatment **(F)**. Co-localization of GFP-ΔN and GPF-ΔC with endogenous BRG1 in the presence of 2 μM doxorubicin treatment for 10 min **(G)**. Pearson's coefficient for the interaction of GFP-ΔN and GFP-ΔC with endogenous with BRG1 in the absence of doxorubicin treatment **(H)**. Pearson's coefficient for the interaction of GFP-ΔN and GFP-ΔC with endogenous with BRG1 in the presence of doxorubicin treatment. In all these experiments, HeLa cells were treated with 2 μM doxorubicin for 10 min and n ≥ 40 cells were analyzed. Star indicates significance with **p*-value < 0.05, ***p*-value < 0.005, ****p* value <0.0001. The wild-type data used in the analysis has been shown in **Figure 2**. The scale in the images is 20 μm.

reference genome (hg38) with the BOWTIE2 tool with default settings. The aligned files were marked for duplicates by PicardMarkduplicates and filtered on bit-wise flags by SAM tools on the Galaxy platform. Only paired-end reads that were mapped in proper pair were selected for peak calling. Biological replicates of SMARCAL1 and BRG1 were merged in a single BAM file before peak calling. Peak calling was performed by MACS2 (Version 2.1.1. 20160309.0) with default settings. Gene annotation and gene ontology was done using HOMER and clusterProfiler respectively. Venn diagrams were plotted using software (http://bioinformatics.psb.ugent.be/software).

The motif-based sequence analysis was performed with the FASTA format of the identified SMARCAL1 peaks using the MEME Suite tool (Bailey et al., 2009). The motif with the lowest E-value was selected for further study.

Statistical analysis: Statistical analyses were performed by SigmaPlot version 10. Pearson's correlation test was used to compare the distribution of data in studies.

RESULTS

SMARCAL1 and BRG1 co-immunoprecipitate, in the absence and presence of DNA damage: Analysis of the ChIP-seq data performed using HeLa cells (GSE137250) showed that SMARCAL1 was present on 7161 genes while BRG1 was present on 7747 genes. When all the genes occupied by both these proteins were compared and intersected, a set of 6000 genes were identified where both SMARCAL1 and BRG1 were found to be present (**Figure 1A**). Further, motif analysis using MEME-Suite showed SMARCAL1 and BRG1 to be present on either identical or similar DNA motifs across the various genomic locations. (**Figure 1B**). Experimentally, we had previously shown that SMARCAL1 and BRG1 are present simultaneously on *ATM*, *ATR*, *DROSHA*, *DGCR8*, and *DICER* promoters (Patne et al., 2017; Sethy et al., 2018). Based on these data, we hypothesized that SMARCAL1 and BRG1 interact with each other.

To test the hypothesis, we performed co-immunoprecipitation experiments in the absence and presence of doxorubicin using HeLa extracts. The study was performed with HeLa cells both in the absence and presence of doxorubicin. Doxorubicin intercalates between bases of DNA and impedes topoisomerase II movement. This results in double-strand break which is repaired by the double-strand break repair pathway (Yang et al., 2014; Yang et al., 2015).

Co-immunoprecipitation experiments showed that SMARCAL1 and BRG1 interact both in the absence and presence of doxorubicin-induced DNA damage (**Figure 1C**). Further, the interaction between SMARCAL1 and BRG1 was observed both in the absence and presence of apoptosis.

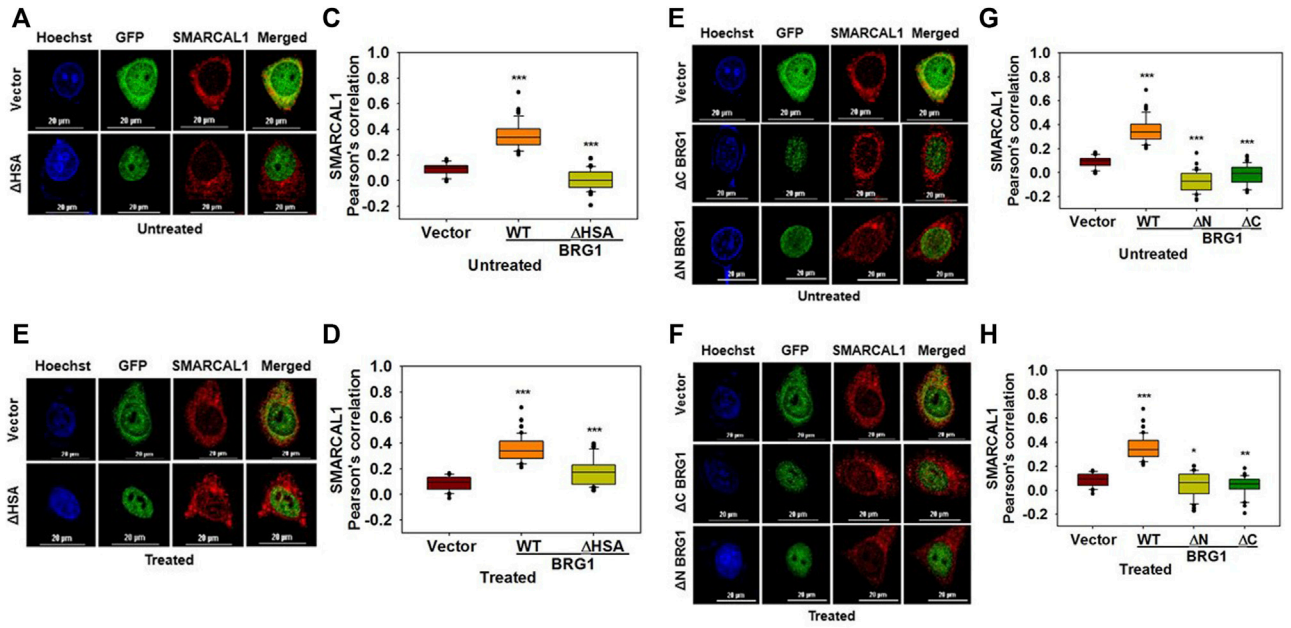

FIGURE 5 | Multiple regions of BRG1 are required for interaction with SMARCAL1 **(A)**. Co-localization of GFP- ΔHSA with endogenous SMARCAL1 in the absence of doxorubicin treatment **(B)** Co-localization of GFP- ΔHSA with endogenous SMARCAL1 in the presence of doxorubicin treatment **(C)**. Pearson's coefficient for the interaction of GFP-ΔHSA with endogenous SMARCAL1 in the absence of doxorubicin treatment **(D)**. Pearson's coefficient for the interaction of GFP-ΔHSA with endogenous SMARCAL1 in the presence of doxorubicin treatment **(E)**. Co-localization of GFP-ΔN and GFP-ΔC with endogenous SMARCAL1 was monitored in the absence of doxorubicin treatment **(F)**. Co-localization of GFP-ΔN and GFP-ΔC with endogenous SMARCAL1 was monitored in the presence of doxorubicin treatment **(G)**. Pearson's coefficient for the interaction of GFP-ΔN and GFP-ΔC with endogenous with SMARCAL1 in the absence of DNA damage **(H)**. Pearson's coefficient for the interaction of GFP-ΔN and GFP-ΔC with endogenous with SMARCAL1 in the presence of DNA damage. In all these experiments, HeLa cells were treated with 2 μM doxorubicin for 10 min and n ≥ 40 cells were analyzed. Star indicates significance with **p*-value < 0.05, ***p*-value < 0.005, ****p* value <0.0001. The wild-type data used in the analysis has been shown inFigure 2.The scale in the images is 20 μm.

SMARCAL1 and BRG1 interact with each other both in the absence and presence of DNA damage: The co-immunoprecipitation experiments do not provide information on whether these proteins are interacting directly or indirectly. Therefore, co-localization and FRET were used to delineate the interaction between BRG1-SMARCAL1 in the absence and presence of 2 μM doxorubicin. As the antibodies for SMARCAL1 and BRG1 were not compatible to screen for endogenous interaction, GFP-SMARCAL1 was overexpressed in HeLa cells and the interaction of the overexpressed protein with endogenous BRG1 was monitored. 48 h post-transfection, the cells were treated with 2 μM doxorubicin for 10 min.

As both SMARCAL1 and BRG1 have been shown to co-localize with γH2AX at the site of DNA damage, we have used this co-localization as a positive control for our studies (Park et al., 2006; Postow et al., 2009). Therefore, we first probed SMARCAL1-γH2AX and BRG1-γH2AX interactions by transfecting HeLa cells with constructs expressing either GFP-BRG1 or GFP-SMARCAL1. In untreated cells, γH2AX foci could not be detected whereas in 2 μM doxorubicin-treated cells γH2AX foci co-localized with both SMARCAL1 and BRG1. In contrast, no interaction was observed in cells transfected with empty GFP-vector in untreated as well as treated conditions (**Supplementary Figure 1A-D**).

Next, we probed the co-localization of SMARCAL1 and BRG1. HeLa cells were transfected with GFP-SMARCAL1, and co-localization studies showed that SMARCAL1 and BRG1 were present in proximity within the cell both in the absence and presence of DNA damage (**Supplementary Figure 2A** and **Figure 2A**, respectively). The Pearson's coefficient in the absence of DNA damage was 0.49 ± 0.08 while it was 0.46 ± 0.07 in the presence of DNA damage (**Supplementary Figure 2B** and **Figure 2B**, respectively), indicating that there is no change in co-localization as a function of DNA damage. Co-localization studies were performed in THP-1 cells also after differentiation using PMA. In this case, we found that BRG1 and SMARCAL1 co-localization was more prominent in the presence of DNA damage (**Supplementary Figure 3A-D**).

In the reverse experiment, HeLa cells were transfected with GFP-BRG1 and the interaction of the overexpressed protein with endogenous SMARCAL1 was studied. These experiments also showed that SMARCAL1 and BRG1 co-localize in the same space within the nucleus both in the absence and presence of doxorubicin-induced DNA damage (**Supplementary Figure 2C** and **Figure 2C** respectively). The Pearson's coefficient in the absence of DNA damage was 0.38 ± 0.12 while it was 0.37 ± 0.1 in the presence of DNA damage, once again indicating that the interaction did not alter as a function of DNA damage (**Supplementary Figure 2D** and **Figure 2D** respectively). A similar result was also obtained with THP-1 cells (**Supplementary Figure 3E-H**).

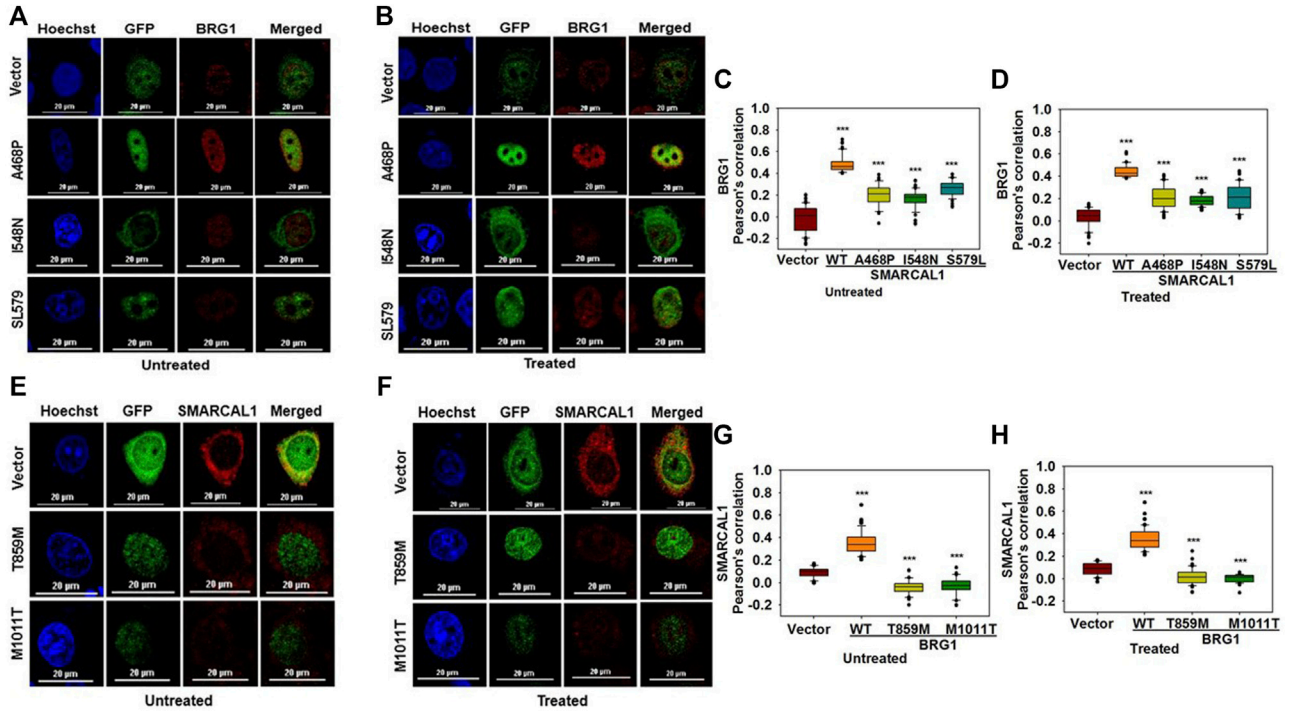

FIGURE 6 | Mutations associated with SIOD and CSS4 impairs the co-localization **(A)**. Co-localization of GFP-SMARCAL1-A468P, GFP-SMARCAL1-I548N, and GFP-SMARCAL1-S579L with BRG1 in the absence of doxorubicin treatment **(B)**. Co-localization of GFP-SMARCAL1-A468P, GFP-SMARCAL1-I548N, and GFP-SMARCAL1-S579L with BRG1 in the presence of 2 μM doxorubicin treatment for 10 min **(C)**. Pearson's coefficient for the interaction in the absence of doxorubicin treatment **(D)**. Pearson's coefficient for the interaction in the presence of doxorubicin treatment **(E)**. Co-localization of GFP-BRG1-T859M and GFP-BRG1-M1011T with SMARCAL1 in the absence of doxorubicin treatment **(F)**. Co-localization of GFP-BRG1-T859M and GFP-BRG1-M1011T with SMARCAL1 in the presence of doxorubicin treatment **(G)**. Pearson's coefficient for the interaction in the absence of doxorubicin treatment **(H)** Pearson's coefficient for the interaction in the presence of doxorubicin treatment. In all these experiments, HeLa cells were treated with 2 μM doxorubicin for 10 min and n ≥ 60 cells for GFP-SMARCAL1-A468P and BRG1, n ≥ 50 cells for GFP-SMARCAL1- I548N and BRG1, and n ≥ 90 cells for GFP-SMARCAL1-S579L and BRG1 were analyzed. Star indicates significance with **p*-value < 0.05, ***p*-value < 0.005, ****p* value <0.0001. The wild-type data used in the analysis has been shown in **Figure 2**. The scale in the images is 20 μm.

To further confirm the interaction we used acceptor photobleaching FRET (Shimi et al., 2004; Weems et al., 2015). The FRET experiment showed that GFP-SMARCAL1 and BRG1 interact with each other with a FRET efficiency of 12.84 ± 1.03% in the absence of DNA damage showing a statistically significant increase of approximately 3-fold as compared to the vector control (**Figures 2E,F**). The FRET efficiency in the presence of DNA damage the efficiency was 13.3 ± 2.72%, which was approximately 2-fold higher as compared to the vector control (**Figures 2E,F**). The FRET efficiency was also calculated in THP-1 cells also showed that GFP-SMARCAL1 and BRG1 interact with each other with a FRET efficiency of 68.2 ± 11.94% in control cells and 73.14 ± 13.23% in the presence of DNA damage (**Supplementary Figure 4A-C**). These FRET efficiencies were found to be statistically significant over the vector alone controls.

In the reverse experiment, BRG1 was overexpressed, and FRET with endogenous SMARCAL1 was monitored. Here, too, the FRET efficiency was 12.56 ± 1.04% in the absence of DNA damage and was 13.11 ± 2.16% in doxorubicin-treated cells (**Supplementary Figure 2E,F**). These FRET efficiencies were once again found to be statistically significant as compared to the vector control (**Supplementary Figure 2E,F**).

Thus, both the co-localization and FRET results suggest that SMARCAL1 and BRG1 physically interact with each other. This data has been used in all the further analyses.

The ATPase activity of SMARCAL1 and BRG1 is required for their co-localization: As both BRG1 and SMARCAL1 are ATP-dependent chromatin remodelers, the importance of their ATPase activity in mediating the interaction with each other was next investigated. To understand the importance of ATPase activity for the interaction, K464A mutant of SMARCAL1 and K785R mutant of BRG1 transfected into HeLa cells as these K464A in SMARCAL1 and K785R in BRG1 is required for ATPase activity of these proteins (Khavari et al., 1993; Gupta et al., 2015).

HeLa cells were transfected with GFP-SMARCAL1 K464A, as this mutant lacks ATPase activity (Gupta et al., 2015), and its interaction was studied with the endogenous wild-type BRG1. The co-localization showed a decrease in the interaction of SMARCAL1 K464A and BRG1 compared to the wild type SMARCAL1 and BRG1 both in the absence and presence of DNA damage (**Figure 3A–D**). Similarly, the co-localization between GFP-BRG1 K785R and endogenous wild-type SMARCAL1 also decreased significantly both in the absence and presence of DNA damage (**Figure 3E–H**).

The results show that the ATPase activity of both the proteins was needed for co-localization with each other.

The HARP domains of SMARCAL1 are required for interaction with BRG1: To delineate the domains of SMARCAL1 required for interaction with BRG1, four deletion constructs were made - ΔHARP1 lacking the HARP1 domain, ΔHARP2 lacking the HARP2 domain, ΔN lacking the entire N-terminal domain, and ΔC lacking the C-terminal domain containing the helicase motifs (**Supplementary Figure 5A**). Each of these mutants was transfected into HeLa cells and the interaction with BRG1 in the absence and presence of doxorubicin-induced DNA damage was studied using co-localization. Of the four deletion constructs, ΔC localized only to the cytoplasm both in the absence and presence of DNA damage (**Figure 4E,F**). It has been reported that a nuclear localization signal is presented within the helicase motifs (Coleman et al., 2000). Therefore, ΔC possibly lacks the signal to move into the nucleus. The interaction of BRG1 with ΔHARP1, ΔHARP2, and ΔN was found to be impaired with the Pearson's correlation maximally reduced in the case of ΔHARP2 deletion construct both in the absence and presence of DNA damage (**Figure 4A–H**), thus, indicating that the HARP domains might be playing an important role in SMARCAL1-BRG1 interaction.

Multiple regions of BRG1 are required for interaction with SMARCAL1: To study the interaction of BRG1 with SMARCAL1, three deletion constructs of BRG1 were made- ΔHSA lacking the HSA domain, ΔN lacking the entire N-terminus domain, and ΔC lacking the C-terminal domain containing the helicase motifs (**Supplementary Figure 5B**). Co-localization experiments showed that none of the deletion mutants of BRG1 were able to interact with SMARCAL1 both in the absence and presence of DNA damage (**Figure 5A–H**). Further, the Pearson's correlation values of BRG1 mutants were either equal to the vector-only control or showed a negative correlation (**Figure 5A–H**).

Thus, the HARP domains of SMARCAL1 are required for interaction with BRG1 while multiple regions of BRG1 possibly mediate the interaction with SMARCAL1.

Mutations associated with SIOD and CSS4 impairs the co-localization: Mutations in SMARCAL1 cause Schmike Immuno-osseous Dysplasia (SIOD) while mutations in BRG1 are associated with Coffin-Siris Syndrome (CSS4) (Boerkoel et al., 2002; Tsurusaki et al., 2012).

To understand whether mutations that cause SIOD also lead to loss of co-localization, we studied the interaction of three mutations present in SIOD patients-A468P, I548N, and S579L with BRG1. All these three mutants are present in the Rec A-like Domain1 and cannot hydrolyze ATP (Gupta et al., 2015). HeLa cells were transfected with constructs expressing these three mutant proteins and the co-localization with BRG1 was analyzed in the absence and presence of DNA damage. Experimental results showed that the co-localization between the mutant SMARCAL1 proteins and BRG1 decreased as compared to the wild-type SMARCAL1 and BRG1 both in the absence and presence of DNA damage (**Figure 6A–D**), suggesting that the mutations have impaired the interaction between the two proteins.

Next, to understand whether CSS4-associated mutants can interact with SMARCAL1, the co-localization of two CSS4-associated mutants-T859M and M1011T-with SMARCAL1 was studied. Experimental results showed that neither of the two mutant proteins was able to co-localize with SMARCAL1 or showed a negative correlation (**Figure 6E–H**).

Thus, mutations that cause SIOD4-or CSS4- lead to reduced co-localization, indicating that phenotypes observed in these syndromes might also be a consequence of the loss in protein-protein interaction.

DISCUSSION

The DNA damage response pathway begins with the sensing of the DNA damage, followed by the recruitment of proteins to the site of DNA damage. The ATP-dependent chromatin remodeling proteins are recruited to the site of DNA damage wherein they remodel the chromatin allowing for the repair process to occur. For example, RSC, an ATP-dependent chromatin remodeler in *S. cerevisiae*, has been found to be recruited to the DSB generated by HO endonuclease at the *MAT* locus wherein it mediates H2A phosphorylation as well as strand resection (Kent et al., 2007). INO80, another ATP-dependent chromatin remodeler, too has been shown to be recruited to DSB generated by HO endonuclease in *S. cerevisiae* (Tsukuda et al., 2005; Panday et al., 2015).

BRG1 and SMARCAL1, both members of the ATP-dependent chromatin remodeling protein family, are known to participate in the repair process. Both have been shown to co-localize with γH2AX, considered as one of the markers of DNA damage (Rogakou et al., 1998; Fillingham et al., 2006). Studies have shown that SMARCAL1 interacts with RPA (Ciccia et al., 2009) and mediates fork regression (Bétous et al., 2012) while BRG1 has been shown to modulate DNA double-strand break repair (Park et al., 2006; Lee et al., 2010; Qi et al., 2015). Studies have also shown that in HeLa cells, SMARCAL1 and BRG1 transcriptionally co-regulate each other on induction of doxorubicin-mediated DNA damage (Haokip et al., 2016). This transcriptional co-regulation is required for the recruitment of 53BP1 and thus, for DNA damage repair (Patne et al., 2017; Sethy et al., 2018).

In this paper, we have now shown that SMARCAL1 and BRG1 interact with each other directly both in the absence and presence of DNA damage. The HARP domains of SMARCAL1, which are known to mediate the annealing helicase activity of the protein (Ghosal et al., 2011), are needed for interaction with BRG1 and thus, suggesting that these domains might have an additional function in mediating the protein-protein interaction. In contrast, a single domain of BRG1 could not be identified. The experimental results demonstrate that multiple regions of the protein might be involved in the interaction with SMARCAL1.

The defining feature of the ATP-dependent chromatin remodeling proteins is the ATPase activity they exhibit in the presence of DNA/nucleosome substrate (Quinn et al., 1996; Muthuswami et al., 2000). The ATPase activity, we show, is also required for the protein-protein interaction both in the absence and presence of doxorubicin-induced DNA damage. Thus, the ATPase dead mutant of SMARCAL1, K464A (Gupta et al., 2015), fails to interact with BRG1. Similarly, the ATPase dead mutant of BRG1, K785R (Khavari et al., 1993), showed impaired interaction with

SMARCAL1. This was intriguing and led us to examine the interaction in SIOD-and CSS4-associated mutants. Co-localization studies showed that the interaction of the SIOD-associated mutants with BRG1 was impaired. Similarly, the CSS4-associated mutants showed impaired co-localization with SMARCAL1. The SIOD-associated mutants lie outside the HARP domain. Studies using ADAAD, the bovine homolog of SMARCAL1, have shown that these residues are needed for maintaining the global conformation of the protein (Gupta et al., 2015). Thus, the loss in the interaction with the cognate protein partner might be a consequence of the altered conformation of the mutant proteins.

The interaction of BRG1 and SMARCAL1 is interesting because both are ATP-dependent chromatin remodeling proteins. Though two ATP-dependent chromatin remodeling proteins have been shown to mediate gene regulation of the same subset of genes (Patne et al., 2017; Yang et al., 2017; Sethy et al., 2018), and proteomic studies have identified that two ATP-dependent chromatin remodeling proteins might be interacting (Rowbotham et al., 2011), this is the first study validating the interaction between two ATP-dependent chromatin remodeling proteins. We hypothesize that the interaction between the two proteins is required for transcriptional co-regulation of genes both in the absence and presence of DNA damage. The loss of interaction observed in both SIOD-associated and CSS4-associated mutants might be one of the reasons for the observed pathophysiology of these diseases.

The importance of the ATPase activity for this interaction is interesting but not surprising. Previously it has been shown that the ATPase activity of both BRG1 and SMARCAL1 is needed for the transcriptional regulation of *ATM*, *ATR*, *DROSHA*, *DGCR8* and *DICER* on induction of DNA damage by doxorubicin treatment in HeLa cells. ChIP-reChIP experiments showed that both BRG1 and SMARCAL1 are present simultaneously on the promoter (Haokip et al., 2016; Patne et al., 2017; Sethy et al., 2018). Further, mutations in the helicase motifs in SMARCAL1 have been shown to cause alterations in the protein conformation (Nongkhlaw et al., 2012; Gupta et al., 2015; Bansal et al., 2018). Thus, it is possible that the ATPase dead mutants of BRG1 and SMARCAL1 have altered protein conformation that precludes the interaction between them.

In the presence of DNA damage, BRG1 and SMARCAL1, possibly together, with γH2AX, mediate DNA damage response. Though now we know that SMARCAL1-γH2AX, BRG1-γH2AX, and SMARCAL1-BRG1 co-localize, this experimental setup did not allow us to show whether the proteins are present simultaneously at the site of DNA damage. Therefore, we can only hypothesize that the three proteins are possibly forming a trimeric complex at the site of DNA damage. The direct interaction between SMARCAL1-γH2AX or BRG1-γH2AX to form a trimeric complex needs to be confirmed in future. The other avenue for exploration is to delineate whether BRG1 in complex with SMARCAL1 and/or γH2AX is post-translationally modified. In our experiments, we found that SMARCAL1 pulls down BRG1 that is of higher molecular weight while this band is absent when the protein is immunoprecipitated with antibodies against γH2AX. BRG1 is known to be modified by ATM (Kwon et al., 2015). Further, pATM has been shown to co-localize with BRG1 on *ATM, ATR, DROSHA, DGCR8* and *DICER* promoters (Sethy et al., 2018). High-resolution mass spectrometry has also identified that BRG1 can be acetylated; however, the relevance of acetylation has not yet been understood (Choudhary et al., 2009). We, therefore, hypothesize that in the cells there could be at least two forms of BRG1 complex. In one complex, BRG1 is possibly post-translationally modified while in the other complex it is in unmodified form. For example, it is possible that on the promoters, where BRG1 is in the same space with SMARCAL1 and pATM, it is phosphorylated by ATM. Further experiments are needed to decipher the modification and the relevance with respect to function.

It has been recently shown that loss-of-function mutations in *Fancm* and *Brca1* leads to synthetic lethality (Panday et al., 2021). Like SMARCAL1, FANCM and BRCA1 are also required for repair of stalled replication fork. Studies have shown that depletion of SMARCAL1 in BRCA1/2 deficient cells leads to reduction in genomic instability (Taglialatela et al., 2017). It is, thus, possible that a similar synthetic lethality exists between SMARCAL1 and BRG1, that can be exploited for generation of small molecule inhibitors for cancer. Indeed, one such molecule, Active DNA-dependent ATPase A inhibitor (ADAADi) targets the ATPase domain of both SMARCAL1 and BRG1 and has been shown to be effective against breast cancer cells lines as well as prostate tumors developed in mouse models (Dutta et al., 2012; Wu et al., 2016; Muthuswami et al., 2019). Identification of many more such molecules might help in augmenting the repertoire of inhibitors leading to development of chemotherapeutic drugs.

DATA AVAILABILITY STATEMENT

The datasets presented in this study can be found in online repositories. The names of the repository/repositories and accession number(s) can be found below: https://www.ncbi.nlm.nih.gov/geo/, GSE137250.

AUTHOR CONTRIBUTIONS

Conceptualization, RM. Methodology, RM, RR, and DB; Investigation, DB, RR, and KP; Writing—original draft, RM, DB; Writing—review and editing, RM, and DB. Funding acquisition, RM; Supervision, RM.

FUNDING

This work was supported by grants from the Council of Scientific and Industrial Research (Grant # No. 37 (1696)/17/EMR-II) and Department of Biotechnology (BRB/PR10355/BRB/10/1342/2014) to RM. Additional support was provided by UPE-II, and DST-PURSE (PAC-JNU-DST-PURSE-462 (phase II)). DB and RR were supported by UGC non-net fellowship.

SUPPLEMENTARY MATERIAL

The Supplementary Material for this article can be found online at: https://www.frontiersin.org/articles/10.3389/fcell.2022.870815/full#supplementary-material

Bailey, T. L., Boden, M., Buske, F. A., Frith, M., Grant, C. E., Clementi, L., et al. (2009). MEME SUITE: Tools for Motif Discovery and Searching. *Nucleic Acids Res.* 37, W202–W208. doi:10.1093/nar/gkp335

Bansal, R., Arya, V., Sethy, R., Rakesh, R., and Muthuswami, R. (2018). RecA-Like Domain 2 of DNA-Dependent ATPase A Domain, a SWI2/SNF2 Protein, Mediates Conformational Integrity and ATP Hydrolysis. *Biosci. Rep.* 38, BSR20180568. doi:10.1042/BSR20180568

Bansbach, C. E., Bétous, R., Lovejoy, C. A., Glick, G. G., and Cortez, D. (2009). The Annealing Helicase SMARCAL1 Maintains Genome Integrity at Stalled Replication Forks. *Genes Dev.* 23, 2405–2414. doi:10.1101/gad.1839909

Bétous, R., Mason, A. C., Rambo, R. P., Bansbach, C. E., Badu-Nkansah, A., Sirbu, B. M., et al. (2012). SMARCAL1 Catalyzes Fork Regression and Holliday Junction Migration to Maintain Genome Stability during DNA Replication. *Genes Dev.* 26, 151–162. doi:10.1101/gad.178459.111

Boerkoel, C. F., Takashima, H., John, J., Yan, J., Stankiewicz, P., Rosenbarker, L., et al. (2002). Mutant Chromatin Remodeling Protein SMARCAL1 Causes Schimke Immuno-Osseous Dysplasia. *Nat. Genet.* 30, 215–220. doi:10.1038/ng821

Choudhary, C., Kumar, C., Gnad, F., Nielsen, M. L., Rehman, M., Walther, T. C., et al. (2009). Lysine Acetylation Targets Protein Complexes and Co-Regulates Major Cellular Functions. *Science* 325, 834–840. doi:10.1126/science.1175371

Ciccia, A., Bredemeyer, A. L., Sowa, M. E., Terret, M.-E., Jallepalli, P. V., Harper, J. W., et al. (2009). The SIOD Disorder Protein SMARCAL1 Is an RPA-Interacting Protein Involved in Replication Fork Restart. *Genes Dev.* 23, 2415–2425. doi:10.1101/gad.1832309

Clapier, C. R., and Cairns, B. R. (2009). The Biology of Chromatin Remodeling Complexes. *Annu. Rev. Biochem.* 78, 273–304. doi:10.1146/annurev.biochem.77.062706.153223

Coleman, M. A., Eisen, J. A., and Mohrenweiser, H. W. (2000). Cloning and Characterization of HARP/SMARCAL1: A Prokaryotic HepA-Related SNF2 Helicase Protein from Human and Mouse. *Genomics* 65, 274–282. doi:10.1006/geno.2000.6174

Conaway, R. C., and Conaway, J. W. (2009). The INO80 Chromatin Remodeling Complex in Transcription, Replication and Repair. *Trends Biochem. Sci.* 34, 71–77. doi:10.1016/j.tibs.2008.10.010

Côté, J., Quinn, J., Workman, J. L., and Peterson, C. L. (1994). Stimulation of GAL4 Derivative Binding to Nucleosomal DNA by the Yeast SWI/SNF Complex. *Science* 265, 53–60.

Dutta, P., Tanti, G. K., Sharma, S., Goswami, S. K., Komath, S. S., Mayo, M. W., et al. (2012). Global Epigenetic Changes Induced by SWI2/SNF2 Inhibitors Characterize Neomycin-Resistant Mammalian Cells. *PLoS One* 7, e49822. doi:10.1371/journal.pone.0049822

Fillingham, J., Keogh, M.-C., and Krogan, N. J. (2006). γH2AX and its Role in DNA Double-Strand Break repairThis Paper Is One of a Selection of Papers Published in This Special Issue, Entitled 27th International West Coast Chromatin and Chromosome Conference, and Has Undergone the Journal's Usual Peer Review Process. *Biochem. Cell Biol.* 84, 568–577. doi:10.1139/o06-072

Flaus, A., Martin, D. M. A., Barton, G. J., and Owen-Hughes, T. (2006). Identification of Multiple Distinct Snf2 Subfamilies with Conserved Structural Motifs. *Nucleic Acids Res.* 34, 2887–2905. doi:10.1093/nar/gkl295

Ghosal, G., Yuan, J., and Chen, J. (2011). The HARP Domain Dictates the Annealing Helicase Activity of HARP/SMARCAL1. *EMBO Rep.* 12, 574–580. doi:10.1038/embor.2011.74

Gupta, M., Mazumder, M., Dhatchinamoorthy, K., Nongkhlaw, M., Haokip, D. T., Gourinath, S., et al. (2015). Ligand-Induced Conformation Changes Drive ATP Hydrolysis and Function in SMARCAL1. *FEBS J.* 282, 3841–3859. doi:10.1111/febs.13382

Haokip, D. T., Goel, I., Arya, V., Sharma, T., Kumari, R., Priya, R., et al. (2016). Transcriptional Regulation of ATP-Dependent Chromatin Remodeling Factors: SMARCAL1 and BRG1 Mutually Co-Regulate Each Other. *Sci. Rep.* 6, 20532. doi:10.1038/srep20532

Hargreaves, D. C., and Crabtree, G. R. (2011). ATP-Dependent Chromatin Remodeling: Genetics, Genomics and Mechanisms. *Cell Res.* 21, 396–420. doi:10.1038/cr.2011.32

Kent, N. A., Chambers, A. L., and Downs, J. A. (2007). Dual Chromatin Remodeling Roles for RSC during DNA Double Strand Break Induction and Repair at the Yeast MAT Locus. *J. Biol. Chem.* 282, 27693–27701. doi:10.1074/jbc.M704707200

Khavari, P. A., Peterson, C. L., Tamkun, J. W., Mendel, D. B., and Crabtree, G. R. (1993). BRG1 Contains a Conserved Domain of the SWI2/SNF2 Family Necessary for Normal Mitotic Growth and Transcription. *Nature* 366, 170–174. doi:10.1038/366170a0

Kwon, S.-J., Park, J.-H., Park, E.-J., Lee, S.-A., Lee, H.-S., Kang, S. W., et al. (2015). ATM-Mediated Phosphorylation of the Chromatin Remodeling Enzyme BRG1 Modulates DNA Double-Strand Break Repair. *Oncogene* 34, 303–313. doi:10.1038/onc.2013.556

Lee, H.-S., Park, J.-H., Kim, S.-J., Kwon, S.-J., and Kwon, J. (2010). A Cooperative Activation Loop Among SWI/SNF, γ-H2AX and H3 Acetylation for DNA Double-Strand Break Repair. *EMBO J.* 29, 1434–1445. doi:10.1038/emboj.2010.27

Muthuswami, R., Bailey, L., Rakesh, R., Imbalzano, A. N., Nickerson, J. A., and Hockensmith, J. W. (2019). BRG1 is a Prognostic Indicator and a Potential Therapeutic Target for Prostate Cancer. *J. Cell. Physiol.* 234, 15194–15205. doi:10.1002/jcp.28161

Muthuswami, R., Truman, P. A., Mesner, L. D., and Hockensmith, J. W. (2000). A Eukaryotic SWI2/SNF2 Domain, an Exquisite Detector of Double-Stranded to Single-Stranded DNA Transition Elements. *J. Biol. Chem.* 275, 7648–7655. doi:10.1074/jbc.275.11.7648

Nongkhlaw, M., Gupta, M., Komath, S. S., and Muthuswami, R. (2012). Motifs Q and I are Required for ATP Hydrolysis but Not for ATP Binding in SWI2/SNF2 Proteins. *Biochemistry* 51, 3711–3722. doi:10.1021/bi2014757

Osley, M. A., Tsukuda, T., and Nickoloff, J. A. (2007). ATP-Dependent Chromatin Remodeling Factors and DNA Damage Repair. *Mutat. Res.* 618, 65–80. doi:10.1016/j.mrfmmm.2006.07.011

Panday, A., Willis, N. A., Elango, R., Menghi, F., Duffey, E. E., Liu, E. T., et al. (2021). FANCM Regulates Repair Pathway Choice at Stalled Replication Forks. *Mol. Cell* 81, 2428–2444. e6. doi:10.1016/j.molcel.2021.03.044

Panday, A., Xiao, L., and Grove, A. (2015). Yeast High Mobility Group Protein HMO1 Stabilizes Chromatin and is Evicted during Repair of DNA Double Strand Breaks. *Nucleic Acids Res.* 43, 5759–5770. doi:10.1093/nar/gkv498

Park, J.-H., Park, E.-J., Lee, H.-S., Kim, S. J., Hur, S.-K., Imbalzano, A. N., et al. (2006). Mammalian SWI/SNF Complexes Facilitate DNA Double-Strand Break Repair by Promoting γ-H2AX Induction. *EMBO J.* 25, 3986–3997. doi:10.1038/sj.emboj.7601291

Patne, K., Rakesh, R., Arya, V., Chanana, U. B., Sethy, R., Swer, P. B., et al. (2017). BRG1 and SMARCAL1 Transcriptionally Co-Regulate DROSHA, DGCR8 and DICER in Response to Doxorubicin-Induced DNA Damage. *Biochim. Biophys. Acta* 1860, 936–951. doi:10.1016/j.bbagrm.2017.07.003

Postow, L., Woo, E. M., Chait, B. T., and Funabiki, H. (2009). Identification of SMARCAL1 as a Component of the DNA Damage Response. *J. Biol. Chem.* 284, 35951–35961. doi:10.1074/jbc.M109.048330

Qi, W., Wang, R., Chen, H., Wang, X., Xiao, T., Boldogh, I., et al. (2015). BRG1 Promotes DNA Double-Strand Break Repair by Facilitating the Replacement of RPA with RAD51. *J. Cell Sci.* 128, 317–330. doi:10.1242/jcs.159103

Quinn, J., Fyrberg, A. M., Ganster, R. W., Schmidt, M. C., and Peterson, C. L. (1996). DNA-Binding Properties of the Yeast SWI/SNF Complex. *Nature* 379, 844–847. doi:10.1038/379844a0

Reisman, D. N., Sciarrotta, J., Wang, W., Funkhouser, W. K., and Weissman, B. E. (2003). Loss of BRG1/BRM in Human Lung Cancer Cell Lines and Primary Lung Cancers: Correlation with Poor Prognosis. *Cancer Res.* 63, 560–566.

Rogakou, E. P., Pilch, D. R., Orr, A. H., Ivanova, V. S., and Bonner, W. M. (1998). DNA Double-Stranded Breaks Induce Histone H2AX Phosphorylation on Serine 139. *J. Biol. Chem.* 273, 5858–5868. doi:10.1074/jbc.273.10.5858

Rowbotham, S. P., Barki, L., Neves-Costa, A., Santos, F., Dean, W., Hawkes, N., et al. (2011). Maintenance of Silent Chromatin through Replication Requires SWI/SNF-Like Chromatin Remodeler SMARCAD1. *Mol. Cell* 42, 285–296. doi:10.1016/j.molcel.2011.02.036

Roy, N., Malik, S., Villanueva, K. E., Urano, A., Lu, X., Von Figura, G., et al. (2015). Brg1 Promotes Both Tumor-Suppressive and Oncogenic Activities at Distinct Stages of Pancreatic Cancer Formation. *Genes Dev.* 29, 658–671. doi:10.1101/gad.256628.114

Sethy, R., Rakesh, R., Patne, K., Arya, V., Sharma, T., Haokip, D. T., et al. (2018). Regulation of ATM and ATR by SMARCAL1 and BRG1. *Biochim. Biophys. Acta Gene Regul. Mech.* 1861, 1076–1092. doi:10.1016/j.bbagrm.2018.10.004

Shen, X., Mizuguchi, G., Hamiche, A., and Wu, C. (2000). A Chromatin Remodelling Complex Involved in Transcription and DNA Processing. *Nature* 406, 541–544. doi:10.1038/35020123

Shimi, T., Koujin, T., Segura-Totten, M., Wilson, K. L., Haraguchi, T., and Hiraoka, Y. (2004). Dynamic Interaction between BAF and Emerin Revealed by FRAP, FLIP, and FRET Analyses in Living HeLa Cells. *J. Struct. Biol.* 147, 31–41. doi:10.1016/j.jsb.2003.11.013

Taglialatela, A., Alvarez, S., Leuzzi, G., Sannino, V., Ranjha, L., Huang, J.-W., et al. (2017). Restoration of Replication Fork Stability in BRCA1- and BRCA2-Deficient Cells by Inactivation of SNF2-Family Fork Remodelers. *Mol. Cell* 68, 414–430. e8. doi:10.1016/j.molcel.2017.09.036

Trotter, K. W., and Archer, T. K. (2008). The BRG1 Transcriptional Coregulator. *Nucl. Recept Signal* 6, e004. doi:10.1621/nrs.06004

Tsukuda, T., Fleming, A. B., Nickoloff, J. A., and Osley, M. A. (2005). Chromatin Remodelling at a DNA Double-Strand Break Site in *Saccharomyces C. Nature* 438, 379–383. doi:10.1038/nature04148

Tsurusaki, Y., Okamoto, N., Ohashi, H., Kosho, T., Imai, Y., Hibi-Ko, Y., et al. (2012). Mutations Affecting Components of the SWI/SNF Complex Cause Coffin-Siris Syndrome. *Nat. Genet.* 44, 376–378. doi:10.1038/ng.2219

Wang, P., Song, X., Cao, D., Cui, K., Wang, J., Utpatel, K., et al. (2020). Oncogene-Dependent Function of BRG1 in Hepatocarcinogenesis. *Cell Death Dis.* 11, 91. doi:10.1038/s41419-020-2289-3

Weems, J. C., Slaughter, B. D., Unruh, J. R., Hall, S. M., McLaird, M. B., Gilmore, J. M., et al. (2015). Assembly of the Elongin A Ubiquitin Ligase is Regulated by Genotoxic and Other Stresses. *J. Biol. Chem.* 290, 15030–15041. doi:10.1074/jbc.M114.632794

Wong, A. K., Shanahan, F., Chen, Y., Lian, L., Ha, P., Hendricks, K., et al. (2000). BRG1, a Component of the SWI-SNF Complex, Is Mutated in Multiple Human Tumor Cell Lines. *Cancer Res.* 60, 6171–6177.

Wu, Q., Lian, J. B., Stein, J. L., Stein, G. S., Nickerson, J. A., and Imbalzano, A. N. (2017). The BRG1 ATPase of Human SWI/SNF Chromatin Remodeling Enzymes as a Driver of Cancer. *Epigenomics* 9, 919–931. doi:10.2217/epi-2017-0034

Wu, Q., Sharma, S., Cui, H., LeBlanc, S. E., Zhang, H., Muthuswami, R., et al. (2016). Targeting the Chromatin Remodeling Enzyme BRG1 Increases the Efficacy of Chemotherapy Drugs in Breast Cancer Cells. *Oncotarget* 7, 27158–27175. doi:10.18632/oncotarget.8384

Yang, F., Kemp, C. J., and Henikoff, S. (2015). Anthracyclines Induce Double-Strand DNA Breaks at Active Gene Promoters. *Mutat. Res.* 773, 9–15. doi:10.1016/j.mrfmmm.2015.01.007

Yang, F., Teves, S. S., Kemp, C. J., and Henikoff, S. (2014). Doxorubicin, DNA Torsion, and Chromatin Dynamics. *Biochim. Biophys. Acta* 1845, 84–89. doi:10.1016/j.bbcan.2013.12.002

Yang, P., Oldfield, A., Kim, T., Yang, A., Yang, J. Y. H., and Ho, J. W. K. (2017). Integrative Analysis Identifies Co-Dependent Gene Expression Regulation of BRG1 and CHD7 at Distal Regulatory Sites in Embryonic Stem Cells. *Bioinformatics* 33, 1916–1920. doi:10.1093/bioinformatics/btx092

Conflict of Interest: The authors declare that the research was conducted in the absence of any commercial or financial relationships that could be construed as a potential conflict of interest.

Publisher's Note: All claims expressed in this article are solely those of the authors and do not necessarily represent those of their affiliated organizations, or those of the publisher, the editors and the reviewers. Any product that may be evaluated in this article, or claim that may be made by its manufacturer, is not guaranteed or endorsed by the publisher.

frontiers | Frontiers in Genetics

REVIEW
published: 24 June 2022
doi: 10.3389/fgene.2022.914404

DNA N6-Methyladenine Modification in Eukaryotic Genome

Hao Li[1,2,3†], *Ning Zhang*[1,2,3†], *Yuechen Wang*[1,4], *Siyuan Xia*[1,4], *Yating Zhu*[1], *Chen Xing*[1], *Xuefeng Tian*[1,2] *and Yinan Du*[1]*

[1]School of Basic Medical Sciences, Anhui Medical University, Hefei, China, [2]First School of Clinical Medicine, Anhui Medical University, Hefei, China, [3]First Affiliated Hospital of Anhui Medical University, Hefei, China, [4]Second School of Clinical Medicine, Anhui Medical University, Hefei, China

DNA methylation is treated as an important epigenetic mark in various biological activities. In the past, a large number of articles focused on 5 mC while lacking attention to N6-methyladenine (6 mA). The presence of 6 mA modification was previously discovered only in prokaryotes. Recently, with the development of detection technologies, 6 mA has been found in several eukaryotes, including protozoans, metazoans, plants, and fungi. The importance of 6 mA in prokaryotes and single-celled eukaryotes has been widely accepted. However, due to the incredibly low density of 6 mA and restrictions on detection technologies, the prevalence of 6 mA and its role in biological processes in eukaryotic organisms are highly debated. In this review, we first summarize the advantages and disadvantages of 6 mA detection methods. Then, we conclude existing reports on the prevalence of 6 mA in eukaryotic organisms. Next, we highlight possible methyltransferases, demethylases, and the recognition proteins of 6 mA. In addition, we summarize the functions of 6 mA in eukaryotes. Last but not least, we summarize our point of view and put forward the problems that need further research.

Keywords: methylation, DNA modification, N6-methyladenine, eukaryotic genome, epigenetics

OPEN ACCESS

Edited by:
Dileep Vasudevan, Institute of Life Sciences (ILS), India

Reviewed by:
Fengquan Zhou, Johns Hopkins Medicine, United States
Tao P. Wu, Baylor College of Medicine, United States
Natalia de Miguel, CONICET Instituto Tecnológico de Chascomús (INTECH), Argentina

***Correspondence:**
Yinan Du
duyinannan@126.com

†These authors have contributed equally to this work

Specialty section:
This article was submitted to Epigenomics and Epigenetics, a section of the journal Frontiers in Genetics

Received: *06 April 2022*
Accepted: *08 June 2022*
Published: *24 June 2022*

Citation:
Li H, Zhang N, Wang Y, Xia S, Zhu Y, Xing C, Tian X and Du Y (2022) DNA N6-Methyladenine Modification in Eukaryotic Genome. Front. Genet. 13:914404. doi: 10.3389/fgene.2022.914404

INTRODUCTION

DNA methylation is one of the most important epigenetic modifications, and is involved in various biological progresses. Previously, research mainly focused on 5-methylcytosine (5 mC). 5 mC is the earliest and best-studied DNA methylation modification in eukaryotes and for most eukaryotes, the abundance of 5 mC in CpGs is over 50% (Chen et al., 2018; Schmitz et al., 2019). In vertebrates, the detected 5 mC level of CpGs is over 70% (Feng et al., 2010). 5 mC is widely involved in transcription suppression, transposon suppression, genomic imprinting, X chromosome inactivation, and epigenetic memory (Bird, 2002; Chen et al., 2016; Wu and Zhang, 2017). Compared with 5 mC N6-methyladenine (6 mA) was considered to exist only in prokaryotes for a long time and has recently been discovered in some eukaryotes with a low prevalence. In prokaryotes, 6 mA plays an important role in distinguishing host DNA from exogenous DNA (Razin, 1984) and controls many biological functions, such as DNA replication, transcription, mismatch repair, chromosome replication, nucleoid organization and segregation, phase variation, bacterial conjugation, and bacterial virulence (Reisenauer et al., 1999; Wion and Casadesús, 2006; Vasu and Nagaraja, 2013). With the development of detection techniques, 6 mA was reported to be present in an increasing number of eukaryotes, including *Chlamydomonas* (Fu et al., 2015), *C. elegans* (Greer et al., 2015; Ma et al., 2019), *Tetrahymena* (Wang et al., 2017), ciliates (Beh et al., 2019), fungi(Mondo et al., 2017), *Arabidopsis Thaliana* (Liang et al., 2018), rice(Zhou et al., 2018), *Drosophila* (Zhang et al.,

TABLE 1 | Advantages and disadvantages of 6 mA detection methods.

Detection methods	Sensitivity	Specificity	Detecting at single-base resolution	Implement ability	Weaknesses
6 mA-IPseq	relatively low	low	no	relatively low cost, easy to conduct	interferences of m1A, m6A, and enrichment of unmethylated DNA fragments
6 mA-REseq	relatively low	high	yes	relatively low cost, easy to conduct	limitation of specific restriction sites
HPLC-MS/MS	high	high	no	relatively complex operation, a requirement for instrument	possible bacterial contamination of enzymes
SMRT	high	relatively low	yes	incredibly costly	interferences of 1 and 6 mA, high false positive rate
Deep leaning	relatively high	relatively high	yes	low cost, save time	low confidence, limitations of the model derived from experimental data

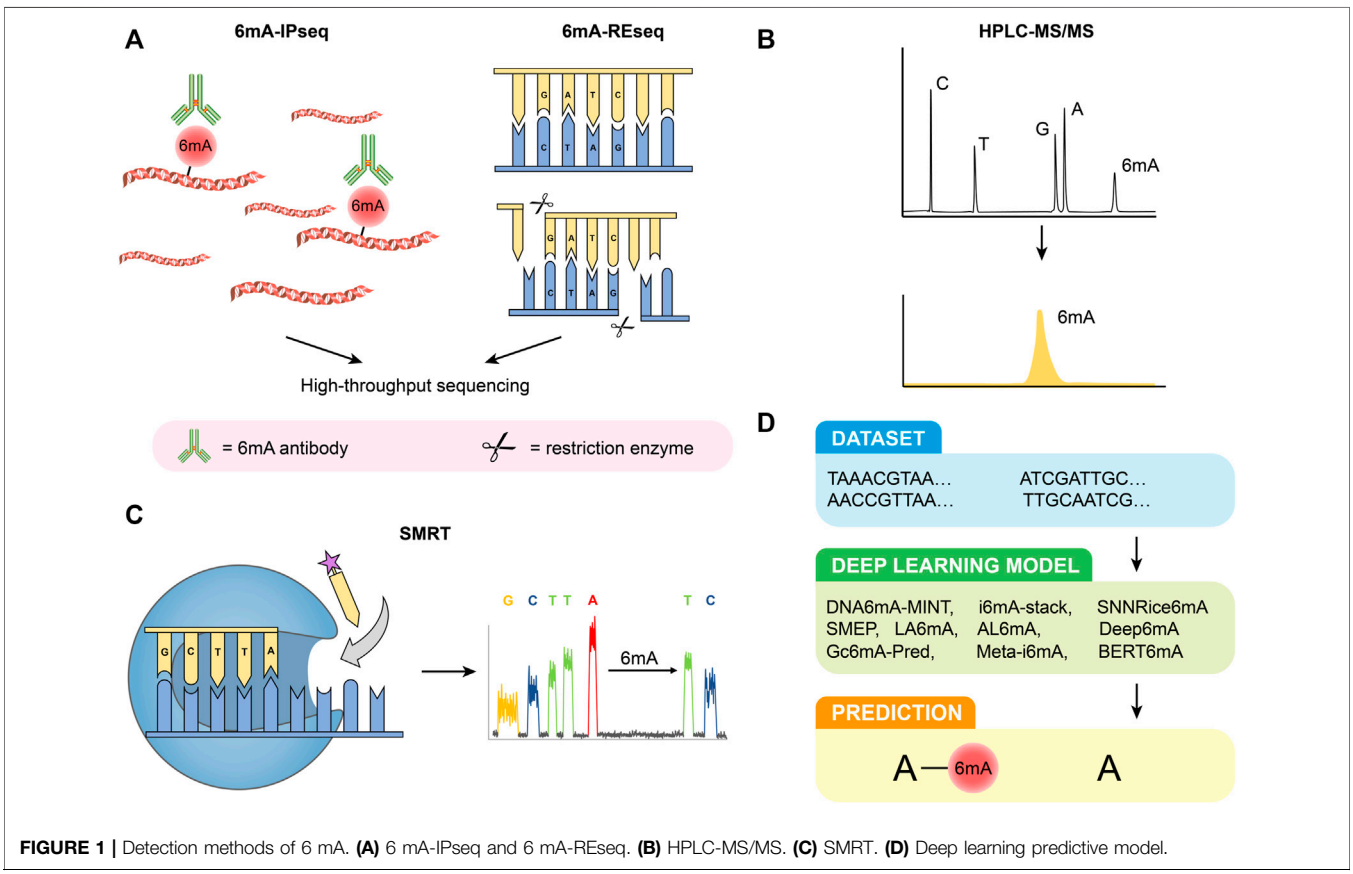

FIGURE 1 | Detection methods of 6 mA. **(A)** 6 mA-IPseq and 6 mA-REseq. **(B)** HPLC-MS/MS. **(C)** SMRT. **(D)** Deep learning predictive model.

2015; Shah et al., 2019), mice (Yao et al., 2017; Kweon et al., 2019), rats (Kigar et al., 2017), zebrafish (Liu et al., 2016b), and humans(Wu et al., 2016; Xiao et al., 2018; Hao et al., 2020).

It has been demonstrated that 6 mA plays an increasingly important role in eukaryotes. Recently, studies of 6 mA methylation have gradually advanced, and a growing number of methyltransferases have been discovered. However, enzymes involved in 6 mA demethylation in eukaryotes are still scarce, and the proteins identifying 6 mA sites remain to be explored. In this review, we first discuss the advantages and disadvantages of 6 mA detection technologies and the prevalence of 6 mA in eukaryotic organisms. Then, we highlight the possible methyltransferases, demethylases, and proteins recognizing 6 mA. Finally, we summarize the functions of 6 mA and put forward the problems that need further research.

DETECTION OF 6 MA

Over the past few decades, multiple methods have been developed to detect 5 mC at a single-gene level or whole-genome level based on sodium bisulfite transformation, chromatography, methylation sensitive restriction enzymes, 5 mC methyl-binding proteins or antibodies to 5 mC, as well as rapid and inexpensive biosensors for detection (Lv et al., 2021; Martisova et al., 2021). The detection methods of 6 mA and 5 mC have many

similar principles. However, due to the low abundance of 6 mA and possible bacterial contamination, the sensitivity and reliability of detection technologies are challenged. Here, we discuss experimental tools and bioinformatics tools for 6 mA detection and their advantages, disadvantages, and limitations (**Table 1**).

6 mA-IPseq

6 mA-immunoprecipitation sequencing (6 mA-IPseq) is a common method of methylation detection. It enriches methylated genomic fragments using a specific 6 mA antibody and then identifies DNA motifs by sequencing (**Figure 1A**) (Fu et al., 2015). The cost of 6 mA-IPseq is relatively low, however, the inability of 6 mA antibodies to precisely locate methylation sites limits the application of this method (Jeong et al., 2016). Recently, investigators reported the preference of 6 mA antibody to unmodified adenine, which indicated the possible false positive results caused by enrichment of unmethylated DNA (Douvlataniotis et al., 2020). In addition, N6-methyladenosine (m6A) or m1A in RNA also disturbs the test (Douvlataniotis et al., 2020). Furthermore, during cell culture, bacterial DNA containing 6 mA may be incorporated into samples DNA (Schiffers et al., 2017). Therefore, 6 mA-IPseq requires high-quality DNA samples without bacterial contamination.

6 mA-REseq

Restriction enzyme-based 6 mA sequencing (6 mA-REseq) relies on a collection of restriction enzymes that digest DNA motifs without specific methylation (**Figure 1A**). Genomic DNA treated with restriction enzymes is fragmented by sonication, end-repaired, and then ligated to DNA adapters. After PCR amplification, the DNA library can be prepared for high throughput sequencing. The unmethylated sequence motifs are enriched at the end of the sequencing reads while methylated motifs are present in the inner part of the reads. The ratio of internal motifs to terminal motifs reveals the relative methylation to unmethylation ratio (Fu et al., 2015). However, the application of 6 mA-REseq is limited to specific restriction sites, and incomplete digestion caused by other reasons may also lead to false positive results (Laird, 2010; Shanmuganathan et al., 2013).

HPLC-MS/MS

High-performance liquid chromatography coupled with tandem mass spectrometry (HPLC-MS/MS) is a highly sensitive and specific method for 6 mA detection. Before being analyzed by HPLC-MS/MS, purified DNA samples are first digested by commercial enzymes. Thereafter the digested DNA can be effectively separated in the chromatographic separation system due to the different physical and chemical properties of each component. Next, they are ionized by atmospheric pressure ionization (API) techniques and then entered into the mass spectrometer, identified by MS/MS based on mass-to-charge ratio (m/z) (Vogeser and Seger, 2008; Liu and Wang, 2021) (**Figure 1B**). HPLC-MS/MS can accurately quantify the signal of each nucleoside even if the samples are contaminated by RNA(Song et al., 2005). However, the result of HPLC-MS/MS can be easily disturbed by bacterial contamination in samples and commercial enzymes (Schiffers et al., 2017; Koh et al., 2018; O'Brown et al., 2019). As a result, strict aseptic conditions and appropriate experimental control are necessary to ensure the accuracy and validity of the results.

SMRT

Single-molecule real-time sequencing (SMRT) is based on DNA polymerases and fluorescence-labeled deoxyribonucleoside triphosphates (**Figure 1C**) (Morgan et al., 2009; Flusberg et al., 2010). In zero-mode waveguides, different fluorescently labeled deoxyribonucleoside triphosphates (dNTPs) are incorporated into the DNA chain by DNA polymerase. The type of dNTPs is determined by the type of fluorescence, and base modifications of DNA can be directly revealed by changes in inter-pulse duration (IPD) values, which means the interval between fluorescence pulses (Flusberg et al., 2010). The development of SMRT provides a more powerful tool for the direct detection of modified nucleotides in DNA. However, the high false positive rate (FPR) of SMRT, especially when the abundance of 6 mA/A is low, has attracted the attention of researchers (Zhu et al., 2018; O'Brown et al., 2019; Douvlataniotis et al., 2020). SMRT cannot distinguish between 6 and 1 mA, and modifications of flanking cytosine may also cause interference (Schadt et al., 2013; Douvlataniotis et al., 2020). The high FPR of SMRT is dependent on the 6 mA rate over the adenines (6 mA/A) in the genome and the sequencing depth and coverage (average of IPD values for each strand of the genome reference). Considering the low level of 6 mA/A in eukaryotes, deep coverage is indispensable to attain a low FPR (Zhu et al., 2018). In addition, whole genome-amplified DNA (WGA DNA, unmethylated DNA) is also recommended as a control to reduce FPR (Yang et al., 2020). SMRT is also suggested to be used in combination with other detection methods.

Deep Learning Predictive Model

Compared with traditional laboratory experiments, bioinformatics tools have significant advantages in terms of price and time cost (**Figure 1D**). At present, there are many deep learning models used for predicting 6 mA, such as DNA6mA-MINT (Rehman and Chong, 2020), i6mA-stack (Khanal et al., 2021), SNNRice6mA (Yu and Dai, 2019), SMEP (Wang et al., 2021), Deep6mA (Li et al., 2021b), LA6mA, AL6mA (Zhang et al., 2021), GC6mA-Pred (Cai et al., 2022), Meta-i6mA (Hasan et al., 2021), and BERT6mA (Tsukiyama et al., 2022). Based on neural networks, Yu and Dai. (2019). proposed a new method called SNNRice6mA to identify 6 mA sites in rice DNA, which showed over 90% sensitivity, specificity, and accuracy. However, the accuracy of SNNRice6mA for cross-species studies decreased significantly, from 93% and 92% in two types of rice to 61.81% in *Mus musculus*. Other algorithms also have their characteristics. For example, Deep6mA presents an accuracy of more than 90% in predicting plants such as *Arabidopsis* (Li et al., 2021b). LA6mA and AL6mA capture location information from DNA sequences through a self-attention mechanism (Zhang et al., 2021). GC6mA-Pred mainly identifies 6 mA sites in the rice genome and outperforms several prediction models, including DNA6MA-MINT, on independent datasets (Cai

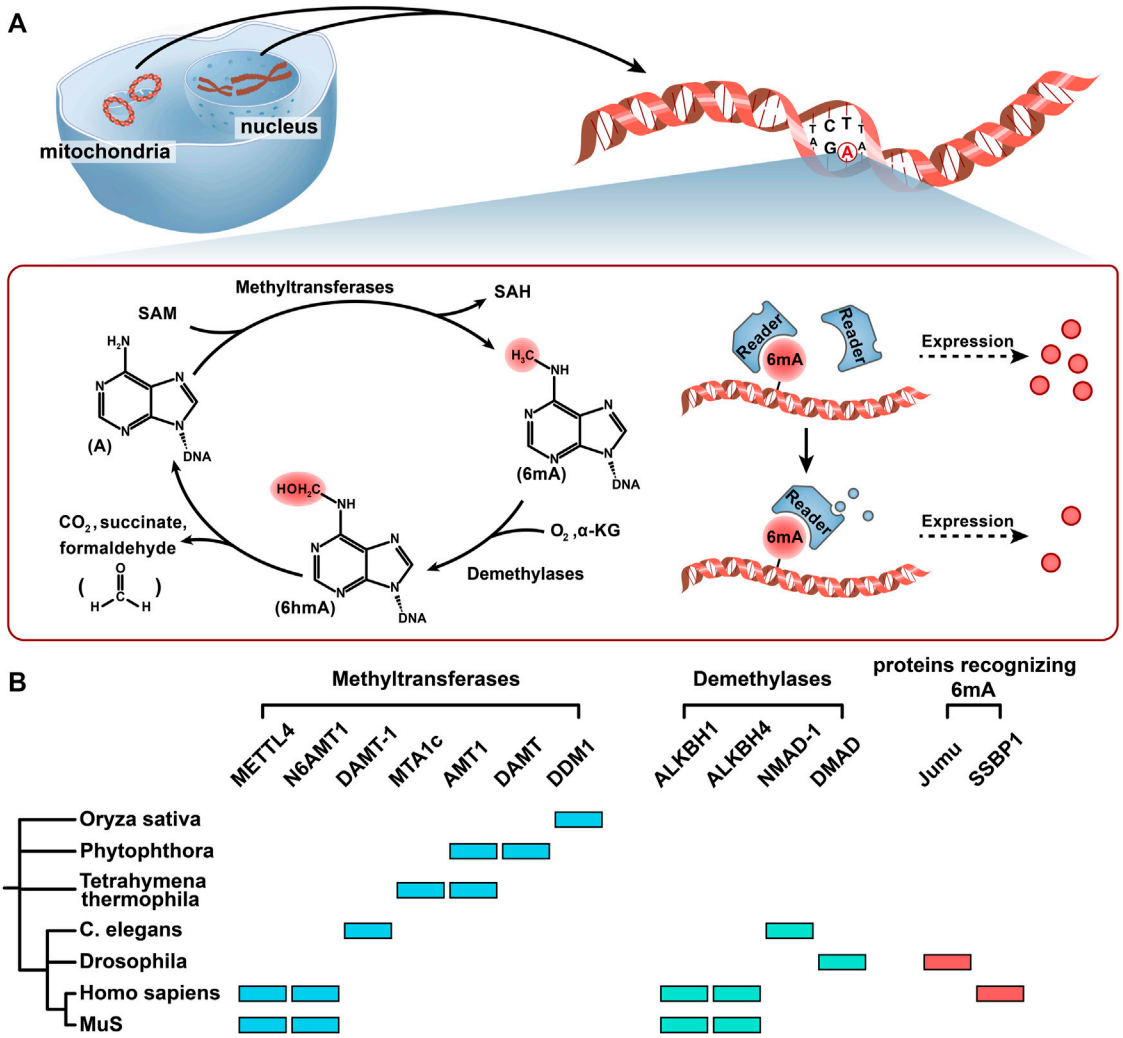

FIGURE 2 | Methylation and demethylation of 6 mA. **(A)** The methyl group on SAM was added to the sixth position of the adenine ring primarily with the help of methyltransferases. Under the catalysis of demethylase ALKBH1, 6 mA is oxidized to the 6 hmA intermediate by Fe^{2+}, O_2, and α-KG, and then 6 hmA spontaneously degrades to adenine and generates formaldehyde without the catalysis of demethylase. Readers (proteins recognizing 6 mA) may recognize the 6 mA modification and manipulate the fate of 6 mA-modified genes in different cellular contexts. **(B)** Seven kinds of 6 mA methyltransferases, four kinds of 6 mA demethylases, and two kinds of proteins recognizing 6 mA in 7 different organisms are shown in a simplified phylogenetic tree. Color codes represent the methyltransferases, demethyltransferases, and proteins recognizing 6 mA in the corresponding organism and proteins.

et al., 2022). These methods present many advantages; however, there are also some problems. BETR6mA was less effective in species with small sample sizes and required pretraining and fine-tuning(Tsukiyama et al., 2022). Although deep learning models present high accuracy and sensitivity in particular species, they are doubtful when they are extrapolated to other species. In the future, with the continuous optimization of deep learning models, they will play an important role in predicting 6 mA sites.

Prevalence of 6 mA

Chemical modification of nucleotide bases in DNA conveys added information to the genetic code. As the most common chemical modification, 5 mC is widely present in higher eukaryotes, such as plants, protozoans, metazoans, and some fungi (Schmitz et al., 2019). In most species of plants, such as tomatoes and oranges, 5 mC is tissue-specific and varies during the growth of plants (Chachar et al., 2021). In vertebrates, the genomes are extensively methylated, where the detected 5 mC of CpGs is more than 70% (Feng et al., 2010). In the mammalian genome, 5 mC primarily occurs within the CpG dinucleotide context, and 60%–80% of CpGs are methylated (Smith and Meissner, 2013; Luo et al., 2018a). However, it was almost undetectable in *Drosophila* and *C. elegans* Chen et al., 2018). In fungi, Bewick et al. (2019). analyzed the prevalence of 5 mC in 40 fungal species and discovered that the level of 5 mC in *Basidiomycota* was the highest whether in a genomic location or sequence context. Whereas 5mC was nonexistent in common fungi such as *Saccharomyces cerevisiae* (a species of yeast) *and*

Aspergillus nidulans. In addition, fungi were reported to lack canonical gene-body methylation, which meant 5 mC was not evenly distributed.

Compared to 5 mC, 6 mA was detected extensively in prokaryotes (**Figure 2A**). In eukaryotes, the existence of 6 mA is controversial. Recently, some research has shown the existence of 6 mA in eukaryotes, including protozoans, metazoans, plants, and fungi. In different biological genomes, the abundance of 6 mA is quite different. In 2020, Lizarraga et al. reported that 6 mA accounted for 2.5% of the total adenine in the parasite *Trichomonas vaginalis*. They also demonstrated that 6 mA was mainly located in intergenic regions (94% of 6 mA-IPseq peaks). Among the 6 mA peaks located in genes (6%), most were distributed between the coding region (48%) and the transcription termination sites (TTSs; 43%), with only 9% found in the TSSs (Lizarraga et al., 2020). In *Drosophila*, the 6 mA level peaked (~0.07%, 6 mA/A) at the 0.75-h embryonic stage and then decreased to a low level (~0.001%, 6 mA/A) at 4–16 h embryonic stages (Zhang et al., 2015). However, in a more recent publication, it was demonstrated that the real level of 6 mA/A in total genomic DNA (gDNA) was 2 parts per million (p.p.m.) (CI, 1–10 p.p.m.) suggesting that previous measurements could be affected by bacterial contamination (Kong et al., 2022). In *Bdelloid rotifer*, 6 mA existed on 17,886 adenines (0.0236% of total adenines) (Rodriguez et al., 2022). In *C. elegans,* 6 mA accounted for 0.7% of the total adenine in the genome by SMRT sequencing (equivalent to 0.3% adenine methylated), which was further confirmed by UHPLC-MS/MS (Greer et al., 2015). In *Tetrahymena*, 6 mA was highly enriched in the NATN motif at linkers and transcription start sites (TSSs) (Wang et al., 2017; Luo. et al., 2018b). However, 6mASCOPE showed that the 6 mA/A level of VATN sites was 2–3 times higher than that of NATN sites (Kong et al., 2022). Compared to protozoans and metazoans, 6 mA has been less researched in plants and fungi. In 2018, Zhang et al. (2018). adopted multiple methods, including LC-MC/MC, 6 mA-IPseq, and 6 mA-REseq, and revealed that the 6 mA level ranged from 0.15% to 0.55% in rice seedlings. In addition, they also found that 6 mA was widely distributed in the *Japonica* and *Indica* genomes and enriched in promoters and exons. In *Arabidopsis*, Liang et al. (2020). reported that the level of 6 mA was up to 0.048% (6 mA/A) by LC-MS/MS. Kong et al. (2022). quantified the 6 mA/A level in 21-day-old Arabidopsis seedlings (approximately 2,500 p.p.m. 6 mA/A by LC-MS/MS). However, using 6 mASCOPE, they found that Arabidopsis only contributed to 4.21% of the total 6 mA events (3 p.p.m.; CI, 1–10 p.p.m.) and others were probably from four soil bacteria (Proteobacteria, Actinobacteria, Bacteroidetes, and Firmicutes). In sea buckthorn (*Hippophae rhamnoides Linn.*), the level of 6 mA was 0.016% by using nanopore sequencing at single-base resolution (Zhang et al., 2022a). Fu et al. 2015. reported that 6 mA-marked genes accounted for 84% of all genes in *Chlamydomonas*, and 6 mA was enriched in TSS. The existence of 6 mA has also been reported in Fig (*Ficus Carica L.*) (Usai et al., 2021). In fungi, Mondo et al. researched almost all the phyla of early-diverging fungi (EDF) and the Dikarya phyla and found that the abundance of 6 mA in EDF accounted for 2.8% of all adenines by SMRT, whereas the 6 mA level in the Dikarya could be a false positive by 6 mA-IPseq (Mondo et al., 2017). In EDF, 6 mA was symmetrically methylated, mainly present in the ApT context, and had a high density in methylated adenine clusters (MACs), whereas none of these were found in the Dikarya. In contrast to other EDFs, the 6 mA level in the arbuscular mycorrhizal fungi (AMF; Glomeromycotina) genome was 0.12%–0.17%, which was lower than that in other EDFs and similar to that in Dikarya and other eukaryotes (Chaturvedi et al., 2021).

The discovery of 6 mA modification in mammalian DNA has become a major focus of scientists. During embryogenesis in pigs, the level of 6 mA undergoes dynamic changes (Liu et al., 2016b). 6 mA gradually accumulated, reaching a maximum of ~0.17%, and then decreased to 0.05%. They also reported a low abundance of 6 mA in adult pig tissues. Similarly, 6 mA was detected in mouse embryonic stem cells (ESCs). In the H2A. X deposition regions, the 6 mA level presented an abundance of ~25–30 p.p.m. (Wu et al., 2016). In contrast, the level of 6 mA showed a linear increase in the embryonic states of mice and zebrafish (Fernandes et al., 2021). However, another group of researchers could not detect 6 mA in mouse ESCs or other tissues, which aroused extensive discussion (Schiffers et al., 2017). 6 mA existed in all of the brain regions and significantly increased up to 25.5 p.p.m. in the PFC upon stress. In 2018, Xiao et al. (2018). reported that the density of 6 mA was 0.051% in the human genome by SMRT sequencing, and the LC-MS/MS result was ~0.056%. It was also reported that the 6 mA reached a level of 1,000 p.p.m. in glioblastoma stem cells and primary glioblastoma (Xie et al., 2018). However, the 6 mA level was found to be only 2 p.p.m. (CI, 1–16 p.p.m.) and 3 p.p.m. (CI, 1–13 p.p.m.) by 6mASCOPE in the two glioblastoma species, suggesting that the 6 mA level in human cells might be overestimated (Kong et al., 2022). Zhang et al. 2022b. identified 2,373 unstable methylated genes containing 6 mA and 5 mC modifications after comparing the methylated genes in HCC (hepatocellular carcinoma) and adjacent liver tissues. These results suggest that 6 mA may play an important role in human disease. Recently, 6 mA was found to be enriched in mitochondrial DNA (mtDNA) in humans. However, the distribution characteristics of 6 mA in mtDNA are debated. Koh et al. (2018). reported that 6 mA was enriched in the heavy strand of mtDNA and arranged throughout the entire mtDNA with no bias toward any specific region. In contrast, Hao et al. (2020). discovered that 6 mA was distributed in the promoter region and enriched in the ND2, COI, and ND4–ND6 regions.

The discussion above has demonstrated the existence of 6 mA in plants, protozoans, metazoans, and some fungi; however, some investigators believe that the current evidence is still insufficient due to bacterial contamination, interfering factors, and high FPR (Liu et al., 2017; O'Brown et al., 2019; Douvlataniotis et al., 2020). They believe that 6 mA should be considered a methylation modification only in basal fungi, ciliates, and green algae but not in animals or plants (Bochtler and Fernandes, 2021). Kong et al. (2022). developed a metagenomic method (a machine learning algorithm) and found that commensal or soil bacteria could explain the majority of 6 mA in insect and plant samples, and there is no evidence of the high 6 mA abundance in

Drosophila, Arabidopsis, or humans. They also reported that even *E. coli plasmids* with Dam methyltransferase mutations were 6 mA-enriched, thus interfering with the evaluation of possible 6 mA methyltransferases and demethylases. Some researchers are optimistic about the existence of 6 mA. Using contamination-free UHPLC-MS/MS technology, they reported the presence of 6 mA in 3 cultured human cell lines (HEK293T, human mesenchymal stem cells, and human ESCs) without mycoplasma contamination (Liu et al., 2020).

DNA Methylation and Demethylation of 6 mA

In eukaryotic DNA methylation and demethylation, "writers" (methyltransferase), "erasers" (demethylases), and "readers" (recognition protein) play central roles. An in-depth study of these three enzymes contributes to revealing the epigenetic mechanism of methylation modification. Here, we discuss 6 mA methyltransferases and demethylases and summarize the candidate proteins recognizing 6 mA that have been discovered thus far (**Figure 2B**).

"Writers"-Methyltransferases of 6 mA

The methyl groups of 5 mC and 6 mA are catalyzed by methyltransferases *via* S-adenosylmethionine (SAM). 5 mC is formed by two kinds of methyltransferases to establish and maintain 5 mC formation together. For example, in mice and humans, Dnmt3 and Dnmt1 are responsible for the establishment and maintenance of 5 mC, respectively (Chen and Zhang, 2020). They add the methyl group on SAM to the fifth position of the cytosine ring, forming 5 mC methylation. Notably, in other organisms, their methyltransferases are mostly homologous with these two enzymes, such as MET1 and DRM2 in plants, and Dnmt5 and Dnmt1 in fungi (Schmitz et al., 2019).

For 6 mA, the methyl group on SAM was added to the sixth position of the adenine ring primarily with the help of the MT-70 methyltransferase family (Li et al., 2019; Joshi et al., 2021; Boulias and Greer, 2022). MT-A70 was considered to have evolved from M.MunI-like DNA 6 mA methyltransferases of bacteria (Wang et al., 2019). The 6 mA methyltransferases reported in eukaryotes are mainly members of the MT-A70 family, such as methyltransferase like 4 (METTL4) in most mammals, DAMT-1 in *C. elegans*, TAMT-1 and MTA1c in *Tetrahymena thermophila,* and DAMT in *Phytophthora* (a kind of fungi) (**Figure 2B**) (Greer et al., 2015; Luo et al., 2018b; Chen et al., 2018; Hao et al., 2020). Greer et al. indicated that DAMT-1 was a 6 mA methyltransferase in *C. elegans.* The evidence showed that 6 mA was significantly decreased after knocking down DAMT-1, which suppressed the transgenerational phenotypes, and the mutation of DPPW (the catalytic domain of DAMT-1) inhibited the increase in 6 mA (Greer et al., 2015). In *Thermophila ciliates,* MTA1c (a complex of MTA1, MTA9, p1, and p2) was reported as a 6 mA methyltransferase and had a special favor for the ApT context. In addition, Beh et al. (2019). found that MAT1 and MAT9 did not have the domain necessary for binding to DNA. Only in the presence of p1 and p2 can MTA1c catalyze 6 mA methylation. In *T. thermophila*, Wang et al. (2019). reported a methyltransferase named AMT1, which contained the catalytic motif DPPW. In rice, DDM1 played an important role in 6 mA methylation, and its mutations affected the development of rice by downregulating the expression levels of *GHD7*, *BRD1*, and *DWF7* (Zhang et al., 2018b). In *Phytophthora*, it was reported that the 6 mA level was significantly reduced and there was a greater loss in the second peak of the bimodal methylation pattern around the TSS in the DAMT mutant, which suggested that DAMT might contribute to 6 mA modification and prefer to the methylation gene bodies after the TSS (Chen et al., 2018). In almost all EDFs, including AMF, AMT1 was found to be a methyltransferase, and the ApT context was symmetrically methylated in the genome (Chaturvedi et al., 2021).

In mammals, the presence of 6 mA methyltransferase is controversial. In Mettl4 knockout (KO) mouse ESCs, the abundance of 6 mA dropped from an average of 8.6 p.p.m. in wild-type (WT) ESCs to an undetectable level (Kweon et al., 2019). The level of 6 mA in spleen genomic DNA also decreased with the inactivation of METTL4, which contains the catalytic motif DPPW. Furthermore, METTL4 was discovered to accumulate in mitochondria and suppress transcription at the mitochondrial promoter region by regulating 6 mA. In contrast, Chen et al. (2020). could not detect 6 mA in 293T cells, and alterations in METTL4 expression levels did not affect 6 mA detection. N-6 adenine-specific DNA methyltransferase 1 (N6AMT1) was reported as a methyltransferase in humans, containing a catalytic conserved motif NPPY (Xiao et al., 2018). The study indicated that silencing or overexpressing N6AMT1 could regulate the level of 6 mA in the human genome. However, another study found that N6AMT1 cannot function as a methyltransferase in glioblastoma (Xie et al., 2018). Structural analysis showed that N6AMT1 has the potential ability to catalyze adenine methylation in DNA. Nevertheless, the negative charges surrounding the active site make it difficult to bind to the negatively charged phosphate backbone of a DNA substrate (Li et al., 2019; Woodcock et al., 2019). One possible explanation is that N6AMT1 can bind to DNA in combination with some kind of partner proteins; however, such a hypothesis has not been confirmed in eukaryotes.

Remarkably, new evidence indicated that 6 mA modification in mammalian DNA is not methyltransferase-generated but DNA polymerase dependent. Musheev et al. (2020). showed that 6 mA was not dependent on methyltransferases but was incorporated by DNA polymerases, and one source of 6 mA may be m6A in RNA. Another study revealed that DNA polymerase lambda (Pol λ) contributed to 6 mA modification in DNA via nonhomologous end joining (NHEJ) repair (Liu et al., 2021a). The complex origins of 6 mA in mammals are not fully understood.

"Erasers"-Demethylases of 6 mA

The removal of 5 mC is a classic demethylation process. The multistep erasure of 5 mC relies on the oxidation and removal of multiple methylation enzymes. A typical example is the demethylation of 5 mC mediated by TET in mammals (Fritz and Papavasiliou, 2010; Young et al., 2015; Wu and Zhang, 2017).

Under the catalysis of TET, Fe^{2+}, O_2, and α-KG oxidized 5 mC to 5 hmC, 5fC, and 5caC successively (Tahiliani et al., 2009; He et al., 2011; Ito et al., 2011). In addition, SIDML2 in tomatoes, ROS1 in *Arabidopsis*, and T7H in fungi were all reported to be involved in 5 mC demethylation (Li et al., 2015; Lang et al., 2017; Zhang et al., 2018a).

Regarding 6 mA, studies on demethylases are more in-depth in mammals and less in other eukaryotic organisms, especially in plants and fungi (Chachar et al., 2021). Its removal is primarily dependent on the alpha-ketoglutarate-dependent dioxygenase (AlkB) family, which contains conserved Fe^{2+} and 2OG (2-oxoglutarate, α-KG)-dependent dioxygenase domains. It was reported that ALKBH1 could convert 6 mA to N6-hydroxymethyladenine (6 hmA), and 6 hmA could spontaneously degrade to adenine and generate formaldehyde without the catalysis of ALKBH1 (**Figure 2B**) (Xiao et al., 2018; Zhang et al., 2020). This is different from the methylation of 5 hmC, which does not produce formaldehyde due to nucleophilic attacks, such as exogenous thiols (Liutkeviciute et al., 2009; Schiesser et al., 2013). HALKBLH1 in the human ALKBH (hALKBH) family contains Flip0 at the N-terminus, a nucleotide recognition cap (NRL) containing Flip1 and Flip2, and a catalytic center. Key amino acid residues in NRL potentially determine the specific recognition and demethylation of hALKBH (Tian et al., 2020). In *C. elegans,* Greer et al. (2015). indicated that the mutant NMAD-1 could decrease demethylation ability, which suggested a new kind of demethylase. The methyltransferase of the 6 mA signature called DPPW in NMAD-1 was important for substrate recognition and catalytic activity. It was shown that in NMAD-1 mutant worms, their fertility was inhibited across generations. Xiao et al. (2018). reported that the ALKBH family might also be involved in the demethylation of 6 mA in *C. elegans*. In addition to the AlkB family, the TET family also plays an important role in the removal of 6 mA. In *Drosophila,* DMAD (*Drosophila* DNA 6 mA demethylase), a member of the TET family, is involved in the demethylation of 6 mA. It was demonstrated that DMAD had a core catalytic domain called DSBH (double-stranded β-helix) fold present in all AlkB family members and specifically inhibited modification of 6 mA, which played an important role in promoting GSC (germline stem cell) differentiation and resulted in the loss of germ cells (Zhang et al., 2015).

ALKBH1 is a demethylase in humans and mice. It was reported that ALKBH1 could precisely regulate the 6 mA level in mouse ESCs (Wu et al., 2016). The results of Li et al. (2020). also revealed the role of ALKBH1 as a DNA demethylase in mice. In humans, the expression of *ALKBH1* influenced the prevalence of 6 mA (Xiao et al., 2018). Furthermore, the role of ALKBH1 in human mitochondria was identified. The level of mitochondrial 6 mA in ALKBH1-KO cells was slightly higher than that in ALKBH1-WT cells (Koh et al., 2018). In addition, the demethylation effect of ALKBH1 was also reported in glioblastoma. The preference of ALKBH1 was demonstrated by a pull-down assay and ALKBH1 ChIP-seq (Xie et al., 2018). However, some reports indicated that ALKBH1 knockout had no impact on 6 mA levels in mouse ESCs and HEK293T cells, implicating the complexity of DNA demethylation (Liu et al., 2016a; Liu et al., 2020). ALKBH4 is orthologous to DMAD (6 mA demethylase in *Drosophila*) and NMAD-1 (6 mA demethylase in *C. elegans*). Its potential role in DNA demethylation in mice has been reported (Kweon et al., 2019). However, more evidence is still needed to confirm its role as a 6 mA demethylase.

"Readers"-Proteins Recognizing 6 mA

Proteins that specifically recognize 5 mC-methylated DNA have been identified in the last century, such as MeCP2, a polypeptide containing both the methyl-CpG binding domain (MBD) and transcriptional inhibition domain (TRD) in mammals (Hendrich and Bird, 1998).

He et al. (2019). found a kind of protein in the Fox family called Jumu, which could recognize and bind 6 mA-modified DNA in *Drosophila* (**Figure 2B**). Jumu can regulate early embryogenesis by inducing 6 mA-labeled genes called *Zelda*. Zelda was reported to positively regulate a group of miRNAs in *Drosophila* embryos by binding to *cis*-regulatory enhancers and affecting the expression of transcriptional regulators thereafter (Fu et al., 2014). After the Jumu-mutated oocytes combined with normal sperm, 72% of the embryos failed to develop into larvae. However, a zygote combined with mutant sperm and normal oocytes can develop normally, and most dead mutant embryos do not show a segmentation phenotype. Their study demonstrated the importance of the 6 mA-binding protein for the regulation of biological activity. Similarly, single-stranded DNA-binding protein 1 (SSBP1), containing HNRNP and YTH domains, was also considered another protein recognizing 6 mA in human mitochondria, which preferentially binds to ssDNA along the heavy chain, consistent with the position of 6 mA enrichment. The presence of 6 mA decreased the melting temperature of dsDNA, thus collecting SSBP1 into the heavy chain of mitochondria. (Koh et al., 2018; Shen et al., 2022). In addition, under hypoxic stress, the abundance of 6 mA in mitochondrial DNA was significantly increased, thus promoting the inhibition of mtDNA transcription by repressing the binding of mitochondrial transcription factor A (TFAM) (Hao et al., 2020). During the differentiation of trophoblast stem cells in mice, the expression of 6 mA in SIDD was significantly increased, which obstructed the binding of SATB1 to chromatin (Li et al., 2020). Some scholars questioned whether 6 mA could actively repel SATB1 binding because the dramatic bending of the DNA helix inhibited the binding of SATB (Li et al., 2021a; Boulias and Greer, 2022). Although these reports have shown the existence of proteins recognizing 6 mA, the downstream process after recognition is still not fully understood.

Function of 6 mA

5 mC has attracted much attention, and multiple biological functions of 5 mC have been demonstrated, including transcription suppression, transposon suppression, genomic imprinting, X chromosome inactivation, and epigenetic memory (Bird, 2002; Chen et al., 2016; Wu and Zhang, 2017). However, research on 6 mA is still limited. In this section, we

summarize several widely recognized functions of 6 mA in eukaryotes.

6 mA and Gene Expression

In different organisms, the prevalence of 6 mA showed different effects on gene expression. It has been confirmed that 6 mA promotes gene expression in *Oxytricha* (Beh et al., 2019), rice (Zhang et al., 2018b), *Chlamydomonas* (Fu et al., 2015; Mondo et al., 2017), and fungi(Mondo et al., 2017) but not in mammals (Wu et al., 2016). The 6 mA level in *Oxytricha* was decreased by mutating the methyltransferase MTA1; however, only a few genes were significantly altered. The genes with a lower or greater loss of 6 mA markers near the TSS in mutants had little change in transcription, which meant drastic changes in the 6 mA level had a low effect on the level of overall transcription across the genome (Beh et al., 2019). This may be because the MTA1 mutant did not completely eliminate 6 mA or other DNA methylation modes in the genome can sufficiently buffer genes from changes in transcription. Similarly, in fungi, 6 mA might promote the likelihood of gene expression, and the level of actual gene expression may be regulated independently to maintain the stability of genome transcription (Mondo et al., 2017). The level of 6 mA-modified genes in wild-type rice was significantly higher than that in mutant rice (Zhang et al., 2018b). The R2R3-MYB protein in *Arabidopsis*, one of the largest transcription factors in the MYB family, has a significantly reduced affinity when binding to 6 mA-modified DNA compared to unmodified DNA (Wang et al., 2020). In *Chlamydomonas*, 6 mA near the TSS region marks active transcription genes(Fu et al., 2015). Sheng et al. also reported that the change in the 6 mA level in TSS was correlated with the expression of highly differentially expressed genes (DEGs) (Sheng et al., 2021). Although many reports have shown that 6 mA can promote gene expression in various eukaryotes, there is evidence supporting that 6 mA blocks the transcription of mammalian genes. For instance, the accumulation of 6 mA located on the X chromosome and Chr13 in mammals and the 6 mA density of young full-length line-1 transposons affected the inhibition of gene expression levels (Wu et al., 2016). In another study of 6 mA in mammalian mitochondria, the transcription of heavy and light chains with 6 mA modification at the promoter region was also inhibited *in vitro* (Hao et al., 2020). However, 6 mA was considered a marker of actively transcribed genes in human liver tissues (Cui et al., 2022). For the mechanism of 6 mA affecting gene transcription, one possible explanation is regulating the combination of genes and their transcription factors. It was reported that the decrease in 6 mA in the promoter of BMP2 could enhance the binding of October4 (octamer-binding transcription factor 4) and then activate BMP2 transcription (Ouyang et al., 2021). The detailed process and relevant molecules remain to be further studied.

6 mA and Nucleosome

Research has shown that 6 mA can assist in nucleosome localization. In *Chlamydia*, 6 mA near TSS sites presents periodic distribution and distributes between the small bodies that connect the nucleus, which may help nucleosome localization. If the distance between the two adjacent 6 mA sites is longer than the length of a nucleosome, the nucleosome is likely to be located between the two adjacent 6 mA sites (Fu et al., 2015). In ciliates, 6 mA is directly detrimental to nucleosome occupancy in local, quantitative, and intrinsic features *in vivo* (Luo. et al., 2018b; Beh et al., 2019). Similarly, Wang et al. reported that 6 mA and nucleosome distributions downstream of TSS had two damped oscillations with periods of ~200 bp but opposite phases (Wang et al., 2017; Wang et al., 2019). However, 6 mA did not exhibit the ability to affect nucleosome occupancy *in vitro* due to endogenous chromatin assembly factors (such as trans-acting factors), DNA sequences, and chromatin remodeling complexes (Wang et al., 2017; Beh et al., 2019). Another reason is that 6 mA can change the curvature and stiffness of DNA, which is not conducive to the formation of small nucleosomes (Luo et al., 2018b). The relationship between 6 mA and nucleosomes in the eukaryotes mentioned above is similar to the function of 5 mC (Huff and Zilberman, 2014; Wang et al., 2017). The dense 5 mC on DNA could alter the major and minor grooves and not facilitate the curvature of DNA within nucleosomes, which would make the nucleosomes unstable (Pérez et al., 2012; Jimenez-Useche et al., 2013). The results suggest that different types of methylation modifications may affect nucleosome location. 6 mA modification and nucleosome localization may also regulate gene transcription and thus participate in a series of processes in eukaryotes. In starved *T. thermophila*, the amplitude (peak-to-trough distance) of nucleosome distribution was increased, whereas the amplitude of 6 mA distribution was decreased. This was probably because DNA replication and transcription perturbed nucleosomes. More highly methylated 6 mA sites were found in linker DNA, which could reinforce nucleosome stacking and stabilize it (Sheng et al., 2021). This suggests that the interaction of 6 mA and nucleosomes may play an important role in epigenetic processes. It was also reported that the decrease in 6 mA in the BMP2 promoter could promote the binding of October4 (octamer-binding transcription factor 4) to the BMP2 promoter and then increase BMP2 transcription (Ouyang et al., 2021). In another study, 6 mA was reported to promote heterochromatin formation in human glioblastoma *via* H3K9me3 histone modification (Xie et al., 2018). The effect of this relationship between 6 mA and nucleosome localization on gene transcription requires further in-deep research.

6 mA and Stress

Under the influence of 6 mA, eukaryotes have different tolerances to environmental stresses. In *Tetrahymena,* the global level of 6 mA was reduced, and the percentage of highly asymmetric 6 mA was increased under starvation (from 0.18% to 1.45% in vegetative cells and 0.12%–0.93% in starved cells). As mentioned above, upon starvation, the change in 6 mA located 1 kb downstream of TSS was correlated with the expression of DEGs (log2-fold change), and the nucleosome positioning degree was also increased in starved cells (Sheng et al., 2021). In rice, dysfunction of heat shock transcription factor A1 (HsfA1) and heat shock protein 70 (HSP 70) induced by 6 mA modifications decreases the sensitivity to heat stress. In

addition, the increase in 6 mA density led to a decrease in cold resistance and increased salt and heat resistance (Zhang et al., 2018b). Under hypoxia, METTL4 was upregulated in mitochondria, leading to upregulation of 6 mA levels. This may be regulated by HIF1α and balance the increased ROS to adapt to hypoxia in mammals. (Hao et al., 2020). The hypoxic stress-induced HIF pathway may play an important role in human diseases (Jain et al., 2018; Guo et al., 2020; Liu et al., 2021b; Liu et al., 2022).

In addition, changes in mammalian environmental stress can cause changes in 6 mA, which means that neuronal activities may affect the prevalence and abundance of 6 mA. Evidence shows that 6 mA exists in the mammalian brain and increases upon stress, which is negatively correlated with LINE transposon expression. In the prefrontal cortex (PFC), 6 mA significantly accumulated and underwent dynamic changes upon chronic stress exposure. A negative correlation between 6 mA and the expression of some neuronal genes was also reported(Yao et al., 2017). Consistent with this, another group found that 6 mA was upregulated and negatively correlated with Hrt2a gene expression in the amygdala upon early life stress in rats (Kigar et al., 2017). Under hypoxic conditions, after ALKBH1 knockdown, genes in the hypoxia pathway were downregulated, and DNA damage and p53 pathway genes were upregulated in glioblastoma (Xie et al., 2018). However, which factors and pathways regulate gene expression changes under hypoxic conditions has not been discussed.

6 mA and Embryogenesis

6 mA may play an important role in embryonic development. The dynamic change was observed in the embryonic stage of *Drosophila*, and it may be regulated by DMAD, whose overexpression led to the loss of germ cells, including GSCs. This finding supported that DMAD may play a role in promoting GSC differentiation. (Zhang et al., 2015). Recently, evidence indicated that 6 mA was possibly related to mammalian embryogenesis. As mentioned earlier, the 6 mA density in pig embryos rose to ~0.17% and then decreased to ~0.05% during embryogenesis, suggesting the possible biological function of 6 mA (Liu et al., 2016b). In zebrafish embryos, the level of 6 mA increased to a maximum of ~0.1% and then gradually decreased to approximately 0.006% (Liu et al., 2016b). However, another study showed that the level of 6 mA presented a linear increase in the embryonic states of mice and zebrafish (Fernandes et al., 2021). In mice, 6 mA is most abundant in the lungs, spleen, and brain, especially in the prefrontal cortex (PFC); therefore, it may play an important role in regulating the development of the nervous system and may be associated with certain neurological disorders (Fernandes et al., 2021). 6 mA was also detected in mouse ESCs. The authors found that 6 mA accumulated in the young long interspersed element 1 (LINE-1) and blocked transcription of their neighboring genes (Wu et al., 2016). Consistent with this conclusion, Li et al. (2020). also reported dynamic changes in 6 mA during early embryogenesis. The evidence showed that 6 mA mainly existed in intergenic regions, such as LINE-1s and modulated the ESC-to-TSC (trophoblast stem cell) transition by antagonizing SATB1 (a well-known SIDD regulating protein expressed in TSC).

6 mA and Human Disease

The extent of DNA methylation is related to the pathogenesis and progression of many diseases. 5 mC modification of DNA is closely related to hypertension (Han et al., 2016). Recently, the relationship between 6 mA and hypertension has also been revealed (Guo et al., 2020). In human and mouse hypertension models, leukocyte 6 mA DNA level was significantly decreased and returned to normal after successful treatment. The prevalence of 6 mA can regulate the expression of key genes and modify cell functions, which accelerates the pathological progress of human diseases. The investigators demonstrated the potential protective role of ALKBH1-mediated 6 mA level in Ang II-induced vascular remodeling. The silencing of ALKBH1 increased the prevalence of 6 mA in VSMCs and inhibited Ang II-induced phenotypic transformation, proliferation, and migration of VSMCs, mediated by the HIF1α-dependent pathway (Guo et al., 2020). In another study of patients with chronic kidney disease (CKD) in the clinical setting, Ouyang et al. (2021). found that the 6 mA level of leukocytes decreased significantly as the severity of vascular calcification (VC) increased. In addition, the mRNA expression of ALKBH1 was significantly upregulated in patients with CKD with VC, which could cause the change of 6 mA level in leukocytes(Chaudhary, 2022). The possible mechanism is that ALKBH1 reduces 6 mA density in the BMP2 promoter of VSMCs and thus promotes the binding of October4. BMP2 transcription is activated and induces an increase in RUNX2 expression thereafter, ultimately resulting in osteogenic reprogramming of VSMCs and VC progression. Using October4-knockout mice, they found that October4 could downregulate BMP2 expressions which could alleviate calcification effect of ALKBH1 overexpression (Rong et al., 2014; Ouyang et al., 2021). Another study reported that ALKBH1 promoted adipogenic differentiation and contributed to the accumulation of adipose tissue. The results showed that ALKBH1 decreased the 6 mA levels of HIF-1α and GYS1 and then activated the HIF-1 pathway (Liu et al., 2022).

Abnormal dynamic regulation of 6 mA has been reported in many cancers. 6 mA methyltransferases such as N6AMT1 have been shown to inhibit tumor progression (Xiao et al., 2018; Shen et al., 2022). A recent study showed that the density of 6 mA in highly expressed genes was significantly higher, and the 6 mA density was decreased in LINE and SINE gene repetition regions in HCC, which might lead to chromosome defects or rearrangements similar to 5 mC, thus promoting the development of cancer (Cui et al., 2022). However, how 6 mA affects subsequent biological processes has not been reported and is worth further investigation. Xiao et al. reported that 6 mA contents were decreased in primary gastric and liver cancers. Loss of 6 mA promoted tumorigenesis, which was related to the regulation of N6AMT1 and ALKBH1 (Xiao et al., 2018). Similarly, depletion of 6 mA led to the accumulation of sensor proteins such as ASXL1, which contributed to the onset and metastasis of aggressive tumors (Kweon et al., 2019). In glioblastoma, the dynamic regulation of 6 mA was related to tumor progression. The regulation of 6 mA methylation at specific sites by methyltransferases and demethylases has an impact on the proliferation, self-renewal, and formation

capacity of tumors (Xie et al., 2018). In the occurrence of triple-negative breast cancer (TNBC), overexpression of *ALKBH1* or downregulation of *N6AMT1* can reduce the resistance of TNBC cells to olaparib (a PARP inhibitor targeting DNA repair). This may be due to the decreased level of 6 mA can reduce the expression of *LINP1*. Meanwhile, the overexpression of γ-H2AX (a marker of DNA damage) regulated by N6AMT1 in TNBC cells was significantly reduced, suggesting that 6 mA plays an important role in DNA damage repair (Sheng et al., 2020). Notably, intratumor bacteria were discovered in many human solid tumors (Nejman et al., 2020). Therefore, it is necessary to avoid possible bacterial contamination while detecting 6 mA in the tumor genome.

DISCUSSION

6 mA plays an important biological role in prokaryotes. Although many studies have indicated the presence of 6 mA in eukaryotes, bacterial contamination and other false positives of nonspecific methylation of DNA or RNA are still the primary factors affecting the prevalence and even the actual presence of 6 mA in eukaryotes. Therefore, it is necessary to use cross-validation of different detection methods to guarantee accuracy. Some methods to minimize the error were also proposed. To test bacterial contamination, amplification of prokaryotic 16 S rRNA genes by PCR using universal 16 S primers is recommended (Liang et al., 2020). Digesting RNA may also be taken into consideration to decrease interference. In the future, we hope more research will focus on developing a new generation of detection techniques that can exclude bacterial contamination and address false positives. In addition, existing publications need to be re-evaluated to determine 6 mA abundance and actual enzymes involved in 6 mA methylation, demethylation and cognition.

The incredibly low abundance of 6 mA reported in eukaryotes raises questions about its biological functions. The abundance of 6 mA presents dynamic changes during embryogenesis and under environmental stress. In addition, it varies among eukaryotes and even in different tissues and cells of the same organism. The large variation in 6 mA abundance among different reports is possibly due to bacterial contamination and different detection methods, or it may be related to the types, development stages, and nutritional status of cells. The level of 6 mA and the underlying factors that influence it need further confirmation. Importantly, researchers need to take action to prevent the results from interfering with bacterial contamination.

The enzymes of the MT-A70 family are common methyltransferases in eukaryotes. Recently, new evidence has shown that 6 mA is DNA polymerase-dependent (discussed earlier). Researchers have suggested that 6 mA plays a role in minimizing the incorporation of 8-oxo-2′-deoxyguanosine (8-oxoG) opposite to adenine by DNA polymerases and thus contributes to DNA damage repair based on the existing evidence. It is a noteworthy hypothesis, and we look forward to witnessing more promising discoveries in this direction. Demethylase has been studied extensively in metazoans but is relatively rare in plants and fungi. Under the catalysis of the demethylase ALKBH1, 6 mA is oxidized to 6 hmA, which can spontaneously degrade to adenine and generate formaldehyde without the catalysis of demethylase. However, the specific processes of other demethylases remain to be explored. In addition, there has been little focus on 6 mA binding proteins, and their potential function may be underestimated. Proteins that recognize 6 mA may assist methyltransferase and demethylase without domains that recognize 6 mA-modified DNA to regulate the expression of 6 mA and may have dramatic effects on various biological processes. In conclusion, the prevalence of 6 mA in eukaryotes is regulated by methyltransferases and demethylases; however, the existing studies on factors and pathways involving the process are limited. In addition, whether there are other enzymes that synergistically mediate the abundance of 6 mA in eukaryotes reminds to be explored. Recently, the relationship between 6 mA regulated by the methylase N6AMT1 and demethylase ALKBH1 and the occurrence of human diseases has been reported, which leads to a new research boom. We expect to see more breakthroughs in "writers," "erasers," and "readers" and shed light on the dynamics and roles of 6 mA in living organisms in the future.

Interestingly, dynamic changes in 6 mA abundance and specific enrichment of 6 mA suggest a link between 6 mA modification and specific biological processes, such as gene expression, nucleosome localization, stress, development of embryogenesis, and human diseases. 6 mA may promote the expression of modified genes; however, in some eukaryotes, the overall transcription level may remain stable due to an independent regulatory mechanism. The same period and opposite phases between 6 mA and nucleosome suggest that the interaction of 6 mA and nucleosome may play an important role in epigenetic processes. In starved *T. thermophila*, the amplitude (peak-to-trough distance) of nucleosome distribution was increased, whereas the amplitude of 6 mA distribution was decreased. This was probably because DNA replication and transcription perturbed nucleosomes, which demonstrated that 6 mA played an important role in eukaryotic metabolic processes and cellular pathways. However, because of technical limitations and possible bacterial contamination, these results need to be treated with caution. In addition, in response to stress and pathological factors resulting in human diseases, the factors regulating 6 mA level and related pathways should be the focus of future research. For humans, we can explore more potential roles of 6 mA, such as being a marker for the development of certain diseases, a target for certain tumors, or a prognosis for certain diseases.

The path of science is fraught with controversy. Owing to the low density and bacterial contamination of 6 mA in eukaryotes, the function of 6 mA eukaryotes has not been accepted until recently. Debates are continuing regarding the presence of 6 mA modification of DNA in eukaryotes. In eukaryotes, the study of 6 mA has just entered the initial stage. As further experimentation and profound discussion are being conducted in this emerging field, the full picture of 6 mA in mammals will be uncovered.

AUTHOR CONTRIBUTIONS

HL and NZ. were responsible for literature collection and writing. SX and YW. helped to prepare the figures, contribute to discussion, and perform the literature search. YZ, CX, and XT. helped write the manuscript and perform the literature search. YD. reviewed and edited the manuscript. All authors read and approved the final manuscript.

FUNDING

This work was funded by the National Natural Science Foundation of China (No. 31701162), the Key Research and Development Program of Anhui Province (No. 202104a07020031), and the College Students' Innovation and Entrepreneurship Training Program of Anhui Province (No. S202110366054).

REFERENCES

Beh, L. Y., Debelouchina, G. T., Clay, D. M., Thompson, R. E., Lindblad, K. A., Hutton, E. R., et al. (2019). Identification of a DNA N6-Adenine Methyltransferase Complex and its Impact on Chromatin Organization. *Cell.* 177 (7), 1781–1796. doi:10.1016/j.cell.2019.04.028

Bewick, A. J., Hofmeister, B. T., Powers, R. A., Mondo, S. J., Grigoriev, I. V., James, T. Y., et al. (2019). Diversity of Cytosine Methylation across the Fungal Tree of Life. *Nat. Ecol. Evol.* 3 (3), 479–490. doi:10.1038/s41559-019-0810-9

Bird, A. (2002). DNA Methylation Patterns and Epigenetic Memory. *Genes. Dev.* 16 (1), 6–21. doi:10.1101/gad.947102

Bochtler, M., and Fernandes, H. (2021). DNA Adenine Methylation in Eukaryotes: Enzymatic Mark or a Form of DNA Damage? *BioEssays* 43 (3), 2000243. doi:10.1002/bies.202000243

Boulias, K., and Greer, E. L. (2022). Means, Mechanisms and Consequences of Adenine Methylation in DNA. *Nat. Rev. Genet.* doi:10.1038/s41576-022-00456-x

Cai, J., Xiao, G., and Su, R. (2022). GC6mA-Pred: A Deep Learning Approach to Identify DNA N6-Methyladenine Sites in the Rice Genome. *Methods* 204, 14–21. doi:10.1016/j.ymeth.2022.02.001

Chachar, S., Liu, J., Zhang, P., Riaz, A., Guan, C., and Liu, S. (2021). Harnessing Current Knowledge of DNA N6-Methyladenosine from Model Plants for Non-model Crops. *Front. Genet.* 12, 668317. doi:10.3389/fgene.2021.668317

Chaturvedi, A., Cruz Corella, J., Robbins, C., Loha, A., Menin, L., Gasilova, N., et al. (2021). The Methylome of the Model Arbuscular Mycorrhizal Fungus, Rhizophagus Irregularis, Shares Characteristics with Early Diverging Fungi and Dikarya. *Commun. Biol.* 4 (1), 901. doi:10.1038/s42003-021-02414-5

Chaudhary, M. (2022). Novel Methylation Mark and Essential Hypertension. *J. Genet. Eng. Biotechnol.* 20 (1), 11. doi:10.1186/s43141-022-00301-y

Chen, H., Gu, L., Orellana, E. A., Wang, Y., Guo, J., Liu, Q., et al. (2020). METTL4 Is an snRNA m6Am Methyltransferase that Regulates RNA Splicing. *Cell. Res.* 30 (6), 544–547. doi:10.1038/s41422-019-0270-4

Chen, H., Shu, H., Wang, L., Zhang, F., Li, X., Ochola, S. O., et al. (2018). Phytophthora Methylomes Are Modulated by 6mA Methyltransferases and Associated with Adaptive Genome Regions. *Genome Biol.* 19 (1), 181. doi:10.1186/s13059-018-1564-4

Chen, K., Zhao, B. S., and He, C. (2016). Nucleic Acid Modifications in Regulation of Gene Expression. *Cell. Chem. Biol.* 23 (1), 74–85. doi:10.1016/j.chembiol.2015.11.007

Chen, Z., and Zhang, Y. (2020). Role of Mammalian DNA Methyltransferases in Development. *Annu. Rev. Biochem.* 89, 135–158. doi:10.1146/annurev-biochem-103019-102815

Cui, H., Rong, W., Ma, J., Zhu, Q., Jiang, B., Zhang, L., et al. (2022). DNA N6-Adenine Methylation in HBV-Related Hepatocellular Carcinoma. *Gene* 822, 146353. doi:10.1016/j.gene.2022.146353

Douvlataniotis, K., Bensberg, M., Lentini, A., Gylemo, B., and Nestor, C. E. (2020). No Evidence for DNA N 6 -methyladenine in Mammals. *Sci. Adv.* 6 (12), eaay3335. doi:10.1126/sciadv.aay3335

Feng, S., Cokus, S. J., Zhang, X., Chen, P.-Y., Bostick, M., Goll, M. G., et al. (2010). Conservation and Divergence of Methylation Patterning in Plants and Animals. *Proc. Natl. Acad. Sci. U.S.A.* 107 (19), 8689–8694. doi:10.1073/pnas.1002720107

Fernandes, S. B., Grova, N., Roth, S., Duca, R. C., Godderis, L., Guebels, P., et al. (2021). N6-Methyladenine in Eukaryotic DNA: Tissue Distribution, Early Embryo Development, and Neuronal Toxicity. *Front. Genet.* 12, 657171. doi:10.3389/fgene.2021.657171

Flusberg, B. A., Webster, D. R., Lee, J. H., Travers, K. J., Olivares, E. C., Clark, T. A., et al. (2010). Direct Detection of DNA Methylation during Single-Molecule, Real-Time Sequencing. *Nat. Methods* 7 (6), 461–465. doi:10.1038/nmeth.1459

Fritz, E. L., and Papavasiliou, F. N. (2010). Cytidine Deaminases: AIDing DNA Demethylation? *Genes. Dev.* 24 (19), 2107–2114. doi:10.1101/gad.1963010

Fu, S., Nien, C.-Y., Liang, H.-L., and Rushlow, C. (2014). Co-activation of microRNAs by Zelda Is Essential for Early Drosophila Development. *Dev. Camb. Engl.* 141 (10), 2108–2118. doi:10.1242/dev.108118

Fu, Y., Luo, G.-Z., Chen, K., Deng, X., Yu, M., Han, D., et al. (2015). N6-methyldeoxyadenosine Marks Active Transcription Start Sites in Chlamydomonas. *Cell.* 161 (4), 879–892. doi:10.1016/j.cell.2015.04.010

Greer, E. L., Blanco, M. A., Gu, L., Sendinc, E., Liu, J., Aristizábal-Corrales, D., et al. (2015). DNA Methylation on N6-Adenine in *C. elegans*. *Cell.* 161 (4), 868–878. doi:10.1016/j.cell.2015.04.005

Guo, Y., Pei, Y., Li, K., Cui, W., and Zhang, D. (2020). DNA N6-Methyladenine Modification in Hypertension. *Aging* 12 (7), 6276–6291. doi:10.18632/aging.103023

Han, L., Liu, Y., Duan, S., Perry, B., Li, W., and He, Y. (2016). DNA Methylation and Hypertension: Emerging Evidence and Challenges. *Brief. Funct. Genomics* 15 (6), 460–469. doi:10.1093/bfgp/elw014

Hao, Z., Wu, T., Cui, X., Zhu, P., Tan, C., Dou, X., et al. (2020). N6-Deoxyadenosine Methylation in Mammalian Mitochondrial DNA. *Mol. Cell* 78 (3), 382–395. doi:10.1016/j.molcel.2020.02.018

Hasan, M. M., Basith, S., Khatun, M. S., Lee, G., Manavalan, B., and Kurata, H. (2021). Meta-i6mA: an Interspecies Predictor for Identifying DNA N6-Methyladenine Sites of Plant Genomes by Exploiting Informative Features in an Integrative Machine-Learning Framework. *Briefings Bioinforma.* 22 (3), bbaa202. doi:10.1093/bib/bbaa202

He, S., Zhang, G., Wang, J., Gao, Y., Sun, R., Cao, Z., et al. (2019). 6mA-DNA-binding Factor Jumu Controls Maternal-To-Zygotic Transition Upstream of Zelda. *Nat. Commun.* 10 (1), 2219. doi:10.1038/s41467-019-10202-3

He, Y.-F., Li, B.-Z., Li, Z., Liu, P., Wang, Y., Tang, Q., et al. (2011). Tet-mediated Formation of 5-carboxylcytosine and its Excision by TDG in Mammalian DNA. *Science* 333 (6047), 1303–1307. doi:10.1126/science.1210944

Hendrich, B., and Bird, A. (1998). Identification and Characterization of a Family of Mammalian Methyl-CpG Binding Proteins. *Mol. Cell. Biol.* 18 (11), 6538–6547. doi:10.1128/mcb.18.11.6538

Huff, J. T., and Zilberman, D. (2014). Dnmt1-independent CG Methylation Contributes to Nucleosome Positioning in Diverse Eukaryotes. *Cell.* 156 (6), 1286–1297. doi:10.1016/j.cell.2014.01.029

Ito, S., Shen, L., Dai, Q., Wu, S. C., Collins, L. B., Swenberg, J. A., et al. (2011). Tet Proteins Can Convert 5-methylcytosine to 5-formylcytosine and 5-carboxylcytosine. *Science* 333 (6047), 1300–1303. doi:10.1126/science.1210597

Jain, T., Nikolopoulou, E. A., Xu, Q., and Qu, A. (2018). Hypoxia Inducible Factor as a Therapeutic Target for Atherosclerosis. *Pharmacol. Ther.* 183, 22–33. doi:10.1016/j.pharmthera.2017.09.003

Jeong, H. M., Lee, S., Chae, H., Kim, R., Kwon, M. J., Oh, E., et al. (2016). Efficiency of Methylated DNA Immunoprecipitation Bisulphite Sequencing for Whole-Genome DNA Methylation Analysis. *Epigenomics* 8 (8), 1061–1077. doi:10.2217/epi-2016-0038

Jimenez-Useche, I., Ke, J., Tian, Y., Shim, D., Howell, S. C., Qiu, X., et al. (2013). DNA Methylation Regulated Nucleosome Dynamics. *Sci. Rep.* 3, 2121. doi:10.1038/srep02121

Joshi, S., Ujaoney, A. K., Ghosh, P., Deobagkar, D. D., and Basu, B. (2021). N6-methyladenine and Epigenetic Immunity of Deinococcus Radiodurans. *Res. Microbiol.* 172 (1), 103789. doi:10.1016/j.resmic.2020.10.004

Khanal, J., Lim, D. Y., Tayara, H., and Chong, K. T. (2021). i6mA-stack: A Stacking Ensemble-Based Computational Prediction of DNA N6-Methyladenine (6mA) Sites in the Rosaceae Genome. *Genomics* 113 (1 Pt 2), 582–592. doi:10.1016/j.ygeno.2020.09.054

Kigar, S. L., Chang, L., Guerrero, C. R., Sehring, J. R., Cuarenta, A., Parker, L. L., et al. (2017). N6-methyladenine Is an Epigenetic Marker of Mammalian Early Life Stress. *Sci. Rep.* 7 (1), 18078. doi:10.1038/s41598-017-18414-7

Koh, C. W. Q., Goh, Y. T., Toh, J. D. W., Neo, S. P., Ng, S. B., Gunaratne, J., et al. (2018). Single-nucleotide-resolution Sequencing of humanN6-Methyldeoxyadenosine Reveals Strand-Asymmetric Clusters Associated with SSBP1 on the Mitochondrial Genome. *Nucleic acids Res.* 46 (22), 11659–11670. doi:10.1093/nar/gky1104

Kong, Y., Cao, L., Deikus, G., Fan, Y., Mead, E. A., Lai, W., et al. (2022). Critical Assessment of DNA Adenine Methylation in Eukaryotes Using Quantitative Deconvolution. *Science* 375 (6580), 515–522. doi:10.1126/science.abe7489

Kweon, S.-M., Chen, Y., Moon, E., Kvederaviciutė, K., Klimasauskas, S., and Feldman, D. E. (2019). An Adversarial DNA N6-Methyladenine-Sensor Network Preserves Polycomb Silencing. *Mol. Cell* 74 (6), 1138–1147. doi:10.1016/j.molcel.2019.03.018

Laird, P. W. (2010). Principles and Challenges of Genome-wide DNA Methylation Analysis. *Nat. Rev. Genet.* 11 (3), 191–203. doi:10.1038/nrg2732

Lang, Z., Wang, Y., Tang, K., Tang, D., Datsenka, T., Cheng, J., et al. (2017). Critical Roles of DNA Demethylation in the Activation of Ripening-Induced Genes and Inhibition of Ripening-Repressed Genes in Tomato Fruit. *Proc. Natl. Acad. Sci. U.S.A.* 114 (22), E4511–E4519. doi:10.1073/pnas.1705233114

Li, W., Shi, Y., Zhang, T., Ye, J., and Ding, J. (2019). Structural Insight into Human N6amt1-Trm112 Complex Functioning as a Protein Methyltransferase. *Cell. Discov.* 5, 51. doi:10.1038/s41421-019-0121-y

Li, W., Zhang, T., and Ding, J. (2015). Molecular Basis for the Substrate Specificity and Catalytic Mechanism of Thymine-7-Hydroxylase in Fungi. *Nucleic Acids Res.* 43 (20), gkv979–10038. doi:10.1093/nar/gkv979

Li, X., Zhang, Z., Luo, X., Schrier, J., Yang, A. D., and Wu, T. P. (2021a). The Exploration of N6-Deoxyadenosine Methylation in Mammalian Genomes. *Protein Cell.* 12 (10), 756–768. doi:10.1007/s13238-021-00866-3

Li, Z., Jiang, H., Kong, L., Chen, Y., Lang, K., Fan, X., et al. (2021b). Deep6mA: A Deep Learning Framework for Exploring Similar Patterns in DNA N6-Methyladenine Sites across Different Species. *PLoS Comput. Biol.* 17 (2), e1008767. doi:10.1371/journal.pcbi.1008767

Li, Z., Zhao, S., Nelakanti, R. V., Lin, K., Wu, T. P., Alderman, M. H., et al. (2020). N6-methyladenine in DNA Antagonizes SATB1 in Early Development. *Nature* 583 (7817), 625–630. doi:10.1038/s41586-020-2500-9

Liang, Z., Riaz, A., Chachar, S., Ding, Y., Du, H., and Gu, X. (2020). Epigenetic Modifications of mRNA and DNA in Plants. *Mol. plant* 13 (1), 14–30. doi:10.1016/j.molp.2019.12.007

Liang, Z., Shen, L., Cui, X., Bao, S., Geng, Y., Yu, G., et al. (2018). DNA N-Adenine Methylation in *Arabidopsis thaliana*. *Dev. Cell* 45 (3), 406–416. doi:10.1016/j.devcel.2018.03.012

Liu, B., Liu, X., Lai, W., and Wang, H. (2017). Metabolically Generated Stable Isotope-Labeled Deoxynucleoside Code for Tracing DNA N6-Methyladenine in Human Cells. *Anal. Chem.* 89 (11), 6202–6209. doi:10.1021/acs.analchem.7b01152

Liu, B., and Wang, H. (2021). Detection of N6-Methyladenine in Eukaryotes. *Adv. Exp. Med. Biol.* 1280, 83–95. doi:10.1007/978-3-030-51652-9_6

Liu, F., Clark, W., Luo, G., Wang, X., Fu, Y., Wei, J., et al. (2016a). ALKBH1-Mediated tRNA Demethylation Regulates Translation. *Cell.* 167 (3), 816–828. doi:10.1016/j.cell.2016.09.038

Liu, J., Zhu, Y., Luo, G.-Z., Wang, X., Yue, Y., Wang, X., et al. (2016b). Abundant DNA 6mA Methylation during Early Embryogenesis of Zebrafish and Pig. *Nat. Commun.* 7, 13052. doi:10.1038/ncomms13052

Liu, X., Lai, W., Li, Y., Chen, S., Liu, B., Zhang, N., et al. (2020). N6-methyladenine Is Incorporated into Mammalian Genome by DNA Polymerase. *Cell. Res.* 31, 94–97. doi:10.1038/s41422-020-0317-6

Liu, X., Lai, W., Li, Y., Chen, S., Liu, B., Zhang, N., et al. (2021a). N6-methyladenine Is Incorporated into Mammalian Genome by DNA Polymerase. *Cell. Res.* 31 (1), 94–97. doi:10.1038/s41422-020-0317-6

Liu, X., Xie, P., Hao, N., Zhang, M., Liu, Y., Liu, P., et al. (2021). HIF-1-regulated Expression of Calreticulin Promotes Breast Tumorigenesis and Progression through Wnt/β-Catenin Pathway Activation. *Proc. Natl. Acad. Sci. U.S.A.* 118 (44), 44118. doi:10.1073/pnas.2109144118

Liu, Y., Chen, Y., Wang, Y., Jiang, S., Lin, W., Wu, Y., et al. (2022). DNA Demethylase ALKBH1 Promotes Adipogenic Differentiation via Regulation of HIF-1 Signaling. *J. Biol. Chem.* 298 (1), 101499. doi:10.1016/j.jbc.2021.101499

Liutkevičiūtė, Z., Lukinavičius, G., Masevičius, V., Daujotytė, D., and Klimašauskas, S. (2009). Cytosine-5-methyltransferases Add Aldehydes to DNA. *Nat. Chem. Biol.* 5 (6), 400–402. doi:10.1038/nchembio.172

Lizarraga, A., O'Brown, Z. K., Boulias, K., Roach, L., Greer, E. L., Johnson, P. J., et al. (2020). Adenine DNA Methylation, 3D Genome Organization, and Gene Expression in the Parasite Trichomonas Vaginalis. *Proc. Natl. Acad. Sci. U.S.A.* 117 (23), 13033–13043. doi:10.1073/pnas.1917286117

Luo, C., Hajkova, P., and Ecker, J. R. (2018a). Dynamic DNA Methylation: In the Right Place at the Right Time. *Science* 361 (6409), 1336–1340. doi:10.1126/science.aat6806

Luo, G.-Z., Hao, Z., Luo, L., Shen, M., Sparvoli, D., Zheng, Y., et al. (2018b). N6-methyldeoxyadenosine Directs Nucleosome Positioning in Tetrahymena DNA. *Genome Biol.* 19 (1), 200. doi:10.1186/s13059-018-1573-3

Lv, H., Dao, F. Y., Zhang, D., Yang, H., and Lin, H. (2021). Advances in Mapping the Epigenetic Modifications of 5-methylcytosine (5mC), N6-methyladenine (6mA), and N4-methylcytosine (4mC). *Biotech Bioeng.* 118 (11), 4204–4216. doi:10.1002/bit.27911

Ma, C., Niu, R., Huang, T., Shao, L.-W., Peng, Y., Ding, W., et al. (2019). N6-methyldeoxyadenine Is a Transgenerational Epigenetic Signal for Mitochondrial Stress Adaptation. *Nat. Cell. Biol.* 21 (3), 319–327. doi:10.1038/s41556-018-0238-5

Martisova, A., Holcakova, J., Izadi, N., Sebuyoya, R., Hrstka, R., and Bartosik, M. (2021). DNA Methylation in Solid Tumors: Functions and Methods of Detection. *Ijms* 22 (8), 4247. doi:10.3390/ijms22084247

Mondo, S. J., Dannebaum, R. O., Kuo, R. C., Louie, K. B., Bewick, A. J., LaButti, K., et al. (2017). Widespread Adenine N6-Methylation of Active Genes in Fungi. *Nat. Genet.* 49 (6), 964–968. doi:10.1038/ng.3859

Morgan, R. D., Dwinell, E. A., Bhatia, T. K., Lang, E. M., and Luyten, Y. A. (2009). The MmeI Family: Type II Restriction-Modification Enzymes that Employ Single-Strand Modification for Host Protection. *Nucleic acids Res.* 37 (15), 5208–5221. doi:10.1093/nar/gkp534

Musheev, M. U., Baumgärtner, A., Krebs, L., and Niehrs, C. (2020). The Origin of Genomic N6-Methyl-Deoxyadenosine in Mammalian Cells. *Nat. Chem. Biol.* 16 (6), 630–634. doi:10.1038/s41589-020-0504-2

Nejman, D., Livyatan, I., Fuks, G., Gavert, N., Zwang, Y., Geller, L. T., et al. (2020). The Human Tumor Microbiome Is Composed of Tumor Type-specific Intracellular Bacteria. *Science* 368 (6494), 973–980. doi:10.1126/science.aay9189

O'Brown, Z. K., Boulias, K., Wang, J., Wang, S. Y., O'Brown, N. M., Hao, Z., et al. (2019). Sources of Artifact in Measurements of 6mA and 4mC Abundance in Eukaryotic Genomic DNA. *BMC genomics* 20 (1), 445. doi:10.1186/s12864-019-5754-6

Ouyang, L., Su, X., Li, W., Tang, L., Zhang, M., Zhu, Y., et al. (2021). ALKBH1-demethylated DNA N6-Methyladenine Modification Triggers Vascular Calcification via Osteogenic Reprogramming in Chronic Kidney Disease. *J. Clin. investigation* 131 (14), 46985. doi:10.1172/JCI146985

Pérez, A., Castellazzi, C. L., Battistini, F., Collinet, K., Flores, O., Deniz, O., et al. (2012). Impact of Methylation on the Physical Properties of DNA. *Biophysical J.* 102 (9), 2140–2148. doi:10.1016/j.bpj.2012.03.056

Razin, A. (1984). "DNA Methylation Patterns: Formation and Biological Functions," in *DNA Methylation: Biochemistry and Biological Significance*. Editors A. Razin, H. Cedar, and A. D. Riggs (New York, NY: Springer New York), 127–146. doi:10.1007/978-1-4613-8519-6_7

Rehman, M. U., and Chong, K. T. (2020). DNA6mA-MINT: DNA-6mA Modification Identification Neural Tool. *Genes.* 11 (8), 898. doi:10.3390/genes11080898

Reisenauer, A., Kahng, L. S., McCollum, S., and Shapiro, L. (1999). Bacterial DNA Methylation: a Cell Cycle Regulator? *J. Bacteriol.* 181 (17), 5135–5139. doi:10.1128/jb.181.17.5135-5139.1999

Rodriguez, F., Yushenova, I. A., DiCorpo, D., and Arkhipova, I. R. (2022). Bacterial N4-Methylcytosine as an Epigenetic Mark in Eukaryotic DNA. *Nat. Commun.* 13 (1), 1072. doi:10.1038/s41467-022-28471-w

Rong, S., Zhao, X., Jin, X., Zhang, Z., Chen, L., Zhu, Y., et al. (2014). Vascular Calcification in Chronic Kidney Disease Is Induced by Bone Morphogenetic Protein-2 via a Mechanism Involving the Wnt/-Catenin Pathway. *Cell. Physiol. Biochem.* 34 (6), 2049–2060. doi:10.1159/000366400

Schadt, E. E., Banerjee, O., Fang, G., Feng, Z., Wong, W. H., Zhang, X., et al. (2013). Modeling Kinetic Rate Variation in Third Generation DNA Sequencing Data to Detect Putative Modifications to DNA Bases. *Genome Res.* 23 (1), 129–141. doi:10.1101/gr.136739.111

Schiesser, S., Pfaffeneder, T., Sadeghian, K., Hackner, B., Steigenberger, B., Schröder, A. S., et al. (2013). Deamination, Oxidation, and C-C Bond Cleavage Reactivity of 5-hydroxymethylcytosine, 5-formylcytosine, and 5-carboxycytosine. *J. Am. Chem. Soc.* 135 (39), 14593–14599. doi:10.1021/ja403229y

Schiffers, S., Ebert, C., Rahimoff, R., Kosmatchev, O., Steinbacher, J., Bohne, A.-V., et al. (2017). Quantitative LC-MS Provides No Evidence for m6dA or m4dC in the Genome of Mouse Embryonic Stem Cells and Tissues. *Angew. Chem. Int. Ed.* 56 (37), 11268–11271. doi:10.1002/anie.201700424

Schmitz, R. J., Lewis, Z. A., and Goll, M. G. (2019). DNA Methylation: Shared and Divergent Features across Eukaryotes. *Trends Genet.* 35 (11), 818–827. doi:10.1016/j.tig.2019.07.007

Shah, K., Cao, W., and Ellison, C. E. (2019). Adenine Methylation in Drosophila Is Associated with the Tissue-specific Expression of Developmental and Regulatory Genes. *G3 (Bethesda, Md* 9 (6), 1893–1900. doi:10.1534/g3.119.400023

Shanmuganathan, R., Basheer, N. B., Amirthalingam, L., Muthukumar, H., Kaliaperumal, R., and Shanmugam, K. (2013). Conventional and Nanotechniques for DNA Methylation Profiling. *J. Mol. Diagnostics* 15 (1), 17–26. doi:10.1016/j.jmoldx.2012.06.007

Shen, C., Wang, K., Deng, X., and Chen, J. (2022). DNA N6-Methyldeoxyadenosine in Mammals and Human Disease. *Trends Genet.* 38, 454–467. doi:10.1016/j.tig.2021.12.003

Sheng, X., Wang, J., Guo, Y., Zhang, J., and Luo, J. (2020). DNA N6-Methyladenine (6mA) Modification Regulates Drug Resistance in Triple Negative Breast Cancer. *Front. Oncol.* 10, 616098. doi:10.3389/fonc.2020.616098

Sheng, Y., Pan, B., Wei, F., Wang, Y., and Gao, S. (2021). Case Study of the Response of N 6 -Methyladenine DNA Modification to Environmental Stressors in the Unicellular Eukaryote Tetrahymena Thermophila. *mSphere* 6 (3), e0120820. doi:10.1128/mSphere.01208-20

Smith, Z. D., and Meissner, A. (2013). DNA Methylation: Roles in Mammalian Development. *Nat. Rev. Genet.* 14 (3), 204–220. doi:10.1038/nrg3354

Song, L., James, S. R., Kazim, L., and Karpf, A. R. (2005). Specific Method for the Determination of Genomic DNA Methylation by Liquid Chromatography-Electrospray Ionization Tandem Mass Spectrometry. *Anal. Chem.* 77 (2), 504–510. doi:10.1021/ac0489420

Tahiliani, M., Koh, K. P., Shen, Y., Pastor, W. A., Bandukwala, H., Brudno, Y., et al. (2009). Conversion of 5-methylcytosine to 5-hydroxymethylcytosine in Mammalian DNA by MLL Partner TET1. *Science* 324 (5929), 930–935. doi:10.1126/science.1170116

Tian, L.-F., Liu, Y.-P., Chen, L., Tang, Q., Wu, W., Sun, W., et al. (2020). Structural Basis of Nucleic Acid Recognition and 6mA Demethylation by Human ALKBH1. *Cell. Res.* 30 (3), 272–275. doi:10.1038/s41422-019-0233-9

Tsukiyama, S., Hasan, M. M., Deng, H.-W., and Kurata, H. (2022). BERT6mA: Prediction of DNA N6-Methyladenine Site Using Deep Learning-Based Approaches. *Briefings Bioinforma.* 23, bbac053. doi:10.1093/bib/bbac053

Usai, G., Vangelisti, A., Simoni, S., Giordani, T., Natali, L., Cavallini, A., et al. (2021). DNA Modification Patterns within the Transposable Elements of the Fig (Ficus Carica L.) Genome. *Plants* 10 (3), 451. doi:10.3390/plants10030451

Vasu, K., and Nagaraja, V. (2013). Diverse Functions of Restriction-Modification Systems in Addition to Cellular Defense. *Microbiol. Mol. Biol. Rev.* 77 (1), 53–72. doi:10.1128/MMBR.00044-12

Vogeser, M., and Seger, C. (2008). A Decade of HPLC-MS/MS in the Routine Clinical Laboratory - Goals for Further Developments. *Clin. Biochem.* 41 (9), 649–662. doi:10.1016/j.clinbiochem.2008.02.017

Wang, B., Luo, Q., Li, Y., Yin, L., Zhou, N., Li, X., et al. (2020). Structural Insights into Target DNA Recognition by R2R3-MYB Transcription Factors. *Nucleic acids Res.* 48 (1), 460–471. doi:10.1093/nar/gkz1081

Wang, Y., Chen, X., Sheng, Y., Liu, Y., and Gao, S. (2017). N6-adenine DNA Methylation Is Associated with the Linker DNA of H2A.Z-Containing Well-Positioned Nucleosomes in Pol II-Transcribed Genes in Tetrahymena. *Nucleic acids Res.* 45 (20), 11594–11606. doi:10.1093/nar/gkx883

Wang, Y., Sheng, Y., Liu, Y., Zhang, W., Cheng, T., Duan, L., et al. (2019). A Distinct Class of Eukaryotic MT-A70 Methyltransferases Maintain Symmetric DNA N6-Adenine Methylation at the ApT Dinucleotides as an Epigenetic Mark Associated with Transcription. *Nucleic acids Res.* 47 (22), 11771–11789. doi:10.1093/nar/gkz1053

Wang, Y., Zhang, P., Guo, W., Liu, H., Li, X., Zhang, Q., et al. (2021). A Deep Learning Approach to Automate Whole-genome Prediction of Diverse Epigenomic Modifications in Plants. *New Phytol.* 232 (2), 880–897. doi:10.1111/nph.17630

Wion, D., and Casadesús, J. (2006). N6-methyl-adenine: an Epigenetic Signal for DNA-Protein Interactions. *Nat. Rev. Microbiol.* 4 (3), 183–192. doi:10.1038/nrmicro1350

Woodcock, C. B., Yu, D., Zhang, X., and Cheng, X. (2019). Human HemK2/KMT9/N6AMT1 Is an Active Protein Methyltransferase, but Does Not Act on DNA *In Vitro*, in the Presence of Trm112. *Cell. Discov.* 5, 50. doi:10.1038/s41421-019-0119-5

Wu, T. P., Wang, T., Seetin, M. G., Lai, Y., Zhu, S., Lin, K., et al. (2016). DNA Methylation on N6-Adenine in Mammalian Embryonic Stem Cells. *Nature* 532 (7599), 329–333. doi:10.1038/nature17640

Wu, X., and Zhang, Y. (2017). TET-mediated Active DNA Demethylation: Mechanism, Function and beyond. *Nat. Rev. Genet.* 18 (9), 517–534. doi:10.1038/nrg.2017.33

Xiao, C.-L., Zhu, S., He, M., Chen, D., Zhang, Q., Chen, Y., et al. (2018). N6-Methyladenine DNA Modification in the Human Genome. *Mol. Cell* 71 (2), 306–318. doi:10.1016/j.molcel.2018.06.015

Xie, Q., Wu, T. P., Gimple, R. C., Li, Z., Prager, B. C., Wu, Q., et al. (2018). N-methyladenine DNA Modification in Glioblastoma. *Cell.* 175 (5), 1228–1243. doi:10.1016/j.cell.2018.10.006

Yang, S., Wang, Y., Chen, Y., and Dai, Q. (2020). MASQC: Next Generation Sequencing Assists Third Generation Sequencing for Quality Control in N6-Methyladenine DNA Identification. *Front. Genet.* 11, 269. doi:10.3389/fgene.2020.00269

Yao, B., Cheng, Y., Wang, Z., Li, Y., Chen, L., Huang, L., et al. (2017). DNA N6-Methyladenine Is Dynamically Regulated in the Mouse Brain Following Environmental Stress. *Nat. Commun.* 8 (1), 1122. doi:10.1038/s41467-017-01195-y

Young, J. I., Züchner, S., and Wang, G. (2015). Regulation of the Epigenome by Vitamin C. *Annu. Rev. Nutr.* 35, 545–564. doi:10.1146/annurev-nutr-071714-034228

Yu, H., and Dai, Z. (2019). SNNRice6mA: A Deep Learning Method for Predicting DNA N6-Methyladenine Sites in Rice Genome. *Front. Genet.* 10, 1071. doi:10.3389/fgene.2019.01071

Zhang, G., Diao, S., Song, Y., He, C., and Zhang, J. (2022a). Genome-wide DNA N6-Adenine Methylation in Sea Buckthorn (Hippophae Rhamnoides L.) Fruit Development. *Tree Physiol.* doi:10.1093/treephys/tpab177

Zhang, G., Huang, H., Liu, D., Cheng, Y., Liu, X., Zhang, W., et al. (2015). N6-methyladenine DNA Modification in Drosophila. *Cell.* 161 (4), 893–906. doi:10.1016/j.cell.2015.04.018

Zhang, H., Lang, Z., and Zhu, J.-K. (2018a). Dynamics and Function of DNA Methylation in Plants. *Nat. Rev. Mol. Cell. Biol.* 19 (8), 489–506. doi:10.1038/s41580-018-0016-z

Zhang, L., Rong, W., Ma, J., Li, H., Tang, X., Xu, S., et al. (2022b). Comprehensive Analysis of DNA 5-Methylcytosine and N6-Adenine Methylation by Nanopore Sequencing in Hepatocellular Carcinoma. *Front. Cell. Dev. Biol.* 10, 827391. doi:10.3389/fcell.2022.827391

Zhang, M., Yang, S., Nelakanti, R., Zhao, W., Liu, G., Li, Z., et al. (2020). Mammalian ALKBH1 Serves as an N6-mA Demethylase of Unpairing DNA. *Cell. Res.* 30 (3), 197–210. doi:10.1038/s41422-019-0237-5

Zhang, Q., Liang, Z., Cui, X., Ji, C., Li, Y., Zhang, P., et al. (2018b). N6-Methyladenine DNA Methylation in Japonica and Indica Rice Genomes and its Association with Gene Expression, Plant Development, and Stress Responses. *Mol. plant* 11 (12), 1492–1508. doi:10.1016/j.molp.2018.11.005

Zhang, Y., Liu, Y., Xu, J., Wang, X., Peng, X., Song, J., et al. (2021). Leveraging the Attention Mechanism to Improve the Identification of DNA N6-Methyladenine Sites. *Briefings Bioinforma.* 22, 351. doi:10.1093/bib/bbab351

Zhou, C., Wang, C., Liu, H., Zhou, Q., Liu, Q., Guo, Y., et al. (2018). Identification and Analysis of Adenine N6-Methylation Sites in the Rice Genome. *Nat. plants* 4 (8), 554–563. doi:10.1038/s41477-018-0214-x

Zhu, S., Beaulaurier, J., Deikus, G., Wu, T. P., Strahl, M., Hao, Z., et al. (2018). Mapping and Characterizing N6-Methyladenine in Eukaryotic Genomes Using Single-Molecule Real-Time Sequencing. *Genome Res.* 28 (7), 1067–1078. doi:10.1101/gr.231068.117

Conflict of Interest: The authors declare that the research was conducted in the absence of any commercial or financial relationships that could be construed as a potential conflict of interest.

frontiers | Frontiers in Genetics

REVIEW
published: 11 July 2022
doi: 10.3389/fgene.2022.906662

Functions and Interactions of Mammalian KDM5 Demethylases

Egor Pavlenko[1†], *Till Ruengeler*[1†], *Paulina Engel*[1] *and Simon Poepsel*[1,2*]

[1]University of Cologne, Center for Molecular Medicine Cologne (CMMC), Faculty of Medicine and University Hospital, Cologne, Germany, [2]Cologne Excellence Cluster for Cellular Stress Responses in Ageing-Associated Diseases (CECAD), University of Cologne, Cologne, Germany

Mammalian histone demethylases of the KDM5 family are mediators of gene expression dynamics during developmental, cellular differentiation, and other nuclear processes. They belong to the large group of JmjC domain containing, 2-oxoglutarate (2-OG) dependent oxygenases and target methylated lysine 4 of histone H3 (H3K4me1/2/3), an epigenetic mark associated with active transcription. In recent years, KDM5 demethylases have gained increasing attention due to their misregulation in many cancer entities and are intensively explored as therapeutic targets. Despite these implications, the molecular basis of KDM5 function has so far remained only poorly understood. Little is known about mechanisms of nucleosome recognition, the recruitment to genomic targets, as well as the local regulation of demethylase activity. Experimental evidence suggests close physical and functional interactions with epigenetic regulators such as histone deacetylase (HDAC) containing complexes, as well as the retinoblastoma protein (RB). To understand the regulation of KDM5 proteins in the context of chromatin, these interactions have to be taken into account. Here, we review the current state of knowledge on KDM5 function, with a particular emphasis on molecular interactions and their potential implications. We will discuss and outline open questions that need to be addressed to better understand histone demethylation and potential demethylation-independent functions of KDM5s. Addressing these questions will increase our understanding of histone demethylation and allow us to develop strategies to target individual KDM5 enzymes in specific biological and disease contexts.

Keywords: KDM5, gene regulation, epigenetics, histone demethylation, JmjC oxygenases

OPEN ACCESS

Edited by:
Laxmi Narayan Mishra, Regeneron Pharmaceuticals, Inc., United States

Reviewed by:
Xin Cui, Georgia State University, United States
Arun Sikarwar, Dayalbagh Educational Institute, India

***Correspondence:**
Simon Poepsel
spoepsel@uni-koeln.de

[†]*These authors have contributed equally to this work*

Specialty section:
This article was submitted to Epigenomics and Epigenetics, a section of the journal Frontiers in Genetics

Received: *28 March 2022*
Accepted: *06 June 2022*
Published: *11 July 2022*

Citation:
Pavlenko E, Ruengeler T, Engel P and Poepsel S (2022) Functions and Interactions of Mammalian KDM5 Demethylases. Front. Genet. 13:906662. doi: 10.3389/fgene.2022.906662

INTRODUCTION

Chromatin structure and its chemical modifications are central to the coordination of transcriptional activity and other nuclear processes. Post-translational modifications (PTMs) of histone proteins that form the core of nucleosomes, the basic organizing unit of chromatin, are key in these processes and tightly linked to chromatin regulation (Strahl and Allis, 2000). Histone PTMs are markers of regulatory genomic elements and functional chromatin states. Accordingly, the prevalence of histone PTMs is highly dynamic and reflects cellular states and their transitions. For example, during cellular differentiation, the landscape of histone PTMs undergoes characteristic changes that correlate with the re-shaping of transcription patterns (Li et al., 2007). A key notion in epigenetics is that histone PTMs are introduced and removed by enzymes that act in a spatio-temporally defined manner. Thus, their faithful regulation is required for normal development and cellular differentiation (Margueron and Reinberg, 2011).

Protein domains that specifically recognize histone PTMs, so-called 'reader' domains, are important for these regulatory mechanisms. Reader domains recruit associated proteins and multi-protein complexes to their genomic targets, but also couple recruitment to local allosteric activation or inhibition of associated enzymes (Torres and Fujimori, 2015). The assembly, composition, and dynamic chromatin interactions of multi-subunit complexes give rise to the complexity of chromatin regulation that is still only beginning to be elucidated. Key to these intricate mechanisms are the interactions to recruit and locally regulate chromatin modifying enzymes as well as their dynamic interplay to control chromatin structure, transcription and other processes.

Deciphering the diverse roles of histone PTMs in different biological contexts remains a substantial challenge and thus is subject of intense research. While detailed molecular mechanisms and implications remain poorly understood in many instances, the most prevalent histone PTMs are reasonably well described. Methylation of lysine 4 of histone H3 (H3K4me1/2/3) is generally associated with genomic regions marked by high transcriptional activity. Alternatively, when present alongside trimethylated lysine 27 of histone H3 (H3K27me3), this PTM is associated with a poised state allowing for rapid transcriptional activation or repression, particularly during early development (Santos-Rosa et al., 2002; Heintzman et al., 2007; Kim and Buratowski, 2009; Rada-Iglesias et al., 2011). Accordingly, factors that interact with methylated H3K4 are involved in transcriptional regulation, such as general transcription factors (Vermeulen et al., 2007), chromatin remodelers such as the BAF and NURF complexes (Wysocka et al., 2006; Local et al., 2018) or methyltransferase complexes such as KMT2 (Park et al., 2010; Eberl et al., 2013).

ACTIVITY AND FUNCTIONS OF KDM5 DEMETHYLASES

The four human members of the KDM5 family, KDM5A-D, each of which has a highly similar mouse homolog, are part of a large group of Jumonji C (JmjC) domain containing, 2-oxoglutarate (2-OG)- and Fe(II)-dependent dioxygenases that comprises numerous enzymes, among them many with chromatin associated functions. Interestingly, the biological function of JmjC domain dioxygenases, as well as their use of and responsiveness to metabolites such as 2-OG, fumarate and succinate, mediate key roles in cancer biology, in particular cancer metabolism (Xu et al., 2011; Losman et al., 2020). The idea that JmjC dioxygenases may have histone lysine demethylating activities was based on the discoveries of DNA demethylation by the dioxygenase AlkB (Trewick et al., 2002), and the hydroxylation of hypoxia-inducible factor (HIF) by EGLN (Bruick and McKnight, 2001; Jaakkola et al., 2001). Indeed, following the first report of a JmjC domain histone demethylase (Tsukada et al., 2006), all four human KDM5 enzymes were shown to specifically demethylate lysine 4 of histone H3 (H3K4) in a series of landmark studies (Christensen et al., 2007; Iwase et al., 2007; Klose et al., 2007; Seward et al., 2007; Tahiliani et al., 2007). The catalytic activity of JmjC domain demethylases involves the decarboxylation of the cofactor 2-OG to succinate and CO_2, as well as the hydroxylation of methylated lysine, leading to the spontaneous decomposition of an unstable hemi-aminal intermediate into demethylated lysine and formaldehyde (Walport et al., 2012) (**Figure 1A**). KDM5 demethylases are generally considered to specifically demethylate the di- and trimethylated state of H3K4 (H3K4me2/3), leading to the hypothesis that the coordination with the activity of the H3K4me1/2-specific demethylase LSD1 may be required for the complete demethylation of H3K4 (Christensen et al., 2007; Klose et al., 2007; Seward et al., 2007; Tahiliani et al., 2007). However, *in vitro* data suggests that demethylation of H3K4me1 by KDM5 enzymes is also possible (Metzger et al., 2010; Kristensen et al., 2012). How specific targeting of different methylation states of H3K4 is brought about, and whether there are mechanisms regulating this specificity is currently unknown.

Members of the KDM5 family of proteins had been known to perform regulatory roles in transcription before their demethylase activity was established. For example, an early report described KDM5B as a co-repressor of developmental transcription factors such as paired box 9 (PAX9) and brain-factor 1 (BF-1) (Tan et al., 2003). Since H3K4 methylation had been recognized as a feature of active chromatin (Litt et al., 2001), an obvious mechanism of KDM5 enzymes was the demethylation of H3K4me2/3 facilitating transcriptional repression. In agreement with this hypothesis, human KDM5 proteins were shown to cause an overall decrease in cellular levels of H3K4me3 when overexpressed (Christensen et al., 2007; Iwase et al., 2007; Klose et al., 2007). Aspects of KDM5 function, such as HOX gene repression by KDM5A (Christensen et al., 2007) and promotion of neuronal viability by KDM5C (Iwase et al., 2007), could be directly linked to their demethylase activity. However, it was also noted in these early studies that KDM5 function may partly be mediated independently of their catalytic activity. For example, KDM5A knock-out mouse embryonic fibroblasts did display transcriptional repression of KDM5A targets even when a catalytically inactive KDM5A was expressed (Klose et al., 2007).

A growing body of literature illustrates the diverse roles of KDM5 demethylases in gene regulation, differentiation and developmental processes. KDM5 proteins help to control cellular differentiation in a number of contexts, but the reported mechanisms and implications vary and seem contradictory at times. For example, loss of KDM5B is associated with embryonic stem cell (ESC) differentiation *in vitro* (Xie et al., 2011) and was shown to antagonize terminal ESC differentiation by balancing cell proliferation and differentiation (Dey et al., 2008). At the same time, the enzyme was required for neuronal differentiation in another study (Schmitz et al., 2011). All three studies have in common, however, that lineage-specific gene expression during differentiation was impaired upon KDM5 depletion (Dey et al., 2008; Schmitz et al., 2011; Xie et al., 2011). In the context of its interactions with the retinoblastoma protein (RB) it was suggested that KDM5A can contribute to the transcriptional activation of genes involved in cellular

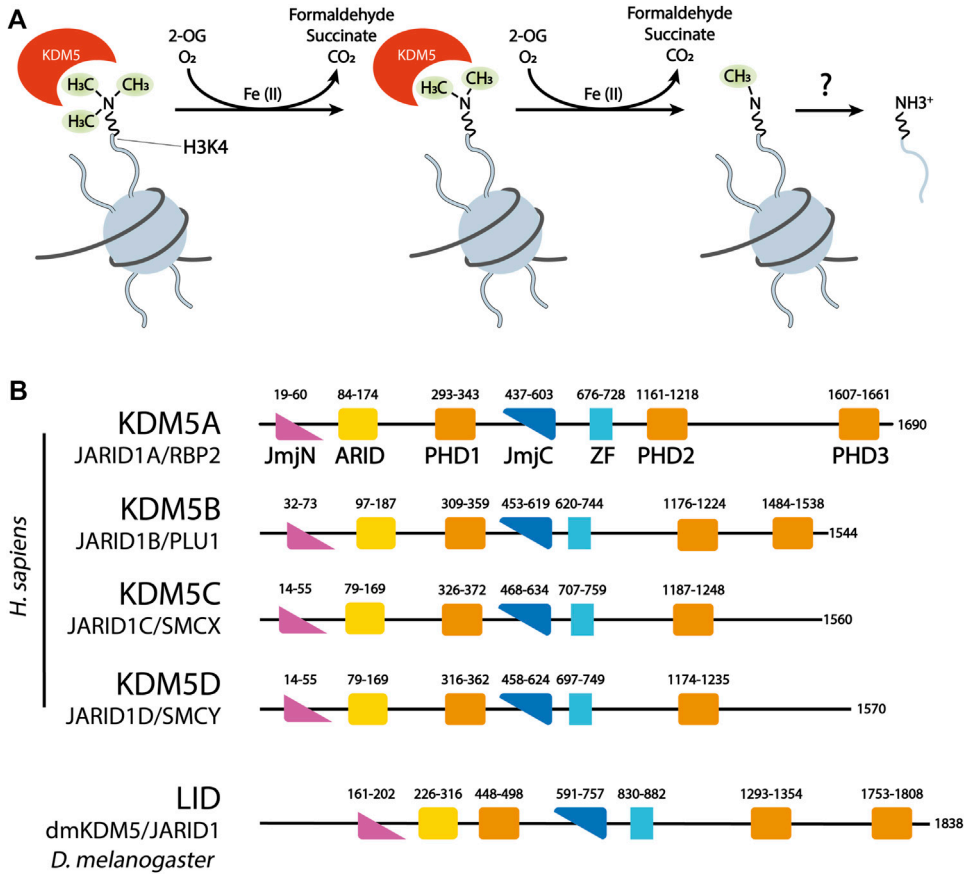

FIGURE 1 | (A) KDM5 demethylases remove methyl groups from H3K4 in a sequential manner, using the dioxygenase activity of their catalytic JmjC domain. 2-Oxoglutarate (2-OG) is decarboxylated to succinate. Formaldehyde, one of the products of demethylation, is commonly detected in quantitative assays of JmjC demethylase activity. **(B)** Domain organization of the four human KDM5 demethylases and the *Drosophila* KDM5 homolog Lid. ZF = C5HC2 Zinc Finger. Numbers correspond to the amino acid numbering of each KDM5 protein.

differentiation (Benevolenskaya et al., 2005), illustrating that KDM5 function is not limited to repressive effects on transcription. KDM5 enzymes have also been implicated in cell cycle control. For example, KDM5A and C genomic occupancy and demethylase activity were required for transcriptional activity of cell cycle regulators during adipocyte differentiation (Brier et al., 2017). The observation that, in the same experimental system, other genes marked by low H3K4me3 levels at their promoters were repressed by KDM5s, underscores the significance of cellular and genomic context for the implications of KDM5 occupancy and activity.

The single KDM5 homologs in *Drosophila melanogaster* and *Caenorhabditis elegans*, called Little imaginal discs (Lid) and retinoblastoma binding protein related 2 (RBR-2), respectively, are required for normal development (Gildea et al., 2000; Christensen et al., 2007). Mammalian KDM5 enzymes show distinct developmental defects upon their deletion, hinting at specific and partially non-redundant roles of these proteins in development. For example, loss of KDM5B leads to defects of respiratory function and neuronal development in mice (Albert et al., 2013). Furthermore, KDM5 enzymes were shown to be involved in DNA replication (Liang et al., 2011; Rondinelli et al., 2015; Gaillard et al., 2021), DNA repair (Gong et al., 2017; Kumbhar et al., 2021) and metabolic pathways (Chang et al., 2019). Comprehensive reviews discuss the functions of KDM5 and other demethylases in development and differentiation in more detail (Pedersen and Helin, 2010; Kooistra and Helin, 2012; Dimitrova et al., 2015; Punnia-Moorthy et al., 2021).

KDM5 DEMETHYLASES IN HUMAN DISEASES

A number of observations provide evidence of a critical role of KDM5 demethylases in diverse disease settings. For instance, KDM5C mutations are frequently found in X-linked intellectual disability (Jensen et al., 2005; Hatch and Secombe, 2021), linking KDM5C function to developmental regulation. Aberrant levels, in particular the amplification and/or overexpression of KDM5 demethylases in many types of cancer, including gastric (Zeng et al., 2010), breast (Yamane et al., 2007; Yamamoto et al., 2014), prostate (Xiang et al.,2007), lung cancer (Oser et al., 2019) and

leukemia (Xue et al., 2020) strongly link KDM5 demethylases to cancer biology. KDM5C was identified as a potential cancer driver (Bailey et al., 2018), and KDM5 inhibition has a strong inhibitory effect on tumor growth in tissue culture and *in vivo* models (Yamane et al., 2007; Vinogradova et al., 2016; Vogel et al., 2019). In some instances, specific roles have been identified by which KDM5 demethylases control tumor phenotypes and therapeutic response. Both KDM5A and KDM5B have been shown to be key determinants of a dynamic, phenotypic heterogeneity in cancer, defining differentiation, proliferation and responsiveness of cell populations to therapeutic intervention. One observation was a marked transcriptional heterogeneity of cancer cells depending on KDM5A and B functions (Hinohara et al., 2018). KDM5A was further identified as a critical factor characterizing drug tolerant persister cancer cells that mediated intrinsic resistance towards chemotherapy in a non-small cell lung cancer (SCLC) cell line (Sharma et al., 2010; Vinogradova et al., 2016). Melanoma cells were shown to be composed of heterogeneous cancer cells that, when expressing high levels of KDM5B, are resistant to therapy such as MAPK inhibition, giving rise to tumor repopulation after initial therapy (Roesch et al., 2010). KDM5B was also identified as a regulator of cancer stem cell properties in oral cancers (Facompre et al., 2016). These studies established KDM5 demethylases as regulators of epigenetic plasticity in human cells that are likely to be of significant interest for future drug development efforts.

In addition, several other mechanisms have been suggested to underlie KDM5 involvement in cancer. By participating in DNA damage response pathways, some KDM5 demethylases may be important mediators of genome stability, for example in renal cancer (Li et al., 2014; Gong et al., 2017). In melanoma, KDM5B was shown to induce an anti-tumor immune response and was required for immune evasion of cells in an *in vivo* model (Zhang et al., 2021). Moreover, KDM5 demethylases are involved in cell cycle regulation (Hou et al., 2012), invasion (Teng et al., 2013), differentiation (Oser et al., 2019) and metabolism (Roesch et al., 2013) of cancer cells. Taken together, KDM5 demethylases perform diverse roles that in many cases favor the pathogenesis and therapy resistance of various cancers. At the same time, the observed complexity of KDM5 functions strongly suggests that KDM5 activities may also serve tumor suppressive functions in some instances (Li et al., 2016a), e.g., facilitating genome stability (Li et al., 2014), underlining the need to understand the underlying mechanisms for context-dependent KDM5 targeting by therapeutic agents. The accumulating evidence of KDM5 function in cancer is discussed in detail in a number of excellent, recent reviews (Hojfeldt et al., 2013; Johansson et al., 2016; Harmeyer et al., 2017; Plch et al., 2019; Yang et al., 2021). As a consequence of the above findings, there has been an increasing interest in developing potent and specific inhibitors against KDM5 demethylases for use in a clinical setting (Johansson et al., 2016; Kaniskan et al., 2018). Major obstacles remain to be addressed on the way towards efficient and specific therapeutic approaches targeting KDM5s. For example, KDM5 inhibitors are mostly competitors of the cofactor 2-OG that as a metabolite is present at high concentrations, hampering competitive inhibition (Kaniskan et al., 2018). Moreover, the catalytic domains and 2-OG binding pockets are structurally highly similar within the KDM5 family, leading to difficulties in specifically targeting individual KDM5 enzymes (Horton et al., 2016; Johansson et al., 2016; Vinogradova et al., 2016). Of note, compound screens and activity assays so far have relied on peptide substrates and truncated KDM5 proteins that can be readily purified in amounts required for these high-throughput approaches. However, the binding of their natural chromatin substrates, as well as allosteric regulatory mechanisms may uncover novel targets of small molecules.

MECHANISMS OF KDM5 FUNCTION

KDM5 Structure, Chromatin Interactions and Activity Regulation

KDM5 demethylases are multi-domain proteins that share a common domain architecture. The four human KDM5 family members have an almost identical arrangement of protein domains, with the exception that KDM5C and D lack the most C-terminal plant homeodomain (PHD)—type zinc finger (**Figure 1B**). Catalytic activity is mediated by a composite JmjN/JmjC domain that, together with a helical domain surrounding a C5HC2 zinc finger motif required for demethylation (Yamane et al., 2007), make up a compact catalytic core (**Figure 2A**) (Johansson et al., 2016). The DNA binding AT-rich interactive (ARID) and the first PHD domain are partially dispensable for the catalytic activity of a truncated construct of KDM5B in the context of peptidic substrates (Johansson et al., 2016), but likely play important roles in the allosteric regulation of KDM5 demethylase activity (see below and (Klein et al., 2014; Torres et al., 2015)). The catalytic cores of KDM5A, B and C have been explored in detail structurally via x-ray crystallography and functionally with biochemical approaches (Horton et al., 2016; Johansson et al., 2016; Vinogradova et al., 2016). These structures have provided valuable information on the architecture of the active site and surrounding protein domains, and have enabled the detailed analysis of inhibitor binding and their modes of action. Additional structural information is still required on how the substrate histone tail is engaged with the active site, potentially providing an explanation for the requirement of the C5HC2 Zn finger for catalytic activity. The regions C-terminal of the catalytic core are less well described, comprising two to three more PHD domains, as well as a region that is predicted to be rich in α-helices adopting a coiled-coil arrangement (**Figure 2B**). A structural study of human full-length KDM5B using small-angle X-ray scattering (SAXS), hydrogen deuterium exchange mass spectrometry and negative-stain electron microscopy combined with homology modeling approaches showed that the C-terminal half of the protein indeed displayed a coiled-coil structure (Dorosz et al., 2019). KDM5B was shown to adopt an overall elongated conformation with the catalytic and most C-terminal regions linked flexibly by a coiled-coil, spectrin-like domain. This overall structural arrangement is in agreement with structure predictions using the Alphafold algorithm (Jumper et al., 2021) (**Figure 2B**).

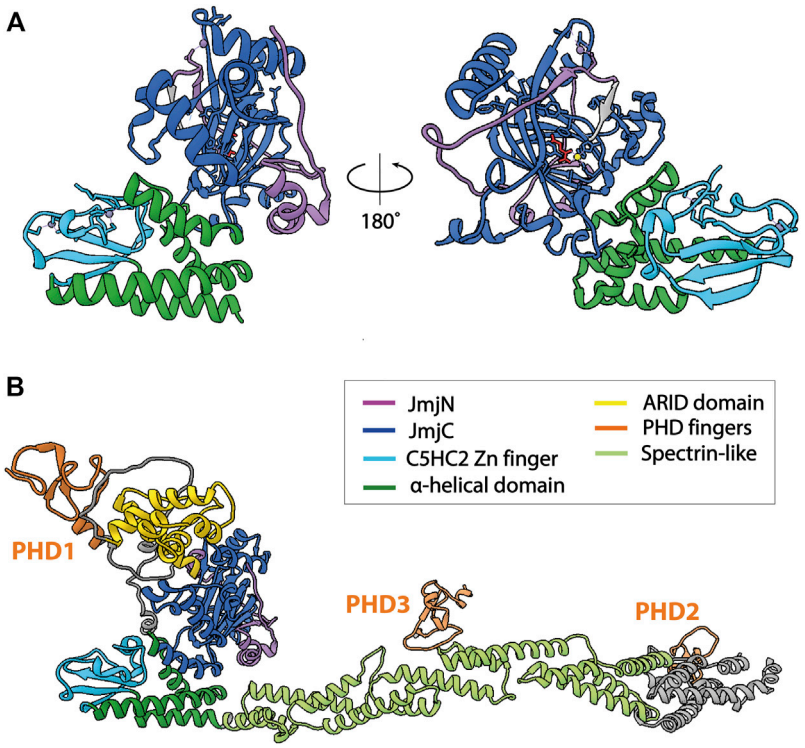

FIGURE 2 | Structures of KDM5B. The catalytic cores of KDM5 enzymes are structurally highly similar, therefore only structures of KDM5B are shown. **(A)** Atomic model of the catalytic core of KDM5B [PDB 5A1F (Johansson et al., 2016)]. The construct crystallized was composed of the JmjN and JmjC domains, as well as the α-helical domain including the C5HC2 Zn finger. The ARID and PHD1 domains were not included. The α-helical domain and the C5HC2 Zn-finger are required for demethylase activity, whereas the ARID and PHD1 domains are dispensable for the demethylation of peptide substrates by truncated KDM5s. **(B)** Alphafold2 prediction of full-length KDM5B (AF-Q9UGL1-F1), showing the predicted arrangement of the protein domains C-terminal of the catalytic core in an extended conformation, in agreement with experimental data (Dorosz et al., 2019). Of note, other conformations cannot be excluded due to the flexibility of the coiled-coil domain. Structural predictions of other KDM5s show a more compact orientation of the C-terminal part, with the PHD2 domain being located in close proximity to the N-terminal, catalytic core. Unstructured regions with low prediction confidence were omitted from the figure for clarity.

The PHD1 domain that is positioned C-terminal of the catalytic JmjN/C domains plays an important role in substrate engagement and activity regulation of KDM5A and B. This domain has a binding preference towards unmodified H3 peptides (Zhang et al., 2014) and may also interact with methylated H3K9 (Klein et al., 2014). Interestingly, engagement of H3 peptides unmethylated at K4 confers allosteric activation of KDM5A and B demethylase activities (Klein et al., 2014; Torres et al., 2015). For KDM5A, it was shown that this activation mechanism involves a conformational rearrangement of the active site (Longbotham et al., 2019). The mechanistic details of how this regulation is brought about structurally, in particular in the context of full-length KDM5 enzymes and chromatin substrates, remain to be elucidated. Functionally, since fully demethylated H3K4 is the final product of KDM5 activity, potentially in coordination with the H3K4me1 specific lysine demethylase LSD1, sequestering the product of catalysis may prevent re-methylation of H3K4. The observed allosteric activation could also imply a feed-forward mechanism propagating demethylated H3K4. Similar mechanisms are known for other chromatin modifiers such as Polycomb repressive complex 2 (PRC2) (Margueron et al., 2009; Poepsel et al., 2018). Indeed, H3 tail binding by PHD1 was required for the stimulation of breast cancer cell migration upon KDM5B overexpression (Klein et al., 2014), indicating a physiological relevance of this interaction. The yeast ortholog of KDM5 demethylases, Jhd1, was shown to depend on its PHD domain for chromatin engagement in cells (Huang et al., 2010).

Apart from the active site and PHD1 domains, the PHD3 and ARID domains are likely to contribute to chromatin engagement of KDM5 enzymes (**Figure 3A**). PHD2 has not yet been biochemically or structurally characterized in detail and did not show histone tail binding. The C-terminal PHD domain of KDM5B was shown to preferentially bind H3K4me2/3, the substrates of KDM5 enzymes, and may therefore play a role in substrate recognition (Klein et al., 2014) (**Figure 3A**). DNA binding of the ARID domains may serve as an additional anchor point on chromatin. Since the ARID domain is located in the vicinity of the JmjN/C domain, it could be involved in substrate nucleosome recognition (**Figure 3A**). However, in the conformation that was resolved by X-ray crystallography, DNA binding would be precluded sterically (Horton et al., 2016; Vinogradova et al., 2016), suggesting that, in the context of nucleosomes, the protein may adopt a different conformation

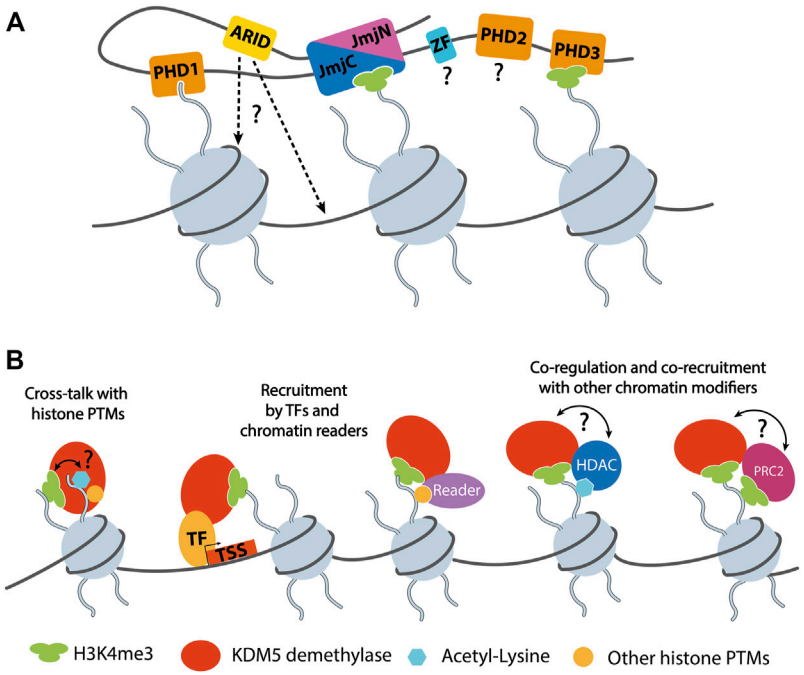

FIGURE 3 | (A) Schematic representation of KDM5 interactions with chromatin. The catalytic composite JmjN/C domain binds the substrate H3 tail harboring methylated H3K4 (depicted as H3K4me3 for simplicity). Two of the PHD domains, PHD1 and 3, were shown to interact with unmethylated and trimethylated H3K4, respectively. The ARID domains are known DNA binding domains with a role in KDM5 chromatin targeting. How DNA binding is mediated in the context of full-length KDM5 proteins is currently unknown, since the arrangement of JmjC and ARID domains seems to be incompatible with the binding of nucleosomal DNA, according to homology models (Horton et al., 2016). The roles and potential chromatin interactions of the C5HC2 and PHD2 Zn fingers are unknown. Note that the depiction of three nucleosomes was chosen for clarity. It is not known how many nucleosomes are bound by a single KDM5 protein simultaneously. **(B)** Functional KDM5 interactions on chromatin. So far, only the binding of unmethylated H3K4 has been shown to regulate the demethylase activity of KDM5s. Given the potential interactions with HDACs, a direct or indirect responsiveness to other histone PTMs such as acetylated lysines, is conceivable. KDM5 proteins are recruited by transcription factors (TFs), reader domain proteins, or mediated by the association with other epigenetic regulators such as HDAC complexes or PRC2. The interaction and functional interplay of KDM5s with HDAC complexes and PRC2 suggests a potential mutual regulation of demethylase and other chromatin modifying activities. Such a direct interplay remains to be demonstrated experimentally.

compatible with DNA binding. The binding preferences of the KDM5A and B ARID domains have been determined experimentally (Scibetta et al., 2007; Tu et al., 2008) and were shown to be important for H3K4 demethylation by KDM5A in cells (Tu et al., 2008).

Despite detailed structural analyses of individual domains of KDM5 demethylases, their contribution to the activity and function of the complete proteins remain incompletely understood. This is in part due to a lack of high-resolution structural information on full-length KDM5 enzymes. Interactions with chromatin and other binding partners have not been elucidated yet, hampering the investigation of KDM5 function in the context of chromatin. Therefore, it will be key to consider full-length KDM5 for future structural and functional analyses.

KDM5 demethylases take part in nuclear processes as diverse as transcriptional repression, replication and DNA repair (see above). Accordingly, they perform roles within diverse chromatin settings regarding the identity, regulatory state, and function of the respective genomic region. Additionally, KDM5 demethylases, like other chromatin modifying enzymes, function via their catalytic activity or independently of catalysis. These aspects underline the complexity of KDM5 biology, the molecular basis of which has so far remained poorly defined. For example, H3K4me2/3 demethylation can have various consequences depending on the local context. Since H3K4me2/3 is highly enriched in actively transcribed promoter regions, an obvious consequence of demethylation would be reduced transcriptional activity, as was shown in a number of instances (Christensen et al., 2007; Dey et al., 2008). However, H3K4me2/3 removal may also have a positive effect on transcription, e.g. by reducing spurious transcription from within gene bodies, as described for KDM5B, thereby facilitating productive transcriptional elongation and increasing the transcriptional output (Xie et al., 2011). Moreover, changes in H3K4me3 levels not always correlate with transcriptional activation, and association of KDM5B with H3K4me3-bearing promoters was shown to lead to repression or activation, depending on the genomic context (Kidder et al., 2014; Brier et al., 2017). Demethylase activity may also be required for establishing and maintaining PTM configurations specific for functional elements within the genome. For example, a possible product of KDM5 activity, H3K4me1, is a characteristic feature of enhancer regions (Heintzman et al., 2007). While the importance

of H3K4me1 for enhancer function is controversial, H3K4 demethylation may help shape its genomic distribution, safeguarding the integrity of epigenetic regulatory pathways. Accordingly, demethylation by KDM5C was shown to facilitate enhancer activity and function through its localized activity at enhancers, potentially through the removal of H3K4me3, thereby reducing aberrant enhancer over-activation (Outchkourov et al., 2013; Shen et al., 2016). A similar role in maintaining the functional integrity of gene regulatory elements was shown for KDM5B controlling the local distribution of H3K4me3 in mouse ESCs. Consequently, loss of KDM5B in this system compromised promoter and enhancer function, as well as transcriptional dynamics during differentiation (Kidder et al., 2014).

In summary, mechanistic knowledge on KDM5 demethylase activity, regulation and function is still relatively scarce, despite their implications in key cellular processes and disease. Defining mechanisms of recruitment, chromatin engagement and activity will be essential to decipher how the diverse roles of KDM5 demethylases are controlled. In addition to their internal structure and interactions with nucleosomal substrates and DNA, intermolecular interactions with other chromatin associated factors are of key importance for KDM5 function. Our current knowledge of how these interactions impact KDM5 function will therefore be reviewed below.

INTERACTIONS OF KDM5 DEMETHYLASES

Retinoblastoma Protein

The retinoblastoma protein (RB) was the first known interaction partner of KDM5 demethylases. In fact, KDM5A was initially identified in a screen for RB binders, hence the name RB binding protein 2 (RBP2) (Defeojones et al., 1991). Since then, a number of studies have explored their functional relationship. RB is best known as a tumor suppressor dysfunctional in many types of human cancers including retinoblastoma (Friend et al., 1986), breast (Lee et al., 1988), and lung cancer (Harbour et al., 1988). Consequently, intense research has been addressing its function, particularly in cell cycle regulation. RB prevents progression from G1 to S phase (Weinberg, 1995) by binding and inhibiting E2F transcription factors (TFs), leading to the repression of E2F target genes and ultimately inducing cell cycle arrest. RB interactions depend on the phosphorylation state of its multiple phosphorylation sites. Hypophosphorylated RB is associated with an active state competent of blocking cell cycle progression. Upon phosphorylation by cyclin-dependent kinases (CDKs), RB releases E2F inhibition, allowing for cell cycle progression (Chen et al., 1989; Harbour et al., 1999). Besides the hyperphosphorylated, inactive state, individual phosphorylation events can modulate RB structure, interactions, and specific functions (Sanidas et al., 2019).

While early research largely focused on its impact on cell proliferation, it has since become clear that RB is involved in a multitude of other processes through E2F-dependent or -independent mechanisms. For example, RB is involved in DNA repair, replication, apoptosis, and the regulation of G2/M phase progression (Brehm et al., 1999; Wu et al., 2003; Macaluso et al., 2005). Accordingly, many RB interactors have been identified, including chromatin-modifying proteins such as histone deacetylases (HDACs) (Luo et al., 1998) and histone methyltransferases (Nielsen et al., 2001) [for review, see (Dick and Rubin, 2013)]. Key interactions are mediated by the large pocket domain, encompassing residues 379–928 (Sellers and Kaelin, 1997). This domain harbors two conserved interaction interfaces, one that is typically engaged by E2F TFs and a binding cleft that has been shown to bind an LxCxE consensus sequence present in viral oncoproteins such as the SV40 large T-antigen, adenovirus E1A and human papilloma virus (HPV) E7 protein (Lee et al., 1998; Kim et al., 2001). Interestingly, the latter interaction site was shown to be important for RB interactions on chromatin, e.g., with HDACs (Brehm et al., 1998; Isaac et al., 2006). Beyond the conserved LxCxE RB interacting motif, surrounding residues and other interaction interfaces contribute to the association of individual proteins with RB (Singh et al., 2005).

The interaction of KDM5A with RB is mediated through two possibly independent sites: its LxCxE motif (LFCDE in KDM5A, aa 1373–1377) and a part loosely termed non-T/E1A region (NTE1A), located C-terminal of the LxCxE motif (Kim et al., 1994). The NTE1A nomenclature indicates that this binding site differs from the classical sites on RB targeted by viral proteins. The cellular interaction of RB and KDM5A remained difficult to demonstrate for some time, but was eventually confirmed by co-immunoprecipitation and detected within transcriptionally active regions during cellular differentiation (Benevolenskaya et al., 2005). KDM5B has a strong overall similarity with KDM5A, including an identical distribution of protein domains (**Figure 1B**). Accordingly, KDM5B also interacts with RB in cells, but lacks an LxCxE consensus sequence for RB binding. Instead, the NTE1A region of KDM5B is required for RB interactions in cells, which was suggested to stabilize hypophosphorylated RB (Roesch et al., 2005). In agreement with this observation, KDM5A colocalized with RB in regions enriched for hypophosphorylated RB (Benevolenskaya et al., 2005). Interactions of KDM5C or D with RB have, to our knowledge, so far not been observed. It is unclear in how far the functional relationship with RB is conserved throughout the KDM5 family.

The interplay of RB/KDM5 has particularly been studied in the contexts of cancer and differentiation. In melanoma, where slow-cycling cancer cells show high KDM5B expression, RB/KDM5B interactions may be involved in tumor suppression (Roesch et al., 2006). In both cancer and developmental contexts, phenotypes caused by RB dysfunction could be rescued by inhibiting KDM5A, leading to the hypothesis that at least part of the functional link between RB and KDM5A may be based on antagonizing roles (Benevolenskaya et al., 2005; Lin et al., 2011). For example, interfering with KDM5A expression or inhibiting its demethylase activity reduced tumor initiation and growth in RB-deficient mice, significantly expanding life span (Lin et al., 2011; McBrayer et al., 2018), and decreased cellular heterogeneity in a small cell lung cancer (SCLC) cell line (Varaljai et al., 2015). In RB-

deficient SCLC, KDM5A activity was shown to be required for the maintenance of the neuroendocrine phenotype and to promote cancer cell proliferation (Oser et al., 2019). These observations could be explained by an inhibitory effect of RB on histone demethylation by KDM5A, either in a direct or indirect manner, and highlight the therapeutic promise of inhibiting KDM5 demethylases, e.g., in RB-deficient cancers.

It was suggested that RB functions that promote cellular differentiation and transcriptional activation are independent of its interactions with E2F TFs, instead requiring its association with KDM5A (Sellers et al., 1998; Benevolenskaya et al., 2005; Lin et al., 2011) with some evidence thus suggesting a role of KDM5A as a transcriptional activator (Benevolenskaya et al., 2005). More recent studies suggest that the release of the transcriptional repression of metabolic regulators by KDM5A may be responsible for the restoration of differentiation upon KDM5A knock-out in RB-deficient cells (Varaljai et al., 2015). Altogether, studies on the relationship of KDM5A and RB in RB-dependent differentiation pathways indicate that the immediate effects of RB/KDM5A complexes on transcriptional activity depend on the target genes, involving divergent mechanisms that may imply either antagonistic or synergistic effects between these regulators (Benevolenskaya et al., 2005; Lopez-Bigas et al., 2008; Varaljai et al., 2015).

In the context of cellular senescence, evidence suggests that RB functionally cooperates with KDM5A and KDM5B to promote cell cycle arrest and senescence phenotypes. Here, upon down-regulation of RB, an increase of H3K4me3 levels was observed at RB-dependent E2F target genes and the loss of H3K4me2/3 at E2F target genes during senescence induction was dependent on KDM5A demethylase activity and its RB binding region (Chicas et al., 2012). A similar functional relationship was determined in a mouse embryonic fibroblast model of cellular senescence (Nijwening et al., 2011), suggesting a common and potentially redundant (Chicas et al., 2012) role of KDM5A and KDM5B in RB-dependent senescence induction. Of note, these observations hinting at a localized correlation of RB binding and KDM5-dependent H3K4 demethylation would not be immediately incompatible with the idea that RB inhibits KDM5 demethylase activity, suggesting that the RB/KDM5 interplay may depend on the experimental model and biological pathway. Also, the latter findings focus on E2F-dependent RB targets, whereas other studies on the RB/KDM5A axis during cellular differentiation (Benevolenskaya et al., 2005; Lopez-Bigas et al., 2008; Varaljai et al., 2015) consider E2F-independent functions of RB. It should be noted that diverse mechanisms may affect the distribution of H3K4me3, including histone methyltransferases or nucleosome remodelers, complicating direct causal conclusions in complex cellular systems.

In summary, there is compelling evidence of direct interactions and a close interplay of RB and KDM5 demethylases, in particular KDM5A and B. Both a synergistic relationship, e.g. during senescence induction, and the mutual inhibition of catalytic activity and regulatory functions have been suggested. It seems that the biological context plays an important role in determining the manifestations of this cross-talk. Given the significance of RB and KDM5 demethylases in development and disease, mechanistic studies will be of great interest to elucidate the molecular basis of these associations and their regulation. It will be of key importance to decipher which implications are mediated by the function of stable RB/KDM5 complexes, and which are the consequences of altered RB and KDM5 functions and activities. For example, it is unclear whether KDM5/RB complexes can bind and demethylate nucleosomes, and how they are recruited to their genomic targets. Since the functions and mechanisms of KDM5/RB complexes seem to vary significantly, elucidating the molecular determinants of RB interactions with different KDM5 family members and in distinct contexts will be of particular importance. Moreover, since the demethylase activity of KDM5A and B underlies their tumor-promoting roles (Vinogradova et al., 2016) and KDM5A/B inhibition is particularly promising in RB-deficient tumor cells (Oser et al., 2019), a potential mechanism of KDM5 inhibition by RB may lead the way towards novel approaches to interfere with oncogenic activities of KDM5 demethylases in defined contexts. Interestingly, while phosphorylation is the best known PTM regulating RB function, other PTMs such as lysine methylation also contribute to RB regulation (Munro et al., 2010; Saddic et al., 2010; Carr et al., 2011; Cho et al., 2012). To our knowledge, non-histone substrates of KDM5 enzymes have so far not been discovered, leaving open the question whether RB demethylation is a possible mechanism underlying the RB/KDM5 interplay.

Histone Deacetylase Complexes

Regulatory complexes interact physically and functionally on chromatin, coordinating their catalytic activities and recruitment. These interactions provide a complex framework for the local, context-dependent reshaping of chromatin (Blackledge et al., 2014). Understanding the interplay of KDM5 enzymes with epigenetic multi-protein complexes may provide valuable clues regarding their distinct cellular functions despite a similar domain organization (Christensen et al., 2007; Klose et al., 2007; Lee et al., 2007). Numerous studies report on such interactions, with histone deacetylase (HDAC)-containing complexes consistently shown to physically associate with KDM5 demethylases. Most HDACs, just like many chromatin modifying enzymes, reside within larger multi-protein complexes that regulate histone lysine acetylation levels (Seto and Yoshida 2014; Park et al., 2020). Histone acetylation facilitates chromatin dynamics or recruits regulators via reader domains such as bromodomains, ultimately promoting transcriptional activity (Zeng and Zhou, 2002). Consequently, histone deacetylation is associated with transcriptional repression (Hu et al., 2000; Huang et al., 2000), suggesting a functional overlap with H3K4 demethylation. Available evidence suggests that the dynamic association of KDM5 demethylases and HDAC complexes on chromatin contributes to their genomic targeting, thereby potentially coordinating H3K4 demethylation and histone deacetylation, leading to transcriptional repression (Hayakawa et al., 2007). KDM5 enzymes were shown to interact with three major HDAC complexes: the nucleosome remodeling and deacetylase (NuRD), SIN3B-containing, and CoREST complexes.

The NuRD and SIN3B-containing HDAC complexes are key chromatin regulators associated with transcriptional repression (Silverstein and Ekwall, 2005; McDonel et al., 2009). While they share the core components HDAC1/2 and RBBP4/7, they differ in their additional subunits, with SAP18/30, SDS30, MRG15 (MORF4L1), EMSY, GATAD1 and PHF12 as part of SIN3B-containing complexes (Grzenda et al., 2009; Varier et al., 2016) and CHD3/4, MBD2/3 and MTA1/2/3 present in NuRD complex variants (Seto and Yoshida, 2014; Millard et al., 2016). Using immunoprecipitation and density gradient fractionation, FLAG-tagged KDM5A was shown to associate with subunits of both the NuRD and SIN3B complexes. The detected assemblies could be physically separated and their co-precipitation with KDM5A was differentially disrupted by deletions of KDM5A, hinting at distinct interfaces selecting for interactions with either the SIN3B or the NuRD complex (Nishibuchi et al., 2014). A suggested interactor of both KDM5A and NuRD, Zinc finger MYND domain-containing protein 8 (ZMYND8), links the recruitment of KDM5A and the NuRD complex to sites of DNA damage, suggesting a role of KDM5A beyond transcriptional regulation (Gong et al., 2017). Interestingly, ZMYND8 was also reported to directly interact with KDM5C (Shen et al., 2016) and KDM5D (Li et al., 2016b), contributing to their genomic localization and functionally cooperating with these KDM5 enzymes. Both reports, however, suggest the ZMYND8-mediated recruitment of KDM5C and D to different genomic elements, namely enhancers (Shen et al., 2016) and transcription start sites (Li et al., 2016b), respectively. The molecular cues that specify these apparently divergent recruitment events have so far remained unclear. Also, it is not known in the case of KDM5C and KDM5D whether the association with ZMYND8 also implies interactions with HDACs or other chromatin regulators such as NuRD. The physical association of KDM5B with the NuRD complex subunits MBD3, LSD1 and HDAC1 was shown using immuno-purification approaches (Li et al., 2011). Additional studies verified the interaction with HDAC1 and further ChIP analysis revealed that KDM5B colocalizes with NuRD complex subunits on chromatin (Klein et al., 2014).

Immunoprecipitation experiments identified KDM5A to directly interact with MORF-related gene on chromosome 15 (MRG15/MORF4L1), a subunit of SIN3B complexes (Hayakawa et al., 2007). Large-scale proteomics studies strongly support KDM5A being a stable component of complexes that include SIN3B, MRG15, HDAC1/2, RBBP4/7, as well as PHF12, EMSY (c11orf30), and GATAD1 (Vermeulen et al., 2010; Malovannaya et al., 2011). The association with this complex facilitates KDM5A recruitment to specific genomic loci, in particular promoter regions with high levels of H3K4me3. Interestingly, genomic occupancy of this KDM5A-containing complex was associated with transcriptional activation of a subset of genes, with an enrichment of pro-proliferative genes. The involvement of KDM5A demethylase activity was not investigated in this study (Varier et al., 2016). ChIP-Seq analyses suggested that KDM5B and the *Drosophila* KDM5 homolog Lid also interact with MRG15, a chromatin organizer that binds methylated histone H3K36me3 (Zhang et al., 2006), leading to KDM5B and Lid recruitment to H3K36me3-bearing regions (Moshkin et al., 2009). Further studies on Lid support the notion that a functional interplay between KDM5 demethylases and SIN3 HDAC complexes may be evolutionarily conserved. In biochemical studies Lid was copurified with the HDAC1 homolog RPD3 as part of a larger multi-protein complex that also contained MRG15. This interaction did not affect the catalytic activity of Lid while having an inhibitory effect on RPD3 HDAC activity (Lee et al., 2009; Di Stefano et al., 2011). Functional and biochemical analyses further support the idea that SIN3 and Lid cooperate in transcriptional regulation during development (Gajan et al., 2016). Since KDM5C or D have not been detected so far as interactors of the above SIN3B complexes, this mechanism may be a distinguishing feature among KDM5 family members in mammals.

The CoREST complex is a transcriptional repressor of neuronal and stem cell fate genes, consisting of the RE1-silencing transcription factor (REST), HDAC1/2, lysine-specific demethylase 1 (LSD1/KDM1A) and RCOR1/2/3 (Wang et al., 2007; Foster et al., 2010; Song et al., 2020). CoREST was co-purified with affinity-tagged KDM5C (Tahiliani et al., 2007; Nishibuchi et al., 2014), and chromatin immunoprecipitation (ChIP) analyses with REST coupled with KDM5C depletion experiments showed overlapping genomic targets (Tahiliani et al., 2007). Biochemical analysis of KDM5C showed no significant changes in enzyme activity in this context. In agreement with these findings, dysregulation or mutations of either KDM5C or REST are linked to neuronal disorders such as X-linked intellectual disability, autosomal recessive intellectual disability and autism (Santos et al., 2006; Najmabadi et al., 2011).

LSD1 (KDM1A) stands out as another potential interactor of KDM5A since its lysine demethylase activity targets the same histone H3 residue as KDM5 demethylases. As opposed to KDM5 enzymes, however, demethylation by LSD1 is restricted to H3K4me1 (Shi et al., 2005). It is therefore a tempting idea that KDM5 demethylases and LSD1 may cooperate to fully demethylate H3K4. Indeed, ChIP analyses of KDM5B support the notion that both demethylases function cooperatively in the context of NuRD to demethylate H3K4 (Li et al., 2011). A large fraction of genomic regions in mouse ESCs occupied by KDM5B was found to be co-occupied by LSD1 and vice versa, supporting a partial and context-dependent co-operation of both enzymes (Kidder et al., 2014). However, direct experimental evidence of cooperative demethylation by KDM5 demethylases and LSD1 is lacking. LSD1 shares key interactors with KDM5 demethylases, e.g. by interacting with the CoREST and NuRD complexes in some contexts (Wang et al., 2009; Pilotto et al., 2015; Song et al., 2020). Cross-talk between these two enzymes may therefore take place within the molecular framework of larger multi-subunit complexes.

Genetic analyses of knock-out experiments suggested that interactions of LSD1 and the *Drosophila* KDM5 homolog Lid have variable implications depending on the chromatin environment. On one hand, Lid antagonized LSD1 silencing function and limited the spreading of heterochromatin beyond euchromatin-heterochromatin boundaries. On the other hand, both enzymes seemed to function cooperatively in the context of

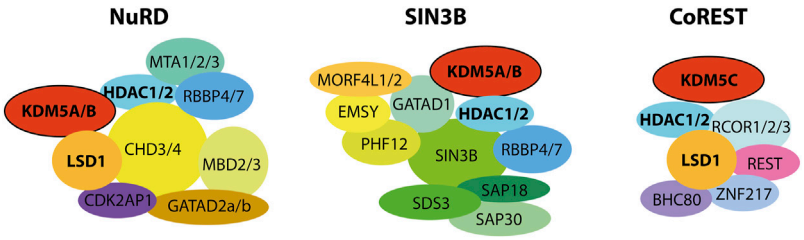

FIGURE 4 | KDM5 demethylases were shown to physically and functionally interact with HDAC complexes. Interactions with the NuRD and SIN3B complexes have been shown for the mammalian KDM5A and B proteins, as well as *Drosophila* Lid. CoREST interactions were shown for KDM5C, with implications for neuronal development. Note that, for reasons of clarity, the stoichiometry and detailed subunit composition of the complexes was neglected. For NuRD and SIN3B, composition and dynamics of subunits are subject to research and have not been definitely established. The placement of subunits and their proximity to each other and to the KDM5 proteins does not reflect experimentally verified proximity within the respective complexes.

regulating Notch target genes by synergistically removing H3K4 methylation marks (Di Stefano et al., 2011). KDM5A was also shown to associate with the Recombination signal Binding Protein for immunoglobulin kappa J (RBP-J) co-repressor complex (Liefke et al., 2010), further supporting the link between KDM5A and Notch signaling, since the RPB-J corepressor complex is an important negative regulator of the Notch pathway, which controls important cell fate decisions. Interestingly, a functional interplay of RBP-J complexes with SIN3B- and MRG15-containing HDAC complexes is involved in the control of Notch signaling in *Drosophila melanogaster* (Moshkin et al., 2009; Liefke et al., 2010), supporting the links between SIN3B, HDACs and KDM5 demethylases. It will be interesting to see whether the involvement of KDM5 demethylases in a conserved pathway such as Notch signaling is also reflected on the molecular level in conserved interactions and molecular mechanisms. In support of a conserved role of KDM5 in Notch signaling, KDM5A repressed Notch dependent neuroendocrine differentiation in SCLC (Oser et al., 2019).

Another context in which KDM5 interactions with HDACs have been described is the transcriptional control of the circadian clock, where KDM5A was shown to be involved through direct interactions with the transcription factors Circadian locomotor output cycles protein kaput (CLOCK) and aryl hydrocarbon receptor nuclear translocator-like protein 1 (ARNTL, also known as BMAL1). Additional results suggested that KDM5A in complex with CLOCK and BMAL1 inhibits HDAC1 activity (DiTacchio et al., 2011). For HDAC4 and other class IIa HDACs, some experimental evidence suggests a possible interaction with KDM5B in the context of breast cancer and other cell lines (Barrett et al., 2007).

Taken together, a large body of evidence supports a physical and functional association of KDM5 demethylases with HDAC containing complexes, in particular NuRD, SIN3B and CoREST (**Figure 4**). It can be assumed that these interactions shown to impact KDM5 targeting and regulation are determinants of the diverse functions of individual KDM5 family members. For example, it is conceivable that KDM5C preferably interacts with CoREST, whereas KDM5A and B interact with NuRD and SIN3B (**Figure 4**). More detailed and targeted studies will have to be designed to address this hypothesis in the future. Other key open questions regard the interfaces within and between the respective complexes, defining which proteins and protein domains are directly involved. For example, it is not clear whether HDAC1/2, common catalytic subunits of KDM5 interacting complexes, are direct interactors stabilizing the association. Moreover, it will be pivotal to investigate the potential mutual regulation and coordination of demethylase and HDAC activities, as well as how interactions affect chromatin binding and genomic targeting. All of these questions require that detailed biochemical and structural studies are performed to pinpoint the molecular foundations of this regulatory interplay. Additionally, targeted functional studies will be required complementary to these mechanistic approaches to shed light on the implications within cellular and organismic contexts.

Other Epigenetic Regulators

In addition to HDAC complexes, other epigenetic regulators likely contribute to KDM5 function through direct interactions. For example, a direct and functional interaction of KDM5A with Polycomb Repressive Complex 2 (PRC2) showcases the complexity of epigenetic regulation (Pasini et al., 2008). PRC2 is a key chromatin regulator that catalyzes the methylation of H3K27, resulting in the H3K27me3 mark associated with silent chromatin domains (Uckelmann and Davidovich, 2021). In particular, bivalent developmental genes, i.e. bearing both H3K4 and H3K27 methylation marks, are targets of both KDM5A and PRC2 binding. This interaction may suggest that PRC2 recruits KDM5A to target genes, but could also represent a basis of a coordinated demethylation of H3K4 and trimethylation of H3K27, ultimately promoting gene silencing (Pasini et al., 2008). In agreement with this, knock-out of KDM5B results in phenotypes reminiscent of Polycomb defects, pointing at a potential functional relationship (Albert et al., 2013). This functional cooperation, however, does not necessarily have to require physical interaction. The lysine methyltransferase KMT1C is generally considered to repress transcription by methylating H3K9me1/me2. *Via* co-immunoprecipitation KDM5A was identified as a binding partner of KMT1C. Similar to PRC2, KMT1C was suggested to stabilize KDM5A binding to chromatin and promote a coordination of enzymatic

activity, resulting in transcriptional repression (Chaturvedi et al., 2012). KDM5D is the least studied KDM5 demethylase overall. Nonetheless, purification of FLAG-tagged KDM5D revealed a direct association with Polycomb group RING finger protein 6 (PCGF6), which is a component of non-canonical PRC1 complexes. Interestingly, it was shown that upon binding PDGF6, the demethylase activity of KDM5D was increased (Lee et al., 2007).

Transcription Factors

In addition to interactions between epigenetic regulators mediating their context-dependent function, KDM5s are recruited to specific genomic sites by sequence-specific transcription factors (TFs). TFs can function individually or cooperatively, and can recruit further effector proteins (Spitz and Furlong, 2012; Lambert et al., 2018). Patterns of chromatin occupancy by KDM5 demethylases in various cell types indicate that TFs may directly recruit KDM5s to target genes (Varier et al., 2016). Accordingly, KDM5B was shown to bind the TFs PAX9 and BF-1 (also known as FOXG1b) in yeast two-hybrid interaction assays and LMO2 in Co-IP experiments. Generally, these proteins function as transcriptional repressors, playing a pivotal role in embryonic tissue and progenitor cell proliferation, respectively. KDM5B significantly increased the transcriptional repression in biochemical assays, corroborating the potential functional implications of these interactions (Tan et al., 2003; Roesch et al., 2008). While the mechanism was not explicitly stated, it is conceivable that PAX9, BF-1 and LMO2 may recruit KDM5B to genomic target sites, but also locally modulate its demethylase activity. Moreover, KDM5B is a co-regulator of various nuclear receptors, such as estrogen receptors, androgen receptors and progesterone receptors (Krishnakumar and Kraus, 2010; Catchpole et al., 2011; Vicent et al., 2013; Klein et al., 2014). KDM5C was shown to co-immunoprecipitate with the TFs c-Myc and ELK1, and c-Myc interactions were also detected for KDM5B and C upon their overexpression (Outchkourov et al., 2013). C-Myc had been described as a functional binding partner of KDM5A and KDM5B, as well as Lid (Secombe et al., 2007). In multiple myeloma, KDM5A was shown to support c-Myc-dependent transcriptional activation, although through an indirect mechanism mediated by direct interactions with the transcription machinery (Ohguchi et al., 2021). Clearly, TFs play an important role in specifying the localized activity and function of KDM5 demethylases. How TFs perform this recruitment function, and whether they exclusively bind to KDM5 proteins directly or within the context of larger, chromatin associated regulator complexes, remains to be studied in detail.

DISCUSSION

Histone demethylases of the KDM5 family display properties characteristic of many epigenetic regulators, making their exploration both challenging and fascinating. Functionally, KDM5 demethylases play diverse and seemingly contradictory roles that strongly depend on the biological context. For example, besides their repressive effect on transcription mediated by H3K4 demethylation, KDM5 demethylases can also facilitate transcriptional activation. Catalytic activity is directly responsible for some, but dispensable for other functions. Ongoing discussions regarding the direct causal effects of histone PTMs such as H3K4 methylation on transcriptional regulation (Cruz et al., 2018; Rada-Iglesias, 2018), and the requirement or dispensability of the activity of chromatin modifying enzymes (Dorighi et al., 2017) illustrate that fundamental processes in epigenetics still require clarification. Finally, dynamic interactions and, most probably, the regulatory interplay with chromatin features such as DNA, histone PTMs, as well as other chromatin associated regulators, define the contexts in which KDM5 demethylases perform their diverse roles. In order to decipher these roles, the molecular foundations of chromatin association and the molecular interactions and cross-talk of KDM5 enzymes with their interaction partners in the chromatin context have to be defined and mechanistically understood.

Over the last years, it has become clear that chromatin-associated processes are mediated by an intricate and dynamic interplay of proteins and their assemblies. Chromatin-modifying enzymes take part in these processes and have to be regulated such that their activity is locally and temporally defined. Establishing the underlying mechanisms is a key challenge towards elucidating the function of chromatin modifying enzymes. Mechanistically, this challenge comes down to deciphering the molecular cues that constitute a biochemical environment instructing catalytic regulation. Chromatin modifying enzymes are typically part of multi-subunit complexes harboring subunits that exert regulatory and targeting roles. Well-known examples are NuRD and PRC2 (Margueron and Reinberg, 2011; Allen et al., 2013). In these cases, subunit composition is one determinant of context-dependent activity, creating a dazzling complexity of regulatory mechanisms that are only beginning to be understood in molecular detail (Poepsel et al., 2018; Kasinath et al., 2021). In contrast to the above examples, KDM5 demethylases have not been described as constitutive members of multi-subunit complexes and it is not clear whether their cellular function strictly relies on their incorporation into such complexes. However, the experimental evidence reviewed here clearly shows that KDM5 function is intricately linked to other regulatory factors on chromatin. Also, it has become clear that KDM5 demethylases perform diverse roles that depend on the biological context. Intermolecular interactions on chromatin are likely to define these contexts and thus are essential for understanding KDM5 function at a molecular level. We will next outline critical gaps in our knowledge, key questions and how they might be approached at different levels in future studies.

Defining Molecular Context

As we have seen, KDM5 demethylases engage in various processes, located at different sites within the genome, and these functions are reflected in diverse molecular interactions. KDM5A being a key regulator of Notch signaling in SCLC (Oser et al., 2019) is one example illustrating the opportunities

associated with deciphering the underlying mechanisms. An important aspect of future efforts will be to further explore which direct interactions take place where in the genome, or within a given process. Most commonly, interactors of KDM5 demethylases have been identified via immunoprecipitation, often in the context of ectopically expressed, affinity-tagged KDM5 proteins or interaction partners. Using this approach, it can be challenging to derive direct physical interactions, since the association may be mediated by co-precipitated proteins and therefore be indirect. Furthermore, a pool of KDM5 is isolated from cultured cells and, thus, the identified interactions may reflect a convolution of various contexts. Future studies should therefore aim at defining the KDM5 interactome in specific contexts, identifying direct physical interactions. Such efforts may be guided by a combination of modern proteomic approaches such as proximity biotinylation or cross-linking mass spectrometry (CL/MS). Using proximity biotinylation, interaction partners are labelled depending on their spatial proximity through the spatially restrained activity of biotinylating enzymes or short-lived, reactive biotinyl moieties (Ummethum and Hamperl, 2020). A key aspect of these approaches is the ability to detect potential interactions in the context of live cells, preserving transient interactions that may be disrupted by extraction and wash procedures. CL/MS is a field of rapid technological development that enables the determination of direct interactions. In CL/MS, interactions are mapped to individual amino acids that are covalently linked by a chemical cross-linking reagent with a defined linker length (Sinz, 2018). CL/MS can now be applied to complex samples providing insights at the interactomic level (Yu and Huang, 2018), but can also yield detailed information on the topology of endogenous, multi-subunit complexes when coupled to affinity purification approaches (Schmidt and Urlaub, 2017; Mashtalir et al., 2018). Importantly, key interactions may rely on the chromatin environment, e.g. through contacts with DNA, nucleosomes, or chromatin bound TFs, and might therefore be disrupted during extraction procedures associated with classical immunoprecipitation protocols. Advanced protocols aiming at elucidating interactions in the context of intact, endogenous chromatin provide promising starting points to further explore KDM5 interactions in their native environment (Lambert et al., 2012). It is very important that such approaches are complemented with each other and with additional methods in order to confirm these results, e.g. in a reconstituted, biochemical system or through functional cellular assays. Furthermore, investigating distinct KDM5 functions of course also requires robust cellular or *in vivo* systems that enable appropriate read-outs of these functions, as well as consequences of perturbing defined interactions (see below).

Interactions and Regulatory Mechanisms

Detailed mechanisms are typically derived from structural and biochemical approaches that define interaction interfaces at high resolution, including conformational rearrangements of protein domains and allosteric regulatory effects on enzymatic activities. While there are first studies reporting the regulation of KDM5A and B activity through chromatin contacts (Klein et al., 2014; Longbotham et al., 2019), no direct regulatory interactions between KDM5 demethylases and other chromatin regulators have been demonstrated yet. The coordinated functions of KDM5 demethylases, RB, and HDAC complexes suggest that the underlying interaction may very well imply the regulation of demethylase activity or a mutual regulatory cross-talk between different chromatin modifying enzymes. Such direct relationships should be explored in detail using biochemical reconstitution approaches, allowing for the high-resolution structural determination of interfaces and the systematic analysis of enzyme kinetics. On the basis of these mechanistic insights, targeted experiments can be designed that manipulate defined interactions rather than knock-downs or the deletions of large portions of the proteins that likely disrupt their function at large. Furthermore, chromatin binding by KDM5 demethylases has not yet been defined. The size and flexibility of chromatin-associated complexes were main factors hampering detailed structural analyses in the past. The development of structural methods such as single-particle cryogenic electron microscopy in recent years has made such challenging complexes more and more amenable to structure elucidation. Structure-function studies on chromatin modifying complexes such as PRC2 have since revealed molecular details of their chromatin association, recruitment, and activity regulation (Poepsel et al., 2018; Kasinath et al., 2021). Given the clear implications of KDM5 demethylases in cancer, there is a strong need of elucidating regulatory and recruitment mechanisms of individual KDM5 demethylases to provide potential starting points for developing therapeutic approaches targeting distinct KDM5 members and their functions, particularly in cancer. Mechanistic studies on the targeted activity of KDM5 demethylases in the context of chromatin will also reveal the basis of localized demethylation in distinct genomic regions, thus explaining, for example, the H3K4 demethylation at enhancers or promoters, leading to opposing effects on the transcriptional activity of target genes (Outchkourov et al., 2013).

Functional Implications

Finally, experimental systems for the investigation of KDM5 function have to be developed or further improved to enable mechanistic insights. For example, ChIP-seq or related approaches such as CUT&Tag allow for the detailed analysis of KDM5 occupancy within the genome, as well as the co-occupancy with other chromatin regulators and the distribution of chromatin marks such as histone PTMs. It will be critical to design experimental approaches that enable the acute and rapid manipulation of KDM5 function for the interrogation of their activity, chromatin occupancy, and function within defined time-frames, reducing pleiotropic effects imposed by approaches that, for example, depend on the selection of single cell clones lacking a KDM5 protein or expressing a mutant protein. Functional read-outs should deliver information that reflects these time-frames while providing insights at sufficient detail and confidence. With respect to the roles of KDM5 demethylases in disease, it would be of great value to link discrete processes and regulatory mechanisms to molecular disease phenotypes. Therefore, appropriate

experimental models that faithfully recapitulate key pathological features have to be used to determine the impact of defined molecular interactions and mechanisms on disease processes and provide a testing ground for KDM5-centered therapeutic approaches.

CONCLUSION

KDM5 demethylases are key epigenetic regulators involved in cellular differentiation, proliferation and development. These implications along with accumulating evidence suggesting KDM5 demethylases as promising targets in cancer therapy, call for a detailed investigation of the mechanisms that define their diverse functions. Targeting and regulatory interactions provide the molecular context in which KDM5 demethylases play their roles. RB and HDAC complexes are central interactors that coordinate with KDM5 demethylases in diverse ways. Future efforts will elucidate the molecular details and mechanistic implications of these interactions. Since RB is also an interactor of HDACs and HDAC complexes (Brehm et al., 1998; Lai et al., 2001), it will be of interest to determine whether RB takes part in HDAC interactions together with KDM5 demethylases. Finally, distinct interactions with chromatin regulators may not only define diverse functions of individual KDM5 demethylases, but could also provide hints to how these enzymes have diversified functionally within the KDM5 protein family. Taken together, these questions will continue to inspire novel experimental studies that will enhance our understanding of KDM5 demethylase biology and epigenetic mechanisms in general.

AUTHOR CONTRIBUTIONS

EP, TR, PE, and SP performed literature research and wrote the manuscript. EP and SP prepared the figures.

FUNDING

EP, TR, PE, and SP are funded by CMMC core funding (JRG XI), TR and SP are supported by the Deutsche Forschungsgemeinschaft (DFG, German Research Foundation)—SFB1430—Project-ID 424228829.

ACKNOWLEDGMENTS

We sincerely apologize to our colleagues whose work was not included in this review by mistake or due to content and space limitations.

REFERENCES

Albert, M., Schmitz, S. U., Kooistra, S. M., Malatesta, M., Torres, C. M., Rekling, J. C., et al. (2013). The Histone Demethylase Jarid1b Ensures Faithful Mouse Development by Protecting Developmental Genes from Aberrant H3K4me3. *Plos Genet.* 9 (4), 15. doi:10.1371/journal.pgen.1003461

Allen, H. F., Wade, P. A., and Kutateladze, T. G. (2013). The NuRD Architecture. *Cell. Mol. Life Sci.* 70 (19), 3513–3524. doi:10.1007/s00018-012-1256-2

Bailey, M. H., Tokheim, C., Porta-Pardo, E., Sengupta, S., Bertrand, D., Weerasinghe, A., et al. (2018). Comprehensive Characterization of Cancer Driver Genes and Mutations. *Cell* 173 (2), 371–+. doi:10.1016/j.cell.2018.02.060

Barrett, A., Santangelo, S., Tan, K., Catchpole, S., Roberts, K., Spencer-Dene, B., et al. (2007). Breast Cancer Associated Transcriptional Repressor PLU-1/JARID1B Interacts Directly with Histone Deacetylases. *Int. J. Cancer* 121 (2), 265–275. doi:10.1002/ijc.22673

Benevolenskaya, E. V., Murray, H. L., Branton, P., Young, R. A., and Kaelin, W. G. (2005). Binding of pRB to the PHD Protein RBP2 Promotes Cellular Differentiation. *Mol. Cell* 18 (6), 623–635. doi:10.1016/j.molcel.2005.05.012

Blackledge, N. P., Farcas, A. M., Kondo, T., King, H. W., McGouran, J. F., Hanssen, L. L. P., et al. (2014). Variant PRC1 Complex-dependent H2A Ubiquitylation Drives PRC2 Recruitment and Polycomb Domain Formation. *Cell* 157 (6), 1445–1459. doi:10.1016/j.cell.2014.05.004

Brehm, A., Miska, E. A., McCance, D. J., Reid, J. L., Bannister, A. J., and Kouzarides, T. (1998). Retinoblastoma Protein Recruits Histone Deacetylase to Repress Transcription. *Nature* 391 (6667), 597–601. doi:10.1038/35404

Brehm, A., Nielsen, S. J., Miska, E. A., McCance, D. J., Reid, J. L., Bannister, A. J., et al. (1999). The E7 Oncoprotein Associates with Mi2 and Histone Deacetylase Activity to Promote Cell Growth. *Embo J.* 18 (9), 2449–2458. doi:10.1093/emboj/18.9.2449

Brier, A. S. B., Loft, A., Madsen, J. G. S., Rosengren, T., Nielsen, R., Schmidt, S. F., et al. (2017). The KDM5 Family Is Required for Activation of Pro-proliferative Cell Cycle Genes during Adipocyte Differentiation. *Nucleic Acids Res.* 45 (4), 1743–1759. doi:10.1093/nar/gkw1156

Bruick, R. K., and McKnight, S. L. (2001). A Conserved Family of Prolyl-4-Hydroxylases that Modify HIF. *Science* 294 (5545), 1337–1340. doi:10.1126/science.1066373

Carr, S. M., Munro, S., Kessler, B., Oppermann, U., and La Thangue, N. B. (2011). Interplay between Lysine Methylation and Cdk Phosphorylation in Growth Control by the Retinoblastoma Protein. *Embo J.* 30 (2), 317–327. doi:10.1038/emboj.2010.311

Catchpole, S., Spencer-Dene, B., Hall, D., Santangelo, S., Rosewell, I., Guenatri, M., et al. (2011). PLU-1/JARID1B/KDM5B Is Required for Embryonic Survival and Contributes to Cell Proliferation in the Mammary Gland and in ER+ Breast Cancer Cells. *Int. J. Oncol.* 38 (5), 1267–1277. doi:10.3892/ijo.2011.956

Chang, S., Yim, S., and Park, H. (2019). The Cancer Driver Genes IDH1/2, JARID1C/KDM5C, and UTX/KDM6A: Crosstalk between Histone Demethylation and Hypoxic Reprogramming in Cancer Metabolism. *Exp. Mol. Med.* 51, 17. doi:10.1038/s12276-019-0230-6

Chaturvedi, C. P., Somasundaram, B., Singh, K., Carpenedo, R. L., Stanford, W. L., Dilworth, F. J., et al. (2012). Maintenance of Gene Silencing by the Coordinate Action of the H3K9 Methyltransferase G9a/KMT1C and the H3K4 Demethylase Jarid1a/KDM5A. *Proc. Natl. Acad. Sci. U. S. A.* 109 (46), 18845–18850. doi:10.1073/pnas.1213951109

Chen, P. L., Scully, P., Shew, J. Y., Wang, J. Y. J., and Lee, W. H. (1989). Phosphorylation of the Retinoblastoma Gene-Product Is Modulated during the Cell-Cycle and Cellular-Differentiation. *Cell* 58 (6), 1193–1198. doi:10.1016/0092-8674(89)90517-5

Chicas, A., Kapoor, A., Wang, X. W., Aksoy, O., Evertts, A. G., Zhang, M. Q., et al. (2012). H3K4 Demethylation by Jarid1a and Jarid1b Contributes to Retinoblastoma-Mediated Gene Silencing during Cellular Senescence. *Proc. Natl. Acad. Sci. U. S. A.* 109 (23), 8971–8976. doi:10.1073/pnas.1119836109

Cho, H. S., Hayami, S., Toyokawa, G., Maejima, K., Yamane, Y., Suzuki, T., et al. (2012). RB1 Methylation by SMYD2 Enhances Cell Cycle Progression through an Increase of RB1 Phosphorylation. *Neoplasia* 14(6), 476-+. doi:10.1593/neo.12656

Christensen, J., Agger, K., Cloos, P. A. C., Pasini, D., Rose, S., Sennels, L., et al. (2007). RBP2 Belongs to a Family of Demethylases, Specific for Tri- and

Dimethylated Lysine 4 on Histone 3. *Cell* 128 (6), 1063–1076. doi:10.1016/j.cell.2007.02.003

Cruz, C., Della Rosa, M., Krueger, C., Gao, Q., Horkai, D., King, M., et al. (2018). Tri-methylation of Histone H3 Lysine 4 Facilitates Gene Expression in Ageing Cells. *Elife* 7. doi:10.7554/eLife.34081

Defeojones, D., Huang, P. S., Jones, R. E., Haskell, K. M., Vuocolo, G. A., Hanobik, M. G., et al. (1991). Cloning of Cdnas for Cellular Proteins that Bind to the Retinoblastoma Gene-Product. *Nature* 352 (6332), 251–254. doi:10.1038/352251a0

Dey, B. K., Stalker, L., Schnerch, A., Bhatia, M., Taylor-Papidimitriou, J., and Wynder, C. (2008). The Histone Demethylase KDM5b/JARID1b Plays a Role in Cell Fate Decisions by Blocking Terminal Differentiation. *Mol. Cell. Biol.* 28 (17), 5312–5327. doi:10.1128/mcb.00128-08

Di Stefano, L., Walker, J. A., Burgio, G., Corona, D. F. V., Mulligan, P., Naar, A. M., et al. (2011). Functional Antagonism between Histone H3K4 Demethylases *In Vivo*. *Genes & Dev.* 25 (1), 17–28. doi:10.1101/gad.1983711

Dick, F. A., and Rubin, S. M. (2013). Molecular Mechanisms Underlying RB Protein Function. *Nat. Rev. Mol. Cell Biol.* 14 (5), 297–306. doi:10.1038/nrm3567

Dimitrova, E., Turberfield, A. H., and Klose, R. J. (2015). Histone Demethylases in Chromatin Biology and beyond. *Embo Rep.* 16 (12), 1620–1639. doi:10.15252/embr.201541113

DiTacchio, L., Le, H. D., Vollmers, C., Hatori, M., Witcher, M., Secombe, J., et al. (2011). Histone Lysine Demethylase JARID1a Activates CLOCK-BMAL1 and Influences the Circadian Clock. *Science* 333 (6051), 1881–1885. doi:10.1126/science.1206022

Dorighi, K. M., Swigut, T., Henriques, T., Bhanu, N. V., Scruggs, B. S., Nady, N., et al. (2017). Mll3 and Mll4 Facilitate Enhancer RNA Synthesis and Transcription from Promoters Independently of H3K4 Monomethylation. *Mol. Cell* 66(4), 568-+. doi:10.1016/j.molcel.2017.04.018

Dorosz, J., Kristensen, L. H., Aduri, N. G., Mirza, O., Lousen, R., Bucciarelli, S., et al. (2019). Molecular Architecture of the Jumonji C Family Histone Demethylase KDM5B. *Sci. Rep.* 9. doi:10.1038/s41598-019-40573-y

Eberl, H. C., Spruijt, C. G., Kelstrup, C. D., Vermeulen, M., and Mann, M. (2013). A Map of General and Specialized Chromatin Readers in Mouse Tissues Generated by Label-free Interaction Proteomics. *Mol. Cell* 49 (2), 368–378. doi:10.1016/j.molcel.2012.10.026

Facompre, N. D., Harmeyer, K. M., Sole, X., Kabraji, S., Belden, Z., Sahu, V., et al. (2016). JARID1B Enables Transit between Distinct States of the Stem-like Cell Population in Oral Cancers. *Cancer Res.* 76 (18), 5538–5549. doi:10.1158/0008-5472.can-15-3377

Foster, C. T., Dovey, O. M., Lezina, L., Luo, J. L., Gant, T. W., Barlev, N., et al. (2010). Lysine-Specific Demethylase 1 Regulates the Embryonic Transcriptome and CoREST Stability. *Mol. Cell. Biol.* 30 (20), 4851–4863. doi:10.1128/mcb.00521-10

Friend, S. H., Bernards, R., Rogelj, S., Weinberg, R. A., Rapaport, J. M., Albert, D. M., et al. (1986). A Human Dna Segment with Properties of the Gene that Predisposes to Retinoblastoma and Osteosarcoma. *Nature* 323 (6089), 643–646. doi:10.1038/323643a0

Gaillard, S., Charasson, V., Ribeyre, C., Salifou, K., Pillaire, M. J., Hoffmann, J. S., et al. (2021). KDM5A and KDM5B Histone-Demethylases Contribute to HU-Induced Replication Stress Response and Tolerance. *Biol. Open* 10 (5). doi:10.1242/bio.057729

Gajan, A., Barnes, V. L., Liu, M. Y., Saha, N., and Pile, L. A. (2016). The Histone Demethylase dKDM5/LID Interacts with the SIN3 Histone Deacetylase Complex and Shares Functional Similarities with SIN3. *Epigenetics Chromatin* 9. doi:10.1186/s13072-016-0053-9

Gildea, J. J., Lopez, R., and Shearn, A. (2000). A Screen for New Trithorax Group Genes Identified Little Imaginal Discs, the *Drosophila melanogaster* Homologue of Human Retinoblastoma Binding Protein 2. *Genetics* 156 (2), 645–663.

Gong, F., Clouaire, T., Aguirrebengoa, M., Legube, G., and Miller, K. M. (2017). Histone Demethylase KDM5A Regulates the ZMYND8-NuRD Chromatin Remodeler to Promote DNA Repair. *J. Cell Biol.* 216 (7), 1959–1974. doi:10.1083/jcb.201611135

Grzenda, A., Lomberk, G., Zhang, J. S., and Urrutia, R. (2009). Sin3: Master Scaffold and Transcriptional Corepressor. *Biochimica Biophysica Acta-Gene Regul. Mech.* 1789 (6-8), 443–450. doi:10.1016/j.bbagrm.2009.05.007

Harbour, J. W., Lai, S. L., Whangpeng, J., Gazdar, A. F., Minna, J. D., and Kaye, F. J. (1988). Abnormalities in Structure and Expression of the Human Retinoblastoma Gene in Sclc. *Science* 241 (4863), 353–357. doi:10.1126/science.2838909

Harbour, J. W., Luo, R. X., Santi, A. D., Postigo, A. A., and Dean, D. C. (1999). Cdk Phosphorylation Triggers Sequential Intramolecular Interactions that Progressively Block Rb Functions as Cells Move through G1. *Cell* 98 (6), 859–869. doi:10.1016/s0092-8674(00)81519-6

Harmeyer, K. M., Facompre, N. D., Herlyn, M., and Basu, D. (2017). JARID1 Histone Demethylases: Emerging Targets in Cancer. *Trends Cancer* 3 (10), 713–725. doi:10.1016/j.trecan.2017.08.004

Hatch, H. A. M., and Secombe, J. (2021). Molecular and Cellular Events Linking Variants in the Histone Demethylase KDM5C to the Intellectual Disability Disorder Claes-Jensen Syndrome. *Febs J.* doi:10.1111/febs.16204

Hayakawa, T., Ohtani, Y., Hayakawa, N., Shinmyozu, K., Saito, M., Ishikawa, F., et al. (2007). RBP2 Is an MRG15 Complex Component and Down-Regulates Intragenic Histone H3 Lysine 4 Methylation. *Genes Cells* 12 (6), 811–826. doi:10.1111/j.1365-2443.2007.01089.x

Heintzman, N. D., Stuart, R. K., Hon, G., Fu, Y. T., Ching, C. W., Hawkins, R. D., et al. (2007). Distinct and Predictive Chromatin Signatures of Transcriptional Promoters and Enhancers in the Human Genome. *Nat. Genet.* 39 (3), 311–318. doi:10.1038/ng1966

Hinohara, K., Wu, H. J., Vigneau, S., McDonald, T. O., Igarashi, K. J., Yamamoto, K. N., et al. (2018). KDM5 Histone Demethylase Activity Links Cellular Transcriptomic Heterogeneity to Therapeutic Resistance. *Cancer Cell* 34(6), 939-+. doi:10.1016/j.ccell.2018.10.014

Hojfeldt, J. W., Agger, K., and Helin, K. (2013). Histone Lysine Demethylases as Targets for Anticancer Therapy. *Nat. Rev. Drug Discov.* 12 (12), 917–930. doi:10.1038/nrd4154

Horton, J. R., Engstrom, A., Zoeller, E. L., Liu, X., Shanks, J. R., Zhang, X., et al. (2016). Characterization of a Linked Jumonji Domain of the KDM5/JARID1 Family of Histone H3 Lysine 4 Demethylases. *J. Biol. Chem.* 291 (6), 2631–2646. doi:10.1074/jbc.M115.698449

Hou, J. L., Wu, J., Dombkowski, A., Zhang, K. Z., Holowatyj, A., Boerner, J. L., et al. (2012). Genomic Amplification and a Role in Drug-Resistance for the KDM5A Histone Demethylase in Breast Cancer. *Am. J. Transl. Res.* 4 (3), 247–256.

Hu, E., Chen, Z. X., Fredrickson, T., Zhu, Y., Kirkpatrick, R., Zhang, G. F., et al. (2000). Cloning and Characterization of a Novel Human. Class I Histone Deacetylase that Functions as a Transcription Repressor. *J. Biol. Chem.* 275 (20), 15254–15264. doi:10.1074/jbc.M908988199

Huang, E. Y., Zhang, J. S., Miska, E. A., Guenther, M. G., Kouzarides, T., and Lazar, M. A. (2000). Nuclear Receptor Corepressors Partner with Class II Histone Deacetylases in a Sin3-independent Repression Pathway. *Genes & Dev.* 14 (1), 45–54.

Huang, F., Chandrasekharan, M. B., Chen, Y. C., Bhaskara, S., Hiebert, S. W., and Sun, Z. W. (2010). The JmjN Domain of Jhd2 Is Important for its Protein Stability, and the Plant Homeodomain (PHD) Finger Mediates its Chromatin Association Independent of H3K4 Methylation. *J. Biol. Chem.* 285 (32), 24548–24561. doi:10.1074/jbc.M110.117333

Isaac, C. E., Francis, S. M., Martens, A. L., Julian, L. M., Seifried, L. A., Erdmann, N., et al. (2006). The Retinoblastoma Protein Regulates Pericentric Heterochromatin. *Mol. Cell. Biol.* 26 (9), 3659–3671. doi:10.1128/mcb.26.9.3659-3671.2006

Iwase, S., Lan, F., Bayliss, P., de la Torre-Ubieta, L., Huarte, M., Qi, H. H., et al. (2007). The X-Linked Mental Retardation Gene SMCX/JARID1C Defines a Family of Histone H3 Lysine 4 Demethylases. *Cell* 128 (6), 1077–1088. doi:10.1016/j.cell.2007.02.017

Jaakkola, P., Mole, D. R., Tian, Y. M., Wilson, M. I., Gielbert, J., Gaskell, S. J., et al. (2001). Targeting of HIF-alpha to the von Hippel-Lindau ubiquitylation complex by O-2-regulated prolyl hydroxylation. *Science* 292 (5516), 468–472. doi:10.1126/science.1059796

Jensen, L. R., Amende, M., Gurok, U., Moser, B., Gimmel, V., Tzschach, A., et al. (2005). Mutations in the JARID1C Gene, Which Is Involved in Transcriptional Regulation and Chromatin Remodeling, Cause X-Linked Mental Retardation. *Am. J. Hum. Genet.* 76 (2), 227–236. doi:10.1086/427563

Johansson, C., Velupillai, S., Tumber, A., Szykowska, A., Hookway, E. S., Nowak, R. P., et al. (2016). Structural Analysis of Human KDM5B Guides Histone

Demethylase Inhibitor Development. *Nat. Chem. Biol.* 12(7), 539-+. doi:10.1038/nchembio.2087

Jumper, J., Evans, R., Pritzel, A., Green, T., Figurnov, M., Ronneberger, O., et al. (2021). Highly Accurate Protein Structure Prediction with AlphaFold. *Nature* 596(7873), 583-+. doi:10.1038/s41586-021-03819-2

Kaniskan, H. U., Martini, M. L., and Jin, J. (2018). Inhibitors of Protein Methyltransferases and Demethylases. *Chem. Rev.* 118 (3), 989–1068. doi:10.1021/acs.chemrev.6b00801

Kasinath, V., Beck, C., Sauer, P., Poepsel, S., Kosmatka, J., Faini, M., et al. (2021). JARID2 and AEBP2 Regulate PRC2 in the Presence of H2AK119ub1 and Other Histone Modifications. *Science* 371 (6527). doi:10.1126/science.abc3393

Kidder, B. L., Hu, G. Q., and Zhao, K. (2014). KDM5B Focuses H3K4 Methylation Near Promoters and Enhancers during Embryonic Stem Cell Self-Renewal and Differentiation. *Genome Biol.* 15 (2), 19. doi:10.1186/gb-2014-15-2-r32

Kim, H. Y., Ahn, B. Y., and Cho, Y. (2001). Structural Basis for the Inactivation of Retinoblastoma Tumor Suppressor by SV40 Large T Antigen. *Embo J.* 20 (1-2), 295–304. doi:10.1093/emboj/20.1.295

Kim, T., and Buratowski, S. (2009). Dimethylation of H3K4 by Set1 Recruits the Set3 Histone Deacetylase Complex to 5 ' Transcribed Regions. *Cell* 137 (2), 259–272. doi:10.1016/j.cell.2009.02.045

Kim, Y. W., Otterson, G. A., Kratzke, R. A., Coxon, A. B., and Kaye, F. J. (1994). Differential Specificity for Binding of Retinoblastoma Binding-Protein-2 to Rb, P107, and Tata-Binding Protein. *Mol. Cell. Biol.* 14 (11), 7256–7264. doi:10.1128/mcb.14.11.7256

Klein, B. J., Piao, L. H., Xi, Y. X., Rincon-Arano, H., Rothbart, S. B., Peng, D. N., et al. (2014). The Histone-h3k4-specific Demethylase KDM5B Binds to its Substrate and Product through Distinct PHD Fingers. *Cell Rep.* 6 (2), 325–335. doi:10.1016/j.celrep.2013.12.021

Klose, R. J., Yan, Q., Tothova, Z., Yamane, K., Erdjument-Bromage, H., Tempst, P., et al. (2007). The Retinoblastoma Binding Protein RBP2 Is an H3K4 Demethylase. *Cell* 128 (5), 889–900. doi:10.1016/j.cell.2007.02.013

Kooistra, S. M., and Helin, K. (2012). Molecular Mechanisms and Potential Functions of Histone Demethylases. *Nat. Rev. Mol. Cell Biol.* 13 (5), 297–311. doi:10.1038/nrm3327

Krishnakumar, R., and Kraus, W. L. (2010). PARP-1 Regulates Chromatin Structure and Transcription through a KDM5B-dependent Pathway. *Mol. Cell* 39 (5), 736–749. doi:10.1016/j.molcel.2010.08.014

Kristensen, L. H., Nielsen, A. L., Helgstrand, C., Lees, M., Cloos, P., Kastrup, J. S., et al. (2012). Studies of H3K4me3 Demethylation by KDM5B/Jarid1B/PLU1 Reveals Strong Substrate Recognition *In Vitro* and Identifies 2,4-Pyridine-Dicarboxylic Acid as an *In Vitro* and in Cell Inhibitor. *Febs J.* 279 (11), 1905–1914. doi:10.1111/j.1742-4658.2012.08567.x

Kumbhar, R., Sanchez, A., Perren, J., Gong, F. D., Corujo, D., Medina, F., et al. (2021). Poly(ADP-ribose) Binding and macroH2A Mediate Recruitment and Functions of KDM5A at DNA Lesions. *J. Cell Biol.* 220 (7). doi:10.1083/jcb.202006149

Lai, A., Kennedy, B. K., Barbie, D. A., Bertos, N. R., Yang, X. J., Theberge, M. C., et al. (2001). RBP1 Recruits the mSIN3-Histone Deacetylase Complex to the Pocket of Retinoblastoma Tumor Suppressor Family Proteins Found in Limited Discrete Regions of the Nucleus at Growth Arrest. *Mol. Cell. Biol.* 21 (8), 2918–2932. doi:10.1128/mcb.21.8.2918-2932.2001

Lambert, J. P., Pawson, T., and Gingras, A. C. (2012). Mapping Physical Interactions within Chromatin by Proteomic Approaches. *Proteomics* 12 (10), 1609–1622. doi:10.1002/pmic.201100547

Lambert, S. A., Jolma, A., Campitelli, L. F., Das, P. K., Yin, Y. M., Albu, M., et al. (2018). The Human Transcription Factors. *Cell* 172 (4), 650–665. doi:10.1016/j.cell.2018.01.029

Lee, E., To, H., Shew, J. Y., Bookstein, R., Scully, P., and Lee, W. H. (1988). Inactivation of the Retinoblastoma Susceptibility Gene in Human-Breast Cancers. *Science* 241 (4862), 218–221. doi:10.1126/science.3388033

Lee, J. O., Russo, A. A., and Pavletich, N. P. (1998). Structure of the Retinoblastoma Tumour-Suppressor Pocket Domain Bound to a Peptide from HPV E7. *Nature* 391 (6670), 859–865. doi:10.1038/36038

Lee, M. G., Norman, J., Shilatifard, A., and Shiekhattar, R. (2007). Physical and Functional Association of a Trimethyl H3K4 Demethylase and Ring6a/MBLR, a Polycomb-like Protein. *Cell* 128 (5), 877–887. doi:10.1016/j.cell.2007.02.004

Lee, N., Erdjument-Bromage, H., Tempst, P., Jones, R. S., and Zhang, Y. (2009). The H3K4 Demethylase Lid Associates with and Inhibits Histone Deacetylase Rpd3. *Mol. Cell. Biol.* 29 (6), 1401–1410. doi:10.1128/mcb.01643-08

Li, B., Carey, M., and Workman, J. L. (2007). The Role of Chromatin during Transcription. *Cell* 128 (4), 707–719. doi:10.1016/j.cell.2007.01.015

Li, N., Dhar, S. S., Chen, T. Y., Kan, P. Y., Wei, Y., Kim, J. H., et al. (2016a). JARID1D Is a Suppressor and Prognostic Marker of Prostate Cancer Invasion and Metastasis. *Cancer Res.* 76 (4), 831–843. doi:10.1158/0008-5472.can-15-0906

Li, N., Li, Y. Y., Lv, J., Zheng, X. D., Wen, H., Shen, H. J., et al. (2016b). ZMYND8 Reads the Dual Histone Mark H3K4me1-H3K14ac to Antagonize the Expression of Metastasis-Linked Genes. *Mol. Cell* 63 (3), 470–484. doi:10.1016/j.molcel.2016.06.035

Li, Q., Shi, L., Gui, B., Yu, W. H., Wang, J. M., Zhang, D., et al. (2011). Binding of the JmjC Demethylase JARID1B to LSD1/NuRD Suppresses Angiogenesis and Metastasis in Breast Cancer Cells by Repressing Chemokine CCL14. *Cancer Res.* 71 (21), 6899–6908. doi:10.1158/0008-5472.can-11-1523

Li, X., Liu, L., Yang, S. D., Song, N., Zhou, X., Gao, J., et al. (2014). Histone Demethylase KDM5B Is a Key Regulator of Genome Stability. *Proc. Natl. Acad. Sci. U. S. A.* 111 (19), 7096–7101. doi:10.1073/pnas.1324036111

Liang, Z. H., Diamond, M., Smith, J. A., Schnell, M., and Daniel, R. (2011). Proliferating Cell Nuclear Antigen Is Required for Loading of the SMCX/KMD5C Histone Demethylase onto Chromatin. *Epigenetics Chromatin* 4. doi:10.1186/1756-8935-4-18

Liefke, R., Oswald, F., Alvarado, C., Ferres-Marco, D., Mittler, G., Rodriguez, P., et al. (2010). Histone Demethylase KDM5A Is an Integral Part of the Core Notch-RBP-J Repressor Complex. *Genes & Dev.* 24 (6), 590–601. doi:10.1101/gad.563210

Lin, W. C., Cao, J., Liu, J. Y., Beshiri, M. L., Fujiwara, Y., Francis, J., et al. (2011). Loss of the Retinoblastoma Binding Protein 2 (RBP2) Histone Demethylase Suppresses Tumorigenesis in Mice Lacking Rb1 or Men1. *Proc. Natl. Acad. Sci. U. S. A.* 108 (33), 13379–13386. doi:10.1073/pnas.1110104108

Litt, M. D., Simpson, M., Gaszner, M., Allis, C. D., and Felsenfeld, G. (2001). Correlation between Histone Lysine Methylation and Developmental Changes at the Chicken Beta-Globin Locus. *Science* 293 (5539), 2453–2455. doi:10.1126/science.1064413

Local, A., Huang, H., Albuquerque, C. P., Singh, N., Lee, A. Y., Wang, W., et al. (2018). Identification of H3K4me1-Associated Proteins at Mammalian Enhancers. *Nat. Genet.* 50(1), 73-+. doi:10.1038/s41588-017-0015-6

Longbotham, J. E., Chio, C. M., Dharmarajan, V., Trnka, M. J., Torres, I. O., Goswami, D., et al. (2019). Histone H3 Binding to the PHD1 Domain of Histone Demethylase KDM5A Enables Active Site Remodeling. *Nat. Commun.* 10, 12. doi:10.1038/s41467-018-07829-z

Lopez-Bigas, N., Kisiel, T. A., DeWaal, D. C., Holmes, K. B., Volkert, T. L., Gupta, S., et al. (2008). Genome-wide Analysis of the H3K4 Histone Demethylase RBP2 Reveals a Transcriptional Program Controlling Differentiation. *Mol. Cell* 31 (4), 520–530. doi:10.1016/j.molcel.2008.08.004

Losman, J. A., Koivunen, P., and Kaelin, W. G. (2020). 2-Oxoglutarate-dependent Dioxygenases in Cancer. *Nat. Rev. Cancer* 20 (12), 710–726. doi:10.1038/s41568-020-00303-3

Luo, R. X., Postigo, A. A., and Dean, D. C. (1998). Rb Interacts with Histone Deacetylase to Repress Transcription. *Cell* 92 (4), 463–473. doi:10.1016/s0092-8674(00)80940-x

Macaluso, M., Montanari, M., Cinti, C., and Giordano, A. (2005). Modulation of Cell Cycle Components by Epigenetic and Genetic Events. *Seminars Oncol.* 32 (5), 452–457. doi:10.1053/j.seminoncol.2005.07.009

Malovannaya, A., Lanz, R. B., Jung, S. Y., Bulynko, Y., Le, N. T., Chan, D. W., et al. (2011). Analysis of the Human Endogenous Coregulator Complexome. *Cell* 145 (5), 787–799. doi:10.1016/j.cell.2011.05.006

Margueron, R., Justin, N., Ohno, K., Sharpe, M. L., Son, J., Drury, W. J., et al. (2009). Role of the Polycomb Protein EED in the Propagation of Repressive Histone Marks. *Nature* 461 (7265), 762–U711. doi:10.1038/nature08398

Margueron, R., and Reinberg, D. (2011). The Polycomb Complex PRC2 and its Mark in Life. *Nature* 469 (7330), 343–349. doi:10.1038/nature09784

Mashtalir, N., D'Avino, A. R., Michel, B. C., Luo, J., Pan, J., Otto, J. E., et al. (2018). Modular Organization and Assembly of SWI/SNF Family Chromatin Remodeling Complexes. *Cell* 175(5), 1272-+. doi:10.1016/j.cell.2018.09.032

McBrayer, S. K., Olenchock, B. A., DiNatale, G. J., Shi, D. D., Khanal, J., Jennings, R. B., et al. (2018). Autochthonous Tumors Driven by Rb1 Loss Have an Ongoing Requirement for the RBP2 Histone Demethylase. *Proc. Natl. Acad. Sci. U. S. A.* 115 (16), E3741–E3748. doi:10.1073/pnas.1716029115

McDonel, P., Costello, I., and Hendrich, B. (2009). Keeping Things Quiet: Roles of NuRD and Sin3 Co-repressor Complexes during Mammalian Development. *Int. J. Biochem. Cell Biol.* 41 (1), 108–116. doi:10.1016/j.biocel.2008.07.022

Metzger, E., Imhof, A., Patel, D., Kahl, P., Hoffmeyer, K., Friedrichs, N., et al. (2010). Phosphorylation of Histone H3T6 by PKC Beta(I) Controls Demethylation at Histone H3K4. *Nature* 464 (7289), 792–U175. doi:10.1038/nature08839

Millard, C. J., Varma, N., Saleh, A., Morris, K., Watson, P. J., Bottrill, A. R., et al. (2016). The Structure of the Core NuRD Repression Complex Provides Insights into its Interaction with Chromatin. *Elife* 5. doi:10.7554/eLife.13941

Moshkin, Y. M., Kan, T. W., Goodfellow, H., Bezstarosti, K., Maeda, R. K., Pilyugin, M., et al. (2009). Histone Chaperones ASF1 and NAP1 Differentially Modulate Removal of Active Histone Marks by LID-RPD3 Complexes during NOTCH Silencing. *Mol. Cell* 35 (6), 782–793. doi:10.1016/j.molcel.2009.07.020

Munro, S., Khaire, N., Inche, A., Carr, S., and La Thangue, N. B. (2010). Lysine Methylation Regulates the pRb Tumour Suppressor Protein. *Oncogene* 29 (16), 2357–2367. doi:10.1038/onc.2009.511

Najmabadi, H., Hu, H., Garshasbi, M., Zemojtel, T., Abedini, S. S., Chen, W., et al. (2011). Deep Sequencing Reveals 50 Novel Genes for Recessive Cognitive Disorders. *Nature* 478 (7367), 57–63. doi:10.1038/nature10423

Nielsen, S. J., Schneider, R., Bauer, U. M., Bannister, A. J., Morrison, A., O'Carroll, D., et al. (2001). Rb Targets Histone H3 Methylation and HP1 to Promoters. *Nature* 412 (6846), 561–565. doi:10.1038/35087620

Nijwening, J. H., Geutjes, E. J., Bernards, R., and Beijersbergen, R. L. (2011). The Histone Demethylase Jarid1b (Kdm5b) Is a Novel Component of the Rb Pathway and Associates with E2f-Target Genes in MEFs during Senescence. *Plos One* 6 (9). doi:10.1371/journal.pone.0025235

Nishibuchi, G., Shibata, Y., Hayakawa, T., Hayakawa, N., Ohtani, Y., Sinmyozu, K., et al. (2014). Physical and Functional Interactions between the Histone H3K4 Demethylase KDM5A and the Nucleosome Remodeling and Deacetylase (NuRD) Complex. *J. Biol. Chem.* 289 (42), 28956–28970. doi:10.1074/jbc.M114.573725

Ohguchi, H., Park, P. M. C., Wang, T. J., Gryder, B. E., Ogiya, D., Kurata, K., et al. (2021). Lysine Demethylase 5A Is Required for MYC-Driven Transcription in Multiple Myeloma. *Blood Cancer Discov.* 2 (4), 370–387. doi:10.1158/2643-3230.bcd-20-0108

Oser, M. G., Sabet, A. H., Gao, W. H., Chakraborty, A. A., Schinzel, A. C., Jennings, R. B., et al. (2019). The KDM5A/RBP2 Histone Demethylase Represses NOTCH Signaling to Sustain Neuroendocrine Differentiation and Promote Small Cell Lung Cancer Tumorigenesis. *Genes & Dev.* 33 (23-24), 1718–1738. doi:10.1101/gad.328336.119

Outchkourov, N. S., Muino, J. M., Kaufmann, K., van Ijcken, W. F. J., Koerkamp, M. J. G., van Leenen, D., et al. (2013). Balancing of Histone H3K4 Methylation States by the Kdm5c/SMCX Histone Demethylase Modulates Promoter and Enhancer Function. *Cell Rep.* 3 (4), 1071–1079. doi:10.1016/j.celrep.2013.02.030

Park, S., Osmers, U., Raman, G., Schwantes, R. H., Diaz, M. O., and Bushweller, J. H. (2010). The PHD3 Domain of MLL Acts as a CYP33-Regulated Switch between MLL-Mediated Activation and Repression. *Biochemistry* 49 (31), 6576–6586. doi:10.1021/bi1009387

Pasini, D., Hansen, K. H., Christensen, J., Agger, K., Cloos, P. A. C., and Helin, K. (2008). Coordinated Regulation of Transcriptional Repression by the RBP2 H3K4 Demethylase and Polycomb-Repressive Complex 2. *Genes & Dev.* 22 (10), 1345–1355. doi:10.1101/gad.470008

Pedersen, M. T., and Helin, K. (2010). Histone Demethylases in Development and Disease. *Trends Cell Biol.* 20 (11), 662–671. doi:10.1016/j.tcb.2010.08.011

Pilotto, S., Speranzini, V., Tortorici, M., Durand, D., Fish, A., Valente, S., et al. (2015). Interplay Among Nucleosomal DNA, Histone Tails, and Corepressor CoREST Underlies LSD1-Mediated H3 Demethylation. *Proc. Natl. Acad. Sci. U. S. A.* 112 (9), 2752–2757. doi:10.1073/pnas.1419468112

Plch, J., Hrabeta, J., and Eckschlager, T. (2019). KDM5 Demethylases and Their Role in Cancer Cell Chemoresistance. *Int. J. Cancer* 144 (2), 221–231. doi:10.1002/ijc.31881

Poepsel, S., Kasinath, V., and Nogales, E. (2018). Cryo-EM Structures of PRC2 Simultaneously Engaged with Two Functionally Distinct Nucleosomes. *Nat. Struct. Mol. Biol.* 25(2), 154-+. doi:10.1038/s41594-018-0023-y

Punnia-Moorthy, G., Hersey, P., Al Emran, A., and Tiffen, J. (2021). Lysine Demethylases: Promising Drug Targets in Melanoma and Other Cancers. *Front. Genet.* 12. doi:10.3389/fgene.2021.680633

Rada-Iglesias, A., Bajpai, R., Swigut, T., Brugmann, S. A., Flynn, R. A., and Wysocka, J. (2011). A Unique Chromatin Signature Uncovers Early Developmental Enhancers in Humans. *Nature* 470(7333), 279-+. doi:10.1038/nature09692

Rada-Iglesias, A. (2018). Is H3K4me1 at Enhancers Correlative or Causative? *Nat. Genet.* 50 (1), 4–5. doi:10.1038/s41588-017-0018-3

Roesch, A., Becker, B., Meyer, S., Wild, P., Hafner, C., Landthaler, M., et al. (2005). Retinoblastoma-binding Protein 2-homolog 1: a Retinoblastoma-Binding Protein Downregulated in Malignant Melanomas. *Mod. Pathol.* 18 (9), 1249–1257. doi:10.1038/modpathol.3800413

Roesch, A., Becker, B., Schneider-Brachert, W., Hagen, I., Landthaler, M., and Vogt, T. (2006). Re-expression of the Retinoblastoma-Binding Protein 2-homolog 1 Reveals Tumor-Suppressive Functions in Highly Metastatic Melanoma Cells. *J. Investigative Dermatology* 126 (8), 1850–1859. doi:10.1038/sj.jid.5700324

Roesch, A., Fukunaga-Kalabis, M., Schmidt, E. C., Zabierowski, S. E., Brafford, P. A., Vultur, A., et al. (2010). A Temporarily Distinct Subpopulation of Slow-Cycling Melanoma Cells Is Required for Continuous Tumor Growth. *Cell* 141 (4), 583–594. doi:10.1016/j.cell.2010.04.020

Roesch, A., Mueller, A. M., Sterapfl, T., Moehle, C., Landthaler, M., and Vogt, T. (2008). RBP2-H1/JARID1B Is a Transcriptional Regulator with a Tumor Suppressive Potential in Melanoma Cells. *Int. J. Cancer* 122 (5), 1047–1057. doi:10.1002/ijc.23211

Roesch, A., Vultur, A., Bogeski, I., Wang, H., Zimmermann, K. M., Speicher, D., et al. (2013). Overcoming Intrinsic Multidrug Resistance in Melanoma by Blocking the Mitochondrial Respiratory Chain of Slow-Cycling JARID1B(high) Cells. *Cancer Cell* 23 (6), 811–825. doi:10.1016/j.ccr.2013.05.003

Rondinelli, B., Schwerer, H., Antonini, E., Gaviraghi, M., Lupi, A., Frenquelli, M., et al. (2015). H3K4me3 Demethylation by the Histone Demethylase KDM5C/JARID1C Promotes DNA Replication Origin Firing. *Nucleic Acids Res.* 43 (5), 2560–2574. doi:10.1093/nar/gkv090

Saddic, L. A., West, L. E., Aslanian, A., Yates, J. R., Rubin, S. M., Gozani, O., et al. (2010). Methylation of the Retinoblastoma Tumor Suppressor by SMYD2. *J. Biol. Chem.* 285 (48), 37733–37740. doi:10.1074/jbc.M110.137612

Sanidas, I., Morris, R., Fella, K. A., Rumde, P. H., Boukhali, M., Tai, E. C., et al. (2019). A Code of Mono-Phosphorylation Modulates the Function of RB. *Mol. Cell* 73 (5), 985–+. doi:10.1016/j.molcel.2019.01.004

Santos, C., Laia, R. R., Madrigal, I., Badenas, C., Pineda, M., and Mila, M. (2006). A Novel Mutation in JARID1C Gene Associated with Mental Retardation. *Eur. J. Hum. Genet.* 14 (5), 583–586. doi:10.1038/sj.ejhg.5201608

Santos-Rosa, H., Schneider, R., Bannister, A. J., Sherriff, J., Bernstein, B. E., Emre, N. C. T., et al. (2002). Active Genes Are Tri-methylated at K4 of Histone H3. *Nature* 419 (6905), 407–411. doi:10.1038/nature01080

Schmidt, C., and Urlaub, H. (2017). Combining Cryo-Electron Microscopy (Cryo-EM) and Cross-Linking Mass Spectrometry (CX-MS) for Structural Elucidation of Large Protein Assemblies. *Curr. Opin. Struct. Biol.* 46, 157–168. doi:10.1016/j.sbi.2017.10.005

Schmitz, S. U., Albert, M., Malatesta, M., Morey, L., Johansen, J. V., Bak, M., et al. (2011). Jarid1b Targets Genes Regulating Development and Is Involved in Neural Differentiation. *Embo J.* 30 (22), 4586–4600. doi:10.1038/emboj.2011.383

Scibetta, A. G., Santangelo, S., Coleman, J., Hall, D., Chaplin, T., Copier, J., et al. (2007). Functional Analysis of the Transcription Repressor PLU-1/JARID1B. *Mol. Cell. Biol.* 27 (20), 7220–7235. doi:10.1128/mcb.00274-07

Secombe, J., Li, L., Carlos, L., and Eisenman, R. N. (2007). The Trithorax Group Protein Lid Is a Trimethyl Histone H3K4 Demethylase Required for dMyc-Induced Cell Growth. *Genes & Dev.* 21 (5), 537–551. doi:10.1101/gad.1523007

Sellers, W. R., and Kaelin, W. G. (1997). Role of the Retinoblastoma Protein in the Pathogenesis of Human Cancer. *J. Clin. Oncol.* 15 (11), 3301–3312. doi:10.1200/jco.1997.15.11.3301

Sellers, W. R., Novitch, B. G., Miyake, S., Heith, A., Otterson, G. A., Kaye, F. J., et al. (1998). Stable Binding to E2F Is Not Required for the Retinoblastoma Protein to

Activate Transcription, Promote Differentiation, and Suppress Tumor Cell Growth. *Genes & Dev.* 12 (1), 95–106. doi:10.1101/gad.12.1.95

Seto, E., and Yoshida, M. (2014). Erasers of Histone Acetylation: The Histone Deacetylase Enzymes. *Cold Spring Harb. Perspect. Biol.* 6 (4). doi:10.1101/cshperspect.a018713

Seward, D. J., Cubberley, G., Kim, S., Schonewald, M., Zhang, L., Tripet, B., et al. (2007). Demethylation of Trimethylated Histone H3 Lys4 *In Vivo* by JARID1 JmjC Proteins. *Nat. Struct. Mol. Biol.* 14 (3), 240–242. doi:10.1038/nsmb1200

Sharma, S. V., Lee, D. Y., Li, B. H., Quinlan, M. P., Takahashi, F., Maheswaran, S., et al. (2010). A Chromatin-Mediated Reversible Drug-Tolerant State in Cancer Cell Subpopulations. *Cell* 141 (1), 69–80. doi:10.1016/j.cell.2010.02.027

Shen, H. J., Xu, W. Q., Guo, R., Rong, B. W., Gu, L., Wang, Z. T., et al. (2016). Suppression of Enhancer Overactivation by a RACK7-Histone Demethylase Complex. *Cell* 165 (2), 331–342. doi:10.1016/j.cell.2016.02.064

Shi, Y. J., Matson, C., Lan, F., Iwase, S., Baba, T., and Shi, Y. (2005). Regulation of LSD1 Histone Demethylase Activity by its Associated Factors. *Mol. Cell* 19 (6), 857–864. doi:10.1016/j.molcel.2005.08.027

Silverstein, R. A., and Ekwall, K. (2005). Sin3: a Flexible Regulator of Global Gene Expression and Genome Stability. *Curr. Genet.* 47 (1), 1–17. doi:10.1007/s00294-004-0541-5

Singh, M., Krajewski, M., Mikolajka, A., and Holak, T. A. (2005). Molecular Determinants for the Complex Formation between the Retinoblastoma Protein and LXCXE Sequences. *J. Biol. Chem.* 280 (45), 37868–37876. doi:10.1074/jbc.M504877200

Sinz, A. (2018). Cross-Linking/Mass Spectrometry for Studying Protein Structures and Protein-Protein Interactions: Where Are We Now and where Should We Go from Here? *Angew. Chemie-International Ed.* 57 (22), 6390–6396. doi:10.1002/anie.201709559

Song, Y., Dagil, L., Fairall, L., Robertson, N., Wu, M. X., Ragan, T. J., et al. (2020). Mechanism of Crosstalk between the LSD1 Demethylase and HDAC1 Deacetylase in the CoREST Complex. *Cell Rep.* 30(8), 2699-+. doi:10.1016/j.celrep.2020.01.091

Spitz, F., and Furlong, E. E. M. (2012). Transcription Factors: from Enhancer Binding to Developmental Control. *Nat. Rev. Genet.* 13 (9), 613–626. doi:10.1038/nrg3207

Strahl, B. D., and Allis, C. D. (2000). The Language of Covalent Histone Modifications. *Nature* 403 (6765), 41–45. doi:10.1038/47412

Tahiliani, M., Mei, P. C., Fang, R., Leonor, T., Rutenberg, M., Shimizu, F., et al. (2007). The Histone H3K4 Demethylase SMCX Links REST Target Genes to X-Linked Mental Retardation. *Nature* 447(7144), 601-+. doi:10.1038/nature05823

Tan, K., Shaw, A. L., Madsen, B., Jensen, K., Taylor-Papadimitriou, J., and Freemont, P. S. (2003). Human PLU-1 Has Transcriptional Repression Properties and Interacts with the Developmental Transcription Factors BF-1 and PAX9. *J. Biol. Chem.* 278 (23), 20507–20513. doi:10.1074/jbc.M301994200

Teng, Y. C., Lee, C. F., Li, Y. S., Chen, Y. R., Hsiao, P. W., Chan, M. Y., et al. (2013). Histone Demethylase RBP2 Promotes Lung Tumorigenesis and Cancer Metastasis. *Cancer Res.* 73 (15), 4711–4721. doi:10.1158/0008-5472.can-12-3165

Torres, I. O., and Fujimori, D. G. (2015). Functional Coupling between Writers, Erasers and Readers of Histone and DNA Methylation. *Curr. Opin. Struct. Biol.* 35, 68–75. doi:10.1016/j.sbi.2015.09.007

Torres, I. O., Kuchenbecker, K. M., Nnadi, C. I., Fletterick, R. J., Kelly, M. J. S., and Fujimori, D. G. (2015). Histone Demethylase KDM5A Is Regulated by its Reader Domain through a Positive-Feedback Mechanism. *Nat. Commun.* 6, 10. doi:10.1038/ncomms7204

Trewick, S. C., Henshaw, T. F., Hausinger, R. P., Lindahl, T., and Sedgwick, B. (2002). Oxidative Demethylation by *Escherichia coli* AlkB Directly Reverts DNA Base Damage. *Nature* 419 (6903), 174–178. doi:10.1038/nature00908

Tsukada, Y., Fang, J., Erdjument-Bromage, H., Warren, M. E., Borchers, C. H., Tempst, P., et al. (2006). Histone Demethylation by a Family of JmjC Domain-Containing Proteins. *Nature* 439 (7078), 811–816. doi:10.1038/nature04433

Tu, S. J., Teng, Y. C., Yuan, C. H., Wu, Y. T., Chan, M. Y., Cheng, A. N., et al. (2008). The ARID Domain of the H3K4 Demethylase RBP2 Binds to a DNA CCGCCC Motif. *Nat. Struct. Mol. Biol.* 15 (4), 419–421. doi:10.1038/nsmb.1400

Uckelmann, M., and Davidovich, C. (2021). Not just a Writer: PRC2 as a Chromatin Reader. *Biochem. Soc. Trans.* 49 (3), 1159–1170. doi:10.1042/bst20200728

Ummethum, H., and Hamperl, S. (2020). Proximity Labeling Techniques to Study Chromatin. *Front. Genet.* 11. doi:10.3389/fgene.2020.00450

Varaljai, R., Islam, A., Beshiri, M. L., Rehman, J., Lopez-Bigas, N., and Benevolenskaya, E. V. (2015). Increased Mitochondrial Function Downstream from KDM5A Histone Demethylase Rescues Differentiation in pRB-Deficient Cells. *Genes & Dev.* 29 (17), 1817–1834. doi:10.1101/gad.264036.115

Varier, R. A., Pau, E. C. D., van der Groep, P., Lindeboom, R. G. H., Matarese, F., Mensinga, A., et al. (2016). Recruitment of the Mammalian Histone-Modifying EMSY Complex to Target Genes Is Regulated by ZNF131. *J. Biol. Chem.* 291 (14), 7313–7324. doi:10.1074/jbc.M115.701227

Vermeulen, M., Eberl, H. C., Matarese, F., Marks, H., Denissov, S., Butter, F., et al. (2010). Quantitative Interaction Proteomics and Genome-wide Profiling of Epigenetic Histone Marks and Their Readers. *Cell* 142 (6), 967–980. doi:10.1016/j.cell.2010.08.020

Vermeulen, M., Mulder, K. W., Denissov, S., Pijnappel, W., van Schaik, F. M. A., Varier, R. A., et al. (2007). Selective Anchoring of TFIID to Nucleosomes by Trimethylation of Histone H3 Lysine 4. *Cell* 131 (1), 58–69. doi:10.1016/j.cell.2007.08.016

Vicent, G. P., Nacht, A. S., Zaurin, R., Font-Mateu, J., Soronellas, D., Le Dily, F., et al. (2013). Unliganded Progesterone Receptor-Mediated Targeting of an RNA-Containing Repressive Complex Silences a Subset of Hormone-Inducible Genes. *Genes & Dev.* 27 (10), 1179–1197. doi:10.1101/gad.215293.113

Vinogradova, M., Gehling, V. S., Gustafson, A., Arora, S., Tindell, C. A., Wilson, C., et al. (2016). An Inhibitor of KDM5 Demethylases Reduces Survival of Drug-Tolerant Cancer Cells. *Nat. Chem. Biol.* 12(7), 531-+. doi:10.1038/nchembio.2085

Vogel, F. C. E., Bordag, N., Zugner, E., Trajkovic-Arsic, M., Chauvistre, H., Shannan, B., et al. (2019). Targeting the H3K4 Demethylase KDM5B Reprograms the Metabolome and Phenotype of Melanoma Cells. *J. Investigative Dermatology* 139(12), 2506-+. doi:10.1016/j.jid.2019.06.124

Walport, L. J., Hopkinson, R. J., and Schofield, C. J. (2012). Mechanisms of Human Histone and Nucleic Acid Demethylases. *Curr. Opin. Chem. Biol.* 16 (5-6), 525–534. doi:10.1016/j.cbpa.2012.09.015

Wang, J. X., Scully, K., Zhu, X., Cai, L., Zhang, J., Prefontaine, G. G., et al. (2007). Opposing LSD1 Complexes Function in Developmental Gene Activation and Repression Programmes. *Nature* 446 (7138), 882–887. doi:10.1038/nature05671

Wang, Y., Zhang, H., Chen, Y. P., Sun, Y. M., Yang, F., Yu, W. H., et al. (2009). LSD1 Is a Subunit of the NuRD Complex and Targets the Metastasis Programs in Breast Cancer. *Cell* 138 (4), 660–672. doi:10.1016/j.cell.2009.05.050

Weinberg, R. A. (1995). THE RETINOBLASTOMA PROTEIN AND CELL-CYCLE CONTROL. *Cell* 81 (3), 323–330. doi:10.1016/0092-8674(95)90385-2

Wu, L. Z., de Bruin, A., Saavedra, H. I., Starovic, M., Trimboli, A., Yang, Y., et al. (2003). Extra-embryonic Function of Rb Is Essential for Embryonic Development and Viability. *Nature* 421 (6926), 942–947. doi:10.1038/nature01417

Wysocka, J., Swigut, T., Xiao, H., Milne, T. A., Kwon, S. Y., Landry, J., et al. (2006). A PHD Finger of NURF Couples Histone H3 Lysine 4 Trimethylation with Chromatin Remodelling. *Nature* 442 (7098), 86–90. doi:10.1038/nature04815

Xiang, Y., Zhu, Z., Han, G., Ye, X., Xu, B., Peng, Z., et al. (2007). JARID1B is a Histone H3 Lysine 4 Demethylase Up-Regulated in Prostate Cancer. *PNAS* 104 (49), 19226–19231. doi:10.1073/pnas.070073510

Xie, L. Q., Pelz, C., Wang, W. S., Bashar, A., Varlamova, O., Shadle, S., et al. (2011). KDM5B Regulates Embryonic Stem Cell Self-Renewal and Represses Cryptic Intragenic Transcription. *Embo J.* 30 (8), 1473–1484. doi:10.1038/emboj.2011.91

Xu, W., Yang, H., Liu, Y., Yang, Y., Wang, P., Kim, S. H., et al. (2011). Oncometabolite 2-Hydroxyglutarate Is a Competitive Inhibitor of Alpha-ketoglutarate-dependent Dioxygenases. *Cancer Cell* 19 (1), 17–30. doi:10.1016/j.ccr.2010.12.014

Xue, S., Lam, Y. M., He, Z. K., Zheng, Y., Li, L., Zhang, Y. H., et al. (2020). Histone Lysine Demethylase KDM5B Maintains Chronic Myeloid Leukemia via Multiple Epigenetic Actions. *Exp. Hematol.* 82, 53–65. doi:10.1016/j.exphem.2020.01.006

Yamamoto, S., Wu, Z. H., Russnes, H. G., Takagi, S., Peluffo, G., Vaske, C., et al. (2014). JARID1B Is a Luminal Lineage-Driving Oncogene in Breast Cancer. *Cancer Cell* 25 (6), 762–777. doi:10.1016/j.ccr.2014.04.024

Yamane, K., Tateishi, K., Klose, R. J., Fang, J., Fabrizio, L. A., Erdjument-Bromage, H., et al. (2007). PLU-1 Is an H3K4 Dernethylase Involved in Transcriptional Repression and Breast Cancer Cell Proliferation. *Mol. Cell* 25 (6), 801–812. doi:10.1016/j.molcel.2007.03.001

Yang, G. J., Zhu, M. H., Lu, X. J., Liu, Y. J., Lu, J. F., Leung, C. H., et al. (2021). The Emerging Role of KDM5A in Human Cancer. *J. Hematol. Oncol.* 14 (1). doi:10.1186/s13045-021-01041-1

Yu, C., and Huang, L. (2018). Cross-Linking Mass Spectrometry: An Emerging Technology for Interactomics and Structural Biology. *Anal. Chem.* 90 (1), 144–165. doi:10.1021/acs.analchem.7b04431

Zeng, J. P., Ge, Z., Wang, L. X., Li, Q., Wang, N., Bjorkholm, M., et al. (2010). The Histone Demethylase RBP2 Is Overexpressed in Gastric Cancer and its Inhibition Triggers Senescence of Cancer Cells. *Gastroenterology* 138 (3), 981–992. doi:10.1053/j.gastro.2009.10.004

Zeng, L., and Zhou, M. M. (2002). Bromodomain: an Acetyl-Lysine Binding Domain. *Febs Lett.* 513 (1), 124–128. doi:10.1016/s0014-5793(01)03309-9

Zhang, P., Du, J. M., Sun, B. F., Dong, X. C., Xu, G. L., Zhou, J. Q., et al. (2006). Structure of Human MRG15 Chromo Domain and its Binding to Lys36-Methylated Histone H3. *Nucleic Acids Res.* 34 (22), 6621–6628. doi:10.1093/nar/gkl989

Zhang, S. M., Cai, W. L., Liu, X. N., Thakral, D., Luo, J. S., Chan, L. H., et al. (2021). KDM5B Promotes Immune Evasion by Recruiting SETDB1 to Silence Retroelements. *Nature* 598(7882), 682-+. doi:10.1038/s41586-021-03994-2

Zhang, Y., Yang, H. R., Guo, X., Rong, N. Y., Song, Y. J., Xu, Y. W., et al. (2014). The PHD1 Finger of KDM5B Recognizes Unmodified H3K4 during the Demethylation of Histone H3K4me2/3 by KDM5B. *Protein & Cell* 5 (11), 837–850. doi:10.1007/s13238-014-0078-4

Conflict of Interest: The authors declare that the research was conducted in the absence of any commercial or financial relationships that could be construed as a potential conflict of interest.

Publisher's Note: All claims expressed in this article are solely those of the authors and do not necessarily represent those of their affiliated organizations, or those of the publisher, the editors and the reviewers. Any product that may be evaluated in this article, or claim that may be made by its manufacturer, is not guaranteed or endorsed by the publisher.

frontiers | Frontiers in Genetics

REVIEW
published: 14 July 2022
doi: 10.3389/fgene.2022.903923

Catching Nucleosome by Its Decorated Tails Determines Its Functional States

Parveen Sehrawat[†], *Rahul Shobhawat*[†] *and Ashutosh Kumar**

Department of Biosciences and Bioengineering, Indian Institute of Technology Bombay, Mumbai, India

The fundamental packaging unit of chromatin, i.e., nucleosome, consists of ~147 bp of DNA wrapped around a histone octamer composed of the core histones, H2A, H2B, H3, and H4, in two copies each. DNA packaged in nucleosomes must be accessible to various machineries, including replication, transcription, and DNA damage repair, implicating the dynamic nature of chromatin even in its compact state. As the tails protrude out of the nucleosome, they are easily accessible to various chromatin-modifying machineries and undergo post-translational modifications (PTMs), thus playing a critical role in epigenetic regulation. PTMs can regulate chromatin states *via* charge modulation on histones, affecting interaction with various chromatin-associated proteins (CAPs) and DNA. With technological advancement, the list of PTMs is ever-growing along with their writers, readers, and erasers, expanding the complexity of an already intricate epigenetic field. In this review, we discuss how some of the specific PTMs on flexible histone tails affect the nucleosomal structure and regulate the accessibility of chromatin from a mechanistic standpoint and provide structural insights into some newly identified PTM–reader interaction.

Keywords: nucleosome, PTMs, histone tails, acetylation, acylation, methylation

OPEN ACCESS

Edited by:
Dileep Vasudevan,
Institute of Life Sciences (ILS), India

Reviewed by:
Sivaraman Padavattan,
National Institute of Mental Health and Neurosciences (NIMHANS), India
Lars Nordenskiöld,
Nanyang Technological University, Singapore
Alexey V. Onufriev,
Virginia Tech, United States

****Correspondence:***
Ashutosh Kumar
ashutoshk@iitb.ac.in

[†]These authors have contributed equally to this work and share first authorship

Specialty section:
This article was submitted to Epigenomics and Epigenetics, a section of the journal Frontiers in Genetics

Received: *24 March 2022*
Accepted: *07 June 2022*
Published: *14 July 2022*

Citation:
Sehrawat P, Shobhawat R and Kumar A (2022) Catching Nucleosome by Its Decorated Tails Determines Its Functional States. Front. Genet. 13:903923. doi: 10.3389/fgene.2022.903923

1 INTRODUCTION

In the eukaryote's nucleus, DNA is packaged into the macromolecular "beads on a string"-like structure called chromatin using highly basic histone proteins. A nucleosome is the basic and efficient unit of this organization in which 145–147 bp of DNA are wrapped around a histone octamer (two molecules of each histone H2A, H2B, H3, and H4). Two pairs of H3–H4 dimer form a tetramer stabilized by a characteristic hydrophobic four-helix bundle structure between H3 and H3′, and then two dimers of H2A–H2B interact with H3–H4 tetramer on each side through a second homologous hydrophobic four-helix bundle structure between H2B and H4, forming a globular octamer from which disordered tails protrude out. Through extensive hydrogen-bonding and electrostatic interactions, histones coordinate with DNA *via* conserved histone fold domains, resulting in the bending of negatively charged DNA over a positively charged octamer surface. This bent conformation of DNA brings the phosphate backbone of the two strands closer, and this energetically constrained conformation is maintained by neutralizing negative charges by positively charged lysine and arginine side chains (Luger et al., 1997).

These strong and extensive interactions render the nucleosome a stable disc that can sterically inhibit the binding of chromatin-associated proteins (CAPs). Virtually all eukaryotic organisms use the inhibitory nature of this packaging to regulate access to DNA. However, the information encoded inside the DNA must be retrieved at appropriate times. Although DNA is very tightly compacted, it still remains accessible to many enzyme machineries that replicate it, repair it, and use it to produce RNA

molecules and proteins. For doing this, chromatin and nucleosomes must be inherently dynamic and highly malleable. Numerous biochemical and structural studies established the dynamic nature of the nucleosome in terms of its conformation and composition. The disordered N-terminal tail of histones have an affinity to DNA, forming a dynamic complex with DNA termed as "fuzzy conformational ensembles," which regulate the chromatin structure and dynamics (Ghoneim, Fuchs, and Musselman 2021; Peng et al., 2021; Shukla, Agarwal, and Kumar 2022). Polach and Widom, (1995) demonstrated the phenomenon of intrinsic structural dynamics of nucleosome known as "DNA breathing," i.e., partially unwrapping and rewrapping of DNA spontaneously. This dynamic unwrapping/rewrapping phenomenon is exploited by several DNA-binding proteins like transcription factors in a tunable and analogous fashion. Using FRET experiments, the Langowski group showed that disassembly of nucleosome is initiated by DNA breathing resulting in a dynamic "octasome," which opens on a 50 μs time scale at an angle of ≈20°. This results in disruption of dimer tetramer interface with H2A–H2B dimer evicting first followed by H3–H4 tetramer removal (Böhm et al., 2011; Gansen et al., 2018).

In addition to DNA breathing, cells have also evolved various other mechanisms to make nucleosomal DNA more accessible: histones posttranslational modifications, histone chaperones, histone variants, and chromatin remodelers. These regulatory mechanisms control the genome function without changing the nucleotide sequence, also referred to as "epigenetic" marks. Histone post-translational modification is the process of covalently attaching adducts like methyl group, acetyl group, phosphate group, and ubiquitin group. These modifications present on free N-terminal tails or inside the histone fold domain affect the structure and dynamics of nucleosomes locally and chromatin globally and provide the binding platform for different groups of proteins like transcription factors, chromatin remodelers, histone-/DNA-modifying enzymes, and chaperones, especially the charge-altering PTMs inside the globular histone octamer core can modify the electrostatic interaction of histone–histone or histone–DNA, thereby altering the structure and dynamics of nucleosomes (Fenley et al., 2018). For instance, phosphorylation in combination with acetylation inside the nucleosomal DNA entry–exit site modulates DNA accessibility by transcription complexes (Brehove et al., 2015). Misregulation of these modifications can cause many diseases like cancer; therefore, regulating this epigenetic mark is necessary for proper functioning. In this review, we have discussed the role of four PTMs (acetylation, acylation, serotonylation, and methylation) present on flexible and intrinsically disordered histone tails in regulating chromatin accessibility and function. Several excellent reviews on other modifications like phosphorylation (Sawicka and Seiser 2014; Treviño, Wang, and Walker 2015), SUMOylation (Ryu and Hochstrasser 2021), and ubiquitination (Mattiroli and Penengo 2021) are good read to get a better understanding.

2 HISTONE TAILS AND PTMS

The nucleosome is a globular structure, but the unstructured N-terminal tail of each histone protrudes out from its core. The pioneering work of Vincent Allfrey in the 1960s and subsequent studies revealed that these tails are subjected to many post-translation modifications like acetylation, methylation, and phosphorylation, thus acting as a hub of chromatin signaling (Millán-Zambrano et al., 2022). Covalent modifications of histone tails can alter the chromatin structure *via* cis-effects or trans-effects. Cis-effects are employed by changing the biophysical properties of modified histone chains, like altering the electrostatic charge or structure of the tail, which in turn affects internucleosomal contacts. For example, histone acetylation on lysine residue exerts its effect by neutralizing the positive charge of histone tails. Charge-neutralized tails generate a localized decondensation of the chromatin fiber, resulting in better availability of DNA double helix to the transcription machinery. Acetylation at H4K16 inhibits the packaging of a nucleosomal array in a compact 30-nm chromatin fiber *in vitro* and further abolishes cross-fiber interactions (Michael et al., 2006). In fact, out of four acetylations possible in the H4 tail, K16 acetylation is unique as only this modification reduces the cation-induced folding of the 12-mer nucleosome array implicating cis-effect of acetyl mark (Allahverdi et al., 2011). Multiscale computational studies supported by NMR experiments revealed that acetylated H4 tails lose local contacts and reduced tail availability for forming critical internucleosomal interactions resulting in the unfolding of chromatin fiber (Collepardo-Guevara et al., 2015; Bascom and Schlick 2018). Similarly, phosphorylation adds a net negative charge generating "charge patches," which result in alteration of nucleosome packaging (Dou and Gorovsky 2000). Bulky groups, such as ADP-ribose and ubiquitin, also affect the arrangements of the histone tails and open up nucleosome arrays.

Histone modifications also act *via* trans-effects, where modification-binding partners are recruited to the chromatin. This is similar to "reading" a specific covalent histone mark by modification reader proteins. For example, the acetylation mark is read by proteins having "bromodomains" (Jacobson et al., 2000). Similarly, methylated lysine or arginine residues are read by chromodomains or similar domains (e.g., MBT and Tudor) to facilitate the modulation of chromatin (Maurer-Stroh et al., 2003). Acetylation, methylation, and phosphorylation were the initially detected and extensively studied modifications. Recent advancement in the high-sensitive mass spectrometry technique has played a pivotal role in revealing a wide array of new modifications, including ubiquitylation, SUMOylation, ADP-ribosylation, a dozen of various acyl groups, serotonylation, and lactylation (Zhao and Garcia 2015). Based on diversity and biological specificity of distinct modifications, Strahl and Allis, (2000) proposed the "histone code" hypothesis, which states that "multiple post-translational modifications form a specific pattern either in combination or sequential fashion on same or different histone tail, to perform a specific downstream function." The key players involved in defining the histone code are the enzymes or proteins that write, read, and then erase these marks in a specific sequence or modification. This fine-tuned action is critical for regulating most nuclear processes, including replication, recombination, DNA damage and repair, transcription, and differentiation.

The crosstalk and specific recognition of histone PTM by its cognate reader define the temporal and spatial modulation of the genome. After the initial discovery of the bromodomain as an acetylation mark reader and chromodomain as a methylation mark reader, several epigenetic studies have identified a diverse repertoire of "readers" regulating the dynamic nature of the chromatin landscape. For example, RAG2 protein of RAG1/2 V(D)J recombinase reads H3K4me3 modification and induces V(D)J recombination at the T- and B-cell receptor gene locus. Mutations in the reader motif of RAG2 impair V(D)J recombination and can result in immunodeficiency syndromes (Matthews et al., 2007). Many chromatin-associating multi-subunit enzymatic complexes contain a set of multiple readers within one or different subunits, and these readers having specificities for different marks can be in close proximities. These complexes can be "writers" or "erasers" [histone acetyltransferases and histone deacetylases] that can redefine the epigenetic landscape by adding or removing modifications at different sites or chromatin remodelers that can alter the structure and dynamics of chromatin. Combinatorial readout of multivalent histone PTMs on the same tail or at a different tail can provide a lock and key type mechanism to carry out a specific biological function at targeted genomic loci. Owing to their fundamental role, any misreading of these epigenetic modifications has been shown to contribute to many human diseases, including cancer and developmental and autoimmune disorders (Chi, Allis, and Wang 2010; Shen and Laird 2013).

In some cases of acute myeloid leukemia, the reader module of H3K9 trimethylation (PHD motif) is found to be fused with nuclear pore protein (NUP98). This fusion protein remains bound to H3K9me3, interfering with the removal of this modification and the addition of H3K27me3, thereby affecting the normal differentiation of progenitor and hematopoietic cells (Wang et al., 2009). In fact, misinterpretation of acetyl marks by their respective reader domains has been implicated in uterine, bladder, cervical, and other tumors (Zhao et al. 2021). Targeting one of the bromodomain protein families BET (bromodomain and extraterminal domain) by small molecules resulted in the reversal of a cancer cell phenotype in the patient-derived NUT midline carcinoma cell line (Filippakopoulos et al., 2010). Understanding the basic aspects of epigenetic control and the genesis of epimutation-induced human disorders requires an understanding of the molecular mechanism and functional importance of PTM–reader interactions. In the following sections, we discuss the molecular mechanism of PTM readout by different reader modules and the functional significance of these newly identified PTM–reader interactions.

3 ACETYLATION

Acetylation of the lysine residue at the ε-amino group was the first PTM discovered in thymus histones by Philips in 1961 (Allfrey et al., 1964). The negative charge on the acetyl group neutralizes the positive charge of the lysine side chain, thereby altering the electrostatic properties of histone proteins. This modification is generally correlated with a transcriptionally active state, and the turnover of this modification is controlled by two groups of enzymes: histone acetyltransferases (HATs) and histone deacetylases (HDACs) (discussed in detail in Marmorstein and Zhou, (2014) and Xia et al. (2020)). This mark is found on all histone tails H2A (K5 and K9), H2B (K5, K12, K15, K16, K20, and K120), H3 (K4, K9, K14, K18, K23, K27, K36, and K56), and H4 (K5, K8, K12, K16, K20, and K91) (Musselman et al., 2012). Although acetylation was discovered about 60 years ago, the first reader of acetylated lysine, a bromodomain, was discovered only in 1999 (Dhalluin et al., 1999). Till now, three types of protein domains able to "read" acetyllysine marks have been identified: bromodomains, DPF domain, and YEATS domain (**Figure 1**). Here, we will discuss these newly identified reader proteins of acetylation mark.

3.1 Recognition of H3K14Ac by the Bromodomain Module of RSC Chromatin Remodeler

Bromodomains are evolutionarily conserved domains that act as histone lysine acetylation readers. In humans, 61 bromodomains in 46 different proteins have been identified, and these proteins are part of transcription-regulating complexes, chromatin remodelers, and PTM writers. Based on the structure and sequence, bromodomains are divided into eight subfamilies (I–VIII) (Filippakopoulos et al., 2012). Even with little sequence homology, all bromodomains have a conserved structural fold consisting of four α-helices (αZ, αA, αB, and αC) (**Figure 1A**). The two highly variable loops, ZA and BC, joining these helices, form a deep hydrophobic acetyllysine binding pocket (Sanchez and Zhou 2009).

One of the yeast chromatin remodelers, the RSC complex, consists of seven bromodomains. Acetylation of histone H3 lysine at the 14th position enhanced RSC binding to nucleosomes and augmented the RSC remodeling activity (Duan and Smerdon 2014; Lorch, Maier-Davis, and Kornberg 2018). Recently, Chen et al. (2020) showed that out of seven bromodomains present in RSC (one in the Sth1 subunit and two each in Rsc1, Rsc2, and Rsc4 subunits), the C-terminal bromodomain of Sth1 is the primary domain responsible for recognizing H3K14Ac. ITC experiments using H3K14Ac containing $H3_{6-21}$ peptide revealed that Rsc1 and Rsc2 have no significant interaction, while Rsc4 (dissociation constant of 263 μM) has a 16-fold weaker interaction than Sth1 bromodomain (dissociation constant of 16 μM). Further ITC results with an array of histone peptides containing different acetylation sites demonstrated that the Sth1 bromodomain could also strongly bind to H3K20Ac with similar K_D as that of H3K14Ac. Sequence analysis of these peptides revealed a conserved feature in both H3K14Ac and H4K20Ac peptides: the following two residues after lysine are hydrophobic, and the third one is a conserved arginine (K(Ac)ΦΦR motif, where Φ represents any hydrophobic amino acid). Mutation at the +1 and +2 position with neutral or polar amino acid and mutation of +3 arginine abolish the interaction between the peptide and Sth1 bromodomain.

Like other bromodomain-containing proteins, Sth1 has a hydrophobic pocket formed by four amphipathic α-helices in

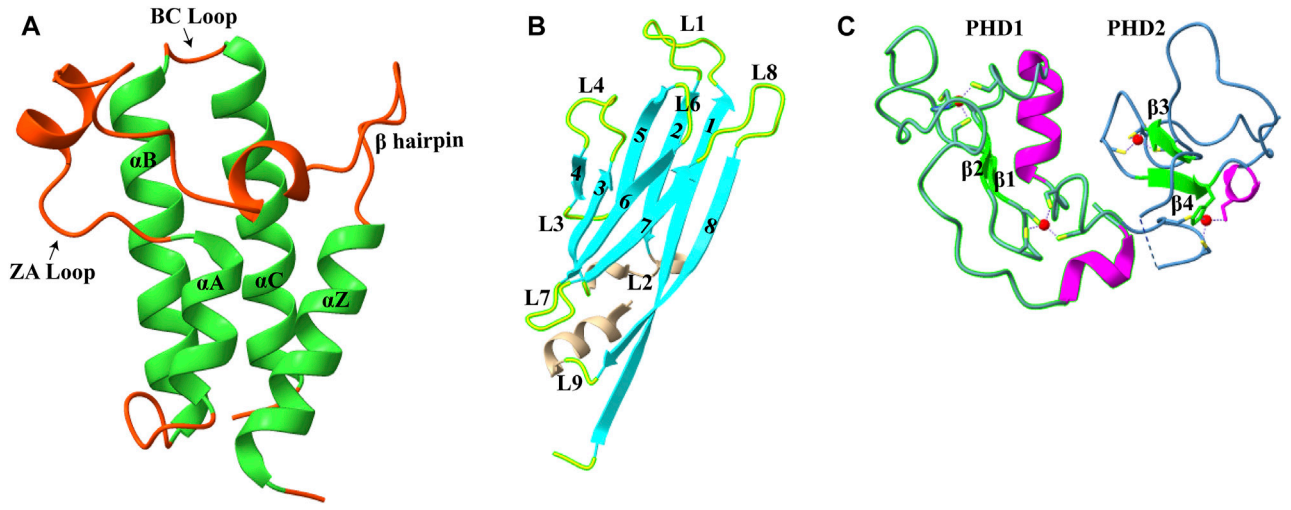

FIGURE 1 | Structures of acetyllysine reader modules **(A)**. Bromodomain of YEATS Sth1 (RSC remodeler): four helices are shown in green (PDB: 6KMB) **(B)**. YEATS domain of AF9 protein (PDB: 4TMP) **(C)**. DPF domain of MOZ protein: antiparallel β-sheets are shown in green, and zinc ions are shown in red color (PDB: 4LJN).

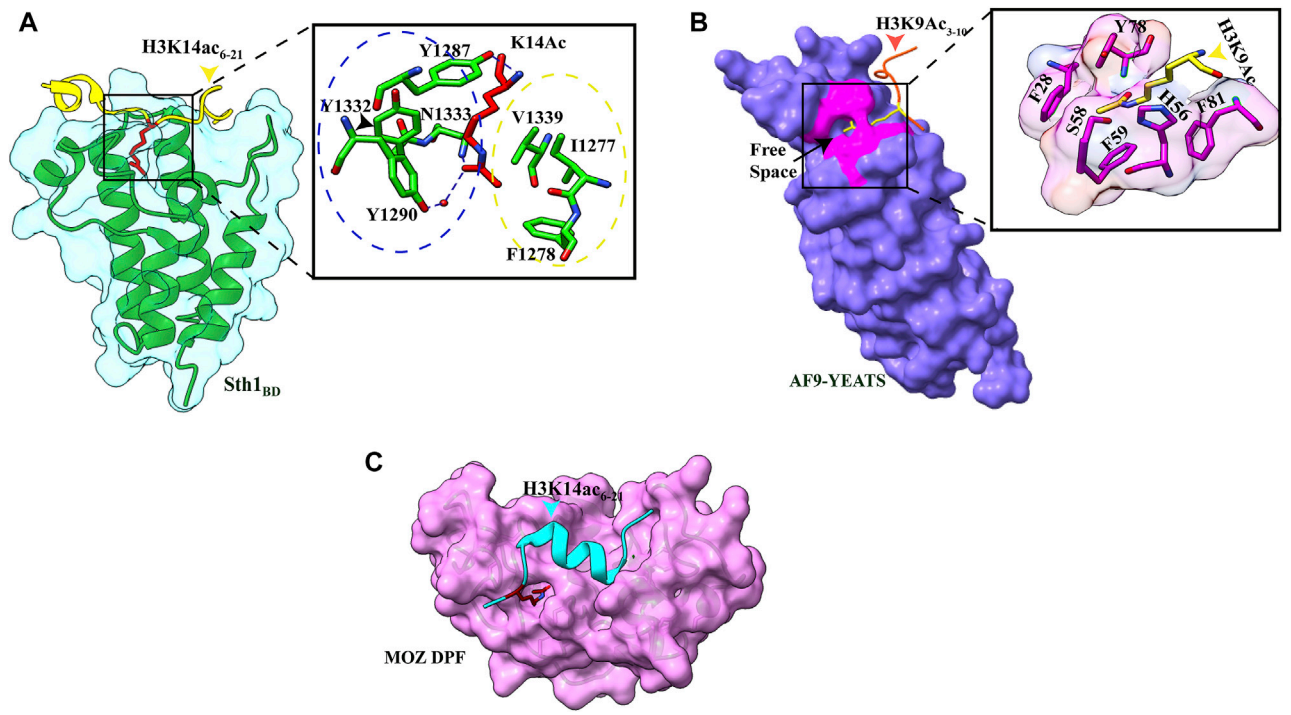

FIGURE 2 | Readout of acetyllysine by different readers. **(A)** Left: overall structure of $Sth1_{BD}$ (green ribbons) with $H3K14ac_{6–21}$ (yellow color, K14 shown as red sticks). Right: close-up view of H3K14ac-binding sites of Sth1. H3K14Ac is shown in red color, and Sth1BD residues are shown in green color. Residues in the blue circle interact with the aliphatic side chain of K14, while residues in the yellow circle interact with the methyl group of acetyl mark. Hydrogen bonds are shown as blue dashed line (PDB ID: 6KMJ). **(B)** Left: overall structure of the AF9 YEATS domain (purple color) with $H3K9Ac_{3–10}$ (orange–red color, K9 shown in yellow color). K9ac (yellow color) can be seen inserted into the narrow end-open pocket. Right: close-up view of interacting residues of H3K9Ac (yellow color) and AF9 residues (pink color). A serine (S58)-lined aromatic cage (F28, H56, F59, Y78, and F81) is formed in which the acetylated lysine snugly fits (PDB ID: 4TMP). **(C)**. Overall structure of $H3K14Ac_{3–15}$ (stick model in cyan color) with MOZDPF (pink surface). K14ac (red color) can be seen inserted in the "dead end" pocket of MOZ protein (PDB ID: 4LLB).

which K14Ac is inserted. In addition to hydrophobic contacts, interactions between the aliphatic side chain of K14 with three aromatic amino acids (Y1287, Y1332, and Y1290), the methyl group of acetyl mark with V1339, I1277, and F1278, and the hydrogen bond between the carbonyl oxygen of the acetyl group and N1333 of Sth1 are responsible for strong affinity (**Figure 2A**).

The other three residues of the K(Ac)ΦΦR motif also make extensive hydrogen bonds and hydrophobic contacts with the Sth1 bromodomain, explaining the specific recognition of this motif by $Sth1_{BD}$. Critical residues of hydrophobic pockets (Y1332 and N1333) are not present in Rsc1 and Rsc2 subunit bromodomains which explains their insignificant interaction with the H3K14Ac peptide (Chen et al., 2020).

More recently, the *C. elegans* homolog of Sth1, SMARCA4, was also shown to be highly selective for H3K14Ac and showed a similar binding affinity. The hydrogen-bonding and hydrophobic interactions are very well conserved in *C. elegans* SMARCA4 bromodomain and $H3_{7-20}$K14Ac-modified peptide complex. In this case also, the K(Ac)ΦΦR motif is involved in the extensive electrostatic, hydrophobic, and hydrogen-bonding interactions that ensure specific and robust binding between SMARCA4 and H3K14Ac-containing peptides (Enríquez et al., 2021).

The RSC complex is the most abundant and well-characterized chromatin remodeler of the SWI/SNF family, comprising about 17 subunits in *Saccharomyces cerevisiae*. Like other remodelers, using its main catalytic subunit Sth1, the RSC complex catalyzes the ATP hydrolysis reaction and uses this energy to evict or side the histone octamer to expose DNA-binding sites on chromatin. At the H3K14Ac-enriched transcription start sites (TSSs), the RSC complex is recruited, which generates a nucleosome-free region enabling RNA Pol II to initiate transcription (Carey, Li, and Workman 2006; Lorch et al., 2011). Also, H3K14Ac is found at UV-irradiated DNA sites, which recruit the RSC complex to facilitate DNA repair by chromatin remodeling (Yu et al., 2005; Duan and Smerdon 2014).

3.2 Recognition of H3K9ac by the YEATS Domain

A study published in 2014 showed YEATS domain as a novel reader of histone acetylation marks. It is an evolutionarily conserved protein module from yeast to humans and is named after its founding domain-containing proteins, Yaf9, ENL, AF9, Taf14, and Sas5 (Masson et al., 2003). Three YEATS domain-containing proteins in *S. cerevisiae* and four proteins in humans are associated with transcription-regulating complexes, chromatin-remodeling complexes, and HAT complexes (Schulze et al., 2009). ITC and pull-down assay revealed that binding of the YEATS domain of AF9 protein to histone H3 tail is acetylation dependent, and the AF9 YEATS domain binds strongly to H3K9Ac (K_D of 3.7 μM) as well as to H3K27Ac (K_D of 7.0 μM) and H3K18Ac (K_D of 11.0 μM), however, to a lesser extent (Li et al., 2014). The crystal structure of YEATS domain with different acetylated histone peptides uncovered a unique serine-lined aromatic sandwich pocket for specific acetyllysine readout. The AF9 YEATS domain adopts an immunoglobin fold in which eight antiparallel β strands form a two-layer β sandwich, and H3K9Ac long side chain is inserted into a serine-lined aromatic cage formed in the cleft of loops L4 and L6 (**Figures 1B**, **2B**). In the AF9 YEATS–H3K9Ac complex, the YEATS domain uses strands β2 and β7 and loops L1, L4, L6, and L8 to form extensive hydrogen bonds and hydrophobic interactions with the T3-S10 segment of H3. In addition to hydrogen and hydrophobic interactions, multiple aromatic residues in the acetyllysine binding pocket are involved in multiple sets of CH–π interactions, which collectively contribute to the stable binding (**Figure 2B**). Key residues involved in the generation of the aromatic cage are highly conserved among different YEATS domain-containing proteins from yeast to humans. The interaction of the YEATS domain and H3 tail is also highly dependent on amino acids flanking the K9, especially arginine, at the eighth position, as mutation at this site resulted in a 200-fold binding decline (Li et al., 2014).

AF9 is subunit of a large protein complex, Super Elongation Complex (SEC), which has been shown to mediate enhanced transcription of several loci in MLL-rearranged leukemias and developmental genes by releasing paused Pol II (Smith, Lin, and Shilatifard 2011). ChIP-seq and CoIP experiments suggested that the YEATS domain (N-terminal part of AF9) is critical for the recruitment of AF9 at the H3K9ac mark around the transcription start sites and C-terminal of AF9 is required for the interaction with other proteins of SEC complex *in vivo*. One of the critical interacting partners of AF9 is DOT1L, an H3K79 methyltransferase, and H3K79me3 mark is associated with active transcription. Several *in vivo* experiments revealed that AF9 is required for DOT1L recruitment at targeted genes and subsequent deposition of H3K79me3 to promote active transcription (Li et al., 2014).

3.3 Recognition of H3K14ac by the DPF Domain

The double PHD finger(DPF) domain, a subgroup of PHD (plant homeodomain) fingers, is a tandem of PHD fingers with a face-to-back orientation where two domains form a single structure. This domain has been found in two protein families, histone acetyltransferase MYST family proteins (MOZ or KAT6A and MORF or KAT6B) and subfamilies of SWI/SNF chromatin remodeler (BAF and PBAF complex). The DPF domain from all these proteins is homologous, and all the key residues are conserved, forming a highly similar secondary structure consisting of two antiparallel β-sheets followed by a C-terminal α-helix which is coordinated by two zinc atoms *via* Cys4-His-Cys3 motif in a cross-brace topology (**Figure 1C**). Two PHD fingers are linked with one another in a face-to-back orientation mediated by the interaction between glutamic acid and arginine in the α-helix of the first PHD finger. Although the PHD finger was originally recognized as a methylation mark reader, the DPF domain of DPF3b was shown to bind H3K14 acetylation mark. The structural aspects of acetyllysine–H3K14Ac interaction are discussed in the next section.

4 ACYLATIONS

The latest advancements in mass spectrometry revealed a wide array of acylation marks in histones apart from classical acetylation modification. These acyl marks include butyrylation (Kbu) (Chen et al., 2007), propionylation (Kpr) (Chen et al., 2007), crotonylation (Kcr) (Tan et al., 2011), succinylation (Ksucc) (Xie et al., 2012), malonylation (Kma) (Xie et al., 2012), 2-hydroxyisobutyrylation (Khib) (Dai et al., 2014), β-hydroxybutyrylation (Kbhb) (Xie et al., 2016),

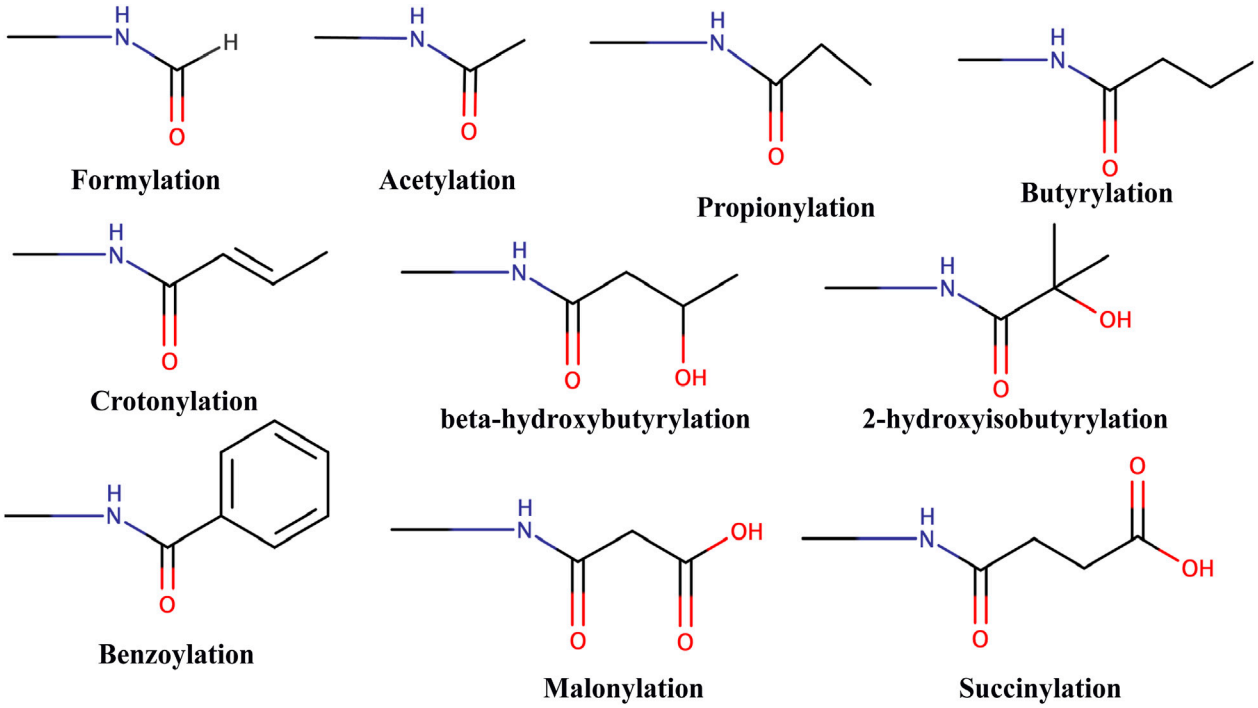

FIGURE 3 | Chemical structure of different types of acylations.

benzoylation (Kbz) (Huang et al., 2018), lactylation (Kla) (Zhang et al., 2019), glutarylation (Kglu) (Bao et al., 2019), and isobutyrylation (Kibu) (Zhu et al., 2021) (**Figure 3**). These modifications are derived from their respective acyl-CoAs, a product of different metabolic pathways. Therefore, these specific marks can identify the metabolic state of the cell and regulate chromatin dynamics and gene expression according to the need of the cell (Nitsch, Shahidian, and Schneider 2021). Also, various new studies suggest that these different acylation marks are important for eliciting specific epigenetic responses (Dutta, Abmayr, and Workman 2016).

Till date, no specific or selective writer, reader, or eraser for non-acetyl acylation modification has been identified so far. A recent study with high-throughput profiling of an acyl-CoA/protein using CoA/AcetylTraNsferase Interaction Profiling (CANTIP) revealed only known acetyl mark-interacting proteins (Levy et al., 2020). In fact, p300 lysine acetyltransferase (also known as KAT3B) has been shown to be able to catalyze the transfer of all types of different acyl groups (Nitsch, Shahidian, and Schneider 2021).

4.1 Recognition of Acyl Marks by Bromodomains

Given that bromodomain is a major protein module that reads lysine acetylation, an initial study found out that the bromodomain of bromodomain-containing protein (BRD4) was able to bind Kbu and Kpr but with very less affinity than Kac (Vollmuth and Geyer 2010). A more comprehensive study where 49 bromodomains were assayed for their binding affinity to different acyl-modified H3 peptides revealed that only bromodomains having larger binding pockets such as CECR2 and BRD9 were able to bind long-chain Kbu modification, and the second bromodomain of TAF1 was able to interact with Kcr, albeit with reduced affinity compared with Kac (Flynn et al., 2015). All these studies implied that bromodomains could read a few acyl marks, but these interactions are not strong and significant compared to acetyl modification.

4.2 Recognition of H3K9acyl/H3K18acyl/H3K27cr by the YEATS Domain

In the crystal structure of the AF9 YEATS domain–H3K9Ac complex, a clear open space at the end of the aromatic sandwich cage led to the hypothesis that this open space can accommodate a large chain of bulkier acyl marks (Li et al., 2014) (**Figure 1B**). Further calorimetric titrations and NMR 2D ^{15}N-^{1}H heteronuclear single quantum coherence (HSQC) spectra revealed that, indeed, the AF9 YEATS domain could bind to the H3 tail peptides, which has crotonylation (cr), propionylation (pr), butyrylation (bu), and formylation (fo) modifications at K9, K18, and K27 positions with no significant binding for the H3K14 site (Li et al., 2016; Zhang et al., 2016). An increase in the hydrocarbon chain beyond the acetyl group resulted in 2.4-, 1.9-, and 1.4-fold binding enhancement for Kcr-, Kpr-, and Kbu-modified peptides, respectively. Similar studies with Taf14 and YEATS2 (subunit of ATAC histone acetyltransferase complex)

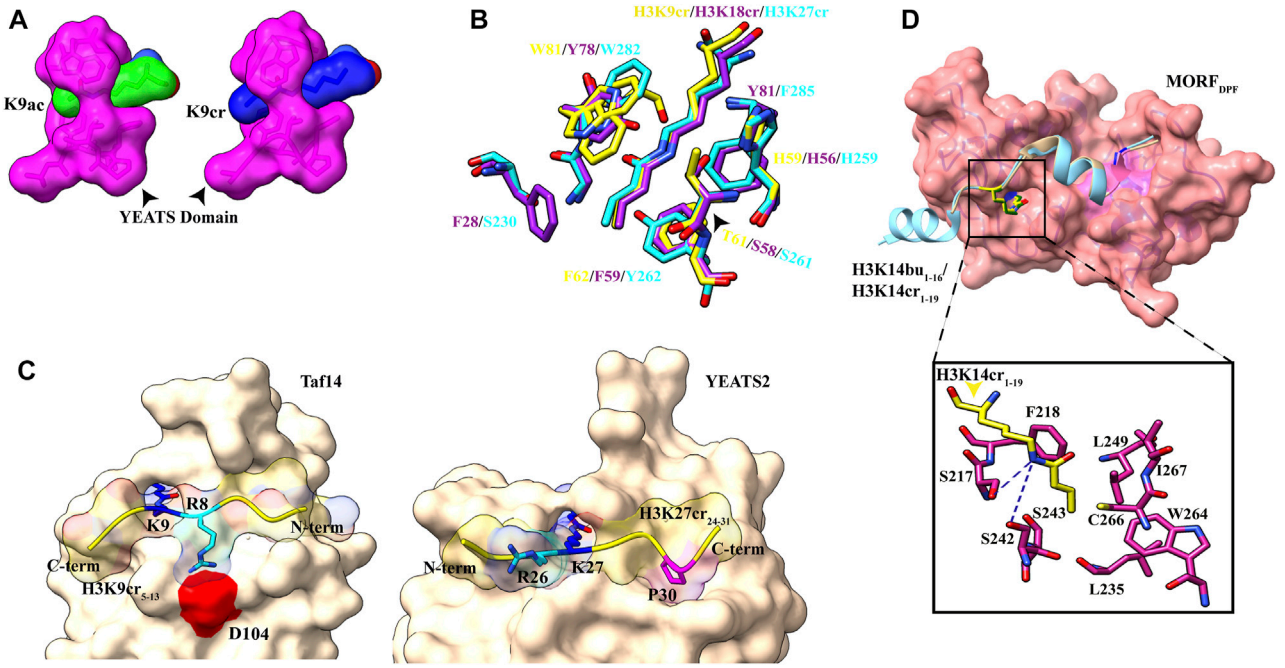

FIGURE 4 | Readout of acyl marks by YEATS and DPF domains. **(A)** Longer chain of the crotonyl group (blue) can be accommodated in the Taf14 YEATS domain (magenta). (PDB ID: 5D7E and 5IOK). **(B)** Superimposition of residues involved in interaction among YEATS domains of different proteins: YEATS2 YEATS domain–H3K27cr (cyan; PDB ID: 5IQL), Taf14 YEATS domain–H3K9cr (yellow; 5IOK), and AF9 YEATS domain–H3K18cr (purple; 5HJD). **(C)** Opposite orientation of H3 peptides across Taf14 (PDB ID: 5IOK) and YEATS2 (PDB ID: 5IQL) proteins. In the Taf14–H3K9cr$_{5-13}$complex, R8 (cyan) interacts with aspartate at 104th position. In YEATS2–H3K27cr$_{24-31}$ complex, R26 (cyan) is facing away from the YEATS domain but proline at 30th position (magenta) makes contacts with the hydrophobic pocket. **(D)** Top: overall structure of the DPF domain of MORF protein with H3K14bu$_{1-16}$ (wheat) and H3K14cr$_{1-19}$ (cyan). Bottom: close-up view of amino acids involved in interaction between crotonylated lysine (yellow) and MORF$_{DPF}$ protein (magenta) (PDB ID: 6OIE and 5B76).

established that the YEATS domain is a Kac reader module with the highest affinity to crotonylation mark (Andrews et al., 2016; D.; Zhao et al., 2016). The crystal structure of all three proteins in complex with H3 tail peptide having crotonylation mark showed a highly similar structure where the extended side chain of Kcr fits comfortably into the narrow end-open pocket of the YEATS domain (**Figure 4A**).

Two conserved aromatic residues in different YEATS domains (F62 and W81 for Taf14, F59 and Y78 for AF9, and Y268 and W282 for YEATS2) make a sandwich arrangement with the planar crotonylamide group, which crosses the β-sandwich cage at a 90° angle in a corkscrew-like manner (**Figure 4B**). This arrangement favors a novel "aromatic–π–aromatic" stacking (also called "π–π–π" stacking) (Klein et al., 2018). Additionally, extensive hydrophobic interactions, the amide–π interactions, the CH–π interactions, and electrostatic interactions (mainly of Cα and Cβ of the alkene moiety with the carbonyl oxygen of Q79) between the side chain of crotonylated lysine and pocket residues significantly contribute to specific recognition of Kcr by the YEATS domain (Krone et al., 2020).

Flanking residues in all three H3K9, H3K18, and H3K27 are conserved, sharing a common motif "$A_{(-2)}R_{(-1)}KS_{(+1)}$." An acidic aspartate residue of Taf14 and AF9 YEATS domains forms charge-stabilized hydrogen-bonding interaction with (*n*–1) arginine of H3K9cr peptide. Interestingly, in the YEATS domain of YEATS2 protein, this acidic aspartate residue is replaced by the neutral asparagine residue, which does not recognize "$R_{(-1)}$." While Taf14 and AF9 YEATS domain prefer H3K9cr and H3 N-terminal residues "K4-Q5-T6-A7-R8" have extensive interactions with loops L6 and L8 surface residues, YEATS2 binds H3K27cr more strongly and oppositely oriented C-terminal residues "S28-A29-P30-A31" fits nicely on the surface of L6 and L8 loops (**Figure 4C**). In the crystal structure of YEATS2, the YEATS domain in complex with H3K27cr revealed a hydrophobic pocket in YEATS2 in which H3P30 fits snugly and facilitates the correct positioning of H3K27cr, explaining the site specificity of YEATS2 (D. Zhao et al., 2016).

A recent study showed the role of histone crotonylation and Taf14 in the yeast metabolic cycle. In the yeast metabolic cycle, acetylation increases in high oxygen consumption state, followed by generation of crotonylation intermediates (Gowans et al., 2019). As the cells shift to a low oxygen consumption state, acetylation mark is replaced by crotonylation marks and in this LOC state H3K9cr and Taf14 repress the pro-growth genes, contrary to earlier studies showing their role in gene expression (Sabari et al., 2015).

4.3 Recognition of H3K14acyl by the DPF Domain

Pull-down assays and ITC experiments using an array of H3K14 bearing different acylations revealed that the DPF domain of DPF2 and MOZ HAT displays more affinity for

H3K14cr, H3K14bu, and H3K14pr than H3K14Ac with crotonylation being the most favored (Xiong et al., 2016). On a similar line, a combination of fluorescence spectroscopy, NMR, and histone peptide pull-down assay established the specificity of the DPF domain of MORF HAT for H3K14cr and H3K14bu (Klein et al., 2017). In all the crystal structures solved for the DPF domain in complex with H3K14cr or H3K14bu, H3 tail peptide has extensive contacts with double PHD finger of the DPF module with segments $H3_{4–11}$ and $H3_{17–25}$ (in case of full length taken) adopting α-helical conformation (Xiong et al., 2016; Klein et al., 2017, 2019). The overall structural analysis revealed binding of the DPF module to acyllysine in a ping-pong-like manner with three characteristic interactions (Klein et al., 2019).

The first PHD domain of the DPF module forms a unique zinc-finger domain in which a hydrophobic pocket is formed at the β-sheet-2 surface. In the MORF (and MOZ) proteins, the hydrophobic pocket is formed by the amino acid residues I228–C230 of β-1, N235–G237 of β-2, and amino acid residues involved in zinc ion coordination S210 (S217), F211 (F218), L242 (L249), W257 (W264), C259 (C266), I260 (I267), and E261 (**Figure 4D**). The planar crotonylation group of H3K14 is inserted snugly into this hydrophobic reader pocket and stably positioned with the help of four water-mediated hydrogen-bonding interactions and four pairs of hydrophobic contacts. The structural and sequence alignment analysis of DPF domains showed that glycine residue G237 of β-strand-2 is a critical component of the hydrophobic pocket due to its free side chain. In classical PHD fingers, this glycine residue is replaced by bulky amino acids like phenylalanine or tyrosine, which fill the pocket and block large chain acylation mark insertion. One of the phenylalanines (F211 in MOZ and F218 in MORF) is in close proximity to the inserted crotonyl group and forms a π–π interaction between the C=C double bond of the crotonyl group and the aromatic ring of phenylalanine. This additional interaction is responsible for selectivity and strengthens the interaction between DPF domain and H3K14cr (Klein et al., 2019). Additionally, H3 residues R2 and K4 are inserted into two "acidic" pockets formed at the surface of β-1 sheet of the second PHD domain and held by hydrogen bonding and electrostatic interactions.

5 SEROTONYLATION

Serotonylation is the attachment of the serotonin molecule to the glutamine residue of proteins. Serotonin [or 5-HT (hydroxy tryptamine)] is a monoamine with an abundant presence and diverse functions varying from neurotransmitter to hormone release and gastrointestinal motility. Additionally, serotonin has been shown to have the ability to covalently modify several proteins, including RacI, small guanosine triphosphatase, and fibronectin and thereby regulate their functions (Walther et al., 2003; Watts, Priestley, and Thompson 2009). The tissue transglutaminase 2 (TGM2) enzyme is responsible for conjugating serotonin to cytosolic proteins *via* the transamidation reaction (Hummerich et al., 2012).

It was previously known that TGMs could modify histones *in vitro* and do so very fast compared to some of the known native substrates (Abad, and Franco 1996). But recently, using the bio-orthogonal metabolic-labeling approach, Farrelly et al. (2019) showed that TGM2 can catalyze serotonylation of glutamine at the fifth position of histone H3 trimethylated lysine 4 (H3K4me3)-marked nucleosomes, resulting in the presence of combinatorial H3K4me3Q5ser *in vivo*.

5.1 Recognition of H3Q5ser by WDR5

In a pull-down assay, WDR5 was captured using H3 peptide with H3K4me3Q5ser dual marks as the bait, suggesting that WDR5 could be a potential reader of this modification (Farrelly et al., 2019). WDR5 is a core subunit of a histone methyltransferase enzyme; the MLL (mixed-lineage leukemia) complex is responsible for trimethylation of H3K4. Further pull-down assays and ITC experiment established that serotonylated H3Q5 enhances the binding of WDR5 by at least two-fold than that of unmodified H3, and H3K4 trimethylation mark has no significant effect on this binding, also supported by the observation that there was no electron density for the trimethyl group of K4 in the crystal structure of WDR5–H3K4me3Q5ser complex (Jie et al., 2022) (**Figure 5B**).

The crystal structure of WDR5–H3Q5ser complex revealed that the serotonyl group is placed in a shallow hydrophobic surface pocket of WDR5. The WDR5–Q5ser interaction is stabilized *via* a network of hydrogen bonds (one between OH group of serotonin with amide group N130 residue of WDR5 and another between amide group of serotonin with WDR5 D172 side chain) and van der Waals contacts (between hydrophobic moiety of serotonyl group and aromatic side chains of Y131, F149, and Y191 of WDR5) (**Figure 5A**). Additionally, R2 of H3 peptide also participates in this complex formation as it is anchored into a negatively charged central channel and interacts with WDR5's F133 and F263 through cation–π interactions (Jie et al., 2022).

In neuroblastoma cells, upon recognition of H3Q5ser modification, WDR5 is recruited to promoter regions of oncogenic genes *GPX1*, *C-MYC*, and *PDCD6* that can promote tumor formation (Jie et al., 2022). Knockdown studies implied that serotonylation of H3Q5 is not dependent on H3K4me3; instead, there was a decrease in the level of H3K4me3 upon WDR5 knockout, also seen in the case of TGM2 knockdown, which may be due to less recruitment of MLL1 complex. H3K4me3Q5ser displays a ubiquitous pattern of tissue expression in mammals, with enrichment observed in the brain and gut, two organ systems responsible for the bulk of 5-HT production. Genome-wide analyses of human serotonergic neurons, developing mouse brain, and cultured serotonergic cells indicate that H3K4me3Q5ser nucleosomes are enriched in euchromatin, are sensitive to cellular differentiation, and correlate with permissive gene expression—phenomena that are linked to the enhanced function of TFIID (Farrelly et al., 2019).

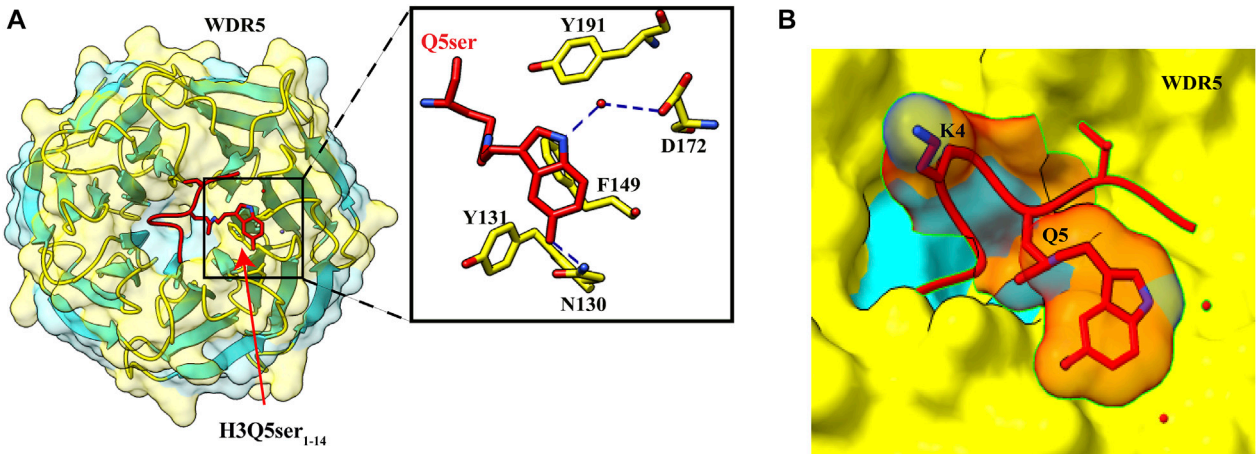

FIGURE 5 | Recognition of H3Q5ser by WDR5. **(A)** Left: overall structure of $WDR5_{22–334}$ in complex with $H3Q5ser_{1–14}$ peptide (red). Right: enlarged view showing residues of $WDR5_{22–334}$ (yellow) interacting with Q5ser (red). Hydrogen bonds are shown with blue dashed lines. **(B)** Lysine at fourth position is protruding away from the WDR5, resulting in no effect of trimethylation of K4 on the Q5ser–WDR5 interaction (PDB ID: 7CFQ).

6 METHYLATION

Histone methylation and its importance in transcription were first observed in the 1960s. There are three lysine methylation states: -mono, -di, and -tri (me1, me2, and me3); since methylation does not change histone's charge configuration, the primary function of these methylations is to interact with effector molecules that specifically recognize these modifications. Generally, all other histone modifications are specific for the active or repressed state, while in methylated chromatin it depends on its methylation state and the modification position. For example, H3K4, H3K36, and H3K79 methylations are considered to mark active transcription (Heintzman et al., 2007), whereas H3K9, H3K27, and H4K20 methylations are associated with silenced chromatin states (Bernstein et al., 2005; Barski et al., 2007).

Methyllysine-specific readers have a peculiar characteristic: they recognize histone modification by an aromatic cage that comprises two to four aromatic amino acids. These aromatic amino acids in some complexes are perpendicular to each other, which helps encircle the entire lysine methylation. The compartment of the aromatic cage defines whether mono-, di-, or tri-methylation state interacts with it. Therefore a small compartment limits its interaction with a higher methylation state because of steric hindrance, while a large compartment favors the interaction with a higher methylation state. Interaction in the compartment between the methylammonium group and the aromatic cage is stabilized by cation–π interactions and the hydrophobic and van der Waal interactions. Amino acids surrounding methyllysine play a vital role in the reader's specificity for a particular methylated lysine. Some readers show very low specificity, while others are specific for a specific methylated state. Beyond caging of the methyllysine, the mechanism of recognition of surrounding residues varies among readers. A number of evolutionarily conserved domains were discovered that interact specifically with the methylated histone. These "reader" proteins contain methyl-lysine-binding motifs, including PHD, chromo, Tudor, PWWP, WD40, BAH, ADD, ankyrin repeat, and MBT domains (**Figure 6**). These readers can distinguish target methyllysine based on their methylation state and surrounding amino acid sequence (Musselman et al., 2012).

6.1 Royal Superfamily

In this superfamily, domains are structurally related and have β-barrel topology. It is believed that they come from a common ancestor, which has the conserved binding ability with the methylated substrate. All the family members consist of a slightly curved β-barrel with three β-strands followed by a short 3_{10} helix, and different members are distinguished based on additional strands or helices. This family includes MBT, Tudor, chromodomain, and PWWP (Yap and Zhou 2010).

6.1.1 Recognition of H4K20me1/me2 by the MBT Domain of L3MBTL1

Isothermal titration calorimetry (ITC) assay using different methylation states of H4K20 peptide revealed that the MBT domain of human L3MBTL1 displays more affinity toward mono- and dimethylation states and does not bind to unmodified and trimethylated histone peptide. However, the binding is relatively of low affinity (K_D = 5–40 μM) and promiscuous (Min et al., 2007). The crystal structure of L3MBT1 with three MBT domains bound to histone peptide of 11 residues (H4 residue 15–25 with H4K20me2) shows the similar structure of all MBT domains assembled in a triangular shape. The structure is consistent with previously known structures of the MBT domain. It consists of four β-strands that form β-barrel and other extended arms of helices and a shorter strand (Wang et al., 2003). L3MBTL1 has three repeats of the MBT domain; however, only the second MBT domain binds

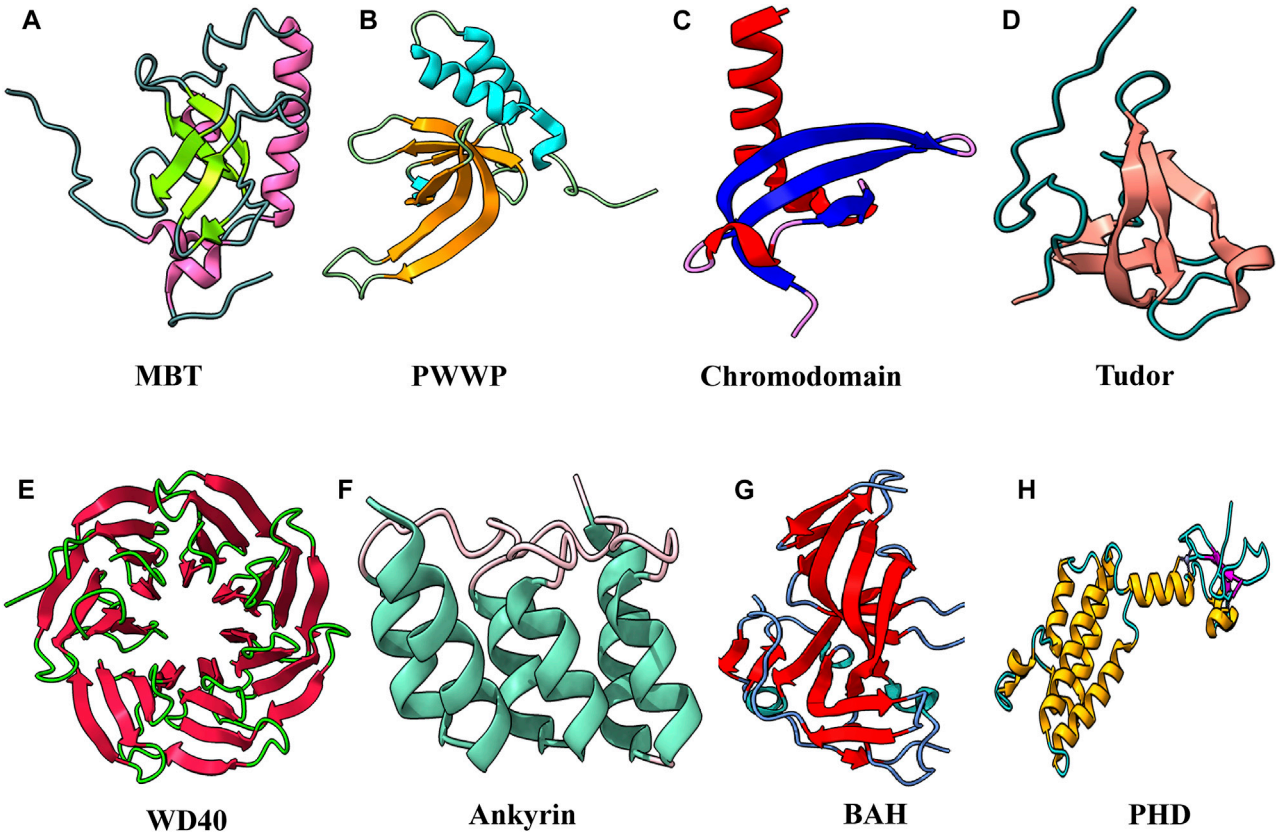

FIGURE 6 | Structural features of domains capable to "read" methyl marks. **(A)** Second MBT domain of human KIAA1617: β-strands in light green and α-helix in pink (PDB ID: 1WJR). **(B)** PWWP domain of Pdp1 (PDB ID: 2L89). **(C)** Chromodomain of MPP8 (PDB ID: 3QO2). **(D)** Tudor domain of human PHF20 (PDB ID: 3SD4). **(E)** WD40 repeats of MYC (PDB ID: 6U8O). **(F)** Ankyrin repeats of human liver-type glutaminase (PDB ID: 5U0K). **(G)** Bromo-adjacent homology domain of human polybromo-1(PDB ID: 6OXB). **(H)** PHD of human BPTF protein (PDB ID: 2F6N).

to methyllysine (Santiveri et al., 2008; Eryilmaz et al., 2009; Li et al., 2007; Min et al., 2007). Superimposition of all three MBT domains revealed that the shorter side chain of cysteine 363 in the aromatic cage of the second MBT was replaced by bulky amino acids in MBT1 and MBT3. Thus, steric hindrance prevents the binding of MBT1 and MBT3 with methylated lysine. It also preferentially reads mono- and dimethylation by the cavity insertion mode, and specificity toward a lower methylation state is because of the aspartate residue present in the aromatic cage. Typical interactions in the aromatic cage are cation–π between aromatic residues and positively charged methylammonium of methyllysine. Additionally, aspartate binds to methylammonium *via* hydrogen bonding in the MBT domain.

In contrast, the flanking residues of the peptide substrate show little interaction with the protein. Only two water-mediated hydrogen bonds are present, first between the backbone carbonyl group of H18 and Y386 of the protein and a second between the carbonyl NH group of K20 and N358 of the protein.

H4K20 methylation was previously linked to chromatin compaction. However, H4K20me1 was found in the actively transcribing genes, contradicting the previously suggested role of methylation in chromatin compaction. A recent study revealed that H4K20me1 nucleosomal arrays were less compacted than H4K20me0 and H4K20me3 nucleosomal arrays, and the H4 tail was more dynamic in K20 mono-methylation. This study suggests that mono-methylation of H4K20 facilitates the opening and accessibility of chromatin (Shoaib et al., 2021).

6.1.2 PWWP Domain

PWWP domain was first identified in the WHSC1 protein that contains the 100–130 amino acid structural motif (Stec et al., 1998). It also has a conserved Pro-Trp-Trp-Pro motif, and it consists of five β-strand barrels packed against the helical bundle. Despite the sequence conservation in different proteins, some variation in the PWWP motif can occur. For example, methyltransferase DNMT3a/b has SWWP (Qiu et al., 2002), and hepatoma-derived growth factor (HDGF) has a PHWP motif instead of a PWWP motif (Sue et al., 2004). It was initially identified as the DNA-binding protein; however, its similarity to the Tudor and chromodomain suggests that it might have the ability to bind methylated lysine. DNMT3a protein responsible for DNA methylation contains the PWWP domain. This domain is also known to interact with methylated histone tails, which led to assumptions that it might have dual binding to histone tails and the dsDNA.

Pdp1 protein, which contains PWWP domains, binds to methylated lysine, and dsDNA was seen by fluorescence polarization assay (FPA) (Qiu et al., 2012). The binding studies showed that PWWP domains of Pdp1 bind to the H3K20 trimethylation. After that, many other PWWP domains were shown to exhibit the binding with methylated lysine. Except for Pdp1, all the proteins containing PWWP domains bind specifically to the H3K36 methylation, suggesting its role as the H3K36 methylation sensor (Vezzoli et al., 2010; van Nuland et al., 2013; Wang et al., 2020). As it binds to the trimethylation state of lysine, it suggests that the binding cavity of the PWWP domain is wider to accommodate the bulkier me3 group than the MBT domain, which can only interact with mono- and dimethylated states. Therefore, this domain shows less specificity for the degree of methylation state.

Structural analysis of Pdp1 revealed that the aromatic cage is formed by Y63, W66, and F94. Cation–π interactions are used by the Pdp1 PWWP domain to recognize the trimethylated lysine at 20th position, and two residues (D97 and N99) from the loop between β3 and β4 form an extensive network of hydrogen bonds with the histone H4 tail residues (R19, K20, and V21) (Qiu et al., 2012). Y63, W66, and F94 amino acid side chains are perpendicularly oriented, forming an aromatic cage accommodating the trimethylammonium group. Mutations of the residues that compose the aromatic cage abolish methylated histone peptide binding.

6.1.3 Recognition of H3K9me3 Marks by HP1 Chromodomain

The chromatin organization modifier domain (chromodomain) is the smallest member of this superfamily. The structural motif is based on the HP1 fold, consisting of three curved antiparallel β-sheets followed by the α-helix (Ball et al., 1997). There are approximately 55 proteins identified which contain chromodomain. These chromodomain-containing proteins were associated with chromatin silencing. These proteins are divided into two groups: canonical (based on HP1 structure) group includes polycomb proteins Cbx1-9, CMT1-3, and CYD; and noncanonical, including CHD1-8, RBBP1, and HRP1.

HP1 and polycomb proteins recognize H3K9me3 (Jacobs and Khorasanizadeh 2002) and H3K27me3 (Min, Zhang, and Xu 2003), respectively, through their ARKS/T motif. The histone tail inserted between two strands forms the complete β-barrel in both proteins. This insertion of the histone tail is stabilized by the electrostatic interactions and the hydrogen bond between the backbone. This interaction involves seven amino acids preceding methyllysine and one following amino acid. This recognition method prefers the recognition of trimethylation over mono- and dimethylation. Recent cryo-EM structure of H3K9me3 di-nucleosome with HP1α, HP1β, and HP1γ revealed how heterochromatin is organized. In this structure, di-nucleosomes trimethylated at K9 are bridged by two symmetric molecules of HP1. Linker DNA between the nucleosome is not interacting with the HP1, which leaves linker DNA to interact with ACF (ATP-utilizing chromatin assembly and remodeling factor) (Machida et al., 2018).

The noncanonical chromodomain proteins are based on the chromo ATPase/helicase-DNA-binding (CHD) protein. They contain two chromodomains, both at the N-terminal, for example, SNF2-type helicase, which is involved in chromatin remodeling. CHD7 specifically recognizes H3K1me1 as the enhancer for the gene.

6.1.4 Recognition of H3K4me3K9me3 Bivalent Mark by the Tudor Domain of Spindlin1

Tudor domains are structurally diverse and mediate protein–protein interactions. Tudor domains interact with all methylation states. This domain consists of approximately 60 amino acids of four or five β-strands which form a β-barrel structure followed by one or two helices (Selenko et al., 2001). Tudor domain-containing protein interacts with the H3K4me3 (Wang et al., 2011; Yang et al., 2012), H3K9me2 (Arita et al., 2012), H3K36me3 (Cai et al., 2013), and H4K20me3 (Hirano et al., 2012). Almost 30 known proteins have this Tudor domain, including JMJD2, 53BP1, SGF29, Spindlin1, UHRF1, PHF1, OHF19, LBR, and TDRD3 (which recognizes methylated arginine residues). Proteins in this family are involved in various biochemical processes like DNA methylation, nonhomologous end joining, DNA damage and repair, transcription activation and repression, and rRNA expression.

To meet the growing demand for ribosomes in rapidly growing cells, more copies of rRNA are produced at a greater transcription rate. The repressive histone methylation marks present on H3K9/K27 and H4K20 in the heterochromatin region are linked to rRNA transcription suppression. Because it has been established that H3K4 methylation is required for active gene expression, the cell must establish H3K4 methylation and H3K9 demethylation to convert the suppressed rRNA expression to active expression. Although H3K4 and H3K9 trimethylation are mutually exclusive, bivalent H3K4me3 and H3K9me3 have been documented in specific cell types (Mikkelsen et al., 2007; Bilodeau et al., 2009; Rugg-Gunn et al., 2010; Matsumura et al., 2015). It was previously reported that KDM4A and KDM4C recognize the H3K4me3 *via* their Tudor domain and help in the demethylation of H3K9me3. This study suggests that these methylation marks can coexist on the same H3 N-terminal tail and functionally crosstalk (Huang et al., 2006; Yamamoto, and Fujimori 2016). It was also previously known that euchromatin rRNA genes contain bivalent mark H3K4me3K9me3 (Murayama et al., 2008). So for rRNA synthesis, the bivalent mark of H3K4 and H3K9 trimethylation is needed.

The Tudor domain is found in Spindlin1, a protein that aids in rRNA expression. Splindin1 creates a complex with C11orf84 that recognizes the bivalent mark on the histone H3 tail. Tudor 2 domain residues F141, W151, Y170, and Y177 form an aromatic pocket for trimethylated K4, whereas Tudor 1 domain residues W62, W72, Y91, and Y98, as well as Tudor 3 domain residue F251, recognize trimethylated K9 (**Figure 7A**) (Du et al., 2021). In addition to cation–π interactions formed by dual methylated lysine, the N-terminal amino group of H3A1 forms a hydrogen bond with the side-chain carboxylate group of D189, and guanidino moiety of H3R2 is ion-paired with

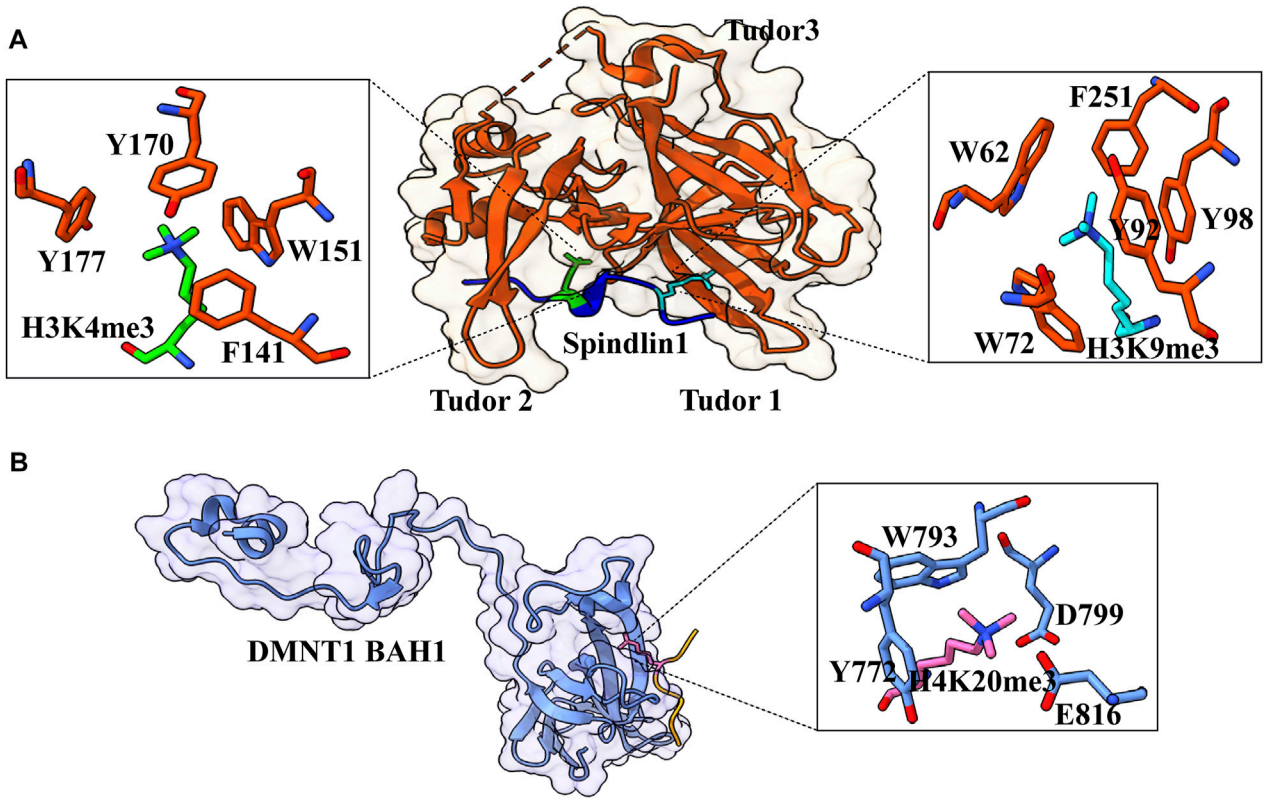

FIGURE 7 | Interaction details of Spindlin1 and DNMT1 with trimethylated histone peptides. **(A)** Structure of Spindlin1 with H3K4me3K9me3 peptide; Spindlin1 shown in orange, H3K4me3 in green and H3K9me3 in cyan. Key residues involved in the interactions are depicted as a ball-stick model shown in an enlarged view (PDB ID: 7CNA). **(B)** Structure of DNMT1 BAH1 with H4K20me3 peptide; DNMT1 BAH1 is shown in light blue and H4K20me3 in pink (PDB ID: 7LMK).

the side-chain carboxylate group of D184 (Du et al., 2021). This bivalent recognition further helps in the dislocation of HP1 from the rRNA chromatin, which relaxes the chromatin and helps in the recruitment of RNA polymerase I, which leads to the expression of rRNA. Spindlin1 Tudor 3 domain is responsible for the binding to C11orf84, while the other two Tudor domains act in concert to recognize a noncanonical bivalent histone mark H3K4me3K9me3.

6.2 The WD40 Repeats

WD40 repeats are present in proteins showing very diverse protein–protein interactions. WD repeats usually have 40–60 amino acids and conserved tryptophan–aspartate (WD) residue. This motif can be found in each blade of a WDR domain. The structural plasticity of WDR domains allows them to keep their β-propeller fold even after deletion of WD repeats, which can range from five to eight but are generally seven (Böcskei, and Polgár 1998; Juhász et al., 2005). Each of these repeats folds into a four-stranded β-sheet, and these propellers are large, usually containing ~300 amino acids.

SET1 methyltransferase (catalyze methylation of H3K4) subunit WDR5 contains seven WD repeats to form the β-propeller structure. SET1 needs WDR5 for its assembly and activity. First, it was found that WDR5 binds to H3K4me2 and me3. However, the crystal structure of WDR5 with the unmodified, mono-, di-, and trimethylated H3K4 reveals that WDR5 interacts with H3R2 and acts as an arginine reader. WRD5 interacts with lysine only through E332, present at the protein's surface. WRD5 anchor as the arginine pocket binds to the unmodified and demethylated arginine residue (Dharmarajan et al., 2012). It was proposed to act as a histone modification intermediate that binds to arginine and presents lysine for methylation.

6.3 Recognition of H3K9me1/me2 by Ankyrin Repeat Domain of G9a

It is a ~33 amino acid repeat, and each repeat consists of helix–loop–helix structure with a β-hairpin/loop region; and in most proteins, 4–7 repeats are present, which stack onto each other to form the right-handed solenoid-like structure that helps in the protein–protein interaction (Sedgwick and Smerdon 1999). A short-distance interaction between inter α-helices helps form the solenoid, forming a typical globular protein shape. The structure of the AR domain is stabilized through inter- and intra-helical hydrophobic and hydrogen bonding *via* polar residues at the N-terminal. Hydrophobic interactions between P5 and H7 form the L-shape of the domain, and hydrogen bond

between T4 and H7 facilitates the formation of β-hairpin with the adjacent loop (Yuan et al., 2004).

The H3K9me1 and H3K9me2 peptides bind to G9a ankyrin repeats with low affinity (K_D = 14 and 6 mM, respectively), with a crystal structure of ankyrin repeats–H3K9me2 peptide complex was solved. The dimethylammonium group of K9me2 is placed into an aromatic pocket lined by three tryptophan residues and glutamate while the H3 peptide is sandwiched between β-turns and the fourth and fifth helices ankyrin repeats (Collins et al., 2008). Peptide residues 9–11, which comprise K9me2, are involved in intermolecular recognition. The formation of complexes is hampered by mutations of certain peptide or aromatic cage residues. G9a's SET domain-mediated methyltransferase activity is unaffected by changes in methyllysine recognition by the ankyrin repeat, indicating that the reading and writing domains work independently.

6.4 The Bromo Adjacent Homology Domain

Bromo adjacent homology (BAH) domain-containing proteins are frequently associated with chromatin functions, and mutations in these domains can result in diseases. BAH has been found to have various roles in chromatin biology, including protein–protein interaction, identification of methylated lysine, and DNA methylation. They have six tandem repeats of the bromodomain at the N-terminus, followed by the repetitive sequence motif of an unknown function; therefore, these are referred to as bromo adjacent homology domains. The majority of BAH domain proteins that have been identified have specific chromatin links, such as nucleosome remodeling and histone and DNA modifications.

BAH has an essential role in DNA methylation, which is an epigenetic mark that catalyzes the addition of the methyl group to the fifth position of cytosine (5-methylcytosine) (Suzuki and Bird 2008). Each round of DNA replication produces hemimethylated DNA, which must be converted to fully methylated DNA before the next round of replication, or the methylation marks will be lost. The family of DNA methyltransferases (Dnmts) mediates the transfer of the methyl group from *S*-adenyl methionine to the fifth position of cytosine at the CpG dinucleotide (Moore, Le, and Fan 2013). DNMT1 has N-terminal regulatory and C-terminal catalytic domains. Human Dnmt1 (1,616 amino acids) has two regions: N-terminal regulatory domain (1–1,139) and C-terminal catalytic domain (1,140–1,616). It also has several regions in N-terminal like CXXC (Bestor 1992), replication focus targeting sequence (RFTS) (Leonhardt et al., 1992), and BAH domain (Callebaut, Courvalin, and Mornon 1999).

H4K20 trimethylation is a significant heterochromatin mark that suppresses repetitive sequences in the human genome. By recognizing H4K20me3 *via* its first Bromo adjacent homology domain, DNMT1 promotes DNA methylation. The structure of DNMT1 with $H4K20me3_{14–25}$ peptide shows that the side chain is inserted into a pocket created by DNMT1 BAH1 Y772, W793, D799, and E816 (**Figure 7B**) (Ren et al., 2021). The side chains of DNMT1 BAH1 D765 and E818 are bidentate hydrogen-bonded to the backbone amides of H4. BAH1 binds to H4K20me3, generating a change in the structure of DNMT1 that allows the autoinhibition linker to be displaced. DNMT1 can break away from the linker's autoinhibition and get activated. H4K20me3 mark is put just after the S-phase of the cell cycle; therefore, H4K20me3 patterns may differ in new histones and parental histone. For a fact, recycled histone H4K20 is extensively methylated throughout replication, but fresh histones are only methylated during the G2/M phase (Ren et al., 2021). In this context, only the parental histones probably facilitate the DNMT1 activation, which lasts beyond the S-phase. This mechanism occurs alongside the UHRF-1-specific S-phase maintenance of DNA methylation (Rothbart et al., 2012).

6.5 PHD Domain

The PHD finger is a short zinc-binding module with a high cysteine content but few secondary structural elements that are now being characterized as a protein–protein or protein–phospholipid interaction domain. The PHD finger is a 50–80 amino acid motif composed of a two-strand antiparallel β-sheet and α-helix linked to the Cys4-His-Cys3 motif in a cross-brace shape by two zinc atoms (Bottomley et al., 2005; Elkin et al., 2005). The structure and function studies on PHD domain-containing proteins like BPFT (Li et al., 2006), IGN2 (Peña et al., 2006), and YNG1 (Taverna et al., 2006), which bind to H3K4 higher methylation state, provide the sequence and methylation state-specific recognition mechanism. Because of their ability to read numerous different post-translational modifications simultaneously, PHD proteins are some of the best examples of the "reader" class of proteins in combinatorial control of transcription. PHD fingers are found on a number of proteins involved in chromatin remodeling. Due to their frequent occurrence near other known chromatin interaction domains (bromodomains, PWWP domains), it was thought that PHD fingers could recognize histone modifications. In the various structures of PHD fingers that have been solved, the H3K4me3 mark can be found on most peptides. The modified histone peptide forms a strand that integrates into the PHD finger's existing antiparallel sheet, and the majority of the complex structures have a similar topology.

7 CONCLUSION

The advancement in mass spectrometry and structural biology field in the past few years has revolutionized the field of epigenetics, resulting in an ever-growing list of PTMs. At the same time, the list of proteins having the capability to write, read, and erase these epigenetic marks is also growing, further expanding the complexity of epigenetics. For example, the identification of several short-chain acylation marks and their readers are critical in linking the metabolic state of the cell to gene regulation as most of the substrates for these PTMs are derived from different metabolic reactions. In the past 20 years, a lot of efforts have been put into understanding the molecular and structural mechanism of PTM readouts by their cognate reader proteins. These studies have identified a wide range of interacting modes, including cation–π and π–π–π stacking interactions (Klein et al., 2018; Du et al., 2021). Selective recognition of PTM by its cognate reader or multivalent

readout of multiple PTMs on the same or different tails by a group of readers targets the protein or protein complex at targeted genomic sites and performs the downstream function. A deep understanding of these PTMs and their recognition by reader proteins is critical as any misregulation of these recognition mechanisms can lead to several human disorders like cancer. In case of misregulation, in-depth characterization of these binding mechanisms can aid in developing specific epigenetic-driven therapeutic targets. From the structural point of view, we have a solid knowledge base of different PTM–reader interactions. However, there are some questions that remain to be explicitly answered, concerning selectivity and specificity, like how the same reader can differentiate between acetyl and acyl modifications *in vivo*. Although a large number of PTMs have been identified and characterized, their reader partner is still to be characterized. Maximum structural studies on reader–PTM interactions till date used only short peptides. Therefore, structural elucidation of reader–PTM interaction at the nucleosomal level and further at the nucleosomal array level remains a major challenge. With improving structural biology tools and computational methods in tandem, it will be easier to overcome the existing limitations and answer questions associated with the molecular mechanism of "decorated tails" recognition by the epigenetic machinery.

AUTHOR CONTRIBUTIONS

AK, PS, and RS: conceptualization, review, and editing; PS and RS: original draft.

REFERENCES

Allahverdi, A., Yang, R., Korolev, N., Fan, Y., Davey, C. A., Liu, C.-F., et al. (2011). The Effects of Histone H4 Tail Acetylations on Cation-Induced Chromatin Folding and Self-Association. *Nucleic Acids Res.* 39 (5), 1680–1691. doi:10.1093/nar/gkq900

Allfrey, V. G., Faulkner, R., and Mirsky, A. E. (1964). ACETYLATION AND METHYLATION OF HISTONES AND THEIR POSSIBLE ROLE IN THE REGULATION OF RNA SYNTHESIS. *Proc. Natl. Acad. Sci. U.S.A.* 51 (5), 786–794. doi:10.1073/pnas.51.5.786

Andrews, F. H., Shinsky, S. A., ShanleShanle, E. K., Bridgers, J. B., Gest, A., TsunTsun, I. K., et al. (2016). The Taf14 YEATS Domain Is a Reader of Histone Crotonylation. *Nat. Chem. Biol.* 12 (6), 396–398. doi:10.1038/nchembio.2065

Arita, K., Isogai, S., Oda, T., Unoki, M., Sugita, K., Sekiyama, N., et al. (2012). Recognition of Modification Status on a Histone H3 Tail by Linked Histone Reader Modules of the Epigenetic Regulator UHRF1. *Proc. Natl. Acad. Sci. U.S.A.* 109 (32), 12950–12955. doi:10.1073/pnas.1203701109

Ball, L. J., MurzinaMurzina, N. V., Broadhurst, R. W., ArcherRaineSingh, S. J., Stott, F. J., Murzin, A. G., et al. (1997). Structure of the Chromatin Binding (Chromo) Domain from Mouse Modifier Protein 1. *EMBO J.* 16 (9), 2473–2481. doi:10.1093/emboj/16.9.2473

Ballestar, E., Abad, C., and Franco, L. (1996). Core Histones Are Glutaminyl Substrates for Tissue Transglutaminase. *J. Biol. Chem.* 271 (31), 18817–18824. doi:10.1074/JBC.271.31.18817

Bao, X., Liu, Z., Zhang, W., Gladysz, K., Fung, Y. M. E., Tian, G., XiongLi, Y., Wong, J. W. H., Yuen, K. W. Y., and Li, X. D.Yi Man Eva Fung; Jason Wing Hon Wong; Karen Wing Yee Yuen (2019). Glutarylation of Histone H4 Lysine 91 Regulates Chromatin Dynamics. *Mol. Cell.* 76 (4), 660–675. doi:10.1016/J.MOLCEL.2019.08.018

Barski, A., Cuddapah, S., Cui, K., Roh, T.-Y., Schones, D. E., Wang, Z., et al. (2007). High-Resolution Profiling of Histone Methylations in the Human Genome. *Cell.* 129 (4), 823–837. doi:10.1016/j.cell.2007.05.009

Bascom, G. D., and Schlick, T. (2018). Chromatin Fiber Folding Directed by Cooperative Histone Tail Acetylation and Linker Histone Binding. *Biophysical J.* 114 (10), 2376–2385. doi:10.1016/j.bpj.2018.03.008

Bernstein, B. E., Kamal, M., Lindblad-Toh, K., Bekiranov, S., BaileyBailey, D. K., Huebert, D. J., et al. (2005). Genomic Maps and Comparative Analysis of Histone Modifications in Human and Mouse. *Cell.* 120 (2), 169–181. doi:10.1016/j.cell.2005.01.001

Bestor, T. H. (1992). Activation of Mammalian DNA Methyltransferase by Cleavage of a Zn Binding Regulatory Domain. *EMBO J.* 11 (7), 2611–2617. doi:10.1002/j.1460-2075.1992.tb05326.x

Bilodeau, S., Kagey, M. H., Frampton, G. M., RahlRahl, P. B., and Young, R. A. (2009). SetDB1 Contributes to Repression of Genes Encoding Developmental Regulators and Maintenance of ES Cell State. *Genes. Dev.* 23 (21), 2484–2489. doi:10.1101/gad.1837309

Böhm, V., Hieb, A. R., Andrews, A. J., Gansen, A., Rocker, A., Tóth, K., et al. (2011). Nucleosome Accessibility Governed by the Dimer/Tetramer Interface. *Nucleic Acids Res.* 39 (8), 3093–3102. doi:10.1093/nar/gkq1279

Bottomley, M. J., Stier, G., Pennacchini, D., Legube, G., Simon, B., Akhtar, A., et al. (2005). NMR Structure of the First PHD Finger of Autoimmune Regulator Protein (AIRE1). *J. Biol. Chem.* 280 (12), 11505–11512. doi:10.1074/jbc.M413959200

Brehove, M., Wang, T., North, J., Luo, Y., Dreher, S. J., Shimko, J. C., et al. (2015). Histone Core Phosphorylation Regulates DNA Accessibility. *J. Biol. Chem.* 290 (37), 22612–22621. doi:10.1074/jbc.M115.661363

Cai, L., RothbartRothbart, S. B., Lu, R., Xu, B., Chen, W.-Y., Tripathy, A., et al. (2013). An H3K36 Methylation-Engaging Tudor Motif of Polycomb-like Proteins Mediates PRC2 Complex Targeting. *Mol. Cell.* 49 (3), 571–582. doi:10.1016/j.molcel.2012.11.026

Callebaut, I., Courvalin, J.-C., and Mornon, J.-P. (1999). The BAH (Bromo-Adjacent Homology) Domain: A Link between DNA Methylation, Replication and Transcriptional Regulation. *FEBS Lett.* 446 (1), 189–193. doi:10.1016/s0014-5793(99)00132-5

Carey, M., Li, B., and Workman, J. L. (2006). RSC Exploits Histone Acetylation to Abrogate the Nucleosomal Block to RNA Polymerase II Elongation. *Mol. Cell.* 24 (3), 481–487. doi:10.1016/j.molcel.2006.09.012

Chen, G., Li, W., Yan, F., Wang, D., and Chen, Y. (2020). The Structural Basis for Specific Recognition of H3K14 Acetylation by Sth1 in the RSC Chromatin Remodeling Complex. *Structure* 28 (1), 111–118. doi:10.1016/j.str.2019.10.015

Chen, Y., Sprung, R., Tang, Y., Ball, H., Sangras, B., Kim, S. C., et al. (2007). Lysine Propionylation and Butyrylation Are Novel Post-Translational Modifications in Histones. *Mol. Cell. Proteomics* 6 (5), 812–819. doi:10.1074/MCP.M700021-MCP200

Chi, P., Allis, C. D., and Wang, G. G. (2010). Covalent Histone Modifications - Miswritten, Misinterpreted and Mis-Erased in Human Cancers. *Nat. Rev. Cancer* 10 (7), 457–469. doi:10.1038/nrc2876

Collepardo-Guevara, R., Portella, G., Vendruscolo, M., Frenkel, D., Schlick, T., and Orozco, M. (2015). Chromatin Unfolding by Epigenetic Modifications Explained by Dramatic Impairment of Internucleosome Interactions: A Multiscale Computational Study. *J. Am. Chem. Soc.* 137 (32), 10205–10215. doi:10.1021/jacs.5b04086

Collins, R. E., Northrop, J. P., Horton, J. R., Lee, D. Y., Zhang, X., Stallcup, M. R., et al. (2008). The Ankyrin Repeats of G9a and GLP Histone Methyltransferases Are Mono- and Dimethyllysine Binding Modules. *Nat. Struct. Mol. Biol.* 15 (3), 245–250. doi:10.1038/nsmb.1384

Dai, L., Peng, C., Montellier, E., Lu, Z., Chen, Y., Ishii, H., et al. (2014). Lysine 2-Hydroxyisobutyrylation Is a Widely Distributed Active Histone Mark. *Nat. Chem. Biol.* 10 (5), 365–370. doi:10.1038/NCHEMBIO.1497

Dhalluin, C., CarlsonL Zeng, C He, J. E. A. K. Aggarwal, Zeng, L., He, C., Aggarwal, A. K., Zhou, M.-M., et al. (1999). Structure and Ligand of a Histone Acetyltransferase Bromodomain. *Nature* 399 (6735), 491–496. doi:10.1038/20974

Dharmarajan, V., Lee, J.-H., Patel, A., Skalnik, D. G., and Cosgrove, M. S. (2012). Structural Basis for WDR5 Interaction (Win) Motif Recognition in Human SET1 Family Histone Methyltransferases. *J. Biol. Chem.* 287 (33), 27275–27289. doi:10.1074/jbc.M112.364125

Dou, Y., and Gorovsky, M. A. (2000). Phosphorylation of Linker Histone H1 Regulates Gene Expression *In Vivo* by Creating a Charge Patch. *Mol. Cell.* 6 (2), 225–231. doi:10.1016/s1097-2765(00)00024-1

Du, Y., Yan, Y., Xie, S., Huang, H., Wang, X., NgNg, R. K., et al. (2021). Structural Mechanism of Bivalent Histone H3K4me3K9me3 Recognition by the Spindlin1/C11orf84 Complex in RRNA Transcription Activation. *Nat. Commun.* 12 (1), 949. doi:10.1038/s41467-021-21236-x

Duan, M.-R., and Smerdon, M. J. (2014). Histone H3 Lysine 14 (H3K14) Acetylation Facilitates DNA Repair in a Positioned Nucleosome by Stabilizing the Binding of the Chromatin Remodeler RSC (Remodels Structure of Chromatin). *J. Biol. Chem.* 289 (12), 8353–8363. doi:10.1074/jbc.m113.540732

Dutta, A., Abmayr, S. M., and Workman, J. L. (2016). Diverse Activities of Histone Acylations Connect Metabolism to Chromatin Function. *Mol. Cell.* 63 (4), 547–552. doi:10.1016/J.MOLCEL.2016.06.038

Elkin, S. K., Ivanov, D., Ewalt, M., Ferguson, C. G., Hyberts, S. G., SunSun, Z.-Y. J. J., et al. (2005). A PHD Finger Motif in the C Terminus of RAG2 Modulates Recombination Activity. *J. Biol. Chem.* 280 (31), 28701–28710. doi:10.1074/jbc.M504731200

Enríquez, P., Krajewski, K., Strahl, B. D., RothbartRothbart, S. B., Dowen, R. H., and Rose, R. B. (2021). Binding Specificity and Function of the SWI/SNF Subunit SMARCA4 Bromodomain Interaction with Acetylated Histone H3K14. *J. Biol. Chem.* 297 (4), 101145. doi:10.1016/j.jbc.2021.101145

Eryilmaz, J., Pan, P., Amaya, A., Dong, A., Adams-Cioaba, M. A., et al. (2009). Structural Studies of a Four-MBT Repeat Protein MBTD1. *PLOS ONE* 4 (10), e7274–7. doi:10.1371/journal.pone.0007274

Farrelly, L. A., Thompson, R. E., Zhao, S., Lepack, A. E., Lyu, Y., BhanuBhanu, N. V., et al. (2019). Histone Serotonylation Is a Permissive Modification that Enhances TFIID Binding to H3K4me3. *Nature* 567 (7749), 535–539. doi:10.1038/s41586-019-1024-7

Fenley, A. T., Anandakrishnan, R., Kidane, Y. H., and OnufrievOnufriev, A. V. (2018). Modulation of Nucleosomal DNA Accessibility via Charge-Altering Post-Translational Modifications in Histone Core. *Epigenetics Chromatin* 11 (1), 11. doi:10.1186/s13072-018-0181-5

Filippakopoulos, P., Picaud, S., Mangos, M., Keates, T., Lambert, J.-P., Barsyte-Lovejoy, D., et al. (2012). Histone Recognition and Large-Scale Structural Analysis of the Human Bromodomain Family. *Cell.* 149 (1), 214–231. doi:10.1016/j.cell.2012.02.013

Filippakopoulos, P., Qi, J., Picaud, S., Shen, Y., Smith, W. B., Fedorov, O., et al. (2010). Selective Inhibition of BET Bromodomains. *Nature* 468 (7327), 1067–1073. doi:10.1038/nature09504

Flynn, E. M., Huang, O. W., Poy, F., Oppikofer, M., BellonBellon, S. F., Tang, Y., et al. (2015). A Subset of Human Bromodomains Recognizes Butyryllysine and Crotonyllysine Histone Peptide Modifications. *Structure* 23 (10), 1801–1814. doi:10.1016/J.STR.2015.08.004

Fülöp, V., Böcskei, Z., and Polgár, L. (1998). Prolyl Oligopeptidase. *Cell.* 94 (2), 161–170. doi:10.1016/s0092-8674(00)81416-6

Gansen, A., Felekyan, S., Kühnemuth, R., Lehmann, K., Tóth, K., Seidel, C. A. M., et al. (2018). High Precision FRET Studies Reveal Reversible Transitions in Nucleosomes between Microseconds and Minutes. *Nat. Commun.* 9 (1), 4628. doi:10.1038/s41467-018-06758-1

Ghoneim, M., Fuchs, H. A., and Musselman, C. A. (2021). Histone Tail Conformations: A Fuzzy Affair with DNA. *Trends Biochem. Sci.* 46 (7), 564–578. doi:10.1016/j.tibs.2020.12.012

Gowans, G. J., Bridgers, J. B., Zhang, J., Dronamraju, R., Burnetti, A., King, D. A., et al. (2019). Recognition of Histone Crotonylation by Taf14 Links Metabolic State to Gene Expression. *Mol. Cell.* 76 (6), 909–921. e3. doi:10.1016/j.molcel.2019.09.029

Heintzman, N. D., StuartStuart, R. K., Hon, G., Fu, Y., ChingHawkins, C. W., HawkinsBarrera, R. D., et al. (2007). Distinct and Predictive Chromatin Signatures of Transcriptional Promoters and Enhancers in the Human Genome. *Nat. Genet.* 39 (3), 311–318. doi:10.1038/ng1966

Hirano, Y., Hizume, K., Kimura, H., Takeyasu, K., Haraguchi, T., and Hiraoka, Y. (2012). Lamin B Receptor Recognizes Specific Modifications of Histone H4 in Heterochromatin Formation. *J. Biol. Chem.* 287 (51), 42654–42663. doi:10.1074/jbc.M112.397950

Huang, H., Zhang, D., Wang, Y., Perez-Neut, M., Han, Z., Zheng, Y. G., et al. (2018). Lysine Benzoylation Is a Histone Mark Regulated by SIRT2. *Nat. Commun.* 9 (1). doi:10.1038/S41467-018-05567-W

Huang, Y., Fang, J., Bedford, M. T., Zhang, Y., and Xu, R.-M. (2006). Recognition of Histone H3 Lysine-4 Methylation by the Double Tudor Domain of JMJD2A. *Science* 312 (5774), 748–751. doi:10.1126/science.1125162

Hummerich, R., Thumfart, J.-O., Findeisen, P., Bartsch, D., and Schloss, P.J; ö; rg-Oliver Thumfart (2012). Transglutaminase-Mediated Transamidation of Serotonin, Dopamine and Noradrenaline to Fibronectin: Evidence for a General Mechanism of Monoaminylation. *FEBS Lett.* 586 (19), 3421–3428. doi:10.1016/j.febslet.2012.07.062

Jacobs, S. A., and Khorasanizadeh, S. (2002). Structure of HP1 Chromodomain Bound to a Lysine 9-Methylated Histone H3 Tail. *Science* 295 (5562), 2080–2083. doi:10.1126/science.1069473

Jacobson, R. H., Ladurner, A. G., King, D. S., and Tjian, R. (2000). Structure and Function of a Human TAF II 250 Double Bromodomain Module. *Science* 288 (5470), 1422–1425. doi:10.1126/science.288.5470.1422

Juhász, T., Szeltner, Z., Fülöp, V., and Polgár, L. (2005). Unclosed β-Propellers Display Stable Structures: Implications for Substrate Access to the Active Site of Prolyl Oligopeptidase. *J. Mol. Biol.* 346 (3), 907–917. doi:10.1016/j.jmb.2004.12.014

Klein, B. J., Jang, S. M., Lachance, C., Mi, W., Lyu, J., Sakuraba, S., et al. (2019). Histone H3K23-specific Acetylation by MORF Is Coupled to H3K14 Acylation. *Nat. Commun.* 10 (1), 4724. doi:10.1038/s41467-019-12551-5

Klein, B. J., Simithy, J., Wang, X., Ahn, J., Andrews, F. H., Zhang, Y., et al. (2017). Recognition of Histone H3K14 Acylation by MORF. *Structure* 25 (4), 650–654. e2. doi:10.1016/j.str.2017.02.003

Klein, B. J., Vann, K. R., Andrews, F. H., Wang, W. W., Zhang, J., Zhang, Y., et al. (2018). Structural Insights into the π-π-π Stacking Mechanism and DNA-Binding Activity of the YEATS Domain. *Nat. Commun.* 9 (1), 4574. doi:10.1038/s41467-018-07072-6

Krone, M. W., Travis, C. R., LeeHannah J Eckvahl, G. Y., Eckvahl, H. J., Houk, K. N., and Waters, M. L. (2020). More Than π-π-π Stacking: Contribution of Amide−π and CH−π Interactions to Crotonyllysine Binding by the AF9 YEATS Domain. *J. Am. Chem. Soc.* 142 (40), 17048–17056. doi:10.1021/jacs.0c06568

Le Masson, I., Yu, D. Y., Jensen, K., Chevalier, A., Courbeyrette, R., Boulard, Y., et al. (2003). Yaf9, a Novel NuA4 Histone Acetyltransferase Subunit, Is Required for the Cellular Response to Spindle Stress in Yeast. *Mol. Cell. Biol.* 23 (17), 6086–6102. doi:10.1128/mcb.23.17.6086-6102.2003

Leonhardt, H., Page, A. W., Weier, H.-U., and Bestor, T. H. (1992). A Targeting Sequence Directs DNA Methyltransferase to Sites of DNA Replication in Mammalian Nuclei. *Cell.* 71 (5), 865–873. doi:10.1016/0092-8674(92)90561-p

Levy, M. J., Montgomery, D. C., Sardiu, M. E., Sardiu, M. E., Montano, J. L., Bergholtz, S. E., et al. (2020). A Systems Chemoproteomic Analysis of Acyl-CoA/Protein Interaction Networks. *Cell. Chem. Biol.* 27 (3), 322–333. e5. doi:10.1016/J.CHEMBIOL.2019.11.011

Li, H., Fischle, W., Wang, W., Duncan, E. M., Liang, L., Murakami-Ishibe, S., et al. (2007). Structural Basis for Lower Lysine Methylation State-specific Readout by MBT Repeats of L3MBTL1 and an Engineered PHD Finger. *Mol. Cell.* 28 (4), 677–691. doi:10.1016/j.molcel.2007.10.023

Li, H., Ilin, S., Wang, W., Duncan, E. M., Wysocka, J., Allis, C. D., et al. (2006). Molecular Basis for Site-specific Read-Out of Histone H3K4me3 by the BPTF PHD Finger of NURF. *Nature* 442 (7098), 91–95. doi:10.1038/nature04802

Li, Y., Sabari, B. R., Panchenko, T., Wen, H., Zhao, D., Guan, H., et al. (2016). Molecular Coupling of Histone Crotonylation and Active Transcription by AF9 YEATS Domain. *Mol. Cell.* 62 (2), 181–193. doi:10.1016/j.molcel.2016.03.028

Li, Y., Wen, H., Xi, Y., Tanaka, K., Wang, H., Peng, D., et al. (2014). AF9 YEATS Domain Links Histone Acetylation to DOT1L-Mediated H3K79 Methylation. *Cell.* 159 (3), 558–571. doi:10.1016/j.cell.2014.09.049

Lorch, Y., Griesenbeck, J., Boeger, H., Maier-Davis, B., and Kornberg, R. D. (2011). Selective Removal of Promoter Nucleosomes by the RSC Chromatin-Remodeling Complex. *Nat. Struct. Mol. Biol.* 18 (8), 881–885. doi:10.1038/nsmb.2072

Lorch, Y., Maier-Davis, B., and Kornberg, R. D. (2018). Histone Acetylation Inhibits RSC and Stabilizes the +1 Nucleosome. *Mol. Cell.* 72 (3), 594–600. doi:10.1016/j.molcel.2018.09.030

Luger, K., MäderMäder, A. W., Richmond, R. K., Sargent, D. F., and Richmond, T. J. (1997). Crystal Structure of the Nucleosome Core Particle at 2.8 Å Resolution. *Nature* 389 (6648), 251–260. doi:10.1038/38444

Machida, S., Takizawa, Y., Ishimaru, M., Sugita, Y., Sekine, S., Nakayama, J.-i., et al. (2018). Structural Basis of Heterochromatin Formation by Human HP1. *Mol. Cell.* 69 (3), 385–397. e8. doi:10.1016/j.molcel.2017.12.011

Marmorstein, R., and Zhou, M.-M. (2014). Writers and Readers of Histone Acetylation: Structure, Mechanism, and Inhibition. *Cold Spring Harb. Perspect. Biol.* 6 (7), a018762, a018762. doi:10.1101/cshperspect.a018762

Matsumura, Y., Nakaki, R., Inagaki, T., Yoshida, A., Kano, Y., Kimura, H., et al. (2015). H3K4/H3K9me3 Bivalent Chromatin Domains Targeted by Lineage-specific DNA Methylation Pauses Adipocyte Differentiation. *Mol. Cell.* 60 (4), 584–596. doi:10.1016/j.molcel.2015.10.025

Matthews, A. G. W., Kuo, A. J., Ramón-Maiques, S., Han, S., Champagne, K. S., Ivanov, D., et al. (2007). RAG2 PHD Finger Couples Histone H3 Lysine 4 Trimethylation with V(D)J Recombination. *Nature* 450 (7172), 1106–1110. doi:10.1038/nature06431

Mattiroli, F., and Penengo, L. (2021). Histone Ubiquitination: An Integrative Signaling Platform in Genome Stability. *Trends Genet.* 37 (6), 566–581. doi:10.1016/j.tig.2020.12.005

Maurer-Stroh, S. Nicholas J. Dickens, Dickens, N. J., Hughes-Davies, L., Kouzarides, T., Eisenhaber, F., and Ponting, C. P. (2003). The Tudor Domain 'Royal Family': Tudor, Plant Agenet, Chromo, PWWP and MBT Domains. *Trends Biochem. Sci.* 28 (2), 69–74. doi:10.1016/S0968-0004(03)00004-5

Mikkelsen, T. S., Ku, M., Jaffe, D. B., Issac, B., Lieberman, E., Giannoukos, G., et al. (2007). Genome-Wide Maps of Chromatin State in Pluripotent and Lineage-Committed Cells. *Nature* 448 (7153), 553–560. doi:10.1038/nature06008

Millán-Zambrano, G., Burton, A., Bannister, A. J., and Schneider, R. (2022). Histone Post-Translational Modifications - Cause and Consequence of Genome Function. *Nat. Rev. Genet.*. doi:10.1038/s41576-022-00468-7

Min, J., Allali-Hassani, A., Nady, N., Qi, C., Ouyang, H., Liu, Y., et al. (2007). L3MBTL1 Recognition of Mono- and Dimethylated Histones. *Nat. Struct. Mol. Biol.* 14 (12), 1229–1230. doi:10.1038/nsmb1340

Min, J., Zhang, Y., and Xu, R.-M. (2003). Structural Basis for Specific Binding of Polycomb Chromodomain to Histone H3 Methylated at Lys 27. *Genes. Dev.* 17 (15), 1823–1828. doi:10.1101/gad.269603

Moore, L. D., Le, T., and Fan, G. (2013). DNA Methylation and its Basic Function. *Neuropsychopharmacol* 38 (1), 23–38. doi:10.1038/npp.2012.112

Murayama, A., Ohmori, K., Fujimura, A., Minami, H., Yasuzawa-Tanaka, K., Kuroda, T., et al. (2008). Epigenetic Control of RDNA Loci in Response to Intracellular Energy Status. *Cell.* 133 (4), 627–639. doi:10.1016/j.cell.2008.03.030

Musselman, C. A., Lalonde, M.-E., Côté, J., and Kutateladze, T. G. (2012). Perceiving the Epigenetic Landscape through Histone Readers. *Nat. Struct. Mol. Biol.* 19 (12), 1218–1227. doi:10.1038/nsmb.2436

Nitsch, S., Zorro Shahidian, L., and Schneider, R. (2021). Histone Acylations and Chromatin Dynamics: Concepts, Challenges, and Links to Metabolism. *EMBO Rep.* 22 (7), e52774. doi:10.15252/EMBR.202152774

Pack, L. R., Yamamoto, K. R., and Fujimori, D. G. (2016). Opposing Chromatin Signals Direct and Regulate the Activity of Lysine Demethylase 4C (KDM4C). *J. Biol. Chem.* 291 (12), 6060–6070. doi:10.1074/jbc.M115.696864

Peña, P. V., Davrazou, F., Shi, X., Walter, K. L., VerkhushaVerkhusha, V. V., Gozani, O., et al. (2006). Molecular Mechanism of Histone H3K4me3 Recognition by Plant Homeodomain of ING2. *Nature* 442 (7098), 100–103. doi:10.1038/nature04814

Peng, Y., Li, S., Onufriev, A., Landsman, D., and Panchenko, A. R. (2021). Binding of Regulatory Proteins to Nucleosomes Is Modulated by Dynamic Histone Tails. *Nat. Commun.* 12 (1), 5280. doi:10.1038/s41467-021-25568-6

Polach, K. J., and Widom, J. (1995). Mechanism of Protein Access to Specific DNA Sequences in Chromatin: A Dynamic Equilibrium Model for Gene Regulation. *J. Mol. Biol.* 254 (2), 130–149. doi:10.1006/jmbi.1995.0606

Qiu, C., Sawada, K., Zhang, X., and Cheng, X. (2002). The PWWP Domain of Mammalian DNA Methyltransferase Dnmt3b Defines a New Family of DNA-Binding Folds. *Nat. Struct. Biol.* 9 (3), 217–224. doi:10.1038/nsb759

Qiu, Y., Zhang, W., Zhao, C., Wang, Y., Wang, W., Zhang, J., et al. (2012). Solution Structure of the Pdp1 PWWP Domain Reveals its Unique Binding Sites for Methylated H4K20 and DNA. *Biochem. J.* 442 (3), 527–538. doi:10.1042/BJ20111885

Ren, W., Fan, H., Grimm, S. A., Kim, J. J., Li, L., Guo, Y., et al. (2021). DNMT1 Reads Heterochromatic H4K20me3 to Reinforce LINE-1 DNA Methylation. *Nat. Commun.* 12 (1), 2490. doi:10.1038/s41467-021-22665-4

Rothbart, S. B., Krajewski, K., Nady, N., Tempel, W., XueBadeaux, S., Badeaux, A. I., et al.Wolfram Tempel (2012). Association of UHRF1 with Methylated H3K9 Directs the Maintenance of DNA Methylation. *Nat. Struct. Mol. Biol.* 19 (11), 1155–1160. doi:10.1038/nsmb.2391

Rugg-Gunn, P. J., Cox, B. J., Ralston, A., Rossant, J., and Rossant, Janet (2010). Distinct Histone Modifications in Stem Cell Lines and Tissue Lineages from the Early Mouse Embryo. *Proc. Natl. Acad. Sci. U.S.A.* 107 (24), 10783–10790. doi:10.1073/pnas.0914507107

Ryu, H.-Y., and Hochstrasser, M. (2021). Histone Sumoylation and Chromatin Dynamics. *Nucleic Acids Res.* 49 (11), 6043–6052. doi:10.1093/nar/gkab280

Sabari, B. R., Tang, Z., Huang, H., Yong-Gonzalez, V., Molina, H., KongKong, H. E., et al. (2015). Intracellular Crotonyl-CoA Stimulates Transcription through P300-Catalyzed Histone Crotonylation. *Mol. Cell.* 58 (2), 203–215. doi:10.1016/j.molcel.2015.02.029

Sanchez, R., and Zhou, M-M. (2009). The Role of Human Bromodomains in Chromatin Biology and Gene Transcription. *Curr. Opin. Drug Discov. Dev.* 12 (5), 659–665. Available at: https://pubmed.ncbi.nlm.nih.gov/19736624.

Santiveri, C. M., Lechtenberg, B. C., Allen, M. D., Sathyamurthy, A., JaulentJaulent, A. M., Freund, S. M. V., et al. (2008). The Malignant Brain Tumor Repeats of Human SCML2 Bind to Peptides Containing Monomethylated Lysine. *J. Mol. Biol.* 382 (5), 1107–1112. doi:10.1016/j.jmb.2008.07.081

Sattler, M., Selenko, P., Sprangers, R., Stier, G., Bühler, D., and Fischer, U. (2001). SMN Tudor Domain Structure and its Interaction with the Sm Proteins. *Nat. Struct. Biol.* 8 (1), 27–31. doi:10.1038/83014

Sawicka, A., and Seiser, C. (2014). Sensing Core Histone Phosphorylation - a Matter of Perfect Timing. *Biochimica Biophysica Acta (BBA) - Gene Regul. Mech.* 1839 (8), 711–718. doi:10.1016/j.bbagrm.2014.04.013

Schulze, J. M., Wang, A. Y., and Kobor, M. S. (2009). YEATS Domain Proteins: a Diverse Family with Many Links to Chromatin Modification and transcription. This Paper Is One of a Selection of Papers Published in This Special Issue, Entitled CSBMCB's 51st Annual Meeting - Epigenetics and Chromatin Dynamics, and Has Undergone the Journal's Usual Peer Review Process. *Biochem. Cell. Biol.* 87 (1), 65–75. doi:10.1139/o08-111

Sedgwick, S. G., and Smerdon, S. J. (1999). The Ankyrin Repeat: A Diversity of Interactions on a Common Structural Framework. *Trends Biochem. Sci.* 24 (8), 311–316. doi:10.1016/S0968-0004(99)01426-7

Shen, H., and Laird, P. W. (2013). Interplay between the Cancer Genome and Epigenome. *Cell.* 153 (1), 38–55. doi:10.1016/j.cell.2013.03.008

Shoaib, M., Chen, Q., Shi, X., Nair, N., Prasanna, C., Yang, R., et al. (2021). Histone H4 Lysine 20 Mono-Methylation Directly Facilitates Chromatin Openness and Promotes Transcription of Housekeeping Genes. *Nat. Commun.* 12 (1), 4800. doi:10.1038/s41467-021-25051-2

Shogren-KnaakShogren-Knaak, M., Ishii, H., Sun, J.-M., Pazin, M. J., Davie, J. R., and Peterson, C. L. (2006). Histone H4-K16 Acetylation Controls Chromatin Structure and Protein Interactions. *Science* 311 (5762), 844–847. doi:10.1126/science.1124000

Shukla, S., Agarwal, P., and Kumar, A. (2022). Disordered Regions Tune Order in Chromatin Organization and Function. *Biophys. Chem.* 281 (February), 106716. doi:10.1016/j.bpc.2021.106716

Smith, E., Lin, C., and Shilatifard, A. (2011). The Super Elongation Complex (SEC) and MLL in Development and Disease. *Genes. Dev.* 25 (7), 661–672. doi:10.1101/gad.2015411

Stec, I., Wright, T. J., van Ommende Boer, G.-J. B., de Boer, P. A. J., van Haeringen, A., Moorman, A. F. M., et al. (1998). WHSC1, a 90 Kb SET Domain-Containing Gene, Expressed in Early Development and Homologous to a Drosophila Dysmorphy Gene Maps in the Wolf-Hirschhorn Syndrome Critical Region and Is Fused to IgH in T(1;14) Multiple Myeloma. *Hum. Mol. Genet.* 7 (7), 1071–1082. doi:10.1093/hmg/7.7.1071

Strahl, B. D., and Allis, C. D. (2000). The Language of Covalent Histone Modifications. *Nature* 403 (6765), 41–45. doi:10.1038/47412

Sue, S.-C., Chen, J.-Y., Lee, S.-C., Wu, W.-g., and Huang, T.-h. (2004). Solution Structure and Heparin Interaction of Human Hepatoma-Derived Growth Factor. *J. Mol. Biol.* 343 (5), 1365–1377. doi:10.1016/j.jmb.2004.09.014

Suzuki, M. M., and Bird, A. (2008). DNA Methylation Landscapes: Provocative Insights from Epigenomics. *Nat. Rev. Genet.* 9 (6), 465–476. doi:10.1038/nrg2341

Tan, M., Luo, H., Lee, S., Jin, F., Yang, J. S., Montellier, E., et al. (2011). Identification of 67 Histone Marks and Histone Lysine Crotonylation as a New Type of Histone Modification. *Cell.* 146 (6), 1016–1028. doi:10.1016/J.CELL.2011.08.008

Taverna, S. D., Ilin, S., Rogers, R. S., Tanny, J. C., Lavender, H., Li, H., et al. (2006). Yng1 PHD Finger Binding to H3 Trimethylated at K4 Promotes NuA3 HAT Activity at K14 of H3 and Transcription at a Subset of Targeted ORFs. *Mol. Cell.* 24 (5), 785–796. doi:10.1016/j.molcel.2006.10.026

Treviño, L. S., Wang, Q., and Walker, C. L. (2015). Phosphorylation of Epigenetic "readers, Writers and Erasers": Implications for Developmental Reprogramming and the Epigenetic Basis for Health and Disease. *Prog. Biophysics Mol. Biol.* 118 (1–2), 8–13. doi:10.1016/j.pbiomolbio.2015.02.013

van Nuland, R., van Schaik, F. M., Simonis, M., van Heesch, S., Cuppen, E., Boelens, R., et al. (2013). Nucleosomal DNA Binding Drives the Recognition of H3K36-Methylated Nucleosomes by the PSIP1-PWWP Domain. *Epigenetics Chromatin* 6 (1), 12. doi:10.1186/1756-8935-6-12

Vezzoli, A., Bonadies, N., Allen, M. D., Freund, S. M. V., Santiveri, C. M., KvinlaugKvinlaug, B. T., et al. (2010). Molecular Basis of Histone H3K36me3 Recognition by the PWWP Domain of Brpf1. *Nat. Struct. Mol. Biol.* 17 (5), 617–619. doi:10.1038/nsmb.1797

Vollmuth, F., and Geyer, M. (2010). Interaction of Propionylated and Butyrylated Histone H3 Lysine Marks with Brd4 Bromodomains. *Angew. Chem. Int. Ed.* 49 (38), 6768–6772. doi:10.1002/ANIE.201002724

Walther, D. J., Peter, J.-U., Winter, S., Höltje, M., Paulmann, N., Grohmann, M., et al. (2003). Serotonylation of Small GTPases Is a Signal Transduction Pathway that Triggers Platelet α-Granule Release. *Cell.* 115 (7), 851–862. doi:10.1016/s0092-8674(03)01014-6

Wang, G. G., Song, J., Wang, Z., Dormann, H. L., Casadio, F., Li, H., et al. (2009). Haematopoietic Malignancies Caused by Dysregulation of a Chromatin-Binding PHD Finger. *Nature* 459 (7248), 847–851. doi:10.1038/nature08036

Wang, H., Farnung, L., Dienemann, C., and Cramer, P. (2020). Structure of H3K36-Methylated Nucleosome-PWWP Complex Reveals Multivalent Cross-Gyre Binding. *Nat. Struct. Mol. Biol.* 27 (1), 8–13. doi:10.1038/s41594-019-0345-4

Wang, W., Chen, Z., Mao, Z., Zhang, H., Ding, X., Chen, S., et al. (2011). Nucleolar Protein Spindlin1 Recognizes H3K4 Methylation and Stimulates the Expression of RRNA Genes. *EMBO Rep.* 12 (11), 1160–1166. doi:10.1038/embor.2011.184

Wang, W. K., Tereshko, V., Boccuni, P., MacGrogan, D., Nimer, S. D., and PatelPatel, D. J. (2003). Malignant Brain Tumor Repeats. *Structure* 11 (7), 775–789. doi:10.1016/S0969-2126(03)00127-8

Watts, S. W., PriestleyPriestley, J. R. C., and ThompsonThompson, J. M. (2009). Serotonylation of Vascular Proteins Important to Contraction. *PloS One* 4 (5), e5682. doi:10.1371/journal.pone.0005682

Xia, C., Tao, Y., Li, M., Che, T., and Qu, J. (2020). Protein Acetylation and Deacetylation: An Important Regulatory Modification in Gene Transcription (Review). *Exp. Ther. Med.* 20 (4), 2923–2940. doi:10.3892/etm.2020.9073

Xie, Z., Dai, J., Dai, L., Tan, M., Cheng, Z., Wu, Y., et al. (2012). Lysine Succinylation and Lysine Malonylation in Histones. *Mol. Cell. Proteomics* 11 (5), 100–107. doi:10.1074/MCP.M111.015875

Xie, Z., Zhang, D., Chung, D., Tang, Z., Huang, H., Dai, L., et al. (2016). Metabolic Regulation of Gene Expression by Histone Lysine β-Hydroxybutyrylation. *Mol. Cell.* 62 (2), 194–206. doi:10.1016/J.MOLCEL.2016.03.036

Xiong, X., Panchenko, T., Yang, S., Zhao, S., Yan, P., Zhang, W., et al. (2016). Selective Recognition of Histone Crotonylation by Double PHD Fingers of MOZ and DPF2. *Nat. Chem. Biol.* 12 (12), 1111–1118. doi:10.1038/nchembio.2218

Yang, N., Wang, W., Wang, Y., Wang, M., Zhao, Q., Rao, Z., et al. (2012). Distinct Mode of Methylated Lysine-4 of Histone H3 Recognition by Tandem Tudor-like Domains of Spindlin1. *Proc. Natl. Acad. Sci. U.S.A.* 109 (44), 17954–17959. doi:10.1073/pnas.1208517109

Yap, K. L., and Zhou, M.-M. (2010). Keeping it in the Family: Diverse Histone Recognition by Conserved Structural Folds. *Crit. Rev. Biochem. Mol. Biol.* 45 (6), 488–505. doi:10.3109/10409238.2010.512001

Yu, Y., Teng, Y., Liu, H., Reed, S. H., and Waters, R. (2005). UV Irradiation Stimulates Histone Acetylation and Chromatin Remodeling at a Repressed Yeast Locus. *Proc. Natl. Acad. Sci. U.S.A.* 102 (24), 8650–8655. doi:10.1073/pnas.0501458102

Yuan, C., Li, J., Mahajan, A., Poi, M. J., Byeon, I.-J. L., and Tsai, M.-D. (2004). Solution Structure of the Human Oncogenic Protein Gankyrin Containing Seven Ankyrin Repeats and Analysis of its Structure–Function Relationship,. *Biochemistry* 43 (38), 12152–12161. doi:10.1021/bi049116o

Zhang, D., Tang, Z., Huang, H., Zhou, G., Cui, C., Weng, Y., et al. (2019). Metabolic Regulation of Gene Expression by Histone Lactylation. *Nature* 574 (7779), 575–580. doi:10.1038/S41586-019-1678-1

Zhang, Q., Zeng, L., Zhao, C., Ju, Y., Konuma, T., and Zhou, M.-M. (2016). Structural Insights into Histone Crotonyl-Lysine Recognition by the AF9 YEATS Domain*Structure* 24, 1606–1612. doi:10.1016/j.str.2016.05.023

Zhao, D., Guan, H., Zhao, S., Mi, W., Wen, H., Li, Y., et al. (2016). YEATS2 Is a Selective Histone Crotonylation Reader. *Cell. Res.* 26, 629–632. doi:10.1038/cr.2016.49

Zhao, S., Allis, C. D., and Wang, G. G. (2021). The Language of Chromatin Modification in Human Cancers. *Nat. Rev. Cancer* 21 (7), 413–430. doi:10.1038/s41568-021-00357-x

Zhao, Y., and Garcia, B. A. (2015). Comprehensive Catalog of Currently Documented Histone Modifications. *Cold Spring Harb. Perspect. Biol.* 7 (9), a025064. doi:10.1101/cshperspect.a025064

ZhaoZhao, J., Chen, W., Pan, Y., Zhang, Y., Sun, H., Wang, H., et al. (2021). Structural Insights into the Recognition of Histone H3Q5 Serotonylation by WDR5. *Sci. Adv.* 7 (25), eabf4291. doi:10.1126/sciadv.abf4291

Zhu, Z., Han, Z., Halabelian, L., Yang, X., Ding, J., Zhang, N., et al. (2021). Identification of Lysine Isobutyrylation as a New Histone Modification Mark. *Nucleic Acids Res.* 49 (1), 177–189. doi:10.1093/NAR/GKAA1176

Conflict of Interest: The authors declare that the research was conducted in the absence of any commercial or financial relationships that could be construed as a potential conflict of interest.

Publisher's Note: All claims expressed in this article are solely those of the authors and do not necessarily represent those of their affiliated organizations, or those of the publisher, the editors, and the reviewers. Any product that may be evaluated in this article, or claim that may be made by its manufacturer, is not guaranteed or endorsed by the publisher.

frontiers | Frontiers in Genetics

ORIGINAL RESEARCH
published: 18 July 2022
doi: 10.3389/fgene.2022.887088

Heterogeneity of Organization of Subcompartments in DSB Repair Foci

*Natnael G. Abate and Michael J. Hendzel**

Departments of Oncology and Cell Biology, Faculty of Medicine and Dentistry, University of Alberta, Edmonton, AB, Canada

Cells assemble compartments around DNA double-strand breaks (DSBs). The assembly of this compartment is dependent on the phosphorylation of histone H2AX, the binding of MDC1 to phosphorylated H2AX, and the assembly of downstream signaling and repair components. The decision on whether to use homologous recombination or nonhomologous end-joining repair depends on competition between 53BP1 and BRCA1. A major point of control appears to be DNA replication and associated changes in the epigenetic state. This includes dilution of histone H4 dimethylation and an increase in acetylation of lysine residues on H2A and H4 that impair 53BP1 binding. In this article, we examined more closely the spatial relationship between 53BP1 and BRCA1 within the cell cycle. We find that 53BP1 can associate with early S-phase replicated chromatin and that the relative concentration of BRCA1 in DSB-associated compartments correlates with increased BRCA1 nuclear abundance as cells progress into and through S phase. In most cases during S phase, both BRCA1 and 53BP1 are recruited to these compartments. This occurs for both IR-induced DSBs and breaks targeted to an integrated LacO array through a LacI-Fok1-mCherry fusion protein. Having established that the array system replicates this heterogeneity, we further examined the spatial relationship between DNA repair components. This enabled us to precisely locate the DNA containing the break and map other proteins relative to that DNA. We find evidence for at least three subcompartments. The damaged DNA, single-stranded DNA generated from end resection of the array, and nuclease CtIP all localized to the center of the compartment. BRCA1 and 53BP1 largely occupied discrete regions of the focus. One of BRCA1 or 53BP1 overlaps with the array, while the other is more peripherally located. The array-overlapping protein occupied a larger volume than the array, CtIP, or single-stranded DNA (ssDNA). Rad51 often occupied a much larger volume than the array itself and was sometimes observed to be depleted in the array volume where the ssDNA exclusively localizes. These results highlight the complexity of molecular compartmentalization within DSB repair compartments.

Keywords: DNA double-stand break, fluorescence microscopy, homologous recombination (HR) pathway, nonhomologous end-joining (NHEJ), DNA repair, cell nucleus, nuclear compartmentalization

OPEN ACCESS

Edited by:
Christophe Thiriet, UMR6286 Unité de fonctionnalité et Ingénierie des Protéines (UFIP), France

Reviewed by:
Arvind Panday, Harvard Medical School, United States
Stephanie Panier, Max Planck Institute for Biology of Ageing, Germany

****Correspondence:***
Michael J. Hendzel
mhendzel@ualberta.ca

Specialty section:
This article was submitted to Epigenomics and Epigenetics, a section of the journal Frontiers in Genetics

Received: *01 March 2022*
Accepted: *26 May 2022*
Published: *18 July 2022*

Citation:
Abate NG and Hendzel MJ (2022) Heterogeneity of Organization of Subcompartments in DSB Repair Foci. Front. Genet. 13:887088. doi: 10.3389/fgene.2022.887088

INTRODUCTION

The preservation of genetic information is critical for cell and species survival. DNA double-strand breaks (DSBs) can compromise the integrity of this genetic information. Consequently, cells have evolved a complex DNA damage response that senses damage and orchestrates the proper repair and maintenance of genetic sequence. Upon DSB formation, the cell organizes up to 1.5 million base pairs surrounding the DSB into a nuclear compartment characterized by a histone mark, phosphorylated serine 139 of histone H2AX (γH2AX) (Iacovoni et al., 2010; Caron et al., 2012; Aymard et al., 2014; Aymard and Legube, 2016). This compartment acts as a repair site and source of signaling for cell cycle arrest until the DSB is repaired (Jackson, 2002; Bekker-Jensen and Mailand, 2010; Hustedt and Durocher, 2017). The compartment is initiated by the recruitment of the MRN complex (MRE11, RAD50, and NBS1) to the break (Lavin, 2004; Lee and Paull, 2005). The MRN complex can recognize the DSB and activate Ataxia-telangiectasia-mutated (ATM) kinase, which will phosphorylate histone H2AX at serine 139 to generate γH2AX (Stucki and Jackson, 2004; Bekker-Jensen et al., 2005). ATM kinase can also phosphorylate mediator of DNA damage checkpoint (MDC1), forming a complex with γH2AX to recruit E3 ligase ring finger 8 (RNF8) (Huen et al., 2007; Kolas et al., 2007; Mailand et al., 2007). Ubiquitylation mediated through RNF8 recruits E3 ligase ring finger 168 (RNF168) (Kolas et al., 2007; Mailand et al., 2007; Doil et al., 2009; Stewart et al., 2009). RNF168-mediated ubiquitylation that occurs on histone H2A K13/15 is directly recognized by 53BP1 at DNA DSB, while polyubiquitylation by RNF8/UBC13 generates K63-linked ubiquitin chains that can bind BRCA1 A complex through ubiquitin-interacting motifs in RAP80 (Kolas et al., 2007; Mailand et al., 2007; Sobhian et al., 2007; Wang et al., 2007; Mattiroli et al., 2012; Fradet-Turcotte et al., 2013).

Among the epigenetic changes that regulate the repair pathway, those that impact the competition between 53BP1 and BRCA1 and the downstream effectors are of particular interest because they dictate the repair outcome. Upon recruitment of 53BP1 to DNA DSB sites, 53BP1 can recruit other effector proteins such as RIF1 and PTIP1 (Gong et al., 2009; Zimmermann et al., 2013), while BRCA1 can form a complex with CtIP and MRN to promote 5′–3′ end resection and recruit PALB2/BRCA2 complex to promote Rad51 loading onto the 3′ (Chen et al., 2008; Escribano-Díaz et al., 2013; Simonetta et al., 2018; Krais et al., 2021). 53BP1 and BRCA1 compete to determine the DSB repair pathway choice (Bouwman et al., 2010; Bunting et al., 2010). This may be reflected in their spatial organization within DSB-associated compartments. BRCA1 is proposed to displace 53BP1 from chromatin near the DSB, consistent with super-resolution fluorescence microscopy experiments revealing peripheral localization of 53BP1 accompanied by accumulation of BRCA1 toward the interior of the compartment (Chapman et al., 2012; Feng et al., 2015). However, transmission electron microscopy revealed a peripheral localization of chromatin in DSB-associated compartments (Strickfaden et al., 2015). This suggested that repair might take place on the periphery of the compartment, and its central domain may function in sequestering molecules away from the break.

To better understand how the organization of repair proteins within the DSB-associated compartment relates to DSB repair pathway choice, we need to know the location of the DNA containing the break. At present, visualizing γH2AX using specific antibodies is the best method to identify DNA DSB sites. However, chromatin immunoprecipitation experiments have demonstrated that histones and γH2AX may be displaced from the actual site of the break (Arnould et al., 2021), and consequently, we cannot determine the exact position of the DNA break using γH2AX. This complicates interpreting the relationship between how molecules are organized within the repair compartment and how this organization relates to function. This uncertainty is increased if liquid compartments are forming in association with the break.

Liquid–liquid unmixing and phase separation are emerging mechanisms of generating membraneless compartments within the nucleus (Razin and Gavrilov, 2020; Nesterov et al., 2021). Poly(ADP-ribose) can initiate phase separation at DNA damage sites and plays an important role in regulating phase separation in the cytoplasm (Altmeyer et al., 2015; Rack et al., 2021). Similarly, both RNA and 53BP1 have been proposed to initiate phase separation within DSB-associated compartments (Kilic et al., 2019; Pessina et al., 2019; Guo et al., 2021; Zhang et al., 2022). In this light, it is important to appreciate that the sites of steady-state accumulation of these proteins may reflect their preferred partitioning into a distinct solvent microenvironment and may not reflect the sites of action on the broken DNA or association with chromatin. In other words, differences in localization may not simply reflect differences in distribution along the chromatin fiber. Thus, it is critical to know the location of the break site(s) within the compartment. This is possible using a model DSB system where integrated arrays of the Lac operon sequence are inserted into the genome and specifically targeted by a fusion protein of the LacI DNA-binding domain and the Fok1 endonuclease domain. The incorporation of a fluorescent protein tag on this fusion protein enables the direct visualization of the break site, and the organization of DNA damage response proteins can be studied in relation to DSB.

In this study, we demonstrated that there are multiple classes of DSB repair compartments based on BRCA1 and 53BP1 abundance and organization. These morphological classifications correlate well with cell cycle progression-associated changes in 53BP1 foci abundance reported previously (Chapman et al., 2013; Escribano-Díaz et al., 2013; Feng et al., 2015; Michelena et al., 2021; Swift et al., 2021). This might be explained by epigenetic changes accompanying the replication of chromatin. However, in contrast to our expectations, we found that 53BP1 can colocalize with newly replicated DNA following ionizing radiation treatment. There is an ongoing increase in 53BP1 nuclear concentration throughout the cell cycle, while BRCA1 increases rapidly at the onset of the S phase. Typically, both proteins were present in individual foci, but the relative abundance in foci correlated with BRCA1 expression, rather than 53BP1, and total BRCA1 nuclear

abundance until late S phase, where 53BP1 formed few foci and had a more prominent nuclear staining outside of foci. After demonstrating the conservation of DSB compartment heterogeneity in the model Lac array DSB system, we examined the relationship between 53BP1, BRCA1, and downstream effectors relative to the location of the DSB (Tang et al., 2013; Arnould et al., 2021). This array system contains 265 tandem repeat LacI binding sites where DSBs can be generated by a LacI–Fok1 fusion protein that is further tagged with mCherry to enable visualization of the array. This allows unambiguous positioning of the damaged DNA. We found that the damaged DNA is located centrally and is the compartment enriched in ssDNA and DNA end resection factors. In contrast, NHEJ and HR factors exist in larger volumes that vary in their spatial relationship with the array. Deconvolution of confocal images suggests that there are at least three subcompartments in the DSB repair compartment—the DNA containing the break, biomolecules associated with 53BP1, and biomolecules associated with BRCA1. While either 53BP1 or BRCA1, but not both, can be found on arrays in individual cells, these compartments, unlike ssDNA and CtIP, extend beyond the dimensions of the array and are further surrounded by the complementary BRCA1-rich or 53BP1-rich compartment. Moreover, since cells containing more centralized 53BP1 have lower DNA content than those with centralized BRCA1, BRCA1 displacement of 53BP1 from the center of the focus may depend on S-phase progression. Since DNA is found in all three compartments, subcompartments could arise through decorating the chromatin fiber or through liquid–liquid unmixing into separate compartments through phase separation.

MATERIALS AND METHODS

Cell Culture

WT U2OS and U2OS expressing the Lac array were maintained in Dulbecco's modified Eagle medium (DMEM) with 10% FBS and 1% penicillin–streptomycin at 37°C. All cells were maintained in sterile cell culture and tested for mycoplasma.

Immunofluorescence

Cells were grown on a glass coverslip in a 35-mm tissue culture dish. DSB formation was initiated and then cells were fixed 1 h later with 4% paraformaldehyde for at least 10 min at room temperature. Following fixation, the fixative was removed and 1–2 ml of 1× PBS was added. PBS was removed and cells were permeabilized by adding 1–2 ml of PBS 0.5% Triton X-100 for at least 5 min. Cells were rinsed two times with 1× PBS and left in 1× PBS. Cells were incubated with a primary antibody by placing the coverslip cell side down on a 30-µl drop of antibody on Parafilm, avoiding air bubbles, for 45 min. The cover of a 35-mm dish was left on top to minimize dehydration. Cells were rinsed once with 1× PBS with 0.1% Triton X-100 to permeabilize the membrane of the cells and then rinsed again with 1× PBS and left in 1× PBS. Cells were incubated with a secondary antibody by placing the coverslip cell side down on a 30-µl drop of antibody on a Parafilm for 45 min. After 45 min, cells were rinsed once with 1× PBS with 0.1% Triton X-100 and twice with 1× PBS. Coverslips were then mounted cell side down onto slides with mounting media (20 µl; 90% glycerol, 10% PBS, 0.1% *p*-phenylenediamine, and multichannel TetraSpeck microspheres) per coverslip.

Initiating DNA Double-Strand Breaks

U2OS 265 cells were gifted from the Roger Greenberg's laboratory (Tang et al., 2013). Cells were grown on a glass coverslip and treated with 0.5 mM Shield1 and 10 mM 4-OHT for 1 h before fixation with 4% paraformaldehyde (Shield1 [632189], Takara; 4-OHT [68047-06–03], Sigma-Aldrich). Cells were washed with PBS and permeabilized with 0.5% Triton X-100 in PBS for 5 min and incubated with primary antibody for 45 min and washed with PBS. Then, incubated with secondary antibody for another 45 min and washed with PBS. Coverslips were mounted on slides using mounting media (90% glycerol, 10% PBS, and 0.1% *p*-phenylenediamine).

Antibodies, Chemicals, and Reagents

Conjugated 53BP1 rabbit polyclonal antibody was obtained from Novus (NB100-309AF488); BRCA1 mouse monoclonal antibody (5C-6934) from Santa Cruz; BRCA1 rabbit polyclonal antibody (07-434) and γH2AX mouse monoclonal antibody (2535291) from Millipore; rabbit polyclonal antibody (39117) from Active Motif; RAD51 rabbit polyclonal antibody (20-001) from Bio Academia; CtIP mouse monoclonal antibody (61141) and RPA rabbit polyclonal antibody (AB76420) from Abcam; RAP80 rabbit polyclonal antibody (14466), RIF1 rabbit polyclonal antibody (A300-569A), mouse monoclonal antibody (200-301-H50), and BrdU mouse monoclonal antibody (B5002) from Rockland; EdU Click-iT (C10338) from Sigma-Aldrich; Alexa 488 goat anti-mouse antibody (A11OC1) from Molecular Probes; Cy5 goat anti-mouse antibody (195-175-166), anti-rabbit antibody (111-175-144), and Cy3 goat anti-mouse antibody (115-165-146) from Jackson.

BrdU-ssDNA

U2OS 265 cells were preincubated with 10 µM BrdU for 18 h, followed by 1-h incubation with Shield1 and 4-OHT. Cells were fixed with 4% paraformaldehyde for 10 min at room temperature. Cells were washed with PBS and permeabilized with 0.5% Triton X-100 in PBS for 5 min and incubated with anti-mouse BrdU antibody (B5002) overnight.

EdU Pulse Labeling

U2OS WT cells were grown on a glass coverslip in a 35-mm tissue culture plate. Cells were treated with 10 µM 5′-ethynyl-2-deoxyuridine (EdU) for 30 min and 6 h, irradiated with 2 Gy, and then fixed after 1 h with 4% paraformaldehyde. Cells were washed with PBS and permeabilized with 0.5% Triton X-100 in PBS for 5 min. Cells were again washed with PBS and incubated with EdU Click-IT reaction (Imaging Kit, Invitrogen) using Alexa 488 Azide dye for 1 h to label the newly replicated chromatin.

Image Acquisition and Quantification

Images were captured using a Leica SP8 laser scanning confocal microscope (100× 1.4 N.A. oil immersion objective). Tetra beads

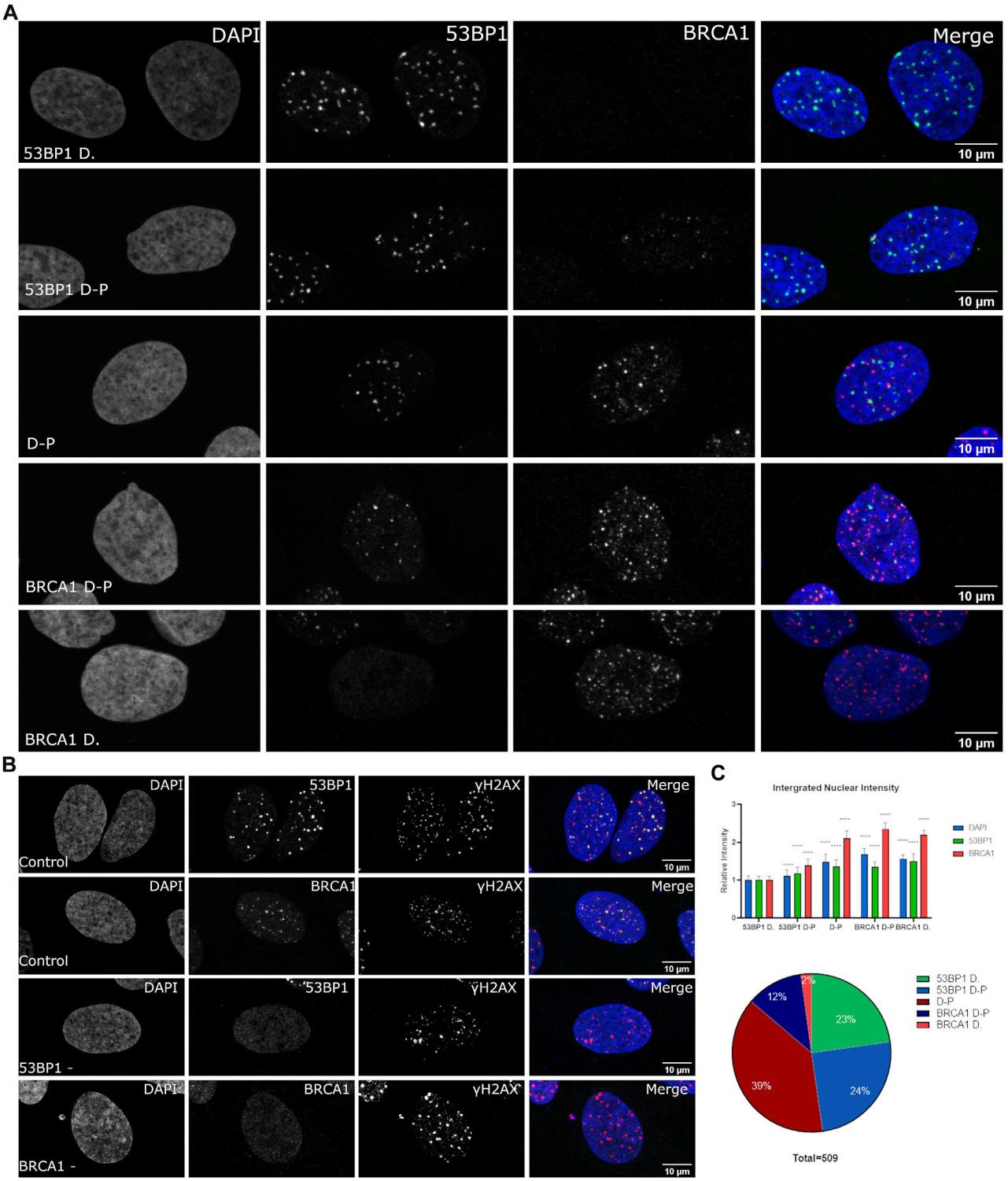

FIGURE 1 | Variation in BRCA1 and 53BP1 recruitment in asynchronous cell populations. WT U2OS cells were fixed 1 h post 2 Gy irradiation and immunostained with antibodies for 53BP1, BRCA1, and γH2AX showing heterogeneity in recruitment to DSB. **(A)** Cells were classified subjectively into five categories based on their relative abundance of BRCA1 and 53BP1 in foci: 53BP1-dominant cell (53BP1 D), 53BP1-dominant double-positive cell (53BP1 D–P), 53BP1–BRCA1–positive cell (D–P), BRCA1 dominant double-positive cell (BRCA1 D–P), and BRCA1-dominant cell (BRCA1 D). Cells were normalized using the intensity values of the 53BP1-dominant category, where cells predominately are in G1 with low DAPI intensity. **(B)** DNA double-strand breaks were confirmed in cells that were negative for 53BP1 foci and cells that were negative for BRCA1 foci using γH2AX as a marker for DSB foci. **(C)** The DNA, BRCA1, and 53BP1 were measured for 509 cells obtained from four

(*Continued*)

FIGURE 1 | separate experiments. These were then plotted for the total nuclear content using the integrated nuclear intensity of each normalized to the 53BP1-dominant category. The proportion of cells in each category is also shown. Quantification of different categories. Error bars represent mean ± SD, ns represents nonsignificant ($p \geq 0.01$), *$p \leq 0.1$, **$p \leq 0.01$, ***$p \leq 0.001$, ****$p \leq 0.0001$ obtained from pair-wise comparisons of each value relative to the 53BP1-dominant category using a Student's *t* test. The scale bar represents 10 μm.

were added for image corrections and to assess and correct channel alignment. Between 5 and 10 z-plane images were acquired with 200–400 nm step size using a 405-nm laser for DAPI and a white light laser for Alexa 488, Cy3, mCherry, and Cy5. To excite DAPI, 405 nm laser was used, 488 nm excitation was used for Alexa 488-labeled antibodies, 594 nm excitation for mCherry, 561 nm excitation for Cy3, and 649 nm excitation for Cy5. Images were analyzed using Bitplane Imaris and ImageJ software. DAPI intensity was used to quantify DNA and identify the cell cycle position and observe the relative difference between 53BP1 and BRCA1. Quantification of images was done post-baseline subtraction to remove any background signal. Maximum intensity projection images were used to generate the summed nuclear intensities. Radial profile plots were obtained using ImageJ in which an area was selected and a radial increase of 75 nm per pixel.

RESULTS

Heterogeneity in 53BP1 and BRCA1 Recruitment

53BP1 and BRCA1 play a critical role in the cell cycle-dependent regulation of DNA repair. 53BP1 is often used interchangeably with histone H2AX phosphorylation to enumerate DSBs despite cell cycle-dependent relationships on 53BP1 foci abundance being reported (Escribano-Díaz et al., 2013; Feng et al., 2015; Michelena et al., 2021; Swift et al., 2021). We sought to assess the heterogeneity in their association with sites of DNA DSBs within asynchronous cell populations. We conducted immunofluorescence using wild type U2OS cells and specific antibodies directed against 53BP1 and BRCA1. We treated cells with 2Gy radiation, fixed 1 h post-treatment, and determined differences in DSB-associated compartments between individual cells. We classified individual cells based on their apparent dominance of 53BP1 versus BRCA1 in merged datasets and then quantified the relative nuclear content of BRCA1, 53BP1, and DNA (**Figure 1A**). To obtain the nuclear DNA content, we measured the integrated nuclear intensity of DAPI, 53BP1, and BRCA1. To confirm the presence of DSBs in cells that contained either no 53BP1 or no BRCA1 foci, cells were costained for phosphorylated H2AX. These cells show abundant DSBs despite the failure to recruit one of 53BP1 or BRCA1 (**Figure 1B**). Cells that strongly recruit 53BP1 but have very little or no BRCA1 in foci were found to have the lowest DNA content and low BRCA1 total nuclear intensity (**Figure 1C**). The progression toward BRCA1 dominance correlates with increased BRCA1 total nuclear intensity and DNA content. 53BP1 concentration also increases with DNA content but is abundant in all categories. These results demonstrate the considerable heterogeneity of DSB foci composition in both individual cells and in a population and, in general, correlate well with the reported loss of 53BP1 during the progression into S phase (Escribano-Díaz et al., 2013; Feng et al., 2015). Note that the BRCA1-dominant double-positive (BRCA1 D-P) category had slightly higher BRCA1 content and DNA content than the BRCA1-dominant category. This suggests that this arises later in the cell cycle than in the BRCA1-dominant category and is consistent with the recovery of 53BP1 binding in G2 (Simonetta et al., 2018). Other features of this subset are the presence of BRCA1 single-positive foci and a more apparent nucleoplasmic signal for 53BP1 relative to the G1- and early S-phase cells.

Changes in DSB Repair Focus Composition During S-Phase Progression

To better understand the transition from 53BP1-dominated foci to BRCA1-dominated foci in relation to the cell cycle, we pulse-labeled cells with 5′-ethinyl-2′deoxyurdine (EdU) for 30 min prior to irradiation and then fixed cells 1 h after irradiation. This enables the differences in BRCA1 and 53BP1 content to be characterized relative to progression through S phase (**Figure 2A,B**). Notably, 53BP1-dominant and 53BP1-dominant double-positive (53BP1 D-P) phenotypes both do not incorporate EdU and differ primarily in BRCA1 total nuclear concentration (**Figure 2C**). In the 53BP1-dominant category, BRCA1 generates very weak nuclear staining and is difficult to detect. Consistent with these cells being pre-replicative, they have the lowest amount of DNA and are not distinguishable based on DNA content (**Figure 2C**). The early S-phase cells show label incorporation broadly throughout the interior of the nucleus (**Figure 2A**, patterns 1,2), while this labeling pattern gets increasingly coarse as cells progress through S phase (**Figure 2A**, patterns 3–5, **Figure 2B**). The late S-phase cells are easily identified based on the replication of heterochromatin being visible as comparatively large domains of incorporation, often in perinuclear or perinucleolar regions (**Figure 2B**). Note that in these cells, we can assume that most of the remaining chromatin has been replicated. These cells are notable for their reduction in the number of 53BP1-positive foci and a more diffuse nuclear 53BP1 signal outside of DSB sites (**Figure 2A**). However, even in these cells, there are consistently examples of foci that are strongly biased toward 53BP1 (circles in **Figure 2B**). In S-phase cells, there are BRCA1-positive, 53BP1-negative/low foci, foci that are double-positive, and 53BP1-positive, BRCA1-negative/low foci. The final class of cells is positive for both, but negative for EdU incorporation (circled in **Figure 2A**). These correspond to the BRCA1 D-P phenotype in **Figure 1** and reflect G2 cells based on their DNA content.

A loss of 53BP1 foci has been previously associated with progression through S phase (Pei et al., 2011; Saredi et al., 2016). A number of epigenetic mechanisms associated with

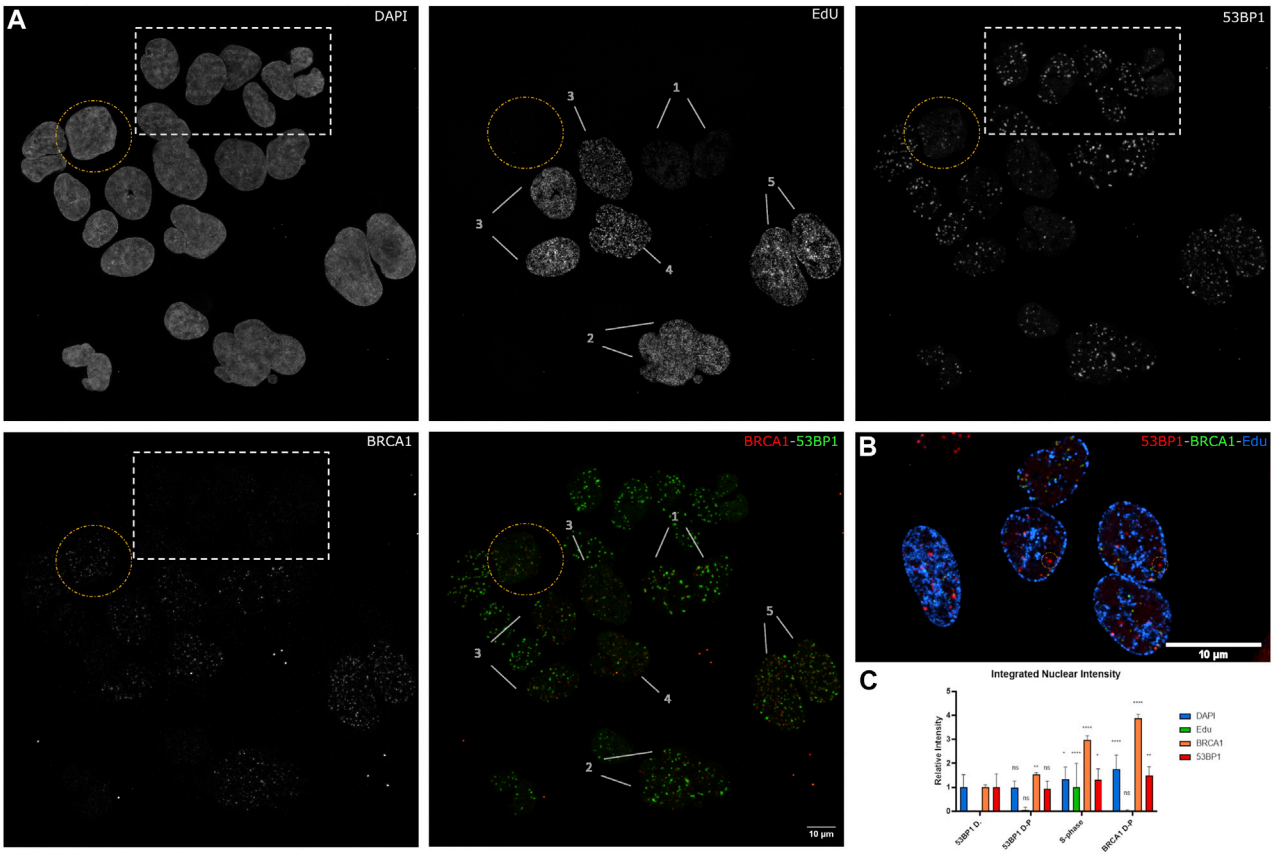

FIGURE 2 | The relationship between S-phase progression, BRCA1, and 53BP1. **(A)** U2OS cells were pulse labeled with EdU 30 min before 2 Gy irradiation. Cells were fixed 1 h postirradiation and immunostained with Click-IT reaction, 53PB1, and BRCA1. **(1–5)** indicate increasing progression through S phase. The yellow circle highlights a BRCA1-dominant non-S-phase cell. The white box indicates 53BP1-dominant non-S-phase cells and **(1–5)** indicate progression through S phase with **1** being the earliest stage and **5** being the latest stage. **(B)** Examples of late S-phase cells showing 53BP1-rich foci. **(C)** Quantification of BRCA1, 53BP1, and DNA intensities with S phase categorized as one and normalized to 53BP1-dominant category. Error bars represent mean ± SD, ns represents nonsignificant ($p \geq 0.01$), $^{*}p \leq 0.1$, $^{**}p \leq 0.01$, $^{***}p \leq 0.001$, $^{****}p \leq 0.0001$ obtained from pair-wise comparisons of each value relative to the 53BP1-dominant category using a Student's *t* test. Note that multiwavelength fluorescent TetraSpeck microspheres were added for alignment corrections. These are present as small fluorescent dots outside of the cells in all channels. The scale bar represents 10 µm.

DNA replication, including dilution of histone H4 lysine 20 methylation as newly synthesized histones are deposited, the Tip60-dependent acetylation of histone H2A on lysines 13 and 15, and the MOF-dependent acetylation of H4 lysine 16 (Akhtar and Becker, 2000; Li et al., 2010; Jacquet et al., 2016). Consistent with this, Pellegrino et al. (2017) examined the distribution of 53BP1 foci relative to EdU incorporated into newly synthesized DNA and found that 53BP1 foci did not colocalize with newly replicated chromatin. Thus, we would predict that in early S phase, where 53BP1 foci are prominent, they will localize to unreplicated DNA, and the replicated chromatin will be refractory to 53BP1 assembly. Although this epigenetic change has been shown to reduce 53BP1 occupancy in the presence or absence of BRCA1, these epigenetic differences may not be sufficient to prevent the binding of 53BP1 to newly replicated DNA in S phase (Michelena et al., 2021). **Figure 3A** shows the relationship between EdU incorporation, BRCA1, and 53BP1 in an early S-phase nucleus. Examples of EdU-labeled chromatin that are double positive for BRCA1 and 53BP1 are highlighted with yellow circles. Examples of 53BP1 located on unreplicated chromatin are illustrated with white circles. We analyzed EdU incorporation at the centers of 53BP1 intensity versus centers of BRCA1 intensity. These results show considerable overlap in the range of EdU concentrations associated with BRCA1 and 53BP1. While there is a tendency for BRCA1 foci to be more closely associated with sites of EdU incorporation, 53BP1 can associate with replicated chromatin and BRCA1 is found in unlabelled regions. Rather than being determined by the underlying chromatin state, the abundance of BRCA1-rich foci correlates more strongly with BRCA1 abundance (**Figure 3**, see also **Figures 1C**, **2A,C** note the concordant increase in 53BP1 concentration outside of foci). To better understand how BRCA1 total nuclear concentration changes during S-phase progression, we pulsed cells for 6 h in the absence of DNA damage, divided cells into fully labeled, partially labeled early in S phase, and partially labeled late (late S-phase staining pattern with reduced EdU incorporation). Plotting the integrated nuclear intensity revealed a rapid increase in BRCA1 content as labeling increased in the partially labeled

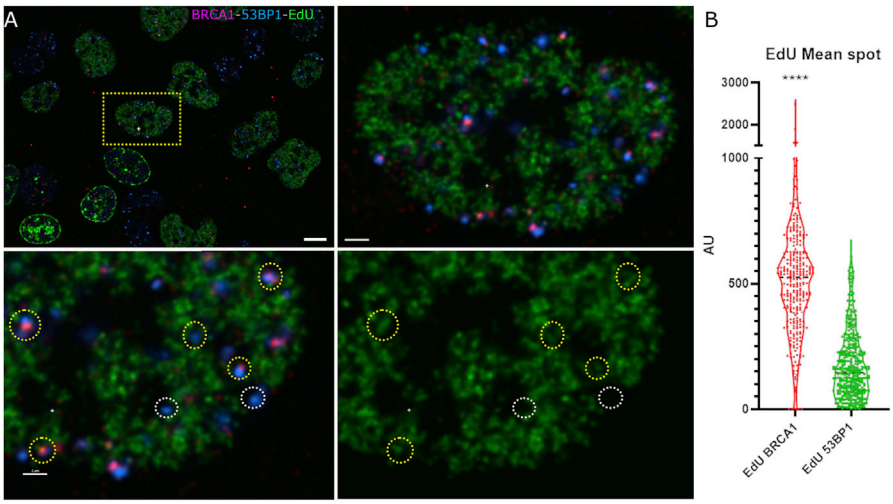

FIGURE 3 | 53BP1-rich foci are found in association with newly replicated chromatin in early S phase. **(A)** U2OS cells pulse labeled with EdU and irradiated were examined for newly replicated chromatin distribution (EdU, green), 53BP1 (blue), and BRCA1 (red). An early S-phase cell is highlighted in the upper left panel showing the field of labeled cells. The top right panel shows a higher magnification view of the same cell. The bottom two panels show a subregion of this nucleus with (left) and without (right) the 53BP1 and BRCA1 channels. The yellow circles highlight chromatin that is positive for 53BP1. These same foci show varying amounts of BRCA1. The white circles highlight 53BP1 foci that clearly reside in regions that have not been replicated. **(B)** Violin plot showing the EdU mean intensity in BRCA1 versus 53BP1 foci in early S-phase cells where EdU is indicative of DNA replication. Quantification of EdU BRCA1 mean intensity versus EdU 53BP1 mean intensity, $^{****}p \leq 0.0001$. The scale bar represents 2 μm.

early S-phase cells. This suggests that limited BRCA1 concentrations may influence focus composition in early S phase in addition to changes in epigenetic state that favor BRCA1 binding over 53BP1.

Spatial Relationships of 53BP1 and BRCA1 to the DSB Site

Super-resolution studies of DNA DSBs reveal that individual classes of proteins are not homogeneously distributed throughout the focus (Reindl et al., 2017, 2022; Schwarz et al., 2019; Michelena et al., 2021). For example, BRCA1 and 53BP1 occupy distinct regions of the compartment (Chapman et al., 2012; Mok and Henderson, 2012; Schwarz et al., 2019). Understanding these relationships is complicated by cell cycle-dependent differences in BRCA1 and 53BP1 spatial organization in foci. It is further complicated by the lack of knowledge of where the broken DNA resides within the focus. We sought to examine the spatial organization of individual DSB compartments by exploiting a system where an array of Lac repressor DNA-binding sequences are inserted into U2OS cells. An inducible and rapidly degradable fusion protein containing the LacI DNA-binding domain fused to the Fok1 nuclease domain and mCherry allows us to rapidly induce DSBs and identify the location of the break sites within the assembled focus. We first confirmed that the same distributions of 53BP1 and BRCA1 could be observed in the array system as we observed for IR-induced DSBs. **Figure 4A** shows that the induction of the nuclease results in the labeling of a single spot within the nucleus that enriches the LacI fusion protein. We found evidence for the same classes of foci as we observed in the asynchronous cell population. Both BRCA1 D-P and 53BP1 D-P foci were observed with the dominant protein localizing more centrally. Notably, both BRCA1 and 53BP1 show localization that overlaps with and extends beyond the array. This can be seen in the radial profile distribution of BRCA1-dominant and 53BP1-dominant foci (**Figure 4C**). The array is most centrally localized while the major array-associated protein (53BP1 or BRCA1) associates with the array but extends beyond it. The minor component (53BP1 or BRCA1) shows a maximum that is well outside the position of the array, consistent with the more peripheral localization observed in images. The radial distribution profiles also reveal that these compartments are larger in the 53BP1-dominant foci versus the BRCA1-dominant foci. We confirmed the presence of DSBs using phosphorylated histone H2AX as a marker (**Figure 4B**). Thus, the array system behaves similarly to the IR-induced breaks and is suitable for more careful analysis of the relationships between these proteins and the break site.

The Location of the Damaged DNA Relative to DSB-Associated Nanocompartments

The ability to directly detect the location of the DSB using the Lac repressor fusion protein allowed us to further assess spatial relationships relative to the break site. First, we addressed the location of DNA end resection. Cells were labeled with BrdU, and then the nuclease expression was induced. One hour later, cells were stained with an anti-BrdU antibody. In the absence of DNA denaturation, this detects only ssDNA and enables the identification of regions of the genome undergoing resection during DSB repair. We found that the BrdU always localized within the array volume (**Figure 5A**). This argues

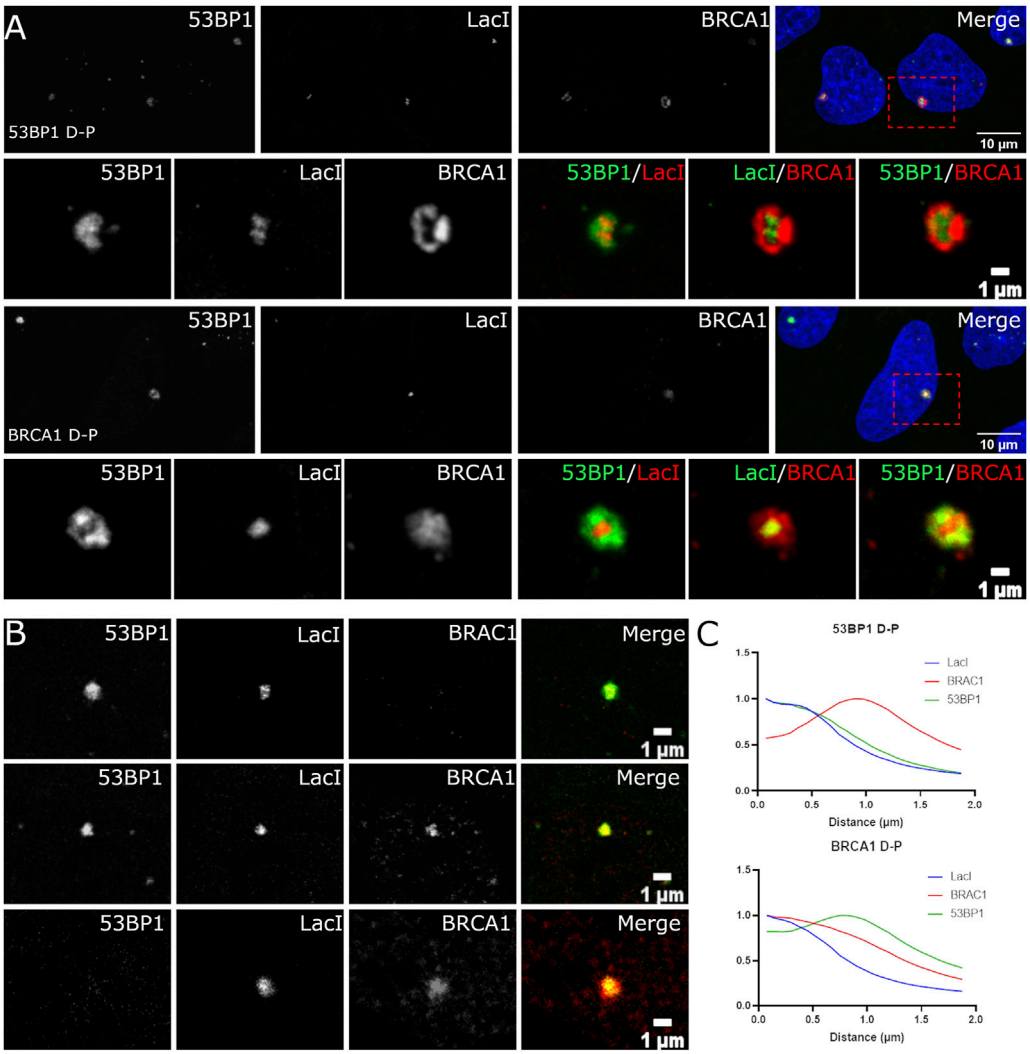

FIGURE 4 | Localization of BRCA1 and 53BP1 relative to the site of the damaged DNA. **(A)** U2OS 265 cells were fixed 1 h post-treatment with 4-OHT and Shield1 to induce DSB formation and then immune stained with 53BP1 and BRCA1. Examples of 53BP1- and BRCA1-dominant double-positive foci are shown. The panel on the far right in rows 1 and 3 show the nucleus with DAPI in blue, BRCA1 in red, and 53BP1 in green. The highlighted region is shown enlarged in the corresponding panels underneath. **(B)** The foci were categorized based on the relative difference in DSB occupancy: 53BP1-dominant cell (53BP1 D), 53BP1-dominant double-positive cell (53BP1 D-P), 53BP1–BRCA1-positive cell (D-P), BRCA1-dominant double-positive cell (BRCA1 D-P), and BRCA1-dominant cell (BRCA1 D). **(C)** Radial profile plots of 30 DSB over three experiments reveal three overlapping distributions that differ in the centralization of BRCA1 or 53BP1. The scale bar represents 10 μm for images illustrating the nucleus (top panel) and scale bar represents 1 μm for individual breaks.

against a separate ssDNA compartment formed at DNA damage sites. 53BP1 was found on the periphery of the array in BrdU-positive cells. In contrast, we could observe BrdU-positive cells where BRCA1 was surrounding the array as well as BrdU-positive cells where BRCA1 associates with the array. When BRCA1 colocalized with the array and the BrdU, BRCA1 appeared to occupy a larger volume encompassing part of the periphery of the array. This indicates that the resected single-stranded DNA does not form a separate compartment from the double-stranded DNA when undergoing end resection, but that there may be a larger regulatory microenvironment that surrounds the array. We concluded that the ssDNA occupies a similar spatial space as the Lac repressor bound to the LacI repeats.

We next determined the location of CtIP, which is associated with BRCA1 and promotes the initiation of DNA end resection. CtIP was exclusively found within the volume of the array (**Figure 5B**). Notably, there remained two categories of BRCA1 distribution. We found that 32/84 recruit BRCA1 and CtIP where BRCA1 colocalized with CtIP on the array, while 52/84 exhibit BRCA1 on the periphery despite CtIP association with the array. Similar to the observations with BrdU, CtIP appears confined to the array while BRCA1 can extend beyond the array volume (**Figure 4B**). The CtIP localization is consistent with the BrdU labeling of single-stranded DNA and suggests that DNA end resection takes place directly on the DNA without spatial reorganization. It is also consistent with distinct BRCA1

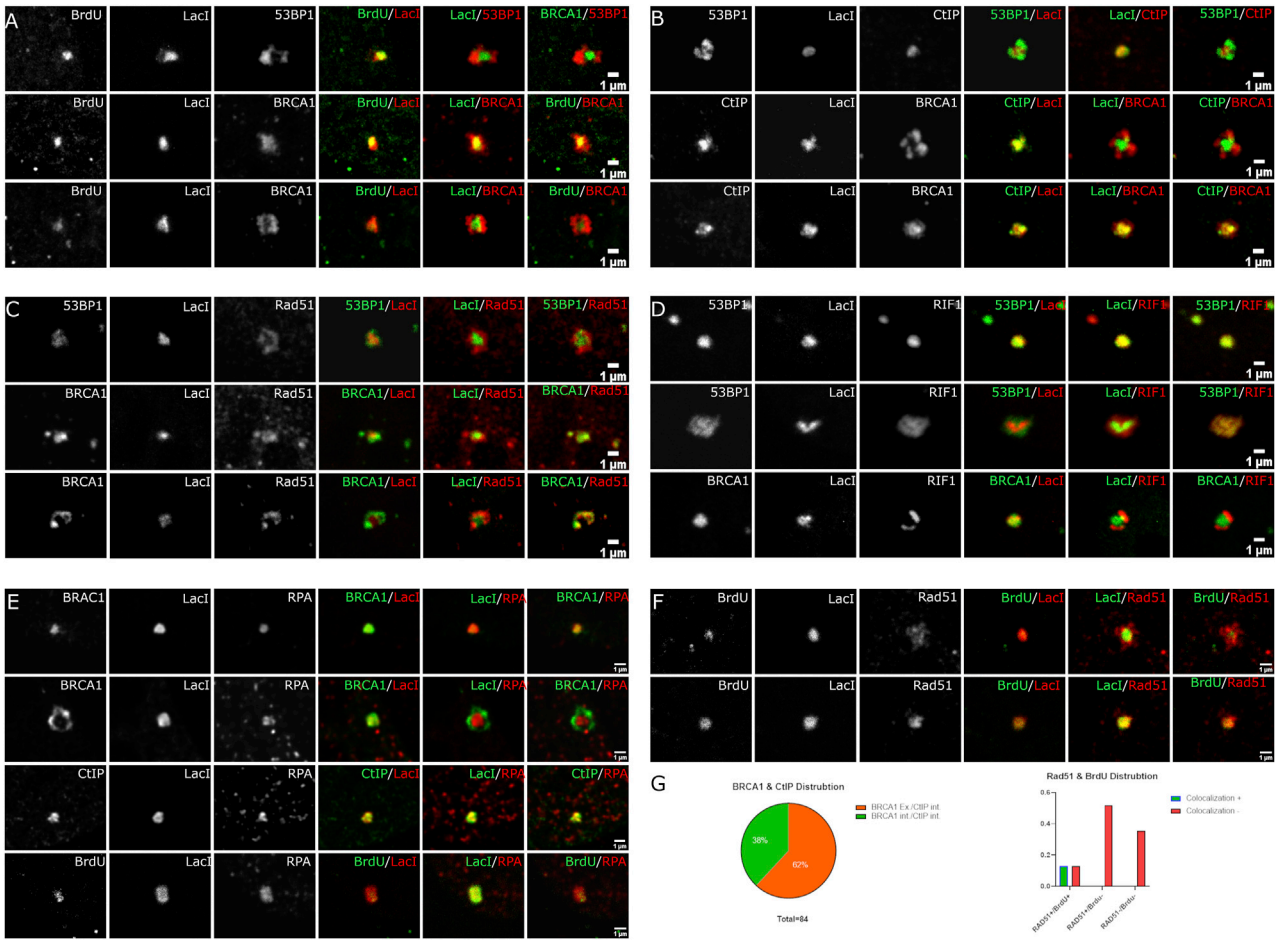

FIGURE 5 | Spatial localization of BrdU labeling, CtIP, RAD51, Rif1, and RPA relative to LacI and the DSB compartment. U2OS 265 Fok1 induced DSB and fixed 1 h post-treatment and stained with antibodies recognizing 53BP1, BRCA1, BrdU, CtIP, Rad51, Rif1, and RPA. For the BrdU experiment, cells were labeled with BrdU for 18 h prior to treatment with Shield1 and 4-OHT. **(A)** BrdU distribution is compared to LacI. **(B)** CtIP localization is compared to LacI. Recruitment of Rad51 versus 53BP1 and BRCA1 relative to LacI **(C)** and Rif1 recruitment relative to 53BP1, BRCA1, and LacI **(D)**. **(E)** Localization of RPA compared with BRCA1, CtIP, and BrdU. **(F)** Different occupancy of Rad51 relative to end resection. **(G)** BRCA1 and CtIP distribution at DSB sites. BRCA1 exterior and CtIP interior versus BRCA1 interior and CtIP interior localizing to LacI. Rad51 and BrdU colocalization at the site of DNA break. The scale bar represents 1 µm.

complexes accumulating at DSBs and the BRCA1-independent activity of CtIP (Reczek et al., 2013; Polato et al., 2014).

We next assessed the relationship between Rad51 and the array (**Figure 5C**). Rad51 differed from CtIP and BrdU. We observed more than one organization of Rad51 relative to the array site. Rad51 could be associated predominantly with the periphery of the array or partially overlapping the array. We did not observe complete localization within the array volume, unlike BrdU and CtIP. This indicates that Rad51 is accumulating beyond the regions containing single-stranded DNA. It is unclear whether it is forming filaments in these regions.

Finally, we examined the 53BP1-associated inhibitor of DNA end resection, RIF1 (**Figure 5D**). RIF1 behaved as expected. In cells where 53BP1 encompasses the array volume, RIF1 also colocalized to the same volume. In cells where 53BP1 is associated with the peripheral regions of the array and excluded from the volume containing the array, RIF1 is also excluded from the array volume. When compared with BRCA1, like 53BP1, RIF1 localizes in a complementary rather than overlapping volume. This suggests that RIF1 localization is exclusively defined by 53BP1, consistent with their complex formation (Zimmermann et al., 2013).

There Are at Least Three Subcompartments in DSB-Associated Foci

The different distributions of 53BP1, BRCA1, single-stranded DNA, effector proteins, and the site of the DNA targeted with DSBs suggested that there may be more than two compartments associated with DNA DSB repair foci. To assess this further, we used deconvolution of laser scanning confocal images to improve resolution. **Figure 6** shows BRCA1 (red), 53BP1 (green), and the Lac repressor–Fok1 fusion protein bound to the array (blue). BRCA1 and 53BP1 occupy distinct regions of the compartment independent of which is more centrally located. While the centrally located protein overlaps with the volume of the

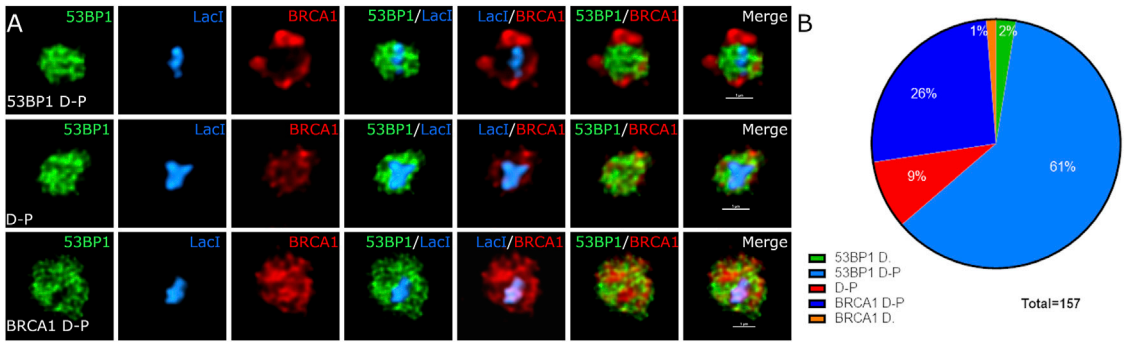

FIGURE 6 | The site of DNA damage and relative proteins occupy specific spatially resolved sites. U2OS 265 cells were treated with 4-OHT and Shield1 to allow the translocation of mCherry–Fok1–Lac repressor to induce the DSB. Antibodies targeting 53BP1 and BRCA1 were used to determine recruitment to the DSB. **(A)** BRCA1 in green, 53BP1 in red, and Lac repressor in blue. Lightning—adaptive deconvolution (Leica)—was used to improve the resolution and image quality. **(B)** The proportion of cells in 53BP1-dominant cell (53BP1 D), 53BP1-dominant double-positive cell (53BP1 D-P), 53BP1–BRCA1-positive cell (D-P), BRCA1-dominant double-positive cell (BRCA1 D-P), and BRCA1-dominant cell (BRCA1 D) is also shown. The images were further magnified 400% using interpolation. The scale bar represents 1 μm.

array, the protein typically does not completely occupy the same volume as the array and extends beyond the array volume. This suggests that there are at least three subcompartments within the focus including the damaged DNA, represented by the array location, the primary responding pathway, occupying the array-proximal volume, and the competing pathway factors, displaced to the outer volume of the compartment.

DISCUSSION

In this study, we investigated the variation in the organization and content of 53BP1 and BRCA1 in asynchronous cell populations upon DSB formation and demonstrated that there are sufficient similarities and differences to enable classification based on phenotype. When doing so, we find similar results to cell cycle-dependent studies demonstrating a gradual loss of 53BP1 foci during S-phase progression (Michelena et al., 2021). 53BP1 is a chromatin-binding protein that recognizes histone H4K20 mono/dimethylation through its Tudor domain and RNF168-mediated H2A K13/K15 ubiquitination through its UDR domain (Pei et al., 2011; Fradet-Turcotte et al., 2013). Inhibition of 53BP1 binding to chromatin may occur through epigenetic changes, including inhibitory histone acetylations and/or replication-dependent dilution of H4K20 methylation. During the S/G2 phase, Tip60 can acetylate H2A K13/15, which inhibits RNF168-mediated ubiquitination, and hMOF can acetylate H4K16, which inhibits the binding of 53BP1 to H4K20 methylation (Taipale et al., 2005; Mattiroli et al., 2012; Jacquet et al., 2016). Since histone H4 is deposited in an unmethylated form, dilution of the H4K20 methylation required for 53BP1 binding occurs during S phase. This is also correlated with the loss of 53BP1 binding (Saredi et al., 2016; Simonetta et al., 2018). The persistence of 53BP1 on newly replicated DNA early in S phase suggests that these replication-associated epigenetic changes are not sufficient to prevent 53BP1-rich focus assembly. Rather, our results suggest that BRCA1 nuclear concentration likely also plays a role. BRCA1 is cell cycle regulated in its expression (Jin et al., 1997; Choudhury et al., 2004). Consistent with this, we found that cells that assembled 53BP1-dominated foci split into two populations based on the amount of BRCA1 expression during G1. During S-phase progression, cells increasingly show BRCA1-rich foci as BRCA1 nuclear concentrations increase. The BARD1–BRCA1 complex can recognize H4K20me0 and H2A K15 ubiquitination to promote HR in S/G2 phase to preferentially bind newly replicated chromatin at the expense of 53BP1 (Saredi et al., 2016; Nakamura et al., 2019; Becker et al., 2021). The combination of increased expression and increased affinity of the BRCA1–BARD1 complex may be critical to mediate this reduction in 53BP1 occupancy. This is consistent with the observation that 53BP1 binding to S-phase damage sites is increased upon BRCA1 knockdown (Chapman et al., 2013; Escribano-Díaz et al., 2013; Michelena et al., 2021). Overall, the results are most consistent with an active competition based on the relative affinities of 53BP1 versus BRCA1 for the different epigenetic states pre- and postreplication, but argue that these modifications bias, rather than dictate, the outcome of this competition.

Our principal objective in this study was to understand protein organization within the DSB-associated compartment. For this purpose, we employed an integrated array system where we could induce a targeted DSB and, most importantly, know the location of the DNA containing the DSB. This allowed us to evaluate DSB compartment assembly in relation to the damage site rather than define localization relative to other DNA damage response proteins. Typically, phosphorylated histone H2AX is used to identify the site of a DNA DSB. However, phosphorylated histone H2AX is typically excluded from the site of the break (Arnould et al., 2021). A second advantage of the system is that the array is sufficiently large that it is easily identified, and subcompartments are characterized without a requirement for super-resolution microscopy approaches. We had previously used electron spectroscopic imaging, an analytical transmission electron microscopy capable of identifying DNA and RNA based

on its abundance of phosphorus, to demonstrate that chromatin is compartmentalized within DSB repair foci (Strickfaden et al., 2015). Our observation that chromatin was enriched on the exterior of foci with 53BP1-rich centers suggested that this could be a site of sequestration away from the repair site. By knowing the location of the DNA DSB, we can now rule this out. The electron microscopy results, however, suggest that chromatin density is much lower in the interior of the focus. While there is evidence from super-resolution microscopy experiments that BRCA1 centralizes and displaces 53BP1 to the periphery (Chapman et al., 2012), we observed that the opposite organization, with centralized 53BP1 and peripherally located BRCA1, also exists within populations of asynchronous cells. While this could reflect an early stage in a process of displacement, this appears unlikely given that this organization correlates with overall DNA content, which further correlates with BRCA1 abundance. Hence, we favor a model where both can bind, that their affinity is modulated by replication-dependent epigenetic changes in the chromatin template, and influenced by the relative expression of each protein. Similar conclusions were recently reached by Michelena et al. (2021).

The central region of the compartment containing the array was determined to be the site of DNA end resection and single-stranded DNA accumulation. BrdU labeling revealed that the single-stranded DNA co-occupied the same volume as the array. If liquid–liquid phase separation occurs within DSB compartments, the separation of single-stranded DNA into a separate compartment could conceivably take place, so this is important to establish. CtIP has also been shown to colocalize with BRCA1 by structured illumination microscopy (Chapman et al., 2012), consistent with our results obtained on the array; however, we found instances where the two signals appeared independent. This could reflect an abundance of the BRCA1 A complex (Kim et al., 2007; Sobhian et al., 2007; Wang et al., 2007) relative to BRCA1/CtIP complexes, or it could reflect BRCA1-independent CtIP localization (Sobhian et al., 2007; Polato et al., 2014). In these instances, BRCA1 was positioned external to CtIP. Rad51, unlike CtIP, tended to localize on the immediate periphery of the array as well as associate with it. It may be that the 1-h time point precedes the assembly of Rad51 into filaments and that it accumulates prior to assembly. As expected, the 53BP1-associated protein RIF1 colocalized with 53BP1 and could exist either on the array or, more commonly, displaced from the region containing the array.

Triple-labeling experiments revealed that the array occupies a distinct space that only partially overlaps with BRCA1 or 53BP1-rich domains. It is notable that BRCA1 and 53BP1, when localized to the array, also encompass it, while CtIP or BrdU (ssDNA) are constrained within the volume of the array. It was also surprising to observe Rad51 surrounding the array rather than confined to the array volume. It may be that this reflects an early point in the assembly onto ssDNA. This suggests the existence of at least three microenvironments within the DNA damage focus. Ultrastructural studies would assist in the interpretation of DSB repair focus organization.

DATA AVAILABILITY STATEMENT

The raw data supporting the conclusions of this article will be made available by the authors, without undue reservation.

AUTHOR CONTRIBUTIONS

The experiments were designed by NGA and MJH. The experiments were completed and analyzed by NGA with support from MJH. The manuscript was written by NGA and MJH.

FUNDING

This work was supported by the Canadian Institutes of Health Research.

ACKNOWLEDGMENTS

We thank members of the Hendzel laboratory and the Department of Oncology Cell Imaging Facility for experimental support. This work was funded by the Canadian Institute of Health Research (CIHR). We thank Dr. Roger Greenberg (University of Pennsylvania) for the kind gift of U2OS 265 cells expressing the mCherry–LacI–Fok1 construct and Ismail Ismail for advice and reagents. MJH is a Canada Research Chair in the Cell Biology and Dynamics of the Genome.

REFERENCES

Akhtar, A., and Becker, P. B. (2000). Activation of Transcription through Histone H4 Acetylation by MOF, an Acetyltransferase Essential for Dosage Compensation in Drosophila. *Mol. Cell* 5 (2), 367–375. doi:10.1016/s1097-2765(00)80431-1

Altmeyer, M., Neelsen, K. J., Teloni, F., Pozdnyakova, I., Pellegrino, S., Grøfte, M., et al. (2015). Liquid Demixing of Intrinsically Disordered Proteins Is Seeded by poly(ADP-Ribose). *Nat. Commun.* 6. doi:10.1038/ncomms9088

Arnould, C., Rocher, V., Finoux, A.-L., Clouaire, T., Li, K., Zhou, F., et al. (2021). Loop Extrusion as a Mechanism for Formation of DNA Damage Repair Foci. *Nature* 590, 660–665. doi:10.1038/s41586-021-03193-z

Aymard, F., Bugler, B., Schmidt, C. K., Guillou, E., Caron, P., Briois, S., et al. (2014). Transcriptionally Active Chromatin Recruits Homologous Recombination at DNA Double-Strand Breaks. *Nat. Struct. Mol. Biol.* 21, 366–374. doi:10.1038/nsmb.2796

Aymard, F., and Legube, G. (2016). A TAD Closer to ATM. *Mol. Cell. Oncol.* 3, e1134411. doi:10.1080/23723556.2015.1134411

Becker, J. R., Clifford, G., Bonnet, C., Groth, A., Wilson, M. D., and Chapman, J. R. (2021). BARD1 Reads H2A Lysine 15 Ubiquitination to Direct Homologous Recombination. *Nature* 596, 433–437. doi:10.1038/s41586-021-03776-w

Bekker-Jensen, S., Lukas, C., Melander, F., Bartek, J., and Lukas, J. (2005). Dynamic Assembly and Sustained Retention of 53BP1 at the Sites of DNA Damage Are Controlled by Mdc1/NFBD1. *J. Cell Biol.* 170, 201–211. doi:10.1083/jcb.200503043

Bekker-Jensen, S., and Mailand, N. (2010). Assembly and Function of DNA Double-Strand Break Repair Foci in Mammalian Cells. *DNA Repair* 9, 1219–1228. doi:10.1016/j.dnarep.2010.09.010

Bouwman, P., Aly, A., Escandell, J. M., Pieterse, M., Bartkova, J., van der Gulden, H., et al. (2010). 53BP1 Loss Rescues BRCA1 Deficiency and Is Associated with Triple-Negative and BRCA-Mutated Breast Cancers. *Nat. Struct. Mol. Biol.* 17, 688–695. doi:10.1038/nsmb.1831

Bunting, S. F., Callén, E., Wong, N., Chen, H.-T., Polato, F., Gunn, A., et al. (2010). 53BP1 Inhibits Homologous Recombination in Brca1-Deficient Cells by Blocking Resection of DNA Breaks. *Cell* 141, 243–254. doi:10.1016/j.cell.2010.03.012

Caron, P., Aymard, F., Iacovoni, J. S., Briois, S., Canitrot, Y., Bugler, B., et al. (2012). Cohesin Protects Genes against γH2AX Induced by DNA Double-Strand Breaks. *PLoS Genet.* 8, e1002460. doi:10.1371/journal.pgen.1002460

Chapman, J. R., Barral, P., Vannier, J.-B., Borel, V., Steger, M., Tomas-Loba, A., et al. (2013). RIF1 Is Essential for 53BP1-dependent Nonhomologous End Joining and Suppression of DNA Double-Strand Break Resection. *Mol. Cell* 49, 858–871. doi:10.1016/j.molcel.2013.01.002

Chapman, J. R., Sossick, A. J., Boulton, S. J., and Jackson, S. P. (2012). BRCA1-associated Exclusion of 53BP1 from DNA Damage Sites Underlies Temporal Control of DNA Repair. *J. Cell Sci.* 125, 3529–3534. doi:10.1242/jcs.105353

Chen, L., Nievera, C. J., Lee, A. Y.-L., and Wu, X. (2008). Cell Cycle-dependent Complex Formation of BRCA1·CtIP·MRN Is Important for DNA Double-Strand Break Repair. *J. Biol. Chem.* 283, 7713–7720. doi:10.1074/jbc.M710245200

Choudhury, A. D., Xu, H., and Baer, R. (2004). Ubiquitination and Proteasomal Degradation of the BRCA1 Tumor Suppressor Is Regulated during Cell Cycle Progression. *J. Biol. Chem.* 279, 33909–33918. doi:10.1074/jbc.M403646200

Doil, C., Mailand, N., Bekker-Jensen, S., Menard, P., Larsen, D. H., Pepperkok, R., et al. (2009). RNF168 Binds and Amplifies Ubiquitin Conjugates on Damaged Chromosomes to Allow Accumulation of Repair Proteins. *Cell* 136, 435–446. doi:10.1016/j.cell.2008.12.041

Escribano-Díaz, C., Orthwein, A., Fradet-Turcotte, A., Xing, M., Young, J. T. F., Tkáč, J., et al. (2013). A Cell Cycle-dependent Regulatory Circuit Composed of 53BP1-RIF1 and BRCA1-CtIP Controls DNA Repair Pathway Choice. *Mol. Cell* 49, 872–883. doi:10.1016/j.molcel.2013.01.001

Feng, L., Li, N., Li, Y., Wang, J., Gao, M., Wang, W., et al. (2015). Cell Cycle-dependent Inhibition of 53BP1 Signaling by BRCA1. *Cell Discov.* 1. doi:10.1038/celldisc.2015.19

Fradet-Turcotte, A., Canny, M. D., Escribano-Díaz, C., Orthwein, A., Leung, C. C. Y., Huang, H., et al. (2013). 53BP1 Is a Reader of the DNA-Damage-Induced H2A Lys 15 Ubiquitin Mark. *Nature* 499, 50–54. doi:10.1038/nature12318

Gong, Z., Cho, Y.-W., Kim, J.-E., Ge, K., and Chen, J. (2009). Accumulation of Pax2 Transactivation Domain Interaction Protein (PTIP) at Sites of DNA Breaks via RNF8-dependent Pathway Is Required for Cell Survival after DNA Damage. *J. Biol. Chem.* 284, 7284–7293. doi:10.1074/jbc.M809158200

Guo, Q., Shi, X., and Wang, X. (2021). RNA and Liquid-Liquid Phase Separation. *Non-coding RNA Res.* 6, 92–99. doi:10.1016/j.ncrna.2021.04.003

Huen, M. S. Y., Grant, R., Manke, I., Minn, K., Yu, X., Yaffe, M. B., et al. (2007). RNF8 Transduces the DNA-Damage Signal via Histone Ubiquitylation and Checkpoint Protein Assembly. *Cell* 131, 901–914. doi:10.1016/j.cell.2007.09.041

Hustedt, N., and Durocher, D. (2017). The Control of DNA Repair by the Cell Cycle. *Nat. Cell Biol.* 19, 1–9. doi:10.1038/ncb3452

Iacovoni, J. S., Caron, P., Lassadi, I., Nicolas, E., Massip, L., Trouche, D., et al. (2010). High-resolution Profiling of γH2AX Around DNA Double Strand Breaks in the Mammalian Genome. *Embo J.* 29, 1446–1457. doi:10.1038/emboj.2010.38

Jackson, S. P. (2002). Sensing and Repairing DNA Double-Strand Breaks. *Carcinogenesis* 23, 687–696. doi:10.1043/carcin/23.5.687

Jacquet, K., Fradet-Turcotte, A., Avvakumov, N., Lambert, J.-P., Roques, C., Pandita, R. K., et al. (2016). The TIP60 Complex Regulates Bivalent Chromatin Recognition by 53BP1 through Direct H4K20me Binding and H2AK15 Acetylation. *Mol. Cell* 62, 409–421. doi:10.1016/j.molcel.2016.03.031

Jin, Y., Xu, X. L., Yang, M.-C. W., Wei, F., Ayi, T.-C., Bowcock, A. M., et al. (1997). Cell Cycle-dependent Colocalization of BARD1 and BRCA1 Proteins in Discrete Nuclear Domains. *Proc. Natl. Acad. Sci.* 94 (22), 12075–12080. doi:10.1073/pnas.94.22.12075

Kilic, S., Lezaja, A., Gatti, M., Bianco, E., Michelena, J., Imhof, R., et al. (2019). Phase Separation of 53 BP 1 Determines Liquid-like Behavior of DNA Repair Compartments. *Embo J.* 38. doi:10.15252/embj.2018101379

Kim, H., Chen, J., and Yu, X. (2007). Ubiquitin-Binding Protein RAP80 Mediates BRCA1-dependent DNA Damage Response. *Science* 316, 1202–1205. doi:10.1126/science.1139621

Kolas, N. K., Chapman, J. R., Nakada, S., Ylanko, J., Chahwan, R., Sweeney, F. D., et al. (2007). Orchestration of the DNA-Damage Response by the RNF8 Ubiquitin Ligase. *Science* 318 (5856), 1637–1640. doi:10.1126/science.1150034

Krais, J. J., Wang, Y., Patel, P., Basu, J., Bernhardy, A. J., and Johnson, N. (2021). RNF168-mediated Localization of BARD1 Recruits the BRCA1-PALB2 Complex to DNA Damage. *Nat. Commun.* 12. doi:10.1038/s41467-021-25346-4

Lavin, M. F. (2004). The Mre11 Complex and ATM: A Two-Way Functional Interaction in Recognising and Signaling DNA Double Strand Breaks. *DNA Repair* 3, 1515–1520. doi:10.1016/j.dnarep.2004.07.001

Lee, J.-H., and Paull, T. T. (2005). ATM Activation by DNA Double-Strand Breaks through the Mre11-Rad50-Nbs1 Complex. *Science* 308 (5721), 551–554. doi:10.1126/science.1108297

Li, X., Corsa, C. A. S., Pan, P. W., Wu, L., Ferguson, D., Yu, X., et al. (2010). MOF and H4 K16 Acetylation Play Important Roles in DNA Damage Repair by Modulating Recruitment of DNA Damage Repair Protein Mdc1. *Mol. Cell Biol.* 30, 5335–5347. doi:10.1128/mcb.00350-10

Mailand, N., Bekker-Jensen, S., Faustrup, H., Melander, F., Bartek, J., Lukas, C., et al. (2007). RNF8 Ubiquitylates Histones at DNA Double-Strand Breaks and Promotes Assembly of Repair Proteins. *Cell* 131, 887–900. doi:10.1016/j.cell.2007.09.040

Mattiroli, F., Vissers, J. H. A., van Dijk, W. J., Ikpa, P., Citterio, E., Vermeulen, W., et al. (2012). RNF168 Ubiquitinates K13-15 on H2A/H2AX to Drive DNA Damage Signaling. *Cell* 150, 1182–1195. doi:10.1016/j.cell.2012.08.005

Michelena, J., Pellegrino, S., Spegg, V., and Altmeyer, M. (2021). Replicated Chromatin Curtails 53BP1 Recruitment in BRCA1-Proficient and BRCA1-Deficient Cells. *Life Sci. Alliance* 4, e202101023–10. doi:10.26508/LSA.202101023

Mok, M. T. S., and Henderson, B. R. (2012). Three-dimensional Imaging Reveals the Spatial Separation of γH2AX-MDC1-53BP1 and RNF8-Rnf168-BRCA1-A Complexes at Ionizing Radiation-Induced Foci. *Radiotherapy Oncol.* 103, 415–420. doi:10.1016/j.radonc.2012.04.009

Nakamura, K., Saredi, G., Becker, J. R., Foster, B. M., Nguyen, N. v., Beyer, T. E., et al. (2019). H4K20me0 Recognition by BRCA1-BARD1 Directs Homologous Recombination to Sister Chromatids. *Nat. Cell Biol.* 21, 311–318. doi:10.1038/s41556-019-0282-9

Nesterov, S. v., Ilyinsky, N. S., and Uversky, V. N. (2021). Liquid-liquid Phase Separation as a Common Organizing Principle of Intracellular Space and Biomembranes Providing Dynamic Adaptive Responses. *Biochimica Biophysica Acta (BBA) - Mol. Cell Res.* 1868, 119102. doi:10.1016/j.bbamcr.2021.119102

Pei, H., Zhang, L., Luo, K., Qin, Y., Chesi, M., Fei, F., et al. (2011). MMSET Regulates Histone H4K20 Methylation and 53BP1 Accumulation at DNA Damage Sites. *Nature* 470, 124–128. doi:10.1038/nature09658

Pessina, F., Giavazzi, F., Yin, Y., Gioia, U., Vitelli, V., Galbiati, A., et al. (2019). Functional Transcription Promoters at DNA Double-Strand Breaks Mediate RNA-Driven Phase Separation of Damage-Response Factors. *Nat. Cell Biol.* 21, 1286–1299. doi:10.1038/s41556-019-0392-4

Polato, F., Callen, E., Wong, N., Faryabi, R., Bunting, S., Chen, H.-T., et al. (2014). CtIP-mediated Resection Is Essential for Viability and Can Operate Independently of BRCA1. *J. Exp. Med.* 211, 1027–1036. doi:10.1084/jem.20131939

Rack, J. G. M., Liu, Q., Zorzini, V., Voorneveld, J., Ariza, A., Honarmand Ebrahimi, K., et al. (2021). Mechanistic Insights into the Three Steps of poly(ADP-Ribosylation) Reversal. *Nat. Commun.* 12. doi:10.1038/s41467-021-24723-3

Razin, S. v., and Gavrilov, A. A. (2020). The Role of Liquid-Liquid Phase Separation in the Compartmentalization of Cell Nucleus and Spatial Genome Organization. *Biochem. Mosc.* 85, 643–650. doi:10.1134/S0006297920060012

Reczek, C. R., Szabolcs, M., Stark, J. M., Ludwig, T., and Baer, R. (2013). The Interaction between CtIP and BRCA1 Is Not Essential for Resection-Mediated DNA Repair or Tumor Suppression. *J. Cell Biol.* 201, 693–707. doi:10.1083/jcb.201302145

Reindl, J., Girst, S., Walsh, D. W. M., Greubel, C., Schwarz, B., Siebenwirth, C., et al. (2017). Chromatin Organization Revealed by Nanostructure of Irradiation Induced γH2AX, 53BP1 and Rad51 Foci. *Sci. Rep.* 7. doi:10.1038/srep40616

Reindl, J., Kundrat, P., Girst, S., Sammer, M., Schwarz, B., and Dollinger, G. (2022). Dosimetry of Heavy Ion Exposure to Human Cells Using Nanoscopic Imaging of Double Strand Break Repair Protein Clusters. *Sci. Rep.* 12. doi:10.1038/s41598-022-05413-6

Saredi, G., Huang, H., Hammond, C. M., Alabert, C., Bekker-Jensen, S., Forne, I., et al. (2016). H4K20me0 Marks Post-replicative Chromatin and Recruits the TONSL-Mms22l DNA Repair Complex. *Nature* 534, 714–718. doi:10.1038/nature18312

Schwarz, B., Friedl, A. A., Girst, S., Dollinger, G., and Reindl, J. (2019). Nanoscopic Analysis of 53BP1, BRCA1 and Rad51 Reveals New Insights in Temporal Progression of DNA-Repair and Pathway Choice. *Mutat. Research/Fundamental Mol. Mech. Mutagen.* 816-818, 111675–111818. doi:10.1016/j.mrfmmm.2019.111675

Simonetta, M., de Krijger, I., Serrat, J., Moatti, N., Fortunato, D., Hoekman, L., et al. (2018). H4K20me2 Distinguishes Pre-replicative from Post-replicative Chromatin to Appropriately Direct DNA Repair Pathway Choice by 53BP1-RIF1-Mad2l2. *Cell Cycle* 17, 124–136. doi:10.1080/15384101.2017.1404210

Sobhian, B., Shao, G., Lilli, D. R., Culhane, A. C., Moreau, L. A., Xia, B., et al. (2007). RAP80 Targets BRCA1 to Specific Ubiquitin Structures at DNA Damage Sites. *Science* 316, 1198–1202. doi:10.1126/science.1139516

Stewart, G. S., Panier, S., Townsend, K., Al-Hakim, A. K., Kolas, N. K., Miller, E. S., et al. (2009). The RIDDLE Syndrome Protein Mediates a Ubiquitin-Dependent Signaling Cascade at Sites of DNA Damage. *Cell* 136, 420–434. doi:10.1016/j.cell.2008.12.042

Strickfaden, H., Xu, Z. Z., and Hendzel, M. J. (2015). Visualization of miniSOG Tagged DNA Repair Proteins in Combination with Electron Spectroscopic Imaging (ESI). *JoVE* 103. doi:10.3791/52893

Stucki, M., and Jackson, S. P. (2004). MDC1/NFBD1: A Key Regulator of the DNA Damage Response in Higher Eukaryotes. *DNA Repair* 3, 953–957. doi:10.1016/j.dnarep.2004.03.007

Swift, M. L., Beishline, K., Flashner, S., and Azizkhan-Clifford, J. (2021). DSB Repair Pathway Choice Is Regulated by Recruitment of 53BP1 through Cell Cycle-dependent Regulation of Sp1. *Cell Rep.* 34, 108840. doi:10.1016/j.celrep.2021.108840

Taipale, M., Rea, S., Richter, K., Vilar, A., Lichter, P., Imhof, A., et al. (2005). hMOF Histone Acetyltransferase Is Required for Histone H4 Lysine 16 Acetylation in Mammalian Cells. *Mol. Cell Biol.* 25, 6798–6810. doi:10.1128/mcb.25.15.6798-6810.2005

Tang, J., Cho, N. W., Cui, G., Manion, E. M., Shanbhag, N. M., Botuyan, M. V., et al. (2013). Acetylation Limits 53BP1 Association with Damaged Chromatin to Promote Homologous Recombination. *Nat. Struct. Mol. Biol.* 20, 317–325. doi:10.1038/nsmb.2499

Wang, B., Matsuoka, S., Ballif, B. A., Zhang, D., Smogorzewska, A., Gygi, S. P., et al. (2007). Abraxas and RAP80 Form a BRCA1 Protein Complex Required for the DNA Damage Response. *Science* 316, 1194–1198. doi:10.1126/science.1139476

Zhang, L., Geng, X., Wang, F., Tang, J., Ichida, Y., Sharma, A., et al. (2022). 53BP1 Regulates Heterochromatin through Liquid Phase Separation. *Nat. Commun.* 13, 360. doi:10.1038/s41467-022-28019-y

Zimmermann, M., Lottersberger, F., Buonomo, S. B., Sfeir, A., and de Lange, T. (2013). 53BP1 Regulates DSB Repair Using Rif1 to Control 5′ End Resection. *Science* 339, 700–704. doi:10.1126/science.1231573

Conflict of Interest: The authors declare that the research was conducted in the absence of any commercial or financial relationships that could be construed as a potential conflict of interest.

Publisher's Note: All claims expressed in this article are solely those of the authors and do not necessarily represent those of their affiliated organizations or those of the publisher, the editors and the reviewers. Any product that may be evaluated in this article, or claim that may be made by its manufacturer, is not guaranteed or endorsed by the publisher.

frontiers | Frontiers in Genetics

TYPE Original Research
PUBLISHED 26 August 2022
DOI 10.3389/fgene.2022.876862

OPEN ACCESS

EDITED BY
Dileep Vasudevan,
Institute of Life Sciences (ILS), India

REVIEWED BY
Davit Potoyan,
Iowa State University, United States
Shinpei Yamaguchi,
Osaka University, Japan

*CORRESPONDENCE
Michael J. Hendzel,
mhendzel@ualberta.ca

SPECIALTY SECTION
This article was submitted to Epigenomics and Epigenetics, a section of the journal Frontiers in Genetics

RECEIVED 15 February 2022
ACCEPTED 18 July 2022
PUBLISHED 26 August 2022

CITATION
Roemer A, Mohammed L, Strickfaden H, Underhill DA and Hendzel MJ (2022), Mechanisms governing the accessibility of DNA damage proteins to constitutive heterochromatin. *Front. Genet.* 13:876862. doi: 10.3389/fgene.2022.876862

Mechanisms governing the accessibility of DNA damage proteins to constitutive heterochromatin

Anastasia Roemer, Lanah Mohammed, Hilmar Strickfaden, D. Alan Underhill and Michael J. Hendzel*

Department of Oncology, Faculty of Medicine and Dentistry, University of Alberta, Edmonton, AB, Canada

Chromatin is thought to regulate the accessibility of the underlying DNA sequence to machinery that transcribes and repairs the DNA. Heterochromatin is chromatin that maintains a sufficiently high density of DNA packing to be visible by light microscopy throughout the cell cycle and is thought to be most restrictive to transcription. Several studies have suggested that larger proteins and protein complexes are attenuated in their access to heterochromatin. In addition, heterochromatin domains may be associated with phase separated liquid condensates adding further complexity to the regulation of protein concentration within chromocenters. This provides a solvent environment distinct from the nucleoplasm, and proteins that are not size restricted in accessing this liquid environment may partition between the nucleoplasm and heterochromatin based on relative solubility. In this study, we assessed the accessibility of constitutive heterochromatin in mouse cells, which is organized into large and easily identifiable chromocenters, to fluorescently tagged DNA damage response proteins. We find that proteins larger than the expected 10 nm size limit can access the interior of heterochromatin. We find that the sensor proteins Ku70 and PARP1 enrich in mouse chromocenters. At the same time, MRE11 shows variability within an asynchronous population that ranges from depleted to enriched but is primarily homogeneously distribution between chromocenters and the nucleoplasm. While larger downstream proteins such as ATM, BRCA1, and 53BP1 are commonly depleted in chromocenters, they show a wide range of concentrations, with none being depleted beyond approximately 75%. Contradicting exclusively size-dependent accessibility, many smaller proteins, including EGFP, are also depleted in chromocenters. Our results are consistent with minimal size-dependent selectivity but a distinct solvent environment explaining reduced concentrations of diffusing nucleoplasmic proteins within the volume of the chromocenter.

KEYWORDS

constitutive heterochromatin, accessibility, phase separation, diffusion, cell nucleus, live cell imaging microscopy, DNA damage (DDR), double-strand break (DSB) repair

Introduction

Pericentric heterochromatin is the region of chromatin juxtaposed to the centromeres and is composed of major satellite repeats (Guenatri et al., 2004). In mouse nuclei, pericentric heterochromatin forms cytologically visible "chromocenters" with DNA stains such as DAPI (Probst & Almouzni, 2008). Chromocenters are epigenetically distinguished by H3K9me3 marks written by the histone methyltransferases SUV39H1 and H2 (Müller-Ott et al., 2014). H3K9me3 marks recruit HP1 proteins, which might facilitate chromatin compaction by dimerizing and/or oligomerizing to bridge nucleosomes (Larson et al., 2017; Machida et al., 2018; Keenen et al., 2021). Pericentric heterochromatin is critical for genome stability, and when disrupted, chromosomal abnormalities, defects in segregation, and increased tumorigenesis are observed in mouse models (Peters et al., 2001; Taddei et al., 2001). Studying the distribution of transcriptional regulators relative to chromatin density using epigenetic modifications to classify chromatin compartments revealed an inverse correlation between chromatin density and protein size, with only the smallest proteins freely accessing heterochromatic regions associated with repressive marks (Miron et al., 2020). Further, Maeshima et al. (2015) investigated the importance of small transcription factor size (about 5 nm) in accessing the condensed interior of topologically associated domains (TADs). They demonstrate in silico that 5 nm spherical objects have free movement in condensed chromatin, 10 nm objects have attenuated movement, and objects larger than 15 nm are excluded entirely (Maeshima et al., 2015). Hihara et al. (2012) similarly used computer simulation to model the movement of EGFP pentamers modelled as 13 nm spheres through nucleosomes modelled as 10 nm spheres. They found that the modelled EGFP pentamers showed attenuated movement and penetration into 10 nm spheres when modelled at high concentrations expected of compact chromatin. Gorisch et al. (2005) used FITC-labelled dextrans of sizes 42, 77, 148, 282, 464, and 2500 kDa dextrans to compare how molecular weight (MW) affects molecule concentration in chromocenters, which is a predicted size range of approximately 6.5–51 nm. They showed reduced access of the dextrans 282 kDa and above in HeLa cell heterochromatin, and this accessibility was increased by increasing chromatin acetylation. An attractive model due to its intuitive simplicity is that size-based accessibility resulting from chromatin compaction restricts availability to the interior (Bancaud et al., 2009). In this model, diffusion into heterochromatin is limited by the size of pores between chromatin fibres or nucleosomes. Size-based accessibility could compromise genomic stability if the sensor proteins MRE11, Ku70/80, and PARP1 exceed this size limit. For example, a complex of Ku70/80 will be 150 kDa (Walker et al., 2001), three times the mass of a typical transcription factor (Maeshima et al., 2015) and has an approximate height and width of 7 and 12 nm (Rivera-Calzada et al., 2007). Thus, it is important to understand if there is significant size-dependence in chromocenter accessibility and, if there is, how this relates to sizes of DNA damage sensing and repair machinery.

DNA double-strand breaks (DSBs) in pericentric heterochromatin are repaired primarily by the homologous repair (HR) pathway or non-homologous end joining (NHEJ) pathway in a cell cycle-dependent manner (Tsouroula et al., 2016). In S and G2, DSBs relocate to the periphery of chromocenters and undergo HR, but in G1, DSBs remain in the chromocenter core and undergo NHEJ (Tsouroula et al., 2016). This suggests that proteins involved in NHEJ repair do not have difficulty accessing the interior of chromocenters. However, chromatin decompaction has been proposed as necessary for DSB repair in heterochromatin (Ayoub et al., 2008; Goodarzi et al., 2009; Noon et al., 2010). The relaxation of chromatin structure in response to DNA double-strand breaks could be a requirement for this accessibility.

Beyond to the potential of molecular size to restrict accessibility to chromocenters, numerous recent studies suggest that chromocenters behave as phase-separated compartments (Larson et al., 2017; Strom et al., 2017, 2021; Larson & Narlikar, 2018; Strickfaden et al., 2019; Wang et al., 2019; Erdel et al., 2020), which could provide an alternative mechanism for reducing the concentration of a diffusing protein below that of the surrounding nucleoplasm. Phase separation is emerging as a mechanism to generate membraneless compartments contributing to the subcellular organization of biomolecules. Phase separation occurs when molecules in a solution capable of multivalent interactions reach a critical concentration and undergo unmixing from the solvent to form a stable microenvironment termed a condensate (Boeynaems et al., 2018). By this mechanism, molecules that favourably interact with the environment of the condensate may enter freely, but molecules with unfavourable interactions will be depleted. Interestingly, some small inert proteins and molecules, including EGFP (Bancaud et al., 2009) and the YFP trimer construct (89 kDa) used by Strom et al. (2017), are depleted from chromocenters relative to the surrounding nucleoplasm despite EGFP being smaller than most transcription factors with a molecular weight (MW) of 27 kDa, a diameter of 2.4 nm, and a length of 4.2 nm (Hink et al., 2000) This is unlikely to be explained simply by differences in density and increased volume exclusion in the chromocenters since the measured density of chromocenters is 208 mg/mL while the surrounding nucleoplasm measures 136 mg/mL (Imai et al., 2017) in living cells.

In this study, we examined the chromocenter concentrations and diffusion of multiple DNA double-strand break sensor, mediator, and effector proteins in living murine cells without DNA damage using fluorescent protein-tagged transfected proteins. This informs us about the ability of proteins

involved in sensing and repairing DNA through both the NHEJ and HR pathways to access the interior of chromocenters. We compared the relative nucleoplasmic and chromocenter concentrations and measured diffusion coefficients of selected proteins to determine if accessibility or diffusion rates within chromocenters are directly correlated with apparent molecular weight. We find that there is no clear relationship between molecular weight and the extent of depletion within chromocenters. Nonetheless, DDR proteins did show substantial differences in concentration within chromocenters, and many showed a large range of concentrations within cell populations. Chromatin density alone did not explain the depletion of proteins from chromocenters. When we compared the accessibility of EGFP in living cells with recombinant GFP perfused into fixed cells, only the living cells showed depletion of EGFP relative to the surrounding nucleoplasm. The sensor proteins PARP1 and Ku70 were typically enriched in chromocenters, while MRE11 distribution varied between cells with individual cells found to be enriched, depleted, or evenly distributed across the cell population. Since MRE11 can bind PAR (Haince et al., 2008), we tested the effect of PARP1/2 inhibition and found no impact on the distribution of MRE11, indicating that this was not due to an increase in DNA damage or PAR accumulation in chromocenters. Importantly, all proteins examined showed some ability to access the interior of chromocenters demonstrating that DNA damage-associated chromatin decondensation is not required for large DDR proteins to have access to nuclear heterochromatin domains.

Materials and methods

Cell culture

C3H/10 T1/2 cells from ATCC (ATCC CCl-226) were cultured in α-Minimal Essential Medium (Gibco™) supplemented with 10% FBS (Gibco™) and 1% Penicillin-Streptomycin (Gibco™). Cells were maintained in an incubator at 37°C with 5% CO_2 and humidity. C3H/10 T1/2 cells are a female cell line with fibroblastic morphology in cell culture that was established from 14 to 17 day old C3H mouse embryos but have mesenchymal stem cell-like properties, including the ability to differentiate into distinct cell lineages (Date et al., 2004).

Transfection

Cells seeded in MatTek dishes were transfected at 60–70% confluency using the Qiagen Effectene transfection kit with some modifications to the protocol. First, 800 ng of DNA was incubated with 3 µL of Enhancer and 100 µL of DNA-condensation buffer (buffer EC) for 15 min rather than the recommended 2–5 min, followed by the addition of 5 µL of Effectene and incubation for 20 min rather than the recommended 5–10. Subsequently, the transfection reagent was added to the cells and cells were left to incubate At 37°C with 5% CO_2 overnight before imaging the following day.

Cell imaging

The following day, the transfection medium containing the transfection reagent was replaced with fresh media following a wash step with 1× PBS. Hoechst 33342 was then incubated with the cells at a concentration of 1 µg/mL for 30 min at 37 C to visualize DNA. Next, the medium containing Hoechst 33342 was removed, and cells were washed with 1× PBS before replacement with fresh medium. Fluorescent tagged protein expression in live cells was visualized with a PerkinElmer Ultraview ERS spinning disc confocal microscope equipped with a Hamamatsu Electron Multiplication Charge-Coupled detector device using a 100× 1.4 NA DIC plan-apochromat oil immersion objective lens. In addition, some images were captured using a Leica Falcon SP8 laser scanning confocal microscope with hybrid detectors using an 86× 1.2 NA water plan-apochromat objective lens. Live cell environmental conditions were maintained for both microscopes throughout imaging with a 37°C and CO_2-controlled live-cell chamber.

PARPi treatment

For experiments with BMN 673 and ABT 888 PARP1/2 inhibitors, inhibitors were added to cells at a concentration of 10 µM 1 h before imaging and present throughout the experiment.

Incubation of fixed cells with recombinant EGFP and fluorescent dextrans

CH3/10T1/2 cells were grown to 60–70% confluence and then fixed with 4% paraformaldehyde for 10 min. They were subsequently permeabilized with 0.5% Triton X for 10 min and stained with Hoechst 33342 for 30 min to visualize DNA. Purified Pierce™ recombinant GFP protein was diluted to 0.05 µg/µL in 1× PBS and added to cells. They were then allowed to equilibrate for 1 h before imaging by the Leica Falcon SP8 laser scanning confocal microscope with hybrid detectors using an 86× 1.2 NA water plan-apochromat objective lens. FITC labelled 70 kDa (Product no. 46945), and 500 kDa dextrans (Product no. 46947) and TRITC labelled 155 kDa dextrans (Product no. T1287) were obtained from Sigma Aldrich. 70 kDa dextrans were used at a concentration of 0.13 µg/µl in 1× PBS, 155 kDa dextrans at a concentration of

0.29 μg/μL, and 500 kDa dextrans at a concentration of 0.93 μg/μL to keep molarity consistent with the purified GFP. They were then added to cells and allowed to equilibrate for a minimum of 30 min before imaging with the Leica Falcon SP8 laser scanning confocal microscope using an 86× 1.2 NA water plan-apochromat objective lens.

Quantification of chromocenter partitioning

To capture the relative fluorescent intensity of proteins in the chromocenters relative to the surrounding nucleoplasm, an area within chromocenters was measured for intensity and compared to the intensity of a same-sized area in the nucleoplasm. The intensity was measured using FIJI by creating circular regions of interest and measuring integrated intensity following background subtraction (https://fiji.dc). Analysis was performed in Microsoft Excel 365. Some proteins were observed to form nuclear foci. Cells with foci were more common with increased expression and were excluded from analysis for all proteins with the exception of Rad51 and RNF 168, where foci were present at all expression levels. Consequently, the analyzed cell population was biased towards low protein expression. An *n* of 30 cells was used for the quantification of each protein.

Fluorescent correlation spectroscopy and diffusion calculation

Fluorescent correlation spectroscopy (FCS) measurements were performed using the Leica Falcon SP8 laser scanning confocal microscope with an 86× 1.2 NA water plan-apochromat objective lens and hybrid detectors. Cells were transfected following the above-described protocol and stained with Hoechst 33342 to visualize DNA. Before imaging, the culture medium was replaced with phenol red-free DMEM to reduce phenol red-derived fluorescence. During FCS measurements, cells were maintained at 37°C and 5% CO_2 in a live-cell environmental chamber. FCS measurements were collected for 5 s with three repetitions at each spatial point. Curve fitting was calculated with the Leica Application Suite X software with photobleaching correction and spark removal at sensitivity level 20 using the diffusion with triplet model with triplet amplitude set to 0.10 and triplet time set to 0.010 to remove triplets from fitting. A single component fit was optimal for all proteins except for RNF168 and 53BP1, for which a single component or two-component fit appeared equal, so a one-component fit was maintained for consistency. The final diffusion value was calculated from measurements collected on three separate days from at least 30 cells. Unambiguously incorrect measurements were removed from the overall calculation. These occurred when zero or near zero molecules were detected despite detection in subsequent acquisitions at the same location.

Graphs were created in RStudio using the ggplot2 package (Wickham, 2016).

Results

PARP1-GFP and Ku70-GFP sensor proteins display enrichment in chromocenters while MRE11-YFP displays heterogenous behavior

Poly (ADP-ribose) polymerase 1 (PARP1) and Ku70 (XRCC6) are both sensors of DNA damage. PARP1-catalyzes poly(ADP-ribosyl)ation, which is an initial step in the DNA damage response that facilitates both Ku70/80 recruitment, the initial step in the NHEJ pathway, and MRE11 recruitment, the nuclease that initiates end resection required for the homologous recombination (HR) repair pathway (Rivera-Calzada et al., 2007; Haince et al., 2008; Yu et al., 2012). PARP1, MRE11, and Ku proteins have all been ascribed the role of DNA double-strand break sensor (Ray Chaudhuri and Nussenzweig, 2017; Huang & Zhou, 2020), where they initiate the DNA double-strand break signalling and repair response. As the sensing of double-stranded breaks is essential to their subsequent repair, we wanted to test the ability of these three critical proteins to access the interior of chromocenters. For example, the Ku heterodimer is approximately 12 × 7 × 7 nm (Walker et al., 2001). The GFP tag may increase this to 15 nm or more; hence, Ku should be excluded based upon a 10 nm diameter pore size. To test the accessibility of chromocenters to sensor proteins, mouse cells were transfected with plasmids encoding the protein of interest fused to a fluorescent protein. To visualize the behaviour of transfected proteins, images were collected in living cells, and chromocenter location was determined by staining DNA with Hoechst 33342. Images were collected by spinning disk or laser scanning confocal microscopy. Both PARP1-GFP and Ku70-GFP visually display enrichment in chromocenters, while MRE11-YFP displayed heterogeneous behaviour (Figures 1A,C). Quantification of protein concentration in chromocenters was assessed relative to the nucleoplasm using the integrated intensity of the fluorescent protein tag. PARP1 and Ku70 both showed enrichment in the chromocenters, with PARP1 showing the strongest enrichment (Figure 1B). Ku70 showed subtle depletion in a subset of cells. The ability of Ku70 to enrich in the chromocenter implies that it is not too large to enter chromocenters, where it can then interact with DNA or proteins to accumulate beyond the nucleoplasmic concentration. In the case of MRE11, there are subsets of cells that are either clearly depleted, clearly enriched, or homogeneously distributed (Figure 1C). Interestingly, NBS1, part of the MRE11/NBS1/Rad50 (MRN) complex, is consistently depleted from chromocenters (Figure 1B).

We previously demonstrated that MRE11 binds to poly(ADP-ribose)(PAR) and is responsible for the rapid

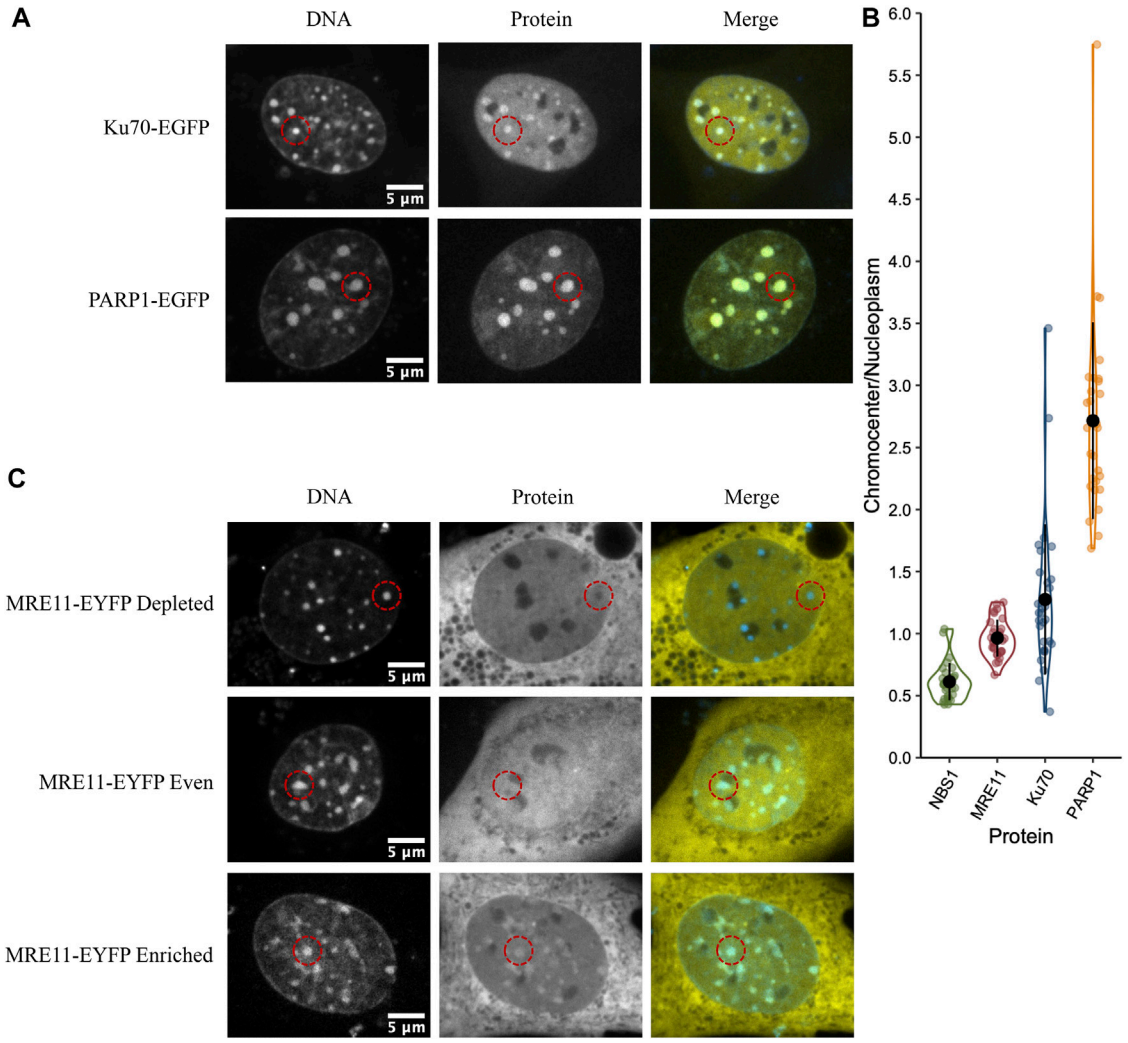

FIGURE 1
DNA damage sensors PARP1 and Ku70 are enriched in chromocenters while the DNA damage sensor MRE11 displays heterogeneous behaviour. **(A)** CH3/10T1/2 cells were transfected with either PARP1-EGFP or Ku70-EGFP and stained with Hoechst 33342 to visualize DNA. **(B)** Quantification of relative fluorescent protein chromocenter intensity for proteins NBS1-EGFP, MRE11-YFP, Ku70-EGFP, and PARP1-EGFP (*n* = 30 cells for each protein). **(C)** CH3/10T1/2 cells were transfected with MRE11-YFP and stained with Hoechst 33342 to visualize DNA. Depleted, homogenous, and enriched distributions of MRE11-YFP are illustrated.

recruitment of MRE11 to sites of DNA damage (Haince et al., 2008). Based on the accumulation of PARP1 in chromocenters, we tested if MRE11-YFP enrichment in chromocenters is due to PARylation within chromocenters. The PARP1 and 2 inhibitors BMN 673 (Talazoparib, 10 µM) or ABT 888 (Veliparib, 10 µM) were incubated with cells for 1 h before imaging (Krietsch et al., 2012; Caron et al., 2019). Both inhibit PARP1 and 2 catalysis of poly (ADP-ribosyl)ation (PARylation) (Donawho et al., 2007; Shen et al., 2013). Neither BMN 673 nor ABT 888 prevented the accumulation of MRE11 in chromocenters nor affected the heterogeneous distribution of MRE11-YFP across the cell population (Figures 2A,B). Since PARP1, Ku70, and MRE11 all show the ability to enter into chromocenters, the results are inconsistent with a 10 nm exclusion limit, and size-based exclusion appears not to be a limitation to the sensing of DNA double-strand breaks in heterochromatin.

Mediator and effector proteins show heterogeneous accessibility that does not correlate with HR or NHEJ pathway involvement

The large downstream mediators of DNA damage repair could rely on changes in chromatin accessibility as a result of early chromatin remodelling events (Poirier et al., 1982; Goodarzi

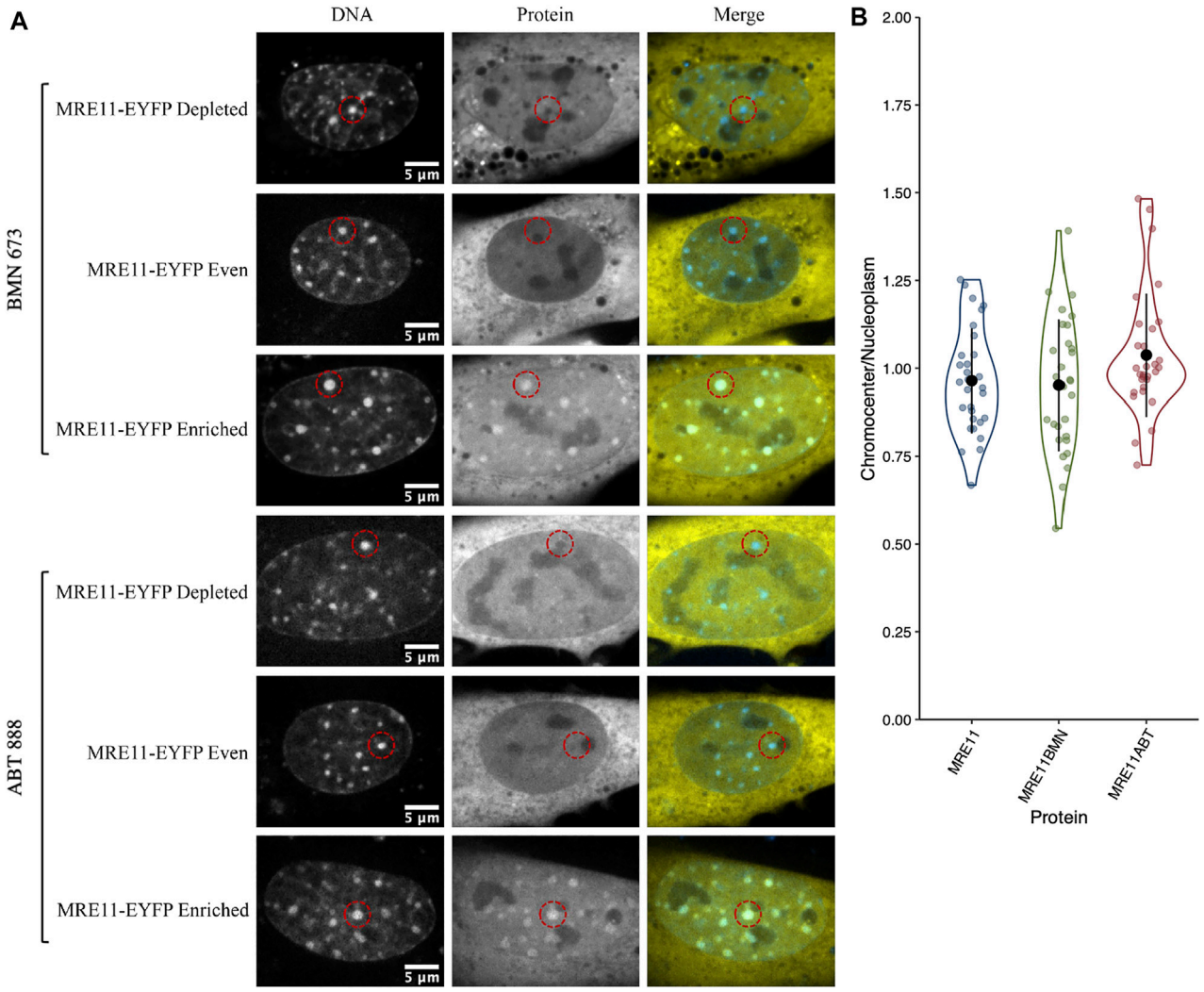

FIGURE 2
MRE11-YFP chromocenter heterogeneity is not dependent on poly (ADP-ribosyl)ation **(A)** CH3/10T1/2 cells were transfected with MRE11-YFP, Hoechst 3 3342 was added to visualize DNA, and then incubated with either BMN 673 or ABT 888 at a concentration of 10 μM for 1 h before imaging. An example of depleted, homogenous, and enriched distributions are provided for both inhibitor groups **(B)** Graph shows quantification of relative chromocenter intensity for each group. MRE11-YFP control is included for direct comparison. Each protein has $n = 30$. MRE11-YFP control is not significantly different from either MRE11-YFP treated with BMN 673 ($p = 0.77$) or MRE11-YFP treated with ABT 888 ($p = 0.087$).

et al., 2008, 2009; Noon et al., 2010; Rack et al., 2021). Consequently, we wanted to test their ability to diffuse into the interior of chromocenters in the absence of DNA damage and the associated chromatin remodelling. Transiently expressed proteins were assessed for their relative concentration in chromocenters (Table 1 and Figure 3). For proteins below approximately 200 kDa in size, there does not appear to be any relationship with accessibility (Table 1 and Figure 3). Notably, most of these proteins show depletion in mouse chromocenters, suggesting that some concentration regulation is taking place. In this respect, the depletion of EGFP alone is salient. BRCA1 and PARP3 have a very similar depletion to EGFP despite BRCA1 being, for example, almost 10X the mass of EGFP alone.

There may be a reduction in the space available for the diffusion of the largest proteins studied. BRCA1-GFP (235 kDa), 53BP1-GFP (241 kDa), MDC1-GFP (254 kDa), and ATM-His-Flag-GFP (~380 kDa) are all depleted from chromocenters (Table 1 and Figure 3). The most striking was 53BP1, which did not show any examples of accumulation within chromocenters. It was also distinctive for a second reason—its appearance in nuclei revealed additional regions of depletion that corresponded to DNA depleted regions of the nucleus outside of the nucleolus. Expression of a fluorescently tagged splicing factor

TABLE 1 Accessibility of DNA damage mediators to chromocenters.

Protein/Dye name	Size (kDa)	Chromocenter status in MEF cells (visual appearance)	Measured chromocenter concentration relative to the nucleoplasm (Min, Max)	Foci formation	Foci publications	Protein dimensions from alpha fold structures (Å) (Jumper et al., 2021) [uniprot accession]
EGFP	27	Depleted	0.79 (0.54, 0.87)	No	N/A	35.47, 41.70, 57.41 [P42212]
Rad51-EGFP	64	Even	0.93 (0.20, 2.8)	short rods	(Tarsounas et al., 2003; Galkin et al., 2005)	103.94, 63.64, 45.69 [Q06609]
Rad52-EGFP	73	Depleted	0.72 (0.28, 2.3)	No	N/A	82.20, 111.39, 134.04 [P43351]
RNF8-EGFP	83	Depleted	0.76 (0.21, 3.7)	No	N/A	205.89, 87.54, 63.38 [O76064]
Tip60-EGFP	86	Depleted	0.75 (0.53, 1.6)	Yes	Wu et al. (2009)	91.57, 86.88, 64.58 [Q92993]
PARP3-EGFP	87	Depleted	0.69 (0.46, 0.90)	No	N/A	103.68, 99.78, 60.30 [Q9Y6F1]
RNF 168-EGFP	92	Enriched	7.0 (1.4, 12)	Yes		177.85, 130.39, 97.67 [Q8IYW5]
PARP2-EGFP	93	Enriched	1.8 (1.2, 3.3)	No	N/A	101.61, 95.84, 83.60 [Q9UGN5]
Rap80-EGFP	107	Enriched	1.2 (0.93, 1.5)	Yes	Soo Lee et al. (2016)	176.16, 135.35, 119.35 [Q96RL1]
NBS1-EGFP	112	Depleted	0.61 (0.43, 1.0)	Yes		123.30, 136.58, 148.48 [O60934]
BRCA1-EGFP	235	Depleted	0.66 (0.31, 1.0)	No	N/A	179.77, 169.90, 181.71 [P38398]
53BP1-EGFP	241	Depleted	0.49 (0.26, 0.80)	Yes	(Kilic et al., 2019; Lukas et al., 2011)	155.69, 163.43, 188.04 [Q12888]
MDC1-EGFP	254	Depleted	0.62 (0.32, 1.2)	Yes		155.48, 181.29, 223.16 [Q14676]
ATM-His-Flag-EGFP	~380	Depleted	0.67 (0.35, 1.2)	No	N/A	82.45, 116.01, 212.66 *From PDBe 6K9K (Xiao et al., 2019)

(SRp20) revealed these to be splicing factor compartments (Figure 3B). 53BP1 has been reported to undergo phase separation *in vitro* and is proposed to participate in forming phase separated compartments surrounding DNA double-strand breaks in cells (Kilic et al., 2019). This could confer poor solubility in liquid compartments that differ from the surrounding nucleoplasm. The nucleolus is also clearly depleted in 53BP1 and has a distinct liquid environment (Figure 3B) (Brangwynne et al., 2011; Feric et al., 2016; Frottin et al., 2019; Lafontaine et al., 2021). We also used the program CIDER to analyze our mediator proteins. We found no obvious differences between them except that 53BP1 has a lower ratio of positively charged residues to negatively charged residues (data not shown) (Holehouse et al., 2015). Notably, except for 53BP1, all DNA damage response proteins have cells within the population that show a near homogeneous distribution between nucleoplasm and chromocenter or examples of cells with protein enrichment in the chromocenter. These results indicate that none of these proteins are too large to enter into chromocenters. However, the large range of relative chromocenter concentrations observed for most of these proteins and the reduced concentration of EGFP in chromocenters suggest mechanisms beyond size-dependent filtering and excluded volume effects reduce the concentrations of freely diffusing nucleoplasmic proteins within the chromocenter volume.

Diffusion properties of example DNA damage response proteins

Slower diffusion through chromocenters with increasing sizes of EGFP multimers has been proposed to reflect dependence on size (Baum et al., 2014). For globular proteins in solution, an eight-fold increase in mass is predicted to decrease the diffusion rate two-fold. To test whether we observe size-dependent diffusion with the DNA damage proteins, we performed fluorescent correlation spectroscopy (FCS) across a size range with EGFP, RNF168-EGFP, PARP1-EGFP, 53BP1-

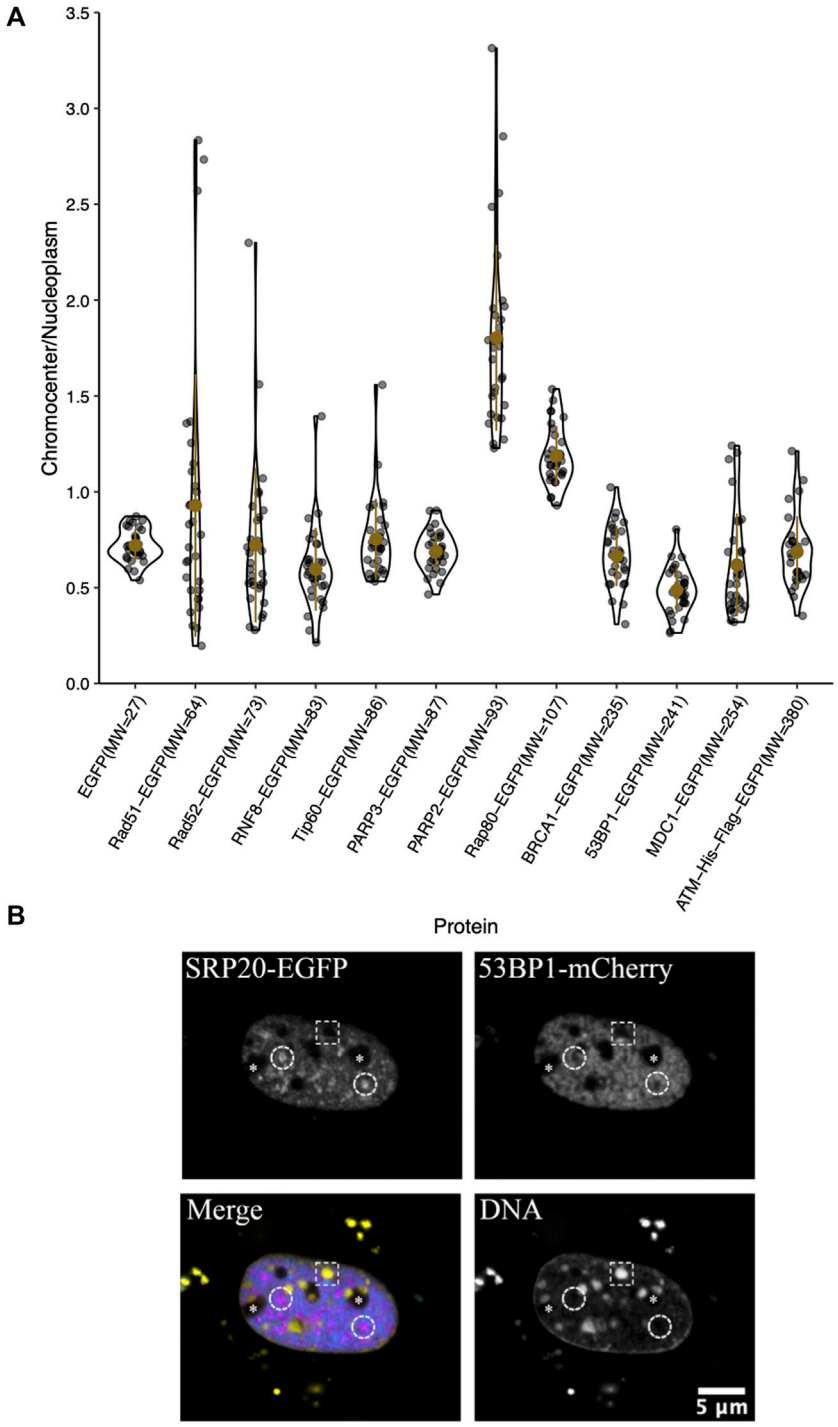

FIGURE 3
Chromocenter localization of mediator and effector proteins. **(A)** Graph showing quantification of relative chromocenter intensity for mediator and effector proteins. Cells were transfected with a plasmid encoding the protein of interest and stained with Hoechst 33342 to visualize DNA (n = 30 for each protein). **(B)** A cell expressing the splicing factor SRp20-EGFP and 53BP1-mCherry and counterstained with Hoechst 33342 to contrast the chromatin. The dashed circles indicate the positions of splicing factor compartments while the dashed rectangle illustrates the position of a chromocenter. Asterisks indicate the positions of nucleoli.

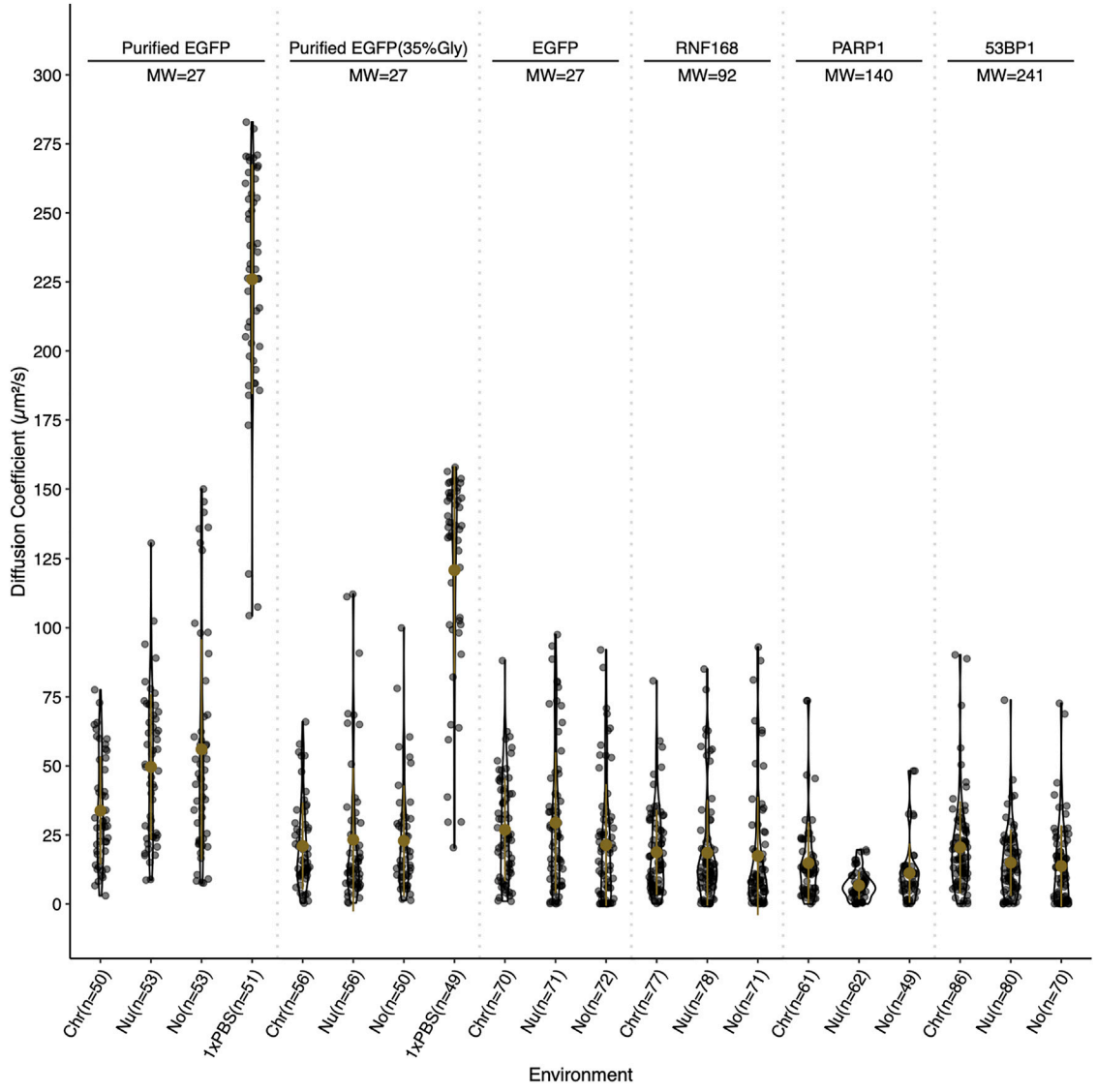

FIGURE 4
Relative diffusion of EGFP and selected DNA damage response proteins. Diffusion coefficients for EGFP, RNF168-EGFP, PARP1-EGFP, and 53BP1-EGFP in live cells, and purified EGFP in 0 and 35% glycerol in fixed cells. Diffusion coefficients are reported in $\mu m^2/s$ and were determined by fluorescent correlation spectroscopy. Diffusion coefficients are reported for the chromocenter (Chr), the nucleoplasm (Nu), the nucleolus (No), and for purified EGFP in 1× PBS (1×PBS). Live cell measurements were gathered at 37°C and fixed cell measurements were collected at 18°C. Both live and fixed cells were stained with Hoechst 33342 to visualize DNA.

EGFP, and purified GFP perfused through fixed cells in 1× PBS and 35% glycerol PBS. Values in the nucleolus were also measured and reported. In fixed cells, the calculated diffusion coefficients reflect the density of chromocenters compared to the nucleoplasm, as the average diffusion coefficient for EGFP in chromocenters is 34 $\mu m^2/s$. In contrast, in the nucleoplasm, it is 50 $\mu m^2/s$. However, EGFP in live cells reveals no significant difference, with the chromocenter having a mean diffusion coefficient of 27 $\mu m^2/s$ and the nucleoplasm having 29 $\mu m^2/s$. We tested purified GFP diffusion in 35% glycerol because of a previous report that in media containing 40% glycerol, the rotational diffusion of GFP in solution is similar to that of GFP in live cells (Erdel et al., 2020). We found that after the addition of glycerol, the mean diffusion coefficient in the solution was reduced from 226 to 121 $\mu m^2/s$. The diffusion coefficient in chromocenters began to more closely resemble that in living cells at 21 $\mu m^2/s$ in 35% glycerol and 34 $\mu m^2/s$ in 1× PBS. This is consistent with the viscosity of the nucleoplasm being approximately equivalent to 30–40% glycerol. While EGFP showed an expected mobility reduction in chromocenters

relative to the nucleoplasm, RNF168-EGFP, PARP1-EGFP, and 53BP1-EGFP FCS all measured a faster mean diffusion coefficient in the chromocenters compared to the nucleoplasm (Figure 4). RNF168-EGFP and 53BP1-EGFP had similar behaviour, with a mean diffusion coefficient of 19 $\mu m^2/s$ in chromocenters for RNF168-EGFP and 20 $\mu m^2/s$ for 53BP1-EGFP, and mean nucleoplasmic diffusion coefficients of 19 and 15 $\mu m^2/s$, respectively (Figure 4). These are about two-fold slower than EGFP but correspond to almost four-fold (RNF168-EGFP) and almost 10-fold (53BP1-EGFP) difference in mass. This is consistent with the free diffusion of 53BP1-EGFP monomers but suggests that RNF168 may form a larger diffusing complex than predicted by its molecular weight as a monomer. Interestingly, PARP1-EGFP had a mean diffusion coefficient of 15 $\mu m^2/s$, which is about twice the mean diffusion coefficient measured in the nucleoplasm of 6.7 $\mu m^2/s$ (Figure 4). One potential explanation for an unexpectedly higher diffusion rate inside chromocenters is that these proteins are diffusing along the chromatin fibre within chromocenters rather than undertaking 3D diffusion in the associated liquid phase. A second explanation is that these molecules diffuse as larger complexes in the nucleoplasm.

Non-specific DNA binding may contribute to the abundance of large proteins in chromocenters

The initial results indicate that even large proteins can diffuse into the interior of chromocenters. Collombet et al. (2021) examined the accessibility of the inactive X chromosome territory to RNA polymerase II using single-molecule tracking methods. They showed that RNA polymerase II could freely diffuse into and through the inactive X chromosome territory. The principal difference explaining its depletion within the inactive X chromosome territory is the absence of binding to chromatin within the inactive X territory. Therefore, we wondered if the depletion of proteins we observed resulted from a failure to be retained in chromocenters rather than depletion by barriers to diffusion that prevented entry. We tested a fusion protein of BRCA1 with the LacI DNA binding domain (274 kDa). The specific DNA binding site for LacI is not natively endogenous in the mammalian genome resulting in LacI being unable to bind DNA specifically, yet LacI is known to have non-specific DNA binding to search the genome for its target sequence (Kao-Huang et al., 1977; Hammar et al., 2012; Stracy et al., 2021). Interestingly, we found that the fusion of the LacI DNA binding domain to BRCA1 increased its concentration in chromocenters. As previously described, BRCA1-GFP is depleted from chromocenters with a mean concentration of 66% of the nucleoplasm, whereas BRCA1-LacI-mCherry was enriched to 120% of the nucleoplasmic concentration (Figures 5A,B). This is consistent with non-specific DNA binding contributing to the accumulation of BRCA1 in mouse chromocenters. To further test this, we examined the fusion of the LacI DNA binding domain to EGFP. In contrast to the BRCA1 fusion, however, the fusion of the LacI DNA binding domain to EGFP did not result in a significant difference in EGFP accumulation in chromocenters. Both forms of the protein were depleted relative to the surrounding nucleoplasm (Figures 5A,B). The result with the EGFP fusion suggests that DNA binding is not a determinant of EGFP distribution but may contribute to BRCA1 distribution. One possible explanation for this is that modelling two DNA binding domains joined by a flexible linker predicts enhanced affinity for DNA over those of the two individual domains because both can interact with the DNA (Zhou, 2001). BRCA1 also binds DNA (Paull et al., 2001; Simons et al., 2006) and combined with the LacI domain, synergy in binding could explain the differences between the LacI fusion with EGFP versus BRCA1-mCherry.

Depletion of EGFP and dextrans cannot be explained by chromatin-mediated volume exclusion

Compaction of chromatin into heterochromatin domains logically results in an increased excluded volume since the chromatin must occupy some of the available space (Bancaud et al., 2009). Therefore, we wanted to test if the depletion of inert molecules such as EGFP from chromocenters could be explained simply by a reduction in available space from increased chromatin occupancy. We placed paraformaldehyde-fixed permeabilized CH3/10T1/2 cells with purified GFP in 1× PBS and compared chromocenter partitioning to live cells transiently expressing EGFP. We observed a clear difference between the two groups, with purified GFP having a near homogeneous distribution across the nucleoplasm (Figures 6A,B). We repeated the experiment with 70, 155, and 500 kDa dextrans to further validate this result. Above 2 kDa, dextrans behave as random coils in solution, allowing the prediction of molecular dimensions based on the radius of gyration (R_G) (Basedow & Ebert, 1979), which is about 8.5, 12.7, and 22.8 nm for the 70, 155, and 500 kDa dextrans, respectively (Oliver & Deen, 1994). Interestingly, despite the large variation in size, there is no significant difference between the dextrans, with each being around 20% depleted from chromocenters relative to the nucleoplasm (Figures 6A,B). Notably, the dextrans are significantly less depleted than EGFP concentrations in chromocenters of living cells, despite the smallest dextran being approximately twice the size of EGFP (Figures 6A,B). This result demonstrates that the observed depletion of proteins from chromocenters cannot be explained solely by volume exclusion effects.

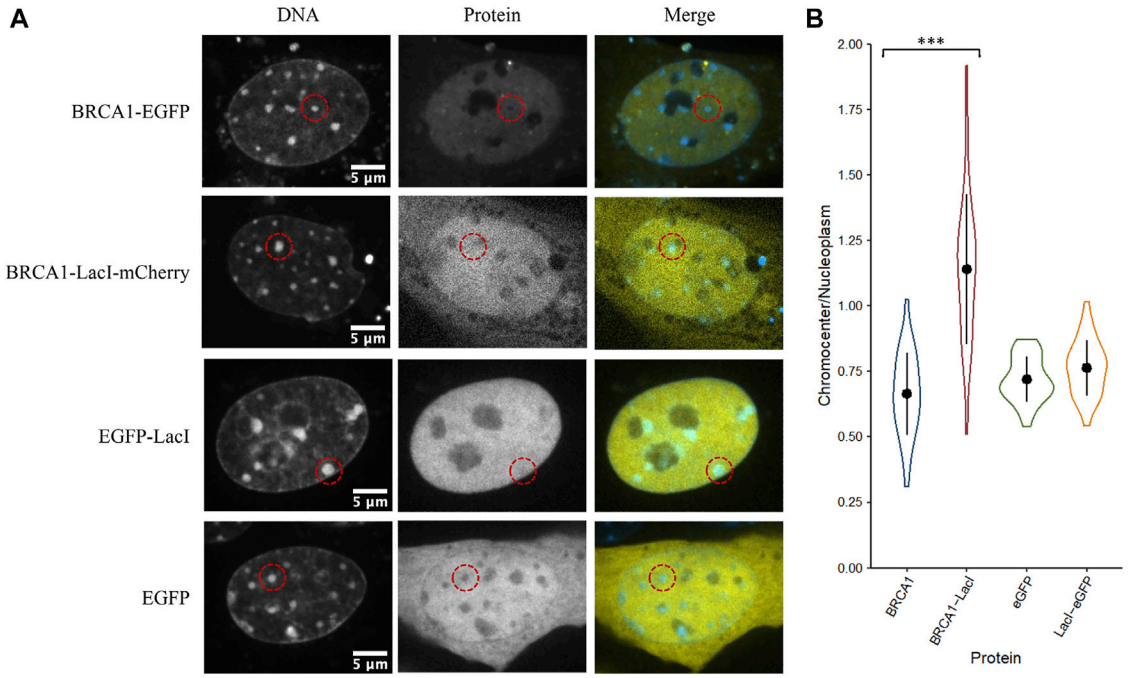

FIGURE 5
The LacI DNA binding domain may alter the ability of BRCA1 to access chromocenters. **(A)** CH3/10T1/2 cells were stained with Hoechst 33342 to visualize DNA and transfected with plasmids encoding either BRCA1-GFP, BRCA1-LacI-mCherry, LacI-EGFP, or EGFP. **(B)** Quantification of relative chromocenter intensity for each protein. BRCA1-EGFP is significantly different from BRCA1-LacI-mCherry (p = 1.3E−09). EGFP is not significantly different from LacI-EGFP (p = 0.088) (n = 30 for each protein).

Spontaneous nuclear focus formation upon expressing DNA damage response proteins

Another mechanism for selectivity independent of size is liquid-liquid phase separation. For example, 53BP1 has been shown to undergo liquid-liquid unmixing to form 53BP1-rich condensates *in vitro*. This reflects a preference for self-interaction over interaction with the solvent (nucleoplasm). Focus formation, particularly upon increased expression, may reflect a potential for differential solubility in distinct solvent environments that are expected to form due to liquid-liquid phase separation. We observed that many of the proteins that we transfected formed nuclear foci. Out of the 17 proteins tested, eight formed nuclear domains that concentrated the fluorescently tagged protein; those eight were Rad51-GFP, Tip60-GFP, RNF168-GFP, Rap80-GFP, NBS1-GFP, MRE11-YFP, 53BP1-GFP, and MDC1-GFP (Figure 7A). Phase separation capacity of proteins is often conferred by regions of disorder (Boeynaems et al., 2018), so to gather a preliminary sense of which proteins may phase separate, we used the program Predictor of Natural Disordered Regions (PONDR®) with the VSL2 algorithm to predict disordered regions in proteins that form foci. With the exception of Rad51, each of these proteins contains disordered regions (Figure 7B). Notably, Rad51 does not form foci. Rather, at very low nucleoplasmic concentrations, we find that Rad51 forms short filaments in the nucleoplasm, consistent with previous studies (van der Heijden et al., 2007; Forget & Kowalczykowski, 2010). Foci formation in a subpopulation of cells is expected because of the presence of DNA double-strand breaks even in the absence of external DNA damage sources. However, proteins that form large numbers of small foci are good candidates for forming LLPS condensates. Demonstrating whether or not this reflects phase separation will require future *in vitro* experiments to determine if any of these proteins can initiate liquid unmixing independently.

Discussion

The condensed state of chromatin in chromocenters has long been thought to contribute to defining the accessibility of molecules. Heterochromatin has increased mutation rates compared to euchromatic regions (Schuster-Böckler & Lehner, 2012). One suggestion to explain this is decreased repair due to lower rates of transcription-coupled nucleotide excision repair (TCR), but another is the attenuated ability of the repair machinery to access heterochromatic regions (Schuster-

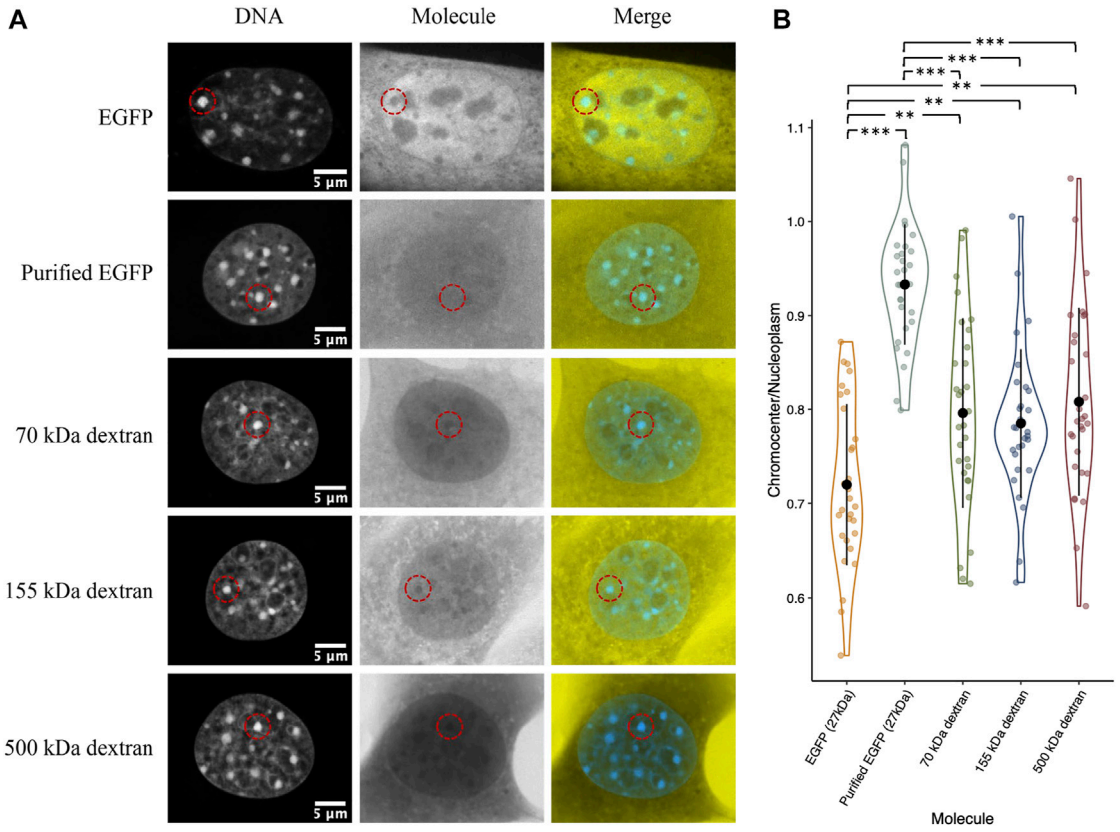

FIGURE 6
Distribution of purified recombinant GFP and fluorescent dextrans in fixed permeabilized cells. **(A)** CH3/10T1/2 cells were either fixed with paraformaldehyde and permeabilized with Triton X followed by perfusion with purified EGFP or the indicated dextrans diluted in 1× PBS. For comparison, a cell transfected with a plasmid encoding EGFP and imaged live is also shown. Both groups were stained with Hoechst 33342 for DNA visualization. **(B)** Quantification of chromocenter concentration relative to the surrounding nucleoplasm.

Böckler & Lehner, 2012; Roberts & Gordenin, 2014). Indeed, H2AX phosphorylation (γH2AX), which is dependent on the large Ataxia Telangiectasia Mutated (ATM) kinase, is reduced in heterochromatic regions in both yeast and mammalian cells (Kim et al., 2007). The concept of chromatin-mediated regulation of accessibility was originally established based on the differential digestion kinetics of active and inactive genes (Weintraub and Groudine, 1976). The association of DNase I sensitivity with the acetylation state of chromatin domains further implicated chromatin folding in regulating genome accessibility (Hebbes et al., 1994) and is consistent with experiments examining the ability of different sized fluorescent dextrans to diffuse into chromatin of differing density (Görisch et al., 2005). Current models propose that chromatin is compacted by interactions with itself (Hansen et al., 2021), and compaction may be further facilitated by proteins and RNA (Thakur et al., 2019; Wang et al., 2019; Fan et al., 2020; Li et al., 2020). Recent studies into the material states of chromatin indicate that chromatin exists in a gel (solid) state (Erdel, 2020; Strickfaden et al., 2020; Hansen et al., 2021). This predicts the existence of pores between crosslinked chromatin fibres. Thus, we might expect that steric hindrance in condensed regions of chromatin could participate in genome regulation. Consistent with this, an inverse relationship between size and localization to constitutive, facultative, and euchromatic regions of mouse nuclei was recently reported, and larger transcriptional complexes were found to be absent in constitutive heterochromatin regions of fixed cells (Miron et al., 2020).

When we examined the distribution of DNA break sensor proteins PARP1, MRE11, and Ku70, we observed variable behaviour for MRE11 and enrichment for both PARP1 and Ku70. In the case of Ku70, the Ku70/80 heterodimer is 11 × 7 × 7 nm and would be expected to have difficulty entering mouse chromocenters if they had a pore size of only 10 nm. PARP1 was significantly enriched in mouse chromocenters. Ku and PARP1 have previously been reported to associate with heterochromatin (el Ramy et al., 2009; Quénet et al., 2008; Song et al., 2001). Accumulation within chromocenters is expected to reflect binding to chromatin within

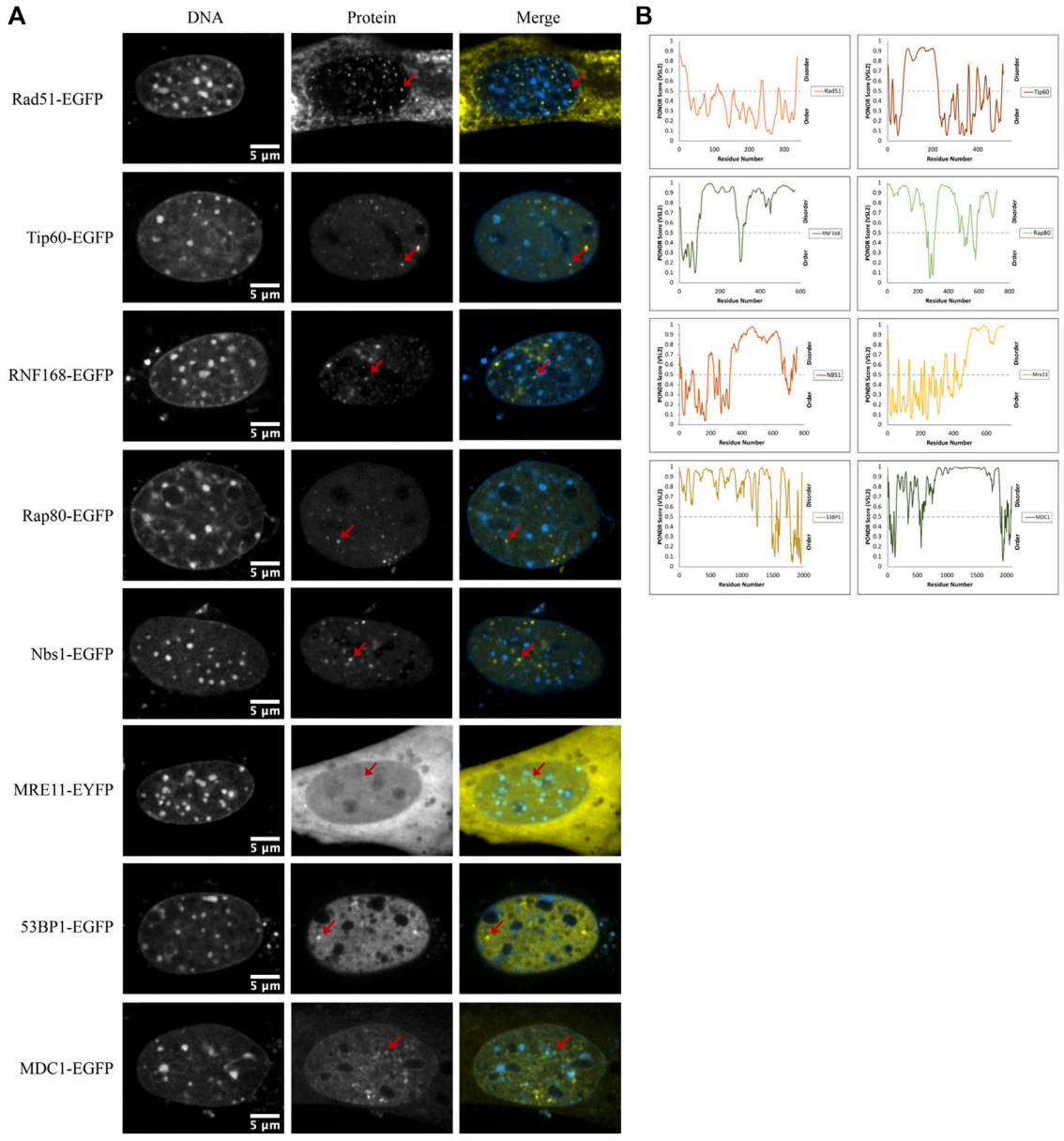

FIGURE 7
DNA damage sensors, mediators, and effectors form nuclear foci. **(A)** Example images of Rad51-EGFP, Tip60-EGFP, RNF168-EGFP, Rap80-EGFP, NBS1-EGFP, MRE11-YFP, 53BP1-EGFP, and MDC1-EGFP transfected CH3/10T1/2 cells stained with Hoechst 33342 displaying nuclear foci. **(B)** PONDR® scores for each protein predicted by the VSL2 algorithm. A score greater than 0.5 predicts disorder for that region of the protein.

chromocenters, although differential solubility in distinct solvent environments could also explain the enrichment of any of these proteins. In either case, the observed ability of these proteins to diffuse into chromocenters would require that the gel be sufficiently porous to enable these protein complexes to diffuse through their interior. Thus, the pore size must exceed 10 nm diameter.

The case of MRE11 is particularly interesting and, together with the partitioning of NBS1, suggests that the concentrations of diffusing nucleoplasmic proteins are regulated in some manner. MRE11 can be depleted, homogeneous, or enriched within mouse chromocenters. This enrichment was not due to poly(ADP-ribose) as PARP inhibitors did not affect MRE11 distribution. MRE11 forms a complex with NBS1 and Rad50. NBS1 was consistently depleted and to a greater extent than MRE11. This suggests that either the complex is excluded more than MRE11 alone or that these proteins show differential regulation of chromocenter concentration without complex

assembly. Importantly, the results indicate that the initial detection of DNA damage within chromocenters is not limited by steric exclusion of sensor proteins since they all show some access to the interior of the mouse chromocenter.

Further supporting the potential physical accessibility barrier to large molecules like ATM, DSB repair in heterochromatin is reported to depend upon chromatin decondensation mediated by the phosphorylation of KAP1 (Goodarzi et al., 2008). Similarly, PARP activation will drive chromatin decondensation, recruitment of chromatin remodelling complexes, and histone displacement (Poirier et al., 1982; Rouleau et al., 2004; Liu & Yu, 2015; Strickfaden et al., 2016). Thus, it may be that some of the mediator and effector proteins involved in DSB repair require chromatin remodelling to increase the porosity of heterochromatin to function there. Work from Tsouroula et al. (2016) establishes that during S/G2, DSBs occurring within chromocenters are relocated to the periphery of chromocenters to undergo repair by HR. In addition, Rad51 assembly occurs on the periphery of chromocenters. In comparison, independent of the cell cycle, DSBs repaired by NHEJ remain within the chromocenter (Tsouroula et al., 2016). Thus, it was of particular interest to assess the ability of ATM and similarly large downstream proteins such as MDC1, 53BP1, and BRCA1 to diffuse into the chromocenter interior. While we did observe that these larger proteins showed greater depletion from mouse chromocenters, in no case did we see evidence for complete exclusion from chromocenters. For example, ATM exists as a dimer in the absence of DNA damage. A monomer of ATM has an approximate height of 20 nm and width of 10 nm (Xiao et al., 2019). The chromocenters are no more than 40% depleted in ATM relative to the surrounding nucleoplasm, with a mean value of 67%. This indicates that significant quantities of even these larger DNA damage response proteins enter chromocenters.

To determine if the movement of the DNA damage response proteins through chromocenters correlated with expected size, we performed fluorescent correlation spectroscopy (FCS) to measure diffusion coefficients across a size range of the proteins. We found that although GFP had an expected small reduction in diffusion within chromocenters. Amongst the other proteins tested, there was not a strong correlation between predicted size and diffusion. For example, 53BP1-EGFP and RNF168-EGFP have the same mean diffusion coefficient in chromocenters. This could reflect the assembly of complexes for RNF168-EGFP. The difference in diffusion coefficient relative to EGFP for 53BP1 is approximately two-fold, while the difference in the predicted size of monomers is approximately 10-fold. Thus, this is close to the expected difference (eight-fold) in mass to account for the reduced diffusion of 53BP1-EGFP relative to EGFP. Nonetheless, 53BP1 diffusion is slightly faster than what we might expect. This is particularly true when considering that the diffusion coefficient measured in the nucleoplasm is slower than in chromocenters. Two possible explanations are that 53BP1 diffuses as a dimer or oligomer in the nucleoplasm but diffuses as monomers through the chromocenters. Purified GFP in permeabilized fixed cells reflected the increased density of the environment with a slower mean diffusion coefficient in the chromocenters compared to the nucleoplasm, as expected because of the higher mass density present in chromocenters (Imai et al., 2017).

One of the most striking features of these results is the wide range in chromocenter concentrations observed for individual proteins. For example, MDC1 and 53BP1 are both depleted from chromocenters. However, we measured concentrations that ranged from 32 to 120% of the nucleoplasmic concentration for MDC1 and from 26 to 67% for 53BP1. For EGFP alone, we observed a range of 53–87% concentration relative to the nucleoplasm. Notably, we found no examples where EGFP was not depleted. However, when we examined fixed and permeabilized cells, we found that purified GFP incubated with permeabilized fixed cells showed near homogeneous distribution between the nucleoplasm and chromocenters. This argues against a volume exclusion effect dictating differences in chromocenter accessibility observed in living cells. That is, the volume occupied by chromatin, and therefore inaccessible to free GFP, is retained during fixation and permeabilization. We expect similar results between living and fixed cells if volume exclusion is responsible for reduced EGFP concentration in the chromocenters of living cells. Another possibility is that the barrier is imposed by a solvent difference arising from the presence of a phase-separated liquid compartment. This barrier would not be expected to be maintained following fixation and detergent extraction. Its removal could explain the failure to maintain a reduced concentration of GFP in the chromocenters of fixed and permeabilized cells. Supporting this interpretation is that the nucleolus is a well-established phase separated compartment in the nucleus (Brangwynne et al., 2011; Feric et al., 2016; Frottin et al., 2019; Lafontaine et al., 2021), and much less depletion was observed for recombinant GFP in the nucleoli of fixed cells relative to the striking depletion in living cells.

Several membraneless compartments in the nucleus are well established as liquid-liquid phase separated (LLPS) condensates, including the nucleolus and nuclear speckles (Boeynaems et al., 2018). Chromocenters are also considered a membraneless compartment, and recent work has established that several key factors in pericentric heterochromatin formation have phase separation capacity *in vitro*. The primary and most explored example of this is heterochromatin protein 1 α (HP1 α), which has been demonstrated to have phase separation capacity *in vitro* (Larson et al., 2017). One current model of heterochromatin formation is that HP1α, which binds H3K9 tri- and dimethylation written by SUV39H1, dimerizes and oligomerizes to bridge nucleosomes compacting chromatin and, at a critical concentration, separates into a heterochromatin phase (Larson et al., 2017). A phase

separation role is also supported by work with HP1a in *Drosophila* (Strom et al., 2017). The histone methyltransferase KMT5C that writes H4K20 methylation marks in heterochromatin has liquid-like behaviour in chromocenters in that it exchanges freely within the chromatin but does not exchange freely with the nucleoplasm upon partial bleaching of chromocenters (Strickfaden et al., 2019). Further, another important heterochromatin protein, methyl CpG binding protein 2 (MeCP2), has been suggested to drive heterochromatin condensate formation in association with DNA, and mutations that disrupt the ability of MeCP2 to form condensates *in vitro* are found in patients with the neurodevelopmental disorder Rett syndrome (Li et al., 2020). Work on transcription factor kinetics with single-molecule tracking has recently demonstrated that rather than the previously bi-exponential behaviour with non-specific binding and specific binding, kinetics are better described with a third classification representing IDR-based constraint (Garcia et al., 2021a; Garcia et al., 2021b). It was found that the accumulation of glucocorticoid receptors at distinct regions in the nucleus could not be attributed solely to direct DNA binding events. Rather, there was a second subpopulation reliant on the presence of the transcription factor's IDR through multivalent interactions consistent with an association with a liquid phase separated compartment (Garcia et al., 2021b). This result supports the idea of the chromocenter as having a liquid phase separated compartment as it supports the accumulation of proteins within the compartment based on their non-specific interaction with other compartment components.

Rad51 forms filaments when overexpressed, and free nucleoplasmic concentrations appear to be kept low because of this propensity to polymerize. Tip60, RNF168, Rap80, and NBS1 all showed the presence of numerous small domains. Interestingly, 53BP1, characterized as a protein capable of initiating liquid-liquid phase separation, formed fewer of these structures. Further studies are required to determine if these are liquid condensates and their concentration dependence. Past work has demonstrated that condensed chromatin behaves as a solid-like gel and may act as a scaffold around which phase separation can occur (Strickfaden et al., 2020) and is supported by the observation that chromatin transitions to a gel-like state upon heterochromatin domain formation during differentiation (Eshghi et al., 2021). In this model, a phase separated condensate would exist around the solid-like gel and would regulate the movement of molecules through the chromocenter (Strickfaden et al., 2020). Differential solubility in a distinct liquid nuclear microenvironment rather than physical exclusion appears to be a better explanation for the relative partitioning of DNA damage response proteins in the nucleoplasm relative to mouse chromocenters. A phase separated condensate model of chromocenters could explain why size alone does not determine the relative abundance of these proteins. In this model, the partition coefficient, reflecting the relative solubility in the two liquid phases, will define the distribution. While this merely changes how the understanding of this distribution should be pursued through mutational analysis, it puts additional demands on the analysis of all proteins that are enriched in liquid compartments. For example, it will be important to distinguish between partitioning through weak multivalent interactions that lead to preferential accumulation in a distinct solvent environment from accumulation mediated by high or low specificity binding to the chromatin, which will also result in accumulation beyond the concentration found freely diffusing within the nucleoplasm.

Data availability statement

The raw data supporting the conclusions of this article will be made available by the authors, without undue reservation.

Author contributions

MH designed and conceived the experiments with input from DU, HS, and AR. AR and LM collected and analyzed the data. AR and MH wrote the manuscript.

Acknowledgments

We thank members of the Hendzel laboratory and the Department of Oncology Cell Imaging Facility for experimental support. This work was funded by the Canadian Institute of Health Research (CIHR). Michael J. Hendzel is a Canada Research Chair in the Cell Biology and Dynamics of the Genome.

Conflict of interest

The authors declare that the research was conducted in the absence of any commercial or financial relationships that could be construed as a potential conflict of interest.

Publisher's note

References

Ayoub, N., Jeyasekharan, A. D., Bernal, J. A., and Venkitaraman, A. R. (2008). HP1-β mobilization promotes chromatin changes that initiate the DNA damage response. *Nature* 453 (7195), 682–686. doi:10.1038/nature06875

Bancaud, A., Huet, S., Daigle, N., Mozziconacci, J., Beaudouin, J., and Ellenberg, J. (2009). Molecular crowding affects diffusion and binding of nuclear proteins in heterochromatin and reveals the fractal organization of chromatin. *EMBO J.* 28 (24), 3785–3798. doi:10.1038/emboj.2009.340

Basedow, A. M., and Ebert, K. H. (1979). Production, characterization, and solution properties of dextran fractions of narrow molecular weight distributions. *J. Polym. Sci. C. Polym. Symp.* 66, 101–115. doi:10.1002/polc.5070660113

Baum, M., Erdel, F., Wachsmuth, M., and Rippe, K. (2014). Retrieving the intracellular topology from multi-scale protein mobility mapping in living cells. *Nat. Commun.* 5. doi:10.1038/ncomms5494

Boeynaems, S., Alberti, S., Fawzi, N. L., Mittag, T., Polymenidou, M., Rousseau, F., et al. (2018). Protein phase separation: A new phase in cell Biology. *Trends Cell Biol.* 28 (6), 420–435. doi:10.1016/j.tcb.2018.02.004

Brangwynne, C. P., Mitchison, T. J., and Hyman, A. A. (2011). Active liquid-like behavior of nucleoli determines their size and shape in *Xenopus laevis* oocytes. *Proc. Natl. Acad. Sci. U. S. A.* 108 (11), 4334–4339. doi:10.1073/pnas.1017150108

Caron, M. C., Sharma, A. K., O'Sullivan, J., Myler, L. R., Ferreira, M. T., Rodrigue, A., et al. (2019). Poly(ADP-ribose) polymerase-1 antagonizes DNA resection at double-strand breaks. *Nat. Commun.* 10 (1), 2954. doi:10.1038/s41467-019-10741-9

Date, T., Doiguchi, Y., Nobuta, M., and Shindo, H. (2004). Bone morphogenetic protein-2 induces differentiation of multipotent C3H10T1/2 cells into osteoblasts, chondrocytes, and adipocytes in vivo and in vitro. *J. Orthop. Sci.* 9 (5), 503–508. doi:10.1007/s00776-004-0815-2

Donawho, C. K., Luo, Y., Luo, Y., Penning, T. D., Bauch, J. L., Bouska, J. J., et al. (2007). ABT-888, an orally active poly(ADP-ribose) polymerase inhibitor that potentiates DNA-damaging agents in preclinical tumor models. *Clin. Cancer Res.* 13 (9), 2728–2737. doi:10.1158/1078-0432.CCR-06-3039

Erdel, F. (2020). Biophysical mechanisms of chromatin patterning. *Curr. Opin. Genet. Dev.* 61, 62–68. doi:10.1016/j.gde.2020.03.006

Erdel, F., Rademacher, A., Vlijm, R., Tünnermann, J., Frank, L., Weinmann, R., et al. (2020). Mouse heterochromatin adopts digital compaction states without showing hallmarks of HP1-driven liquid-liquid phase separation. *Mol. Cell* 78 (2), 236–249. e7. doi:10.1016/j.molcel.2020.02.005

Eshghi, I., Eaton, J. A., and Zidovska, A. (2021). Interphase chromatin undergoes a local sol-gel transition upon cell differentiation. *Phys. Rev. Lett.* 126 (22), 228101. doi:10.1103/PhysRevLett.126.228101

Fan, C., Zhang, H., Fu, L., Li, Y., Du, Y., Qiu, Z., et al. (2020). Rett mutations attenuate phase separation of MeCP2. *Cell Discov.* 6, 38. doi:10.1038/s41421-020-0172-0

Feric, M., Vaidya, N., Harmon, T. S., Mitrea, D. M., Zhu, L., Richardson, T. M., et al. (2016). Coexisting liquid phases underlie nucleolar subcompartments. *Cell* 165 (7), 1686–1697. doi:10.1016/j.cell.2016.04.047

Forget, A. L., and Kowalczykowski, S. C. (2010). Single-molecule imaging brings Rad51 nucleoprotein filaments into focus. *Trends Cell Biol.* 20 (5), 269–276. doi:10.1016/j.tcb.2010.02.004

Frottin, F., Schueder, F., Tiwary, S., Gupta, R., Körner, R., Schlichthaerle, T., et al. (2019). The nucleolus functions as a phase-separated protein quality control compartment. *Science* 365 (6451), 342–347. doi:10.1126/science.aaw9157

Galkin, V. E., Esashi, F., Yu, X., Yang, S., West, S. C., and Egelman, E. H. (2005). BRCA2 BRC motifs bind RAD51-DNA filaments. *Proc. Natl. Acad. Sci. U. S. A.* 102, 8537–8542. doi:10.1073/pnas.0407266102

Garcia, D. A., Fettweis, G., Presman, D. M., Paakinaho, V., Jarzynski, C., Upadhyaya, A., et al. (2021a). Power-law behavior of transcription factor dynamics at the single-molecule level implies a continuum affinity model. *Nucleic Acids Res.* 49 (12), 6605–6620. doi:10.1093/nar/gkab072

Garcia, D. A., Johnson, T. A., Presman, D. M., Fettweis, G., Wagh, K., Rinaldi, L., et al. (2021b). An intrinsically disordered region-mediated confinement state contributes to the dynamics and function of transcription factors. *Mol. Cell* 81 (7), 1484–1498.e6. e6. doi:10.1016/j.molcel.2021.01.013

Goodarzi, A. A., Noon, A. T., Deckbar, D., Ziv, Y., Shiloh, Y., Löbrich, M., et al. (2008). ATM signaling facilitates repair of DNA double-strand breaks associated with heterochromatin. *Mol. Cell* 31 (2), 167–177. doi:10.1016/j.molcel.2008.05.017

Goodarzi, A. A., Noon, A. T., and Jeggo, P. A. (2009). The impact of heterochromatin on DSB repair. *Biochem. Soc. Trans.* 37 (3), 569–576. doi:10.1042/BST0370569

Görisch, S. M., Wachsmuth, M., Tóth, K. F., Lichter, P., and Rippe, K. (2005). Histone acetylation increases chromatin accessibility. *J. Cell Sci.* 118 (24), 5825–5834. doi:10.1242/jcs.02689

Guenatri, M., Bailly, D., Maison, C., and Almouzni, G. (2004). Mouse centric and pericentric satellite repeats form distinct functional heterochromatin. *J. Cell Biol.* 166 (4), 493–505. doi:10.1083/jcb.200403109

Haince, J. F., McDonald, D., Rodrigue, A., Déry, U., Masson, J. Y., Hendzel, M. J., et al. (2008). PARP1-dependent kinetics of recruitment of MRE11 and NBS1 proteins to multiple DNA damage sites. *J. Biol. Chem.* 283 (2), 1197–1208. doi:10.1074/jbc.M706734200

Hammar, P., Leroy, P., Mahmutovic, A., Marklund, E. G., Berg, O. G., and Elf, J. (2012). The lac repressor displays facilitated diffusion in living cells. *Science* 336 (6088), 1595–1598. doi:10.1126/science.1221648

Hansen, J. C., Maeshima, K., and Hendzel, M. J. (2021). The solid and liquid states of chromatin. *Epigenetics Chromatin* 14 (1), 50. doi:10.1186/s13072-021-00424-5

Hebbes, T. R., Clayton, A. L., Thorne, A. W., and Crane-Robinson, C. (1994). Core histone hyperacetylation co-maps with generalized DNase I sensitivity in the chicken β-globin chromosomal domain. *EMBO J.* 13 (8), 1823–1830. doi:10.1002/j.1460-2075.1994.tb06451.x

Hihara, S., Pack, C. G., Kaizu, K., Tani, T., Hanafusa, T., Nozaki, T., et al. (2012). Local nucleosome dynamics facilitate chromatin accessibility in living mammalian cells. *Cell Rep.* 2 (6), 1645–1656. doi:10.1016/j.celrep.2012.11.008

Hink, M. A., Griep, R. A., Borst, J. W., van Hoek, A., Eppink, M. H. M., Schots, A., et al. (2000). Structural dynamics of green fluorescent protein alone and fused with a single chain Fv protein. *J. Biol. Chem.* 275 (23), 17556–17560. doi:10.1074/jbc.M001348200

Holehouse, A. S., Ahad, J., Das, R. K., and Pappu, R. v. (2015). Cider: Classification of intrinsically disordered ensemble regions. *Biophysical J.* 108 (2), 228a. doi:10.1016/j.bpj.2014.11.1260

Huang, R. X., and Zhou, P. K. (2020). DNA damage response signaling pathways and targets for radiotherapy sensitization in cancer. *Signal Transduct. Target. Ther.* 5 (1), 60. doi:10.1038/s41392-020-0150-x

Imai, R., Nozaki, T., Tani, T., Kaizu, K., Hibino, K., Ide, S., et al. (2017). Density imaging of heterochromatin in live cells using orientation-independent-DIC microscopy. *Mol. Biol. Cell* 28 (23), 3349–3359. doi:10.1091/mbc.E17-06-0359

Jumper, J., Evans, R., Pritzel, A., Green, T., Figurnov, M., Ronneberger, O., et al. (2021). Highly accurate protein structure prediction with AlphaFold. *Nature* 596 (7873), 583–589. doi:10.1038/S41586-021-03819-2

Kao-Huang, Y., Revzint, A., Butlert, A. P., O'conner, P., Noble, D. W., and von Hippel, P. H. (1977). Non-specific DNA binding of genome-regulating proteins as a biological control mechanism: Measurement of DNA-bound *Escherichia coli* lac repressor in vivo*. *(minicells/repressor-DNA interactions/effective Ion. act. inE. coli/reprressor-inducer-operator-DNA Bind. constants)* 74 (10), 4228–4232. doi:10.1073/pnas.74.10.4228

Keenen, M. M., Brown, D., Brennan, L. D., Renger, R., Khoo, H., Carlson, C. R., et al. (2021). HP1 proteins compact dna into mechanically and positionally stable phase separated domains. *ELife* 10, e64563. doi:10.7554/eLife.64563

Kilic, S., Lezaja, A., Gatti, M., Bianco, E., Michelena, J., Imhof, R., et al. (2019). Phase separation of 53 BP 1 determines liquid-like behavior of DNA repair compartments. *EMBO J.* 38 (16), e101379. doi:10.15252/embj.2018101379

Kim, J. A., Kruhlak, M., Dotiwala, F., Nussenzweig, A., and Haber, J. E. (2007). Heterochromatin is refractory to γ-H2AX modification in yeast and mammals. *J. Cell Biol.* 178 (2), 209–218. doi:10.1083/jcb.200612031

Krietsch, J., Caron, M. C., Gagné, J. P., Ethier, C., Vignard, J., Vincent, M., et al. (2012). PARP activation regulates the RNA-binding protein NONO in the DNA damage response to DNA double-strand breaks. *Nucleic Acids Res.* 40 (20), 10287–10301. doi:10.1093/nar/gks798

Lafontaine, D. L. J., Riback, J. A., Bascetin, R., and Brangwynne, C. P. (2021). The nucleolus as a multiphase liquid condensate. *Nat. Rev. Mol. Cell Biol.Nature Res.* 22 (3), 165–182. doi:10.1038/s41580-020-0272-6

Larson, A. G., Elnatan, D., Keenen, M. M., Trnka, M. J., Johnston, J. B., Burlingame, A. L., et al. (2017). Liquid droplet formation by HP1α suggests a role for phase separation in heterochromatin. *Nature* 547 (7662), 236–240. doi:10.1038/nature22822

Larson, A. G., and Narlikar, G. J. (2018). The role of phase separation in heterochromatin formation, function, and regulation. *Biochemistry* 57 (17), 2540–2548. doi:10.1021/acs.biochem.8b00401

Li, C. H., Coffey, E. L., Dall'Agnese, A., Hannett, N. M., Tang, X., Henninger, J. E., et al. (2020). MeCP2 links heterochromatin condensates and neurodevelopmental disease. *Nature* 586 (7829), 440–444. doi:10.1038/s41586-020-2574-4

Liu, C., and Yu, X. (2015). *ADP-ribosyltransferases and poly ADP-ribosylation*.

Machida, S., Takizawa, Y., Ishimaru, M., Sugita, Y., Sekine, S., Nakayama, J. i., et al. (2018). Structural basis of heterochromatin formation by human HP1. *Mol. Cell* 69 (3), 385–397. e8. doi:10.1016/j.molcel.2017.12.011

Maeshima, K., Kaizu, K., Tamura, S., Nozaki, T., Kokubo, T., and Takahashi, K. (2015). The physical size of transcription factors is key to transcriptional regulation in chromatin domains. *J. Phys. Condens. Matter* 27 (6), 064116. doi:10.1088/0953-8984/27/6/064116

Miron, E., Oldenkamp, R., Brown, J. M., S Pinto, D. M., Shan Xu, C., Faria, A. R., et al. (2020). Chromatin arranges in chains of mesoscale domains with nanoscale functional topography independent of cohesin. *Sci. Adv.* 6, eaba8811. doi:10.1126/sciadv.aba8811

Müller-Ott, K., Erdel, F., Matveeva, A., Mallm, J., Rademacher, A., Hahn, M., et al. (2014). Specificity, propagation, and memory of pericentric heterochromatin. *Mol. Syst. Biol.* 10 (8), 746. doi:10.15252/msb.20145377

Noon, A. T., Shibata, A., Rief, N., Löbrich, M., Stewart, G. S., Jeggo, P. A., et al. (2010). 53BP1-dependent robust localized KAP-1 phosphorylation is essential for heterochromatic DNA double-strand break repair. *Nat. Cell Biol.* 12 (2), 177–184. doi:10.1038/ncb2017

Oliver, J. D., and Deen, W. M. (1994). Random-coil model for glomerular sieving of dextran. *Bull. Math. Biol.* 56 (3).

Paull, T. T., Cortez, D., Bowers, B., Elledge, S. J., and Gellert, M. (2001). Direct DNA binding by Brca1. *Proc. Natl. Acad. Sci. U. S. A.* 98 (11), 6086–6091. doi:10.1073/pnas.111125998

Peters, A., O'Carroll, D., Scherthan, H., Mechtler, K., Sauer, S., Schöfer, C., et al. (2001). Loss of the Suv39h histone methyltransferases imapirs mammalian heterochromatin and genome stability. *Cell* 107(3):323–337. doi:10.1016/S0092-8674(01)00542-6

Poirier, G. G., de Murciat, G., Jongstra-Bilent, J., Niedergangt, C., and Mandelo, P. (1982). Poly(ADP-ribosyl)ation of polynucleosomes causes relaxation of chromatin structure [nucleosome superstructure/electron microscopy/poly(ADP-ribose) polymerase/histone HI modification]. *Proc. Natd Acad. Sci. U. S. A.* 79.

Probst, A. v., and Almouzni, G. (2008). Pericentric heterochromatin: Dynamic organization during early development in mammals. *Differentiation.* 76 (1), 15–23. doi:10.1111/j.1432-0436.2007.00220.x

Quénet, D., Gasser, V., Fouillen, L., Cammas, F., Cianferani, S., Losson, R., et al. (2008). The histone subcode: poly(ADP-ribose) polymerase-1 (Parp-1) and parp-2 control cell differentiation by regulating the transcriptional intermediary factor TIF1beta and the heterochromatin protein HP1alpha. *FASEB J.* 22 (11), 3853–3865. doi:10.1096/fj.08-113464

Rack, J. G. M., Liu, Q., Zorzini, V., Voorneveld, J., Ariza, A., Honarmand Ebrahimi, K., et al. (2021). Mechanistic insights into the three steps of poly(ADP-ribosylation) reversal. *Nat. Commun.* 12 (1), 4581. doi:10.1038/s41467-021-24723-3

Ramy, R., Magroun, N., Messadecq, N., Gauthier, L. R., Boussin, F. D., Kolthur-Seetharam, U., et al. (2009). Functional interplay between parp-1 and SirT1 in genome integrity and chromatin-based processes. *Cell. Mol. Life Sci.* 66 (19), 3219–3234. doi:10.1007/s00018-009-0105-4

Ray Chaudhuri, A., and Nussenzweig, A. (2017). The multifaceted roles of PARP1 in DNA repair and chromatin remodelling. *Nat. Rev. Mol. Cell Biol.* 18 (10), 610–621. doi:10.1038/nrm.2017.53

Rivera-Calzada, A., Spagnolo, L., Pearl, L. H., and Llorca, O. (2007). Structural model of full-length human Ku70-Ku80 heterodimer and its recognition of DNA and DNA-PKcs. *EMBO Rep.* 8 (1), 56–62. doi:10.1038/sj.embor.7400847

Roberts, S. A., and Gordenin, D. A. (2014). Hypermutation in human cancer genomes: Footprints and mechanisms. *Nat. Rev. Cancer* 14 (12), 786–800. doi:10.1038/nrc3816

Rouleau, M., Aubin, R. A., and Poirier, G. G. (2004). Poly(ADP-ribosyl)ated chromatin domains: Access granted. *J. Cell Sci.* 117 (6), 815–825. doi:10.1242/jcs.01080

Schuster-Böckler, B., and Lehner, B. (2012). Chromatin organization is a major influence on regional mutation rates in human cancer cells. *Nature* 488 (7412), 504–507. doi:10.1038/nature11273

Shen, Y., Rehman, F. L., Feng, Y., Boshuizen, J., Bajrami, I., Elliott, R., et al. (2013). BMN673, a novel and highly potent PARP1/2 inhibitor for the treatment of human cancers with DNA repair deficiency. *Clin. Cancer Res.* 19 (18), 5003–5015. doi:10.1158/1078-0432.CCR-13-1391

Simons, A. M., Horwitz, A. A., Starita, L. M., Griffin, K., Williams, R. S., Glover, J. N. M., et al. (2006). BRCA1 DNA-binding activity is stimulated by BARD1. *Cancer Res.* 66 (4), 2012–2018. doi:10.1158/0008-5472.CAN-05-3296

Song, K., Jung, Y., Jung, D., and Lee, I. (2001). Human Ku70 interacts with heterochromatin protein 1alpha. *J. Biol. Chem.* 276 (11), 8321–8327. doi:10.1074/jbc.M008779200

Soo Lee, N., Jin Chung, H., Kim, H. J., Yun Lee, S., Ji, J. H., Seo, Y., et al. (2016). TRAIP/RNF206 is required for recruitment of RAP80 to sites of DNA damage. *Nat. Commun.* 7, 10463. doi:10.1038/ncomms10463

Stracy, M., Schweizer, J., Sherratt, D. J., Kapanidis, A. N., Uphoff, S., and Lesterlin, C. (2021). Transient non-specific DNA binding dominates the target search of bacterial DNA-binding proteins. *Mol. Cell* 81 (7), 1499–1514.e6. e6. doi:10.1016/j.molcel.2021.01.039

Strickfaden, H., McDonald, D., Kruhlak, M. J., Haince, J. F., Th'Ng, J. P. H., Rouleau, M., et al. (2016). Poly(ADP-ribosyl)ation-dependent transient chromatin decondensation and histone displacement following laser microirradiation. *J. Biol. Chem.* 291 (4), 1789–1802. doi:10.1074/jbc.M115.694992

Strickfaden, H., Missiaen, K., Hendzel, M. J., and Alan Underhill, D. (2019). KMT5C displays robust retention and liquid-like behavior in phase separated heterochromatin. *BioRxiv*. doi:10.1101/776625

Strickfaden, H., Tolsma, T. O., Sharma, A., Underhill, D. A., Hansen, J. C., and Hendzel, M. J. (2020). Condensed chromatin behaves like a solid on the mesoscale in vitro and in living cells. *Cell* 183 (7), 1772–1784.e13. e13. doi:10.1016/j.cell.2020.11.027

Strom, A. R., Biggs, R. J., Banigan, E. J., Wang, X., Chiu, K., Herman, C., et al. (2021). Hp1α is a chromatin crosslinker that controls nuclear and mitotic chromosome mechanics. *ELife* 10, e63972. doi:10.7554/eLife.63972

Strom, A. R., Emelyanov, A. v., Mir, M., Fyodorov, D. v., Darzacq, X., and Karpen, G. H. (2017). Phase separation drives heterochromatin domain formation. *Nature* 547 (7662), 241–245. doi:10.1038/nature22989

Taddei, A., Maison, C., Roche, D., and Almouzni, G. (2001). Reversible disruption of pericentric heterochromatin and centromere function by inhibiting deacetylases. *Nat. Cell Biol.* 3, 114–120. doi:10.1038/35055010

Tarsounas, M., Davies, D., and West, S. C. (2003). BRCA2-dependent and independent formation of RAD51 nuclear foci. *Oncogene* 22, 1115–1123. doi:10.1038/sj.onc.1206263

Thakur, J., Fang, H., Llagas, T., Disteche, C. M., and Henikoff, S. (2019). Architectural RNA is required for heterochromatin organization. *BioRxiv*. doi:10.1101/784835

Tsouroula, K., Furst, A., Rogier, M., Heyer, V., Maglott-Roth, A., Ferrand, A., et al. (2016). Temporal and spatial uncoupling of DNA double-strand break repair pathways within mammalian heterochromatin. *Mol. Cell* 63 (2), 293–305. doi:10.1016/j.molcel.2016.06.002

van der Heijden, T., Seidel, R., Modesti, M., Kanaar, R., Wyman, C., and Dekker, C. (2007). Real-time assembly and disassembly of human RAD51 filaments on individual DNA molecules. *Nucleic Acids Res.* 35 (17), 5646–5657. doi:10.1093/nar/gkm629

Walker, J. R., Corpina, R. A., and Goldberg, J. (2001). Structure of the Ku heterodimer bound to DNA and its implications for double-strand break repair. *NATURE* 412.

Wang, L., Gao, Y., Zheng, X., Liu, C., Dong, S., Li, R., et al. (2019). Histone modifications regulate chromatin compartmentalization by contributing to a phase separation mechanism. *Mol. Cell* 76 (4), 646–659. e6. doi:10.1016/j.molcel.2019.08.019

Weintraub, H., and Groudine, M. (1976). Chromosomal Subunits in Active Genes Have an Altered Conformation: Globin genes are digested by deoxyribonuclease 1 in red blood cell nuclei but not in fibroblast nuclei. *Sci. Am. Assoc. Adv. Sci.* 193 (4256), 848–856. doi:10.1126/science.94874

Wickham, H. (2016). *ggplot2: Elegant graphics for data analysis*. Springer-Verlag New York.

Wu, Q., Hu, H., Lan, J., Emenari, C., Wang, Z., Chang, K. S., et al. (2009). PML3 orchestrates the nuclear dynamics and function of TIP60. *J. Biol. Chem.* 284 (13), 8747–8759. doi:10.1074/jbc.M807590200

Xiao, J., Liu, M., Qi, Y., Chaban, Y., Gao, C., Pan, B., et al. (2019). Structural insights into the activation of ATM kinase. *Cell Res.* 29 (8), 683–685. doi:10.1038/s41422-019-0205-0

Yu, Z., Vogel, G., Coulombe, Y., Dubeau, D., Spehalski, E., Hébert, J., et al. (2012). The MRE11 GAR motif regulates DNA double-strand break processing and ATR activation. *Cell Res.* 22, 305–320. doi:10.1038/cr.2011.128

Zhou, H. X. (2001). The affinity-enhancing roles of flexible linkers in two-domain DNA-binding proteins. *Biochemistry* 40 (50), 15069–15073. doi:10.1021/bi015795g

frontiers | Frontiers in Genetics

TYPE Review
PUBLISHED 09 September 2022
DOI 10.3389/fgene.2022.926577

OPEN ACCESS

EDITED BY
Christophe Thiriet,
UMR6286 Unité de fonctionnalité et Ingénierie des Protéines (UFIP), France

REVIEWED BY
Jieqiong Lou,
The University of Melbourne, Australia
Zoraya Palomera-Sanchez,
Michoacana University of San Nicolás de Hidalgo, Mexico

*CORRESPONDENCE
Devyani Haldar,
devyani@cdfd.org.in

SPECIALTY SECTION
This article was submitted to Epigenomics and Epigenetics, a section of the journal Frontiers in Genetics

RECEIVED 22 April 2022
ACCEPTED 05 August 2022
PUBLISHED 09 September 2022

CITATION
Aricthota S, Rana PP and Haldar D (2022), Histone acetylation dynamics in repair of DNA double-strand breaks. *Front. Genet.* 13:926577. doi: 10.3389/fgene.2022.926577

Histone acetylation dynamics in repair of DNA double-strand breaks

Shalini Aricthota, Paresh Priyadarshan Rana and Devyani Haldar*

Laboratory of Chromatin Biology and Epigenetics, Centre for DNA Fingerprinting and Diagnostics, Hyderabad, Telangana, India

Packaging of eukaryotic genome into chromatin is a major obstacle to cells encountering DNA damage caused by external or internal agents. For maintaining genomic integrity, the double-strand breaks (DSB) must be efficiently repaired, as these are the most deleterious type of DNA damage. The DNA breaks have to be detected in chromatin context, the DNA damage response (DDR) pathways have to be activated to repair breaks either by non-homologous end joining and homologous recombination repair. It is becoming clearer now that chromatin is not a mere hindrance to DDR, it plays active role in sensing, detection and repair of DNA damage. The repair of DSB is governed by the reorganization of the pre-existing chromatin, leading to recruitment of specific machineries, chromatin remodelling complexes, histone modifiers to bring about dynamic alterations in histone composition, nucleosome positioning, histone modifications. In response to DNA break, modulation of chromatin occurs *via* various mechanisms including post-translational modification of histones. DNA breaks induce many types of histone modifications, such as phosphorylation, acetylation, methylation and ubiquitylation on specific histone residues which are signal and context dependent. DNA break induced histone modifications have been reported to function in sensing the breaks, activating processing of breaks by specific pathways, and repairing damaged DNA to ensure integrity of the genome. Favourable environment for DSB repair is created by generating open and relaxed chromatin structure. Histone acetylation mediate de-condensation of chromatin and recruitment of DSB repair proteins to their site of action at the DSB to facilitate repair. In this review, we will discuss the current understanding on the critical role of histone acetylation in inducing changes both in chromatin organization and promoting recruitment of DSB repair proteins to sites of DNA damage. It consists of an overview of function and regulation of the deacetylase enzymes which remove these marks and the function of histone acetylation and regulators of acetylation in genome surveillance.

KEYWORDS

chromatin, histone acetyltransferase (HAT), histone deacetylase (HDAC), histone modifications, chromatin remodelling, homologous recombination, DNA double-strand break repair pathway choice

Introduction

Genomic integrity is constantly compromised by DNA damage arising from exposure to endogenous and exogenous genotoxic agents. Double-strand breaks (DSBs) are the most dangerous form of DNA damage that are caused from exposure to ionizing radiation (IR), the collapse of DNA replication forks or during processing of certain types of DNA lesion. If not detected and repaired rapidly, these can cause mutations, chromosomal rearrangements, genomic instability, cell death or diseases like cancer (Jackson and Bartek, 2009; Ciccia and Elledge, 2010; Kieffer and Lowndes, 2022). Two major evolutionarily conserved pathways have evolved to protect organisms from DSB, non-homologous end joining (NHEJ) and homologous recombination (HR). The NHEJ pathway repairs the damaged DNA ends by direct religation, whereas in HR, the intact sister chromatid (present at S-phase and G2 phase) is used as a template for repair (Lieber, 2010; Chapman et al., 2012). However, a fundamental question remains on how one of these specific pathways is chosen although several factors influencing the DNA repair pathway choice such as chromatin structure, DNA end resection, cell cycle phase and transcription have been identified (Chapman et al., 2012; Aymard et al., 2014; Hustedt and Durocher, 2016). Studies over last three decades have shown how cells detect and repair DSBs and established that in addition to the proteins directly involved in DNA repair, chromatin structure surrounding the DSB and the factors regulating it, plays a conserved active role in facilitating DNA damage signalling and repair (Lukas et al., 2011; Soria et al., 2012; Mohan et al., 2021). The ability of cells to mount an effective DNA damage response is regulated by the chromatin dynamics of the region surrounding the DSB.

In eukaryotic cells, DNA is wrapped into chromatin in the nuclei. Nucleosome, the basic unit of chromatin, is comprised of 147 base pairs of DNA and a histone octamer with two H2A–H2B dimer and one H3–H4 tetramers (Jenuwein and Allis, 2001; Luger et al., 1997). The N- and C-terminal tails of these histone proteins can be post-translationally modified via acetylation, phosphorylation, methylation, SUMOylation, and ubiquitination (Strahl and Allis, 2000; Kouzarides, 2007). The repair of DSB is governed by the reorganization of the pre-existing chromatin, resulting in recruitment of damage sensors and chromatin remodelers to bring about dynamic alterations in histone modifications leading to recruitment of repair proteins (Soria et al., 2012; Wilson and Durocher, 2017; Mohan et al., 2021). In response to DNA break, modulation of chromatin occurs via various mechanisms including post-translational modification of histones. Upon DBS formation, post-translational modifications like phosphorylation, acetylation, methylation and ubiquitylation are known to be induced on specific histone residues near the DSB, which are signal and context dependent (Kouzarides, 2007; Miller and Jackson, 2012; Van and Santos, 2018). DNA break induced histone modifications have been reported to function in sensing the lesion, activating pathways for processing and repair of breaks to maintain genomic integrity. Formation of DSB induces chromatin decondensation, which is evident from the reports showing increased sensitivity of damaged DNA to micrococcal nuclease (Telford and Stewart, 1989). Several studies have shown that dynamic regulation of histone acetylation via histone acetylases and Histone deacetylases play crucial role in regulating chromatin structure flanking the DSB and is required for activation of the DNA damage response and DSB repair. In response to DSBs, formation of open, relaxed chromatin domains occur which are spatially localized to the area surrounding the break (Figure 1). These relaxed chromatin structures are created through the joint action of the chromatin remodellers and histone acetyltransferases (Qi et al., 2016). The resulting destabilization of nucleosomes at the DSB by chromatin remodeller and histone modifiers, is needed for the subsequent recruitment of the DNA repair proteins. The DSBs are then repaired either by non-homologous end joining and homologous recombination. Histone acetylation increases chromatin assessibility and therefore has been shown to play a positive role in DSB repair pathway. However, there are reports on requirement of HDAC complexes, for efficient DNA repair by NHEJ (Jazayeri et al., 2004; Miller et al., 2010; Miller and Jackson, 2012). Therefore, understanding about chromatin dynamics at DSBs and the precise role chromatin environment plays to influence the process of DSB repair is not fully understood. Further, there is emerging evidence that the different chromatin structures in the cell, such as heterochromatin and euchromatin, utilize distinct remodeling complexes and pathways to facilitate DSB repair (Caridi et al., 2017). Interestingly, the metabolic state of the cell at the time when DSB occur also influence DNA damage signalling and repair (Sivanand et al., 2017; Vadla et al., 2020). The processing and repair of DSB is therefore critically influenced by the nuclear architecture in which the lesion arises. At the damaged DNA, histone acetylation level changes through signal dependent recruitment and regulation of histone acetyltransferases and histone deacetylases which function in coordination with the ATP dependent remodellers. In this review, we will discuss how chromatin architecture of the region where the DSB is localized alters via dynamic changes in histone acetylation to generate a repair conducive platform to maintain genomic integrity.

DNA damage response

Double-strand breaks can form directly by breakage of both the strands, or collapse of stalled replication forks. DSBs are quickly detected by mobilizing and recruiting the sensing factors to recognize these lesions and activating the DNA damage checkpoint (Smolka et al., 2007). The signaling pathways begins with the activation of sensors ATM, ATR and DNA-

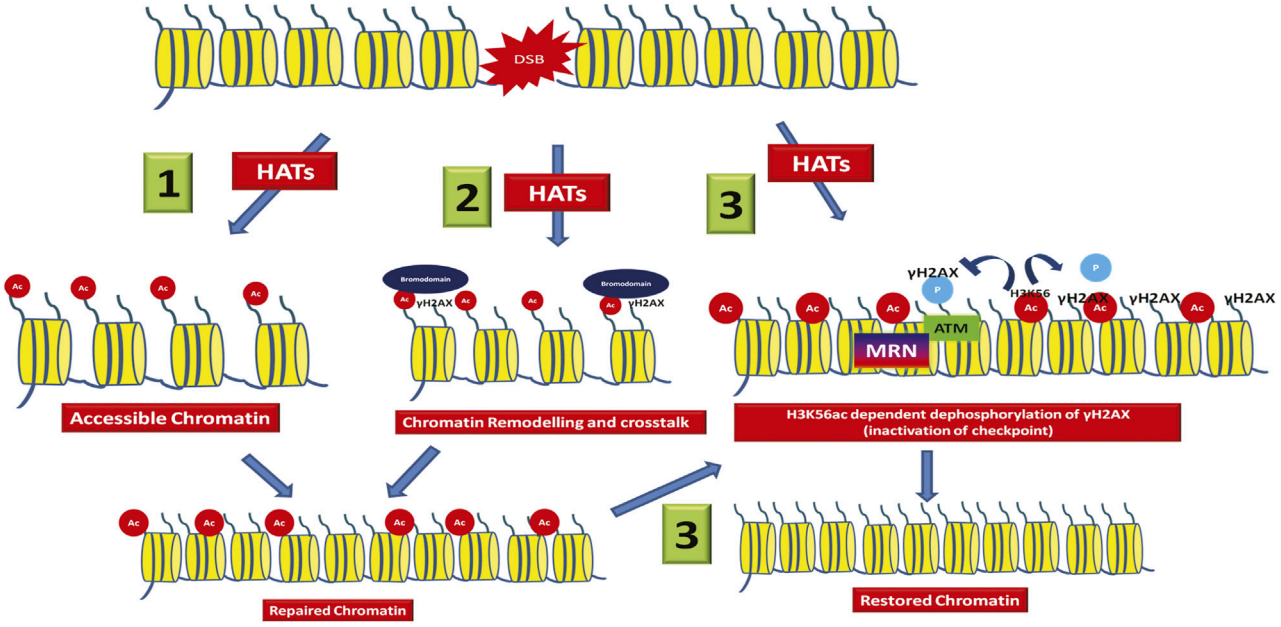

FIGURE 1
Different roles of histone acetylation at the DSB. At the DSB, acetylation of histones by the action of histone acetyltransferases leads to- 1) Charge based increase in chromatin accessibility leading to recruitment of repair factors. 2) The acetylated histones are recognized by acetyl readers like bromodomain containing proteins, which in turn leads to chromatin remodelling around the break and DDR factor recruitment. 3) Some modifications like H3K56ac helps in inactivation of checkpoint and therefore leads to chromatin restoration to its native state.

PKCs (Matsuoka et al., 2007). The primary mark for DSB is phosphorylation of H2AX, spreads to megabases around the DSB and triggers downstream processes (Rogakou et al., 1998; Rogakou et al., 1999). One of the earliest cellular responses to DSBs is the rapid recruitment of the ATM kinase and phosphorylation of histone H2AX (known as γH2AX) on either side of the DSB which acts a platform for landing of multiple repair factors to the chromatin (Bonner et al., 2008). For example, initial phosphorylation of H2AX (γH2AX) recruits scaffold protein MDC1 (Stucki et al., 2005) forming a docking platform that promote the recruitment and retention of other DNA repair proteins onto the chromatin at DSBs, including the MRN complex, the RNF8 ubiquitin ligase and the BRCA1, Ku70/80, and 53BP1 proteins (Kolas et al., 2007; Mailand et al., 2007; Melander et al., 2008). In response to DSBs, formation of open, relaxed chromatin domains occur which are spatially localized to the area surrounding the break the relaxed chromatin is created through the joint action created through the joint action of the chromatin remodellers and histone acetyltransferases such as SWI/SNF complexes, Tip60, p300, etc., respectively (Papamichos-Chronakis and Peterson, 2013; Qi et al., 2016). The resulting destabilization of nucleosomes at the DSB by chromatin remodeller and modifiers is needed for ubiquitination of the chromatin by the RNF8 ubiquitin ligase, and for the subsequent recruitment of the NHEJ or HR factors.

The metabolic state and cell cycle stage also affects DSB formation and the response to DSB varies accordingly. Repair via homologous recombination pathway depends on presence of a sister chromatid as template. Hence, the HR pathways is functional during the S/G2 phase, whereas, the NHEJ pathway is active throughout the cell cycle. Recognition of damaged DNA ends by Ku70/80 leads to recruitment of other factors for NHEJ (Kieffer and Lowndes, 2022). Similarly, the HR pathway requires the processing of the DNA by MRN complex and other proteins like RPA, CtIP, Exo1 followed by recruitment of BRCA1 and other HR factors. Checkpoint mediators like 53BP1 of NHEJ pathway and BRCA1 of HR pathways compete against each other to make the pathway choice (Powell and Kachnic, 2003; Panier and Boulton, 2014) (Figure 3). The repair pathway choice refers to the preference of HR vs. NHEJ pathway for repairing a DSB according to the availability of template DNA and the complexity of the damage (Chapman et al., 2012; Mohan et al., 2021). The γH2AX and the MRN complex is involved in crosstalk with histone modifications for efficient loading of chromatin remodelers and repair factors at the sites of DSBs. The external environment can affect HR machinery via affecting the chromatin modification marks. For example, a low pH environment requires the acetylation level to drop to certain extent for HR to successfully commence upon DSB formation (Vadla et al., 2020). Even the chromatin landscape

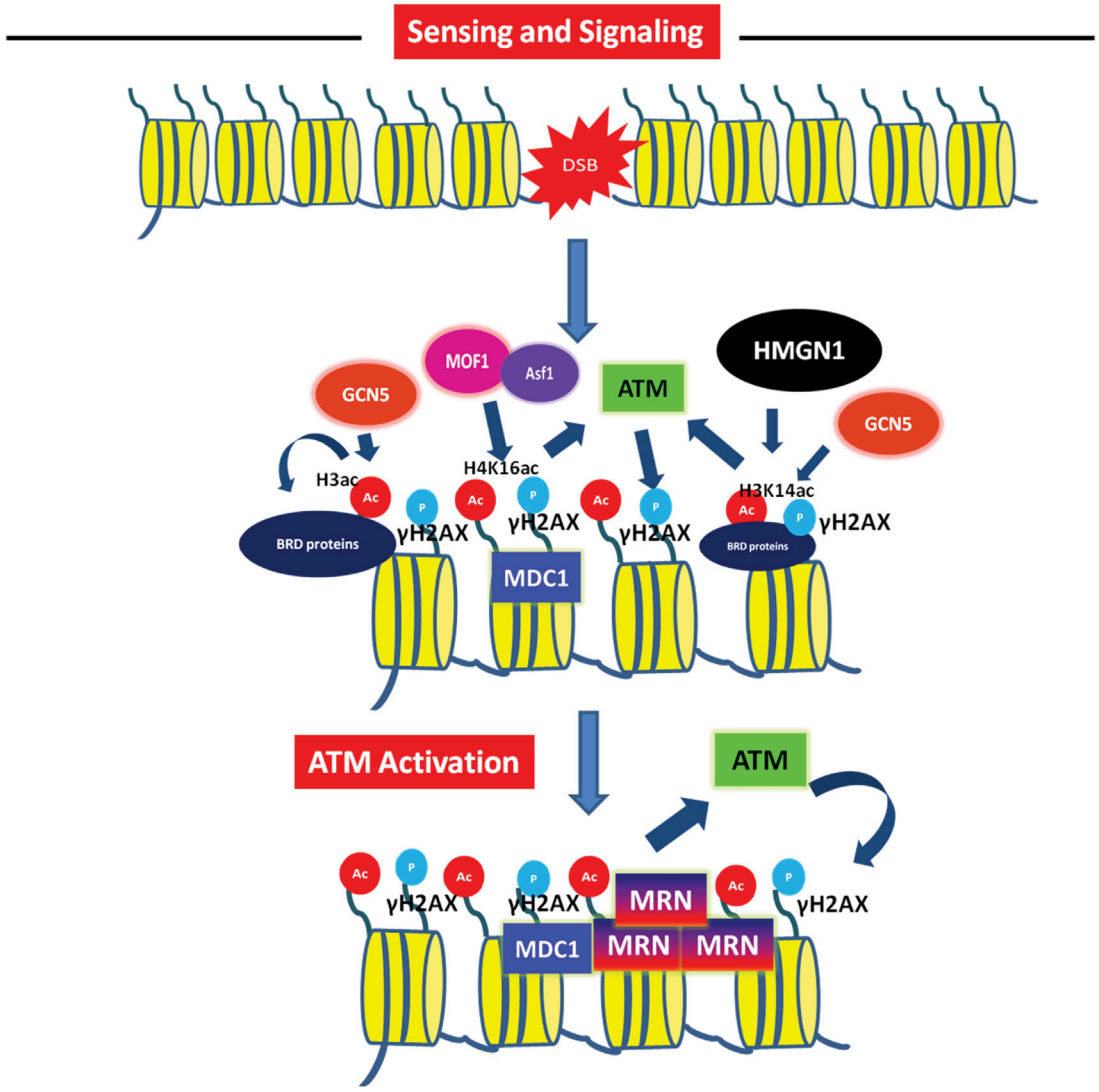

FIGURE 2
Role of acetylation in sensing and signalling of double-strand breaks Acetylation mediated activation of DNA damage checkpoint leading to DNA damage recognition- The checkpoint sensor ATM phosphorylates H2AX, leading to recruitment of MDC1. This MDC1 recruitment *via* interaction with γH2AX is facilitated by H4K16 acetylation mark established by MOF1 (with help of Asf1 histone chaperon) at the DSB. The H3K14ac by GCN5 and docking of MDC1 promotes ATM activation and spreading of γH2AX mark. This leads to recruitment of pathway specific factors like the MRN complex.

around a break, like heterochromatin or euchromatin, can influence the repair machinery, calling in the specific repair factors (Caridi et al., 2017; Aleksandrov et al., 2020). The activation of ATM and DNA-PKCs can be influenced by the chromatin remodelers recruited to specific histone marks. There are multiple modes of ATM activation as depicted in Figure 2 and also described in individual histone modifications sections. In addition to these canonical sensors, currently, the role of histone deacetylase SIRT6 has come into light regarding its interaction with CHD4 as a DSB sensor. It involves chromatin relaxation and HP1 release from H3K9me3 for HR machineries to access the damaged DNA (Hou et al., 2020; Meng et al., 2020; Onn et al., 2020), linking heterochromatin regulation to DSB sensing and repair. After the establishment of chromatin marks and recruitment of repair factors, the chromatin remodelers like SWI/SNF and RSC (Remodelling the Structure of Chromatin) complex slide the nucleosomes to make the DNA damage accessible. This demonstrates the importance of chromatin modifications in signalling of DNA damage and making the repair pathway choice.

Histone acetylation and DSB repair

The various post-translational modification of histones at the DSB can act as a barrier *via* compaction or can make chromatin accessible via decompaction during the process of damage signalling as well as repair (Aleksandrov et al., 2020). Acetylation of histones is one such dynamic chromatin modification regulated by the concerted action of HAT and HDAC (Gong and Miller, 2013; Roos and Krumm, 2016). Acetylation of lysine residues changes the charge at the DNA-nucleosome interface, leading to more open and accessible chromatin (Dhar et al., 2017). The histone acetyltransferases can be grouped into five subfamilies, namely HAT1/KAT1 (yHAT1), Gcn5/PCAF (yGcn5, hGCN5, hPCAF), Myst (yEsa1, ySas2, hMOZ, hMOF, hTIP60, etc), p300/CBP (hp300, hCBP), and Rtt109 (yrtt109) (Carrozza et al., 2003; Utley and Cote, 2003). Among these, p300/CBP subfamily is metazoan specific while Rtt109 is yeast specific (Marmorstein and Zhou, 2014). Histone acetylation is reversed by histone deacetylases, an action that restores the positive charge of the lysine. There are four classes of HDAC: Classes I and II contain enzymes that are most closely related to yeast scRpd3 and scHda1, respectively, class IV has only a single member, HDAC11, while class III (referred to as sirtuins) are homologous to yeast scSir2 (Glozak and Seto, 2007). This latter class, in contrast to the other three classes, requires a specific cofactor for its activity, NAD+ (Glozak and Seto, 2007; Greiss and Gartner, 2009).

The acetylation modifications at the N-terminus of the histones are most commonly studied as they are highly accessible at the tails and mediate binding of reader chromatin proteins (Kouzarides, 2007; Soria et al., 2012). Five reversible acetylable lysines are present at the N-terminus of histone H3 namely, 9, 14, 18, 23, and 27, whereas four acetylable lysines are present at positions 5, 8, 12, and 16 at the N-terminus of Histone H4 (North and Verdin, 2004; Wang et al., 2007; Ma and Schultz, 2008; Hulin et al., 2016; Khilji et al., 2021; Song et al., 2021; Wu et al., 2022). Interestingly, covalent modifications also occur within the globular domain of histones, especially at positions that are in close contact with the nucleosomal DNA wrapped around each octamer. One example of such acetylation is histone H3 lysine 56 (H3K56ac). The other histones like the linker H1 and the H2A are also modified at lysines with important roles in DSB repair. Table 1 shows the list of all histone lysine acetylation modifications which are regulated in response to DSBs. There are mainly three ways by which lysine acetylation of histones act at the chromatin- Activation of DDR pathway via making chromatin accessible, helping the remodelling of chromatin around DSB to help in DNA repair factor mobility and localization and lastly restoration of chromatin post DNA repair through inactivation of checkpoint (for example, H3K56ac is required for inactivation of checkpoint, also described in H3K56ac section) and later nucleosome packaging to native chromatin state (Figure 1).

The bromo-domain (BRD) containing proteins act as the reader of acetylation marks through which many repair proteins come to the site of damage and thereby mediate repair functions (Marmorstein and Zhou, 2014). The role of histone acetylation and deacetylation in DSB repair was indicated by some of the earliest studies where the HDAC, sirtuins were shown to play a role in recombinational repair. The mutants of Sir proteins and Rad52 were shown to be synthetically sensitive to gamma-irradiation (Tsukamoto et al., 1997). Using two Hybrid assay, the Sir2, Sir3, and Sir4 were found to physically interact with Ku, the NHEJ factor (Tsukamoto et al., 1997). Consistent with this, Sir2 along with other sir proteins relocalize to the site of damage and help in silencing as well as chromatin compaction (Martin et al., 1999; Mills et al., 1999; Guarente, 2000). These proteins relocalize to the sites of damage along with the NHEJ protein Ku (Martin et al., 1999). Subsequently, indications on the role of histone acetylation in DSB repair came in the early 2000. The acetylation of histone H4 at the N-terminus residues catalysed by Esa1 acetyltransferase (mammalian Tip60 homolog) was first shown to be implicated in DSB repair (Bird et al., 2002). Early studies (Qin and Parthun, 2002) and (Tamburini and Tyler, 2005) have shown the role of histone H3 acetylation catalysed by Hat1 acetyltransferase and Gcn5 in the repair of DSB induced by the mating-type switching HO endonuclease. In support of these studies, the deletion of acetyl transferases responsible for the acetylation of these histone residues such as Tip60 in mammals, NuA4 subunit yng2 and gcn5 were also found to have DSB repair defects, genome stability functions, tumor suppressor functions, consistent with the roles of acetylation in DSB repair (Ikura et al., 2000; Choy and Kron, 2002; Kusch et al., 2004; Gorrini et al., 2007; Sun et al., 2010). The first direct evidence on the role of histone acetyltransferases in DSB repair came from the localization studies of Nua4 and Tip60 at the chromatin near DSB (Downs et al., 2004; Murr et al., 2006). NuA4/Tip60 is recruited to DSBs to acetylate Histone H4, H2A as well as H2AX and facilitate chromatin opening (Sun et al., 2010; Jacquet et al., 2016). It also has non-histone targets such as ATM which facilitates the DSB repair signalling (Sun et al., 2005). The human HATs like Mof1, TIP60, CBP, p300, and GCN5 play redundant roles in regulating acetylation at DSBs. Interestingly, ablation of CBP, p300, and Tip60 lead to decreased NHEJ (Van and Santos, 2018). Analysis using experiments such as laser microirradiation and ChIP at I-Sce1 induced DSBs, these acetyltransferases were found to be accumulated at the sites of DSB along with γ-H2AX and NHEJ factors Ku70, Ku80, 53BP1 (Murr et al., 2006; Ogiwara et al., 2011; Jacquet et al., 2016). The histone acetylation and deacetylation landscapes dictate the choice of pathway for repair of DSBs. For example, the histone acetylation mark H4K16 has been shown to counteract binding of 53BP1 leading to resection and repair by HR (Tang et al., 2013). Tip60 mediated H2AK15ac also leads to inhibition of 53BP1 binding at DSBs (Jacquet et al., 2016). These epigenetic

TABLE 1 List of acetyl lysine modifications of Histones with roles in DSB signaling and Repair.

Histone acetylation	Acetyl transferase	Function in DDR	Reference
H1K85ac	PCAF	Decreases immediately post DNA damage. Promotes heterochromatin protein 1 (HP1) recruitment leading to condensed chromatin	Li et al. (2018)
H2AK15ac	Tip60	Peaks at S/G2, reduces at sites specifically repaired by NHEJ. Tip60 dependent H2AK15ac regulates DSB repair pathway choice by inhibiting H2AK15Ub and binding of 53BP1 thus, promoting HR.	Jacquet et al. (2016)
H2AX K5ac	TIP60	Decreases the spread of γH2AX-P upon damage. Aids in NBS1 accumulation at the damaged regions via H2AX exchange, thus aiding in ATM signalling	Kusch et al. (2004); Ikura et al. (2007); Jha et al. (2008); Ikura et al. (2015)
H2AX K36ac	p300/CBP	Constitutive acetylation, does not increase on radiation damage, however, promotes IR survival independently of gH2AX phosphorylation	Jiang et al. (2010)
H2BK120ac	SAGA acetyl transferase	Upon DSB induction H2BK120ub to H2BK120ac switch occurs irrespective of the region of DSB. May help in nucleosome remodelling	Clouaire et al. (2018)
H3K9ac	GCN5, PCAF	Reduces upon DNA damage, helps in localization of Swi/SNF complex to γH2AX containing nucleosomes. Obstructs ATM activation in stem cells leading to IR sensitivity	(Tjeertes et al., 2009; Lee et al., 2010; Meyer et al., 2016)
H3K14ac	GCN5	Increases in response to damage, helps in localization of Swi/SNF complex to γH2AX containing nucleosomes. Stimulated by HMGN1 and required for the activation of ATM.	(Kim et al., 2009; Lee et al., 2010)
H3K18ac	p300/CBP, GCN5	Recruitment of SWI/SNF and Ku at initial timepoints during G1 phase, later deacetylation by Sirt7 leads to loading of 53BP1 to facilitate effective NHEJ.	(Ogiwara et al., 2011; Vazquez et al., 2016; Swift et al., 2021)
H3K56ac	p300/CBP	Both reduction and increase observed post DNA damage, Deacetylated by Sirt6 and Sirt3 promotes NHEJ by recruiting SNF2H and 53BP1 to the DSB sites. Deactivates checkpoint to facilitate recovery and chromatin assembly	(Chen et al., 2008; Das et al., 2009; Tjeertes et al., 2009; Miller et al., 2010; Vempati et al., 2010; Battu et al., 2011; Toiber et al., 2013; Clouaire et al., 2018; Sengupta and Haldar, 2018; Vadla et al., 2020)
H4K5ac, H4K8ac	Tip60-Trap	Repair by HR by facilitating recruitment of MDC1, BRCA1. 53BP1, RAD51	(Murr et al., 2006; Ogiwara et al., 2011; Clouaire et al., 2018)
H4K12ac	p300/CBP	Recruitment of SWI/SNF complex, KU70/80 and repair by NHEJ H4K12ac was reduced at AsiSI induced DSBs	
H4K16ac	Tip60-Trap MOF1	Biphasic response at the DSBs, facilitates both NHEJ and HR. Initial decrease and then increase at later timepoints. Abrogation of MDC1, 53BP1 and BRCA1 foci in the absence of MOF1	(Li et al., 2010; Miller et al., 2010; Sharma et al., 2010)

landscapes are therefore dynamic and becomes crucial when the DSBs occur during the process of other DNA metabolic activities such as DNA replication, transcription, etc. (Aleksandrov et al., 2020). This review will here on focus majorly on histone H3 and H4 acetylation in DSB signalling and repair with crosstalks with other modifications.

Histone H4 acetylation and DSB repair

The role of histone H4 acetylation in the regulation of transcription by opening up chromatin is well known. However, the deletion of enzyme responsible for H4 acetylation, the human Tip60 lead to defective DSB repair capacity post IR treatment suggested the functions of histone H4 acetylation in DSB repair pathway (Ikura et al., 2000). The TIP60 acetyltransferase subunit, acetylates histone H4 at K5, K8, K12, and K16, as well as H2A at K5 and K15 at the DSBs. Histone H4 acetylation reduces the charge dependent histone-DNA interactions and also provides a platform for landing of a class of chromatin proteins that contain bromodomains (Umehara et al., 2010; Plotnikov et al., 2014; Gong et al., 2016). Of the potential H4 acetylation sites, the levels of H4K16ac increase after DNA damage and absence of H4K16ac leads to defective DNA repair (Li et al., 2010; Miller et al., 2010; Sharma et al., 2010). The Myst family acetyltransferase MOF1 catalyses H4K16ac. Upon deletion of MOF1, defective recruitment of MDC1, 53BP1 and BRCA1 was observed at DSBs (Li et al., 2010; Sharma et al., 2010). Reduced MDC1 in MOF1 deletion leads to reduced activation of ATM (Gupta et al., 2005). MOF1 mediated H4K16ac facilitates interaction with acidic patch of H2AX for recruitment of MDC1 and other chromatin remodelling events facilitating effective DNA repair (Figure 2) (Dhar et al., 2017). The

histone chaperone Asf1 interacts with human MOF1 and regulates ATM activation via H4K16ac (Huang et al., 2018b). Asf1 also helps in NHEJ by mediating the phosphorylation of MDC1 by ATM (Lee et al., 2017). Given the role of H4K16ac in activation of ATM i.e., the sensing and signalling step of DSB repair, the H4K16ac kinetics at DSBs and its role in repair is however complicated. Whether acetylation has a positive role in DNA damage repair is still unclear. In budding yeast, Sin3 and Rpd3 dependent deacetylation of H4K16 at the DSBs regulate repair by NHEJ (Jazayeri et al., 2004). Similarly, in mammalian cells, after laser-induced DNA damage, H4K16Ac levels decrease rapidly followed by a steady increase at DSBs (Miller et al., 2010). The deacetylation of H4K16 was coincident with localization of HDAC1 and HDAC2 at the damage sites at initial time points. Depletion of both HDAC1 and HDAC2 results in hyper-acetylation of H4K16Ac and defects in NHEJ in humans as well as mice (Miller et al., 2010). H416ac presents as an obstacle in formation of higher order chromatin structure even though it increases chromatin accessibility. The deacetylation of H4K16ac leads to chromatin compaction which might be required to create a microenvironment for quick access and recruitment of NHEJ factors to the DSB site (Fernandez-Capetillo and Nussenzweig, 2004). The biphasic response of H4K16ac in response to DSB could be due to its role in regulation of DNA repair pathway choice. DNA repair by NHEJ can occurs fast anytime while HR is the preferred pathway only when the sister chromatids are available for repair i.e., specifically in S/G2 phase of the cell cycle and it is slower as compared to NHEJ. The major factor responsible for initiating NHEJ is recruitment of 53BP1 which inhibits DNA end resection. Studies using Nuclear Magnetic Resonance (NMR) and peptides containing specific histone marks has found, acetylation of H4K16 to be inhibitory toward the binding of the tudor domains of 53BP1 to H4K20me2 (Figure 3). Also, the HAT Tip60 has been implicated in the accumulation of BRCA1 at the chromatin while inhibiting 53BP1. The Tip60 complex also binds to H4K20me2 (through the MBTD1 complex) and prevents ubiquitination of H2A by directly acetylating the H2AK15 ubiquitin site, providing an example of how acetylation of a specific residue can inhibit other modification at the same residue (Figure 3). This Tip60-H4K20me2-H2AK15Ub-Ac axis helps promote HR by inhibiting 53BP1 (Tang et al., 2013; Jacquet et al., 2016). The role of H4 acetylation in regulating BRCA1 recruitment is also supported by another recent study where in S/G2 phase, the acetyl CoA generating enzyme ACLY is phosphorylated in response to DSB and leads to H4 acetylation by Tip60 which further recruits BRCA1 (Sivanand et al., 2017). BRDs act as lysine readers at the chromatin and have significant roles in DSB repair (Figure 3). Several BRD proteins like BRD4, ZMYND8, ACF1, TRIM28 (KAP-1), and TRIM33 are recruited to DSBs (Chiu et al., 2017; Gong and Miller, 2018). Some HATs such as p300 and GCN5 also possess BRD domains. CBP/p300 localizes to DSB sites and acetylates H4 at K5, K8, K12, and K16 and this leads to recruitment of NHEJ protein Ku70 and Ku80 to the sites of DSB (Ogiwara et al., 2011). These acetylations also help establish chromatin remodeling events at the break sites by enabling recruitment of SWI/SNF complex (Ogiwara et al., 2011). Recently, it was shown that H4K12ac was significantly reduced at AsiSI induced DSBs (Clouaire et al., 2018). Therefore, the molecular functions of this modification still remains to be explored further. In summary, H4ac in crosstalk with other histone modifications and readers can act as a barrier for the NHEJ pathway, while promotes HR and this dictates the pathway choice for DSB repair. For more detailed overview of Histone H4 acetylation and DSB repair, we refer the readers to other reviews which are specifically on role of histone H4 acetylation (Gong and Miller, 2013; Dhar et al., 2017).

Histone H3 acetylation and DSB repair

The exact role of histone H3 acetylation in DSB repair pathway is less understood. Consistent with the role of acetylation in making chromatin accessible, it was suggested that histone H3 acetylation is required for the recruitment of the SWI/SNF complex in cooperation with γ-H2AX to DSB sites which promotes further nucleosome remodeling to mediate repair (Downs et al., 2004; van Attikum et al., 2004; Lee et al., 2010; Ogiwara et al., 2011).

DNA damage-induced changes in acetylation of mammalian histone H3 N-terminal lysines 9, 14, 18, 23 and 56 was observed by several studies (Das et al., 2009; Tjeertes et al., 2009; Yuan et al., 2009; Lee et al., 2010; Miller et al., 2010; Vempati et al., 2010; Guo et al., 2011). The dynamic nature of acetylation and deacetylation at H3K9, 14, 18, 23, 27 in response to a DSB created by a HO endonuclease was established first by earlier studies (Tamburini and Tyler, 2005), (Lee et al., 2010), where it was shown that histone acetylations at certain residues were first reduced and then increased to support repair and restoration. Additionally, it was shown that the acetylation was not only altered at the site of DNA lesion but also was altered at the donor locus or the sister chromatid. Consistent with this, the acetyl transferase responsible for H3 acetylation like Gcn5 and Esa1 and the histone deacetylases responsible for removal of acetyl mark for example, Rpd3, Sir2, and Hst1 were shown to be localized to the double-strand break during DNA repair (Jazayeri et al., 2004; Tamburini and Tyler, 2005). Histone acetylation marks such as histone H3 at lysine 56 (H3K56ac) is known to be associated with open chromatin. However, on the contrary a prevailing view suggests deacetylation of H3K56 is an early event in the response to DSBs. Certain histone acetylation marks such as H3K56 and H4K16 get activated in phases or waves, showing initial reduction and later on increase at the sites of DSB which indicates the dynamic role of both HATs and HDACs in sensing as well as repair of DSBs.

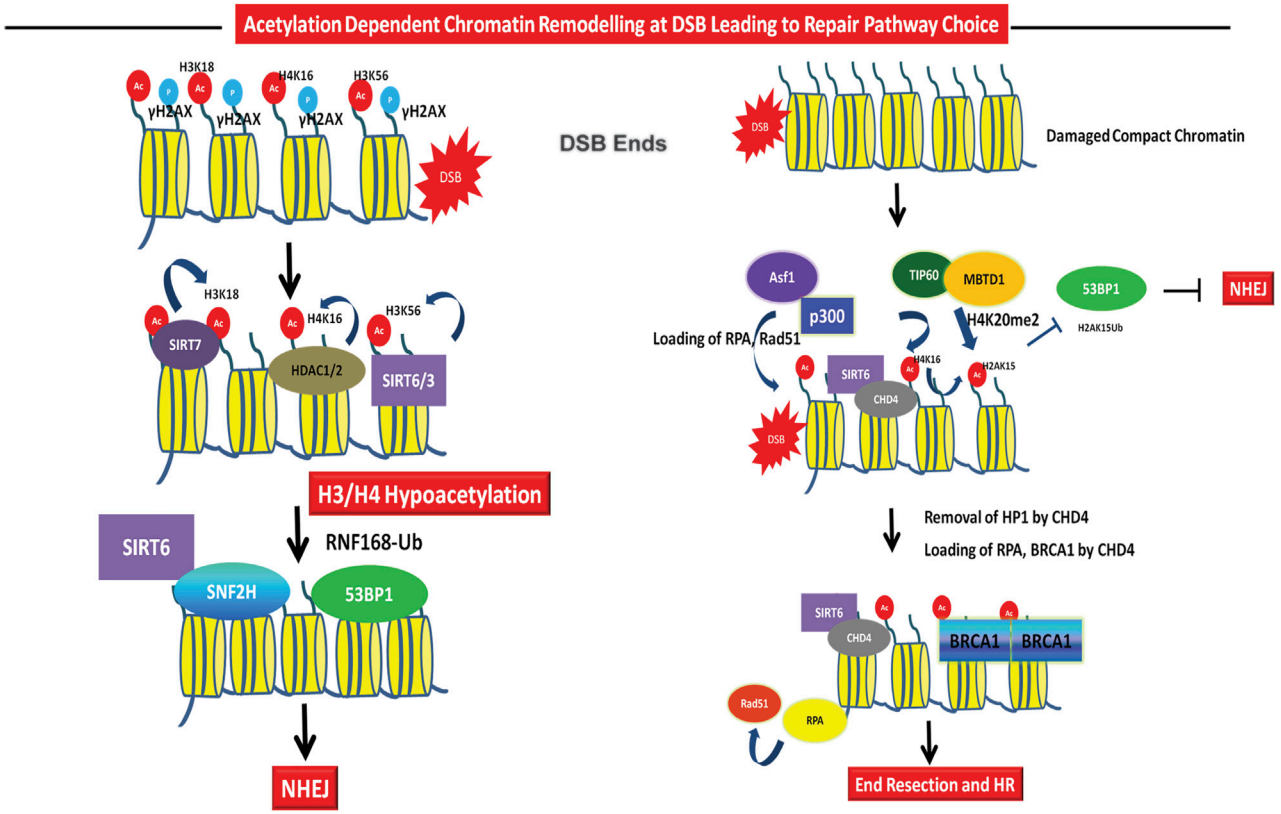

FIGURE 3
Role of acetylation in DSB repair pathway choice. Repair Pathway Choice- The early recruitment of HDACs like SIRT6, SIRT3, and HDAC1/2 leads to deacetylation of H3K56ac, H3K18ac, H4K16ac, etc. leading to chromatin compaction and recruitment of NHEJ factors 53BP1 and Ku70/80. SIRT6 dependent SNF2H recruitment aids in the recruitment of downstream DNA repair factors at G1 to facilitate NHEJ. The repair pathway choice for HR through acetylation is mediated *via* Tip60 dependent ubiquitylation to acetylation switch at H2AK15, through H4K20me3 leading to inhibitory binding to 53BP1 and inhibition of NHEJ. Repair of damage in G2 or at compact chromatin regions require removal of heterochromatin protein like HP1 by CHD4. CHD4 is recruited by SIRT6 and this leads to removal of HP1 leading to chromatin decompaction, recruitment of RPA and BRCA1 to facilitate HR. Asf1 and p300 also facilitates the recruitment of Rad51 and RPA at DSBs.

Histone H3K14ac and DSB Repair

H3K14ac, the H3 tail modification is known to be associated with transcriptionally active chromatin. H3K14ac along with other H3 and H4 tail modifications was first shown to be altered upon DSB repair at an HO endonuclease site triggered by homologous recombination pathway (Tamburini and Tyler, 2005). However, the specific role of H3K14ac in DSB repair is not defined. In fission yeast, H3K14ac is regulated by GCN5 and MST2 acetyl transferases (Wang et al., 2012). The combined deletion of gcn5, mst2 or the mutation of H3K14R (hypo-acetylation mimic) leads to severe sensitivity phenotypes in response to variety of DNA damage-inducing agents such as UV light, bleomycin, MMS (methylmethane sulfonate), and ionizing radiation. H3K14ac is induced at an HO endonuclease DSB site, indicating its active role at the DSB signalling or repair. Consequently, loss of H2A phosphorylation was observed in H3K14R mutant due to the compact chromatin structure and the accessibility of RSC complex was found to be reduced in fission yeast (Wang et al., 2012). In support of this, the RSC complex through its bromodomain regions was shown to be recruited to the chromatin via H3K14ac in budding yeast (Kasten et al., 2004). Further studies show the role of yeast RSC complex in facilitating the recruitment of ATM/ATR complexes (Tel1/Mec1) to the break site and for the induction of phosphorylation of H2A (Liang et al., 2007; Shim et al., 2007). Consistent with the roles of H3K14ac in DDR in yeast, H3K14 was found to be increased in response to IR treatment in mammalian cells in GCN5 dependent manner (Lee et al., 2010). H3K14ac is correlated with active chromatin (Wang et al., 2008). Since, H3K14 is a tail modification, it is downregulated by deletion of a nucleosome binding protein HMGN1. This axis of HMGN1-H3K14ac induces the activation of ATM *via* ATM autophosphorylation in response to IR (Figure 2) (Kim et al., 2009). The role of HMGN1 in the activation of ATM is due to the

global reorganisation of ATM in the nucleus via H3K14ac and not due to local changes in interaction of ATM with HMGN1 or with other chromatin factors (Kim et al., 2009). This is a classic example of the role of histone H3 tail modification in the global nuclear changes leading to DDR signal activation. The specific role of H3K14ac in the DDR pathway is still emerging. Acetylated histones are read by bromodomain containing proteins. Recently, a bromodomain containing protein ZMYND8 is shown to localize to the sites of DSB (Gong and Miller, 2018). Independently, it was shown that ZMYND8 interacts with H3K14ac mark along with H3K4-me1 to regulate transcription of malignant genes (Li et al., 2016). Whether this axis of ZMYND1-H3K18ac is linked to the DDR signalling or repair can be checked in the future. Also, the detailed kinetics of H3K14ac using laser induced site specific damage is needed to further gain knowledge about the specific signalling events orchestrated by this H3 tail modification leading to repair. Since, its crosstalk with other histone modifications in regulating transcription is known, whether this is true for DSB repair could be an interesting question to pursue in the future.

Histone H3K18ac and DSB repair

Several studies reported H3K18ac, one of the histone mark of the N-terminus of histone H3, at the site of DSBs (Schiltz et al., 1999; Tamburini and Tyler, 2005; Ogiwara et al., 2011; Vazquez et al., 2016). p300 and CBP dependent H3K18ac mediates the access of the chromatin remodeling complex SWI/SNF to the DSB site (Ogiwara et al., 2011). Furthermore, DNA damage caused by ionizing radiation resulted in GCN5-mediated H3K18ac. Further, this modification along with acetylation marks at other N-terminal residues in H3 is induced on γH2AX containing nucleosomes leading to the binding of BRG1, the ATPase subunit of SWI/SNF complex (Figure 2). This mechanism helps in spreading of phosphorylation of H2AX on nucleosomes flanking the DSB and thus forms a feedback loop to facilitate DSB repair (Lee et al., 2010). However, the kinetics of H3K18ac at the DSBs was unclear. Recently, interesting details emerged about the kinetics of H3K18ac levels at the DSBs. A rapid increase in H3K18ac was observed post 15 min of IR treatment followed by reduction and this reduction persisted till the end of repair (Vazquez et al., 2016). Incidentally, in response to IR and genotoxic stress, the sirtuin SIRT7 is recruited to DSB sites as early as 1 s and peaks at 1 min to mediate deacetylation of H3K18ac and this fine-tuning is required for the binding of 53BP1 to the chromatin and making an early choice for NHEJ (Figure 3). This loading of SIRT7 to the chromatin is ATM-independent and is dependent upon the sensor PARP (Vazquez et al., 2016). Consistently, the NHEJ efficiency was significantly reduced in SIRT7 knock out cells. SIRT7 deficiency also leads to replication defects and fork collapse. This suggests that H3K18ac role at the chromatin may not be limited to DSB repair in G1. Coincidently, a very recent report introduced a new player, a transcription factor SP1 in the regulation of H3K18ac *via* p300 (Swift et al., 2021). SP1 is required to recruit p300 to the DSB site during G1 phase and induce H3K18ac. The induced H3K18ac is required for recruitment of SWI/SNF complex and NHEJ factor Ku to the DSB. These results at first seem contradictory to the earlier study where deacetylation of H3K18ac is required for NHEJ factor 53BP1 binding. It is therefore hypothesized that, initial opening of chromatin *via* H3K18ac mediated by p300 and SP1 is required for initiating the NHEJ pathway in G1 phase by recruitment of SWI/SNF and Ku80. Further, deacetylation by SIRT7 could be required for 53BP1 loading to restrict resection and finishing DNA repair (Figure 3). In support of this, it was reported that Dicer is upregulated in response to DSBs which sequesters SIRT7 in the cytoplasm at the early timepoints to facilitate chromatin opening via H3K18ac (Zhang et al., 2016; Chen et al., 2017). Subsequent release of SIRT7 leads to deacetylated H3K18 promoting effective repair by NHEJ. Clearly, the role of H3K18ac in the DSB repair pathway needs further investigation. The global role of H3K18ac in the regulation of transcription is known. However, fine tuning the levels of this acetylation at a particular DSB in different cell cycle stages is crucial to mediate the repair.

Histone H3K56ac and DSB repair

Acetylation of the globular domain residue, histone H3K56 in the alpha N helix that is strategically positioned at the DNA entry and exit site in the nucleosome, was first discovered in budding yeast by mass spectrometry (Masumoto et al., 2005; Xu et al., 2005). Structurally, H3K56 faces the major groove of the nucleosomal DNA providing an excellent position to affect histone/DNA interactions when acetylated (Davey and Richmond, 2002; Gershon and Kupiec, 2021). The histone H3K56 is acetylated in the S-phase of the cell cycle specifically behind the replication forks and is deacetylated by the sirtuins at G2/M phase. In yeast, all newly synthesized histone H3 in S phase are acetylated at H3K56 residue (Hyland et al., 2005; Masumoto et al., 2005; Ozdemir et al., 2005; Xu et al., 2005; Xhemalce et al., 2007; Haldar and Kamakaka, 2008). The histone H3K56ac is conserved in mammals and is associated with human cancers (Das et al., 2009). Acetylation of H3K56 leads to increased DNA accessibility by facilitating spontaneous unwrapping at the entry and exit points of the nucleosome. This is supported by many biophysical studies (Neumann et al., 2009; Kim et al., 2015). H3K56ac is regulated by CBP/p300 in humans along with histone chaperone Asf1a and is deacetylated by HDAC1/2, sirtuins, SIRT1, SIRT2, SIRT3, and SIRT6 (Das et al., 2009; Yuan et al., 2009; Vempati et al., 2010).

Role of H3K56ac in yeast DSB repair

The yeast acetyltransferase Rtt109 acetylates H3K56 in collaboration with the chaperones, Asf1 (a H3-H4 chaperone) and Vps75 (Celic et al., 2006; Schneider et al., 2006; Driscoll et al., 2007; Han et al., 2007; Tsubota et al., 2007). Asf1, in complex with H3K14ac-H4, alters the selectivity of Rtt109-Vps75 significantly towards H3K56ac, indicating crosstalk among different H3 acetylations (Cote et al., 2019). The sirtuins ScHst4 and ScHst3 in *S. cerevisiae* and the SpHst4 in *S. pombe* regulate cell cycle progression and heterochromatin silencing and assembly (Brachmann et al., 1995; Freeman-Cook et al., 1999; Haldar and Kamakaka, 2008; Konada et al., 2018). These deacetylases remove and thus, negatively regulate H3K56ac levels during the cell cycle as well as post DNA damage. Several studies showed this modification is required for maintenance of genome integrity (Celic et al., 2006; Maas et al., 2006; Miller et al., 2006; Xhemalce et al., 2007; Haldar and Kamakaka, 2008). The acetylated histone H3K56 promotes replication-coupled nucleosome assembly as well as assembly of nucleosomes following repair by increasing interaction between histone chaperon CAF1, Rtt106 and Asf1 and histones (Chen et al., 2008; Li et al., 2008). This is required for restoration of chromatin structure following DNA replication or repair, as has been depicted by several studies and proposed in the access-repair-restore model, a necessary step for maintenance of genome integrity (Green and Almouzni, 2002). Interestingly, the levels of H3K56ac are maintained in response to DNA damage during S-phase in the checkpoint dependent manner (Masumoto et al., 2005; Thaminy et al., 2007). The tight regulation of this modification is via the downregulation of sirtuins Hst3 and Hst4 in S-phase and post-DNA damage in S-phase (Celic et al., 2006; Haldar and Kamakaka, 2008). Budding yeast Hst3 is regulated by CDK dependent phosphorylation and degradation via SCF (Cdc4) ubiquitination pathway (Delgoshaie et al., 2014; Edenberg et al., 2014). Checkpoint sensor kinase Mec1 regulates Hst3 levels in an intra-S-phase checkpoint kinase Rad53 dependent mechanism (Thaminy et al., 2007). In fission yeast, *S. pombe,* SpHst4 which is the functional homolog of budding yeast hst3, hst4, has also been recently shown by our lab to be degraded in an ubiquitin dependent manner (Aricthota and Haldar, 2021). Notably, the DDK kinase Hsk1 phosphorylates Hst4 at the C-terminus in response to DNA damage caused by methylmethane sulfonate treatment, which thereby is recognized by the SCF (Pof3) complex and ubiquitinated. Hst4 is then targeted for degradation via proteasome. In response to DNA damage caused by methylmethane sulfonate (MMS) treatment.

Deletion of sirtuins Hst3 and Hst4 induces several genome instability phenotypes, including spontaneous DNA double-strand breaks, increased chromosomal loss, impairment of break-induced replication, and increased sensitivity to genotoxic agents (Brachmann et al., 1995; Freeman-Cook et al., 1999; Che et al., 2015). Notably, these phenotypes are suppressed by deletion of histone chaperone Asf1 which is essential for the activity of Rtt109 histone acetyltransferase (HAT) complex or by a non-acetylatable H3K56R mutant, suggesting that constitutive H3K56 hyperacetylation results in genomic instability (Celic et al., 2006; Maas et al., 2006; Driscoll et al., 2007). The absence of H3K56ac is equally harmful for the genome stability as expression of hypoacetylated H3K56R mutant or the absence of Asf1 leads to severe sensitivity in the presence of genotoxic agents such as, methylmethane sulfonate (MMS), campthotecin (CPT), and hydroxyurea (HU), etc., (Lewis et al., 2005; Maas et al., 2006; Haldar and Kamakaka, 2008). Inability to downregulate Hst4 of *S. pombe*, in a phosphorylation defective mutant of Hst4, 4SA-hst4 leads to hypoacetylated H3K56 and this mutant suffers sensitivity and defective recovery from replication stress (Aricthota and Haldar, 2021).

The genome stability defects observed upon perturbation of H3K56ac pathway indicates the role of H3K56ac in the regulation of DDR signalling or repair. Absence of sirtuins Hst3 and Hst4 leads to activation of checkpoint without any exogenous treatment indicating spontaneous and persistent DNA damage. Similar results were obtained in the absence of rtt109 deletion indicating that dynamic regulation of H3K56ac functions in the DDR pathway (Driscoll et al., 2007). Studies have indicated that rtt109, asf1 functions in the same pathway as asf1 in the response to genotoxic drug treatments (Recht et al., 2006; Driscoll et al., 2007). High levels of H2A phosphorylation was seen in cells with hyperacetylated as well as hypoacetylated genome (Simoneau et al., 2015; Aricthota and Haldar, 2021). Also, high recombination foci (Rad52 foci) were observed in the absence of exogenous damage in these cells, indicating cells with deregulated H3K56ac pathway face spontaneous DNA damage possibly due to defects in repairing the replicative DNA damage (Wurtele et al., 2012; Konada et al., 2018). The absence of H3K56ac in rtt109 and h3K56R conditions leads to persistent Rad51 foci which could be due to inability to resolve the damage downstream of Rad51. The DNA damage checkpoint gets deactivated once the damage is repaired i.e., during recovery. The absence of H3K56ac by deletion of Rtt109 or Asf1, leads to activated checkpoint post damage removal and due to this, cells are unable to re-enter cell cycle (Chen et al., 2008; Tsabar et al., 2016). This cell cycle re-entry mechanism is conserved in *S. pombe*, as the non-degradable phospho-mutant of hst4 (4SA-hst4) shows hypoacetylation of H3K56ac and defective recovery from replication stress (Aricthota and Haldar, 2021). These defects could be due to the role of chromatin reassembly functions of H3K56ac in deactivating the checkpoint.

The role of H3K56ac in HR in yeast is not established due to the absence of sensitivity of the mutants of this pathway in response to acute IR treatment. Also, it was observed that acute exposure to IR did not induce H3K56ac in *S. cerevisiae* (Masumoto et al., 2005). Further, cells lacking Rtt109 or Asf1 are capable of repairing a single HO-induced DSB. The genetic interaction data of *hst3hst4* mutants with the HR pathway genes in yeast suggests that Rad51 is not required for the survival of these mutants. However, the survival depends on the Rad52 and MRN complex (Munoz-Galvan et al., 2013). These data suggest that H3K56ac pathway is specifically required in a branch of HR repair which is not dependent on Rad51. One such example is the repair by break induced replication (BIR), which is needed to repair single ended DSBs (Che et al., 2015). Since, H3K56ac only occurs during S-phase of the cell cycle, it is assumed that it is not required for DNA repair activities outside S-phase. However, the H3K56R mutants were found to be sensitive to prolonged bleomycin treatment which induces DSBs and is repaired by Rad51 pathway, indicating that H3K56ac role in DSB repair still needs to be studied. In *S. cerevisaie*, H3K56ac has been implicated in the formation of meiotic breaks (Karanyi et al., 2019). Further supporting the possible role of H3K56ac in HR, the downregulation of Hst4 was also observed in response to MMS and HU but not in bleomycin treatment (which induce DSBs), indicating that only early S-phase fork stalling leads to induction of H3K56ac. The molecular role of Hst3/Hst4 and H3K56ac pathway in the DNA repair mechanisms induced by these damaging agents warrants further investigation. Also, it was shown in the fungus Neurospora, the role of H3K56ac and rtt109 in the regulation of Quelling and DNA damage-induced small RNA (qiRNA) production *via* homologous recombination. The H3K56ac was found at the site specific DSB break site in this study (Zhang et al., 2014).

H3K56ac is also required for the stability of advancing replication forks. Impairment of nucleosome assembly pathways through deletion of Asf1 or Caf1 leads to defective DSB repair during DNA replication (Lewis et al., 2005). Absence of asf1, rtt109 leads to increased recombination, as sister chromatid exchanges increase (Prado et al., 2004). The balance of acetylation and deacetylation of H3K56 during DNA replication is required to help the recombination machinery in choosing the right sister chromatid for the recombination during HR (Munoz-Galvan et al., 2013). Since, sister chromatid recombination is the major pathway for repair of replication induced DSBs, this could explain the sensitivity of H3K56ac pathway mutants to HU, CPT, etc., replicative stress causing agents. Overall, the accurate, timely and dynamic regulation of histone H3 lysine 56ac is the key to cell survival upon DNA damage.

Role of H3K56ac in human DSB repair

The core domain modification, histone H3K56ac is conserved in mammals and is associated with human cancers (Das et al., 2009). It is regulated by CBP/p300 in humans along with histone chaperone Asf1a and is deacetylated by HDAC1/2, Sirtuins, SIRT1, SIRT2, SIRT3, and SIRT6 (Das et al., 2009; Yuan et al., 2009; Vempati et al., 2010). The role of H3K56ac in human DSB repair is a long studied question and still elusive. It is a DNA damage responsive modification as its level alter upon exposure to DNA damage. However, there are conflicting reports on the H3K56ac levels upon treatment of specific cell lines with same DNA damaging agents and therefore, the function and regulation of H3K56ac in DSB repair has been controversial in human. Some studies have shown that the level of H3K6ac increases in response to DNA damage (Das et al., 2009; Yuan et al., 2009; Vempati et al., 2010). However, other studies have shown that H3K56 is actively deacetylated at sites of DNA breaks (Tjeertes et al., 2009; Miller et al., 2010). Treatment of cells with PIKK inhibitors such as wortmanin leads to reduced H3K9ac and H3K56ac without any exogenous DNA damage (Tjeertes et al., 2009). This could be due to endogenous DNA damage induced by the inhibition of ATM/ATR kinases. The kinetics of reduction of H3K56ac is very fast and corresponds with the appearance of γH2AX upon treatment with Phleomycin. These seemingly contrasting results could be due to the non-specific signal by the different commercial antibodies available against H3K56ac or speculatively, could be due to difference cellular microenvironment i.e. the cell culture conditions which varied between these laboratories ad (Pal et al., 2016). The other reason for these contrasting results could be the growth conditions of the cell and its effect on the dynamicity of H3K56ac, where the initial level or the pre-exiting modification code/level would determine how the levels of this modification would alter. Recent results indicate that the cellular microenvironment plays a role in controlling the dynamics of HK56ac upon DNA damage in mammalian cells (Vadla et al., 2020). Specifically, the cell density changes and accumulation of metabolites and pH alterations affect the global levels of H3K56ac. Upon DNA damage, H3K56ac increases in low density cells with low initial acetylation, while acetylation decreases in high cell density cells. The gradual increase in H3K56ac from low to high cell density medium was coincident with decreasing levels of SIRT1 and SIRT6 (Vadla et al., 2020). Interestingly, unlike yeast, the global reduction of H3K56ac in response to DNA damage in humans is not dependent on cell cycle effects (Tjeertes et al., 2009). There are instances of similar changes in acetylation in response to damage due to the complex dynamics of DNA damage repair at the chromatin due to differences in DNA repair code generated due to subtle changes in cellular microenvironment. UV treatment leads to rapid hyperacetylation of all histones followed by a hypoacetylated state (Ramanathan and Smerdon, 1986). More recent studies have suggested this biphasic mode of H3K56ac where it decreases immediately upon DNA damage (UVR) and subsequently restored. Additionally, HDAC1 and HDAC2 act at DSBs to deacetylate H3K56ac to promote repair by NHEJ (Miller et al., 2010). The sirtuin, SIRT3 localizes to nucleus and deacetylates H3K56ac immediately to regulate NHEJ pathway via regulating

recruitment of NHEJ protein 53BP1 (Sengupta and Haldar, 2018). This biphasic mode of post-translational modifications is interesting and has been observed for histone H4K16ac as well. Similar to H3K56ac, the linker histone H1K85ac is decreased immediately in response to IR treatment as well as at the site specific DSB to promote chromatin compaction, but increase at later timepoints (Li et al., 2018). H1K85ac promotes Heterochromatin protein 1 (HP1) recruitment at the chromatin which facilitates chromatin compaction. Reducing H1K85ac immediately post DNA damage by HDAC1 leads to chromatin decompaction. However, the role of H1K85ac in DSB repair is dynamic as both H1K85Q and H1K85R mutants are sensitive to IR treatments. HATs and HDACs function in regulating these dynamic modifications in order to remodel chromatin via recruitment of specific remodelers. Various chromatin remodelers, including INO80, the NURD complex, SMARCAD1, p400, CHD4, etc. were shown to be recruited to sites of damage, suggesting the need of chromatin remodeling in order to allow repair (Papamichos-Chronakis and Peterson, 2013; Price and D'Andrea, 2013; Xu and Price, 2011). Previous studies have shown that defects in DNA damage repair in SNF2H knockdown cells could be rescued with chloroquine treatment, a drug that causes chromatin relaxation (Murr et al., 2006; Nakamura et al., 2011). The NAD + dependent sirtuin, SIRT6 is required for the localization of SNF2H to the sites of DSB (Toiber et al., 2013). SIRT6 deacetylates H3K56ac at DSB to regulate SNF2H binding. It was observed that in the absence of SIRT6 and in H3K56Q mutants, SNF2H is unable to open chromatin leading to defective DSB repair signaling by inhibiting recruitment of repair proteins such as RPA, 53BP1, and BRCA1 (Toiber et al., 2013). Subsequent studies have linked SNF2H functioning downstream of RNF168- H2A ubiquitination pathway which regulates key steps in NHEJ at heterochromatic regions (Kato and Komatsu, 2015). Interestingly, SIRT6 also functions in regulating recruitment of another chromatin remodeler, CHD4 at the sites of DNA damage at G2 phase of the cell cycle, specifically at compacted DSB regions. SIRT6-CHD4 competitively binds H3K9me3 which helps in evicting the heterochromatin protein HP1 from the chromatin leading to chromatin decompaction to promote HR (Hou et al., 2020). Earlier reports have suggested that PARP dependent accumulation of CHD4 further recruits HDAC1/2 (Chou et al., 2010; Polo et al., 2010). Whether any other histone acetylation has function in this CHD4-HDAC1/2 pathway forming a repair code to regulate HR is not known. A study has however, shown that knock down of HAT p300 leads to reduced recruitment of CHD4 and their knock down independently lead to reduced HR while NHEJ was not affected. The fact that knock-down of both HATs like p300 and HDACs like sirtuins leads to defective DSB repair suggests the complex role of post-translational modifications in DSB repair. The histone chaperone Asf1 has been shown to regulate homologous recombination via enabling loading of Rad51 to the sites of DSBs (Figure 3) (Huang et al., 2018a). Also, similar to yeast, studies in mammalian cells have shown the role of H3K56ac in recovering from DNA damage via inactivating checkpoint, promoting chromatin reassembly and thus regulating cell-cycle progression (Chen et al., 2008; Battu et al., 2011). Since, Asf1, p300 and SIRT6 regulates H3K56ac, it is plausible to think that H3K56ac function in HR needs further detailed studies where cell cycle effects and time points are accounted for.

Concluding remarks

DNA damage triggers a network of intricate signaling and repair mechanisms which take place in the chromatin context. Starting from detection of the lesion till the restoration of chromatin following repair, proteins involved in all steps of DNA damage response work in close coordination with the regulators of chromatin for making chromatin structure conducive for DDR and DNA repair. Histone modifications and modifiers alter chromatin by loosening contact with DNA thereby relaxing chromatin and recruiting DNA remodeling and repair factors via interaction with their bromodomain. Histones are acetylated on several residues and defect in acetylation of specific residue results in definite phenotypes. However, the molecular functions of these acetylation in DSB repair are not well understood. Further, crosstalk between several modifications are known and it has been proposed that these may form specific repair codes to determine downstream steps of repair pathways. Further research will through light on these mechanisms which will be crucial for understanding the complexities of DSB repair pathways and contribute to development of new therapeutics of diseases resulting from defective DSB repair.

Author contributions

SA, PR, and DH discussed concepts, planned, and wrote the manuscript.

Funding

This study was supported by a grant from the Science and Engineering Research Board (SERB), Ministry of Science and Technology, India (Grant CRG/2020/005724). SA is supported by SERB grant.

Conflict of interest

The authors declare that the research was conducted in the absence of any commercial or financial relationships that could be construed as a potential conflict of interest.

Publisher's note

References

Aleksandrov, R., Hristova, R., Stoynov, S., and Gospodinov, A. (2020). The chromatin response to double-strand DNA breaks and their repair. *Cells* 9(8):1853. doi:10.3390/cells9081853

Aricthota, S., and Haldar, D. (2021). DDK/Hsk1 phosphorylates and targets fission yeast histone deacetylase Hst4 for degradation to stabilize stalled DNA replication forks. *Elife* 10, e70787. doi:10.7554/eLife.70787

Aymard, F., Bugler, B., Schmidt, C. K., Guillou, E., Caron, P., Briois, S., et al. (2014). Transcriptionally active chromatin recruits homologous recombination at DNA double-strand breaks. *Nat. Struct. Mol. Biol.* 21, 366–374. doi:10.1038/nsmb.2796

Battu, A., Ray, A., and Wani, A. A. (2011). ASF1A and ATM regulate H3K56-mediated cell-cycle checkpoint recovery in response to UV irradiation. *Nucleic Acids Res.* 39, 7931–7945. doi:10.1093/nar/gkr523

Bird, A. W., Yu, D. Y., Pray-Grant, M. G., Qiu, Q., Harmon, K. E., Megee, P. C., et al. (2002). Acetylation of histone H4 by Esa1 is required for DNA double-strand break repair. *Nature* 419, 411–415. doi:10.1038/nature01035

Bonner, W. M., Redon, C. E., Dickey, J. S., Nakamura, A. J., Sedelnikova, O. A., Solier, S., et al. (2008). GammaH2AX and cancer. *Nat. Rev. Cancer* 8, 957–967. doi:10.1038/nrc2523

Brachmann, C. B., Sherman, J. M., Devine, S. E., Cameron, E. E., Pillus, L., and Boeke, J. D. (1995). The SIR2 gene family, conserved from bacteria to humans, functions in silencing, cell cycle progression, and chromosome stability. *Genes Dev.* 9, 2888–2902. doi:10.1101/gad.9.23.2888

Caridi, P. C., Delabaere, L., Zapotoczny, G., and Chiolo, I. (2017). And yet, it moves: Nuclear and chromatin dynamics of a heterochromatic double-strand break. *Philos. Trans. R. Soc. Lond. B Biol. Sci.* 372, 20160291. doi:10.1098/rstb.2016.0291

Carrozza, M. J., Utley, R. T., Workman, J. L., and Cote, J. (2003). The diverse functions of histone acetyltransferase complexes. *Trends Genet.* 19, 321–329. doi:10.1016/S0168-9525(03)00115-X

Celic, I., Masumoto, H., Griffith, W. P., Meluh, P., Cotter, R. J., Boeke, J. D., et al. (2006). The sirtuins hst3 and Hst4p preserve genome integrity by controlling histone h3 lysine 56 deacetylation. *Curr. Biol.* 16, 1280–1289. doi:10.1016/j.cub.2006.06.023

Chapman, J. R., Taylor, M. R., and Boulton, S. J. (2012). Playing the end game: DNA double-strand break repair pathway choice. *Mol. Cell* 47, 497–510. doi:10.1016/j.molcel.2012.07.029

Che, J., Smith, S., Kim, Y. J., Shim, E. Y., Myung, K., and Lee, S. E. (2015). Hyper-acetylation of histone H3K56 limits break-induced replication by inhibiting extensive repair synthesis. *PLoS Genet.* 11, e1004990. doi:10.1371/journal.pgen.1004990

Chen, C. C., Carson, J. J., Feser, J., Tamburini, B., Zabaronick, S., Linger, J., et al. (2008). Acetylated lysine 56 on histone H3 drives chromatin assembly after repair and signals for the completion of repair. *Cell* 134, 231–243. doi:10.1016/j.cell.2008.06.035

Chen, X., Li, W. F., Wu, X., Zhang, H. C., Chen, L., Zhang, P. Y., et al. (2017). Dicer regulates non-homologous end joining and is associated with chemosensitivity in colon cancer patients. *Carcinogenesis* 38, 873–882. doi:10.1093/carcin/bgx059

Chiu, L. Y., Gong, F., and Miller, K. M. (2017). Bromodomain proteins: Repairing DNA damage within chromatin. *Philos. Trans. R. Soc. Lond. B Biol. Sci.* 372, 20160286. doi:10.1098/rstb.2016.0286

Chou, D. M., Adamson, B., Dephoure, N. E., Tan, X., Nottke, A. C., Hurov, K. E., et al. (2010). A chromatin localization screen reveals poly (ADP ribose)-regulated recruitment of the repressive polycomb and NuRD complexes to sites of DNA damage. *Proc. Natl. Acad. Sci. U. S. A.* 107, 18475–18480. doi:10.1073/pnas.1012946107

Choy, J. S., and Kron, S. J. (2002). NuA4 subunit Yng2 function in intra-S-phase DNA damage response. *Mol. Cell. Biol.* 22, 8215–8225. doi:10.1128/MCB.22.23.8215-8225.2002

Ciccia, A., and Elledge, S. J. (2010). The DNA damage response: Making it safe to play with knives. *Mol. Cell* 40, 179–204. doi:10.1016/j.molcel.2010.09.019

Clouaire, T., Rocher, V., Lashgari, A., Arnould, C., Aguirrebengoa, M., Biernacka, A., et al. (2018). Comprehensive mapping of histone modifications at DNA double-strand breaks deciphers repair pathway chromatin signatures. *Mol. Cell* 72, 250–262. e256. doi:10.1016/j.molcel.2018.08.020

Cote, J. M., Kuo, Y. M., Henry, R. A., Scherman, H., Krzizike, D. D., and Andrews, A. J. (2019). Two factor authentication: Asf1 mediates crosstalk between H3 K14 and K56 acetylation. *Nucleic Acids Res.* 47, 7380–7391. doi:10.1093/nar/gkz508

Das, C., Lucia, M. S., Hansen, K. C., and Tyler, J. K. (2009). CBP/p300-mediated acetylation of histone H3 on lysine 56. *Nature* 459, 113–117. doi:10.1038/nature07861

Davey, C. A., and Richmond, T. J. (2002). DNA-dependent divalent cation binding in the nucleosome core particle. *Proc. Natl. Acad. Sci. U. S. A.* 99, 11169–11174. doi:10.1073/pnas.172271399

Delgoshaie, N., Tang, X., Kanshin, E. D., Williams, E. C., Rudner, A. D., Thibault, P., et al. (2014). Regulation of the histone deacetylase Hst3 by cyclin-dependent kinases and the ubiquitin ligase SCFCdc4. *J. Biol. Chem.* 289, 13186–13196. doi:10.1074/jbc.M113.523530

Dhar, S., Gursoy-Yuzugullu, O., Parasuram, R., and Price, B. D. (2017). The tale of a tail: Histone H4 acetylation and the repair of DNA breaks. *Philos. Trans. R. Soc. Lond. B Biol. Sci.* 372, 20160284. doi:10.1098/rstb.2016.0284

Downs, J. A., Allard, S., Jobin-Robitaille, O., Javaheri, A., Auger, A., Bouchard, N., et al. (2004). Binding of chromatin-modifying activities to phosphorylated histone H2A at DNA damage sites. *Mol. Cell* 16, 979–990. doi:10.1016/j.molcel.2004.12.003

Driscoll, R., Hudson, A., and Jackson, S. P. (2007). Yeast Rtt109 promotes genome stability by acetylating histone H3 on lysine 56. *Science* 315, 649–652. doi:10.1126/science.1135862

Edenberg, E. R., Vashisht, A. A., Topacio, B. R., Wohlschlegel, J. A., and Toczyski, D. P. (2014). Hst3 is turned over by a replication stress-responsive SCF(Cdc4) phospho-degron. *Proc. Natl. Acad. Sci. U. S. A.* 111, 5962–5967. doi:10.1073/pnas.1315325111

Fernandez-Capetillo, O., and Nussenzweig, A. (2004). Linking histone deacetylation with the repair of DNA breaks. *Proc. Natl. Acad. Sci. U. S. A.* 101, 1427–1428. doi:10.1073/pnas.0307342101

Freeman-Cook, L. L., Sherman, J. M., Brachmann, C. B., Allshire, R. C., Boeke, J. D., and Pillus, L. (1999). The *Schizosaccharomyces pombe* hst4(+) gene is a SIR2 homologue with silencing and centromeric functions. *Mol. Biol. Cell* 10, 3171–3186. doi:10.1091/mbc.10.10.3171

Gershon, L., and Kupiec, M. (2021). The amazing acrobat: Yeast's histone H3K56 juggles several important roles while maintaining perfect balance. *Genes (Basel)* 12, 342. doi:10.3390/genes12030342

Glozak, M. A., and Seto, E. (2007). Histone deacetylases and cancer. *Oncogene* 26, 5420–5432. doi:10.1038/sj.onc.1210610

Gong, F., Chiu, L. Y., and Miller, K. M. (2016). Acetylation reader proteins: Linking acetylation signaling to genome maintenance and cancer. *PLoS Genet.* 12, e1006272. doi:10.1371/journal.pgen.1006272

Gong, F., and Miller, K. M. (2018). Double duty: ZMYND8 in the DNA damage response and cancer. *Cell Cycle* 17, 414–420. doi:10.1080/15384101.2017.1376150

Gong, F., and Miller, K. M. (2013). Mammalian DNA repair: HATs and HDACs make their mark through histone acetylation. *Mutat. Res.* 750, 23–30. doi:10.1016/j.mrfmmm.2013.07.002

Gorrini, C., Squatrito, M., Luise, C., Syed, N., Perna, D., Wark, L., et al. (2007). Tip60 is a haplo-insufficient tumour suppressor required for an oncogene-induced DNA damage response. *Nature* 448, 1063–1067. doi:10.1038/nature06055

Green, C. M., and Almouzni, G. (2002). When repair meets chromatin. First in series on chromatin dynamics. *EMBO Rep.* 3, 28–33. doi:10.1093/embo-reports/kvf005

Greiss, S., and Gartner, A. (2009). Sirtuin/Sir2 phylogeny, evolutionary considerations and structural conservation. *Mol. Cells* 28, 407–415. doi:10.1007/s10059-009-0169-x

Guarente, L. (2000). Sir2 links chromatin silencing, metabolism, and aging. *Genes Dev.* 14, 1021–1026. doi:10.1101/gad.14.9.1021

Guo, R., Chen, J., Mitchell, D. L., and Johnson, D. G. (2011). GCN5 and E2F1 stimulate nucleotide excision repair by promoting H3K9 acetylation at sites of damage. *Nucleic Acids Res.* 39, 1390–1397. doi:10.1093/nar/gkq983

Gupta, A., Sharma, G. G., Young, C. S., Agarwal, M., Smith, E. R., Paull, T. T., et al. (2005). Involvement of human MOF in ATM function. *Mol. Cell. Biol.* 25, 5292–5305. doi:10.1128/MCB.25.12.5292-5305.2005

Haldar, D., and Kamakaka, R. T. (2008). *Schizosaccharomyces pombe* Hst4 functions in DNA damage response by regulating histone H3 K56 acetylation. *Eukaryot. Cell* 7, 800–813. doi:10.1128/EC.00379-07

Han, J., Zhou, H., Li, Z., Xu, R. M., and Zhang, Z. (2007). Acetylation of lysine 56 of histone H3 catalyzed by RTT109 and regulated by ASF1 is required for replisome integrity. *J. Biol. Chem.* 282, 28587–28596. doi:10.1074/jbc.M702496200

Hou, T., Cao, Z., Zhang, J., Tang, M., Tian, Y., Li, Y., et al. (2020). SIRT6 coordinates with CHD4 to promote chromatin relaxation and DNA repair. *Nucleic Acids Res.* 48, 2982–3000. doi:10.1093/nar/gkaa006

Huang, T. H., Fowler, F., Chen, C. C., Shen, Z. J., Sleckman, B., and Tyler, J. K. (2018a). The histone chaperones ASF1 and CAF-1 promote mms22l-TONSL-mediated Rad51 loading onto ssDNA during homologous recombination in human cells. *Mol. Cell* 69, 879–892. doi:10.1016/j.molcel.2018.01.031

Huang, T. H., Shen, Z. J., Sleckman, B. P., and Tyler, J. K. (2018b). The histone chaperone ASF1 regulates the activation of ATM and DNA-PKcs in response to DNA double-strand breaks. *Cell Cycle* 17, 1413–1424. doi:10.1080/15384101.2018.1486165

Hulin, J.-A., Nguyen, T. D. T., Cui, S., Marri, S., Yu, R. T., Downes, M., et al. (2016). Barx2 and Pax7 regulate Axin2 expression in myoblasts by interaction with β-catenin and chromatin remodelling. *Stem Cells* 34, 2169–2182. doi:10.1002/stem.2396

Hustedt, N., and Durocher, D. (2016). The control of DNA repair by the cell cycle. *Nat. Cell Biol.* 19, 1–9. doi:10.1038/ncb3452

Hyland, E. M., Cosgrove, M. S., Molina, H., Wang, D., Pandey, A., Cottee, R. J., et al. (2005). Insights into the role of histone H3 and histone H4 core modifiable residues in *Saccharomyces cerevisiae*. *Mol. Cell. Biol.* 25, 10060–10070. doi:10.1128/MCB.25.22.10060-10070.2005

Ikura, M., Furuya, K., Matsuda, S., Matsuda, R., Shima, H., Adachi, J., et al. (2015). Acetylation of histone H2AX at lys 5 by the TIP60 histone acetyltransferase complex is essential for the dynamic binding of NBS1 to damaged chromatin. *Mol. Cell. Biol.* 35, 4147–4157. doi:10.1128/MCB.00757-15

Ikura, T., Ogryzko, V. V., Grigoriev, M., Groisman, R., Wang, J., Horikoshi, M., et al. (2000). Involvement of the TIP60 histone acetylase complex in DNA repair and apoptosis. *Cell* 102, 463–473. doi:10.1016/s0092-8674(00)00051-9

Ikura, T., Tashiro, S., Kakino, A., Shima, H., Jacob, N., Amunugama, R., et al. (2007). DNA damage-dependent acetylation and ubiquitination of H2AX enhances chromatin dynamics. *Mol. Cell. Biol.* 27, 7028–7040. doi:10.1128/MCB.00579-07

Jackson, S. P., and Bartek, J. (2009). The DNA-damage response in human biology and disease. *Nature* 461, 1071–1078. doi:10.1038/nature08467

Jacquet, K., Fradet-Turcotte, A., Avvakumov, N., Lambert, J. P., Roques, C., Pandita, R. K., et al. (2016). The TIP60 complex regulates bivalent chromatin recognition by 53BP1 through direct H4K20me binding and H2AK15 acetylation. *Mol. Cell* 62, 409–421. doi:10.1016/j.molcel.2016.03.031

Jazayeri, A., McAinsh, A. D., and Jackson, S. P. (2004). *Saccharomyces cerevisiae* Sin3p facilitates DNA double-strand break repair. *Proc. Natl. Acad. Sci. U. S. A.* 101, 1644–1649. doi:10.1073/pnas.0304797101

Jenuwein, T., and Allis, C. D. (2001). Translating the histone code. *Science* 293, 1074–1080. doi:10.1126/science.1063127

Jha, S., Shibata, E., and Dutta, A. (2008). Human Rvb1/Tip49 is required for the histone acetyltransferase activity of Tip60/NuA4 and for the downregulation of phosphorylation on H2AX after DNA damage. *Mol. Cell. Biol.* 28, 2690–2700. doi:10.1128/MCB.01983-07

Jiang, X., Xu, Y., and Price, B. D. (2010). Acetylation of H2AX on lysine 36 plays a key role in the DNA double-strand break repair pathway. *FEBS Lett.* 584, 2926–2930. doi:10.1016/j.febslet.2010.05.017

Karanyi, Z., Hornyak, L., and Szekvolgyi, L. (2019). Histone H3 lysine 56 acetylation is required for formation of normal levels of meiotic DNA breaks in *S. cerevisiae*. *Front. Cell Dev. Biol.* 7, 364. doi:10.3389/fcell.2019.00364

Kasten, M., Szerlong, H., Erdjument-Bromage, H., Tempst, P., Werner, M., and Cairns, B. R. (2004). Tandem bromodomains in the chromatin remodeler RSC recognize acetylated histone H3 Lys14. *EMBO J.* 23, 1348–1359. doi:10.1038/sj.emboj.7600143

Kato, A., and Komatsu, K. (2015). RNF20-SNF2H pathway of chromatin relaxation in DNA double-strand break repair. *Genes (Basel)* 6, 592–606. doi:10.3390/genes6030592

Khilji, S., Li, Y., Chen, J., and Li, Q. (2021). Multi-omics approach to dissect the mechanisms of rexinoid signaling in myoblast differentiation. *Front. Pharmacol.* 12, 746513. doi:10.3389/fphar.2021.746513

Kieffer, S. R., and Lowndes, N. F. (2022). Immediate-early, early, and late responses to DNA double stranded breaks. *Front. Genet.* 13, 793884. doi:10.3389/fgene.2022.793884

Kim, J., Lee, J., and Lee, T. H. (2015). Lysine acetylation facilitates spontaneous DNA dynamics in the nucleosome. *J. Phys. Chem. B* 119, 15001–15005. doi:10.1021/acs.jpcb.5b09734

Kim, Y. C., Gerlitz, G., Furusawa, T., Catez, F., Nussenzweig, A., Oh, K. S., et al. (2009). Activation of ATM depends on chromatin interactions occurring before induction of DNA damage. *Nat. Cell Biol.* 11, 92–96. doi:10.1038/ncb1817

Kolas, N. K., Chapman, J. R., Nakada, S., Ylanko, J., Chahwan, R., Sweeney, F. D., et al. (2007). Orchestration of the DNA-damage response by the RNF8 ubiquitin ligase. *Science* 318, 1637–1640. doi:10.1126/science.1150034

Konada, L., Aricthota, S., Vadla, R., and Haldar, D. (2018). Fission yeast sirtuin Hst4 functions in preserving genomic integrity by regulating replisome component Mcl1. *Sci. Rep.* 8, 8496. doi:10.1038/s41598-018-26476-4

Kouzarides, T. (2007). Chromatin modifications and their function. *Cell* 128, 693–705. doi:10.1016/j.cell.2007.02.005

Kusch, T., Florens, L., Macdonald, W. H., Swanson, S. K., Glaser, R. L., Yates, J. R., 3rd, et al. (2004). Acetylation by Tip60 is required for selective histone variant exchange at DNA lesions. *Science* 306, 2084–2087. doi:10.1126/science.1103455

Lee, H. S., Park, J. H., Kim, S. J., Kwon, S. J., and Kwon, J. (2010). A cooperative activation loop among SWI/SNF, gamma-H2AX and H3 acetylation for DNA double-strand break repair. *EMBO J.* 29, 1434–1445. doi:10.1038/emboj.2010.27

Lee, K. Y., Im, J. S., Shibata, E., and Dutta, A. (2017). ASF1a promotes non-homologous end joining repair by facilitating phosphorylation of MDC1 by ATM at double-strand breaks. *Mol. Cell* 68, 61–75. doi:10.1016/j.molcel.2017.08.021

Lewis, L. K., Karthikeyan, G., Cassiano, J., and Resnick, M. A. (2005). Reduction of nucleosome assembly during new DNA synthesis impairs both major pathways of double-strand break repair. *Nucleic Acids Res.* 33, 4928–4939. doi:10.1093/nar/gki806

Li, N., Li, Y., Lv, J., Zheng, X., Wen, H., Shen, H., et al. (2016). ZMYND8 reads the dual histone mark H3K4me1-H3K14ac to antagonize the expression of metastasis-linked genes. *Mol. Cell* 63, 470–484. doi:10.1016/j.molcel.2016.06.035

Li, Q., Zhou, H., Wurtele, H., Davies, B., Horazdovsky, B., Verreault, A., et al. (2008). Acetylation of histone H3 lysine 56 regulates replication-coupled nucleosome assembly. *Cell* 134, 244–255. doi:10.1016/j.cell.2008.06.018

Li, X., Corsa, C. A., Pan, P. W., Wu, L., Ferguson, D., Yu, X., et al. (2010). MOF and H4 K16 acetylation play important roles in DNA damage repair by modulating recruitment of DNA damage repair protein Mdc1. *Mol. Cell. Biol.* 30, 5335–5347. doi:10.1128/MCB.00350-10

Li, Y., Li, Z., Dong, L., Tang, M., Zhang, P., Zhang, C., et al. (2018). Histone H1 acetylation at lysine 85 regulates chromatin condensation and genome stability upon DNA damage. *Nucleic Acids Res.* 46, 7716–7730. doi:10.1093/nar/gky568

Liang, B., Qiu, J., Ratnakumar, K., and Laurent, B. C. (2007). RSC functions as an early double-strand-break sensor in the cell's response to DNA damage. *Curr. Biol.* 17, 1432–1437. doi:10.1016/j.cub.2007.07.035

Lieber, M. R. (2010). The mechanism of double-strand DNA break repair by the nonhomologous DNA end-joining pathway. *Annu. Rev. Biochem.* 79, 181–211. doi:10.1146/annurev.biochem.052308.093131

Luger, K., Rechsteiner, T. J., Flaus, A. J., Waye, M. M., and Richmond, T. J. (1997). Characterization of nucleosome core particles containing histone proteins made in bacteria. *J. Mol. Biol.* 272, 301–311. doi:10.1006/jmbi.1997.1235

Lukas, J., Lukas, C., and Bartek, J. (2011). More than just a focus: The chromatin response to DNA damage and its role in genome integrity maintenance. *Nat. Cell Biol.* 13, 1161–1169. doi:10.1038/ncb2344

Ma, P., and Schultz, R. M. (2008). Histone deacetylase 1 (HDAC1) regulates histone acetylation, development, and gene expression in preimplantation mouse embryos. *Dev. Biol.* 319, 110–120. doi:10.1016/j.ydbio.2008.04.011

Maas, N. L., Miller, K. M., DeFazio, L. G., and Toczyski, D. P. (2006). Cell cycle and checkpoint regulation of histone H3 K56 acetylation by Hst3 and Hst4. *Mol. Cell* 23, 109–119. doi:10.1016/j.molcel.2006.06.006

Mailand, N., Bekker-Jensen, S., Faustrup, H., Melander, F., Bartek, J., Lukas, C., et al. (2007). RNF8 ubiquitylates histones at DNA double-strand breaks and promotes assembly of repair proteins. *Cell* 131, 887–900. doi:10.1016/j.cell.2007.09.040

Marmorstein, R., and Zhou, M. M. (2014). Writers and readers of histone acetylation: Structure, mechanism, and inhibition. *Cold Spring Harb. Perspect. Biol.* 6, a018762. doi:10.1101/cshperspect.a018762

Martin, S. G., Laroche, T., Suka, N., Grunstein, M., and Gasser, S. M. (1999). Relocalization of telomeric Ku and SIR proteins in response to DNA strand breaks in yeast. *Cell* 97, 621–633. doi:10.1016/s0092-8674(00)80773-4

Masumoto, H., Hawke, D., Kobayashi, R., and Verreault, A. (2005). A role for cell-cycle-regulated histone H3 lysine 56 acetylation in the DNA damage response. *Nature* 436, 294–298. doi:10.1038/nature03714

Matsuoka, S., Ballif, B. A., Smogorzewska, A., McDonald, E. R., 3rd, Hurov, K. E., Luo, J., et al. (2007). ATM and ATR substrate analysis reveals extensive protein networks responsive to DNA damage. *Science* 316, 1160–1166. doi:10.1126/science.1140321

Melander, F., Bekker-Jensen, S., Falck, J., Bartek, J., Mailand, N., and Lukas, J. (2008). Phosphorylation of SDT repeats in the MDC1 N terminus triggers retention of NBS1 at the DNA damage-modified chromatin. *J. Cell Biol.* 181, 213–226. doi:10.1083/jcb.200708210

Meng, F., Qian, M., Peng, B., Peng, L., Wang, X., Zheng, K., et al. (2020). Synergy between SIRT1 and SIRT6 helps recognize DNA breaks and potentiates the DNA damage response and repair in humans and mice. *Elife* 9, e55828. doi:10.7554/eLife.55828

Meyer, B., Fabbrizi, M. R., Raj, S., Zobel, C. L., Hallahan, D. E., and Sharma, G. G. (2016). Histone H3 lysine 9 acetylation obstructs ATM activation and promotes ionizing radiation sensitivity in normal stem cells. *Stem Cell Rep.* 7, 1013–1022. doi:10.1016/j.stemcr.2016.11.004

Miller, K. M., and Jackson, S. P. (2012). Histone marks: Repairing DNA breaks within the context of chromatin. *Biochem. Soc. Trans.* 40, 370–376. doi:10.1042/BST20110747

Miller, K. M., Maas, N. L., and Toczyski, D. P. (2006). Taking it off: Regulation of H3 K56 acetylation by Hst3 and Hst4. *Cell Cycle* 5, 2561–2565. doi:10.4161/cc.5.22.3501

Miller, K. M., Tjeertes, J. V., Coates, J., Legube, G., Polo, S. E., Britton, S., et al. (2010). Human HDAC1 and HDAC2 function in the DNA-damage response to promote DNA nonhomologous end-joining. *Nat. Struct. Mol. Biol.* 17, 1144–1151. doi:10.1038/nsmb.1899

Mills, K. D., Sinclair, D. A., and Guarente, L. (1999). MEC1-dependent redistribution of the Sir3 silencing protein from telomeres to DNA double-strand breaks. *Cell* 97, 609–620. doi:10.1016/s0092-8674(00)80772-2

Mohan, C., Das, C., and Tyler, J. (2021). Histone and chromatin dynamics facilitating DNA repair. *DNA Repair (Amst)* 107, 103183. doi:10.1016/j.dnarep.2021.103183

Munoz-Galvan, S., Jimeno, S., Rothstein, R., and Aguilera, A. (2013). Histone H3K56 acetylation, Rad52, and non-DNA repair factors control double-strand break repair choice with the sister chromatid. *PLoS Genet.* 9, e1003237. doi:10.1371/journal.pgen.1003237

Murr, R., Loizou, J. I., Yang, Y. G., Cuenin, C., Li, H., Wang, Z. Q., et al. (2006). Histone acetylation by Trrap-Tip60 modulates loading of repair proteins and repair of DNA double-strand breaks. *Nat. Cell Biol.* 8, 91–99. doi:10.1038/ncb1343

Nakamura, K., Kato, A., Kobayashi, J., Yanagihara, H., Sakamoto, S., Oliveira, D. V., et al. (2011). Regulation of homologous recombination by RNF20-dependent H2B ubiquitination. *Mol. Cell* 41, 515–528. doi:10.1016/j.molcel.2011.02.002

Neumann, H., Hancock, S. M., Buning, R., Routh, A., Chapman, L., Somers, J., et al. (2009). A method for genetically installing site-specific acetylation in recombinant histones defines the effects of H3 K56 acetylation. *Mol. Cell* 36, 153–163. doi:10.1016/j.molcel.2009.07.027

North, B. J., and Verdin, E. (2004). Sirtuins: Sir2-related NAD-dependent protein deacetylases. *Genome Biol.* 5, 224. doi:10.1186/gb-2004-5-5-224

Ogiwara, H., Ui, A., Otsuka, A., Satoh, H., Yokomi, I., Nakajima, S., et al. (2011). Histone acetylation by CBP and p300 at double-strand break sites facilitates SWI/SNF chromatin remodeling and the recruitment of non-homologous end joining factors. *Oncogene* 30, 2135–2146. doi:10.1038/onc.2010.59210.1038/onc.2010.592

Onn, L., Portillo, M., Ilic, S., Cleitman, G., Stein, D., Kaluski, S., et al. (2020). SIRT6 is a DNA double-strand break sensor. *Elife* 9, e51636. doi:10.7554/eLife.51636

Ozdemir, A., Spicuglia, S., Lasonder, E., Vermeulen, M., Campsteijn, C., Stunnenberg, H. G., et al. (2005). Characterization of lysine 56 of histone H3 as an acetylation site in *Saccharomyces cerevisiae*. *J. Biol. Chem.* 280, 25949–25952. doi:10.1074/jbc.C500181200

Pal, S., Graves, H., Ohsawa, R., Huang, T. H., Wang, P., Harmacek, L., et al. (2016). The commercial antibodies widely used to measure H3 K56 acetylation are non-specific in human and Drosophila cells. *PLoS One* 11, e0155409. doi:10.1371/journal.pone.0155409

Panier, S., and Boulton, S. J. (2014). Double-strand break repair: 53BP1 comes into focus. *Nat. Rev. Mol. Cell Biol.* 15, 7–18. doi:10.1038/nrm3719

Papamichos-Chronakis, M., and Peterson, C. L. (2013). Chromatin and the genome integrity network. *Nat. Rev. Genet.* 14, 62–75. doi:10.1038/nrg3345

Plotnikov, A. N., Yang, S., Zhou, T. J., Rusinova, E., Frasca, A., and Zhou, M. M. (2014). Structural insights into acetylated-histone H4 recognition by the bromodomain-PHD finger module of human transcriptional coactivator CBP. *Structure* 22, 353–360. doi:10.1016/j.str.2013.10.021

Polo, S. E., Kaidi, A., Baskcomb, L., Galanty, Y., and Jackson, S. P. (2010). Regulation of DNA-damage responses and cell-cycle progression by the chromatin remodelling factor CHD4. *EMBO J.* 29, 3130–3139. doi:10.1038/emboj.2010.188

Powell, S. N., and Kachnic, L. A. (2003). Roles of BRCA1 and BRCA2 in homologous recombination, DNA replication fidelity and the cellular response to ionizing radiation. *Oncogene* 22, 5784–5791. doi:10.1038/sj.onc.1206678

Prado, F., Cortes-Ledesma, F., and Aguilera, A. (2004). The absence of the yeast chromatin assembly factor Asf1 increases genomic instability and sister chromatid exchange. *EMBO Rep.* 5, 497–502. doi:10.1038/sj.embor.7400128

Price, B. D., and D'Andrea, A. D. (2013). Chromatin remodeling at DNA double-strand breaks. *Cell* 152, 1344–1354. doi:10.1016/j.cell.2013.02.011

Qi, W., Chen, H., Xiao, T., Wang, R., Li, T., Han, L., et al. (2016). Acetyltransferase p300 collaborates with chromodomain helicase DNA-binding protein 4 (CHD4) to facilitate DNA double-strand break repair. *Mutagenesis* 31, 193–203. doi:10.1093/mutage/gev075

Qin, S., and Parthun, M. R. (2002). Histone H3 and the histone acetyltransferase Hat1p contribute to DNA double-strand break repair. *Mol. Cell. Biol.* 22, 8353–8365. doi:10.1128/MCB.22.23.8353-8365.2002

Ramanathan, B., and Smerdon, M. J. (1986). Changes in nuclear protein acetylation in u.v.-damaged human cells. *Carcinogenesis* 7, 1087–1094. doi:10.1093/carcin/7.7.1087

Recht, J., Tsubota, T., Tanny, J. C., Diaz, R. L., Berger, J. M., Zhang, X., et al. (2006). Histone chaperone Asf1 is required for histone H3 lysine 56 acetylation, a modification associated with S phase in mitosis and meiosis. *Proc. Natl. Acad. Sci. U. S. A.* 103, 6988–6993. doi:10.1073/pnas.0601676103

Rogakou, E. P., Boon, C., Redon, C., and Bonner, W. M. (1999). Megabase chromatin domains involved in DNA double-strand breaks *in vivo*. *J. Cell Biol.* 146, 905–916. doi:10.1083/jcb.146.5.905

Rogakou, E. P., Pilch, D. R., Orr, A. H., Ivanova, V. S., and Bonner, W. M. (1998). DNA double-stranded breaks induce histone H2AX phosphorylation on serine 139. *J. Biol. Chem.* 273, 5858–5868. doi:10.1074/jbc.273.10.5858

Roos, W. P., and Krumm, A. (2016). The multifaceted influence of histone deacetylases on DNA damage signalling and DNA repair. *Nucleic Acids Res.* 44, 10017–10030. doi:10.1093/nar/gkw922

Schiltz, R. L., Mizzen, C. A., Vassilev, A., Cook, R. G., Allis, C. D., and Nakatani, Y. (1999). Overlapping but distinct patterns of histone acetylation by the human coactivators p300 and PCAF within nucleosomal substrates. *J. Biol. Chem.* 274, 1189–1192. doi:10.1074/jbc.274.3.1189

Schneider, J., Bajwa, P., Johnson, F. C., Bhaumik, S. R., and Shilatifard, A. (2006). Rtt109 is required for proper H3K56 acetylation: A chromatin mark associated with the elongating RNA polymerase II. *J. Biol. Chem.* 281, 37270–37274. doi:10.1074/jbc.C600265200

Sengupta, A., and Haldar, D. (2018). Human sirtuin 3 (SIRT3) deacetylates histone H3 lysine 56 to promote nonhomologous end joining repair. *DNA Repair (Amst)* 61, 1–16. doi:10.1016/j.dnarep.2017.11.003

Sharma, G. G., So, S., Gupta, A., Kumar, R., Cayrou, C., Avvakumov, N., et al. (2010). MOF and histone H4 acetylation at lysine 16 are critical for DNA damage response and double-strand break repair. *Mol. Cell. Biol.* 30, 3582–3595. doi:10.1128/MCB.01476-09

Shim, E. Y., Hong, S. J., Oum, J. H., Yanez, Y., Zhang, Y., and Lee, S. E. (2007). RSC mobilizes nucleosomes to improve accessibility of repair machinery to the damaged chromatin. *Mol. Cell. Biol.* 27, 1602–1613. doi:10.1128/MCB.01956-06

Simoneau, A., Delgoshaie, N., Celic, I., Dai, J., Abshiru, N., Costantino, S., et al. (2015). Interplay between histone H3 lysine 56 deacetylation and chromatin modifiers in response to DNA damage. *Genetics* 200, 185–205. doi:10.1534/genetics.115.175919

Sivanand, S., Rhoades, S., Jiang, Q., Lee, J. V., Benci, J., Zhang, J., et al. (2017). Nuclear acetyl-CoA production by ACLY promotes homologous recombination. *Mol. Cell* 67, 252–265. e256. doi:10.1016/j.molcel.2017.06.008

Smolka, M. B., Albuquerque, C. P., Chen, S. H., and Zhou, H. (2007). Proteome-wide identification of *in vivo* targets of DNA damage checkpoint kinases. *Proc. Natl. Acad. Sci. U. S. A.* 104, 10364–10369. doi:10.1073/pnas.0701622104

Song, Z., Yang, L., Hu, W., Yi, J., Feng, F., and Zhu, L. (2021). Effects of histone H4 hyperacetylation on inhibiting MMP2 and MMP9 in human amniotic epithelial cells and in premature rupture of fetal membranes. *Exp. Ther. Med.* 21, 515. doi:10.3892/etm.2021.9946

Soria, G., Polo, S. E., and Almouzni, G. (2012). Prime, repair, restore: The active role of chromatin in the DNA damage response. *Mol. Cell* 46, 722–734. doi:10.1016/j.molcel.2012.06.002

Strahl, B. D., and Allis, C. D. (2000). The language of covalent histone modifications. *Nature* 403, 41–45. doi:10.1038/47412

Stucki, M., Clapperton, J. A., Mohammad, D., Yaffe, M. B., Smerdon, S. J., and Jackson, S. P. (2005). MDC1 directly binds phosphorylated histone H2AX to regulate cellular responses to DNA double-strand breaks. *Cell* 123, 1213–1226. doi:10.1016/j.cell.2005.09.038

Sun, Y., Jiang, X., Chen, S., Fernandes, N., and Price, B. D. (2005). A role for the Tip60 histone acetyltransferase in the acetylation and activation of ATM. *Proc. Natl. Acad. Sci. U. S. A.* 102, 13182–13187. doi:10.1073/pnas.0504211102

Sun, Y., Jiang, X., and Price, B. D. (2010). Tip60: Connecting chromatin to DNA damage signaling. *Cell Cycle* 9, 930–936. doi:10.4161/cc.9.5.10931

Swift, M. L., Beishline, K., and Azizkhan-Clifford, J. (2021). Sp1-dependent recruitment of the histone acetylase p300 to DSBs facilitates chromatin remodeling and recruitment of the NHEJ repair factor Ku70. *DNA Repair (Amst)* 105, 103171. doi:10.1016/j.dnarep.2021.103171

Tamburini, B. A., and Tyler, J. K. (2005). Localized histone acetylation and deacetylation triggered by the homologous recombination pathway of double-strand DNA repair. *Mol. Cell. Biol.* 25, 4903–4913. doi:10.1128/MCB.25.12.4903-4913.2005

Tang, J., Cho, N. W., Cui, G., Manion, E. M., Shanbhag, N. M., Botuyan, M. V., et al. (2013). Acetylation limits 53BP1 association with damaged chromatin to promote homologous recombination. *Nat. Struct. Mol. Biol.* 20, 317–325. doi:10.1038/nsmb.2499

Telford, D. J., and Stewart, B. W. (1989). Micrococcal nuclease: Its specificity and use for chromatin analysis. *Int. J. Biochem.* 21, 127–137. doi:10.1016/0020-711x(89)90100-6

Thaminy, S., Newcomb, B., Kim, J., Gatbonton, T., Foss, E., Simon, J., et al. (2007). Hst3 is regulated by Mec1-dependent proteolysis and controls the S phase checkpoint and sister chromatid cohesion by deacetylating histone H3 at lysine 56. *J. Biol. Chem.* 282, 37805–37814. doi:10.1074/jbc.M706384200

Tjeertes, J. V., Miller, K. M., and Jackson, S. P. (2009). Screen for DNA-damage-responsive histone modifications identifies H3K9Ac and H3K56Ac in human cells. *EMBO J.* 28, 1878–1889. doi:10.1038/emboj.2009.119

Toiber, D., Erdel, F., Bouazoune, K., Silberman, D. M., Zhong, L., Mulligan, P., et al. (2013). SIRT6 recruits SNF2H to DNA break sites, preventing genomic instability through chromatin remodeling. *Mol. Cell* 51, 454–468. doi:10.1016/j.molcel.2013.06.018

Tsabar, M., Waterman, D. P., Aguilar, F., Katsnelson, L., Eapen, V. V., Memisoglu, G., et al. (2016). Asf1 facilitates dephosphorylation of Rad53 after DNA double-strand break repair. *Genes Dev.* 30, 1211–1224. doi:10.1101/gad.280685.116

Tsubota, T., Berndsen, C. E., Erkmann, J. A., Smith, C. L., Yang, L., Freitas, M. A., et al. (2007). Histone H3-K56 acetylation is catalyzed by histone chaperone-dependent complexes. *Mol. Cell* 25, 703–712. doi:10.1016/j.molcel.2007.02.006

Tsukamoto, Y., Kato, J., and Ikeda, H. (1997). Silencing factors participate in DNA repair and recombination in *Saccharomyces cerevisiae*. *Nature* 388, 900–903. doi:10.1038/42288

Umehara, T., Nakamura, Y., Jang, M. K., Nakano, K., Tanaka, A., Ozato, K., et al. (2010). Structural basis for acetylated histone H4 recognition by the human BRD2 bromodomain. *J. Biol. Chem.* 285, 7610–7618. doi:10.1074/jbc.M109.062422

Utley, R. T., and Cote, J. (2003). The MYST family of histone acetyltransferases. *Curr. Top. Microbiol. Immunol.* 274, 203–236. doi:10.1007/978-3-642-55747-7_8

Vadla, R., Chatterjee, N., and Haldar, D. (2020). Cellular environment controls the dynamics of histone H3 lysine 56 acetylation in response to DNA damage in mammalian cells. *J. Biosci.* 45, 19. doi:10.1007/s12038-019-9986-z

van Attikum, H., Fritsch, O., Hohn, B., and Gasser, S. M. (2004). Recruitment of the INO80 complex by H2A phosphorylation links ATP-dependent chromatin remodeling with DNA double-strand break repair. *Cell* 119, 777–788. doi:10.1016/j.cell.2004.11.033

Van, H. T., and Santos, M. A. (2018). Histone modifications and the DNA double-strand break response. *Cell Cycle* 17, 2399–2410. doi:10.1080/15384101.2018.1542899

Vazquez, B. N., Thackray, J. K., Simonet, N. G., Kane-Goldsmith, N., Martinez-Redondo, P., Nguyen, T., et al. (2016). SIRT7 promotes genome integrity and modulates non-homologous end joining DNA repair. *EMBO J.* 35, 1488–1503. doi:10.15252/embj.201593499

Vempati, R. K., Jayani, R. S., Notani, D., Sengupta, A., Galande, S., and Haldar, D. (2010). p300-mediated acetylation of histone H3 lysine 56 functions in DNA damage response in mammals. *J. Biol. Chem.* 285, 28553–28564. doi:10.1074/jbc.M110.149393

Wang, F., Kou, Z., Zhang, Y., and Gao, S. (2007). Dynamic reprogramming of histone acetylation and methylation in the first cell cycle of cloned mouse embryos. *Biol. Reprod.* 77, 1007–1016. doi:10.1095/biolreprod.107.063149

Wang, Y., Kallgren, S. P., Reddy, B. D., Kuntz, K., Lopez-Maury, L., Thompson, J., et al. (2012). Histone H3 lysine 14 acetylation is required for activation of a DNA damage checkpoint in fission yeast. *J. Biol. Chem.* 287, 4386–4393. doi:10.1074/jbc.M111.329417

Wang, Z., Zang, C., Rosenfeld, J. A., Schones, D. E., Barski, A., Cuddapah, S., et al. (2008). Combinatorial patterns of histone acetylations and methylations in the human genome. *Nat. Genet.* 40, 897–903. doi:10.1038/ng.154

Wilson, M. D., and Durocher, D. (2017). Reading chromatin signatures after DNA double-strand breaks. *Philos. Trans. R. Soc. Lond. B Biol. Sci.* 372, 20160280. doi:10.1098/rstb.2016.0280

Wu, F., Xu, L., Tu, Y., Cheung, O. K., Szeto, L. L., Mok, M. T., et al. (2022). Sirtuin 7 super-enhancer drives epigenomic reprogramming in hepatocarcinogenesis. *Cancer Lett.* 525, 115–130. doi:10.1016/j.canlet.2021.10.039

Wurtele, H., Kaiser, G. S., Bacal, J., St-Hilaire, E., Lee, E. H., Tsao, S., et al. (2012). Histone H3 lysine 56 acetylation and the response to DNA replication fork damage. *Mol. Cell. Biol.* 32, 154–172. doi:10.1128/MCB.05415-11

Xhemalce, B., Miller, K. M., Driscoll, R., Masumoto, H., Jackson, S. P., Kouzarides, T., et al. (2007). Regulation of histone H3 lysine 56 acetylation in *Schizosaccharomyces pombe*. *J. Biol. Chem.* 282, 15040–15047. doi:10.1074/jbc.M701197200

Xu, F., Zhang, K., and Grunstein, M. (2005). Acetylation in histone H3 globular domain regulates gene expression in yeast. *Cell* 121, 375–385. doi:10.1016/j.cell.2005.03.011

Xu, Y., and Price, B. D. (2011). Chromatin dynamics and the repair of DNA double strand breaks. *Cell Cycle* 10, 261–267. doi:10.4161/cc.10.2.14543

Yuan, J., Pu, M., Zhang, Z., and Lou, Z. (2009). Histone H3-K56 acetylation is important for genomic stability in mammals. *Cell Cycle* 8, 1747–1753. doi:10.4161/cc.8.11.8620

Zhang, P. Y., Li, G., Deng, Z. J., Liu, L. Y., Chen, L., Tang, J. Z., et al. (2016). Dicer interacts with SIRT7 and regulates H3K18 deacetylation in response to DNA damaging agents. *Nucleic Acids Res.* 44, 3629–3642. doi:10.1093/nar/gkv1504

Zhang, Z., Yang, Q., Sun, G., Chen, S., He, Q., Li, S., et al. (2014). Histone H3K56 acetylation is required for quelling-induced small RNA production through its role in homologous recombination. *J. Biol. Chem.* 289, 9365–9371. doi:10.1074/jbc.M113.528521

Advantages of publishing in Frontiers

OPEN ACCESS
Articles are free to read for greatest visibility and readership

FAST PUBLICATION
Around 90 days from submission to decision

HIGH QUALITY PEER-REVIEW
Rigorous, collaborative, and constructive peer-review

TRANSPARENT PEER-REVIEW
Editors and reviewers acknowledged by name on published articles

Frontiers
Avenue du Tribunal-Fédéral 34
1005 Lausanne | Switzerland

Visit us: www.frontiersin.org
Contact us: frontiersin.org/about/contact

REPRODUCIBILITY OF RESEARCH
Support open data and methods to enhance research reproducibility

DIGITAL PUBLISHING
Articles designed for optimal readership across devices

FOLLOW US
@frontiersin

IMPACT METRICS
Advanced article metrics track visibility across digital media

EXTENSIVE PROMOTION
Marketing and promotion of impactful research

LOOP RESEARCH NETWORK
Our network increases your article's readership